Universitat Jaume I

Escuela de Doctorado de la Universitat Jaume I

Programa de Doctorado en Química Sostenible

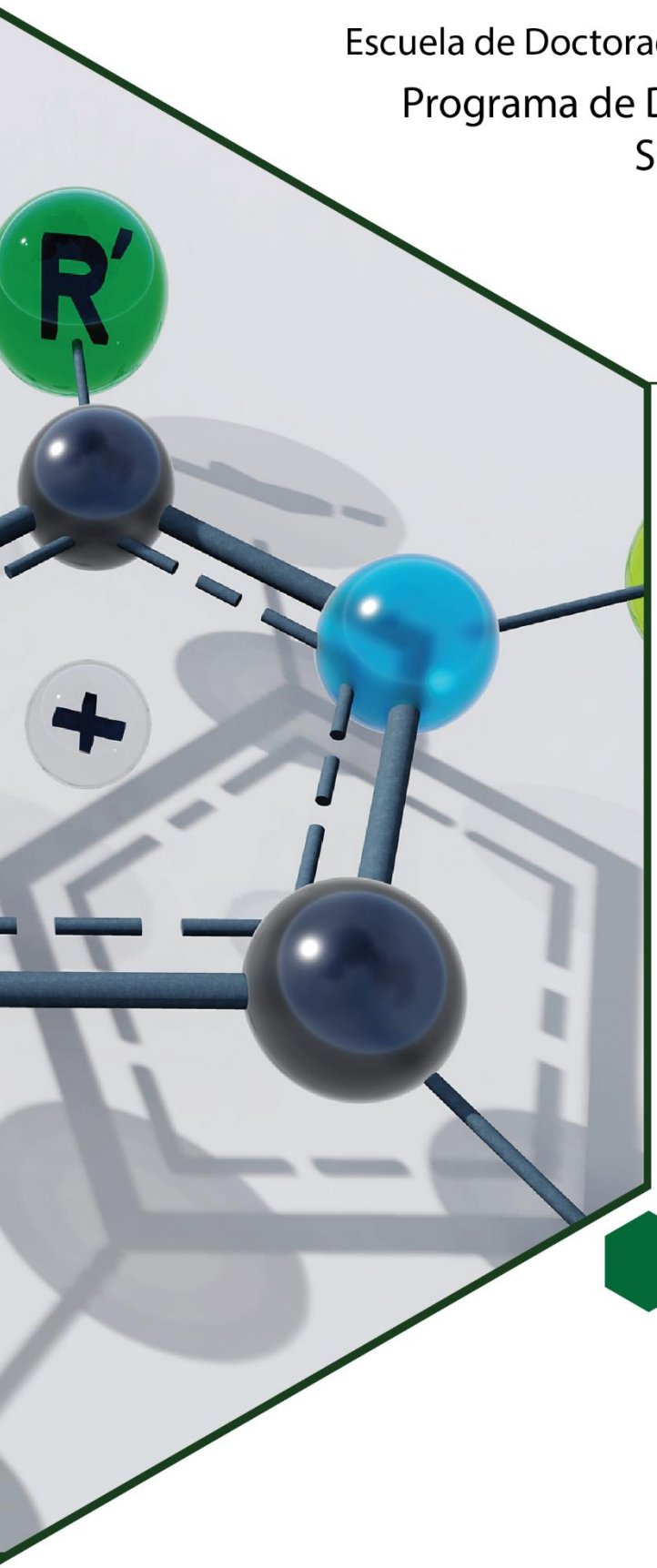

Tesis Doctoral

Materiales poliméricos multifuncionales basados en líquidos iónicos

Estrategias para el desarrollo de aplicaciones avanzadas en Química Sostenible en la UNED de Costa Rica

Autor

David A. Valverde Barquero

Directores

Dr. Eduardo García- Verdugo Cepeda

Dr. Santiago V. Luis Lafuente

Noviembre, 2020

UNIVERSITAT JAUME I

Escuela de Doctorado de la Universitat Jaume I

Programa de Doctorado en Química Sostenible

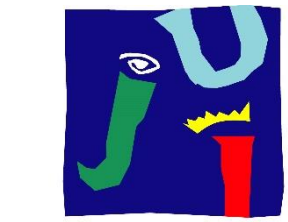

UNIVERSITAT JAUME·I

Tesis Doctoral

Materiales Poliméricos Multifuncionales basados en Líquidos Iónicos. Estrategias para el Desarrollo de Aplicaciones Avanzadas en Química Sostenible en la UNED de Costa Rica

Autor:

David A. Valverde Barquero

Directores:

Dr. Eduardo García-Verdugo Cepeda

Dr. Santiago V. Luis Lafuente

Noviembre, 2020

Programa de Doctorado en

QUÍMICA SOSTENIBLE

Escuela de Doctorado de la Universitat Jaume I

Título de la tesis

Materiales Poliméricos Multifuncionales basados en Líquidos Iónicos. Estrategias para el Desarrollo de Aplicaciones Avanzadas en Química Sostenible en la UNED de Costa Rica

Memoria presentada por **David A. Valverde Barquero** para optar al grado de **Doctor** por la Universitat Jaume I

Doctorando

DAVID ALBERTO\|VALVERDE\|BARQUERO
Firmado digitalmente por DAVID ALBERTO\|VALVERDE\|BARQUERO
Fecha: 2020.12.22 11:44:00 +01'00'

David A. Valverde Barquero

Directores de la Tesis

EDUARDO\|GARCIA VERDUGO\|CEPEDA
Firmado digitalmente por EDUARDO\|GARCIA VERDUGO\|CEPEDA
Nombre de reconocimiento (DN): cn=EDUARDO\|GARCIA VERDUGO\|CEPEDA, serialNumber=18999710P, givenName=EDUARDO, sn=GARCIA VERDUGO CEPEDA, ou=CIUDADANOS, o=ACCV, c=ES
Fecha: 2020.12.22 11:54:25 +01'00'

Dr. Eduardo García-Verdugo Cepeda

SANTIAGO VICENTE\|LUIS\|LAFUENTE
Firmado digitalmente por SANTIAGO VICENTE\|LUIS\|LAFUENTE
Nombre de reconocimiento (DN): cn=SANTIAGO VICENTE\|LUIS\|LAFUENTE, serialNumber=17854184C, givenName=SANTIAGO VICENTE, sn=LUIS LAFUENTE, ou=CIUDADANOS, o=ACCV, c=ES
Fecha: 2020.12.22 12:17:31 +01'00'

Dr. Santiago V. Luis Lafuente

Castellón de la Plana, Noviembre de 2020

Financiación recibida

La realización de esta tesis Doctoral ha sido posible gracias a la concesión de la beca institucional por parte del Consejo de Becas Institucional, adscrita a la iniciativa 6 del Acuerdo de Mejoramiento Institucional (AMI) de la Universidad Estatal a Distancia (UNED) de Costa Rica.

La financiación de la actividad investigadora ha sido posible gracias a los proyectos concedidos por el Ministerio de Economía y Competitividad del Gobierno de España (MECD CTQ2015-68429-R / CTQ RTI 2018-098233-B-C22) y por la Generalitat Valenciana (Prometeo 2016-071).

A quienes siempre me han apoyado…

Agradecimientos

A mis directores el Profesor Dr. Eduardo García-Verdugo y el Profesor Dr. Santiago V. Luis, que durante el desarrollo de la presente tesis doctoral me han permitido desarrollar y enriquecer mi formación académica e investigadora en el área de la Química, mostrando su pasión y rigor científico. Les agradezco su compresión, dedicación y guía en esta investigación, por su ayuda sin importar el momento en que acudí a cada uno de ellos.

Así mismo expreso mi agradecimiento a la Dr. María Isabel Burguete, a la Dr. Belén Altava y al Dr. Víctor Sans por su valiosa disponibilidad durante la realización de esta investigación. Dentro de este grupo quiero agradecer por su amistad y disposición incondicional al Dr. Raúl Porcar.

Doy gracias al Departamento de Química Inorgánica y Orgánica, así como al soporte técnico brindado por el SCIC de la Universitat Jaume I.

Un agradecimiento especial a mis compañeros de laboratorio, mis amigos en este viaje de aventuras Edgar P., Adriana V., Ferran E., Iván M., María M., Daniel N., Roberta P., Bárbara G. A David M., Marikena P., Adrián E., Julián S. y a todos los compañeros que han trabajado a mi lado.

Finalmente y no menos importante, agradezco a la Vicerrectoría Académica, a la Escuela de Ciencias Exactas y Naturales, al Acuerdo de Mejoramiento Institucional (AMI) y al Consejo de Becas Institucional de la UNED de Costa Rica por haberme otorgado la beca doctoral que me ha permitido viajar y residir en España para optar por el grado de Doctor en Química Sostenible.

"Estoy entre aquellos que piensan que la ciencia tiene una gran belleza"

Marie Curie

Abreviaturas

Todas las abreviaturas utilizadas en este trabajo hacen referencia a su acrónimo en inglés.

2-MeTHF	2-metil tetrahidrofurano (*2-methyl tetrahydrofuran*)
3DP	Impresión tridimensional / Impresión 3D (*three-dimensional printing / 3D printing)*
AE	Economía atómica (*Atom Economy*)
AIBN	2,2'-Azobis 2-metilpropionitrilo) (*2,2'-Azobis(2-methylpropionitrile)*)
AM	Fabricación aditiva de materiales (*Additive Manufacturing)*
ATRP	Polimerización por transferencia de átomos (*Atom Transfer Radical Polimerization*)
BAPO	Óxido de fenil*bis*(2,4,6-trimetilbenzoil)fosfina (*phenilbis(2,4,6-trimethylbenzoyl)phosphine oxide*)
BET	Brunauer–Emmett–Teller (*Brunauer–Emmett–Teller*)
BJ	Inyección del pegamento (*Binder Jetting*)
BTB	Azul de bromotimol (*Bromothymol Blue*)
cEF	Factor medioambiental completo (*Complete E Factor*)
ClVB	Clorometilestireno (*Chloromethylstyrene*)
CMDTTC	Tritiocarbonato de cianometil dodecilo (*Cyanomethyl dodecyl trithiocarbonate*)

CRP	Polimerización radicalaria controlada (*Controlled Radical Polymerization*)
CTA	Agente de transferencia de la cadena (*Chain Transfer Agent*)
D	Difusividad (*Diffusivity*)
D*	Relación de Einstein (*Einstein relation*)
$\mathbf{D_a}$	Coeficiente de difusión del anión (*Diffusion Coefficient for the Anion*)
$\mathbf{D_c}$	Coeficiente de difusión del catión (*Diffusion Coefficient for the Cation*)
DED	Deposición directa de la energía (*Direct Energy Deposition*)
DMC	Dimetil carbonato (*Dimethyl carbonate*)
DMF	N,N-dimetilformamida (*N,N-dimethylformamide*)
DMSO	Dimetilsulfóxido (*Dimethyl sulfoxide*)
DPA	Difenilantraceno (*Diphenylanthracene*)
DSC	Calorimetría diferencial de barrido (*Differential Scanning Calorimetry*)
DVB	Divinilbenceno (*Divinyl benzene*)
E Factor	Factor medioambiental (*E-nvironmental Factor*)
$\mathbf{E_{act}}$	Energía de activación (*Activation Energy*)

E_{dis}	Energía de disociación (*Dissociation Energy*)
EGDMA	Etilen glicol dimetacrilato (*Ethylen glycol dimethacrylate*)
EHS	Medioambiente, salud y seguridad (*Environmental, Healt and Safety*)
EP	Polarización de electrodos (*Electrode Polarization*)
ET	Estado de transición *(Transition State)*
Et_2O	Etanol (*Ethanol*)
F_R	Velocidad de flujo (*Flow Rate)*
FRET	Tansferencia de energía de resonancia de Föster (*Förster's resonance energy transfer*)
G-L	Gas-líquido (*Gas-liquid*)
GMA	Glicidil metacrilato (*Glycidyl methacrylate*)
HBD	Donante de enlace de hidrógeno (*Hydrogen Bond Donor*)
HPLC	Cromatografía líquida de alta eficiencia (*High Performance Liquid Chromatography*)
ID	Diámetro interno (*Internal Diameter*)
ILC-SILP	SILP-líquidos iónicos cristalinos (*Ionic Liquid Crystalline-SILP*)
ILs	Líquidos iónicos (*Ionic Liquids*)

IM	Intermedio *(Intermediate)*
IPA	Alcohol isopropílico / (2-propanol) (*Isopropyl alcohol*) / (*2-propanol*)
IR-FT-ATR	Espectroscopía infrarroja por transformada de Fourier-reflexión total atenuada (*Fourier Transform Infrared Spectroscopy - Attenuated total Reflection*)
IR-Raman	Espectroscopía infrarroja -Raman (*Infrared Spectroscopy-Raman*)
k	Constante (*Constant*)
L	Espesor (*Thickness*)
LCA	Análisis del ciclo de vida (*Life Cycle Assessment*)
LCD	Pantalla de Cristal líquido (*Liquid Crystal-Display*)
$\mathbf{L_D}$	Longitud de Debye (*Debye length*)
LEDs	Diodo emisor de luz (*Light-emitting diodes)*
M	Relación del grosor de la muestra al doble de la longitud de Debye (*Ratio of the sample thickness to twice the Debye length*)
ME	Extrusión del material (*Material Extrusion*)
MeOH	Metanol (M*ethanol*)
MJ	Inyección del material (*Material jetting*)
MOFs	*Marcos orgánicos para metales* *(Metal Organic Frameworks)*

***m*-SILLPs**	Líquidos iónicos monolíticos soportados covalentemente (*Monolithic Supported Ionic Liquid like-Phases*)
n	Concentración de carga (*Charge Concentration*)
N°	Número (*Number*)
n_0	Número de densidad (*Number Density*)
NBP	4-(4-nitrobencil)piridina (*4-(4-nitrobenzyl)pyridine*)
NFm	Tejido de nanofibra (*Nanofibers Mats*)
NFs	Nanofibras (*Nanofibers*)
NMP	Polimerización mediada por nitróxido (*Nitroxide-mediated Radical Polymerization*)
NMR	Resonancia magnética nuclear (*Nuclear Resonance Magnetic*)
n_{tot}	Concentración total de iones (*Total concentration of ions*)
OD	Diámetro externo (*Outside Diameter*)
P	Presión *(Pressure)*
PAHT	Poli(acrilamida-homocisteína tiolactona) (*Poly(acrylamide-homocysteine thiolactone)*)
PBF	Fusión de lecho de polvo (*Powder Bed Fusion*)
P_c	Presión crítica *(Critical Pressure)*
PDI	Índice de polidispersidad (*Polydispersity Index*)

PDT	Terapias fotodinámicas (*Photodynamic Therapies*)
PEEK	Poliéter éter cetona (*Polyether ether ketone*)
PEGDMA	Poli(etilenglicol) dimetacrilato (*Poly(ethylene glycol) dimethacrylate*)
PILs	Líquidos iónicos poliméricos (*Polymeric Ionics Liquids*)
PMI	Intensidad de masa en el proceso (*Process Mass Intensity*)
ppm	Partes por millón (*part per million*)
PS-DVB	Poliestireno-estireno / divinilbenceno (*Polystyrene-styrene / Divinyl benzene*)
PSILs	Líquidos iónicos poliméricos soportados (*Polymer Supported Ionic Liquids*)
PTFE	Politetrafluoroetileno (P*olytetrafluoroethylene*)
PVP	Polivinilpirrolidona (*Polyvinylpyrrolidone*)
QD	Punto cuántico (*Quantum Dot*)
QDs-SILLPs	Puntos cuánticos inmovilizados en SILLPs (*Quantum Dots Immobilized on SILLPs*)
RAFT	Fragmentación y transferencia de cadena por adición reversible (*Reversible Addition-Fragmentation Chain Transfer*)
RB	Rosa de Bengala (*Rose Bengal*)
RB-PS-DVB	Rosa de bengala-poliestireno-divinilbenceno (*Rose Bengal-Polystyrene-Divinyl bencene*)

RB-SILLPs	Rosa de Bengala inmovilizado en SILLPs (*Rose Bengal Immobilized on SILLPs*)
Rh6G	Rodamina 6G (*Rhodamine 6G*)
RhB	Rodamina B (*Rhodaine B*)
RME	Eficiencia de masa en la reacción (*Reaction Mass Efficiency*)
r.t	Temperatura ambiente (*Room temperature*)
scCO$_2$	Dióxido de carbono supercrítico (*Supercritical Carbon Dioxide)*
scFs	Fluidos supercríticos (S*upercritical Fluids*)
SCILL	Catalizadores sólidos con capas de líquidos iónicos (*Solid Catalysts with Ionic Liquids Layers*)
SCILs	Catalizadores sólidos con líquidos iónicos (*Solid Catalysts with Ionic Liquids*)
SD	Subdifusivo (*Subdiffusive*)
SDGs	Objetivos del Desarrollo Sostenible (*Sustainable Development Goals*)
sEF	Factor medioambiental simple (*Simple E Factor*)
SEM	Microscopio de barrido electrónico (*Scanning electron microscope*)
SILC/SILCAs	Catalizadores de líquidos iónicos soportados (*Supported Ionic Liquid Catalysis/Catalysts*)
SILF	Líquidos iónicos soportados en películas (*Supported Ionic Liquids Film*)
SILLPs	Líquidos iónicos soportados en fase sólida (*Supported Ionic Liquid like-Phases*)

SILMs	Membranas de líquidos iónicos soportados (*Supported Ionic Liquid Membranes*)
SILnPs	Líquidos iónicos soportados con nanopartículas (*Supported Ionic Liquids Nanoparticles*)
SILPs	Líquidos iónicos soportados en fase sólida (*Supported Ionic Liquid Phases*)
SILs	Líquidos iónicos soportados (*Supported Ionic Liquids*)
SL	Laminación de hoja (*Sheet Lamination*)
SSILP	SILP estructurados (*Structured SILP*)
T	Temperatura *(Temperature)*
T_c	Temperatura crítica (*Critical Temperature)*
TEA	Trietilamina (*Triethylamine*)
TGA	Análisis termogravimétrico (*Thermogravimetric Analysis*)
THF	Tetrahidrofurano (*Tetrahydrofuran*)
T_m	Punto de fusión (*Melting Point*)
TMPTMA	Trimetacrilato de trimetilolpropano (*Trimethylolpropane trimethacrylate*)
TOF	Frecuencia de repetición (*Turnover Frequency*)
TON	Número de repetición (*Turnover Number)*

T_R	Tiempo de residencia (*Residence Time*)
TSILs	Líquidos iónicos con tareas específicas (*Task Specific Ionic Liquids*)
TS-PILs	Líquidos iónicos poliméricos con tareas específicas (*Task Specific-Polymeric Ionic Liquids*)
TTC	Tritiocarbonatos (*Trithiocarbonates)*
US EPA	Agencia de Protección Ambiental de Estados Unidos (*United States Environmental Protection Agency*)
UV	Ultravioleta (*Ultraviolet*)
UV/Vis	Ultravileta/Visible (*Ultraviolet/Visible*)
VFT	Vogel–Fulcher–Tammann (*Vogel–Fulcher–Tammann*)
VOCs	Compuestos orgánicos volátiles (*Volatile Organic Compounds*)
VP	Fotopolimerización en cubeta (*Vat Photopolymerization*)
V_R	Volumen del reactor (*Reactor Volume*)
WCA	Ángulo de contacto con el agua (*Water Contact Angle*)
wt	Peso (*Weight)*
X	Fracción molar (*Molar fraction*)
ZIs	Sales iónicas zwiterionicas (*Zwitterionic Ionic Salts*)

Símbolos

Hz	Hertz (*hertz*)
k_B	Constante de Boltzmann (*Boltzmann constant*)
mM	Milimolar (*millimolar*)
MPa	Mega Pascal (*Mega Pascal*)
Mw	Peso Molar (*Molar weigth*)
q	Carga del cation monovalente (*charge of a monovalent cation*)
ppm	Partes por millón (*parts per millon*)
W	Watts (W*atts*)
w/v	Peso/volumen (*weigth/volume*)
w/w	Peso/peso (*weigth/weigth)*
α	Relajación Cole-Cole (*Cole–Cole relaxation*)
ε	Permitividad dieléctrica (*dielectric permittivity*)
ε*	Permitividad dieléctrica compleja (*complex dielectric permittivity*)

σ	Conductividad (*conductivity*)
σ^*	Conductividad compleja (*complex conductivity*)
$\|\sigma\|$	Módulo de conductividad (*modulus of conductivity*)
τ_{EP}	Tiempo de relajación del electro de polarización (*electrode polarization time relaxation*)
τ_m	Tiempo de relajación asociado con la conductividad (r*elaxation time associated with the conductivity*)
φ	Ángulo de fase (phase angle)
ω	Frecuencia angular (*angular frequency*)
Ø	Diámetro (*diameter*)

Resumen de la Memoria presentada para optar al grado de Doctor

Materiales Poliméricos Multifuncionales basados en Líquidos Iónicos. Estrategias para el desarrollo de aplicaciones avanzadas en Química Sostenible en la UNED de Costa Rica

David A. Valverde Barquero

Esta tesis Doctoral se enmarca en el área de la Química Sostenible y se centra específicamente en el desarrollo de materiales poliméricos multifuncionales basados en líquidos iónicos. El eje central es el diseño, preparación, desarrollo y aplicación de los materiales poliméricos modificados basados en líquidos iónicos, integrando una serie de técnicas novedosas consideradas como herramientas útiles en la Química Sostenible, las cuales pueden ser puestas en práctica en la UNED de Costa Rica.

La memoria de la tesis está estructurada en nueve capítulos. Se ha redactado siguiendo el esquema principal del formato de artículo científico según el trabajo de investigación desarrollado. Los resultados obtenidos permitieron la publicación de dos artículos (citados en el apartado de divulgación de este trabajo) en las revistas "*Physical Chemistry Chemical Physics*" y en "*ChemSusChem*", un tercer artículo aceptado en la "*ACS Sustainable Chemistry & Engineering*", revistas de alto índice de impacto y con gran consideración dentro del área de la Química Sostenible. Además, el trabajo realizado ha permitido la preparación de otros tres manuscritos que serán enviados en breve esperando a ser publicados también en revistas de alto impacto. Cada capítulo del desarrollo incluye un breve resumen en español e inglés, así como una descripción introductoria sobre el tema, la discusión de resultados, las conclusiones, la sección experimental y la información suplementaria. Las abreviaciones y símbolos empleados recurrentemente se acopian al principio del documento por orden alfabético.

Respecto a la organización de los capítulos, se establecieron de tal forma que facilite la comprensión de los resultados y una lectura fluida. En este sentido, inicialmente se encuentra el *Capítulo I. Introducción* el cual incluye de forma

general los temas principales que se tratan en el desarrollo de la tesis. Esto permite ubicar al lector y mostrarle los aspectos teóricos del desarrollo y la importancia de los resultados obtenidos. Este capítulo es una breve revisión bibliográfica sobre la Química Sostenible, líquidos iónicos, líquidos iónicos soportados, catálisis, estrategias avanzadas para aplicaciones en Química Verde (reacciones en flujo continuo, fluidos supercríticos, electrohilado e impresión 3D) y materiales conductores iónicos.

Seguidamente, en el *Capítulo II. Objetivos* se exponen los objetivos generales y específicos de la tesis, con el fin de que el lector centre su atención y comprenda las motivaciones del trabajo.

A partir de este punto, durante seis capítulos se detalla la discusión de los resultados obtenidos sobre los materiales desarrollados y sus potenciales aplicaciones.

En el artículo publicado, llamado en este trabajo como *Capítulo III. Difusividad de iones libres y concentración de carga en membranas de líquidos iónicos poliméricos entrecruzados tipo ionogel basados en sales zwiterionicas sulfonadas e iones de Litio*, se diferencia ligeramente de los demás. En este se describe la síntesis de las mezclas de líquidos iónicos zwiterionicos (ZIs) y $LiNTf_2$, ya que cuentan con propiedades interesantes como su elevada conducción iónica o como fases líquidas en la preparación de membranas basadas en PILs entrecruzados. Los materiales preparados mostraron elevadas conductividades correlacionadas con la composición monomérica y la con la mezcla ZIs:$LiNTf_2$, así como buenas propiedades mecánicas y alta estabilidad térmica.

El *Capítulo IV. Síntesis en flujo continuo para la preparación simple de polímeros esféricos funcionalizados derivados del Poli(acrilamida-tiolactona)*, se reporta la manera simple y rápida la preparación de polímeros esféricos funcionalizados mediante un sistema de flujo continuo. El grupo funcional de la tiolactona

permite la incorporación de dos grupos funcionales adicionales, proporcionando materiales con propiedades interesantes para aplicaciones como la catálisis.

En el *Capítulo V. Preparación y aplicación de tejidos de nanofibras derivados de Líquidos Iónicos Poliméricos*, se desarrolla la preparación y obtención de tejidos de nanofibras por el electrohilado utilizando la mezcla de un líquido iónico polimérico funcionalizado con unidades de amino-homocisteína tiolactona y la poli(vinilpirrolidona). Dado a la presencia del grupo funcional de la tiolactona, los tejidos obtenidos pueden ser modificados mediante procesos de post-funcionalización, lo que permite la introducción de nuevos grupos funcionales y el entrecruzamiento de las nanofibras. Como una primera aproximación, los materiales modificados se utilizaron en diferentes aplicaciones como la detección de aminas volátiles y en catálisis.

Seguidamente el artículo publicado, titulado en esta tesis como *Capítulo VI. Rosa de Bengala inmovilizado sobre "Fases Soportadas relacionadas con los Líquidos Iónicos": Un fotocatalizador eficiente para procesos en discontinuo y en flujo continuo*, se evalúa la actividad fotocatalítica del Rosa de Bengala (RB) inmovilizado sobre materiales conteniendo fases soportadas relacionadas con los líquidos iónicos. Bajo la perspectiva de un fotocatalizador soportado sobre un polímero, este fue diseñado para que desarrollara un papel fundamental en la catálisis. Al ser modificado con unidades semejantes a un líquido iónico, la estructura polimérica no solo mantuvo su carácter inerte hacia el RB sino que controlaba la accesibilidad de los reactivos / sustratos a los centros activos, proporcionando un microambiente específico para la reacción.

El *Capítulo VII. Polímeros Multifuncionales basados en líquidos iónicos y fragmentos de Rosa de Bengala para la conversión de CO_2 a carbonatos*, (artículo aceptado) se desarrollaron sistemas organocatalíticos basados en materiales poliméricos conteniendo fases soportadas relacionadas con los líquidos iónicos, los cuales contenían unidades de Rosa de Bengala. Los materiales se probaron en la

reacción de cicloadición de CO_2 a epóxidos y se demostró que la actividad catalítica puede ser mejorada ajustando y controlando la naturaleza del SILLP. Además, los materiales desarrollados mostraron una gran estabilidad, sin disminución en la actividad catalítica al ser probados en condiciones de flujo continuo.

El último capítulo de resultados, *Capítulo VIII. Impresión 3D como herramienta facilitadora de técnicas emergentes. Conversión catalítica de CO_2 estable y más eficiente en procesos de flujo continuo usando reactores impresos basados en líquidos iónicos soportados*, trata sobre como la impresión 3D a través del diseño digital facilita la obtención de materiales avanzados con geometrías complejas. Los materiales impresos se modificaron con unidades semejantes a los líquidos iónicos lo que permitiendo su empleo como catalizadores eficientes bajo condiciones de flujo continuo en la conversión de CO_2 a ciclocarbonatos. La digitalización del catalizador permite obtener sistemas que presentan las propiedades moleculares de los líquidos iónicos a la vez que la configuración macroscópica permitió mejorar su eficiencia catalítica en términos de productividad, en la reacción de clicoadición de CO_2 en presencia de epóxidos.

Para finalizar, el *Capítulo IX. Conclusiones generales*, se engloban las conclusiones más relevantes derivadas del trabajo desarrollado en cada uno de los manuscritos que integran esta tesis doctoral.

Summary of the Thesis to qualify for the Doctor degree

Multifunctional Polymeric Materials based on Ionic Liquids. Strategies for the development of advanced applications in Sustainable Chemistry in the UNED from Costa Rica

David A. Valverde Barquero.

This Doctoral Thesis is framed in the area of Sustainable Chemistry and focuses specifically on the development of multifunctional polymeric materials based on ionic liquids. The central axis is the design, preparation, development and application of these materials, integrating a series of novel techniques considered enabling tools to develop Sustainable Chemistry, which can be put into practice in the UNED from Costa Rica.

This Thesis has been structured in nine chapters. It has been written following the main outline of the scientific article format according to the research work developed. The obtained results have allowed the publication of two articles (cited in the dissemination section of this work) in the journal "*Physical Chemistry Chemical Physics*" and "*ChemSusChem*", a third article accepted in the "*ACS Sustainable Chemistry & Engineering*", which has a high impact index in the field of Sustainable Chemistry. In addition, the work carried out has allowed the preparation of another four manuscript drafts that will be sent shortly hoping to be published also in high impact specialized journals. Each chapter includes a brief summary in Spanish and English, as well as an introductory description of the topic, discussion of results, conclusions, experimental section and the supplementary information. The abbreviations and symbols frequently used throughout this work are collected at the beginning of the thesis in alphabetical order.

Regarding the order of the chapters, it has been established in such a way to facilitate the understanding of the results and fluent reading. In this sense, initially there is *Chapter I. Introduction* which includes, in a general way, the main topics that are dealt with in the development of the thesis. Aiming to provide the

reader with the basic theoretical aspects and state of art on the field. Thus, this chapter is a brief bibliographic review on Sustainable Chemistry, ionic liquids, supported ionic liquids, catalysis, advances strategies for applications in Green Chemistry (continuous flow reactions, supercritical fluids, electrospinning, and 3D printing) and ionic conductive materials.

Next, in *Chapter II. Objectives*, the general and specifics objectives of this thesis are presented to the reader specifying the main motivations of the work.

From this point on, in the next six chapters the discussion of the results obtained on the materials developed and their potential applications is detailed.

In the published article, called in this work *as Chapter III. Free ion diffusivity and charge concentration on cross-linked Polymeric Ionic Liquid ionogel films based on sulfonated zwitterion salts and Lithium ions,* differs slightly from the others. This chapter describes the synthesis of zwitterionic ionic liquids mixtures with $LiNTf_2$. These mixtures presented interesting properties such as a high and modulable ionic conductivity. A series of composite materials based on the combination of the ionic liquid phases and crosslinked PILs were obtained and characterized. The composites showed a good mechanical properties and high thermal stability. They also displayed high conductivities, which can be correlated with the monomeric mixture used in the reparation of the composite as well as with the nature of **ZIs-1**:$LiNTf_2$ mixture.

The *Chapter IV. Continuous flow system for the simple preparation of functionalized polymeric beads derived from Poly(acrylamide-thiolactone)*, reports on the simple and fast way of the preparation of functionalized spherical polymers based in continuous flow devices. The thiolactone functional group allows the incorporation of different additional functional groups, providing materials with interesting properties for applications such as catalysis.

In the Chapter V. *Preparation and applications of Nanofibers mats derived from Task Specific Polymeric Ionic Liquid*, the preparation of nanofibers mats by electrospinning using a mixture of poly(homocysteine thiolactone) ionic-liquids/poly(vinylpyrrolidone) is described. The presence of the thiolactone functional group allowed the post-functionalisation of the NFs mats simultaneously introducing different functional groups and crosslinking the NFs, while keeping the NFs nanostructure. As a first approximation, the functionalized materials were used in different applications such as the VOC´s sensing and catalysis.

Then the published article, called in this thesis *Chapter VI. Rose Bengal immobilized onto Supported Ionic Liked-like Phases: An Efficient photocatalyst for batch and flow processes,* the photocatalytic activity of the Rose Bengal (RB) immobilized onto Supported Ionic Liked-like Phases is evaluated. In these systems, the polymer is designed to play a pivotal role. The polymeric backbone adequately modified with ionic liquid-like moieties (*Supported Ionic Liquid-like Phases*, SILLPs) is not just an inert support for the dye but controls the accessibility of reagents/substrates to the active sites and provides specific microenvironments for the reaction. The structure of SILLPs can be fine-tuned to adjust the catalytic efficiency of the RB−SILLP composites achieving systems more active and stable than the related systems in absence of IL-like units.

The *Chapter VII. Multifunctional polymers based on ionic liquid and Rose Bengal fragments for the conversion of CO_2 to carbonates* (accepted article) aim to develop organocatalytic systems based on Supported Ionic Liquid-like Phases containing Rose Bengal units. The activity of the supported RB fragments can be fine-tuned by controlling the nature of the SILLPs (i.e. substitution at the imidazolium ring, crosslinking degree of the polymeric matrix, loading, etc.). Such a catalytic system prepared from cheap, simple and commercially available components provides high activity and stability, with no decay in activity for at least ten days of continuous use under flow conditions.

In the last chapter of results, *Chapter VIII. 3D Printing as "enabler" of enabling techniques. Stable and more efficient catalytic CO_2 conversion under continuous flow process using printed reactor based on supported ionic liquids*, it is about how 3D printing through digital design makes it easier to obtain advanced materials with complex geometries. The preparation and optimisation of an epoxy functionalised ink allowed the preparation of 3D objects. The surface of these objects was post-functionalised with IL-like units transferring the catalytic properties to the surface of these 3D objects. The great design freedom provided by this additive manufacturing technology was exploited to design continuous flow reactors with high stability (up to 5 days) and with enhanced activity profiles (up to three orders of magnitude) in comparison with conventional systems. The easy implementation and modification of the reactor design can be used as an essential element for the optimization of the catalytic processes under study.

Finally, *Chapter IX. General Conclusions*, the most relevant conclusions derived from the work developed in each chapter of the thesis that make up this Doctoral Thesis are included.

Divulgación de este trabajo

Los resultados de la presente Tesis Doctoral han permitido la preparación de **dos artículos** publicados, un artículo aceptado y tres en proceso de publicación en revistas de carácter científico:

1. Valverde, D.; García-Bernabé, A.; Andrio, A.; García-Verdugo, E.; Luis. S. V. Compañ, V. **Free ion diffusivity and charge concentration on cross-linked Polymeric Ionic Liquid iongels films based on sulfonated zwitterion salts and Lithium ions.** *Phys. Chem. Chem. Phys.*, **2019**, *21*, 17923-17932.

2. Valverde, D.; Porcar, R.; Prinzi, R.; Burguete, M. I.; García-Verdugo, E., Luis, S. V. **Continuous Flow system for the simple preparation of functionalized polymeric beads derived from Poly(acrylamide-thiolactone).** Manuscrito para enviar a una revista científica.

3. Valverde, D.; Muñoz, I.; Burguete, M. I.; García-Verdugo, E.; Luis, S. V. **Preparation and application of Nanofibers mats derived from Task Specific Polymeric Ionic Liquid.** Manuscrito para enviar a una revista científica.

4. Valverde, D.; Porcar, R.; Izquierdo, D.; Burguete, M. I.; García-Verdugo, E.; Luis, S. V. **Rose Bengal Immobilized onto Supported Ionic Like-Phases: An Efficient Photocatalyst for Batch and Flow Processes**. *Chem.Sus.Chem.*, **2019**, *12*, 1–10.

5. Valverde, D.; Porcar, R.; Lozano, P.; García-Verdugo, E.; Luis, S. V. **Multifunctional polymers based on ionic liquid and Rose Bengal fragments for the conversion of CO_2 to carbonates. Synergies between**

functional groups and residual water. Manuscrito aceptado en la revista *"ACS Sustainable Chemistry & Engineering"*.

6. Valverde, D.; Sans, V.; Burguete, M. I.; García-Verdugo, E.; Luis, S. V. **3D printing as *enabler* of enabling techniques. Stable and more efficient catalytic CO_2 conversion under continuous flow process using reactors based on supported ionic liquids.** Manuscrito para enviar a una revista científica.

Además, parte de las investigaciones realizadas también han sido presentadas en diversos **congresos** y **eventos de carácter científico**, tanto de carácter nacional como internacional:

1. **Valverde, D.**; García-Verdugo, E.; Buguete, M. I.; Luis, S. V. *CO_2 Activation by Organocatalysts Immobilized onto Supported Ionic Liquid-like Phases (SILLPs)*. Comunicación oral. 23 Conferencia de Química, Santiago de Cuba (Cuba), **2020**.

2. **Valverde, D.**; Porcar, R.; Buguete, M. I, García-Verdugo, E.; Luis, S. V. *CO_2 Activation by HBD Organocatalysts Immobilized onto Supported Ionic Liquid-like Phases (SILLPs)*. Póster (premiado). 4th EuCheMs Conference on green and Sustainable Chemistry, Tarragona (España), **2019**.

3. García-Vergugo, E.; Porcar, R.; **Valverde, D.**; Burguete, M. I.; Luis, S. V. *Polymer as Non-Innocent Vector to Develop Efficient Rose Bengal Supported Catalytic.* Comunicación oral. 4th EuCheMs Conference on green and Sustainable Chemistry, Tarragona (España), **2019**.

4. **Valverde, D.**; Muñoz, I.; Prinzi, R.; Porcar, R.; García-Verdugo, E.; Burguete, M. I.; Luis, S. V. *Structured Polymeric Ionic Liquids Fibers Fabricated by Electrospinning and Application in pH Sensing*. Póster. XIII International Workshop on Sensors and Molecular Recognition (XIII IWOSMOR), Valencia (España), **2019**.

5. **Valverde. D.,** Porcar, R.; Altava, B.; Burguete, M. I.; García-Verdugo, E.; Luis, S. V. *Advanced materials for NO_x determination*. Póster. 17th International Conference on Chemistry and the Environment, (17th ICCE), Thessaloniki (Grecia), **2019**.

6. Porcar, R.; García-Verdugo, E.; Burguete, M. I.; Luis, S. V; **Valverde, D**. *Synthesis and Characterization of polymeric ionic Liquids Membranes derived from Poly(Acrilamide Homocysteie Thiolactone) (PAHT) fabricated by electrospinning*. Póster. XXXVII Reunión Bienal de la Real Sociedad Española de Química, Donostia-San Sebastián (España), **2019**.

7. **Valverde, D.**; Porcar, R.; Burguete, M. I.; Lozano, P.; Luis, S. V.; García-Verdugo, E. *Immobilized Hydroxyl Hydrogen Bond Donors onto Supported Ionic Liquid-Like Phases (SILLPs) as efficient Organocatalyst for the Cycloaddition of CO_2 to Epoxides.* Comunicación oral. XXXVII Reunión Bienal de la Real Sociedad Española de Química, Donostia-San Sebastián (España), **2019**.

8. García-Verdugo, E.; **Valverde, D.**; Porcar, R.; Altava, B., Burguete, M. I.; Luis, S. L. *Hierarchically Structured Poymeric Ionic Liquid Membranes obteined by Electrospinning*. Comunicación oral. Electrospinning and related techniques: From design to production of advanced polymer materials devices. EUPOC, Como (Italia), **2019**.

9. **Valverde, D.;** García-Bernabé, A.; Andrio, A.; García-Verdugo, E.; Luis. S. V. Compañ, V. *Free Ion Diffusivity and Charge Concentration in Crosslinked Polymeric Ionic Liquid Films Doped with Sulfonate-Base Zwitterion Imidazolium Salts*. Póster. XV Simposio Jóvenes Investigadores Químicos, RSEQ-Sigma Aldrich (Merck), Toledo (España), **2018**.

10. **Valverde, D.**; Porcar, R.; García-Verdugo, E.; Luis, S. V.; Compañ, V. *Free Ion Diffusivity and Charge Concentration in Crosslinked Polymeric Ionic Liquid Films Doped with sulfonate-base Zwitterion salts*. Póster. 6 th Young Polymer Scientist Conference & Short Course and 10th ECNP International Conference on Nanostructured Polymers and Nanocomposites, Donostia-San Sebastián (España), **2018**.

11. **Valverde, D.**; Altava, B.; Burguete, M. I.; Luis, S.V. *Pseudopeptidic ligands: Synthesis and Cu++ recognition*. Póster. XII International Workshop on Sensors and Molecular Recognition (XII WOSMOR). Valencia (España), **2018**.

12. **Valverde, D.**; Porcar, R.; García-Verdugo, E.; Burguete, M. I.; Luis, S.V. *Design and Study of Multifunctional Compounds Based on Polymeric Materials for Advanced Applications in Green Chemistry.* Póster. XIV Simposio de Investigadores Jóvenes Químicos, RSEQ-Sigma Aldrich (Merck), Badajoz (España), **2017**.

13. Porcar, R.; Montolio, S.; **Valverde, D**.; Prinzi, R.; Burguete, M. I.; García-Verdugo, E.; Luis, S. V. *Design and study of advance materials derived from amine-thiobutrolactone.* Póster. VIII Mediterranean Organic Chemistry Meeting, Palma (España), **2017**.

Índice

"El desarrollo de la Química sigue siendo una necesidad para luchar contra la degradación de nuestro planeta"

Santiago V. Luis

CAPÍTULO I

Introducción

Capítulo I. Introducción

1.1. Sostenibilidad Ambiental y Química Verde

La sociedad se encuentra en un período de cambio fundamental en lo que se refiere a los paradigmas sobre el bienestar económico, la equidad social y la calidad del medio ambiente, impulsado por el crecimiento exponencial de la población y consecuentemente por los retos crecientes a los que se enfrenta la mejora del bienestar humano. La creciente demanda de bienes y servicios ha limitado la capacidad de la humanidad para proteger los ecosistemas que sustentan la vida en la Tierra y por tanto la biodiversidad, siendo uno de los principales problemas de la degradación ambiental el consumo excesivo directo e indirecto de los recursos naturales.[1]

La rápida expansión de la población humana ha resultado en interacciones dinámicas y a veces inesperadas entre la población, el consumo de alimentos, el desarrollo industrial y los daños ambientales. En particular, el impacto ambiental y los daños a la salud por la producción, distribución, uso y desecho de los productos químicos en cantidades cada vez mayores y en un entorno prácticamente cerrado han hecho surgir importantes inquietudes a nivel mundial.[2] Los Objetivos de Desarrollo Sostenible (SDGs, por sus siglas en inglés) para el año 2030, planteados por las Naciones Unidas apuntan a proteger el planeta mientras aspiran a brindar prosperidad para todos. Dichos objetivos se centran en desarrollar ciudades y comunidades sostenibles, reduciendo su impacto ambiental y la gestión y calidad de los recursos.[3]

[1] Shaker, R. R. The Spatial Distribution of Development in Europe and Its Underlying Sustainability Correlations. *Applied Geography*. **2015**, *63*, 304–314.
[2] Horváth, I. T. Introduction: Sustainable Chemistry. *Chem. Rev.* **2018**, *118* (2), 369–371.
[3] Brooks, B. W. Greening Chemistry and Ecotoxicology towards Sustainable Environmental Quality. *Green Chem.* **2019**, *21* (10), 2575–2582.

El cambio climático puede afectar a casi todos los aspectos del desarrollo sostenible, siendo necesario comprender cómo las acciones para abordarlo pueden reforzar o socavar los SDGs. Muchos de los objetivos referentes a alimentos, agua, salud y sistemas de energía están conectados intrínsecamente con el cambio climático. Así, por ejemplo, el progreso en distintos objetivos relacionados con el consumo y la producción sostenible permitirá reducir las emisiones de gases de efecto invernadero. Se debe resaltar que la acción climática requiere esfuerzos para planificar y gestionar mejor los recursos de manera integrada.[4]

Figura 1. Objetivos del Desarrollo Sostenible que representan un desafío actual para la sociedad (modificado de http://www.iynf.org/2018/08/a-guide-to-sustainable-development-and-its-challenges-in-developing-countries).

La conciencia ambiental contemporánea probablemente se deriva del informe "*U Thant Report*" presentado en la 23ª sesión de las Naciones Unidas en 1969.

[4] Nerini, F. F.; Sovacool, B.; Hughes, N.; Cozzi, L.; Cosgrave, E.; Howells, M.; Tavoni, M.; Tomei, J.; Zerriffi, H.; Milligan, B. Connecting Climate Action with Other Sustainable Development Goals. *Nat. Sustain.* **2019**, *2* (8), 674–680.

Posteriormente, en las actas de la conferencia de Estocolmo de 1972 se establecieron algunas definiciones inciales sobre el desarrollo sostenible. Sin embargo, la primera formulación clara de esta idea salió a la luz en la década de 1980. La Comisión de las Naciones Unidas para el Medio Ambiente y el Desarrollo creada en 1983 elaboró el "*Brundtland Report*" incluido en el libro "*Our Common Future*" publicado en 1987.[5] En él se define el desarrollo sostenible como una forma de crecimiento que satisface las necesidades del presente sin comprometer la capacidad de las generaciones futuras para satisfacer sus propias necesidades.[6] El informe desarrolló componentes fundamentales que abarcan la protección del medio ambiente, el crecimiento económico y la equidad social, los cuales están estrechamente relacionados y con frecuencia son mencionados como los tres pilares de la sostenibilidad ambiental.[7]

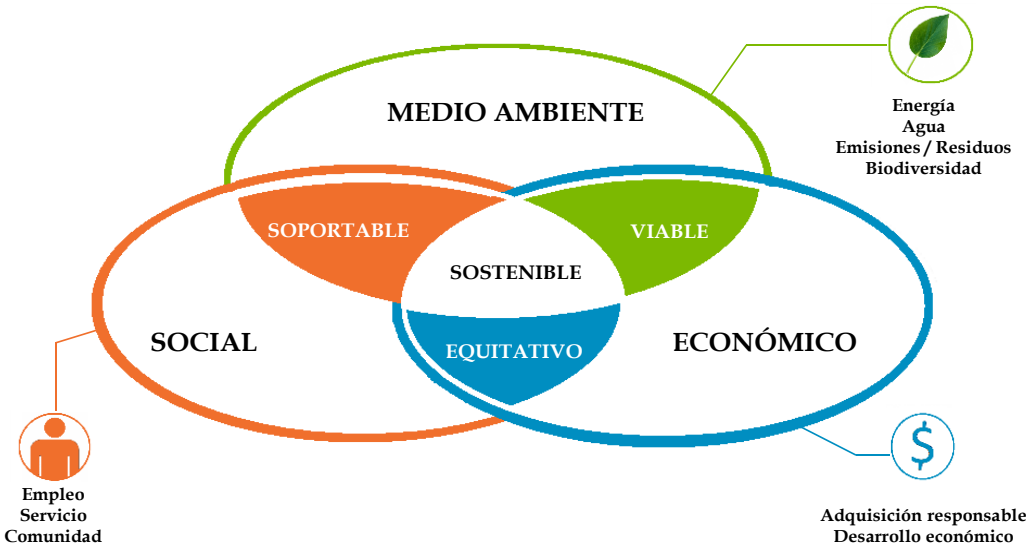

Figura 2. Representación de los tres pilares integrados de la sostenibilidad ambiental: medio ambiente, social y económico (modificado de ref. 5).

[5] Little, J. C.; Hester, E. T.; Carey, C. C. Assessing and Enhancing Environmental Sustainability: A Conceptual Review. *Environ. Sci. Technol.* **2016**, *50* (13), 6830–6845.
[6] Brundtland, G. H. *Report of the World Commission on Environment and Development: Our Common Future*, 1st ed.; United Nations: Oslo, 1987.
[7] Tobiszewski, M.; Mechlińska, A.; Namieśnik, J. Green Analytical Chemistry—Theory and Practice. *Chem. Soc. Rev.* **2010**, *39* (8), 2869–2878.

Es importante resaltar que desde 1992, a partir de la conferencia sobre el Medio Ambiente y Desarrollo de las Naciones Unidas llevada a cabo en Río de Janeiro – Brasil, la Educación para el Desarrollo Sostenible es parte de la agenda 21. En el capítulo 26 se indica que la educación es fundamental para promover el desarrollo sostenible y mejorar la capacidad de las personas para abordar los problemas del medio ambiente y desarrollo.[8]

El concepto de Química Verde se formuló por primera vez a principios de la década de 1990 a partir de la elaboración realizada por Anastas y Warner.[9] En los años transcurridos desde entonces, ha habido una adopción internacional de las aproximaciones allí definidas. Esto ha dado lugar a la creación de una multitud de programas e iniciativas gubernamentales sobre Química Verde alrededor de todo el mundo, con un papel pionero de los programas localizados en Estados Unidos, Reino Unido e Italia que han desempeñado un papel importante en el desarrollo de este campo.[10]

El término "Química Sostenible" designa una finalidad más general: El desarrollo de una química que permita la reducción de la contaminación por las sustancias nocivas para la salud y el medio ambiente, sin merma de las ventajas sociales que aporta la actividad química.[11] La Agencia de Protección Ambiental de Estados Unidos (US EPA por sus siglas en inglés) define la Química Verde o Sostenible como "el diseño de productos y procesos químicos que reducen o eliminan el uso o generación de sustancias peligrosas".[12]

[8] Burmeister, M.; Rauch, F.; Eilks, I. Education for Sustainable Development (ESD) and Chemistry Education. *Chem. Educ. Res. Pract.* **2012**, *13* (2), 59–68.
[9] Anastas, P.; Warner, J. *Green Chemistry: Theory and Practice*, 1st ed.; Oxford University Press: New York, 1998.
[10] Anastas, P.; Eghbali, N. Green Chemistry: Principles and Practice. *Chem. Soc. Rev.* **2010**, *39* (1), 301–312.
[11] Mestres, R. Química Sostenible: Naturaleza, Fines y Ámbito. *Educ. quím.* **2013**, *24*, 103–112.
[12] Dunn, P. J. The Importance of Green Chemistry in Process Research and Development. *Chem. Soc. Rev.* **2012**, *41* (4), 1452–1461.

En el libro "*Green Chemistry: Theory and Practice*" de P. Anastas y J. Warner publicado en 1998, se indica que:[9]

"*La Química Verde se basa en la utilización de un conjunto de principios que reducen o eliminan el uso o generación de sustancias peligrosas en el diseño, fabricación y aplicación de productos químicos*"

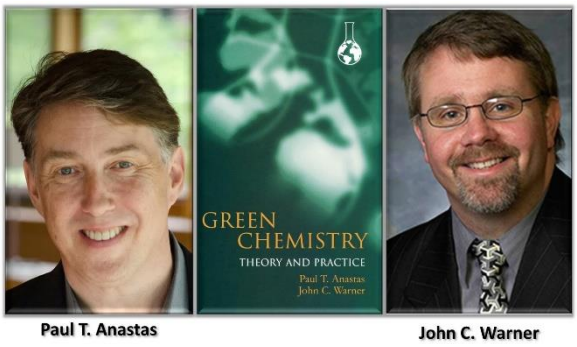

Figura 3. Fotografía de P. Anastas y J. Warner y su libro "*Green Chemistry. Theory and Practice*".

R. Sheldon definió en 2007 la Química Verde como la química que "utiliza eficientemente las materias primas (preferiblemente renovables), elimina los residuos y evita el uso de reactivos y disolventes tóxicos y / o peligrosos en la fabricación y aplicación de productos químicos".[13]

Términos tales como síntesis química benigna, vías alternativas sintéticas para la prevención de la contaminación,[9] o tecnologías sostenibles,[13] describen esencialmente el mismo concepto. Ser capaz de llevar a cabo una transformación o construir un camino eficaz y fiable para la obtención de una molécula de interés es fundamental en síntesis química. La eficiencia no es tan sólo una medida de la calidad científica de un método sintético, sino que debe incluir otras consideraciones de tipo práctico y económico. Los aspectos económicos desempeñan un papel importante en el diseño de síntesis, incluyendo el uso de reactivos y materias primas más accesibles y / o de menor costo. Los aspectos de toxicidad e impacto medioambiental deben incluirse ahora en este análisis de la eficiencia y la elegancia sintética, en particular cuando abordamos el desarrollo práctico e industrial. El concepto de Química Verde ha tenido un gran impacto puesto que transciende el laboratorio de investigación, afectando a la industria, la educación, el medio ambiente y a la sociedad en general.[9]

[13] Sheldon, R. A.; Arends, I.; Hanefeld, U. *Green Chemistry and Catalysis*, 1st ed.; John Wiley & Sons: Weinheim, 2007.

Uno de los aspectos más importantes de la Química Verde es su énfasis en el diseño ya que éste incluye una declaración voluntaria -no accidental- de intencionalidad. Incluye novedad, planificación y concepción sistemática. Este campo ha demostrado cómo los químicos pueden diseñar una nueva generación de productos y procesos que sean rentables y compatibles con la salud humana y el medio ambiente. La planificación cuidadosa de la síntesis química y el diseño molecular permiten crear sinergias que reducen las consecuencias adversas, en lugar de intentar solucionar con posterioridad los problemas generados. Los Doce Principios de Química Verde son "reglas de diseño" para ayudar a los químicos a alcanzar el objetivo intencional de la sostenibilidad.[9]

1.1.1. Principios de la Química Verde

Los Doce Principios de la Química Verde fueron introducidos en 1998 por Paul Anastas y John Warner, como guía para el diseño de nuevos productos y procesos químicos y se aplican a todos los aspectos del ciclo de vida del proceso, desde las materias primas utilizadas hasta la eficiencia y seguridad de la transformación, la toxicidad y la biodegradabilidad de los reactivos utilizados.[10] Estos principios son una categorización de los enfoques fundamentales adoptados para lograr productos y procesos ambientalmente benignos. Al igual que en todos los sistemas multiparamétricos, se realizan compensaciones y equilibrios hacia la optimización basados en las circunstancias específicas de la aplicación.[14]

[14] Anastas, P. T.; Kirchhoff, M. M. Origins, Current Status, and Future Challenges of Green Chemistry. *Acc. Chem. Res.* **2002**, *35* (9), 686–694.

Los Doce Principios de la Química Verde se enuncian a continuación: [9,10,14,15,16]

1. ***Prevención.*** Es mejor prevenir la formación de residuos que tratar o limpiar éstos después de formarse. El diseño de procesos químicos novedosos previamente planificados permite el uso de reactivos y materias primas renovables o alternativas menos peligrosas y no tóxicas.

2. ***Economía atómica.*** Los métodos sintéticos deben ser diseñados para maximizar la incorporación de todos los materiales utilizados durante el proceso en el producto final. Barry Trost[17,18] desarrollo este concepto y describe la eficiencia de conversión de un proceso químico en términos de todos los átomos involucrados que se incorporan en los productos deseados producidos. En un proceso químico ideal, la cantidad de materiales de partida o reactivos es igual a la cantidad de todos los productos generados sin desechar ningún átomo.

3. ***Síntesis química menos peligrosa***. Siempre que sea posible, las metodologías sintéticas deben diseñarse para utilizar y generar sustancias que presentan poca o ninguna toxicidad para la salud humana y el medio ambiente. El uso de compuestos y materiales menos tóxicos o carentes de toxicidad se traduce en la minimización o eliminación de los riesgos para los trabajadores en la industria y los laboratorios de investigación, además de un menor impacto ambiental.

[15] Erythropel, H. C.; Zimmerman, J. B.; Winter, T. M. de; Petitjean, L.; Melnikov, F.; Lam, C. H.; Lounsbury, A. W.; Mellor, K. E.; Janković, N. Z.; Tu, Q.; Pincus, L. N.; Falinsku, M. M.; Shi, W.; Coish, P.; Plata, D. L.; Anastas, P. L. The Green ChemisTREE: 20 Years after Taking Root with the 12 Principles. *Green Chem.* **2018**, *20* (9), 1929–1961.
[16] Anastas, P. T.; Zimmerman, J. B. The Periodic Table of the Elements of Green and Sustainable Chemistry. *Green Chem.* **2019**, *21* (24), 6545–6566.
[17] Trost, B. M. The Atom Economy - A Search for Synthetic Efficiency. *Science.* **1991**, *254* (5037), 1471–1477.
[18] Trost, B. M. Atom Economy - A Challenge for Organic Synthesis: Homogeneous Catalysis Leads the Way. *Angew Chem. Int. Ed. Engl.* **1995**, *34* (3), 259–281.

4. ***Diseñando productos químicos más seguros*.** Los productos químicos deben diseñarse para preservar la eficacia de la función y reducir la toxicidad. A través del conocimiento de la estructura molecular los científicos pueden diseñar las propiedades de un compuesto según su campo de aplicación, por lo que el objetivo de diseñar compuestos químicos seguros es maximizar el equilibrio entre el rendimiento y la función deseada del producto, al mismo tiempo que se garantiza la eliminación o reducción al nivel más bajo de toxicidad y peligrosidad para el ser humano y el ambiente.

5. ***Disolventes y auxiliares más seguros***. El uso de sustancias auxiliares (por ejemplo: disolventes, agentes de separación, etc.) debe hacerse innecesario siempre que sea posible y ser inocuo cuando sea necesario.

   Sustancias auxiliares: estas se pueden definir como aquellas sustancias que ayudan a la manipulación de un producto químico, pero no son parte integral de la molécula misma. La finalidad de estas sustancias es facilitar pasos en los procesos de producción de una molécula o un compuesto químico. Muchas de las sustancias auxiliares han sido utilizadas ampliamente en distintas operaciones unitarias pero rara vez se ha evaluado su necesidad. Esto es muy común con el empleo de disolventes y agentes de separación. A menudo el empleo excesivo de auxiliares puede representar un impacto notable sobre la salud humana y el medio ambiente.

   Disolventes: Muchos disolventes tradicionales son tóxicos y algunos incluso cancerígenos (algunos disolventes halogenados y aromáticos). Todas estas sustancias son utilizadas en grandes cantidades y presentan una extensa gama de aplicaciones. Esos beneficios, sin embargo, se combinan con los riesgos a la salud y también para el medio ambiente, mencionados anteriormente.

6. ***Diseño para la Eficiencia Energética.*** Los requerimientos energéticos de los procesos químicos deben ser identificados por sus impactos ambientales y económicos y tienen que ser minimizados. Los métodos sintéticos deberían ser llevados a temperatura y presión ambiente. La química desempeña un papel importante en el consumo y liberación de energía -en las transformaciones químicas- pero también en muchos procesos de generación, transporte y almacenamiento de energía. Históricamente, la generación y el consumo de energía conllevan un alto impacto ambiental. A diferencia del estado actual, debe de existir un compromiso continuo para que el proceso de generación, transporte y transformación de energía tenga un perfil sostenible para la sociedad, la economía y el ambiente.

7. ***Uso de materias primas renovables.*** Deben utilizarse materias primas renovables siempre que sea técnica y económicamente factible. Desde tiempo atrás ha existido un enfoque significativo de las comunidades científicas, industriales y ambientales sobre el uso de los recursos renovables. La diferencia entre un recurso renovable y no renovable se puede traducir de manera simple como "tiempo". Los recursos renovables se asocian de forma frecuente a materiales biológicos y de origen vegetal; sin embargo, este término puede aplicarse igualmente a sustancias que se regeneran fácilmente dentro de marcos de tiempo accesibles para la vida humana. El dióxido de carbono es un ejemplo de ello: puede generarse a través de una gran variedad de fuentes tanto naturales como antropogénicas, pero puede consumirse igualmente -como materia prima- en un periodo de tiempo dentro de la escala humana. El mismo argumento se puede aplicar al gas metano.

8. ***Reducción de derivados.*** La derivatización innecesaria (uso de grupos de bloqueo, protección / desprotección, modificación temporal del proceso físico / químico) debe minimizarse o evitarse si es posible, ya que tales pasos requieren reactivos adicionales y generan residuos. La derivatización es

particularmente común en la química fina, farmacéutica y en la de los aditivos y colorantes. En estas áreas, el uso de grupos de bloqueo o de protección evitan la desfuncionalización o perdida de actividad del grupo de interés durante el proceso sintético.

9. ***Catálisis.*** Los reactivos catalíticos (tan selectivos como sea posible) son superiores a los reactivos estequiométricos. El papel de los catalizadores es favorecer la transformación deseada sin ser consumidos durante la reacción y sin incorporase en el producto final. Su contribución tiene en cuenta varios factores:

   Selectividad: La catálisis selectiva permite controlar la formación preferente de un solo producto, incluyendo el control de la estereoquímica, lo que lleva a una minimización de los productos secundarios formados y por tanto de los residuos.

   Minimización energética: al reducir la energía de activación de una vía de reacción, no solamente se logra el control de la reacción, sino también disminuye la temperatura necesaria para efectuar la síntesis. En la producción de compuestos químicos básicos a gran escala, el problema energético es uno de los factores más importantes respecto al impacto ambiental y económico.

   Al comparar el proceso catalítico con un proceso estequiométrico, la catálisis ofrece la ventaja de que a pesar de que, en general, el catalizador llevará a cabo un número muy alto de transformaciones antes de desactivarse.

10. ***Diseño para la degradación.*** Los productos químicos deben de diseñarse de tal manera que al final de su función se descompongan en productos de degradación inocuos y no persistan en el medio ambiente. Una preocupación

fundamental en la conservación del medio ambiente son los llamados "productos químicos persistentes" o "bioacumulativos". Esto significa que una vez desechados permanecen como tales, sin degradarse, en el medio ambiente o se incorporan a las plantes y animales, acumulándose en sus sistemas. A menudo la acumulación de estas sustancias es perjudicial para las especies por su toxicidad directa o indirecta.

El diseño de un producto biodegradable debe de evaluar en qué sustancias se descompondrá el producto de partida, ya que sus productos de degradación pueden ser incluso más tóxicos y perjudicar la salud humana y el medio ambiente. Dicho estudio debe de incluir los efectos sobre la salud, los ecosistemas, la vida silvestre y la carga general de contaminación en el medio ambiente.

11. ***Análisis en tiempo real para la prevención de la contaminación.*** Las metodologías analíticas desarrolladas deben permitir la monitorización y control en tiempo real del proceso, antes de la formación de sustancias peligrosas. Ello facilita la prevención y minimización de la generación de sustancias peligrosas en los procesos químicos. Este control debe permitir el detectar la generación de subproductos peligrosos y las reacciones secundarias, de modo que cuando se detecten sustancias tóxicas, incluso a niveles de trazas, sea posible ajustar los parámetros de la reacción para reducir o eliminar la formación de estas sustancias.

12. ***Química inherentemente más segura para la prevención de accidentes.*** Las sustancias químicas y su uso en procesos químicos deben elegirse de tal manera que minimicen la posibilidad de accidentes químicos, incluyendo emanaciones, explosiones e incendios. Los riesgos planteados por la toxicidad, explosividad, y la inflamabilidad, deben de abordarse desde el inicio del diseño de los procesos químicos. A veces, se puede aumentar el

potencial de riesgo, inadvertidamente, al minimizar la generación de residuos, por lo que el proceso debe equilibrar la prevención de la contaminación con la reducción de los riesgos de un accidente químico.

Los enfoques en el diseño de una química inherentemente más segura pueden incluir la utilización de sólidos o sustancias de baja presión de vapor, disminuir el uso de halógenos moleculares en grandes cantidades o incluso usar técnicas como el "*just in time*" que implica la generación y el consumo rápido de sustancias peligrosas para un proceso determinado. El empleo de esta tecnología en la industria puede eliminar la necesidad de grandes inventarios de sustancias peligrosas, minimizando el riesgo significativo de accidentes.

Aunque en la década de 1990 los principios de la Química Verde eran poco utilizados para el desarrollo de experimentos y rara vez eran un tópico en simposios, hoy día representa el foco de muchos grupos de investigación y un eje fundamental en eventos científicos. Los 12 Principios de la Química Verde no solamente sirven como marco para el diseño sino también para la discusión, ya que los Principios establecen el "qué" y el "por qué" de diseñar procesos y productos químicos que reducen o eliminan el uso o generación de sustancias peligrosas.

Es necesario tener en cuenta que estos Principios no son independientes uno del otro, sino más bien un sistema interconectado por el cual se diseñan sinergias que permiten la innovación y el desarrollo de nuevos métodos y tecnologías más eficientes. Una forma resumida de abordar los Principios de la Química Verde fue desarrollada por Poliakoff en 2005, con el acrónimo inglés "*PRODUCTIVELY*": [19]

[19] Tang, S. L. Y.; Smith, R. L.; Poliakoff, M. Principles of Green Chemistry: PRODUCTIVELY. *Green Chem.* **2005**, *7* (11), 761–762.

P - Prevenir los residuos ("***P****revent Wastes"*).

R - Materiales renovables ("***R****enewable materials*").

O – Omitir pasos de derivatización química ("***O****mit derivatization steps*").

D – Productos químicos degradables ("***D****egradable chemical products"*).

U – Uso de Métodos químicos seguros ("***U****se safe synthetic methods*").

C – Procesos catalíticos ("***C****atalytic reagents*").

T – Temperatura y presión Ambiente ("***T****emperature, Pressure ambient*").

I – Monitorización del proceso en tiempo real ("***I****n-process monitoring*").

V – Uso de pocas sustancias auxiliares ("***V****ery few auxiliary substances*").

E – Maximizar la cantidad de producto por unidad de materia prima ("***E****-Factor*").

L – Productos químicos menos tóxicos ("***L****ow toxicity of chemical products*").

Y – Minimizar el potencial de accidentes ("***Y****es, it is safe*").

La madurez del campo ha permitido desarrollar una gran diversidad de aplicaciones en las que la Química Verde es la base y que tienen como filosofía la mejora continua y la sostenibilidad ambiental.[15]

1.1.2. Métricas de Química Verde y Sostenibilidad

Las primeras métricas de Química Verde introducidas en la década de 1990 para cuantificar la eficiencia de una síntesis química fueron la economía atómica (AE, por sus siglas en inglés) y el "*E factor*". En las últimas dos décadas ambas han sido adoptadas tanto por el mundo académico como por la industria. Con el avance de estas tecnologías emergentes, se han propuesto otras formas de medir la sostenibilidad de un proceso basadas en la masa, como el PMI ("*Process Mass Intensity*") o el RME ("*Reaction Mass Effiency*"), sin embargo este tipo de métricas deben de ser complementadas por estudios que midan el impacto ambiental de los desechos tales como el análisis del ciclo de vida (LCA por sus siglas en inglés)

y metodologías estratégicas para determinar la viabilidad económica de los procesos y productos.[20]

La economía atómica es un número teórico que determina la cantidad de átomos (masa) de los reactivos de partida que se incorporan al producto final suponiendo un rendimiento químico del 100%, sin tener en cuenta los disolventes y los productos químicos utilizados en el tratamiento de aislamiento del compuesto final. La AE es una herramienta muy útil en una evaluación rápida del proceso y puede utilizarse para comparar rutas sintéticas alternativas en la obtención del producto prediciendo las cantidades de desechos (una parte) que se pueden generar, sin llevar a cabo procesos experimentales.[21,22]

El "*E(nvironmental) factor*" desarrollado por R. Sheldon, se definió como la relación de masa de los desechos totales generados respecto a la masa de los productos obtenidos (*E factor* = Kg de desechos / kg de productos).[23,24] El *E factor* ideal es igual a cero, esto indica que no hay producción de residuos, por lo que un elevado valor de *E factor* señala una alta generación de desechos en el proceso.[25]

El *E factor* presenta dos diferencias notables respecto al parámetro *AE*. La primera es que tiene en cuenta todos los componentes auxiliares (disolventes o reactivos químicos usados en el tratamiento, entre otros) mientras que la *AE* no los considera. En segundo lugar, la *AE* se emplea en etapas individuales del proceso,

[20] Sheldon, R. A. Metrics of Green Chemistry and Sustainability: Past, Present, and Future. *ACS Sustainable Chem. Eng.* **2018**, *6* (1), 32–48.
[21] Constable, D. J. C.; Curzons, A. D.; Cunningham, V. L. Metrics to 'Green' Chemistry—Which Are the Best? *Green Chem.* **2002**, *4* (6), 521–527.
[22] Sheldon, R. A. E Factors, Green Chemistry and Catalysis: An Odyssey. *Chem. Commun.* **2008**, No. 29, 3352–3365.
[23] Sheldon, R. A. Selective Catalytic Synthesis of Fine Chemicals: Opportunities and Trends. *J. Mol. Catal. A-Chem.* **1996**, *107* (1), 75–83.
[24] Sheldon, R. A. The E Factor 25 Years on: The Rise of Green Chemistry and Sustainability. *Green Chem.* **2017**, *19* (1), 18–43.
[25] Chen, T.-L.; Kim, H.; Pan, S.-Y.; Tseng, P.-C.; Lin, Y.-P.; Chiang, P.-C. Implementation of Green Chemistry Principles in Circular Economy System towards Sustainable Development Goals: Challenges and Perspectives. *Sci. Total. Environ.* **2020**, *716*, 136998.

mientras que el *E Factor* se puede aplicar a un proceso de varios pasos facilitando la evaluación holística de un proceso.[26]

Dentro de los inconvenientes del *E factor* se encuentran en que no diferencia entre los tipos de residuos y que es propenso a la aplicación inconsistente para calcular la cantidad total de desechos, ya que si no se conocen los valores de reciclaje de los disolventes dependerá del evaluador estimarlos, por lo que pueden variar significativamente. Por esta razón el concepto inicial del *E factor* ha evolucionado. Recientemente, se han desarrollado el *sEF* (*simple E factor*) y el *cEF* (*complete E factor*). El *sEF* no tomo en cuenta el agua ni los disolventes y es más adecuado para la exploración de nuevas rutas de proceso en la etapa inicial de desarrollo del proyecto. Por su parte el *cEF* incluye todos los materiales del proceso (materias primas, reactivos, disolventes, agua, etc.) y es apropiado para el análisis de flujo total de residuos del proceso. Este no considera el reciclaje ya que los desarrolladores de los procesos no pueden estimar en que grado los disolventes y el agua se podrán reciclar durante o al final de la cadena de suministro. En general el valor real del *E factor* se encontrará entre el *cEF* y el *sEF*.[27]

Tanto la *AE* como el *E factor* han sido ampliamente usados por la academia y la industria en la exploración de la Química Verde y el uso adecuado de los recursos naturales que permita caminar hacia la sostenibilidad. En este contexto, los esfuerzos llevados a cabo en este trabajo se centran en desarrollar materiales y procesos más eficientes, con un uso de disolventes que genere un menor impacto ambiental, combinando, además, metodologías sintéticas con materiales catalíticos emergentes, sistemas de flujo continuo, fluidos supercríticos, técnicas novedosas de fabricación, etc. Todo esto con el fin de llevar a cabo síntesis orgánicas de forma eficaz, novedosa y sostenible.

[26] A. Sheldon, R. Green Chemistry and Resource Efficiency: Towards a Green Economy. *Green Chem*. **2016**, *18* (11), 3180–3183.
[27] Roschangar, F.; Sheldon, R. A.; Senanayake, C. H. Overcoming Barriers to Green Chemistry in the Pharmaceutical Industry – the Green Aspiration Level™ Concept. *Green Chem.* **2015**, *17* (2), 752–768.

1.2. Disolventes

Hoy en día, la industria química utiliza una gran cantidad de disolventes. En particular, las industrias de química fina y farmacéutica usan toneladas de disolventes por kilogramo de producto final obtenido. Muchos de los disolventes orgánicos manejados en los laboratorios y en la industria son perjudiciales, tóxicos y ambientalmente dañinos y, por tanto, su uso plantea riegos para la salud humana y el medio ambiente.[28]

En las industrias químicas y afines, el empleo de disolventes está asociado con la generación de desechos y con las altas cargas ambientales y económicas resultantes.[29] La selección de un disolvente verde a menudo es difícil, dado que deben conjugarse una serie de condicionantes que en algunos casos son contradictorios. Estos incluyen la eficiencia química, seguridad (inflamabilidad), salud (toxicidad a corto y largo plazo), medio ambiente (biodegradabilidad, ecotoxicidad, solubilidad en el agua, volatilidad, olor, análisis del ciclo de vida), calidad, restricciones industriales (punto de ebullición, congelación, densidad, viscosidad, reciclabilidad) y costo. Por ejemplo, el agua no es el disolvente ideal por su punto de congelación o su alto valor de entalpía de vaporización; mientras que el metanol, a pesar de ser muy económico y biodegradable, es inflamable, volátil y está sujeto a restricciones regulatorias.[30]

Comprender las propiedades de los disolventes es una parte necesaria del desarrollo sostenible, por lo que estos han sido clasificados en función de su impacto sobre la salud y el medio ambiente y de su seguridad.[31] Estas

[28] Clarke, C. J.; Tu, W.-C.; Levers, O.; Bröhl, A.; Hallett, J. P. Green and Sustainable Solvents in Chemical Processes. *Chem. Rev.* **2018**, *118* (2), 747–800.
[29] Subramaniam, B. Exploiting Neoteric Solvents for Sustainable Catalysis and Reaction Engineering: Opportunities and Challenges. *Ind. Eng. Chem. Res.* **2010**, *49* (21), 10218–10229.
[30] Prat, D.; Pardigon, O.; Flemming, H.-W.; Letestu, S.; Ducandas, V.; Isnard, P.; Guntrum, E.; Senac, T.; Ruisseau, S.; Cruciani, P.; Hosek, P. Sanofi's Solvent Selection Guide: A Step Toward More Sustainable Processes. *Org. Process Res. Dev.* **2013**, *17* (12), 1517–1525.
[31] Capello, C.; Fischer, U.; Hungerbühler, K. What is a Green Solvent? A Comprehensive Framework for the Environmental Assessment of Solvents. *Green Chem.* **2007**, *9* (9), 927–934.

clasificaciones son la guía central de selección de disolventes en los procesos químicos. La mayoría son publicadas por compañías farmacéuticas tales como Sanofi,[30] AstraZeneca,[32] Pfizer,[33] y GSK.[34] Por ejemplo, la guía de AstraZeneca clasifica una lista de cuarenta y seis disolventes en base a diez criterios diferentes: dos para seguridad (inflamabilidad y resistividad), uno para salud y siete para medio ambiente, incluyendo el análisis del ciclo de vida del producto. Cada criterio es puntuado entre 1 y 10, con un código de tres colores (verde, amarillo y rojo) para facilitar la identificación de la peligrosidad del disolvente.[32] Los procesos industriales emplean principalmente disolventes orgánicos, por lo que estas guías son útiles para seleccionar un disolvente considerando el papel del mismo en el proceso químico y en la obtención del producto principal.[28]

En las guías desarrollas para determinar qué tan "verde" es un disolvente se utilizan métodos de evaluación como el análisis del ciclo de vida,[35,36,37] y el "*Environmental, Healt and Safety*" (EHS por sus siglas en inglés) utilizado para la identificación de sustancias potencialmente peligrosas.[31] Como complemento a estas metodologías, se han desarrollado herramientas de software (*Ecosolvent*®) que miden las emisiones de CO_2 en la producción del disolvente y otras variables

[32] Diorazio, L. J.; Hose, D. R. J.; Adlington, N. K. Toward a More Holistic Framework for Solvent Selection. *Org. Process Res. Dev.* **2016**, *20* (4), 760–773.
[33] Alfonsi, K.; Colberg, J.; Dunn, P. J.; Fevig, T.; Jennings, S.; Johnson, T. A.; Kleine, H. P.; Knight, C.; Nagy, M. A.; Perry, D. A.; Stefaniak, M. Green Chemistry Tools to Influence a Medicinal Chemistry and Research Chemistry Based Organisation. *Green Chem.* **2008**, *10* (1), 31–36.
[34] Henderson, R. K.; Jiménez-González, C.; Constable, D. J. C.; Alston, S. R.; Inglis, G. G. A.; Fisher, G.; Sherwood, J.; Binks, S. P.; Curzons, A. D. Expanding GSK's Solvent Selection Guide – Embedding Sustainability into Solvent Selection Starting at Medicinal Chemistry. *Green Chem.* **2011**, *13* (4), 854–862.
[35] Lemesle, C.; Frémiot, J.; Beaugendre, A.; Casetta, M.; Bellayer, S.; Duquesne, S.; Schuller, A.-S.; Jimenez, M. Life Cycle Assessment of Multi-Step versus One-Step Coating Processes Using Oil or Bio-Based Resins. *J. Clean. Prod.* **2020**, *242*, 118527.
[36] Chen, Z.; Shen, Q.; Sun, N.; Wei, W. Life Cycle Assessment of Typical Methanol Production Routes: The Environmental Impacts Analysis and Power Optimization. *J. Clean. Prod.* **2019**, *220*, 408–416.
[37] Matharu, A. S.; Lokesh, K. Green Chemistry Principles and Global Drivers for Sustainability – An Introduction. In *Green Chemistry for Surface Coatings, Inks and Adhesives: Sustainable Applications*; Höfer, R., Matharu, A. S., Zhang, Z., Eds.; Green Chemistry Series; The Royal Society of Chemistry: United Kingdom, 2019, pp 1–17.

ambientales.[38] Estas metodologías no sólo pretenden cubrir aspectos sobre el desempeño ambiental, el impacto en la salud o la seguridad en el manejo del disolvente, sino también tener en cuenta cuál podría ser el mejor método para su eliminación al final del uso.

A pesar de que muchos disolventes son altamente volátiles, considerablemente persistentes y altamente tóxicos, tal y como se planteaba en los principios de la Química Verde, los disolventes están intrínsicamente relacionados con la síntesis y los procesos químicos. En general, después de su uso no pueden reutilizarse en el proceso original porque pueden contener contaminantes residuales, por requerimientos de calidad, e incluso por restricciones legales, convirtiéndose en residuos.[38,39]

Ante tal situación, además de la creciente presión legislativa, social y a un sector industrial cada vez más "verde", todos los días se desarrollan e implementan nuevos procesos basados en la sustitución de los disolventes tradicionales por alternativas más ecológicas y sostenibles, en las cuáles, consideraciones como la toxicidad y el reciclaje o el proceder de fuentes renovables y no de combustibles fósiles, influyen directamente en la elección realizada, particularmente a nivel industrial.[40]

Estos disolventes alternativos capaces de reducir el impacto ambiental respecto a los tradicionales pueden llegar a ser disolventes reactivos actuando simultáneamente como sustrato y como medio de reacción, formando parte de la estructura final del producto.[39] Existe una amplia gama de los denominados

[38] Amelio, A.; Genduso, G.; Vreysen, S.; Luis, P.; Bruggen, B. V. der. Guidelines Based on Life Cycle Assessment for Solvent Selection during the Process Design and Evaluation of Treatment Alternatives. *Green Chem.* **2014**, *16* (6), 3045–3063.

[39] Restrepo Rodríguez, J. A. Desarrollo de materiales poliméricos multifuncionales nanoestructurados. Aplicaciones en Química Sostenible. Ph.D. Thesis, Universitat Jaume I, Castellón de la Plana, España, 2010.

[40] Imperato, G.; König, B.; Chiappe, C. Ionic Green Solvents from Renewable Resources. *Eur. J. Org. Chem.* **2007**, *1* (7), 1049–1058.

disolventes benignos que incluyen tanto disolventes de origen natural como sintético,[41,42,43] y que se han utilizado en una amplia gama de aplicaciones.[44,45,46]

El término "disolvente neotérico" se ha utilizado en los últimos años para designar genéricamente a estos nuevos disolventes o a materiales antiguos a los cuales se les ha encontrado nuevas aplicaciones como disolventes.[47] Aunque con lentitud, estos disolventes neotéricos se están integrando en los procesos industriales. Este conjunto incluye disolventes expandidos por gases (*gas expanded solvents*),[28] líquidos poliméricos como el polietilenglicol de bajo peso molecular,[48] disolventes inteligentes capaces de variar su comportamiento en función de estímulos ambientales,[49] disolventes a partir de mezclas eutécticas profundas (*DES*),[50] líquidos iónicos (ILs),[51] fluidos supercríticos como el dióxido

[41] Yang, J.; Tan, J.-N.; Gu, Y. Lactic Acid as an Invaluable Bio-Based Solvent for Organic Reactions. *Green Chem.* **2012**, *14* (12), 3304–3317.
[42] Weldemhret, T. G.; Bañares, A. B.; Ramos, K. R. M.; Lee, W.-K.; Nisola, G. M.; Valdehuesa, K. N. G.; Chung, W.-J. Current Advances in Ionic Liquid-Based Pre-Treatment and Depolymerization of Macroalgal Biomass. *Renew. Energy.* **2020**, *152*, 283–299.
[43] Kunthakudee, N.; Sunsandee, N.; Chutvirasakul, B.; Ramakul, P. Extraction of Lycopene from Tomato with Environmentally Benign Solvents: Box-Behnken Design and Optimization. *Chem. Eng. Commun.* **2020**, *207* (4), 574–583.
[44] Jessop, P. G.; Stanley, R. R.; Brown, R. A.; Eckert, C. A.; Liotta, C. L.; Ngo, T. T.; Pollet, P. Neoteric Solvents for Asymmetric Hydrogenation: Supercritical Fluids, Ionic Liquids, and Expanded Ionic Liquids. *Green Chem.* **2003**, *5* (2), 123–128.
[45] Warr, G. G.; Atkin, R. Solvophobicity and Amphiphilic Self-Assembly in Neoteric and Nanostructured Solvents. *Curr. Opin. Colloid Interface Sci.* **2020**, *45*, 83–96.
[46] Mokhtarpour, M.; Shekaari, H.; Zafarani-Moattar, M. T.; Golgoun, S. Solubility and Solvation Behavior of Some Drugs in Choline Based Deep Eutectic Solvents at Different Temperatures. *J. Mol. Liq.* **2020**, *297*, 111799.
[47] Wilkes, J. S. A Short History of Ionic Liquids—from Molten Salts to Neoteric Solvents. *Green Chem.* **2002**, *4* (2), 73–80.
[48] Mansour, F. R.; Zhou, L.; Danielson, N. D. Applications of Poly(Ethylene)Glycol (PEG) in Separation Science. *Chromatographia.* **2015**, *78* (23), 1427–1442.
[49] Pollet, P.; Eckert, C. A.; Liotta, C. L. Switchable Solvents. *Chem. Sci.* **2011**, *2* (4), 609–614.
[50] Perna, F. M.; Vitale, P.; Capriati, V. Deep Eutectic Solvents and Their Applications as Green Solvents. *Curr. Opin. Green Sustain. Chem.* **2020**. *21*, 27-33.
[51] Habibul, N.; Ilmurat, M.; Habibul, Z.; Hu, Y.; Ma, X. Uptake and Accumulation of Imidazolium Ionic Liquids in Rice Seedlings: Impacts of Alkyl Chain Length. *Chemosphere* **2020**, *242*, 125228.

de carbono ($scCO_2$)[52] y el agua (scH_2O),[53] disolventes fluorados (*FSs*),[54] y disolventes derivados de materias primas renovables tales como el bioetanol,[55] el lactato de etilo,[56] o el 2-metil tetrahidrofurano (2-MeTHF).[57]

Dado que los disolventes constituyen alrededor del 80% del volumen total de los productos químicos utilizados en un proceso,[58] resulta de gran interés el uso de disolventes renovables derivados de la biomasa tales como el glicerol[59,60] y el ácido láctico[61], con los disolventes obtenidos por fermentación siendo fácilmente biodegradables. En la Figura 4 se muestran algunas estructuras de disolventes obtenidos a partir de biomasa renovable.

[52] Morgenstern, D. A.; LeLacheur, R. M.; Morita, D. K.; Borkowsky, S. L.; Feng, S.; Brown, G. H.; Luan, L.; Gross, M. F.; Burk, M. J.; Tumas, W. Supercritical Carbon Dioxide as a Substitute Solvent for Chemical Synthesis and Catalysis. In *Green Chemistry*; ACS Symposium Series; American Chemical Society, 1996; Vol. 626, pp 132–151.
[53] Maxim, F.; Contescu, C.; Boillat, P.; Niceno, B.; Karalis, K.; Testino, A.; Ludwig, C. Visualization of Supercritical Water *pseudo*-Boiling at Widom Line Crossover. *Nat. Commun.* **2019**, *10* (1), 1–11.
[54] Hobbs, H. R.; Thomas, N. R. Biocatalysis in Supercritical Fluids, in Fluorous Solvents, and under Solvent-Free Conditions. *Chem. Rev.* **2007**, *107* (6), 2786–2820.
[55] Al-Azkawi, A.; Elliston, A.; Al-Bahry, S.; Sivakumar, N. Waste paper to Bioethanol: Current and Future Prospective. *Biofpr.* **2019**, *13* (4), 1106–1118.
[56] Tobiszewski, M. Analytical Chemistry with Biosolvents. *Anal. Bioanal. Chem.* **2019**, *411* (19), 4359–4364.
[57] Slater, C. S.; Savelski, M. J.; Hitchcock, D.; Cavanagh, E. J. Environmental Analysis of the Life Cycle Emissions of 2-Methyl Tetrahydrofuran Solvent Manufactured from Renewable Resources. *J. Environ. Sci. Health A.* **2016**, *51* (6), 487–494.
[58] Gu, Y.; Jérôme, F. Bio-Based Solvents: An Emerging Generation of Fluids for the Design of Eco-Efficient Processes in Catalysis and Organic Chemistry. *Chem. Soc. Rev.* **2013**, *42* (24), 9550–9570.
[59] Li, M.; Chen, C.; He, F.; Gu, Y. Multicomponent Reactions of 1,3-Cyclohexanediones and Formaldehyde in Glycerol: Stabilization of Paraformaldehyde in Glycerol Resulted from Using Dimedone as Substrate. *Adv. Synth. Catal.* **2010**, *352* (2–3), 519–530.
[60] Jamale, D. K.; Undare, S. S.; Valekar, N. J.; Sarkate, A. P.; Kolekar, G. B.; Anbhule, P. V. Glycerol Mediated Synthesis, Biological Evaluation, and Molecular Docking Study of 4-(1H-Pyrazol-4-Yl)-Polyhydroquinolines as Potent Antitubercular Agents. *J. Heterocyclic Chem.* **2019**, *56* (2), 608–618.
[61] Gössi, A.; Burgener, F.; Kohler, D.; Urso, A.; Kolvenbach, B. A.; Riedl, W.; Schuur, B. In-Situ Recovery of Carboxylic Acids from Fermentation Broths through Membrane Supported Reactive Extraction Using Membrane Modules with Improved Stability. *Sep. Purif. Technol.* **2020**, *241*, 116694.

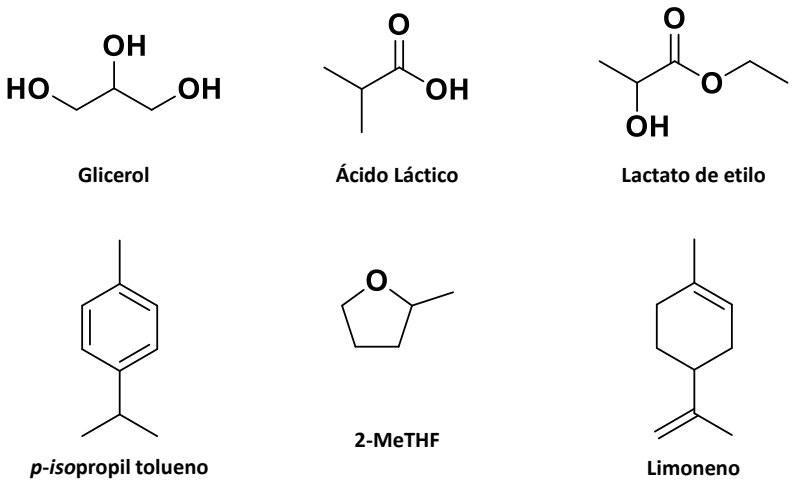

Figura 4. Estructuras de algunos disolventes obtenidos de materias derivadas de biomasa

Desde el punto de vista medio ambiental, el agua es un disolvente muy atractivo. Aún con las limitaciones asociadas a su baja capacidad solvatante para muchos compuestos orgánicos y el coste energético de su destilación, se ha utilizado con éxito en distintas reacciones orgánicas,[62] ofreciendo algunas ventajas que incluyen la facilidad de aislamiento del producto, su no toxicidad y no inflamabilidad y su alta capacidad de calentamiento.[63]

Por supuesto, en aquellos casos donde sea viable, las reacciones sin disolvente representan una alternativa sostenible (*free solvent*).[64,65] A menudo se afirma que el mejor disolvente, es la ausencia de disolvente, porque trae consigo beneficios inmediatos como la disminución del consumo de energía y de los tiempos de

[62] Papadogianakis, G.; Sheldon, R. A. Special Issue on Recent Advances in Catalysis in Green Aqueous Media. *Catal. Today*. **2015**, *247*, 1–3.
[63] Abraham, R.; Prakash, P.; Mahendran, K.; Ramanathan, M. A Novel and Convenient Oxidation-Controlled Procedure for the Synthesis of Oxazolines from TosMIC and Aldehydes in Water – Anti Biofilm Activity. *Arab. J. Chem.* **2020**, *13* (1), 2153–2161.
[64] Pichon, A.; Lazuen-Garay, A.; James, S. L. Solvent-Free Synthesis of a Microporous Metal–Organic Framework. *CrystEngComm*. **2006**, *8* (3), 211–214.
[65] Gawande, M. B.; Bonifácio, V. D. B.; Luque, R.; Branco, P. S.; Varma, R. S. Solvent-Free and Catalysts-Free Chemistry: A Benign Pathway to Sustainability. *ChemSusChem*. **2014**, *7* (1), 24–44.

reacción, la disminución del tamaño de los reactores y la reducción del coste económico.[66]

El empleo de fluidos supercríticos (*SCF* ó *scFs*, por sus siglas en inglés) ha sido estudiado, también, en detalle, puesto que tienen propiedades físicas únicas. Exhiben coeficientes de difusión similares a las de un gas y densidades semejantes a las de un líquido,[67,68] lo que resulta ventajoso a la hora de modelar sus propiedades. No obstante, la necesidad de trabajar con altas presiones representa una limitación importante de este campo frente a otras alternativas.

En este trabajo, como parte del proceso de formación en el campo de la Química Verde, en cada ruta sintética estudiada se analizaron las condiciones sin disolventes y cuando no fue posible, se usaron disolventes sostenibles como reemplazo de los disolventes orgánicos tradicionales. Las transformaciones químicas se llevaron a cabo empleando el menor consumo de energía posible y utilizando disolventes neotéricos para disminuir el impacto ambiental. En este trabajo se emplearon disolventes como: agua, etanol, 2-MeTHF y CO_2 supercrítico.

1.2.1. Líquidos Iónicos: Aspectos Generales y propiedades

Dada su conexión con este trabajo, conviene analizar con más detalle el uso de líquidos iónicos (ILs, por sus siglas en inglés) para reemplazar el uso de los disolventes orgánicos tradicionales.[69] Los ILs son considerados una clase de

[66] Singh, M. S.; Chowdhury, S. Recent Developments in Solvent-Free Multicomponent Reactions: A Perfect Synergy for Eco-Compatible Organic Synthesis. *RSC Adv.* **2012**, *2* (11), 4547–4592.
[67] Kiran, E. Supercritical Fluids and Polymers – The Year in Review – 2014. *J. Supercrit. Fluid.* **2016**, *110*, 126–153.
[68] Hatami, T.; Johner, J. C. F.; Kurdian, A. R.; Meireles, M. A. A. A Step-by-Step Finite Element Method for Solving the External Mass Transfer Control Model of the Supercritical Fluid Extraction Process: A Case Study of Extraction from Fennel. *J. Supercrit. Fluid.* **2020**, *160*, 104797.
[69] Elgharbawy, A. A. M.; Azmi, N. A. N.; Mohd-Salleh, H. Ionic Liquids: Promising Solvents for Halal Industry. *J. Food Res.* **2020**, *4*, 52–62.

disolventes no moleculares,[70] que consisten completamente en iones, pero que, a diferencia de las sales clásicas, son líquidos a temperatura ambiente o cerca de ella.[71] Están formados por cationes orgánicos y aniones que pueden ser orgánicos o inorgánicos. En la Figura 5 se pueden observar los cationes y aniones usados frecuentemente para la preparación de ILs. Por lo general, los cationes, basados en sales de amonio o fosfonio, deben tener un carácter voluminoso y deslocalizado, por lo que el apropiado diseño de sistemas aromáticos de azolio o piridino permite controlar sus propiedades físicas. Los aniones pueden ser muy variados, preferentemente deslocalizados y poco coordinantes, y son responsables de actividad química y la reactividad.[72,73]

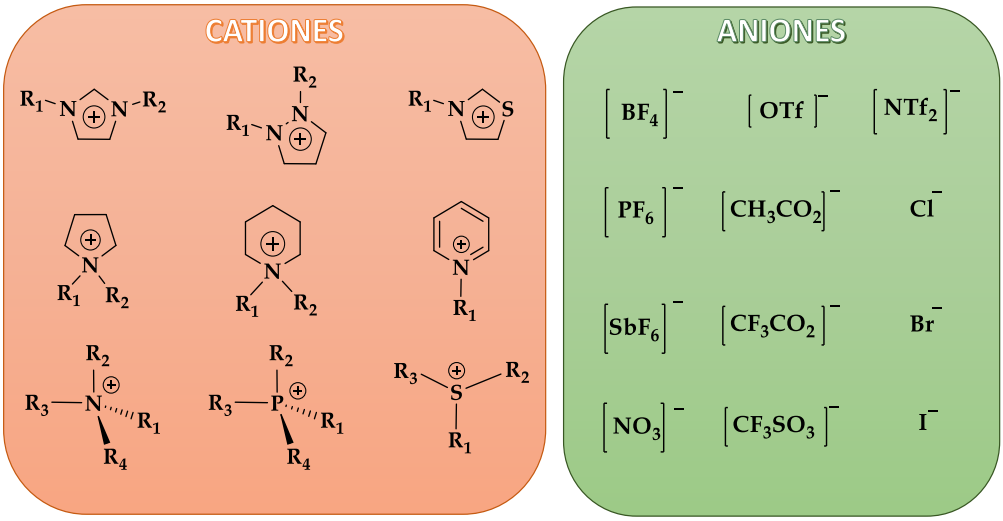

Figura 5. Cationes y aniones comúnmente usados para la preparación de líquidos iónicos.

[70] Sandoval Barrantes, M. Nuevas Estrategias Sostenibles para la Síntesis Enzimática de Oligosacáridos y Glycoconjugados de Interés Biológico. Ph.D. Thesis, Universidad Complutense de Madrid, Madrid, 2012.
[71] Bystrov, S. S.; Matveev, V. V.; Chernyshev, Y. S.; Balevičius, V.; Chizhik, V. I. Molecular Mobility in a Set of Imidazolium-Based Ionic Liquids $[Bmim]^+A^-$ by the NMR-Relaxation Method. *J. Phys. Chem. B.* **2019**, *123* (10), 2362–2372.
[72] Peris Salom, E. Continuous Flow Systems for Multicatalytic Processes Based on Supported Ionic Liquids. Ph.D. Thesis, Universitat Jaume I, Castellón de la Plana, España, 2019.
[73] Salvador, A. R. Líquidos iónicos a temperatura ambiente: Un nuevo medio para las reacciones químicas. *R. Acad. Cienc. Exact. Fís. Nat.* **2008**, *102* (1), 79–90.

El primer líquido iónico fue descrito por Paul Walden en 1914 (Figura 6), cuando realizó la neutralización de la etilamina con ácido nítrico concentrado formando el nitrato de etilamonio ($[EtNH_3]^+$ $[NO_3]^-$).[74] Walden informo sobre las propiedades físicas del compuesto, tales como su bajo punto de fusión (13-14 ^oC).[75] Este IL tenía semejanzas con el agua, ya que era transparente, incoloro, inodoro y sumado a ello tenía una viscosidad razonablemente alta y lo más importante, la conductividad del $[EtNH_3]^+$ $[NO_3]^-$ mostró una interacción pura de aniones y cationes. Sin embargo no fue hasta 1951, cuando se informó sobre la segunda generación de líquidos iónicos al mezclar cloruros de alquilpiridinio con cloruro de aluminio. En este caso, la mayoría de los líquidos ILs no eran estables en presencia de humedad, y su acidez y basicidad no era fácil de regular. [76,77]

Известія Императорской Академіи Наукъ. — 1914.
(Bulletin de l'Académie Impériale des Sciences de St.-Pétersbourg).

Ueber die Molekulargrösse und elektrische Leitfähigkeit einiger geschmolzenen Salze.

(Mit 1 Figur).

Von P. Walden.

Im Nachstehenden will ich meine Untersuchungen über die elektrische Leitfähigkeit und die aus den Kapillaritätskonstanten abgeleiteten Molekulargrösse einiger organischen Ammoniumsalze mitteilen. Gewählt wurden *wasserfreie* Salze, welche bei relativ *niedrigen Temperaturen*, etwa bis zu 100° C. schmelzen. Diese niedrigen Schmelztemperaturen engten die Möglichkeit einer *Wärmespaltung* sowohl des Solvens, als auch des gelösten Salzes in der Salzschmelze ein; sie eröffneten daher die *Reproduzierbarkeit* der bisher nur bei *hohen* Temperaturen, in den *Schmelzen* der wasserfreien *Mineralsalze* gemachten Beobachtungen bei *niedrigen Temperaturen*; sie boten die Möglichkeit dar, mit Hilfe der für gewöhnliche Temperaturen gebräuchlichen Methoden und Apparate alle Messungen durchzuführen. Die Verhältnisse in *diesen* niedrig schmelzenden Salzen näherten sich daher den Versuchsbedingungen, wie sie für die gewöhnlichen wässrigen und nichtwässrigen Lösungsmittel eingehend erforscht worden sind und durch die osmotische Theorie van't Hoffs und die elektrolytische Dissoziationstheorie von Arrhenius beherrscht werden.

Das allgemeine Bild dieser *organischen Salze* bei *niedrigen Temperaturen* (unter, bezw. um 100° C.) entspricht also den Erfahrungen an *anorganischen* (einfachen) *geschmolzenen Salzen bei weit höheren* Temperaturen (etwa zwischen 300—600° C.). Wenn die Salzmolekeln in dem einen, wie in dem andern Fall *assoziiert* sind, und dieser (approximative) Assoziationsgrad bis auf $x = 6 - 9$ ansteigt, so kann von einer *vollkommenen* Dissoziation des geschmolzenen Salzes in die *einfachen Jonen* natürlich *keine Rede sein*; eine elektrolytische Dissoziation ist augenscheinlich vorhanden, sie betrifft aber sicherlich das Vorhandensein von komplexen Jonen neben einfachen (infolge einer stufenweisen Aufspaltung der assoziierten Salzmolekeln). Der Dissoziationsgrad betrifft also beide Arten von Jonen und wird, je nach der Zusammensetzung und dem Typus des binären Salzes (d. h. je nach der Natur des Kations und Anions), verschiedene Werte für die einzelnen Salze annehmen. —

Figura 6. **(a)** Fotografía de Paul Walden, investigador y descubridor de los líquidos iónicos. **(b)** Extracto del primer artículo que describe el $[EtNH_3]^+$ $[NO_3]^-$ como líquido iónico (tomado de ref. 74).

[74] Walden, P. Ueber Die Molekulargrösse Und Elektrische Leitfähigkeit Einiger Geschmolzenen Salze. *Bull. Acad. Imp. Sci. St. Pétersbourg*. **1914**, *8* (6), 405–422.
[75] Plechkova, N. V.; Seddon, K. R. Applications of Ionic Liquids in the Chemical Industry. *Chem. Soc. Rev.* **2007**, *37* (1), 123–150.
[76] Wang, B.; Qin, L.; Mu, T.; Xue, Z.; Gao, G. Are Ionic Liquids Chemically Stable? *Chem. Rev.* **2017**, *117* (10), 7113–7131.
[77] Fedorov, M. V.; Kornyshev, A. A. Ionic Liquids at Electrified Interfaces. *Chem. Rev.* **2014**, *114* (5), 2978–3036.

Desde el estudio llevado a cabo por Wilkes y colaboradores, donde se describe el uso potencial de los líquidos iónicos como electrolitos en baterías, células fotoelectroquímicas y galvanoplastia,[78] se popularizó el estudio de los ILs como medio de reacción y extracción, así como para numerosas aplicaciones industriales.[79] Su uso se ha extendido ampliamente, ya que despiertan gran interés debido a sus propiedades. La mejor distribución y deslocalización de la carga y el mayor tamaño de los iones,[80] en comparación con las sales inorgánicas clásicas, dan como resultado bajos puntos de fusión[81] (sales orgánicas que funden por debajo de los 100 °C), [82] además de propiedades fisicoquímicas únicas y ajustables,[83,84] lo que los diferencia de los disolventes moleculares tradicionales. En este sentido, algunas propiedades fundamentales de los ILs incluyen el ser líquidos a temperatura ambiente,[85] presión de vapor casi nula, por lo que son prácticamente no volátiles,[86] elevada estabilidad térmica y electroquímica, escasa

[78] Wilkes, J. S.; Levisky, J. A.; Wilson, R. A.; Hussey, C. L. Dialkylimidazolium Chloroaluminate Melts: A New Class of Room-Temperature Ionic Liquids for Electrochemistry, Spectroscopy and Synthesis. *Inorg. Chem.* **1982**, *21* (3), 1263–1264.
[79] Ranke, J.; Stolte, S.; Störmann, R.; Arning, J.; Jastorff, B. Design of Sustainable Chemical Products the Example of Ionic Liquids. *Chem. Rev.* **2007**, *107* (6), 2183–2206.
[80] Krasovskiy, V. G.; Chernikova, E. A.; Glukhov, L. M.; Kapustin, G. I.; Koroteev, A. A. Effect of Hydroxyl Groups in a Cation Structure on the Properties of Ionic Liquids. *Russ. J. Phys. Chem.* **2018**, *92* (12), 2379–2385.
[81] Giacalone, F.; Gruttadauria, M. Covalently Supported Ionic Liquid Phases: An Advanced Class of Recyclable Catalytic Systems. *ChemCatChem.* **2016**, *8* (4), 664–684.
[82] Longhi, M.; Arnaboldi, S.; Husanu, E.; Grecchi, S.; Buzzi, I. F.; Cirilli, R.; Rizzo, S.; Chiappe, C.; Mussini, P. R.; Guazzelli, L. A Family of Chiral Ionic Liquids from the Natural Pool: Relationships between Structure and Functional Properties and Electrochemical Enantiodiscrimination Tests. *Electrochim. Acta.* **2019**, *298*, 194–209.
[83] Restrepo, J.; Lozano, P.; Burguete, M. I.; García-Verdugo, E.; Luis, S. V. Gold Nanoparticles Immobilized onto Supported Ionic Liquid-like Phases for Microwave Phenylethanol Oxidation in Water. *Catal. Today.* **2015**, *255*, 97–101.
[84] Montolio, S.; Abarca, G.; Porcar, R.; Dupont, J.; Burguete, M. I.; García-Verdugo, E.; Luis, S. V. Hierarchically Structured Polymeric Ionic Liquids and Polyvinylpyrrolidone Mat-Fibers Fabricated by Electrospinning. *J. Mater. Chem. A.* **2017**, *5* (20), 9733–9744.
[85] Galiński, M.; Lewandowski, A.; Stępniak, I. Ionic Liquids as Electrolytes. *Electrochim. Acta.* **2006**, *51* (26), 5567–5580.
[86] Liu, X.; Chen, Y.; Zeng, S.; Zhang, X.; Zhang, S.; Liang, X.; Gani, R.; Kontogeorgis, G. M. Structure Optimization of Tailored Ionic Liquids and Process Simulation for Shale Gas Separation. *AIChE J.* **2020**, *66* (2), e16794.

inflamabilidad,[87] alta conductividad iónica[88] y capacidad para solvatar compuestos de polaridad muy variable.[89]

El estudio de los ILs como alternativa a los disolventes orgánicos comunes representa un tema de investigación multidisciplinario. La posibilidad de diseñarlos para una amplia variedad de procesos, utilizando las aproximaciones de la Química Verde y las tecnologías limpias, vincula diferentes campos como la química, la biología, la ingeniería, la industria farmacéutica,[90,91] alimentaria[92] y la agricultura.[93] Todas estas características han hecho que representen un elemento fundamental dentro de las tecnologías asociadas a la Química Verde.[94]

Una característica fundamental de los ILs es la posibilidad de ajustar sus propiedades físicas y químicas con la modulación del anión o del catión.[95] Esto ha hecho que a menudo se les denomine "disolventes de diseño" así como la preparación de una variedad prácticamente infinita de compuestos con estas

[87] Nakaya, N.; Hosoya, T.; Miyafuji, H. Ionic Liquids as Formaldehyde-Free Wood Adhesives. *J. Wood. Sci.* **2018**, *64* (6), 794–801.
[88] Jiao, J.; Gai, Q.-Y.; Fu, Y.-J.; Zu, Y.-G.; Luo, M.; Zhao, C.-J.; Li, C.-Y. Microwave-Assisted Ionic Liquids Treatment Followed by Hydro-Distillation for the Efficient Isolation of Essential Oil from Fructus Forsythiae Seed. *Sep. Purif. Technol.* **2013**, *107*, 228–237.
[89] Hollóczki, O.; Firaha, D. S.; Friedrich, J.; Brehm, M.; Cybik, R.; Wild, M.; Stark, A.; Kirchner, B. Carbene Formation in Ionic Liquids: Spontaneous, Induced, or Prohibited? *J. Phys. Chem. B.* **2013**, *117* (19), 5898–5907.
[90] Bica, K.; Shamshina, J.; Hough, W. L.; MacFarlane, D. R.; Rogers, R. D. Liquid Forms of Pharmaceutical Co-Crystals: Exploring the Boundaries of Salt Formation. *Chem. Commun.* **2011**, *47* (8), 2267–2269.
[91] Marrucho, I. M.; Branco, L. C.; Rebelo, L. P. N. Ionic Liquids in Pharmaceutical Applications. *Annu. Rev. Chem. Biomol. Eng.* **2014**, *5* (1), 527–546.
[92] Toledo Hijo, A. A. C.; Maximo, G. J.; Costa, M. C.; Batista, E. A. C.; Meirelles, A. J. A. Applications of Ionic Liquids in the Food and Bioproducts Industries. *ACS Sustainable Chem. Eng.* **2016**, *4* (10), 5347–5369.
[93] Zajac, A.; Kukawka, R.; Pawlowska-Zygarowicz, A.; Stolarska, O.; Smiglak, M. Ionic Liquids as Bioactive Chemical Tools for Use in Agriculture and the Preservation of Agricultural Products. *Green Chem.* **2018**, *20* (21), 4764–4789.
[94] Mallakpour, S.; Dinari, M. Ionic Liquids as Green Solvents: Progress and Prospects. In *Green Solvents II: Properties and Applications of Ionic Liquids*; Mohammad, A., Inamuddin, Dr., Eds.; Springer Netherlands: Dordrecht, 2012; pp 1–32.
[95] P. Wasserscheid *and* T. Welton, *Ionic Liquids in Synthesis,* Vol. *1*, WILEY-VCH, Verlag GmbH & Co. KGaA, Weinheim, Germany 2008.

características.[96,97] Ello facilita la creación a medida de ILs con propiedades específicas para determinadas aplicaciones.[98] Se han reportado una amplia gama de estructuras para líquidos iónicos, siendo los más estudiados los basados en cationes de imidazolio, fosfonio, piridinio y amonio.[99] Aunque se han descrito numerosas aplicaciones,[100,101,102] su alta viscosidad o la lenta difusividad de los gases limitan algunas de sus aplicaciones industriales.

Como hemos mencionado, muchos de los ILs son considerados de bajo impacto ambiental puesto que no generan VOCs,[103] aumentan los rendimientos en los procesos sintéticos y catalíticos y, además, se pueden reutilizar.[104] Sin embargo, no todos los ILs pueden ser clasificados ambientalmente amigables ya que algunos son poco biodegradables[105,106] y se pueden acumular en el agua

[96] Earle, M. J.; Seddon, K. R. Ionic Liquids. Green Solvents for the Future. *Pure Appl. Chem.* **2000**, *72* (7), 1391–1398.
[97] Earle, M. J.; Seddon, K. R. Ionic Liquids: Green Solvents for the Future. In *Clean Solvents, Alternative Media for Chemical Reactions and Processing*; Abraham, M., Moens, L., Eds.; ACS Symposium Series; American Chemical Society: Washington, DC., 2002; Vol. 819, pp 10–25.
[98] Fei, Z.; Dyson, P. J. The Making of iLiquids – the Chemist's Equivalent of the IPhone. *Chem. Commun.* **2013**, *49* (26), 2594.
[99] Olivier-Bourbigou, H.; Magna, L.; Morvan, D. Ionic Liquids and Catalysis: Recent Progress from Knowledge to Applications. *Appl. Catal. A-Gen.* **2010**, *373* (1), 1–56.
[100] Holbrey, J. D.; Rogers, R. D. Green Chemistry and Ionic Liquids: Synergies and Ironies. In *Ionic Liquids: Industrial Applications for Green Chemistry*; Rogerds, R. D., Seddon, K. R., Eds.; ACS Symposium Series; American Chemical Society: United States, 2002; Vol. 818, pp 2–14.
[101] Maase, M. Industrial Applications of Ionic Liquids. In *Ionic Liquids in Synthesis*; Wasserscheid, P., Welton, T., Eds.; John Wiley & Sons, Ltd: United Satates, 2008; Vol. 2, pp 663–687.
[102] Smiglak, M.; Pringle, J. M.; Lu, X.; Han, L.; Zhang, S.; Gao, H.; MacFarlane, D. R.; Rogers, R. D. Ionic Liquids for Energy, Materials, and Medicine. *Chem. Commun.* **2014**, *50* (66), 9228–9250.
[103] Rogers, R. D.; Seddon, K. R. Ionic Liquids-Solvents of the Future? *Science.* **2003**, *302* (5646), 792–793.
[104] Dołżonek, J.; Kowalska, D.; Maculewicz, J.; Stepnowski, P. Regeneration, Recovery, and Removal of Ionic Liquids. In *Encyclopedia of Ionic Liquids*; Zhang, S., Ed.; Springer: Singapore, 2020; pp 1–9.
[105] Coleman, D.; Gathergood, N. Biodegradation Studies of Ionic Liquids. *Chem. Soc. Rev.* **2010**, *39* (2), 600–637.
[106] Mena, I. F.; Diaz, E.; Palomar, J.; Rodriguez, J. J.; Mohedano, A. F. Cation and Anion Effect on the Biodegradability and Toxicity of Imidazolium– and Choline–Based Ionic Liquids. *Chemosphere* **2020**, *240*, 124947.

desencadenando una serie de problemas ambientales.[107,108,109] Algunos son señalados incluso como nocivos. Por ejemplo, las sales de imidazolio con cadenas de alquilo largas son tóxicas mientras que los de cadena corta son poco biodegradables.[110]

Si consideramos la sostenibilidad en el contexto del proceso a realizar, los ILs al mejorar el rendimiento de reacción, la selectividad, la velocidad de extracción y reducir en gran medida los residuos y la energía utilizada en el proceso conllevan claras ventajas frente a los disolventes tradicionales. Sin embargo, es preciso considerar que, por lo general, su preparación implica valores altos del "*E factor*", lo que, además, encarece su coste.[111,112] Su impacto ambiental dependerá también, en gran medida, de la longitud de las cadenas de carbono (estructura del catión) y del anión.[113] Para solventar su potencial ecotoxicidad se ha propuesto la síntesis de ILs biocompatibles, obtenidos a partir de productos

[107] Stolte, S.; Matzke, M.; Arning, J.; Böschen, A.; Pitner, W.-R.; Welz-Biermann, U.; Jastorff, B.; Ranke, J. Effects of Different Head Groups and Functionalised Side Chains on the Aquatic Toxicity of Ionic Liquids. *Green Chem.* **2007**, *9* (11), 1170–1179.
[108] Xia, X.; Wan, R.; Wang, P.; Huo, W.; Dong, H.; Du, Q. Toxicity of Imidazoles Ionic Liquid [C_{16}mim]Cl to Hela Cells. *Ecotox. Environ. Safe.* **2018**, *162*, 408–414.
[109] Wan, R.; Xia, X.; Wang, P.; Huo, W.; Dong, H.; Chang, Z. Toxicity of Imidazoles Ionic Liquid [C_{16}mim]Cl to HepG2 Cells. *Toxicol. in Vitro.* **2018**, *52*, 1–7.
[110] Kunz, W.; Maurer, E.; Klein, R.; Touraud, D.; Rengstl, D.; Harrar, A.; Dengler, S.; Zech, O. Low Toxic Ionic Liquids, Liquid Catanionics, and Ionic Liquid Microemulsions. *J. Disper. Sci. Technol.* **2011**, *32* (12), 1694–1699.
[111] Sheldon, R. A. The E Factor: Fifteen Years On. *Green Chem.* **2007**, *9* (12), 1273–1283.
[112] Deetlefs, M.; Seddon, K. R. Assessing the Greenness of Some Typical Laboratory Ionic Liquid Preparations. *Green Chem.* **2010**, *12* (1), 17–30.
[113] Xu, Y.; Wang, J.; Du, Z.; Li, B.; Juhasz, A.; Tan, M.; Zhu, L.; Wang, J. Toxicity Evaluation of Three Imidazolium-Based Ionic Liquids ([C_6mim]R) on *Vicia faba* Seedlings Using an Integrated Biomarker Response (IBR) Index. *Chemosphere* **2020**, *240*, 124919.

naturales relativamente económicos como aminoácidos,[114,115] carbohidratos[116] y metabolitos naturales como la colina.[117]

Los líquidos iónicos, más allá de ser usados como disolventes alternativos,[118,119] abarcan una amplia gama de aplicaciones en farmacología y medicina,[120] almacenamiento de energía,[121] materiales magnéticos y luminiscentes,[122,123,124] procesos integrados de reacción - separación,[125] absorción y transformación de gases (CO_2[126] y SO_2[127]) biotransformaciones,[128] electro/fotoquímica[129] o

[114] Fiorani, G.; Selva, M.; Perosa, A.; Benedetti, A.; Enrichi, F.; Licence, P.; Easun, T. L. Luminescent Dansyl-Based Ionic Liquids from Amino Acids and Methylcarbonate Onium Salt Precursors: Synthesis and Photobehaviour. *Green Chem.* **2014**, *17* (1), 538–550.
[115] Song, Z.; Liang, Y.; Fan, M.; Zhou, F.; Liu, W. Ionic Liquids from Amino Acids: Fully Green Fluid Lubricants for Various Surface Contacts. *RSC Adv.* **2014**, *4* (37), 19396–19402.
[116] Poletti, L.; Chiappe, C.; Lay, L.; Pieraccini, D.; Polito, L.; Russo, G. Glucose-Derived Ionic Liquids: Exploring Low-Cost Sources for Novel Chiral Solvents. *Green Chem.* **2007**, *9* (4), 337–341.
[117] Mena, I. F.; Diaz, E.; Rodriguez, J. J.; Mohedano, A. F. Biological Oxidation of Choline-Based Ionic Liquids in Sequencing Batch Reactors. *J. Chem. Technol. Biotechnol.* **2020**, *95* (4), 922–931.
[118] Giernoth, R. Task-Specific Ionic Liquids. *Angew. Chem. Int. Ed.* **2010**, *49* (16), 2834–2839.
[119] Giernoth, R. Ionic Liquids with a Twist: New Routes to Liquid Salts. *Angew. Chem. Int. Ed.* **2010**, *49* (33), 5608–5609.
[120] Egorova, K. S.; Gordeev, E. G.; Ananikov, V. P. Biological Activity of Ionic Liquids and Their Application in Pharmaceutics and Medicine. *Chem. Rev.* **2017**, *117* (10), 7132–7189.
[121] Gür, T. M. Review of Electrical Energy Storage Technologies, Materials and Systems: Challenges and Prospects for Large-Scale Grid Storage. *Energy Environ. Sci.* **2018**, *11* (10), 2696–2767.
[122] Yoshida, Y.; Saito, G. Design of Functional Ionic Liquids Using Magneto- and Luminescent-Active Anions. *Phys. Chem. Chem. Phys.* **2010**, *12* (8), 1675–1684.
[123] Estager, J.; Holbrey, J. D.; Swadźba-Kwaśny, M. Halometallate Ionic Liquids – Revisited. *Chem. Soc. Rev.* **2014**, *43* (3), 847–886.
[124] Ogawa, T.; Sameera, W. M. C.; Yoshida, M.; Kobayashi, A.; Kato, M. Luminescent Ionic Liquids Based on Cyclometalated Platinum (II) Complexes Exhibiting Thermochromic Behaviour in Different Colour Regions. *Dalton Trans.* **2018**, *47* (16), 5589–5594.
[125] Villa, R.; Alvarez, E.; Porcar, R.; Garcia-Verdugo, E.; Luis, S. V.; Lozano, P. Ionic Liquids as an Enabling Tool to Integrate Reaction and Separation Processes. *Green Chem.* **2019**, *21* (24), 6527–6544.
[126] Hospital-Benito, D.; Lemus, J.; Moya, C.; Santiago, R.; Palomar, J. Process Analysis Overview of Ionic Liquids on CO_2 Chemical Capture. *Chem. Eng. J.* **2020**, *390*, 124509.
[127] Wang, L.; Zhang, Y.; Liu, Y.; Xie, H.; Xu, Y.; Wei, J. SO_2 Absorption in Pure Ionic Liquids: Solubility and Functionalization. *J. Hazard. Mater.* **2020**, *392*, 122504.
[128] Dupont, J. From Molten Salts to Ionic Liquids: A "Nano" Journey. *Acc. Chem. Res.* **2011**, *44* (11), 1223–1231.
[129] Nese, C.; Unterreiner, A.-N. Photochemical Processes in Ionic Liquids on Ultrafast Timescales. *Phys. Chem. Chem. Phys.* **2010**, *12* (8), 1698–1708.

desempeñando una doble función como disolvente y catalizador en la transformación química.[130,131,132,133]

1.3. Líquidos Iónicos Soportados

Los líquidos iónicos al ser "disolventes de diseño"[134] permiten una amplia gama de aplicaciones,[135,136,137] pero, sin embargo, son productos relativamente caros[138] y en algunos casos pueden ser tóxicos o poco biodegradables, [139,140] provocando que puedan no ser atractivos desde el punto de vista económico y ambiental. Una solución a este problema consiste en inmovilizar los ILs en matrices sólidas, de tal forma que se combinen las ventajas de los líquidos iónicos con las del soporte.

La inmovilización de los ILs en un material se lleva a cabo mediante diferentes estrategias (Figura 7), tales como: la encapsulación, la adsorción, la formación del

[130] Welton, T. Room-Temperature Ionic Liquids. Solvents for Synthesis and Catalysis. *Chem. Rev.* **1999**, *99* (8), 2071–2084.
[131] Hallett, J. P.; Welton, T. Room-Temperature Ionic Liquids: Solvents for Synthesis and Catalysis. 2. *Chem. Rev.* **2011**, *111* (5), 3508–3576.
[132] Li, H.; Bhadury, P. S.; Song, B.; Yang, S. Immobilized Functional Ionic Liquids: Efficient, Green, and Reusable Catalysts. *RSC Adv.* **2012**, *2* (33), 12525–12551.
[133] Doherty, S. Homogeneous Catalysis in Ionic Liquids. In *Catalysis in Ionic Liquids. From Catalyst Synthesis to Application*; Hardacre, C., Parvulescu, V., Eds., RSC Catalysis Series; The Royal Society of Chemistry: United Kingdon, 2014; pp 44–308.
[134] Niedermeyer, H.; Hallett, J. P.; Villar-Garcia, I. J.; Hunt, P. A.; Welton, T. Mixtures of Ionic Liquids. *Chem. Soc. Rev.* **2012**, *41* (23), 7780–7802.
[135] Stark, A. Ionic Liquids in the Biorefinery: A Critical Assessment of Their Potential. *Energy Environ. Sci.* **2010**, *4* (1), 19–32.
[136] Lovelock, K. R. J. Influence of the Ionic Liquid/Gas Surface on Ionic Liquid Chemistry. *Phys. Chem. Chem. Phys.* **2012**, *14* (15), 5071–5089.
[137] Montolio, S.; Gonzáez, L.; Altava, B.; Tenhu, H.; Burguete, M. I.; García-Verdugo, E.; Luis, S. V. LCST-Type Polymers Based on Chiral-Polymeric Ionic Liquids. *Chem. Commun.* **2014**, *50* (73), 10683–10686.
[138] Wilkes, J. S.; Wasserscheid, P.; Welton, T. Introduction. In *Ionic Liquids in Synthesis*; Wasserscheid, P., Welton, T., Eds.; WILEY-VCH Verlag & Co. KGaA: Weinheim, Germany., 2008; Vol. 1, pp 1–6.
[139] Stepnowski, P. Potential Environmental Impact of Imidazolium Ionic Liquids. In *Ionic Liquids IV. Not Just Solvents Anymore.*; Brennecke, J. F., Rogers, R. D., Seddon, K. R., Eds.; ACS Symposium Series 975; American Chemical Society: Washington, DC., 2007; pp 10–20.
[140] Jing, B.; Lan, N.; Qiu, J.; Zhu, Y. Interaction of Ionic Liquids with a Lipid Bilayer: A Biophysical Study of Ionic Liquid Cytotoxicity. *J. Phys. Chem. B.* **2016**, *120* (10), 2781–2789.

par iónico y la unión covalente. Con frecuencia esta última reduce las pérdidas por lixiviación del IL a lo largo de la reacción, además se obtiene un material de fácil recuperación y reutilización.[141]

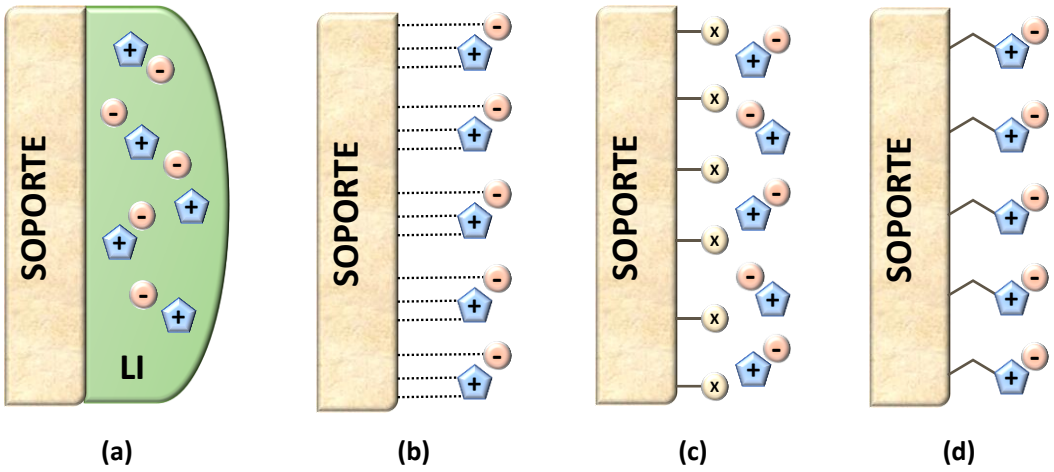

Figura 7. Representación esquemática de los diferentes enfoques para la inmovilización de los ILs en un soporte sólido; **(a)** encapsulación, **(b)** adsorción mediante enlaces electrostáticos, puentes de hidrógeno, fuerzas de Van der Waals, entre otras, **(c)** formación del par iónico usando un soporte funcional con carga positiva o negativo y **(d)** anclaje mediante enlace covalente a través del catión.

Al soportar un IL sobre una matriz sólida, las propiedades de esta también están presentes en el material resultante. La heterogenización del IL ofrece una serie de ventajas típicas de los catalizadores soportados. En general, estos sistemas permiten la reducción de la cantidad de IL utilizado en comparación a los procesos homogéneos, además la separación de los productos obtenidos en la reacción es más sencilla y en consecuencia posibilita la reutilización del

[141] Barbaro, P.; Liguori, F. Ion Exchange Resins: Catalyst Recovery and Recycle. *Chem. Rev.* **2009**, *109* (2), 515–529.

catalizador. Además, soluciona problemas de (eco)toxicidad, facilita la aplicación en reactores de lecho fijo y potencia su uso en procesos de flujo continuo.[142, 143,144]

La inmovilización de una especie química sobre un soporte provoca que sus propiedades se alteren, puesto que el soporte no es una matriz inerte. El soporte no sólo determina la difusión de los reactivos para alcanzar los centros activos, sino que también define el microentorno de dicho centro activo, lo que ha mostrado ser esencial en el desarrollo de catalizadores soportados.[145,146] Lo mismo ocurre con la inmovilización de ILs, que pueden considerarse como una clase muy particular de líquidos iónicos con propiedades específicas ("*Task Specific ILs*" - TSILs).[144,147] Es importante tener en cuenta que los líquidos iónicos soportados (SILs) pueden actuar como catalizadores por sí mismos o utilizarse para inmovilizar especies catalíticas que incluyen complejos metálicos,[148]

[142] Burguete, M. I.; Galindo, F.; García-Verdugo, E.; Karbass, N.; Luis, S. V. Polymer Supported Ionic Liquid Phases (SILPs) versus Ionic Liquids (ILs): How Much Do They Look Alike. *Chem. Commun.* **2007**, No. 29, 3086–3088.
[143] Sans, V.; Karbass, N.; Burguete, M. I.; Compañ, V.; García-Verdugo, E.; Luis, S. V.; Pawlak, M. Polymer-Supported Ionic-Liquid-Like Phases (SILLPs): Transferring Ionic Liquid Properties to Polymeric Matrices. *Chem. Eur. J.* **2011**, *17* (6), 1894–1906.
[144] Montolio, S.; Altava, B.; García-Verdugo, E.; Luis, S. V. Supported ILs and Materials Based on ILs for the Development of Green Synthetic Processes and Procedures. In *Green Synthetic Processes and Procedures*; Ballini, R., Ed.; Green Chemistry Series; Royal Society of Chemistry.: United Kingdom, 2019; pp 289–318.
[145] Altava, B.; Burguete, M. I.; García-Verdugo, E.; Luis, S. V. Chiral Catalysts Immobilized on Achiral Polymers: Effect of the Polymer Support on the Performance of the Catalyst. *Chem. Soc. Rev.* **2018**, *47* (8), 2722–2771.
[146] Altava, B.; Burguete, M. I.; García-Verdugo, E.; Luis, S. V.; Vicent, M. J.; Mayoral, J. A. Supported Chiral Catalysts: The Role of the Polymeric Network. *React. Funct. Polym.* **2001**, *48* (1), 25–35.
[147] Chiappe, C.; Pomelli, C. S. Point-Functionalization of Ionic Liquids: An Overview of Synthesis and Applications. *Eur. J. Org. Chem.* **2014**, 6120–6139.
[148] Riisager, A.; Fehrmann, R.; Wasserscheid, P.; van Hal, R. Supported Ionic Liquid-Phase Catalysis—Heterogenization of Homogeneous Rhodium Phosphine Catalysts. In *Ionic Liquids IIIB: Fundamentals, Progress, Challenges, and Opportunities*; Rogers, R. D., Seddon, K. R., Eds.; ACS Symposium Series; American Chemical Society: Washington, DC., 2005; Vol. 902, pp 334–349.

nanopartículas,[149] organocatalizadores,[150] fotocatalizadores[151] y biocatalizadores.[152] Cuando los SILs funcionan como catalizadores (sin agregar un cocatalizador), tanto la cadena lateral del IL como el anión presente juegan un papel importante en la reacción de catálisis.[153,154,155,156]

Se han utilizado distintas aproximaciones para la preparación de SILs, dando lugar a familias muy diversas. En la aproximación inicial más sencilla, los SILS se prepararon recubriendo con una capa delgada de IL la superficie interior y/ o exterior del soporte sólido, dando lugar a los denominados SILF ("*Supported Ionic Liquids Film*").[157]

Posteriormente se han desarrollado otros materiales relacionados que incluyen: catalizadores basados en líquidos iónicos soportados (SILC/SILCAs),[158]

[149] El Sayed, S.; Bordet, A.; Weidenthaler, C.; Hetaba, W.; Luska, K. L.; Leitner, W. Selective Hydrogenation of Benzofurans Using Ruthenium Nanoparticles in Lewis Acid-Modified Ruthenium-Supported Ionic Liquid Phases. *ACS Catal.* **2020**, *10* (3), 2124–2130.
[150] Jumde, R. P.; Di Pietro, A.; Manariti, A.; Mandoli, A. New Polymer-Supported Mono- and Bis-Cinchona Alkaloid Derivatives: Synthesis and Use in Asymmetric Organocatalyzed Reactions. *Chem. Asian J.* **2015**, *10* (2), 397–404.
[151] Wahlen, J.; De Vos, D. E.; Jacobs, P. A.; Alsters, P. L. Solid Materials as Sources for Synthetically Useful Singlet Oxygen. *Adv. Synth. Catal.* **2004**, *346* (2–3), 152–164.
[152] Lozano, P.; Alvarez, E.; Nieto, S.; Villa, R.; Bernal, J. M.; Donaire, A. Biocatalytic Synthesis of Panthenyl Monoacyl Esters in Ionic Liquids and Deep Eutectic Solvents. *Green Chem.* **2019**, *21* (12), 3353–3361.
[153] Girard, A.-L.; Simon, N.; Zanatta, M.; Marmitt, S.; Gonçalves, P.; Dupont, J. Insights on Recyclable Catalytic System Composed of Task-Specific Ionic Liquids for the Chemical Fixation of Carbon Dioxide. *Green Chem.* **2014**, *16* (5), 2815–2825.
[154] Agrigento, P.; Al-Amsyar, S. M.; Sorée, B.; Taherimehr, M.; Gruttadauria, M.; Aprile, C.; Pescarmona, P. P. Synthesis and High-Throughput Testing of Multilayered Supported Ionic Liquid Catalysts for the Conversion of CO_2 and Epoxides into Cyclic Carbonates. *Catal. Sci. Technol.* **2014**, *4* (6), 1598–1607.
[155] Lambert, R.; Coupillaud, P.; Wirotius, A.-L.; Vignolle, J.; Taton, D. Imidazolium-Based Poly(Ionic Liquid)s Featuring Acetate Counter Anions: Thermally Latent and Recyclable Precursors of Polymer-Supported N-Heterocyclic Carbenes for Organocatalysis. *Macromol. Rapid Commun.* **2016**, *37* (14), 1143–1149.
[156] Jadhav, A. H.; Thorat, G. M.; Lee, K.; Lim, A. C.; Kang, H.; Seo, J. G. Effect of Anion Type of Imidazolium Based Polymer Supported Ionic Liquids on the Solvent Free Synthesis of Cycloaddition of CO_2 into Epoxide. *Catal. Today.* **2016**, *265*, 56–67.
[157] Selvam, T.; Machoke, A.; Schwieger, W. Supported Ionic Liquids on Non-Porous and Porous Inorganic Materials—A Topical Review. *Appl. Catal. A-Gen.* **2012**, *445–446*, 92–101.
[158] Virtanen, P.; Salmi, T.; Mikkola, J.-P. Kinetics of Cinnamaldehyde Hydrogenation by Supported Ionic Liquid Catalysts (SILCA). *Ind. Eng. Chem. Res.* **2009**, *48* (23), 10335–10342.

catalizadores sólidos con IL (SCILs),[159] catalizadores sólidos con capas de IL (SCILL),[160] líquidos iónicos soportados con nanopartículas (SILnPs),[161] SILP-líquidos iónicos cristalinos (ILC-SILP),[162] SILP estructurados (SSILP),[163] líquidos iónicos poliméricos soportados (PSILs)[164] y membranas de líquidos iónicos soportados (SILMs).[165] El uso de esta terminología puede ser confuso ya que las diferencias entre estas familias de SILs no son siempre claras. En la Figura 8 se representan las dos categorías simplificadas consideradas en este trabajo y que se basan en la de interacción que existe entre el IL y el soporte. Estas categorías son:

- SILPs (*"Supported Ionic Liquid Phases"*): consisten en fases líquidas de IL adsorbidas en un soporte sólido, obteniendo una capa sencilla o múltiple de IL físicamente adsorbida en la superficie.[166]

- SILLPs (*"Supported Ionic Liquid Like-Phases"*): son matrices sólidas modificadas covalentemente con unidades estructurales relacionadas con los ILs. Pueden conocerse como "disolventes iónicos sólidos" o como

[159] Gu, Y.; Ogawa, C.; Kobayashi, S. Silica-Supported Sodium Sulfonate with Ionic Liquid: A Neutral Catalyst System for Michael Reactions of Indoles in Water. *Org. Lett.* **2007**, *9* (2), 175–178.
[160] Lijewski, M.; Hogg, J. M.; Swadźba-Kwaśny, M.; Wasserscheid, P.; Haumann, M. Coating of Pd/C Catalysts with Lewis-Acidic Ionic Liquids and Liquid Coordination Complexes – SCILL Induced Activity Enhancement in Arene Hydrogenation. *RSC Adv.* **2017**, *7* (44), 27558–27563.
[161] Sidhpuria, K. B.; Daniel-da-Silva, A. L.; Trindade, T.; Coutinho, J. A. P. Supported Ionic Liquid Silica Nanoparticles (SILnPs) as an Efficient and Recyclable Heterogeneous Catalyst for the Dehydration of Fructose to 5-Hydroxymethylfurfural. *Green Chem.* **2011**, *13* (2), 340–349.
[162] Sobota, M.; Wang, X.; Fekete, M.; Happel, M.; Meyer, K.; Wasserscheid, P.; Laurin, M.; Libuda, J. Ordering and Phase Transitions in Ionic Liquid-Crystalline Films. *ChemPhysChem.* **2010**, *11* (8), 1632–1636.
[163] Ruta, M.; Yuranov, I.; Dyson, P. J.; Laurenczy, G.; Kiwi-Minsker, L. Structured Fiber Supports for Ionic Liquid-Phase Catalysis Used in Gas-Phase Continuous Hydrogenation. *J. Catal.* **2007**, *247* (2), 269–276.
[164] Lin, Y.; Wang, F.; Zhang, Z.; Yang, J.; Wei, Y. Polymer-Supported Ionic Liquids: Synthesis, Characterization and Application in Fuel Desulfurization. *Fuel* **2014**, *116*, 273–280.
[165] Tomé, L. C.; Patinha, D. J. S.; Freire, C. S. R.; Rebelo, L. P. N.; Marrucho, I. M. CO_2 Separation Applying Ionic Liquid Mixtures: The Effect of Mixing Different Anions on Gas Permeation through Supported Ionic Liquid Membranes. *RSC Adv.* **2013**, *3* (30), 12220–12229.
[166] Riisager, A.; Jørgensen, B.; Wasserscheid, P.; Fehrmann, R. First Application of Supported Ionic Liquid Phase (SILP) Catalysis for Continuous Methanol Carbonylation. *Chem. Commun.* **2006**, No. 9, 994–996.

materiales nanoestructurados con microambientes de polaridad modulable similar a los proporcionados por los ILs.[143] En estos materiales el líquido iónico está unido covalentemente a la matriz sólida, lo que resulta en una monocapa de IL unido covalentemente a la superficie.[167]

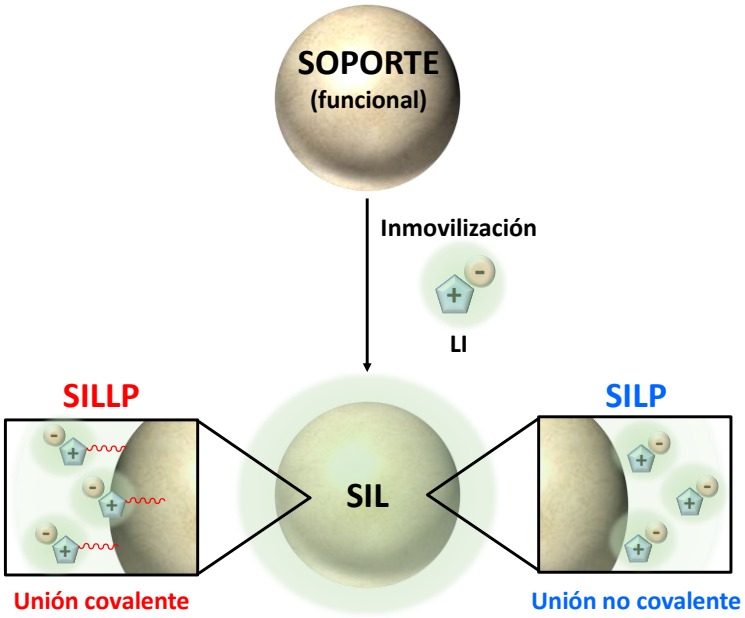

Figura 8. Esquema general para la preparación de materiales basados en **SILs**. Representación esquemática entre el **SILP** (derecha) que consiste en la adsorción física del IL, mientras que el **SILLP** (izquierda) se forma a través de la unión química entre el IL y el soporte sólido (modificado de ref. 72).

El concepto de SILP fue descrito por primera vez en 2003 por Riisager en un trabajo donde se describían sistemas catalíticos en fase sólida basados en un catalizador de rodio-bifosfina disuelto en una fase de IL inmovilizada sobre un soporte de sílice, y que fueron ensayados en un proceso de hidroformilación en continuo.[168]

[167] Sans, V.; Gelat, F.; Karbass, N.; Burguete, M. I.; García-Verdugo, E.; Luis, S. V. Polymer Cocktail: A Multitask Supported Ionic Liquid-Like Species to Facilitate Multiple and Consecutive C-C Coupling Reactions. *Adv. Synth. Catal.* **2010**, *352* (17), 3013–3021.
[168] Riisager, A.; Wasserscheid, P.; van Hal, R.; Fehrmann, R. Continuous Fixed-Bed Gas-Phase Hydroformylation Using Supported Ionic Liquid-Phase (SILP) Rh Catalysts. *J. Catal.* **2003**, *219* (2), 452–455.

La dispersión de una capa delgada de IL sobre una superficie porosa sólida (SILP) permite la inmovilización de ésta en la matriz sólida, produciendo materiales heterogéneos que contienen sobre un líquido que prácticamente no se evapora, debido a la baja presión de vapor de los ILs, incluso a temperaturas elevadas. De nuevo, la variación de los aniones y cationes permite modificar propiedades como reactividad, solubilidad y polaridad en el SILP, adecuando así las características a la aplicación deseada. La modificación "personalizada" de los SILPs permite obtener materiales altamente uniformes con propiedades bien definidas. Sin embargo, una de las desventajas es la tasa de lixiviación del IL por la unión no covalente, por lo que los SILPs se usan preferente en combinación con fases gaseosas en lugar con fases líquidas.[72,143,169,170]

Esta desventaja está ausente cuando la fase de líquido iónico se encuentra anclada covalentemente al soporte, tal como ocurre en los SILLPs. A cambio, el proceso de preparación de los materiales puede ser más largo y costoso. Tanto la estructura química como la morfología de la matriz sólida son factores importantes para determinar sus usos. Dentro de los materiales sólidos comúnmente empleados, tanto para SILPs como para SILLPs, se pueden

[169] Kolding, H.; Fehrmann, R.; Riisager, A. CO_2 Capture Technologies: Current Status and New Directions Using Supported Ionic Liquid Phase (SILP) Absorbers. *Sci. China Chem.* **2012**, *55* (8), 1648–1656.

[170] Khokarale, S. G.; García-Suárez, E. J.; Fehrmann, R.; Riisager, A. Highly Selective Continuous Gas-Phase Methoxycarbonylation of Ethylene with Supported Ionic Liquid Phase (SILP) Catalysts. *ChemCatChem.* **2017**, *9* (10), 1824–1829.

encontrar sílice,[171] alúmina,[172] zeolitas,[173] nanotubos de carbono,[174] o poliestireno,[175] entre otras.

En esta memoria se describe mayoritariamente el trabajo con SILLPs (y con algunos sistemas mixtos). En todos los casos se han utilizado como soportes polímeros de poliestireno entrecruzado (copolímeros de estireno y divinilbenceno). Para la preparación de los líquidos iónicos soportados covalentemente se ha partido de resinas de tipo Merrifield, que consisten en poliestireno clorometilado. Su uso presenta ventajas como una razonable estabilidad térmica y una elevada estabilidad química, altas capacidades de funcionalización y buenas propiedades mecánicas que facilitan su recuperación y reutilización.

1.3.1. Líquidos Iónicos Soportados sobre Resinas Preformadas

1.3.1.1. Polímeros Funcionalizados basados en Resinas Merrifield

En 1963 la contribución de R.B Merrifield[176] a la química sirvió de punto de partida para el desarrollo de la síntesis orgánica en fase sólida. Merrifield demostró que el anclaje de péptidos a soportes insolubles mejoraba en gran medida su síntesis. Teniendo la molécula deseada unida a un sólido, la

[171] Doorslaer, C. V.; Wahlen, J.; Mertens, P.; Binnemans, K.; Vos, D. D. Immobilization of Molecular Catalysts in Supported Ionic Liquid Phases. *Dalton Trans.* **2010**, *39* (36), 8377–8390.
[172] Sánchez Fuentes, C. E.; Guzmán-Lucero, D.; Torres-Rodriguez, M.; Likhanova, N. V.; Bolaños, J. N.; Olivares-Xometl, O.; Lijanova, I. V. CO_2/N_2 Separation Using Alumina Supported Membranes Based on New Functionalized Ionic Liquids. *Sep. Purif. Technol.* **2017**, *182*, 59–68.
[173] Wang, B.; Lai, H.; Yue, Y.; Sheng, G.; Deng, Y.; He, H.; Guo, L.; Zhao, J.; Li, X. Zeolite Supported Ionic Liquid Catalysts for the Hydrochlorination of Acetylene. *Catalysts.* **2018**, *8* (9), 351.
[174] Bains, D.; Singh, G.; Bhinder, J.; Agnihotri, P. K.; Singh, N. Ionic Liquid-Functionalized Multiwalled Carbon Nanotube-Based Hydrophobic Coatings for Robust Antibacterial Applications. *ACS Appl. Bio Mater.* **2020**, *3* (4), 2092–2103.
[175] Kim, D. W.; Chi, D. Y. Polymer-Supported Ionic Liquids: Imidazolium Salts as Catalysts for Nucleophilic Substitution Reactions Including Fluorinations. *Angew. Chem. Int. Ed.* **2004**, *43* (4), 483–485.
[176] Merrifield, R. B. Solid Phase Peptide Synthesis. I. The Synthesis of a Tetrapeptide. *J. Am. Chem. Soc.* **1963**, *85* (14), 2149–2154.

purificación se convertiría en una cuestión trivial al separar la molécula con el soporte por mera filtración.[177,178]

El copolímero de poliestireno y estireno / divinilbenceno (PS-DVB) que tiene grupos clorometilo como puntos de unión, es conocido comercialmente como resina Merrifield y hasta el presente es el polímero más comúnmente empleado como soporte[179] (Figura 9 a). Generalmente, estas matrices de PS-DVB se producen por polimerización en emulsión, obteniéndose una estructura porosa mediante el empleo de plantillas.[180,181] Inicialmente se desarrollaron como resinas de intercambio iónico,[182] y hoy día son los soportes poliméricos insolubles más utilizados para la preparación de catalizadores inmovilizados.[183] Su estabilidad y compatibilidad con una amplia gama de condiciones de reacción, la posibilidad de obtenerlas con distintas morfologías (macroporosa y microporosa), grados de entrecruzamiento y grados de funcionalización, incluyendo una gran variedad de funcionalidades accesibles, los hacen ideales para muchas aplicaciones y para su post-funcionalización [184,185] (Figura 9 b).

[177] Merrifield, R. B. Solid-Phase Peptide Synthesis. In *Advances in Enzymology and Related Areas of Molecular Biology*; Nord, F. F., Ed.; John Wiley & Sons, Ltd: New York, 1969; Vol. 32, pp 221–296.
[178] Akelah, A.; Sherrington, D. C. Application of Functionalized Polymers in Organic Synthesis. *Chem. Rev.* **1981**, *81* (6), 557–587.
[179] Vaino, A. R.; Janda, K. D. Solid-Phase Organic Synthesis: A Critical Understanding of the Resin. *J. Comb. Chem.* **2000**, *2* (6), 579–596.
[180] Gokmen, M. T.; Du Prez, F. E. Porous Polymer Particles—A Comprehensive Guide to Synthesis, Characterization, Functionalization and Applications. *Prog. Polym. Sci.* **2012**, *37* (3), 365–405.
[181] Ji, X.; Griesing, F.; Yan, R.; Sun, B.; Pauer, W.; Zhu, M.; Sun, Y.; Moritz, H.-U. One-Pot Preparation of Poly(Styrene-Co-Divinylbenzene)/Silver Nanoparticles Composite Microspheres with Tunable Porosity and Their Catalytic Degradation of Methylene Blue in Aqueous Solution. *RSC Adv.* **2017**, *7* (79), 50176–50187.
[182] Dardel, F. de; Arden, T. V. Ion Exchangers. In *Ullmann's Encyclopedia of Industrial Chemistry*; WILEY-VCH Verlag & Co. KGaA: Weinheim, Germany., 2002; Vol. 19, pp 473–545.
[183] Lu, J.; Toy, P. H. Organic Polymer Supports for Synthesis and for Reagent and Catalyst Immobilization. *Chem. Rev.* **2009**, *109* (2), 815–838.
[184] Benaglia, M.; Puglisi, A.; Cozzi, F. Polymer-Supported Organic Catalysts. *Chem. Rev.* **2003**, *103* (9), 3401–3430.
[185] Hentze, H.-P.; Antonietti, M. Porous Polymers and Resins for Biotechnological and Biomedical Applications. *Rev. Mol. Biotechnol.* **2002**, *90* (1), 27–53.

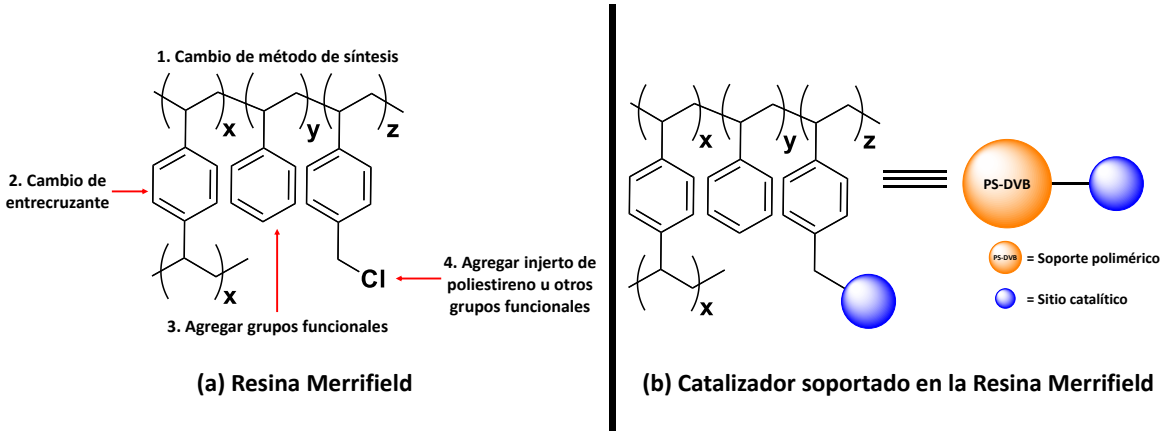

Figura 9. Representación de la estructura polimérica de la resina Merrifield. **(a)** Posibles modificaciones estructurales para mejorar el soporte heterogéneo. **(b)** Inmovilización del catalizador sobre el soporte polimérico de PS-DVB (modificado de ref. 145).

Las resinas de PS-DVB se pueden clasificar morfológicamente en dos tipos: resinas microporosas o de tipo gel y resinas macroporosas o macroreticuladas obtenidas con la finalidad de mejorar sus propiedades como soportes catalíticos. En las resinas de tipo gel o microporosas el porcentaje de DVB puede variar, pero típicamente poseen bajos grados de entrecruzamiento, aproximadamente entre el 0.5% y 20% y para resinas de síntesis combinatoria ronda entre el 0.5% y 2.0%.[186] Basta con un entrecruzamiento superior al 0.2% para que sean insolubles. El material está compuesto por una red amorfa y reticulada de cadenas poliméricas sin ninguna estructura definida. Mediante la adsorción de N_2 y la aplicación de la teoría BED se estima que su área superficial en estado seco es muy baja (10 $m^2\ g^{-1}$) y que no tienen porosidad apreciable en seco por lo que la difusión de moléculas pequeñas a su través es muy lenta. Sin embargo, la resina puede hincharse en un disolvente (Figura 10 a) de polaridad compatible con la del polímero (tolueno, cloroformo, dioxano y THF) produciendo la separación de las cadenas y consecuentemente la formación de espacios o porosidad inducida por el disolvente. Esto permite mejorar la difusión y el acceso de los compuestos

[186] Sherrington, D. C. Preparation, Structure and Morphology of Polymer Supports. *Chem. Commun.* **1998**, No. 21, 2275–2286.

en los centros activos de la matriz polimérica. El porcentaje de hinchamiento suele estar inversamente relacionado con el contenido de DVB o con la relación de reticulación nominal. Cuanto mayor sea el entrecruzamiento de la resina, menor será la capacidad de hinchamiento. Este proceso ocurre desde el exterior hacia el interior. Inicialmente se forma una capa pelicular externa expandida dejando un núcleo central vítreo no hinchado. A medida que pasa el tiempo, el grosor de la capa externa hinchada aumenta y el núcleo vitreo se reduce gradualmente hasta que desaparece. A diferencia de los polímeros lineales, el polímero no se solvata totalmente, ya que las cadenas están conectadas entre sí en al menos en un punto de unión. El disolvente que mejor solvate la red polimérica, provocará que esta se hinche hasta su límite máximo definido por los enlaces entrecruzados.[186,187,188]

En general, las resinas microporosas son más resistentes mecánicamente y se puede alcanzar un mayor grado de funcionalización,[189] pero cuando están hinchadas son blandas y compresibles, de modo que a medida que aumenta la presión en el sistema la resina se comprime restringiendo el acceso a los sitios activos, limitando su uso en columnas empacadas. Estos inconvenientes pueden superarse mediante el uso de resinas macroporosas.

[187] Corain, B.; Kralik, M. Generating Palladium Nanoclusters inside Functional Cross-Linked Polymer Frameworks. *J. Mol. Catal. A-Chem.* **2001**, *173* (1), 99–115.
[188] Corain, B.; Zecca, M.; Jeřábek, K. Catalysis and Polymer Networks — the Role of Morphology and Molecular Accessibility. *J. Mol. Catal. A-Chem.* **2001**, *177* (1), 3–20.
[189] Izquierdo Henríquez, D. Síntesis y propiedades de líquidos iónicos soportados (SILLPs) derivados de imidazolio. Aplicaciones en Biocatálisis. Ph.D. Thesis, Universitat Jaume I, Castellón de la Plana, España, 2013.

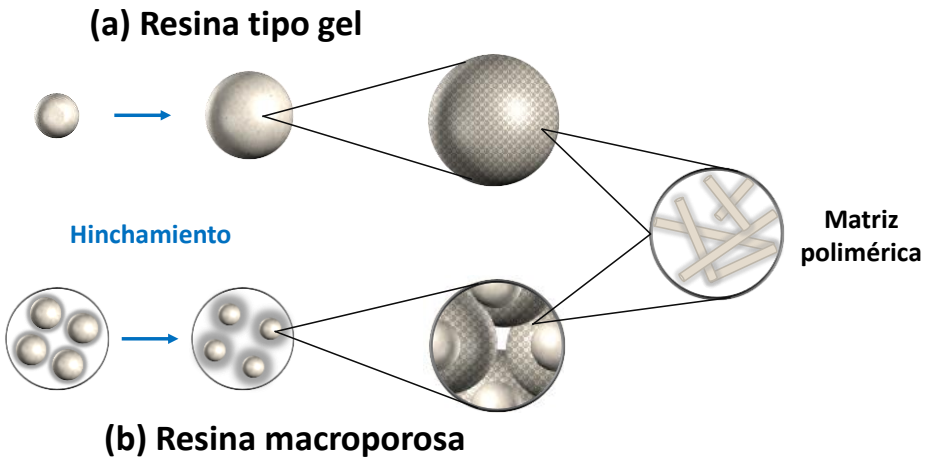

Figura 10. Proceso de hinchamiento de las resinas de tipo gel y macroporosa (modificado de ref. 187).

Para las resinas macroporosas, el porcentaje de entrecruzante es elevado, suele encontrarse entre el 25% y 80% de DVB. El término macroporoso puede resultar engañoso ya que su uso hace referencia a la existencia de una estructura porosa permanente bien desarrollada estando en estado seco. La matriz polimérica consiste en gránulos de cadenas poliméricas reticuladas y entrecruzadas que se agrupan en una estructura continua dejando espacios entre ellos dando lugar a una estructura bastante heterogénea. Estos materiales tienen áreas superficiales más altas en estado seco que normalmente varían entre 50 a 1000 $m^2\ g^{-1}$. Además, no necesitan hincharse en un disolvente para permitir el acceso de reactivos al interior porque poseen una estructura porosa permanente (Figura 10 b).[190]

Por otro lado, cuando el polímero macroporoso se moja con un disolvente compatible, éste, además de llenar el volumen de los poros, hinchará las partículas de microgel que se encuentran dentro de la matriz. Este proceso ocurre con bastante rapidez ya que la estructura permanentemente porosa brinda un acceso rápido al disolvente a través de los poros. Las resinas macroreticulares se

[190] Santora, B. P.; Gagné, M. R.; Moloy, K. G.; Radu, N. S. Porogen and Cross-Linking Effects on the Surface Area, Pore Volume Distribution, and Morphology of Macroporous Polymers Obtained by Bulk Polymerization. *Macromolecules.* **2001**, *34* (3), 658–661.

producen mediante una copolimerización en suspensión en presencia de un porógeno o un diluyente inerte, dando lugar en la separación de fases a la precipitación de un polímero reticulado. Cada perla del material está compuesta por una fase de polímero reticulado y el porógeno que actúa como plantilla para la estructura porosa permanente de la resina. Finalmente, la eliminación del porógeno y el secado producen perlas rígidas y permanentemente porosas.[186,191]

La reactividad de las resinas macroporosas no depende del hinchamiento. Las reacciones pueden llevarse a cabo en una amplia variedad de disolventes sin cambios apreciables en la velocidad de reacción. Sin embargo, en ocasiones, la menor carga alcanzable y la reducida resistencia mecánica de las perlas son problemas que pueden incrementarse en algunos medios de reacción. La actividad de los compuestos soportados resultantes (por ejemplo: catalizadores) dependerá del equilibro entre los sitios activos superficiales e internos.[145,189]

La elección de la matriz polimérica dependerá del uso a realizar. La morfología de los polímeros, la porosidad en la resina de tipo macro, el grado de entrecruzamiento y la selección del disolvente determinan la accesibilidad de los grupos funcionales y la movilidad de los compuestos, todo lo cual debe analizarse a la hora de determinar las condiciones de reacción de un sistema heterogéneo. Estos materiales pueden ser usados para soportar líquidos iónicos covalentemente (SILLPs) de tal forma que funcionen como catalizadores,[192] o

[191] Das, S.; Heasman, P.; Ben, T.; Qiu, S. Porous Organic Materials: Strategic Design and Structure–Function Correlation. *Chem. Rev.* **2017**, *117* (3), 1515–1563.
[192] Burguete, M. I.; Erythropel, H.; Garcia-Verdugo, E.; Luis, S. V.; Sans, V. Base Supported Ionic Liquid-like Phases as Catalysts for the Batch and Continuous-Flow Henry Reaction. *Green Chem.* **2008**, *10* (4), 401–407.

bien, que permitan posteriormente la inmovilización y estabilización de complejos metálicos[193] o enzimas,[194,195] entre otros.

1.3.1.2. Líquidos Iónicos Soportados en Resinas Merrifield

Como se ha mencionado anteriormente, los compuestos soportados presentan las ventajas generales de los materiales sólidos, como la fácil recuperación y la reciclabilidad.[143] En este contexto, este trabajo desarrolla y caracteriza una serie de líquidos iónicos soportados covalentemente sobre soportes poliméricos de PS-DVB.

La inmovilización de ILs sobre las resinas Merrifield es un método sencillo para la obtención de SILLPs.[196] El uso de unidades funcionales de líquidos iónicos en los soportes poliméricos es muy interesante, ya que idealmente, modificarán la naturaleza del material, transfiriendo las propiedades de los ILs a nivel molecular y en la nanoescala. De esta forma se pueden obtener materiales sólidos estructurados diseñados a medida, capaces de presentar la mayoría de las características propias de los ILs como disolventes moleculares, desempeñando un papel activo en la inmovilización y la estabilización de diferentes compuestos.[197]

---

[193] Altava, B.; Burguete, M. I.; García-Verdugo, E.; Karbass, N.; Luis, S. V.; Puzary, A.; Sans, V. Palladium N-Methylimidazolium Supported Complexes as Efficient Catalysts for the Heck Reaction. *Tetrahedron Lett.* **2006**, *47* (14), 2311–2314.

[194] Lozano, P.; García-Verdugo, E.; Karbass, N.; Montague, K.; Diego, T. D.; Burguete, M. I.; Luis, S. V. Supported Ionic Liquid-Like Phases (SILLPs) for Enzymatic Processes: Continuous KR and DKR in SILLP–$ScCO_2$ Systems. *Green Chem.* **2010**, *12* (10), 1803–1810.

[195] García-Verdugo, E.; Lozano, P.; Luis, S. V. Biocatalytic Processes Based on Supported Ionic Liquids. In *Supported Ionic Liquids: Fundamentals and Applications.*; Fehrmann, R., Riisager, A., Haumann, M., Eds.; WILEY-VCH Verlag & Co. KGaA: Weinheim, Germany., 2014; pp 351–368.

[196] Karbass, N.; Sans, V.; Garcia-Verdugo, E.; Burguete, M. I.; Luis, S. V. Pd(0) Supported onto Monolithic Polymers Containing IL-like Moieties. Continuous Flow Catalysis for the Heck Reaction in near-Critical EtOH. *Chem. Commun.* **2006**, No. 29, 3095–3097.

[197] Burguete, M. I.; García-Verdugo, E.; Garcia-Villar, I.; Gelat, F.; Licence, P.; Luis, S. V.; Sans, V. Pd Catalysts Immobilized onto Gel-Supported Ionic Liquid-like Phases (g-SILLPs): A Remarkable Effect of the Nature of the Support. *J. Catal.* **2010**, *269* (1), 150–160.

En nuestro grupo se han preparado y estudiado SILLPs basados en diferentes matrices sólidas de PS-DVB macroporosas o de tipo gel. Estos materiales se han utilizado con éxito como soportes para catalizadores metálicos, sistemas enzimáticos organocatalizadores, y fotocatalizadores, demostrando su utilidad práctica.[143] Sin embargo, una cuestión fundamental es el conocer qué tan similares son los microentornos creados por las superficies funcionalizadas a los existentes en los líquidos iónicos.

Los estudios usando pireno como sonda fluorescente han demostrado un aumento cuantitativo de la polaridad de los SILLPs en comparación con los polímeros de PS-DVB sin modificar, proporcionando valores notablemente similares a los de los ILs correspondientes.[143] Aunque, como cabía esperar, el anclaje covalente provoca que se pierdan ciertas propiedades del IL como la conductividad y la viscosidad, la introducción de las unidades relacionadas con el IL transfiere otras características importantes, como acidez o hidrofilicidad, al soporte. Además, la eliminación de la lixiviación en los SILLPs, respecto a los SILPs, favorece su uso en sistemas que utilizan fases líquidas y en procesos de flujo continuo.[198]

Una de las variables a tener en cuenta durante la modificación de las resinas Merrifield, es la carga de los grupos clorometilo. Por ejemplo, al emplear una resina de alta carga se podrá inmovilizar una mayor cantidad de IL respecto a una de baja carga, pero el tener una mayor cantidad de líquido iónico soportado no implica que las propiedades finales del material sean mejores.[189]

En este trabajo se han preparado SILLPs derivados de imidazolio utilizando soportes poliméricos de PS-DVB con grupos clorometilo. Inicialmente el grupo imidazol, mediante una adición nucleofílica, reacciona como agente alquilante

[198] Martín, S.; Porcar, R.; Peris, E.; Burguete, M. I.; García-Verdugo, E.; Luis, S. V. Supported Ionic Liquid-like Phases as Organocatalysts for the Solvent-Free Cyanosilylation of Carbonyl Compounds: From Batch to Continuous Flow Process. *Green Chem.* **2014**, *16* (3), 1639–1647.

con los grupos clorometilo de la resina, dando lugar a la formación de los grupos cloruro de imidazolio correspondientes (Figura 11).

En el trabajo con sistemas soportados, una limitación importante es el adecuado seguimiento del progreso de las reacciones en fase sólida. Los procedimientos utilizados van desde el análisis elemental (análisis de nitrógeno en la resina o de cloro en la solución después del tratamiento con amina) hasta métodos espectroscópicos (IR-FT-ATR o IR-Raman). Otra posibilidad es el uso de sondas colorimétricas que son rápidas, de fácil aplicación y no requieren instrumentación costosa. Así, por ejemplo, la reacción de la 4-(4-nitrobencil)piridina (NBP) permite detectar la presencia de grupos clorometilo. Cuando las resinas basadas en PS-DVB, se sumergen en una disolución de NBP en CH_2Cl_2 / DMF y trietilamina (TEA), los polímeros desarrollan un color que

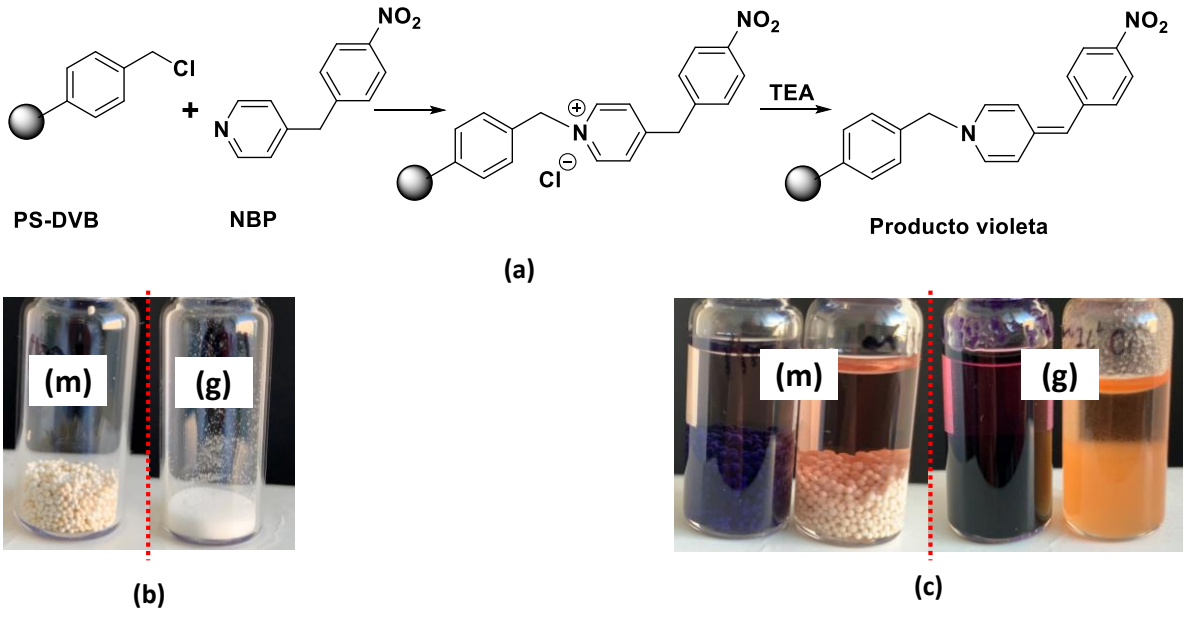

Esquema 1. **(a)** Esquema de reacción entre la resina de PS-DVB clorometilada y NBP, para obtener un producto coloreado (modificado de ref. 199). **(b)** Resina Merrifield macroporosa (m) y tipo gel (g). **(c)** Resina Merrifield (m) y (g) tratadas con NBP. Prueba positiva para la presencia de grupos clorometilo (color violeta) y prueba negativa (color blanco).

varía desde el rosa hasta el violeta, según la carga (alta o baja) de la resina (Esquema 1).[199]

El intercambio del anión o los cambios en los sustituyentes en el anillo de imidazol / imidazolio pueden utilizarse para modificar las propiedades del SILLP. Pero esto puede lograse igualmente a través de cambios en la cadena polimérica que ofrece un vector de diseño adicional para optimizar las propiedades microscópicas y macroscópicas. Esto permite disponer de materiales que pueden ayudar a la activación de un catalizador, generar intermediarios catalíticos, mejorar la estabilidad de los catalizadores, influir en la selectividad de la reacción, etc. En la Figura 11, se puede observar el grado de modularidad que tiene un SILLP.

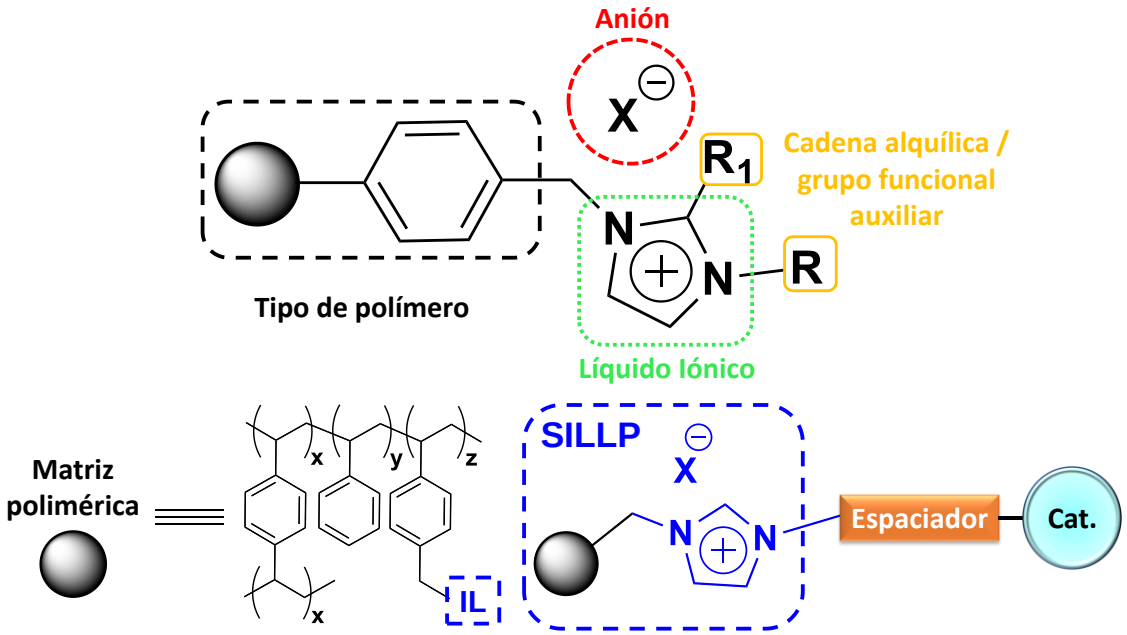

Figura 11. Representación esquemática de un SILLP soportado en una resina Merrifield y sus posibles modificaciones estructurales utilizadas para ajustar sus propiedades (modificado de ref. 72).

[199] Galindo, F.; Altava, B.; Burguete, M. I.; Gavara, R.; Luis, S. V. A Sensitive Colorimetric Method for the Study of Polystyrene Merrifield Resins and Chloromethylated Macroporous Monolithic Polymers. *J. Comb. Chem.* **2004**, *6* (6), 859–861.

Estos SILLPs se han utilizado como organocatalizadores en diversas aplicaciones,[200,201] ya que los ILs pueden actuar por sí mismos como agentes catalíticos, según el catión y anión que lo formen. También pueden ser empleados para estabilizar nanopartículas ya que proveen estabilidad y mantienen la actividad catalítica de éstas.[202,203,204] Las enzimas también pueden ser inmovilizadas en un SILLP, a través de interacciones hidrofóbicas, fuerzas de Van der Waals o enlaces por puentes de hidrógeno, contribuyendo a evitar la desnaturalización de la enzima.[194,205,206]

*1.3.2. Líquidos Iónicos Monolíticos Soportados (m-***SILLPs***)*

Los materiales monolíticos se han desarrollado rápidamente durante los últimos 20 años, habiéndose desarrollado numerosas aplicaciones químicas en particular en el campo de las separaciones. Su historia se remonta a finales de 1960, cuando se investigaron alternativas para las columnas empaquetadas con polímeros u óxidos inorgánicos en cromatografía líquida y de gases, para lo cual se desarrolló un material de tipo hidrogel a base de metacrilato con bajos grados de reticulación (aproximadamente 0.2%). Entre las principales ventajas de los

[200] Montroni, E.; Lombardo, M.; Quintavalla, A.; Trombini, C.; Gruttadauria, M.; Giacalone, F. A Liquid–Liquid Biphasic Homogeneous Organocatalytic Aldol Protocol Based on the Use of a Silica Gel Bound Multilayered Ionic Liquid Phase. *ChemCatChem.* **2012**, *4* (7), 1000–1006.
[201] Risi, C. D.; Bortolini, O.; Brandolese, A.; Carmine, G. D.; Ragno, D.; Massi, A. Recent Advances in Continuous-Flow Organocatalysis for Process Intensification. *React. Chem. Eng.* **2020**, 1–36.
[202] Burguete, M. I.; García-Verdugo, E.; Luis, S. V.; Restrepo, J. A. Preparation of Polymer-Supported Gold Nanoparticles Based on Resins Containing Ionic Liquid-like Fragments: Easy Control of Size and Stability. *Phys. Chem. Chem. Phys.* **2011**, *13* (33), 14831–14838.
[203] Jiao, N.; Li, Z.; Wang, Y.; Liu, J.; Xia, C. Palladium Nanoparticles Immobilized onto Supported Ionic Liquid-like Phases (SILLPs) for the Carbonylative Suzuki Coupling Reaction. *RSC Adv.* **2015**, *5* (34), 26913–26922.
[204] Restrepo, J.; Porcar, R.; Lozano, P.; Burguete, M. I.; García-Verdugo, E.; Luis, S. V. Microwave-Assisted Selective Oxidation of 1-Phenyl Ethanol in Water Catalyzed by Metal Nanoparticles Immobilized onto Supported Ionic Liquidlike Phases. *ACS Catal.* **2015**, *5* (8), 4743–4750.
[205] Basso, A.; Serban, S. Industrial Applications of Immobilized Enzymes—A Review. *Mol. Catal.* **2019**, *479*, 110607.
[206] Elgharbawy, A. A. M.; Moniruzzaman, M.; Goto, M. Recent Advances of Enzymatic Reactions in Ionic Liquids: Part II. *Biochem. Eng. J.* **2020**, *154*, 107426.

materiales monolíticos se encuentra el transporte rápido de masa que se logra entre el soporte monolítico y el líquido circundante.[207]

En 1992, Svec y Fréchet publicaron un artículo donde describieron la generación de materiales poliméricos monolíticos vía polimerización *in situ*. Para la obtención de los monolitos utilizaron glicidilmetacrilato y etilenglicol dimetacrilato como monómero y reticulante respectivamente, además de ciclohexanol y dodecanol como agentes porogénicos y un iniciador térmico radicalario (AIBN). A través de la ruptura homolítica del iniciador, tiene lugar el crecimiento de las cadenas poliméricas para formar los núcleos que en pasos sucesivos se transforman en cadenas interconectadas para finalmente formar el monolito que se puede adaptar a la forma del molde correspondiente. Las primeras separaciones con estos soportes no fueron muy eficientes o rápidas sin embargo, demostraron su potencial para la separación de compuestos.[208,209,210,211]

Los monolitos porosos ofrecen muchas ventajas para distintas aplicaciones.[146,212,213] En nuestro grupo se han preparado monolitos poliméricos porosos tubulares basados en mezclas que contienen estireno y divinilbenceno (DVB) como monómeros estructurales y clorometilestireno (ClVB) como monómero funcional. La presencia de un agente porogénico permite obtener una estructura monolítica porosa. Los grupos clorometilo presentes pueden ser

[207] Buchmeiser, M. R. Polymeric Monolithic Materials: Syntheses, Properties, Functionalization and Applications. *Polymer*. **2007**, *48* (8), 2187–2198.
[208] Svec, Frantisek.; Frechet, J. M. J. Continuous Rods of Macroporous Polymer as High-Performance Liquid Chromatography Separation Media. *Anal. Chem.* **1992**, *64* (7), 820–822.
[209] Svec, F.; Frechet, J. M. J. Kinetic Control of Pore Formation in Macroporous Polymers. Formation of "Molded" Porous Materials with High Flow Characteristics for Separations or Catalysis. *Chem. Mater.* **1995**, *7* (4), 707–715.
[210] Viklund, C.; Svec, F.; Fréchet, J. M. J.; Irgum, K. Monolithic, "Molded", Porous Materials with High Flow Characteristics for Separations, Catalysis, or Solid-Phase Chemistry: Control of Porous Properties during Polymerization. *Chem. Mater.* **1996**, *8* (3), 744–750.
[211] Svec, F.; Fréchet, J. M. J. New Designs of Macroporous Polymers and Supports: From Separation to Biocatalysis. *Science.* **1996**, *273* (5272), 205–211.
[212] Urban, J. Current Trends in the Development of Porous Polymer Monoliths for the Separation of Small Molecules. *J. Sep. Sci.* **2016**, *39* (1), 51–68.
[213] Svec, F. Monolithic Columns: A Historical Overview. *Electrophoresis.* **2017**, *38* (22–23), 2810–2820.

sustituidos, como en las resinas Merrifield, para soportar otros grupos funcionales como por ejemplo unidades de imidazolio (Figura 12).[214]

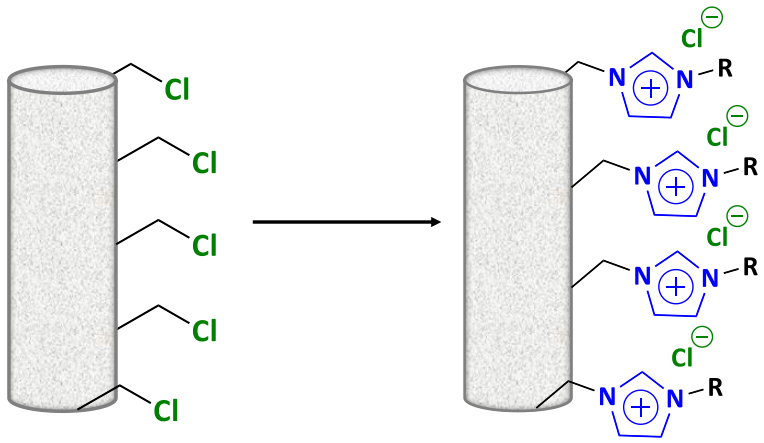

Figura 12. Representación esquemática de la preparación de un m-SILLP por post-funcionalización de un soporte polimérico monolítico poroso de DVB-ClVB.

Las propiedades macroscópicas de estos monolitos poliméricos porosos pueden modularse mediante una adecuada selección de la composición monomérica y por su modificación posterior con diferentes fragmentos semejantes a los ILs. Las unidades de IL unidas covalentemente (*m*-SILLP) pueden transferir al soporte muchas de sus características intrínsecas, lo que se refleja en los cambios observados en la hidrofilia de la superficies poliméricas.[215] Así, membranas de *m*-SILLP han sido utilizados en la separación de mezclas de agua y aceite en condiciones de ultrafiltración,[214] ofreciendo una solución a la separación de aguas residuales oleosas.[216] En aplicaciones catalíticas, no muestran los problemas

[214] Porcar, R.; Nuevo, D.; García-Verdugo, E.; Lozano, P.; Sanchez-Marcano, J.; Burguete, M. I.; Luis, S. V. New Porous Monolithic Membranes Based on Supported Ionic Liquid-like Phases for Oil/Water Separation and Homogenous Catalyst Immobilisation. *Chem. Commun.* **2018**, *54* (19), 2385–2388.
[215] Lozano, P.; García-Verdugo, E.; Piamtongkam, R.; Karbass, N.; Diego, T. D.; Burguete, M. I.; Luis, S. V.; Iborra, J. L. Bioreactors Based on Monolith-Supported Ionic Liquid Phase for Enzyme Catalysis in Supercritical Carbon Dioxide. *Adv. Synth. Catal.* **2007**, *349* (7), 1077–1084.
[216] Cao, C.-X.; Yuan, J.; Cheng, J.-P.; Han, B.-H. Synthesis of Porous Polymer/Tissue Paper Hybrid Membranes for Switchable Oil/Water Separation. *Sci. Rep.* **2017**, *7* (1), 1–9.

habituales de difusión en la matriz polimérica dado a su porosidad, por lo que pueden funcionar como microreactores estables adaptables a sistemas de flujo continuo, ofreciendo importantes ventajas sobre los procesos discontinuos o con reactores empaquetados con polímeros.[217] Estos materiales reúnen las propiedades de los ILs y la de los polímeros monolíticos porosos funcionales, y proporcionan nuevas vías de desarrollo para una síntesis orgánica más eficiente y sostenible.

1.3.3. Líquidos Iónicos Poliméricos (PILs)

Los líquidos iónicos poliméricos (PILs) han surgido durante la última década como un tema interdisciplinario en múltiples campos de la investigación. Su interés se debe a la amplia gama de propiedades fisicoquímicas y la variabilidad de diseños de estructuras químicas accesibles, modificando los monómeros y la naturaleza de la cadena polimérica.[218]

Los PILs son macromoléculas formados por unidades de ILs unidos a través de una cadena polimérica,[219] en la Figura 13 se pueden observar las posibles combinaciones de aniones, polianiones, cationes, policationes y especies zwiterionicas que se pueden fabricar.[143,220,221,222] El término PILs se suele restringir a polímeros no entrecruzados y preferentemente cuando se utilizan

[217] Jas, G.; Kirschning, A. Continuous Flow Techniques in Organic Synthesis. *Chem. Eur. J.* **2003**, *9* (23), 5708–5723.
[218] Yuan, J.; Mecerreyes, D.; Antonietti, M. Poly(Ionic Liquid)s: An Update. *Prog. Polym. Sci.* **2013**, *38* (7), 1009–1036.
[219] Yuan, J.; Antonietti, M. Poly(Ionic Liquid)s: Polymers Expanding Classical Property Profiles. *Polymer.* **2011**, *52* (7), 1469–1482.
[220] Meek, K. M.; Elabd, Y. A. Sulfonated Polymerized Ionic Liquid Block Copolymers. *Macromol. Rapid Commun.* **2016**, *37* (14), 1200–1206.
[221] Guo, Z.-Y.; Hai, X.; Wang, Y.-T.; Shu, Y.; Chen, X.-W.; Wang, J.-H. Core–Corona Magnetic Nanospheres Functionalized with Zwitterionic Polymer Ionic Liquid for Highly Selective Isolation of Glycoprotein. *Biomacromolecules.* **2018**, *19* (1), 53–61.
[222] Li, X.; Lv, C.; Jia, X.; Cheng, M.; Wang, K.; Hu, Z. Nanoparticle Based on Poly(Ionic Liquid) as an Efficient Solid Immobilization Catalyst for Aldol Reaction and Multicomponent Reaction in Water. *ACS Appl. Mater. Interfaces.* **2017**, *9* (1), 827–835.

como electrolitos poliméricos. Esta nueva clase de polielectrolitos expande las propiedades y aplicaciones de los ILs, ya que al combinar las características únicas de éstos con las de los polímeros,[223] se logra una mayor resistencia mecánica, flexibilidad y durabilidad, así como un mejor control dimensional sobre la estructura, es decir sobre la arquitectura molecular.[143,224]

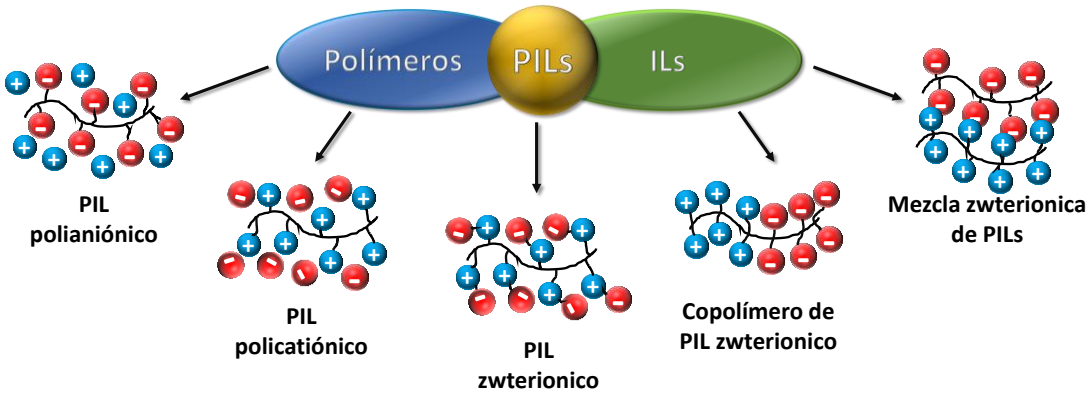

Figura 13. Representación de las algunas disposiciones estructurales de los PILs (modificado de ref. 143).

Los ILs se pueden crear a través de un IL polimerizable, obteniendo un polielectrolito macromolecular que posee unidades repetitivas de monómero de IL catiónicas o aniónicas (Figura 14) y a diferencia de los polielectrolitos clásicos que son solubles en agua y se disocian en soluciones acuosas, la mayoría de los PILs son insolubles agua, mientras que se solubilizan en disolventes orgánicos polares. Esto se debe principalmente al carácter hidrófobo del contraión y las interacciones culómbicas reducidas.[225,226]

[223] Nishimura, N.; Ohno, H. 15th Anniversary of Polymerised Ionic Liquids. *Polymer*. **2014**, *55* (16), 3289–3297.
[224] Green, O.; Grubjesic, S.; Lee, S.; Firestone, M. A. The Design of Polymeric Ionic Liquids for the Preparation of Functional Materials. *J. Macromol. Sci. Polymer Rev.* **2009**, *49* (4), 339–360.
[225] Mecerreyes, D. Polymeric Ionic Liquids: Broadening the Properties and Applications of Polyelectrolytes. *Prog. Polym. Sci.* **2011**, *36* (12), 1629–1648.
[226] Qian, W.; Texter, J.; Yan, F. Frontiers in Poly(Ionic Liquid)s: Syntheses and Applications. *Chem. Soc. Rev.* **2017**, *46* (4), 1124–1159.

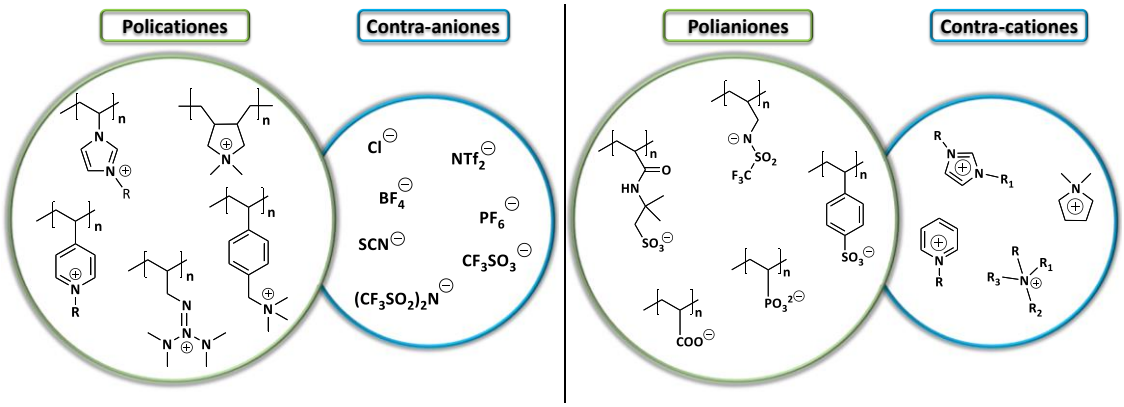

Figura 14. Estructuras químicas para la preparación de materiales basados en PILs.

Cuando los PILs se preparan conteniendo el catión en la cadena polimérica, tanto las estructuras como las propiedades se pueden ajustar fácilmente mediante intercambio aniónico, que experimentalmente es mucho más sencillo que la reestructuración de la cadena polimérica. El PIL se puede transformar incluso entre un estado hidrofílico o hidrófobo a través de la metátesis del contraión con una sal externa. Tal modularidad permite una amplia gama de condiciones de procesamiento en disolventes polares o no polares. Un PIL soluble o dispersable en un determinado líquido puede interactuar electrostáticamente con otras especies cargadas para asociar el PIL con iones, moléculas, complejos, polímeros o superficies, permitiendo desarrollar nuevas clases de materiales avanzados.[227]

Los PILs pueden sintetizarse mediante polimerización por radicales libres de grupos vinílicos, acrílicos y monómeros de estireno que contienen unidades de IL. La síntesis del polímero por este método ocurre por la adición sucesiva de los monómeros para formar cadenas largas. El mecanismo general implica tres etapas. La primera etapa, llamada iniciación, en donde se generan los radicales libres a partir del iniciador, mediante el uso de una fuente de energía (luz o calor), y seguidamente se forma el radical libre en el monómero. El segundo paso es la propagación, en donde se añaden nuevas unidades monoméricas creciendo la

[227] Zhang, S.-Y.; Zhuang, Q.; Zhang, M.; Wang, H.; Gao, Z.; Sun, J.-K.; Yuan, J. Poly(Ionic Liquid) Composites. *Chem. Soc. Rev.* **2020**, *49* (6), 1726–1755.

cadena polimérica. En esta etapa pueden participar agentes de transferencia de cadena para agregar monómeros distintos a los iniciales. El último proceso es la terminación, donde ocurren todas las reacciones de finalización de radicales posibles.[228]

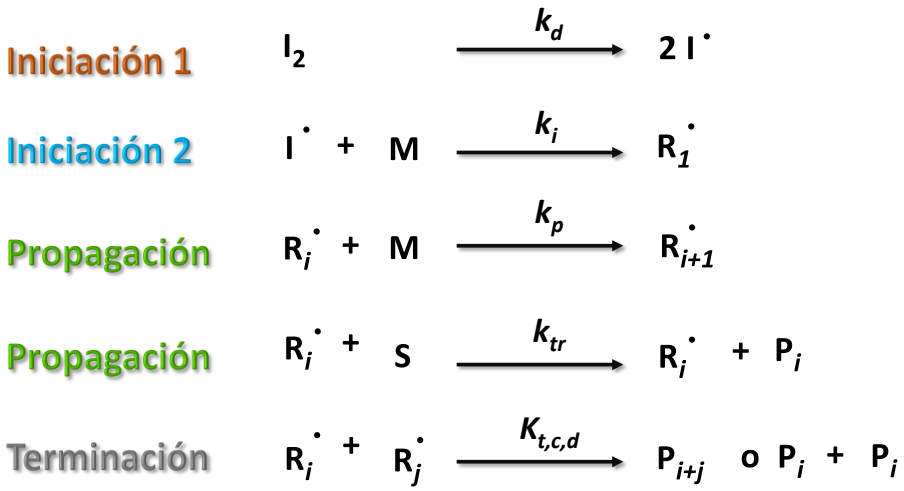

Esquema 2. Representación general del mecanismo de polimerización por radicales libres. R_i: Radical de cadena larga i, I_2: iniciador, M: monómero, S: agente de transferencia, P: polímero (modificado de ref. 228).

En general, al preparar los PILs de manera lineal se obtienen polímeros solubles, aunque se pueden modificar para que sean insolubles, agregando agentes entrecruzantes como el divinilbenceno o diacrilatos.

La polimerización radicalaria tradicionalmente tiene ciertas desventajas referentes al control de la estructura macromolecular (distribución de pesos moleculares), la composición y la estructura polimérica formada, pudiendo obtenerse polímeros del tipo "*random*", alternos o copolímeros. Existen métodos de polimerización radicalaria controlada (CRP) que proporcionan nuevas formas de síntesis que permiten controlar más eficientemente los procesos radicalarios y

[228] Odian, G. *Principles of Polymerization*, 4th ed.; John Wiley & Sons: New Jersey, 2004.

aumentar su versatilidad.[229] Los tres tipos más comunes de CRP son: polimerización mediada por nitróxido (NMP),[230] polimerización por transferencia de átomos (ATRP)[231] y la polimerización por fragmentación y transferencia de cadena por adición reversible (RAFT).[232]

La principal diferencia con la polimerización tradicional es que en CRP las reacciones de terminación se reducen mediante la adición de una agente de control para provocar la desactivación reversible de las cadenas de propagación. En este sentido, en NMP se agregan nitróxidos para desactivar los radicales poliméricos y minimizar la terminación mutua, mientras que en ATRP se usa un catalizador metálico para reducir la frecuencia de las reacciones de terminación. Ambos tipos de reacción se basan en la terminación reversible, mientras que la vía RAFT permite la transferencia reversible de cadena.[230,231,232]

La polimerización vía RAFT fue descrita por primera vez por Rizzardo, Moad y Thang en 1998,[233] e implica añadir una pequeña cantidad de un compuesto de tiocarbonilo que actúa como el agente de transferencia de la cadena (CTA) además de como iniciador. Una vez generadas las especies radicales, el CTA induce reacciones de fragmentación y transferencia de cadena por adición reversible, creando un equilibrio dinámico entre las especies activas e inactivas (Esquema 3).[234] Este equilibrio es el responsable del progreso de la polimerización. Cuando se detiene la polimerización, la mayoría de las cadenas

[229] Moad, G.; Rizzardo, E.; Thang, S. H. Living Radical Polymerization by the RAFT Process. *Aust. J. Chem.* **2005**, *58* (6), 379–410.
[230] Rizzardo, E.; Solomon, D. H. On the Origins of Nitroxide Mediated Polymerization (NMP) and Reversible Addition–Fragmentation Chain Transfer (RAFT)*. *Aust. J. Chem.* **2012**, *65* (8), 945–969.
[231] Matyjaszewski, K. Atom Transfer Radical Polymerization (ATRP): Current Status and Future Perspectives. *Macromolecules.* **2012**, *45* (10), 4015–4039.
[232] Moad, G.; Rizzardo, E.; Thang, S. H. Radical Addition–Fragmentation Chemistry in Polymer Synthesis. *Polymer.* **2008**, *49* (5), 1079–1131.
[233] Chiefari, J.; Chong, Y. K. (Bill); Ercole, F.; Krstina, J.; Jeffery, J.; Le, T. P. T.; Mayadunne, R. T. A.; Meijs, G. F.; Moad, C. L.; Moad, G.; Rizzardo, E.; Thang, S. H. Living Free-Radical Polymerization by Reversible Addition−Fragmentation Chain Transfer: The RAFT Process. *Macromolecules.* **1998**, *31* (16), 5559–5562.
[234] *Handbook of RAFT Polymerization*; Barner-Kowollik, C., Ed.; WILEY-VCH Verlag & Co. KGaA: Weinheim, 2008.

retienen un grupo final de tiocarbonilo,[235] que se puede fragmentar fácilmente para modificaciones adicionales y actuar como precursores de materiales poliméricos más complejos.[236]

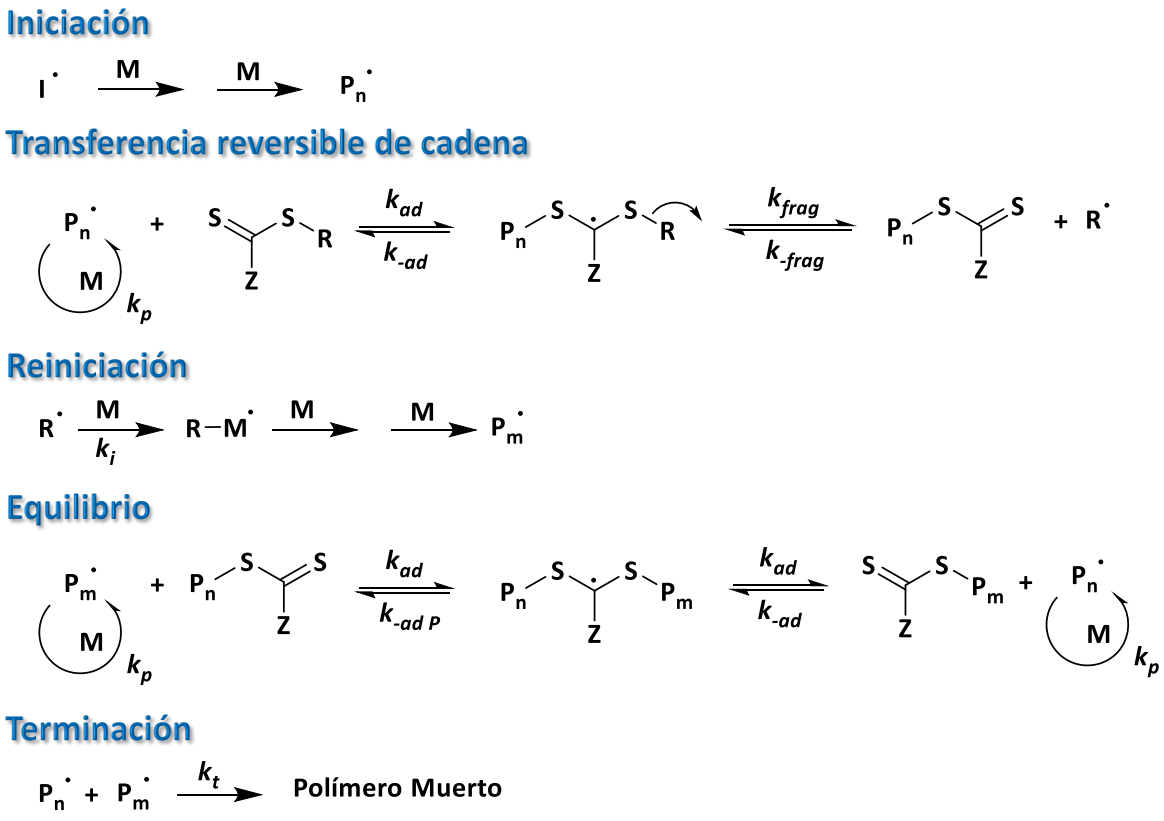

Esquema 3. Mecanismo de reacción mediante polimerización tipo RAFT que incluye los pasos de iniciación, propagación (transferencia reversible de cadena, reiniciación, equilibrio) y terminación. Los coeficientes de velocidad indicados son potencialmente dependientes de la longitud de la cadena. I: iniciador, M: monómero, R: radical RAFT, P: polímero (modificado de ref. 235).

La técnica se basa en una estrategia cinética para controlar el peso molecular y la estructura del polímero resultante. La concentración de los monómeros y el CTA es quien determina el tamaño final de las cadenas poliméricas. En general los

[235] Moad, G.; Rizzardo, E.; Thang, S. H. Living Radical Polymerization by the RAFT Process—A First Update. *Aust. J. Chem.* **2006**, *59* (10), 669–692.
[236] Roth, P. J.; Boyer, C.; Lowe, A. B.; Davis, T. P. RAFT Polymerization and Thiol Chemistry: A Complementary Pairing for Implementing Modern Macromolecular Design. *Macromol. Rapid Commun.* **2011**, *32* (15), 1123–1143.

polímeros obtenidos por la polimerización RAFT se caracterizan por tener un peso molecular determinado y baja polidispersidad (PDI < 1.1). Sumado a ello, la presencia de los grupos terminales de tiocarbonilo permiten continuar con un segundo proceso de polimerización, ya sea agregando nuevos monómeros iguales o diferentes a los iniciales o bien, añadiendo otros grupos funcionales de tal forma que la cadena se pueda extender con bloques estructurales bien definidos modularmente para mejorar sus características.[237]

La polimerización RAFT ofrece una versatilidad mayor respecto a los otros tipos de polimerización en términos de condiciones de reacción, la variedad de monómeros que se pueden usar, la tolerancia a una gran cantidad de funciones y el rango de estructuras complejas que se pueden crear. Permite igualmente añadir unidades relacionadas estructuralmente con los ILs de forma modular y controlada, generando PILs con características únicas.

Los PILs pueden también obtenerse mediante la modificación posterior de un polímero obtenido por polimerización RAFT de un monómero funcional. Por ejemplo, Tang reportó en 2005 la preparación de un PIL por post-modificación del poly(*p*-clorovinilestireno) obtenido por RAFT mediante la cuaternización de las unidades clorometileno usando 1-butilimidazol.[238]

En 2001 Sharples describió una nueva estrategia de síntesis orgánica denominándola como "*click chemistry*". Las reacciones tipo *click* se basan en procesos que transcurren de modo unívoco y cuantitatico preferentemente en condiciones relativamente suaves y que conducen a la formación de enlaces C-C, C-X u otros enlaces de interés.[239,240] Este tipo de reacciones han adquirido gran

[237] Barner-Kowollik, C.; Perrier, S. The Future of Reversible Addition Fragmentation Chain Transfer Polymerization. *J. Polym. Sci. Pol. Chem.* **2008**, *46* (17), 5715–5723.
[238] Tang, J.; Tang, H.; Sun, W.; Radosz, M.; Shen, Y. Poly(Ionic Liquid)s as New Materials for CO_2 Absorption. *J. Polym. Sci. Pol. Chem.* **2005**, *43* (22), 5477–5489.
[239] Kolb, H. C.; Finn, M. G.; Sharpless, K. B. Click Chemistry: Diverse Chemical Function from a Few Good Reactions. *Angew. Chem. Int. Ed.* **2001**, *40* (11), 2004–2021.
[240] Espeel, P.; Du Prez, F. E. "Click"-Inspired Chemistry in Macromolecular Science: Matching Recent Progress and User Expectations. *Macromolecules.* **2015**, *48* (1), 2–14.

importancia en la preparación y modificación de materiales poliméricos debido a la facilidad que ofrece para unir de forma sencilla, rápida y fiable diferentes fragmentos estructurales, a distintas escalas. En este sentido se han producido avances significativos en la aplicación de este enfoque sintético en distintas áreas de investigación que incluyen la bioconjugación,[241] la química biológica,[242] el desarrollo de fármacos[243] y la ciencia de materiales[244] como los PILs.[245]

Entre las diferentes reacciones de tipo *click* que se han desarrollado, las reacciones tiol-eno presentan una gran versatilidad para la síntesis de moléculas pequeñas y polímeros.[246] Estos procesos proporcionan distintas estrategias para la síntesis y modificación de polímeros. El empleo de derivados de tiolactona representa una plataforma sintética para el desarrollo de nuevos materiales multifuncionales, ya que el anillo de tiolactona, a través de una reacción nucleófila de adición al carbonilo, puede ser abierto de tal manera que el grupo tiol pueda usarse en reacciones tiol-eno como la adición de Michael u otros procesos.

La reactividad de la γ-tiolactona (un tioester cíclico de cinco átomos) es muy útil en este sentido. En la Esquema 4 se describe de forma general el proceso de apertura por aminólisis (liberación del tiol por la apertura nucleofílica del anillo)

[241] McKay, C. S.; Finn, M. G. Click Chemistry in Complex Mixtures: Bioorthogonal Bioconjugation. *Chem. Biol.* **2014**, *21* (9), 1075–1101.
[242] Jewett, J. C.; Bertozzi, C. R. Cu-Free Click Cycloaddition Reactions in Chemical Biology. *Chem. Soc. Rev.* **2010**, *39* (4), 1272–1279.
[243] Thirumurugan, P.; Matosiuk, D.; Jozwiak, K. Click Chemistry for Drug Development and Diverse Chemical–Biology Applications. *Chem. Rev.* **2013**, *113* (7), 4905–4979.
[244] Golas, P. L.; Matyjaszewski, K. Marrying Click Chemistry with Polymerization: Expanding the Scope of Polymeric Materials. *Chem. Soc. Rev.* **2010**, *39* (4), 1338–1354.
[245] Mirjafari, A. Ionic Liquid Syntheses via Click Chemistry: Expeditious Routes toward Versatile Functional Materials. *Chem. Commun.* **2018**, *54* (24), 2944–2961.
[246] Hoyle, C. E.; Lowe, A. B.; Bowman, C. N. Thiol-Click Chemistry: A Multifaceted Toolbox for Small Molecule and Polymer Synthesis. *Chem. Soc. Rev.* **2010**, *39* (4), 1355–1387.

seguido de una reacción *click* tiol-alqueno, que se ha usado para la construcción de nuevas arquitecturas poliméricas mediante post-funcionalización.[247,248]

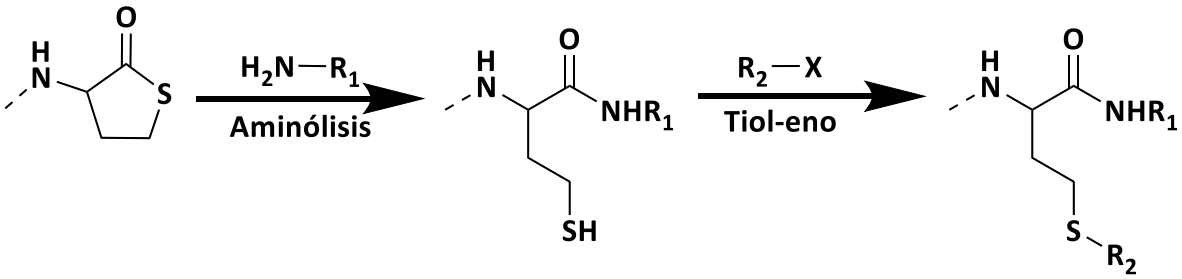

Esquema 4. γ-Tiolactona como precursor de grupos tiol reactivos. El tiol es liberado por aminólisis ymediante una reacción tiol-eno ("*click chemistry*") se incorpora el residuo R_2.

En este sentido, nuestro grupo ha realizado esfuerzos para desarrollar metodologías sintéticas que incluyan PILs funcionalizados con derivados de tiolactona. Así, se ha utilizado la poli(acrilamida-homocisteína tiolactona) (PAHT) como precursor macromolecular para crear PILs avanzados y de fácil acceso a través de la apertura del anillo de tiolactona, seguido de reacciones tiol-eno.[143] Esta estrategia sintética ha permitido obtener polímeros lineales y entrecruzados con morfologías y propiedades fisicoquímicas con aplicaciones en materiales para catálisis y en procesos de separación. [249]

El homopolímero de PAHT se obtuvo mediante polimerización RAFT, mientras que su posterior modificación permitió obtener PILs funcionalizados. En primer lugar se sintetizó el polímero de PAHT a partir del monómero de N-tiolactona

[247] Espeel, P.; Goethals, F.; Driessen, F.; Nguyen, L.-T. T.; Prez, F. E. D. One-Pot, Additive-Free Preparation of Functionalized Polyurethanes via Amine–Thiol–Ene Conjugation. *Polym. Chem.* **2013**, *4* (8), 2449–2456.

[248] Espeel, P.; Du Prez, F. E. One-Pot Double Modification of Polymers Based on Thiolactone Chemistry. In *Multi-Component and Sequential Reactions in Polymer Synthesis*; Theato, P., Ed.; Advances in Polymer Science; Springer International Publishing: Switzerland, 2015; Vol. 269, pp 105–131.

[249] Montolio Breva, S. Nuevos Materiales Basados En SILLPs (Supported Ionic Liquid-like Phases) Para Aplicaciones Avanzadas En La Química y La Ingeniería Sostenible. Ph.D. Thesis., Universitat Jaume I, Castellón de la Plana, España, 2016.

acrilamida, preparado mediante la reacción entre la tiolactona de la D,L-homocisteína y el cloruro de acriloilo. En la reacción de homopolimerización se utilizó el tritiocarbonato de cianometil dodecilo (CMDTTC) como agente de transferencia y el azobisisobutironitrilo (AIBN) como iniciador (Esquema 5). En la reacción se obtuvo una conversión mayor al 95% y un PDI de 1.58. La post-modificación de este PAHT se realizó por aminólisis utilizando ILs conteniendo grupos amino libres y una posterior reacción tiol-eno utilizando grupos acrilatos.[250]

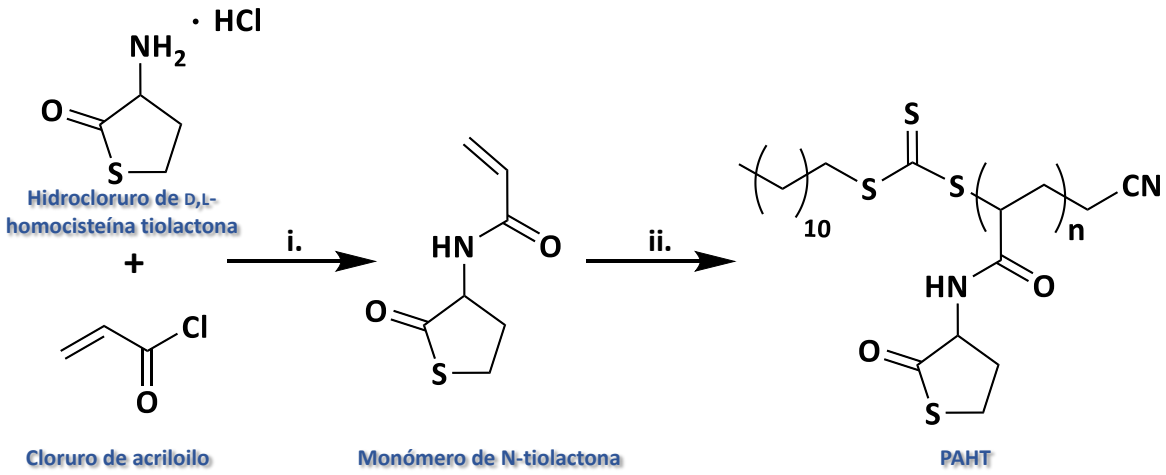

Esquema 5. Síntesis del PAHT a partir del monómero N-tiolactona acrilamida obtenido de la reacción entre la tiolactona de la D,L-homocisteína y el cloruro de acriloilo (modificado de ref. 250)

Inicialmente, el estudio de PILs se dirigió a la preparación de materiales poliméricos porosos para usos en la química analítica (ej. electroforesis) y como electrolitos, pero hoy día se utilizan en

[250] Montolio, S.; Zagorodko, O.; Porcar, R.; Burguete, M. I.; Luis, S. V.; Tenhu, H.; García-Verdugo, E. Poly(Acrylamide-Homocysteine Thiolactone) as a Synthetic Platform for the Preparation of Polymeric Ionic Liquids by Post Ring-Opening-Orthogonal Modifications. *Polym. Chem.* **2017**, *8* (33), 4789–4797.

numerosas aplicaciones: como membranas de separación de gases,[251] en la inmovilización y estabilización de nanopartículas,[252] en materiales sensibles a estímulos externos como pH y al calor[253] o en catálisis.[254,255]

1.4. Catálisis

La catálisis ha tenido una amplia gama de aplicaciones desde hace mucho tiempo hasta hoy día. Aproximadamente, entre el 85% y 90% de todos los procesos químicos incluyen al menos un paso catalítico,[256,257] además es una de las tecnologías más utilizadas en la industria química.[258] Desde los siglos XVI y XVII se han utilizado ampliamente reacciones catalíticas como la producción de bebidas alcohólicas por fermentación, la fabricación de vinagre por oxidación de etanol y la producción de jabón por hidrólisis de grasas. Ostwald, quien recibió el Premio Nobel en Química en 1909, propuso ya en 1895 que un catalizador es una sustancia que cambia la velocidad de reacción sin aparecer en los

[251] Andrzejewska, E. Photoinitiated Polymerization in Ionic Liquids and Its Application. *Polym. Int.* **2017**, *66* (3), 366–381.
[252] Montolio, S.; Vicent, C.; Aseyev, V.; Alfonso, I.; Burguete, M. I.; Tenhu, H.; García-Verdugo, E.; Luis, S. V. AuNP–Polymeric Ionic Liquid Composite Multicatalytic Nanoreactors for One-Pot Cascade Reactions. *ACS Catal.* **2016**, *6* (10), 7230–7237.
[253] Chen, F.; Guo, J.; Xu, D.; Yan, F. Thermo- and pH-Responsive Poly(Ionic Liquid) Membranes. *Polym. Chem.* **2016**, *7* (6), 1330–1336.
[254] Pinaud, J.; Vignolle, J.; Gnanou, Y.; Taton, D. Poly(N-Heterocyclic-Carbene)s and Their CO_2 Adducts as Recyclable Polymer-Supported Organocatalysts for Benzoin Condensation and Transesterification Reactions. *Macromolecules.* **2011**, *44* (7), 1900–1908.
[255] Zhou, X.; Weber, J.; Yuan, J. Poly(Ionic Liquid)s: Platform for CO_2 Capture and Catalysis. *Curr. Opin. Green Sustain. Chem.* **2019**, *16*, 39–46.
[256] Védrine, J. C. Concluding Remarks and Challenges of Heterogeneous Catalysis on Metal Oxides. In *Metal Oxides in Heterogeneous Catalysis*; Védrine, J. C., Ed.; Metal Oxides; Elsevier: Amsterdam, Netherlands, 2018; pp 551–569.
[257] Armor, J. N. A History of Industrial Catalysis. *Catal. Today.* **2011**, *163* (1), 3–9.
[258] Davis, M. E.; Davis, R. J. *Fundamentals of Chemical Reaction Engineering*, 1st ed.; McGraw-Hill: New York, 2003.

productos.[259,260] Por su parte, Berzelius, describió en un artículo publicado en 1936 sus ideas sobre la catálisis, definiéndola como "la descomposición de los cuerpos por la fuerza catalítica".[261;262]

En general, se define un catalizador como una sustancia que acelera una reacción sin consumirse en ella. Lo hace formando enlaces temporales con las moléculas que reaccionan, facilitando a su vez que éstas reaccionen para formar el producto, liberando al catalizador inalterado de modo que está disponible para la siguiente reacción. Así, una reacción catalítica se puede describir como un evento cíclico en el que el catalizador participa y se recupera en su forma original al final del ciclo (Figura 15).[263, 264]

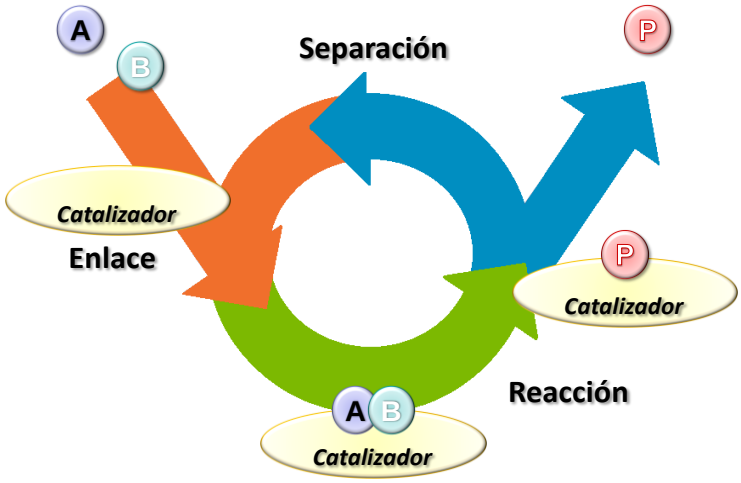

Figura 15. Reacción catalítica entre dos moléculas A y B para obtener el producto P. El ciclo se inicia con la unión de A y B al catalizador, para reaccionan dentro del complejo catalítico formando P. En el paso final, P se separa del catalizador, liberando este último para el siguiente ciclo (modificado de ref. 263).

[259] Leeuwen, P. W. N. M. van. *Homogeneous Catalysis: Understanding the Art*; Springer: Netherlands, 2004.
[260] Ostwald, W., *Z. Phys. Chem.* **1984**, *15*, 705-706.
[261] Kakaei, K.; Esrafili, M. D.; Ehsani, A. Introduction to Catalysis. In *Interface Science and Technology*; Kakaei, K., Esrafili, M. D., Ehsani, A., Eds.; Graphene Surfaces; Elsevier: Amsterdam, Netherlands, 2019; Vol. 27, pp 1–21.
[262] Berzelius, J. J., *Jahres-Bericht*, **1823-1825**, *4*, 60-61.
[263] Chorkendorff, J.; Niemantsverdriet, J. W. *Concepts of Modern Catalysis and Kinetics*; 1st ed.; LEY-VCH Verlag GmbH & Co. KGaA, Weinheim, 2003.
[264] van Santen, R. A. Molecular Catalytic Kinetics Concepts. In *Novel Concepts in Catalysis and Chemical Reactors: Improving the Efficiency for the Future*; Cybulski, A., Moulijn, J. A., Stankiewicz, A., Eds.; WILEY-VCH Verlag & Co. KGaA: Weinheim, Germany., 2010; pp 1–30.

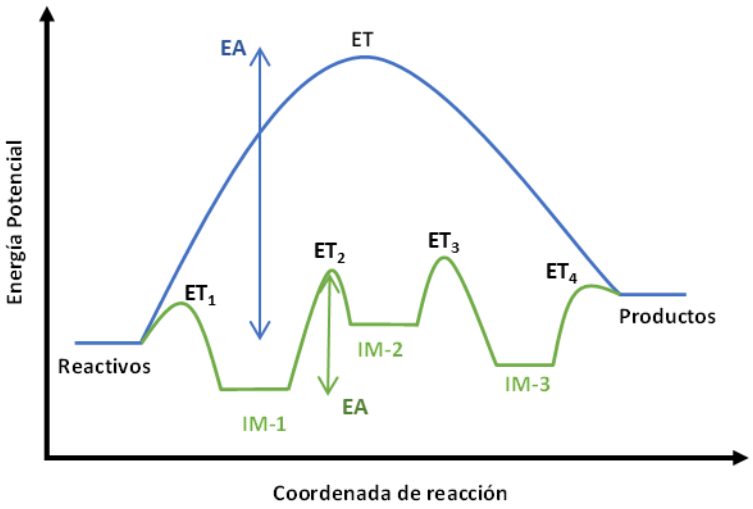

Figura 16. Perfil de una reacción no catalizada (-línea azul-) *versus* un proceso catalítico (-línea verde-). IM: intermedio; ET: estado de transición; EA: energía de activación (modificado de ref. 261).

La eficiencia del catalizador se define en términos de actividad, selectividad y tiempo de vida. Este último está definido por los cambios en la estructura del catalizador que conducen a su desactivación. En la práctica, cuando la desactivación es apreciable, un catalizador debe ser reactivado o reemplazado. Un catalizador ofrece una ruta energética más favorable para la reacción catalizada que la que transcurre en su ausencia, requiriendo una energía de activación menor (Figura 16). Un catalizador solo afecta la velocidad de reacción, no interviene en la termodinámica ni en el equilibrio químico y puede involucrar varios estados de transición, que serán totalmente diferentes a los del mecanismo para el proceso no catalizado.[261,263]

La actividad del catalizador está dada por la frecuencia de repetición ("*Turnover frequency*, TOF") y por el número de repetición ("*Turnover number*", TON). El TOF es una medida de la eficiencia instantánea del catalizador, calculado como la derivada del número de repeticiones del ciclo catalítico con respecto al tiempo por sitio activo (Nº de moles de producto / tiempo x moles de catalizador). El TON (Nº de moles obtenidos de producto / moles de catalizador) especifica el uso límite que se puede hacer de un catalizador para una reacción en condiciones definidas, limitado por el número de reacciones moleculares o ciclos de reacción que ocurren en el centro activo hasta la perdida de actividad. El TON representa

el rendimiento máximo de productos obtenidos por un centro catalítico. En general un catalizador activo tendrá valores altos de TON y TOF.[265]

El uso de nuevos catalizadores permite eliminar grandes cantidades de reactivos que en su disposición final provocarían una gran cantidad de desechos. Frente a los desafíos duales de recursos económicos y medio ambiente, la sustitución de metodologías estequiométricas por alternativas catalíticas favorece tanto la reducción de costes como la economía atómica gracias a la selectividad catalítica, convirtiéndose en una importante fuerza impulsora para el desarrollo sostenible.[266] Así mismo, la catálisis es una herramienta fundamental para alcanzar los 12 principios de la Química Verde,[267,268] y lograr una sociedad moderna más amigable con el medio ambiente y un planeta más sostenible.[9,269]

1.4.1. Tipos de Catálisis

Los catalizadores se pueden encontrar en una amplia variedad de formas y estructuras e incluyen especies tan diferentes como átomos individuales, complejos moleculares, zeolitas, enzimas o polímeros. Además pueden emplearse en entornos sólidos, líquidos o gaseosos. Es habitual distinguir tres grandes subdisciplinas en catálisis: homogénea, heterogénea y biocatálisis.

[265] Kozuch, S.; Martin, J. M. L. "Turning Over" Definitions in Catalytic Cycles. *ACS Catal.* **2012**, *2* (12), 2787–2794.
[266] Zheng, R.; Liu, Z.; Wang, Y.; Xie, Z. Industrial Catalysis: Strategies to Enhance Selectivity. *Chinese J. Catal.* **2020**, *41* (7), 1032–1038.
[267] Anastas, P. T.; Bartlett, L. B.; Kirchhoff, M. M.; Williamson, T. C. The Role of Catalysis in the Design, Development, and Implementation of Green Chemistry. *Catal. Today.* **2000**, *55* (1), 11–22.
[268] Bystrzanowska, M.; Petkov, P.; Tobiszewski, M. Ranking of Heterogeneous Catalysts Metals by Their Greenness. *ACS Sustainable Chem. Eng.* **2019**, *7* (22), 18434–18443.
[269] Liu, J. Single-Atom Catalysis for a Sustainable and Greener Future. *Curr. Opin. Green Sustain. Chem.* **2020**, *22*, 54–64.

1.4.1.1. Catálisis Homogénea

El término catálisis homogénea define un sistema catalítico en el que los sustratos de la reacción y los componentes del catalizador se encuentran en una sola fase, generalmente en estado líquido. Esta definición engloba tanto a reacciones que emplean catalizadores derivados de complejos organometálicos, como a otros sistemas tales como, por ejemplo, la catálisis ácido - base, numerosos procesos enzimáticos, el empleo de organocatalizadores y el de catalizadores poliméricos solubles.[270,271,272,273,274]

En el contexto de la Química Verde, muchos esfuerzos se centran en la transformación de productos derivados de la biorenovables en productos de alto valor añadido. La catálisis homogénea ha jugado un papel muy importante en procesos como la obtención de biodiesel. Algunos de los catalizadores homogéneos comúnmente usados son los ácidos o bases fuertes como NaOH, KOH, $MgSO_4$, H_2SO_4 y HCl.[275,276] La catálisis homogénea se ha utilizado también en otros procesos relacionados con la conversión de biomasa mediante procesos de funcionalización y desfuncionalización o de despolimerización selectiva.[277]

[270] van Leeuwen, P. W. N. M. Homogeneous Metal Catalysis: An Undergraduate Introduction. In *Reference Module in Chemistry, Molecular Sciences and Chemical Engineering*; Reedijk, J., Eds.; Elsevier: Amsterdam, Netherlands, 2016; pp: 1-45.
[271] Kokel, A.; Schäfer, C. Application of Green Chemistry in Homogeneous Catalysis. In *Green Chemistry: An Inclusive Approach*; Török, B., Dransfield, T., Eds.; Elsevier: Amsterdam, Netherlands, 2018; pp 375–414.
[272] Bergbreiter, D. E. Soluble Polymers as Tools in Catalysis. *ACS Macro Lett.* **2014**, *3* (3), 260–265.
[273] Bergbreiter, D. E.; Tian, J.; Hongfa, C. Using Soluble Polymer Supports To Facilitate Homogeneous Catalysis. *Chem. Rev.* **2009**, *109* (2), 530–582.
[274] Fu, Y.-H.; Perales, C.; Eliason, T.; Bergbreiter, D. E. 110th Anniversary: Reversible Solubilization of Polar Polymers and Polymeric Catalysts in Nonpolar Solvents. *Ind. Eng. Chem. Res.* **2019**, *58* (31), 14579–14587.
[275] Singh, K.; Kaloni, D.; Gaur, S.; Kushwaha, S.; Mathur, G. Current Research and Perspectives on Microalgae-Derived Biodiesel. *Biofuels.* **2020**, *11* (1), 1–18.
[276] Chen, Y. W.; Lee, H. V. Recent Progress in Homogeneous Lewis Acid Catalysts for the Transformation of Hemicellulose and Cellulose into Valuable Chemicals, Fuels, and Nanocellulose. *Rev. Chem. Eng.* **2020**, *36* (2), 215–235.
[277] Deuss, P. J.; Barta, K.; Vries, J. G. de. Homogeneous Catalysis for the Conversion of Biomass and Biomass-Derived Platform Chemicals. *Catal. Sci. Technol.* **2014**, *4* (5), 1174–1196.

Los catalizadores homogéneos son altamente selectivos y ajustables, pero a menudo carecen de estabilidad a largo plazo, además la separación del producto final es difícil ya que todos los componentes coexisten en la misma fase.[278] La modificación sintética de los catalizadores moleculares es posible por rutas fácilmente disponibles. Transferir este conocimiento y la reactividad a una superficie sólida abre la puerta a nuevas aplicaciones en catálisis heterogénea.[279]

1.4.1.2. Catálisis Heterogénea

La catálisis heterogénea implica sistemas en los que el catalizador y los reactivos se encuentran en fases físicas diferentes. Los catalizadores típicos suelen ser sólidos inorgánicos como metales, óxidos y sales metálicas, pero también pueden ser materiales orgánicos como hidroperóxidos orgánicos,[280] enzimas soportadas,[281] y polímeros funcionales.[282] En los catalizadores heterogéneos la reacción tiene lugar sobre las superficies accesibles, por lo que en general resulta beneficioso el disponer de un área superficial grande.[283] Es importante tener en cuenta que, tal como se ha mencionado antes, muchos catalizadores homogéneos pueden heterogeneizarse mediante su inmovilización covalente o no covalente

[278] Wang, L.; Polyansky, D. E.; Concepcion, J. J. Self-Assembled Bilayers as an Anchoring Strategy: Catalysts, Chromophores, and Chromophore-Catalyst Assemblies. *J. Am. Chem. Soc.* **2019**, *141* (20), 8020–8024.
[279] Vannucci, A. K.; Alibabaei, L.; Losego, M. D.; Concepcion, J. J.; Kalanyan, B.; Parsons, G. N.; Meyer, T. J. Crossing the Divide between Homogeneous and Heterogeneous Catalysis in Water Oxidation. *PNAS.* **2013**, *110* (52), 20918–20922.
[280] Deutschmann, O.; Knözinger, H.; Kochloefl, K.; Turek, T.; Elvers, B. Heterogeneous Catalysis and Solid Catalysts. In *Ullmann's Encyclopedia of Industrial Chemistry*; WILEY-VCH Verlag & Co. KGaA: Weinheim, Germany., 2009; pp 1–110.
[281] Chado, G. R.; Holland, E. N.; Tice, A. K.; Stoykovich, M. P.; Kaar, J. L. Exploiting the Benefits of Homogeneous and Heterogeneous Biocatalysis: Tuning the Molecular Interaction of Enzymes with Solvents via Polymer Modification. *ACS Catal.* **2018**, *8* (12), 11579–11588.
[282] Sun, Q.; Dai, Z.; Meng, X.; Wang, L.; Xiao, F.-S. Task-Specific Design of Porous Polymer Heterogeneous Catalysts beyond Homogeneous Counterparts. *ACS Catal.* **2015**, *5* (8), 4556–4567.
[283] Nørskov, J. K.; Studt, F.; Abild-Pedersen, F.; Bligaard, T. *Fundamental Concepts in Heterogeneous Catalysis.*, 1st ed.; Wiley: New Jersey, 2014.

sobre distintos soportes como pueden ser materiales de carbono,[284] sílice,[285] zeolitas,[286] MOFs (*Metal Organic Frameworks*)[287] y polímeros.[288,289,290]

Una de las ventajas de la catálisis heterogénea sobre la catálisis homogénea es la facilidad de separación de los reactivos y productos del catalizador, así como su recuperación y reciclaje, acercándola a la implementación de rutas sintéticas verdes;[291] además representa una de las tecnologías más limpias e importantes aplicadas en la industria química.[292] Una ventaja específica de los catalizadores heterogéneos es que pueden ser usados en reacciones de flujo continuo, en lugar de los procesos de tipo discontinuo donde se deben de separar los reactivos y los productos del catalizador en un paso distinto a la reacción, lo que proporciona una menor contaminación del catalizador en los productos.[293] Los reactivos sin reaccionar y los productos transformados se extraen continuamente del sistema de reacción, mientras que el catalizador se mantiene en el reactor quedando expuesto a reactivos frescos. Esta operación de proceso continuo es posible dado

[284] Nethravathi, C.; Anumol, E. A.; Rajamathi, M.; Ravishankar, N. Highly Dispersed Ultrafine Pt and PtRu Nanoparticles on Graphene: Formation Mechanism and Electrocatalytic Activity. *Nanoscale.* **2011**, *3* (2), 569–571.
[285] Zhang, Q.; Yang, X.; Guan, J. Applications of Magnetic Nanomaterials in Heterogeneous Catalysis. *ACS Appl. Nano Mater.* **2019**, *2* (8), 4681–4697.
[286] Dusselier, M.; Davis, M. E. Small-Pore Zeolites: Synthesis and Catalysis. *Chem. Rev.* **2018**, *118* (11), 5265–5329.
[287] Samaniyan, M.; Mirzaei, M.; Khajavian, R.; Eshtiagh-Hosseini, H.; Streb, C. Heterogeneous Catalysis by Polyoxometalates in Metal–Organic Frameworks. *ACS Catal.* **2019**, *9* (11), 10174–10191.
[288] Yashima, E.; Ousaka, N.; Taura, D.; Shimomura, K.; Ikai, T.; Maeda, K. Supramolecular Helical Systems: Helical Assemblies of Small Molecules, Foldamers, and Polymers with Chiral Amplification and Their Functions. *Chem. Rev.* **2016**, *116* (22), 13752–13990.
[289] Choi, S. J.; Choi, E. H.; Song, C.; Ko, Y.-J.; Lee, S. M.; Kim, H. J.; Jang, H.-Y.; Son, S. U. Hyper-Cross-Linked Polymer on the Hollow Conjugated Microporous Polymer Platform: A Heterogeneous Catalytic System for Poly(Caprolactone) Synthesis. *ACS Macro Lett.* **2019**, *8* (6), 687–693.
[290] Shifrina, Z. B.; Matveeva, V. G.; Bronstein, L. M. Role of Polymer Structures in Catalysis by Transition Metal and Metal Oxide Nanoparticle Composites. *Chem. Rev.* **2020**, *120* (2), 1350–1396.
[291] Vaccaro, L. Green Shades in Organic Synthesis. *Eur. J. Org. Chem.* **2020**, *28*, 4273–4283.
[292] Hao, W.; Chen, D.; Li, Y.; Yang, Z.; Xing, G.; Li, J.; Chen, L. Facile Synthesis of Porphyrin Based Covalent Organic Frameworks via an A2B2 Monomer for Highly Efficient Heterogeneous Catalysis. *Chem. Mater.* **2019**, *31* (19), 8100–8105.
[293] Baerns, M. Aspects of Heterogeneous Catalysis and of Its Industrial and Environmental Practice. In *Reference Module in Chemistry, Molecular Sciences and Chemical Engineering*; Reedijk, J., Eds.; Elsevier: Amsterdam, Netherlands, 2014; pp:1-34.

que el catalizador está en una fase distinta a los reactivos y a los productos.[294] La combinación de los catalizadores heterogéneos con las operaciones de flujo continuo han hecho posible el desarrollo de procesos a gran escala en la industria química y petroquímica.[295]

Muchos autores han considerado que la optimización y la compresión mecanística de los catalizadores heterogéneos resultan más difíciles que en los catalizadores homogéneos, debido a su complejidad estructural. Del mismo modo, tiende a considerarse que la catálisis heterogénea es menos eficiente en particular en términos de selectividad, sobre todo enantioselectividad,[296,297] ya que los catalizadores homogéneos suelen ser más selectivos porque cuentan con un solo centro activo, en contraste con la diversidad de centros en un catalizador heterogéneo típico.[298]

Entre los diferentes tipos de catalizadores heterogéneos se encuentran los catalizadores soportados, que consisten en materiales catalíticos (en especial metales) depositados en la superficie de un soporte, el cuál es un sólido poroso e inerte al medio de reacción. Un soporte debe tener buenas propiedades mecánicas; alta estabilidad térmica, con frecuencia delimitada por el tipo de polímero; accesibilidad al centro activo, lo que depende de la estructura del poro y de la fácil difusión del sustrato dentro de la matriz, lo cual -a su vez- depende de la naturaleza del sustrato y del disolvente usados.[39] Es necesario resaltar que una de las características más llamativas de catálisis soportada es la preparación

[294] van Santen, R. A. Heterogeneous Catalysis. In *Modern Heterogeneous Catalysis: An Introduction.*; van Santen, R. A., Ed.; Wiley Online Books; WILEY-VCH Verlag & Co. KGaA: Weinheim, Germany., 2017; pp 1–13.
[295] Liu, X.; Ünal, B.; Jensen, K. F. Heterogeneous Catalysis with Continuous Flow Microreactors. *Catal. Sci. Technol.* **2012**, *2* (10), 2134–2138.
[296] Bonello, J. M.; Williams, F. J.; Lambert, R. M. Aspects of Enantioselective Heterogeneous Catalysis: Structure and Reactivity of (S)-(−)-1-(1-Naphthyl)Ethylamine on Pt{111}. *J. Am. Chem. Soc.* **2003**, *125* (9), 2723–2729.
[297] Fraile, J. M.; García, J. I.; Mayoral, J. A. Recent Advances in the Immobilization of Chiral Catalysts Containing Bis(Oxazolines) and Related Ligands. *Coord. Chem. Rev.* **2008**, *252* (5), 624–646.
[298] Kyriakou, G.; Beaumont, S. K.; Lambert, R. M. Aspects of Heterogeneous Enantioselective Catalysis by Metals. *Langmuir.* **2011**, *27* (16), 9687–9695.

de materiales multicomponentes integrando catalizadores individuales incompatibles entre sí. Esta metodología permite la inmovilización de dos catalizadores que combinados en disolución serían inactivos, al soportarlos se puede lograr el aislamiento suficiente de los sitios activos dando como resultado sistemas multicatalíticos activos que pueden ser usados en reacciones catalíticas multipaso "*one pot*".[299,300]

1.4.1.3. Fotocatálisis

La fotocatálisis se ha inspirado en el proceso natural de fotosíntesis[301,302] y el concepto se remonta a Edmond Becquerel en 1839,[303,304] y tradicionalmente utilizado para dos procesos diferentes. El primero se refiere a cuando un material utiliza energía luminosa para impulsar reacciones termodinámicamente no espontáneas ($\Delta G > 0$), a este proceso se le conoce como fotosíntesis. En este caso, el material puede considerarse como un fotocatalizador solo si el fotón es considerado como un reactante. Ahora bien, cuando el material usa la luz para facilitar reacciones termodinámicamente espontáneas en la dirección directa de la reacción ($\Delta G < 0$), el material se ajusta a la definición de fotocatalizador. Bajo esta situación el material no cambia la termodinámica de la reacción sino que solo afecta a la cinética de ésta, estableciendo nuevas rutas de reacción a través de la absorción de la energía. [305] El término fotocatalizador consiste en la combinación de dos palabras: foto, relacionada con el fotón y el catalizador como la sustancia

[299] van Oers, M.; Rutjes, F.; van Hest, J. Cascade Reactions in Nanoreactors. *Curr. Opin. Biotech.* **2014**, *28*, 10–16.
[300] Voit, B. Sequential One-Pot Reactions Using the Concept of "Site Isolation." *Angew. Chem. Int. Ed.* **2006**, *45* (26), 4238–4240.
[301] Berardi, S.; Drouet, S.; Francàs, L.; Gimbert-Suriñach, C.; Guttentag, M.; Richmond, C.; Stoll, T.; Llobet, A. Molecular Artificial Photosynthesis. *Chem. Soc. Rev.* **2014**, *43* (22), 7501–7519.
[302] Zhu, S.; Wang, D. Photocatalysis: Basic Principles, Diverse Forms of Implementations and Emerging Scientific Opportunities. *Adv. Energy Mater.* **2017**, *7* (23), 1700841.
[303] Becquerel, A. E. *Comptes rendus*. **1839**, *9*, 1839.
[304] Becquerel, A. E. *CR Acad. Sci*. **1839**, *9*, 145.
[305] Yang, X.; Wang, D. Photocatalysis: From Fundamental Principles to Materials and Applications. *ACS Appl. Energy Mater.* **2018**, *1* (12), 6657–6693.

que altera la velocidad de reacción.[306] Independientemente de las diferencias termodinámicas, en este trabajo se ha adoptado la definición concedida por la IUPAC, la cual considera a un fotocatalizador como "*el catalizador capaz de producir, por la absorción de luz, transformaciones químicas de los reactantes. El estado excitado del fotocatalizador interactúa repetidamente con los reactantes formando intermedios reactivos, regenerándose después de cada ciclo*".[307]

Los materiales fotocatalíticos pueden dividirse en tres tipos de acuerdo con la diferencia de energía entre la banda de valencia (HOMO) y la banda de conducción (LUMO), conocida como banda prohibida (Eg.) (Figura 17). Estas categorías son: conductores (Eg.: <1.0 eV), semiconductores (Eg.: <1.5-3.0 eV) y aislantes (Eg.: >5.0 eV).[306] En general, los fotocatalizadores son semiconductores que absorben la luz, generando electrones para que ocurra la reacción de redox.[308]

[306] Ameta, R.; Solanki, M. S.; Benjamin, S.; Ameta, S. C. Photocatalysis. In *Advanced Oxidation Processes for Waste Water Treatment*; Ameta, S. C., Ameta, R., Eds.; Emerging Green Chemical Technology; Academic Press.: London. United Kingdom, 2018; pp 135–175.
[307] McNaught, A. D.; Wilkinson, A.; Jenkins, A. D. *IUPAC Compendium of Chemical Terminology: The Gold Book*; 2nd ed.; International Union of Pure and Applied Chemistry: Research Triangle Park, NC: USA, 2006.
[308] Bensebaa, F. Clean Energy. In *Interface Science and Technology*; Bensebaa, F., Ed.; Nanoparticle Technologies from Lab to Market; Academic Press.: Amsterdam, Netherlands, 2013; Vol. 19, pp 279–383.

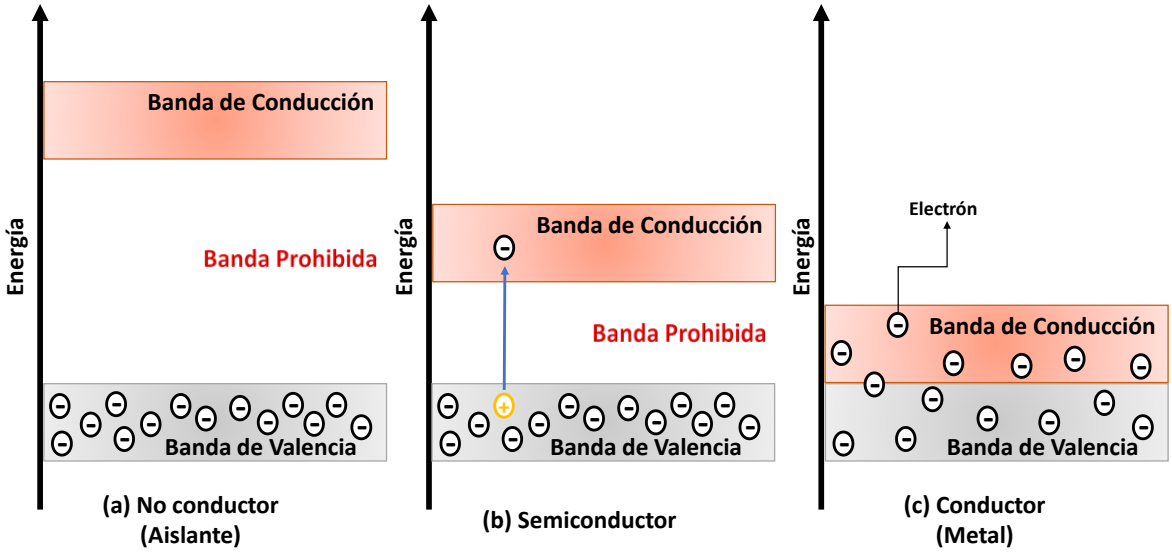

Figura 17. Comparación del salto energético (banda prohibida) entre las bandas de valencia y de conducción en un material **(a)** no conductor, **(b)** semiconductor y **(c)** conductor. En el material conductor el salto energético es prácticamente inexistente; en el semiconductor es muy pequeño y en el material no conductor es muy grande, por lo que se dificulta la promoción de un electrón desde la banda de valencia hasta la banda de conducción (modificado de ref. 306).

Hoy en día, los fotocatalizadores se emplean en numerosas aplicaciones como en producción/conversión de energía,[309,310] en el área biomédica para terapias fotodinámicas (PDT),[311,312] o en el tratamiento de aguas residuales para la eliminación de contaminantes Los fotocatalizadores son especialmente adecuados para las reacciones de remediación ambiental, ya que normalmente no necesitan activación térmica y por tanto, funcionan a temperatura ambiente,

[309] Osterloh, F. E. Photocatalysis versus Photosynthesis: A Sensitivity Analysis of Devices for Solar Energy Conversion and Chemical Transformations. *ACS Energy Lett.* **2017**, *2* (2), 445–453.
[310] Luo, J.; Zhang, S.; Sun, M.; Yang, L.; Luo, S.; Crittenden, J. C. A Critical Review on Energy Conversion and Environmental Remediation of Photocatalysts with Remodeling Crystal Lattice, Surface, and Interface. *ACS Nano.* **2019**, *13* (9), 9811–9840.
[311] Belali, S.; Savoie, H.; O'Brien, J. M.; Cafolla, A. A.; O'Connell, B.; Karimi, A. R.; Boyle, R. W.; Senge, M. O. Synthesis and Characterization of Temperature-Sensitive and Chemically Cross-Linked Poly(N-Isopropylacrylamide)/Photosensitizer Hydrogels for Applications in Photodynamic Therapy. *Biomacromolecules.* **2018**, *19* (5), 1592–1601.
[312] Tanaka, S.; Enoki, T.; Imoto, H.; Ooyama, Y.; Ohshita, J.; Kato, T.; Naka, K. Highly Efficient Singlet Oxygen Generation and High Oxidation Resistance Enhanced by Arsole-Polymer-Based Photosensitizer: Application as a Recyclable Photooxidation Catalyst. *Macromolecules.* **2020**, *53* (6), 2006–2013.

o incluso por debajo de ella y además, también trabajan bien a bajas concentraciones de reactivos.[313,314]

Como en otros casos, las reacciones fotocatalíticas pueden clasificarse en dos tipos según el estado físico de los reactivos y el fotocatalizador. La fotocatálisis homogénea ocurre cuando tanto el semiconductor como los reactivos se encuentran en una misma fase, mientras que en la fotocatálisis heterogénea se encuentran en fases diferentes.[306, 315] La fotocatálisis heterogénea se puede describir mediante cuatro pasos importantes. Inicialmente se absorbe la luz para generar electrones, luego ocurre la separación de cargas en el estado excitado, seguido por la transferencia de electrones y agujeros a la superficie del fotocatalizador y finalmente el uso de las cargas en la superficie para la reacción de reducción-oxidación (redox) (Figura 18).[302] En general, el fotocatalizador heterogéneo facilita las reacciones redox de las especies adsorbidas en su superficie cuando es excitado por la luz incidente.[316]

[313] Schneider, J.; Matsuoka, M.; Takeuchi, M.; Zhang, J.; Horiuchi, Y.; Anpo, M.; Bahnemann, D. W. Understanding TiO_2 Photocatalysis: Mechanisms and Materials. *Chem. Rev.* **2014**, *114* (19), 9919–9986.

[314] Huang, Y.; Li, X.; Le Li, J.; Zhang, B.; Cai, T. An Environmentally Benign and pH-Sensitive Photocatalyst with Surface-Bound Metalloporphyrin for Heterogeneous Catalysis of Controlled Radical Polymerization. *Macromolecules.* **2018**, *51* (20), 7974–7982.

[315] Gisbertz, S.; Pieber, B. Heterogeneous Photocatalysis in Organic Synthesis. *ChemPhotoChem.* **2020**, *4*, 1–21.

[316] Abrams, B. L.; Vesborg, P. C. K. Catalysts for Environmental Remediation - Examples in Photo- and Heterogeneous Catalysis. In *New and Future Developments in Catalysis*; Suib, S. L., Ed.; Catalysis for Remediation and Environmental Concerns; Elsevier: Amsterdam, 2013; pp 63–85.

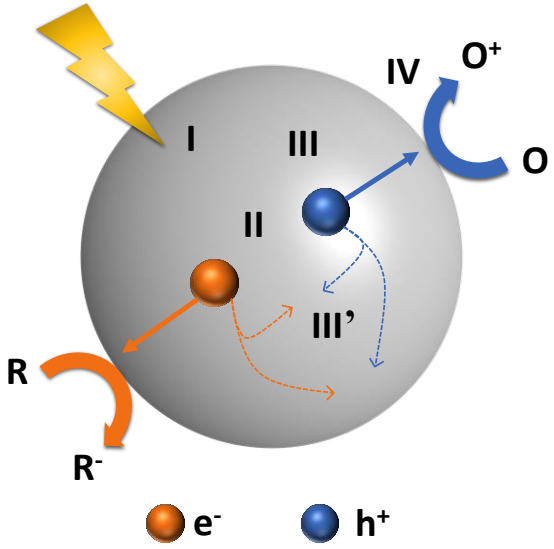

Figura 18. Etapas de la fotocatálisis heterogénea: (**I**) absorción de luz para la generación del par electrón-hueco (e^-/h^+); (**II**) separación de las cargas excitadas; (**III**) transferencia de e^- y h^+ a la superficie del fotocatalizador; (**III'**) recombinación de e^- / h^+; (**IV**) uso de las cargas en la superficie para la reacción redox. **R**: sustancias químicas en reacciones reductoras; **O**: sustancias químicas en reacciones oxidantes (modificado de ref. 302).

Un caso de especial relevancia en este trabajo es la producción de oxígeno singlete, que se puede generar mediante la fotosensibilización. Este es un proceso por el cual se produce una alteración fotoquímica o fotofísica en un compuesto como resultado de la absorción inicial de radiación por parte de un fotosensibilizador.[307] La producción fotoquímica de oxígeno singlete generalmente involucra una molécula orgánica como sensibilizador, encargada de absorber la luz ultravioleta o visible y después de un cruce entre sistemas de singlete a triplete, se transfiere la energía al triplete del estado fundamental del oxígeno molecular.[317] En la formación de oxígeno singlete se utilizan colorantes orgánicos e inorgánicos que ejercen como fotosensibilizadores y que son capaces de activar varios ciclos de reacción, como las quinonas o heterociclos pobres de electrones.[318] Los fotosensibilizadores más comúnmente usados son las

[317] Pibiri, I.; Buscemi, S.; Palumbo-Piccionello, A.; Pace, A. Photochemically Produced Singlet Oxygen: Applications and Perspectives. *ChemPhotoChem.* **2018**, *2* (7), 535–547.
[318] Karbass, N. Desarrollo de procesos químicos respetuosos con el medio ambiente mediante el uso combinado de catalizadores inmovilizados en líquidos iónicos soportados y fluidos supercríticos. Ph.D. Thesis, Universitat Jaume I, Castellón de la Plana, España, 2009.

porfirinas,[319] la fenalenona,[320] el azul de metileno,[321] la eosina Y,[322] y el rosa de bengala.[323,324] En la Figura 19 se pueden observar las estructuras de algunos fotosensibilizadores.

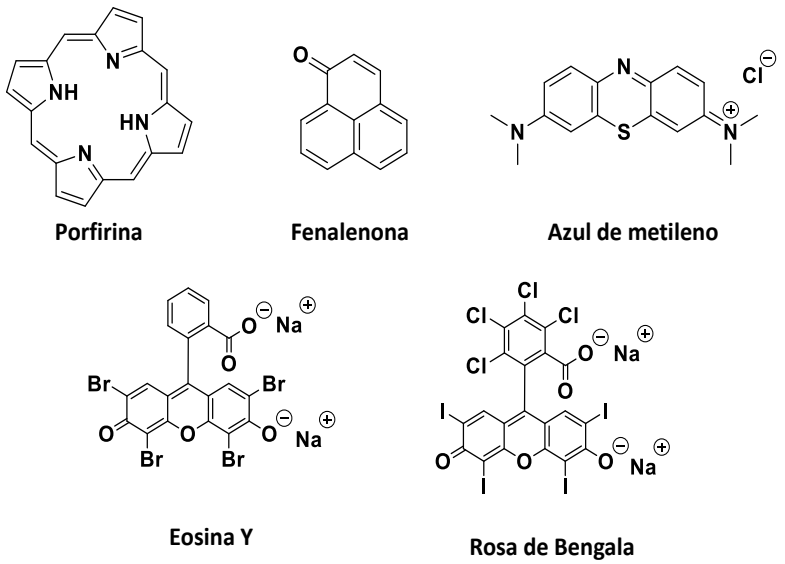

Figura 19. Estructuras de algunos fotosensibilizadores usados en la formación de oxígeno singlete.

Este trabajo, se ha centrado en el desarrollo de fotosensibilizadores soportados sobre polímeros insolubles que permitan llevar a cabo procesos de

[319] Tamaki, Y.; Ishitani, O. Supramolecular Photocatalysts for the Reduction of CO_2. *ACS Catal.* **2017**, *7* (5), 3394–3409.
[320] Espinoza, C.; Trigos, Á.; Medina, M. E. Theoretical Study on the Photosensitizer Mechanism of Phenalenone in Aqueous and Lipid Media. *J. Phys. Chem. A.* **2016**, *120* (31), 6103–6110.
[321] Kohle, F. F. E.; Li, S.; Turker, M. Z.; Wiesner, U. B. Ultrasmall PEGylated and Targeted Core–Shell Silica Nanoparticles Carrying Methylene Blue Photosensitizer. *ACS Biomater. Sci. Eng.* **2020**, *6* (1), 256–264.
[322] Johnson, G. A.; Muthukrishnan, N.; Pellois, J.-P. Photoinactivation of Gram Positive and Gram Negative Bacteria with the Antimicrobial Peptide $(KLAKLAK)_2$ Conjugated to the Hydrophilic Photosensitizer Eosin Y. *Bioconjugate Chem.* **2013**, *24* (1), 114–123.
[323] Wu, L.-L.; Tang, L.; Zhou, S.-G.; Peng, Y.-J.; He, X.-D.; Guan, Z.; He, Y.-H. Rose Bengal-Photosensitized Oxidation of Tertiary Amines for the Synthesis of Bis-1,3-Dicarbonyl Compounds. *Tetrahedron* **2017**, *73* (45), 6471–6478.
[324] Yu, Z.-Y.; Zhao, J.-N.; Yang, F.; Tang, X.-F.; Wu, Y.-F.; Ma, C.-F.; Song, B.; Yun, L.; Meng, Q.-W. Rose Bengal as Photocatalyst: Visible Light-Mediated Friedel–Crafts Alkylation of Indoles with Nitroalkenes in Water. *RSC Adv.* **2020**, *10* (8), 4825–4831.

fotosensibilización heterogénea, de tal forma que se libere oxígeno singlete en el medio de reacción sin que éste se contamine por el fotosensibilizador.[325] En este caso en particular se utilizó el rosa de bengala (su sal disódica) como fotosensibilizador, dado que cuenta con una serie de ventajas como son la intensa absorción de luz en la región visible del espectro (500-600 nm), largos tiempos de vida en el estado excitado, alta estabilidad térmica y fotoquímica y facilidad para inmovilizarlo mediante procesos de adsorción, unión electrostática y covalente sobre diferentes tipos de matrices poliméricas. El rosa de bengala fue uno de los primeros fotosensibilizadores que se utilizó en fase heterogénea y ha sido comercializado como "*Sensitox*". Dicho material fotosensible está formado por la unión covalente del rosa de bengala y un copolímero de estireno y divinilbenceno.[326,327,328]

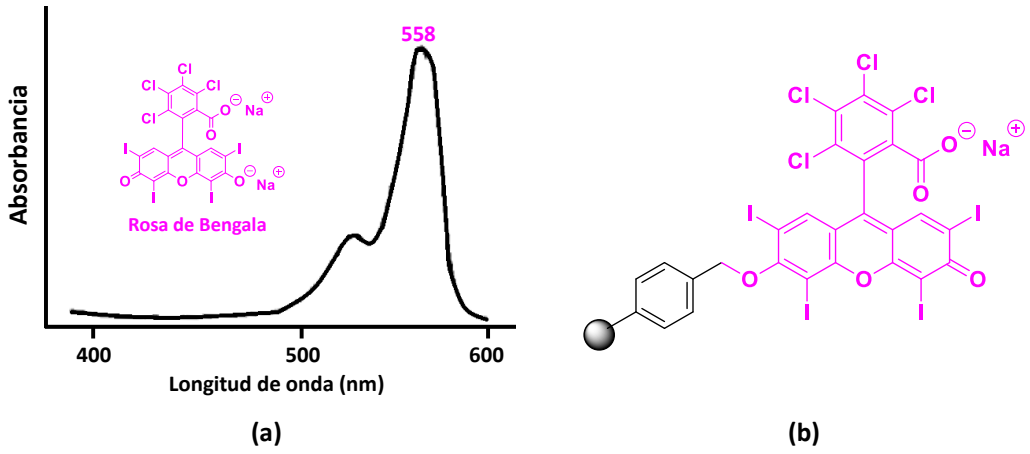

Figura 20. **(a)** Espectro de absorción del rosa de bengala (sal disódica) en una disolución en metanol. **(b)** Estructura química del rosa de bengala soportado en el copolímero de estireno y divinilbenceno, conocido también como catalizador de Neckers ("Sensitox").

[325] Burguete, M. I.; Gavara, R.; Galindo, F.; Luis, S. V. New Polymer-Supported Photocatalyst with Improved Compatibility with Polar Solvents. Synthetic Application Using Solar Light as Energy Source. *Catal. Commun.* **2010**, *11* (13), 1081–1084.
[326] Linden, S. Meei.; Neckers, D. C. Fundamental Properties of Rose Bengal. 25. Bleaching Studies of Rose Bengal Onium Salts. *J. Am. Chem. Soc.* **1988**, *110* (4), 1257–1260.
[327] Neckers, D. C. Rose Bengal. *J. Photoch. Photobio. A.* **1989**, *47* (1), 1–29.
[328] Santos, D. T.; Albarelli, J. Q.; Joyce, K.; Oelgemöller, M. Sensitizer Immobilization in Photochemistry: Evaluation of a Novel Green Support. *J. Chem. Technol. Biotechnol.* **2009**, *84* (7), 1026–1030.

1.5. Estrategias Avanzadas para Aplicaciones en Química Verde

El objetivo principal de la Química Verde es lograr gradualmente la reducción y eliminación de sustancias peligrosas durante el diseño, la fabricación y la aplicación de los productos químicos.[9] Ello ha llevado a los químicos sintéticos y de procesos a desarrollar nuevos sistemas para la síntesis orgánica avanzada, con el empleo de tecnologías emergentes que pueden proporcionar beneficios tanto económicos como ambientales.[329]

En este contexto, las reacciones de múltiples pasos representan un reto único y se han desarrollado enfoques alternativos que imitan los procesos naturales que a menudo integran secuencias multicatalíticas. Tal y como se ha venido mencionando, las condiciones de reacción alternativas ensayadas involucran la integración de varias tecnologías sostenibles como el uso de disolventes neotéricos, incluyendo el uso de fluidos supercríticos[330], la inmovilización de reactivos catalíticos, reacciones multicomponentes,[331] procesos en flujo continuo,[332,333] y la aplicación de técnicas avanzadas para la fabricación de materiales tales como la impresión 3D.[334]

[329] Hjeresen, D. L.; Kirchhoff, M. M.; Lankey, R. L. Green Chemistry: Environment, Economics, and Competitiveness. *Corp. Environ. Strategy.* **2002**, *9* (3), 259–266.
[330] Garcia-Verdugo, E.; Venardou, E.; Thomas, W. B.; Whiston, K.; Partenheimer, W.; Hamley, P. A.; Poliakoff, M. Is It Possible to Achieve Highly Selective Oxidations in Supercritical Water? Aerobic Oxidation of Methylaromatic Compounds. *Adv. Synth. Catal.* **2004**, *346* (2–3), 307–316.
[331] Cioc, R. C.; Ruijter, E.; Orru, R. V. A. Multicomponent Reactions: Advanced Tools for Sustainable Organic Synthesis. *Green Chem.* **2014**, *16* (6), 2958–2975.
[332] Ley, S. V. On Being Green: Can Flow Chemistry Help? *Chem. Rec.* **2012**, *12* (4), 378–390.
[333] *Chemical Reactions and Processes Under Flow Conditions*; Luis, S. V., García-Verdugo, E., Eds.; RSC Green Chemistry; Royal Society of Chemistry: London. United Kingdom, 2010.
[334] Overvelde, J. T. B. How to Print Multi-Material Devices in One Go. *Nature.* **2019**, *575* (7782), 289–290.

1.5.1. Reacciones en flujo continuo

El cambio de paradigma que experimenta actualmente la industria química implica la necesidad de optimizar los procesos químicos para reducir, en la medida de lo posible, las operaciones involucradas, el uso de disolventes, el consumo de energía y para avanzar hacia la utilización de materias primas renovables. La convergencia entre la síntesis orgánica y la ingeniería química ha dado lugar a la química en flujo, permitiendo el reemplazo de los procesos discontinuos -que requieren múltiples operaciones- por procesos catalíticos de flujo continuo altamente flexibles e integrados que permitan la síntesis de compuestos funcionales avanzados y contribuyan a la sostenibilidad ambiental.[335, 336,337,338]

La mayoría de los procesos petroquímicos industriales y otras transformaciones que producen productos químicos a granel se llevan a cabo en flujo. Sin embargo, a pesar de que las ventajas de la química en flujo son ampliamente conocidas, la situación es distinta en las industrias de química fina y farmacéutica. La producción por lotes de muchas metodologías sintéticas utilizadas actualmente, siguen dominando la producción industrial.[333,339]

En este sentido, las ventajas asociadas con la química en flujo continuo incluyen mejoras en la estequiometría de la reacción así como en la transferencia de masa y calor y una intensificación significativa de los procesos (haciendo que estén disponibles 24 horas, 7 días a la semana). La optimización resulta más sencilla,

[335] McQuade, D. T.; Seeberger, P. H. Applying Flow Chemistry: Methods, Materials, and Multistep Synthesis. *J. Org. Chem.* **2013**, *78* (13), 6384–6389.
[336] Myers, R. M.; Fitzpatrick, D. E.; Turner, R. M.; Ley, S. V. Flow Chemistry Meets Advanced Functional Materials. *Chem. Eur. J.* **2014**, *20* (39), 12348–12366.
[337] Jensen, K. F. Flow Chemistry—Microreaction Technology Comes of Age. *AIChE J.* **2017**, *63* (3), 858–869.
[338] Plutschack, M. B.; Pieber, B.; Gilmore, K.; Seeberger, P. H. The Hitchhiker's Guide to Flow Chemistry. *Chem. Rev.* **2017**, *117* (18), 11796–11893.
[339] Luis, S. V.; García-Verdugo, E. Continuous Flow System Using Polymer-Supported Chiral Catalysts. In *Polymeric Chiral Catalyst Design and Chiral Polymer Synthesis*; Itsuno, S., Ed.; John Wiley & Sons, Ltd: New Jersey, 2011; pp 125–156.

ajustando los tiempos de residencia a través de parámetros simples como el flujo, la presión o la temperatura, lo que lleva a tiempos de proceso más cortos, mayor seguridad y reproducibilidad, mezclas eficientes incluso con fases inmiscibles y a una mejora en la calidad del producto. Sumado a ello, el escalado de la producción en los procesos en flujo generalmente es más sencillo que en los procesos discontinuos.[333]

Los procesos de flujo continuo se pueden clasificar en cuatro categorías en función de las condiciones y el tipo de reacción que se lleven a cabo. Tal y como se define a continuación y por simplicidad se utiliza el caso de reactores tubulares:[340,341,342,343]

Tipo I: Es el caso más directo, los reactivos (A y B) se alimentan en el reactor de flujo continuo y estos pasan a través de una columna en la que se producen las reacciones para generar el producto que se recoge continuamente. En este caso, también se obtienen los sustratos sin reaccionar y otros productos secundarios, por lo que al final del proceso se necesitan procedimientos separación y purificación.

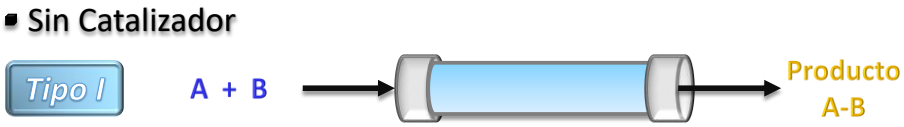

Figura 21. Sistema de flujo continuo Tipo I. Reacción entre los sustratos A y B sin catalizador (modificado de ref. 340).

[340] Tsubogo, T.; Oyamada, H.; Kobayashi, S. Multistep Continuous-Flow Synthesis of (R)- and (S)-Rolipram Using Heterogeneous Catalysts. *Nature.* **2015**, *520* (7547), 329–332.
[341] Kobayashi, S. Flow "Fine" Synthesis: High Yielding and Selective Organic Synthesis by Flow Methods. *Chem. Asian J.* **2016**, *11* (4), 425–436.
[342] *Flow Chemistry: Integrated Approaches for Practical Applications*; Luis, S. V., Garcia-Verdugo, E., Eds.; Green Chemistry; Royal Society of Chemistry: London. United Kingdom, 2020.
[343] Porta, R.; Benaglia, M.; Puglisi, A. Flow Chemistry: Recent Developments in the Synthesis of Pharmaceutical Products. *Org. Process Res. Dev.* **2016**, *20* (1), 2–25.

Tipo II: Uno de los reactivos (B) es soportado y empaquetado en el reactor de flujo continuo. Por lo general suele haber un exceso de B, para que se consuma el segundo sustrato (A). Aunque se puede evitar la contaminación del producto por los reactivos A y B, una de las principales desventajas es que pueden ocurrir reacciones secundarias. Además, cuando se consume el reactivo soportado (B), se debe de cambiar el reactor de flujo.

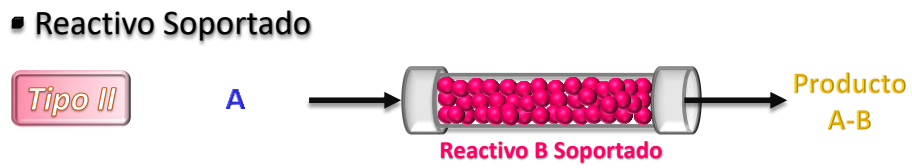

Figura 22. Sistema de flujo continuo Tipo II. Reacción entre el fluido A y el reactivo B soportado (modificado de ref. 340).

Tipo III: El sustrato A reacciona con B en presencia de un catalizador homogéneo. Aunque presenta las ventajas de los procesos catalíticos, es preciso tener en cuenta que el catalizador se eluye contaminando el flujo de salida, por lo que no se pueda evitar el paso adicional de procesamiento para detener la reacción catalítica y eliminar el catalizador. Esto dificulta llevar a cabo una reacción en flujo de múltiples pasos.

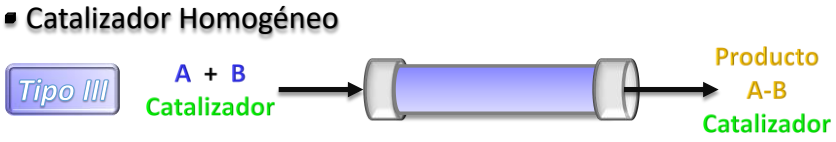

Figura 23. Sistema de flujo continuo Tipo III. Reacción entre los reactivos A y B utilizando un catalizador homogéneo (modificado de ref. 340).

Tipo IV: El sustrato A reacciona con B en presencia de un catalizador heterogéneo empacado en el reactor de flujo continuo. Si la reacción ocurre idealmente, no se requiere la separación del catalizador del producto. Este tipo

de proceso permite la transformación secuencial de compuestos orgánicos mediante la integración de reacciones catalíticas de distinto tipo.

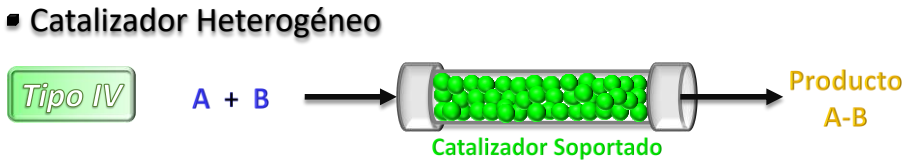

Figura 24. Sistema de flujo continuo Tipo IV. Reacción entre los reactivos A y B utilizando un catalizador heterogéneo (modificado de ref. 340).

Desde la perspectiva de la sostenibilidad, los sistemas de flujo tipo III y IV, son los recomendados para la síntesis orgánica al utilizar catalizadores, ya que conducen al ahorro de energía y a la reducción de residuos. Sin embargo, si se analizan más detalladamente estos sistemas, mientras que en el sistema tipo III los productos están contaminados por el catalizador, en el tipo IV, bajo condiciones ideales de reacción, se obtiene el producto puro.[341,344,345,346,347]

Es importante resaltar que existen diferencias importantes entre los procesos de flujo continuo y por lotes referentes al tiempo de producción y al rendimiento de la reacción. En general en los procesos por lotes la obtención del producto es determinado por el tiempo que se mantiene el recipiente a una temperatura dada y la estequiometría de la reacción es determinada por la concentración de los reactivos y su relación volumétrica. En las reacciones de flujo continuo el volumen del reactor y la velocidad de flujo determinan la velocidad de producción y la estequiometría de la reacción viene definida por la relación de la concentración de los reactivos y la velocidad de flujo. En este último caso, la

[344] Poliakoff, M.; Licence, P. Green Chemistry. *Nature.* **2007**, *450* (7171), 810–812.
[345] Clark, J. H.; Luque, R.; Matharu, A. S. Green Chemistry, Biofuels, and Biorefinery. *Annu. Rev. Chem. Biomol. Eng.* **2012**, *3* (1), 183–207.
[346] Gürsel, I. V.; Noël, T.; Wang, Q.; Hessel, V. Separation/Recycling Methods for Homogeneous Transition Metal Catalysts in Continuous Flow. *Green Chem.* **2015**, *17* (4), 2012–2026.
[347] Atodiresei, I.; Vila, C.; Rueping, M. Asymmetric Organocatalysis in Continuous Flow: Opportunities for Impacting Industrial Catalysis. *ACS Catal.* **2015**, *5* (3), 1972–1985.

producción puede acelerarse mediante el aumento de las velocidades de flujo de los fluidos siempre y cuando la conversión sea completa.[72,333,348,349]

Los reactores de flujo continuo permiten un buen control sobre las condiciones de reacción, la transferencia de calor, la mezcla de los reactivos y el tiempo de residencia (TR). Este último puede ser calculado mediante la relación del volumen del reactor (V_R) y la velocidad de flujo a través de él (F_R) ($TR = V_R / F_R$). La distribución del tiempo de residencia en un reactor es uno de los parámetros más importantes, ya que proporciona información sobre cuánto tiempo han estado los reactivos en el catalizador y por lo tanto define el grado de progreso de una reacción.[350]

Nuestro grupo de trabajo tiene una amplia experiencia en la integración de procesos en flujo multicatalíticos con materiales basados en ILs, SILPs, SILLPs y PILs y que permiten obtener compuestos intermedios de alto valor añadido.[143] El uso de plataformas divergentes ha permitido, además, obtener diversas familias de compuestos a partir de elementos comunes iniciales.[351,352]

[348] Su, Y.; Straathof, N. J. W.; Hessel, V.; Noël, T. Photochemical Transformations Accelerated in Continuous-Flow Reactors: Basic Concepts and Applications. *Chem. Eur. J.* **2014**, *20* (34), 10562–10589.
[349] Gutmann, B.; Cantillo, D.; Kappe, C. O. Continuous-Flow Technology—A Tool for the Safe Manufacturing of Active Pharmaceutical Ingredients. *Angew. Chem. Int. Ed.* **2015**, *54* (23), 6688–6728.
[350] Sans, V.; Karbass, N.; Burguete, M. I.; García-Verdugo, E.; Luis, S. V. Residence Time Distribution, a Simple Tool to Understand the Behaviour of Polymeric Mini-Flow Reactors. *RSC Adv.* **2012**, *2* (23), 8721–8728.
[351] Peris, E.; Porcar, R.; García-Álvarez, J.; Burguete, M. I.; García-Verdugo, E.; Luis, S. V. Divergent Multistep Continuous Synthetic Transformations of Allylic Alcohol Enabled by Catalysts Immobilized in Ionic Liquid Phases. *ChemSusChem.* **2019**, *12* (8), 1684–1691.
[352] Peris, E.; Porcar, R.; Burguete, M. I.; García-Verdugo, E.; Luis, S. V. Supported Ionic Liquid-Like Phases (SILLPs) as Immobilised Catalysts for the Multistep and Multicatalytic Continuous Flow Synthesis of Chiral Cyanohydrins. *ChemCatChem.* **2019**, *11* (7), 1955–1962.

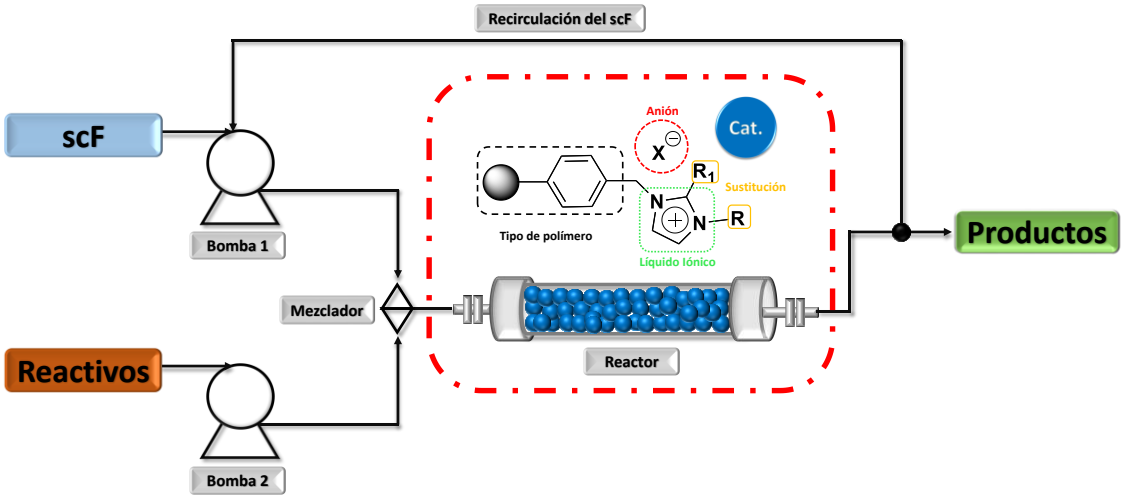

Figura 25. Representación esquemática de un sistema de flujo continuo utilizando fluidos supercríticos y SILLPs derivados de imidazolio como catalizador.

Estas estrategias reúnen las ventajas de los sistemas homogéneos basados en ILs con las proporcionadas por los catalizadores inmovilizados en un soporte insoluble, donde la inmovilización del (bio)catalizador se lleva a cabo mediante su adsorción en la superficie modificada con la unidad semejante al IL o mediante la unión covalente del mismo. Los procesos catalíticos de flujo continuo resultantes (Figura 25) pueden utilizar una fase gaseosa o fluidos supercríticos para suministrar los reactivos al reactor con el IL soportado y de esta forma obtener los productos.[249, 333,355 342,353,354,355]

[353] Werner, S.; Szesni, N.; Kaiser, M.; Haumann, M.; Wasserscheid, P. A Scalable Preparation Method for SILP and SCILL Ionic Liquid Thin-Film Materials. *Chem. Eng. Technol.* **2012**, *35* (11), 1962–1967.

[354] Xin, B.; Hao, J. Imidazolium-Based Ionic Liquids Grafted on Solid Surfaces. *Chem. Soc. Rev.* **2014**, *43* (20), 7171–7187.

[355] García-Verdugo, E.; Altava, B.; Burguete, M. I.; Lozano, P.; Luis, S. V. Ionic Liquids and Continuous Flow Processes: A Good Marriage to Design Sustainable Processes. *Green Chem.* **2015**, *17* (5), 2693–2713.

1.5.2. Fluidos Supercríticos

Un fluido supercrítico (scFs) es aquel que se encuentra por encima de la temperatura y la presión crítica (T_c y P_c).[356,357] En la Figura 26 se representa el diagrama de fase temperatura (T) – presión (P) típico para una sustancia. Cualquier compuesto estable tiene un punto triple y un punto crítico. El primero se refiere a las condiciones de temperatura y presión en la que las fases sólida, líquida y gaseosa se encuentran en equilibrio entre sí. La línea que va desde el punto triple al punto crítico que se encuentra entre las regiones líquida y gaseosa se llama curva de coexistencia gas-líquido (G-L). Al moverse a lo largo de esta curva se encuentra el punto crítico, aquí la expansión térmica hace que la densidad del líquido disminuya mientras que el aumento de la presión provoca que aumente la densidad del gas. En este punto, las densidades de las dos fases son equivalentes por lo que no es posible distinguir una fase de la otra, debido a que tienen propiedades idénticas. Por lo tanto, el punto crítico definido por T_c y P_c, puede describirse como la temperatura y presión máximas aplicadas en donde las fases líquida y gaseosa de una sustancia coexisten en equilibrio. Mas allá del punto crítico no hay distinción entre ambas fases, por lo que la sustancia actúa como un fluido homogéneo (ya no es un sistema bifásico heterogéneo).[358]

Desde el punto de vista macroscópico, la curva de coexistencia G-L termina en el punto crítico. Sin embargo, trabajos recientes demuestran que incluso en condiciones supercríticas hay dos regiones en la que los fluidos exhiben un comportamiento diferente. Bajo estas condiciones hay un máximo en el calor específico y la temperatura o la presión cambian a través de la línea que continua

[356] Hitchen, S. M.; Dean, J. R. Properties of Supercritical Fluids. In *Applications of Supercritical Fluids in Industrial Analysis*; Dean, J. R., Ed.; Springer.: Dordrecht, 1993; pp 1–11.
[357] Cansell, F.; Chevalier, B.; Demourgues, A.; Etourneau, J.; Even, C.; Pessey, V.; Petit, S.; Tressaud, A.; Weill, F. Supercritical Fluid Processing: A New Route for Materials Synthesis. *J. Mater. Chem.* **1999**, *9* (1), 67–75.
[358] Attard, T. M.; Hunt, A. J. Introduction to High-Pressure Solvent Systems. In *Supercritical and Other High-pressure Solvent Systems: For Extraction, Reaction and Material Processing*; Hunt, A. J., Attard, T. M., Eds.; Green Chemistry; Royal Society of Chemistry.: United Kingdom, 2018; pp 1–13.

después de la curva de coexistencia G-L, esta extensión se denomina línea Widom. Esta línea puede verse como la transición desde un comportamiento similar al de un líquido a un comportamiento más similar al de un gas en los fluidos supercríticos.[359,360]

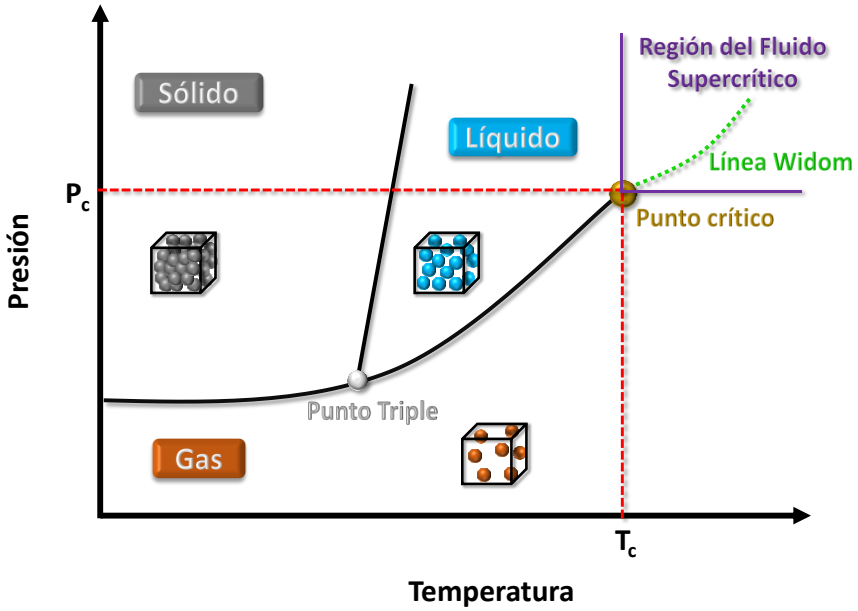

F*igura 26.* Representación general de un diagrama de fase presión – temperatura de una sustancia.

Cuando un compuesto alcanza el punto crítico, se comporta como un gas no ideal. En este punto, los gases son altamente compresibles y se disuelven en grandes cantidades en disolventes orgánicos tradicionales, alterando las

[359] Simeoni, G. G.; Bryk, T.; Gorelli, F. A.; Krisch, M.; Ruocco, G.; Santoro, M.; Scopigno, T. The Widom Line as the Crossover between Liquid-like and Gas-like Behaviour in Supercritical Fluids. *Nature Phys.* **2010**, *6* (7), 503–507.
[360] McMillan, P. F.; Stanley, H. E. Going Supercritical. *Nature Phys.* **2010**, *6* (7), 479–480.

características físicas de la fase líquida en función de la presión.[361] En la tabla 1, se pueden observar los puntos críticos (T_c y P_c) para varios fluidos.[362,363]

Tabla 1. Temperatura y presión crítica de algunos fluidos comunes utilizados en síntesis orgánica.

Disolvente	Temperatura Crítica (°C)	Presión Crítica (atm)
Agua	374.1	218.3
Dióxido de carbono	31.0	72.9
Metanol	240.0	78.6
Etanol	243.0	63.0
Isopropanol	235.2	47.0
Etilenglicol	374.0	75.6
Acetona	235.5	47.0
Tolueno	319.0	41.6
Amoniaco	132.5	112.5

A diferencia de los fluidos en forma líquida o gaseosa, los fluidos supercríticos muestran propiedades fisicoquímicas interesantes en cuanto a su comportamiento de solvatación, sus propiedades dieléctricas, su baja viscosidad y tensión superficial o su alta difusividad. Todas ellas cambian abruptamente cerca de los puntos críticos y se modulan fácilmente variando la temperatura y la presión.[364]

Los fluidos supercríticos, especialmente el H_2O y el CO_2 han encontrado amplias aplicaciones en numerosos campos como en el tratamiento de aguas residuales, la conversión de biomasa, el procesamiento y reciclaje de materiales, la extracción

[361] Hintermair, U.; Franciò, G.; Leitner, W. Continuous Flow Organometallic Catalysis: New Wind in Old Sails. *Chem. Commun.* **2011**, *47* (13), 3691–3701.
[362] Sunol, A. K.; Sunol, S. G. Safer Solvents and Processes. In *Handbook of Solvents*.; Wypych, G., Ed.; ChemTec Publishing: Toronto, 2014; pp 635–785.
[363] Bondesgaard, M.; Becker, J.; Xavier, J.; Hellstern, H.; Mamakhel, A.; Iversen, B. B. Guide to By-Products Formed in Organic Solvents under Solvothermal Conditions. *J. Supercrit. Fluids.* **2016**, *113*, 166–197.
[364] Xu, Y.; Musumeci, V.; Aymonier, C. Chemistry in Supercritical Fluids for the Synthesis of Metal Nanomaterials. *React. Chem. Eng.* **2019**, *4* (12), 2030–2054.

y separación secuencial y en otras aplicaciones en Química Verde. En este último campo, los scFs proporcionan algunas ventajas en la reacciones correspondientes al acelerar la transferencia de masa y energía, por la disminución de la viscosidad y de la tensión superficial.[361,365,364,366] Además, sus propiedades modulables proporcionan herramientas sencillas para la optimización rápida de los parámetros de reacción y facilitan el desarrollo de procesos en flujo continuo eficientes. La posibilidad de combinar los catalizadores soportados con los scFs en condiciones de flujo continuo para transformaciones quimio o enantioselectivas, presenta un gran potencial para el desarrollo de nuevas metodologías sintéticas más eficientes. Esta combinación no solo proporciona una forma de obtener altos rendimientos y un tratamiento simple de los productos, sino que también, en algunos casos, puede aumentar la selectividad de las reacciones.[367]

En los últimos años el dióxido de carbono supercrítico ($scCO_2$) ha recibido cada vez más atención y es estudiado como un fluido supercrítico modelo por razones de disponibilidad y seguridad. Sus características lo convierten en un fluido interesante en el contexto de la catálisis y la Química Verde. Tiene condiciones supercríticas moderadas: T_c: 31 °C y P_c: 74 bar, por lo que la cantidad de energía requerida para generar $scCO_2$ es relativamente baja. Es esencialmente no tóxico, químicamente inerte frente a muchas sustancias, no es inflamable y la simple despresurización permite su eliminación. Como disolvente de polaridad relativamente baja, el espectro de solutos está más limitado a moléculas de

[365] Aymonier, C.; Philippot, G.; Erriguible, A.; Marre, S. Playing with Chemistry in Supercritical Solvents and the Associated Technologies for Advanced Materials by Design. *J. Supercrit. Fluids.* **2018**, *134*, 184–196.
[366] Morin, C.; Loppinet-Serani, A.; Cansell, F.; Aymonier, C. Near- and Supercritical Solvolysis of Carbon Fibre Reinforced Polymers (CFRPs) for Recycling Carbon Fibers as a Valuable Resource: State of the Art. *J. Supercrit. Fluids.* **2012**, *66*, 232–240.
[367] Burguete, M. I.; García-Verdugo, E.; Luis, S. V. Efficient and Selective Chemical Transformations under Flow Conditions: The Combination of Supported Catalysts and Supercritical Fluids. *Beilstein J. Org. Chem.* **2011**, *7* (1), 1347–1359.

volatilidad y polaridad medias, pero esta polaridad puede también ajustarse mediante la manipulación de la temperatura y la presión.[368,369,370]

Aunque es un gas de efecto invernadero, su uso no implica una adición neta a la atmósfera. De hecho, la transformación eficiente del CO_2 en productos de alto valor agregado es una contribución importante para la protección del medio ambiente y el uso de los recursos, y ofrece vías de desarrollo en sectores energéticos e industriales respecto a la captura y transformación de este. En este sentido, se ha prestado especial atención al uso del CO_2 en ciclos supercríticos para la producción combinada de energía y calor, así como en el desarrollo de tecnologías que permitan la conversión de CO_2 en combustibles y productos químicos.[371,372] Así, la reacción de fijación de CO_2 en condiciones pseudo o supercríticas con epóxidos se ha utilizado para generar productos intermedios para química fina, policarbonatos o carbonatos cíclicos (Esquema 6).[373]

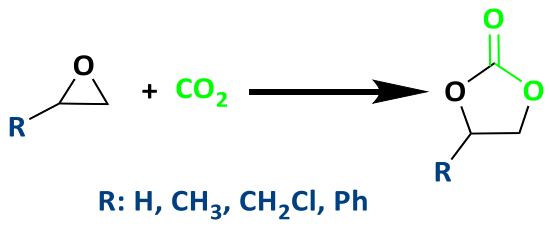

Esquema 6. Representación esquemática de la cicloadición de CO_2 a epóxidos para producir carbonatos cíclicos.

[368] Leitner, W. Supercritical Carbon Dioxide as a Green Reaction Medium for Catalysis. *Acc. Chem. Res.* **2002**, *35* (9), 746–756.
[369] Sheldon, R. A. Green Solvents for Sustainable Organic Synthesis: State of the Art. *Green Chem.* **2005**, *7* (5), 267–278.
[370] Haddleton, A. J.; Bassett, S. P.; Howdle, S. M. Comparison of Polymeric Particles Synthesised Using ScCO2 as the Reaction Medium on the Millilitre and Litre Scale. *J. Supercrit. Fluids.* **2020**, *160*, 104785.
[371] Koytsoumpa, E. I.; Bergins, C.; Kakaras, E. The CO_2 Economy: Review of CO_2 Capture and Reuse Technologies. *J. Supercrit. Fluids.* **2018**, *132*, 3–16.
[372] Nguyen, T. B. H.; Zondervan, E. Methanol Production from Captured CO_2 Using Hydrogenation and Reforming Technologies_ Environmental and Economic Evaluation. *J. CO_2 Util.* **2019**, *34*, 1–11.
[373] Sun, J.; Cheng, W.; Fan, W.; Wang, Y.; Meng, Z.; Zhang, S. Reusable and Efficient Polymer-Supported Task-Specific Ionic Liquid Catalyst for Cycloaddition of Epoxide with CO_2. *Catal. Today.* **2009**, *148* (3), 361–367.

La síntesis de ciclocarbonatos ha sido ampliamente estudiada por poseer una economía atómica del 100%, contribuyendo a reducir las emisiones globales de CO_2 y su conversión en una materia prima útil para la industria química.[374]

En este trabajo se han desarrollado estrategias sintéticas que permiten el uso $scCO_2$ en sistemas de flujo continuo con catalizadores basados en unidades de líquidos iónicos soportados en la cicloadición del CO_2 a epóxidos para producir carbonatos cíclicos. Estos compuestos se utilizan como disolventes apróticos, precursores de materiales poliméricos, intermediarios de una serie de productos para química fina y como electrolitos en baterías.[375,376]

1.5.3. Técnica de electroestirado o electrohilado para la fabricación de nanofibras

El origen de la técnica de electroestirado o electrohilado se remonta más de 60 años y fue observada por Rayleigh en 1897, quien evaluó el efecto de inducir cargas eléctricas en chorros de agua, así como la inestabilidad asimétrica del flujo. En los últimos año, debido a la demanda de materiales con dimensiones a escala nanométrica, la técnica de electrohilado se ha convertido en un proceso atractivo gracias a la habilidad de transformar un amplio rango de materiales en estructuras nanofibrilares a bajo costo y con relativa simplicidad.[377] La técnica es práctica y versátil ya que facilita la producción de fibras multifuncionales a partir

[374] North, M.; Pasquale, R.; Young, C. Synthesis of Cyclic Carbonates from Epoxides and CO_2. *Green Chem.* **2010**, *12* (9), 1514–1539.
[375] Stewart, J. A.; Drexel, R.; Arstad, B.; Reubsaet, E.; Weckhuysen, B. M.; Bruijnincx, P. C. A. Homogeneous and Heterogenised Masked N-Heterocyclic Carbenes for Bio-Based Cyclic Carbonate Synthesis. *Green Chem.* **2016**, *18* (6), 1605–1618.
[376] Zhong, W.; Bobbink, F. D.; Fei, Z.; Dyson, P. J. Polyimidazolium Salts: Robust Catalysts for the Cycloaddition of Carbon Dioxide into Carbonates in Solvent-Free Conditions. *ChemSusChem.* **2017**, *10* (13), 2728–2735.
[377] Duque, L. M.; Rodríguez, L.; López, M. Electrospinning: La Era de las Nanofibras. *Rev. Iberoam. Polim.* **2013**, *14*, 10-27.

de diversos polímeros.[378] Una de las características atractivas del electrohilado es la capacidad de producir una amplia gama de morfologías, la cual está determinada por una compleja interacción entre el flujo de fluido, las fuerzas eléctricas y la evaporación del disolvente.[379] Otra de las propiedades de las fibras obtenidas mediante esta técnica, es que poseen diámetros que van de las submicras a los nanómetros, rangos en los que es posible encontrar características únicas, como un área superficial muy grande en relación al volumen, flexibilidad en la superficie y alta porosidad,[377] lo que las hacen óptimas para una variedad de usos, como por ejemplo: portadoras de medicamentos en la liberación controlada de fármacos, distintas aplicaciones médicas como injertos vasculares, estructuras de soporte en la ingeniería de tejidos y suturas, como soportes biocatalíticos, membranas multifuncionales, sistemas de filtración, biosensores, sensores ópticos y (bio) químicos, células electroquímicas (como membranas o material del electrodo), refuerzos a nanoescala y catálisis.[380]

1.5.3.1. Electrohilado de polímeros

El montaje básico del electrohilado consiste en un capilar a través del cual debe ser expulsada la disolución polimérica, una fuente de alimentación de alto voltaje, un plato colector (lámina de metal o cilindro rotativo conductor) donde se depositarán las fibras después de que se evapora el disolvente (Figura 27 a); la fuente de alimentación que posee dos electrodos está conectada tanto al capilar (ánodo) como al colector (cátodo) de tal manera que se pueda aplicar una diferencia de potencial en ambas partes.[377,380] El capilar con frecuencia está conectado a una jeringa controlada por una bomba que permite alimentar la

[378] Uyar, T.; Besenbacher, F. Electrospinning of Uniform Polystyrene Fibers: The Effect of Solvent Conductivity. *Polymer.* **2008**, *49* (24), 5336–5343.
[379] Eda, G.; Shivkumar, S. Bead Structure Variations during Electrospinning of Polystyrene. *J. Mater. Sci.* **2006**, *41* (17), 5704–5708.
[380] Meli, L.; Miao, J.; Dordick, J. S.; Linhardt, R. J. Electrospinning from Room Temperature Ionic Liquids for Biopolymer Fiber Formation. *Green Chem.* **2010**, *12* (11), 1883–1892.

disolución polimérica a un flujo específico.[380] Algunos equipos están provistos con dos bombas independientes (Figura 27 b), de tal manera que permiten la inyección de dos disoluciones diferentes al mismo tiempo. A este tipo de técnica se conoce como electrohilado coaxial.[377]

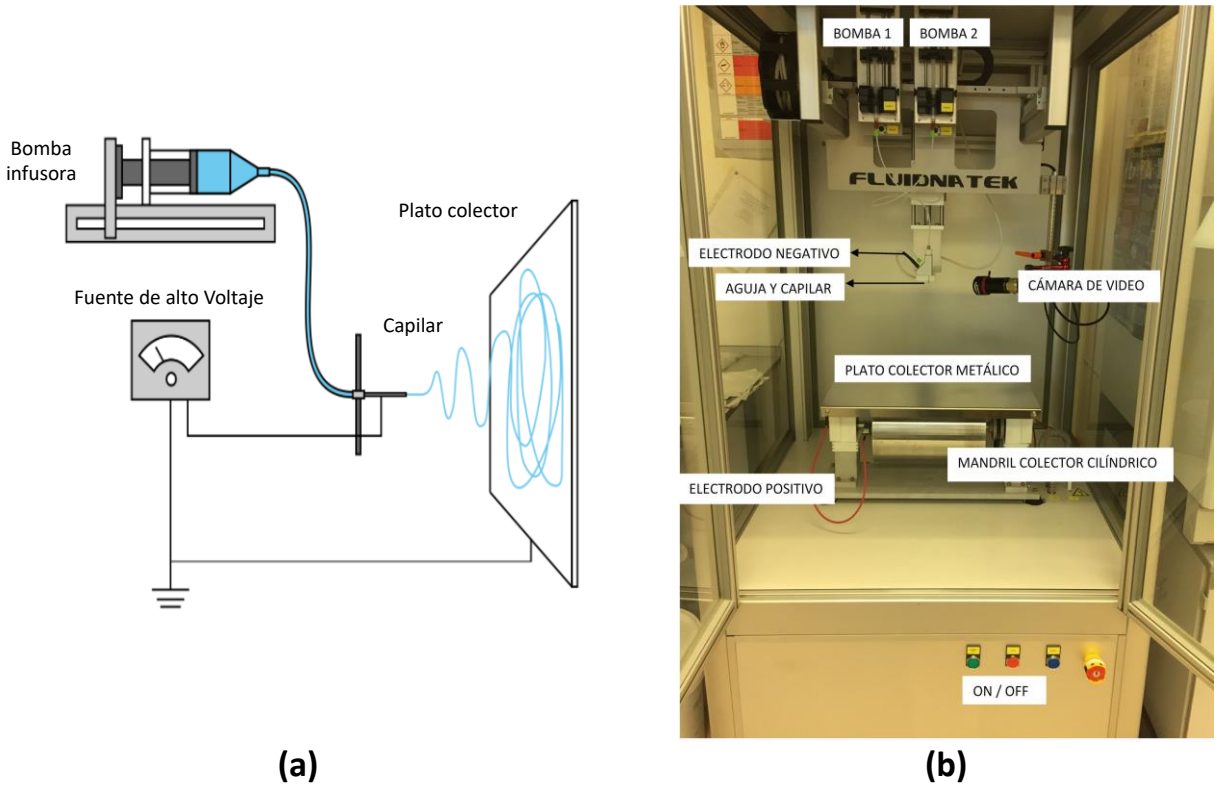

Figura 27. **(a)** Montaje básico de electrohilado (tomado de ref. 377). **(b)** Equipo de electrohilado Fluidnatek LE 100.V1 BioInicia.

La técnica puede ser desarrollada de forma horizontal o vertical y es necesario que el polímero este disuelto en un disolvente que permita una disolución completa del mismo para evitar taponamiento del capilar durante el proceso, pero que a la vez promueva la obtención de fibras homogéneas. Los polímeros tradicionales son dieléctricos, y en presencia de un campo eléctrico pueden considerarse como una distribución de dipolos eléctricos microscópicos compuestos por cargas positivas y negativas cuyos centros no coinciden

perfectamente, que se mantienen en su lugar por acción de las fuerzas atómicas y moleculares y solo pueden cambiar su posición ligeramente en respuesta a fuertes campos eléctricos externos, lo que explica por qué ocurre el estiramiento de la disolución en el proceso. Son llamadas cargas ligadas en contraposición a las cargas libres que determinan la conductividad en un material conductor. En ocasiones para incrementar las propiedades dieléctricas de la disolución, se adicionan algunos disolventes con altas constantes dieléctricas para favorecer la formación de fibras con menos estructuras defectuosas y con diámetros reducidos. Una vez que se tiene la disolución en la jeringa el flujo puede ser inyectado a una velocidad específica de tal manera que se permita crear una gota colgante en la punta de la aguja. A medida que se aplica una diferencia de voltaje, la carga eléctrica se acumula en la superficie de la gota de disolución y cuando la repulsión electrostática dentro de la gota excede la tensión superficial de la disolución que minimiza el área superficial de esta, la gota se deforma formando una forma cónica conocida como cono de Taylor, [377,380] este fenómeno se puede observar en la Figura 28.

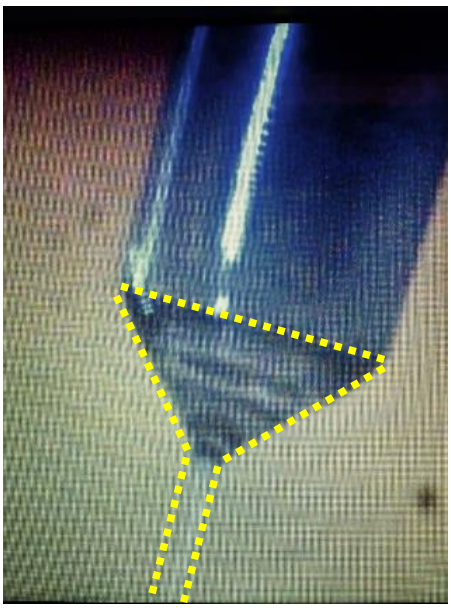

Figura 28. Formación del cono de Taylor de una disolución polimérica.

Después de que en la disolución polimérica se rompan las fuerzas de cohesión que en muchos casos está dominada por la tensión superficial, un chorro de disolución se expulsa en forma de hilo delgado (este es alargado debido a las interacciones electrostáticas entre las cargas cercanas) desde la punta del cono, el cual es atraído hacia el colector siguiendo un camino recto. Durante este proceso el disolvente se evapora y finalmente las fibras se solidifican a su llegada al plato colector. Esta etapa es afectada por una serie de factores que hacen que el hilo generado sea inestable. Dos de estos factores son el modo de eje simétrico donde las fluctuaciones del chorro ocurren alrededor del eje principal y la otra es un eje no simétrico (Figura 29). Estas inestabilidades generan defectos como los "*beads*" (Figura 29 a) que a su vez provocan la disminución de la superficie por unidad de área del proceso.[377, 380]

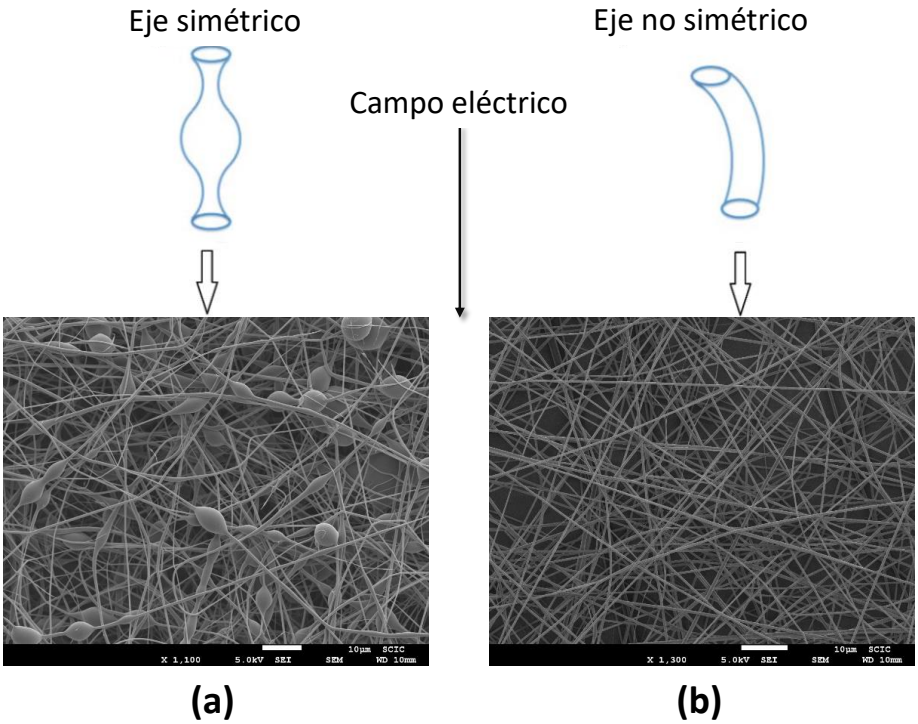

Figura 29. Modos de inestabilidad de flexión simétricos y no simétricos que conducen a una calidad de fibra diferente dependiendo del modo predominante. (**a)** fibras con formación de "beads". **(b)** fibras lisas (modificado de ref.380).

En la actualidad, además del montaje tradicional existen varias modificaciones del electrohilado. Tal y como se indicó anteriormente, una de ellas es el electrohilado coaxial. Esta es una ampliación de la técnica convencional que ha permitido electrohilar simultáneamente diferentes polímeros. Se basa en una boquilla pequeña dentro de otra más grande que resulta en una estructura de fibras conformada por un núcleo y una corteza (Figura 30), esta variación ha convertido a la técnica en una de las mejores opciones para obtener fibras con elementos de diferente naturaleza. Existen otras modificaciones al electrohilado convencional, tales como el electroestirado con camisa de protección, el electrohilado con doble componente y el *forcespinning*.[377]

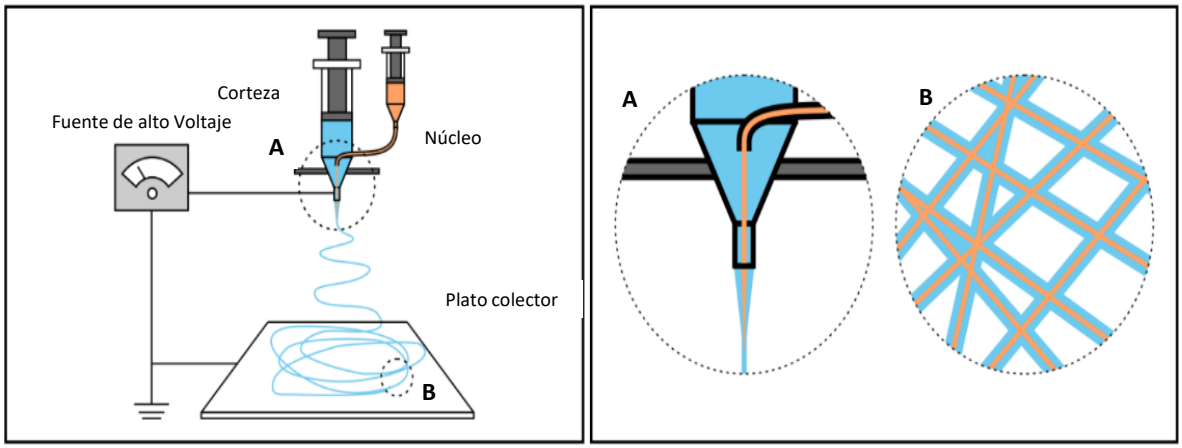

Figura 30. *Esquema del electrohilado coaxial* (tomado de ref. 377).

1.5.3.2 Condiciones y parámetros del electrohilado

Coexisten diversas condiciones y parámetros que se encuentran relacionados con las propiedades y características de las fibras obtenidas por medio del electrohilado por lo que el control de ellas durante la ejecución del proceso es indispensable, a continuación, se desplegarán una serie de parámetros del electroestirado y de la disolución polimérica, así como las condiciones ambientales que se deben de tomar en cuenta para desarrollar esta técnica.

1.5.3.2.1. Parámetros de la disolución polimérica

a) *Concentración de la disolución polimérica.* La concentración de polímero en la disolución influencia tanto la viscosidad como la tensión superficial de ésta. La viscosidad de una disolución de polímero está relacionada también con el entrecruzamiento de las cadenas poliméricas: si las cadenas son menos entrecruzadas la disolución tendrá una viscosidad baja y viceversa. Esta propiedad, además, tiene un efecto significativo sobre el tamaño final y la distribución de las fibras. Si la disolución está muy diluida las fibras de polímero se rompen en gotas antes de llegar al plato colector debido al efecto de la tensión superficial. De igual forma, si la disolución está muy concentrada entonces las fibras no podrán formar el hilo debido a la alta viscosidad, ya que ello dificulta el paso de la disolución a través del capilar.[377, 381]

b) *Tensión superficial.* En algunos trabajos se ha indicado que reduciendo la tensión superficial de una disolución de polímero pueden obtenerse fibras sin la presencia de "*beads*". Este tipo de fuerza reduce el área superficial por unidad de masa, cambiando los chorros por esferas. Al aplicar un alto voltaje se aumenta la superficie oponiéndose a la formación de "*beads*" y favoreciendo chorros más delgados. En este caso es la fuerza viscoelásticaes la que se resiste a cambios rápidos en la forma. El coeficiente de tensión superficial depende del polímero y del disolvente.[377]

c) *Conductividad de la disolución.* Las disoluciones con alta conductividad tienen mayor capacidad de transportar las cargas que aquellas con baja conductividad. La adición de sales o ILs a la disolución incrementa la conductividad. Se ha encontrado que un aumento de la conductividad

[381] Deitzel, J. M.; Kleinmeyer, J.; Harris, D.; Beck Tan, N. C. The Effect of Processing Variables on the Morphology of Electrospun Nanofibers and Textiles. *Polymer.* **2001**, *42* (1), 261–272.

eléctrica de la disolución provoca una disminución significativa en el diámetro de las fibras, mientras que cuando la conductividad es baja se observa un alargamiento insuficiente del chorro lo que impide la producción de fibras uniformes.[377, 380]

d) *Efecto dieléctrico del disolvente.* El disolvente cumple dos papeles importantes al utilizar la técnica de electrohilado. El primero es disolver las moléculas de polímero para formar el chorro con carga eléctrica y el segundo es transportar las moléculas de polímero disuelto hasta el colector. La constante dieléctrica tiene gran influencia en el proceso. Generalmente una disolución con buenas propiedades dieléctricas reduce la formación de "*beads*".[377, 381]

1.5.3.2.2. Parámetros del electrohilado

a) *Diferencia de potencial (voltaje).* El voltaje es uno de los parámetros más importantes dentro del proceso de electrohilado. En la literatura se describe que, en algunos casos, los voltajes altos conllevan el que se transporte más fluido en el chorro, lo que da lugar a fibras con mayores diámetros. En otros estudios, sin embargo, se indica que decrece el diámetro de las fibras y aumenta la probabilidad de obtener hilos con "*beads*". En general, en la mayoría de los casos un voltaje alto permite un mayor estiramiento de la disolución debido a la presencia de un campo eléctrico fuerte.[377]

b) *Flujo de salida.* Un menor flujo de salida provoca que el disolvente tenga más tiempo para evaporarse lo que evita la formación de defectos en las fibras. Sin embargo, hay que señalar que es necesario mantener un volumen mínimo de salida para mantener el cono de Taylor estable.[377]

c) *Distancia entre la punta de la aguja y el colector.* El efecto de la variación de la distancia puede o no tener efecto en la morfología de las fibras. Al trabajar con distancias muy grandes las fibras pueden romperse debido a su propio peso, especialmente si las fibras son de diámetro pequeño. Es necesario una distancia mínima con el fin de dar el tiempo suficiente para que el disolvente se evapore antes de alcanzar el plato colector. Con distancias muy largas o demasiado cortas se puede observar la aparición de "*beads*" o hilos húmedos que promueven la obtención de fibras aplanadas o con forma de cintas.[377]

1.5.3.2.3. Condiciones ambientales

Las condiciones ambientales también ejercen una cierta influencia en esta técnica. Así, la presencia de humedad conduce a la aparición de pequeños poros en la superficie de las fibras obtenidas, ya que el agua condensa en la superficie de éstas. La humedad, por tanto, puede influir en la morfología de las fibras, especialmente cuando se utilizan disolventes volátiles, ya que puede variar la velocidad de evaporación del disolvente de la disolución. Asimismo, la temperatura puede incrementar la tasa de evaporación, ocasionando una reducción en la viscosidad de la disolución. Dependiendo de las condiciones y algunas características del ambiente las fibras pueden tener diversas formas y tamaños.[377,382]

1.5.4. Fabricación avanzada de materiales: Impresión 3D

El diseño exitoso de materiales avanzados y dispositivos funcionales basados en compuestos moleculares es altamente complejo, ya que a menudo requiere de la

[382] Nezarati, R. M.; Eifert, M. B.; Cosgriff-Hernandez, E. Effects of Humidity and Solution Viscosity on Electrospun Fiber Morphology. *Tissue Eng. Part C Methods.* **2013**, *19* (10), 810–819.

creación y adaptación simultánea del diseño de las especies moleculares activas, los materiales de soporte y el desarrollo de geometrías macroscópicas complejas. Esto último, sin embargo, puede facilitarse enormemente mediante el empleo de tecnologías de fabricación como la impresión 3D.[383] Esta técnica ha emergido como un nuevo conjunto de tecnologías con el potencial de revolucionar la fabricación de dispositivos muy diversos al permitir el desarrollo de diseños a medida, a menudo inviables con las técnicas tradicionales. No obstante, el desarrollo de materiales avanzados funcionalizados impresos en 3D, cuyas propiedades están determinadas por la inclusión de las propiedades moleculares, todavía está en desarrollo.[384,385]

El uso de las tecnologías de fabricación aditiva de materiales (AM, por sus siglas en inglés) denominada generalmente como impresión tridimensional (3DP, *idem*), crea estructuras a partir de modelos digitales.[386] Es una herramienta novedosa que funciona depositando múltiples capas individuales de material. Se adiciona una capa sobre otra sucesivamente hasta crear el material con geometrías complejas.[387] La naturaleza aditiva de esta técnica minimiza la cantidad de reactivos empleados, reduciendo potencialmente el uso de energía, la demanda de recursos y las emisiones de CO_2 relacionadas durante todo el ciclo de vida del producto. Se estima que la implementación de la impresión 3D podrá

[383] Wales, D. J.; Cao, Q.; Kastner, K.; Karjalainen, E.; Newton, G. N.; Sans, V. 3D-Printable Photochromic Molecular Materials for Reversible Information Storage. *Adv. Mater.* **2018**, *30* (26), 1800159.
[384] Fantino, E.; Chiappone, A.; Roppolo, I.; Manfredi, D.; Bongiovanni, R.; Pirri, C. F.; Calignano, F. 3D Printing of Conductive Complex Structures with In Situ Generation of Silver Nanoparticles. *Adv. Mater.* **2016**, *28* (19), 3712–3717.
[385] Yang, H.; Leow, W. R.; Wang, T.; Wang, J.; Yu, J.; He, K.; Qi, D.; Wan, C.; Chen, X. 3D Printed Photoresponsive Devices Based on Shape Memory Composites. *Adv. Mater.* **2017**, *29* (33), 1701627.
[386] Ambrosi, A.; Pumera, M. 3D-Printing Technologies for Electrochemical Applications. *Chem. Soc. Rev.* **2016**, *45* (10), 2740–2755.
[387] Gunasekera, D. H. A. T.; Kuek, S.; Hasanaj, D.; He, Y.; Tuck, C.; Croft, A. K.; Wildman, R. D. Three Dimensional Ink-Jet Printing of Biomaterials Using Ionic Liquids and Co-Solvents. *Faraday Discuss.* **2016**, *190* (0), 509–523.

reducir las intensidades en el consumo de energía y las emisiones de CO_2 en un 5% para el 2025.[388]

Desde la invención de la primera impresora 3D de estereolitografía por C. Hull en 1986,[389] se ha eliminado la necesidad de moldes o mecanismos para crear estructuras complejas. Adicionalmente, se ha abierto una amplia gama de aplicaciones en campos como la educación,[390] la industria alimentaria,[391] la oceanografía,[392] la biomedicina (regeneración de tejidos),[393,394] la energía (células solares y sensores eléctricos),[395,396] y la química, con la fabricación a medida de diferentes dispositivos y reactores.[397,398]

Los procesos de impresión 3D se pueden clasificar en siete categorías: inyección de aglutinante (BJ), deposición directa de energía (DED), extrusión del material (ME), inyección del material (MJ), fusión de lecho de polvo (PBF), laminación de hojas (SL) y fotopolimerización (VP). Todas las siglas hacen referencia a su

[388] Gebler, M.; Schoot Uiterkamp, A. J. M.; Visser, C. A Global Sustainability Perspective on 3D Printing Technologies. *Energy Policy.* **2014**, *74*, 158–167.
[389] Hull, C. W. *Apparatus for Production of Three-Dimensional Objects by Stereolithography*. US4575330A, March 11, 1986.
[390] Rossi, S.; Benaglia, M.; Brenna, D.; Porta, R.; Orlandi, M. Three Dimensional (3D) Printing: A Straightforward, User-Friendly Protocol To Convert Virtual Chemical Models to Real-Life Objects. *J. Chem. Educ.* **2015**, *92* (8), 1398–1401.
[391] Sun, J.; Peng, Z.; Zhou, W.; Fuh, J. Y. H.; Hong, G. S.; Chiu, A. A Review on 3D Printing for Customized Food Fabrication. *Procedia Manuf.* **2015**, *1*, 308–319.
[392] Mohammed, J. S. Applications of 3D Printing Technologies in Oceanography. *Methods in Oceanography.* **2016**, *17*, 97–117.
[393] Mironov, V.; Boland, T.; Trusk, T.; Forgacs, G.; Markwald, R. R. Organ Printing: Computer-Aided Jet-Based 3D Tissue Engineering. *Trends Biotechnol.* **2003**, *21* (4), 157–161.
[394] Derby, B. Printing and Prototyping of Tissues and Scaffolds. *Science.* **2012**, *338* (6109), 921–926.
[395] Vak, D.; Hwang, K.; Faulks, A.; Jung, Y.-S.; Clark, N.; Kim, D.-Y.; Wilson, G. J.; Watkins, S. E. 3D Printer Based Slot-Die Coater as a Lab-to-Fab Translation Tool for Solution-Processed Solar Cells. *Adv. Energy Mater.* **2015**, *5* (4), 1401539.
[396] Leigh, S. J.; Bradley, R. J.; Purssell, C. P.; Billson, D. R.; Hutchins, D. A. A Simple, Low-Cost Conductive Composite Material for 3D Printing of Electronic Sensors. *PLoS One.* **2012**, *7* (11), e49365.
[397] Parra-Cabrera, C.; Achille, C.; Kuhn, S.; Ameloot, R. 3D Printing in Chemical Engineering and Catalytic Technology: Structured Catalysts, Mixers and Reactors. *Chem. Soc. Rev.* **2018**, *47* (1), 209–230.
[398] Sun, X.; Yan, Y.; Zhang, L.; Ma, G.; Liu, Y.; Yu, Y.; An, Q.; Tao, S. Direct 3D Printing of Reactive Agitating Impellers for the Convenient Treatment of Various Pollutants in Water. *Adv. Mater. Interfaces.* **2018**, *5* (8), 1701626.

terminología en inglés. Además se pueden utilizar distintos tipos de compuestos tales como polímeros, materiales cerámicos, metales, materiales con propiedades electrónicas, biomateriales y materiales compuestos.[399,400]

Para la elaboración de los materiales creados y utilizados en este trabajo se utilizó la fotopolimerización (Figura 31 a). La VP es un término general incluido en la estereolitografía y procesos relacionados. En este caso específico, la fotopolimerización ocurre en la cubeta donde se encuentran las resinas, las cuales se someten a una reacción química provocada por la irradiación de un láser y de esta forma se obtiene el material sólido (Figura 31 b). La fotopolimerización involucra monómeros / oligómeros, fotoiniciadores, y aditivos tales como estabilizantes, flexibilizantes y disolventes. La fotopolimerización es un proceso fotoquímico que lleva a la unión de pequeños monómeros para formar cadenas poliméricas. En general, se requiere un fotoiniciador que actúe como catalizador para que la reacción tenga una velocidad razonable (Figura 31 c). Los polímeros formados deben tener el entrecruzamiento suficiente para que las moléculas polimerizadas no se vuelvan a disolver en la disolución monomérica. Deben poseer, además, las propiedades mecánicas necesarias para mantener la estructura diseñada bajo las diversas condiciones de trabajo.[399]

[399] Lee, J.-Y.; An, J.; Chua, C. K. Fundamentals and Applications of 3D Printing for Novel Materials. *Appl. Mater. Today.* **2017**, *7*, 120–133.
[400] Williams, C. B.; Mistree, F.; Rosen, D. W. A Functional Classification Framework for the Conceptual Design of Additive Manufacturing Technologies. *J. Mech. Des* **2011**, *133* (12), 1-11.

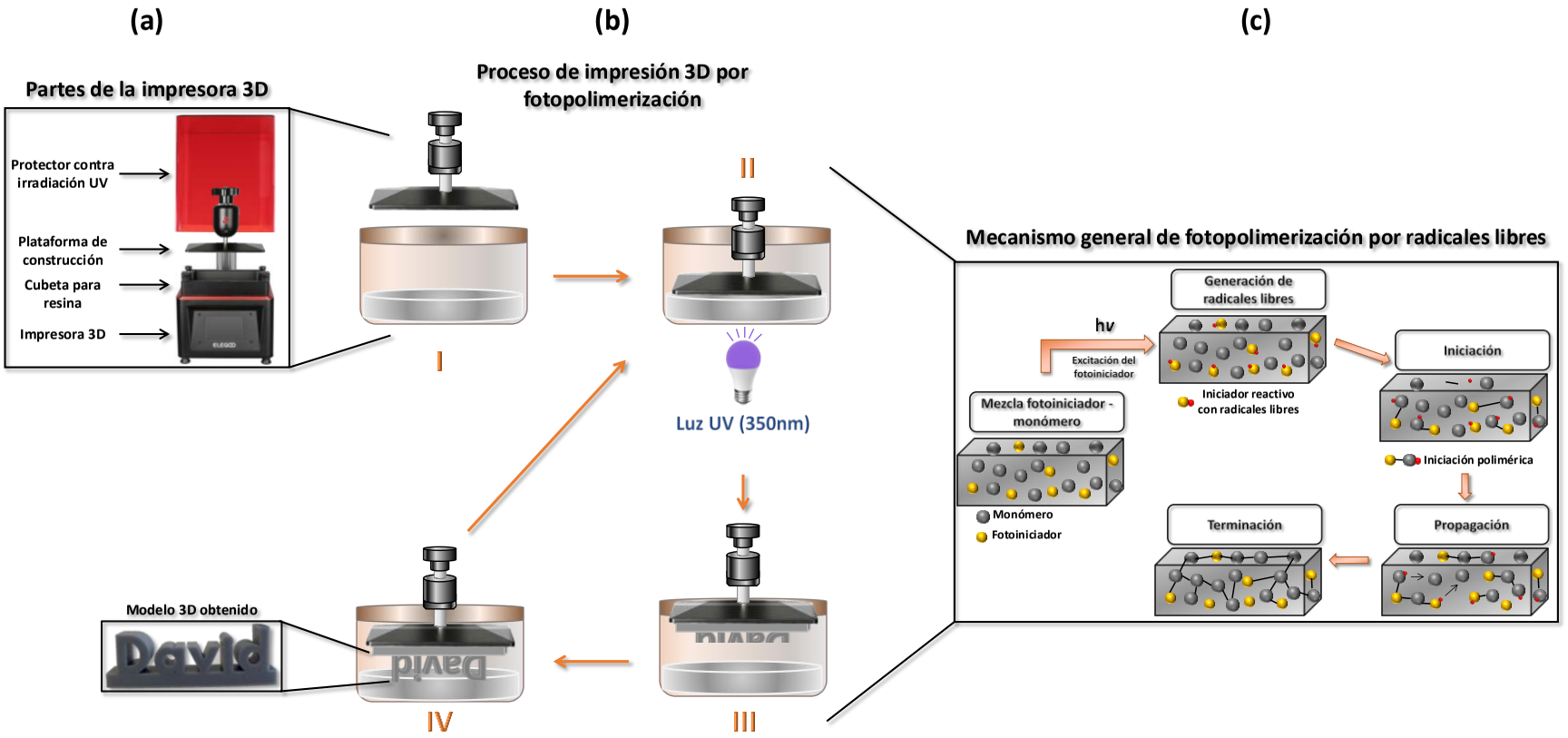

Figura 31. (a) Componentes principales de la impresora 3D. **(b)** Representación esquemática del proceso de impresión 3D por fotopolimerización. (I) Los reactivos utilizados en la preparación de la mezcla monomérica líquida se cargan en la cubeta. (II) La placa se sumerge en la disolución para comenzar el ciclo de impresión, la luz UV (350 nm) irradia la disolución e inicia la reacción fotoquímica para formar la capa de polímero en la placa de construcción. (III) La placa se eleva para terminar de generar la capa polimérica. (IV) El ciclo vuelve a iniciar, sumergiéndose la placa en la disolución y creando una nueva capa, y así continuamente hasta obtener el modelo 3D programado. **(c)** Mecanismo general de fotopolimerización por radicales libres (modificado de ref. 399).

La impresión 3D por fotopolimerización tiene un interés particular por la versatilidad que ofrece la química de los polímeros. Sin embargo, el uso de la polimerización tradicional por radicales libres trae consigo la desventaja de crear materiales con cadenas poliméricas que después de su obtención pueden ser difíciles de modificar. Una solución a esta limitación es utilizar agentes de transferencia de cadena reversible (RAFT), como los tritiocarbonatos (TTC). Estas especies se pueden reactivar bajo la radiación UV/luz visible y en consecuencia permiten la inserción de nuevos monómeros en la red existente o proporcionan polímeros dinámicos para la autocuración o modificación de la cadena polimérica.[401]

En el campo de la química, Cronin ha descrito la aplicación de la impresión 3D a la preparación de materiales de laboratorio (acuñados como "*reactionware*"),[402,403] incluyendo el desarrollo de dispositivos para la síntesis en flujo continuo.[404,405,406] La fabricación de micro y minireactores por 3DP para su aplicación en reacciones en flujo continuo representa, de hecho, una de las aplicaciones más importantes en química.[407] Sin embargo, los la post-modificación de dispositivos preparados por 3DP ha recibido poca atención, aunque nuestro grupo ha descrito la

[401] Bagheri, A.; Engel, K. E.; Bainbridge, C. W. A.; Xu, J.; Boyer, C.; Jin, J. 3D Printing of Polymeric Materials Based on Photo-RAFT Polymerization. *Polym. Chem.* **2020**, *11* (3), 641–647.
[402] Symes, M. D.; Kitson, P. J.; Yan, J.; Richmond, C. J.; Cooper, G. J. T.; Bowman, R. W.; Vilbrandt, T.; Cronin, L. Integrated 3D-Printed Reactionware for Chemical Synthesis and Analysis. *Nature Chem.* **2012**, *4* (5), 349–354.
[403] Kitson, P. J.; Glatzel, S.; Chen, W.; Lin, C.-G.; Song, Y.-F.; Cronin, L. 3D Printing of Versatile Reactionware for Chemical Synthesis. *Nat Protoc.* **2016**, *11* (5), 920–936.
[404] Kitson, P. J.; Rosnes, M. H.; Sans, V.; Dragone, V.; Cronin, L. Configurable 3D-Printed Millifluidic and Microfluidic 'Lab on a Chip' Reactionware Devices. *Lab Chip.* **2012**, *12* (18), 3267–3271.
[405] Mathieson, J. S.; Rosnes, M. H.; Sans, V.; Kitson, P. J.; Cronin, L. Continuous Parallel ESI-MS Analysis of Reactions Carried out in a Bespoke 3D Printed Device. *Beilstein J. Nanotechnol.* **2013**, *4* (1), 285–291.
[406] Dragone, V.; Sans, V.; Rosnes, M. H.; Kitson, P. J.; Cronin, L. 3D-Printed Devices for Continuous-Flow Organic Chemistry. *Beilstein J. Org. Chem.* **2013**, *9* (1), 951–959.
[407] Okafor, O.; Weilhard, A.; Fernandes, J. A.; Karjalainen, E.; Goodridge, R.; Sans, V. Advanced Reactor Engineering with 3D Printing for the Continuous-Flow Synthesis of Silver Nanoparticles. *React. Chem. Eng.* **2017**, *2* (2), 129–136.

impresión 3D de materiales que se han modificado posteriormente para inmovilizar enzimas.[408]

En los materiales con estructuras meso y macroporosos los rendimientos catalíticos están estrechamente relacionados con su forma de obtención ya que éstos definen la estructura porosa. A menudo se preparan por métodos complejos como el autoensamblaje, la deposición química de vapor o utilizando plantillas previamente elaboradas. Estos métodos generalmente son caros, lo que obstaculiza las posibles aplicaciones industriales. A diferencia de las tecnologías de fabricación tradicionales, la impresión 3D es una forma conveniente y eficiente para preparar estructuras 3D complejas. Bajo esta perspectiva, los métodos de 3DP son factibles para la construcción de reactores de tamaños reducidos para las plantas químicas, así como para la preparación de materiales catalíticos, al utilizar el diseño modular para disminuir los costos de diseño y de fabricación.[409,410]

Con el continuo crecimiento de la tecnología 3D, la precisión de la impresión y el rendimiento del material han mejorado significativamente,[411] además ha minimizado notablemente la cantidad de materia prima utilizada para generar el producto final.[412] El 3DP puede ser ampliamente utilizado para desarrollar reactores que integren catalizadores multifuncionales. Esto ofrece una serie de ventajas para el estudio y desarrollo de materiales catalíticos, ya que se pueden formular catalizadores con diferentes estructuras modulables (especialmente

[408] Peris, E.; Okafor, O.; Kulcinskaja, E.; Goodridge, R.; Luis, S. V.; Garcia-Verdugo, E.; O'Reilly, E.; Sans, V. Tuneable 3D Printed Bioreactors for Transaminations under Continuous-Flow. *Green Chem.* **2017**, *19* (22), 5345–5349.
[409] Hurt, C.; Brandt, M.; Priya, S. S.; Bhatelia, T.; Patel, J.; Selvakannan, P.; Bhargava, S. Combining Additive Manufacturing and Catalysis: A Review. *Catal. Sci. Technol.* **2017**, *7* (16), 3421–3439.
[410] Zhou, X.; Liu, C. Three-Dimensional Printing for Catalytic Applications: Current Status and Perspectives. *Adv. Funct. Mater.* **2017**, *27* (30), 1701134.
[411] Hartings, M. R.; Ahmed, Z. Chemistry from 3D Printed Objects. *Nat. Rev. Chem.* **2019**, *3* (5), 305–314.
[412] Díaz-Marta, A. S.; Tubío, C. R.; Carbajales, C.; Fernández, C.; Escalante, L.; Sotelo, E.; Guitián, F.; Barrio, V. L.; Gil, A.; Coelho, A. Three-Dimensional Printing in Catalysis: Combining 3D Heterogeneous Copper and Palladium Catalysts for Multicatalytic Multicomponent Reactions. *ACS Catal.* **2018**, *8* (1), 392–404.

complejas) en menos pasos. Además, la estructura impresa puede mejorar la transferencia de masa y calor, así como optimizar la distribución de los componentes, favoreciendo las propiedades de adsorción y el rendimiento catalítico.[413,414,415] Así, se han alcanzado altas conversiones con catalizadores heterogéneos con geometrías complejas impresas por 3DP,[416] y se han creado sistemas catalíticos con múltiples funciones y que faciliten la separación de los productos obtenidos.[417,418]

Una forma de integrar el 3DP con la catálisis heterogénea es mediante el uso de PILs o SILLPs. Aunque pueden utilizarse diferentes técnicas de polimerización,[419] los materiales de partida derivados de ILs presentan algunos inconvenientes como su alta viscosidad que dificultan el proceso de impresión por inyección. También se ha descrito la impresión 3D de polímeros utilizando monómeros de ILs auto-organizados.[420] Una vía para evitar los problemas de viscosidad, es utilizar otras técnicas de impresión tales como la fotopolimerización en cubeta descrita anteriormente. Esto permite la deposición aditiva de los compuestos y modular el PIL deseado mediante la modificación de

[413] Lefevere, J.; Gysen, M.; Mullens, S.; Meynen, V.; Van Noyen, J. The Benefit of Design of Support Architectures for Zeolite Coated Structured Catalysts for Methanol-to-Olefin Conversion. *Catal. Today*. **2013**, *216*, 18–23.
[414] Michorczyk, P.; Hędrzak, E.; Węgrzyniak, A. Preparation of Monolithic Catalysts Using 3D Printed Templates for Oxidative Coupling of Methane. *J. Mater. Chem. A*. **2016**, *4* (48), 18753–18756.
[415] Couck, S.; Cousin-Saint-Remi, J.; Van der Perre, S.; Baron, G. V.; Minas, C.; Ruch, P.; Denayer, J. F. M. 3D-Printed SAPO-34 Monoliths for Gas Separation. *Micropor. Mesopor. Mat.* **2018**, *255*, 185–191.
[416] Tubío, C. R.; Azuaje, J.; Escalante, L.; Coelho, A.; Guitián, F.; Sotelo, E.; Gil, A. 3D Printing of a Heterogeneous Copper-Based Catalyst. *J. Catal.* **2016**, *334*, 110–115.
[417] Zhou, X.; Liu, C. Three-Dimensional Printing of Porous Carbon Structures with Tailorable Pore Sizes. *Catal. Today*. **2018**, (doi.org/10.1016/j.cattod.2018.05.044).
[418] Zhu, J.; Wu, P.; Chen, L.; He, J.; Wu, Y.; Wang, C.; Chao, Y.; Lu, L.; He, M.; Zhu, W.; Li, H. 3D-Printing of Integrated Spheres as a Superior Support of Phosphotungstic Acid for Deep Oxidative Desulfurization of Fuel. *J. Energy Chem.* **2020**, *45*, 91–97.
[419] Schultz, A. R.; Lambert, P. M.; Chartrain, N. A.; Ruohoniemi, D. M.; Zhang, Z.; Jangu, C.; Zhang, M.; Williams, C. B.; Long, T. E. 3D Printing Phosphonium Ionic Liquid Networks with Mask Projection Microstereolithography. *ACS Macro Lett.* **2014**, *3* (11), 1205–1209.
[420] Ndefru, B. G.; Ringstrand, B. S.; Diouf, S. I.-Y.; Seifert, S.; Leal, J. H.; Semelsberger, T. A.; Dreier, T. A.; Firestone, M. A. Multiscale Additive Manufacturing of Polymers Using 3D Photo-Printable Self-Assembling Ionic Liquid Monomers. *Mol. Syst. Des. Eng.* **2019**, *4* (3), 580–585.

las propiedades de las capas impresas. En la literatura se ha descrito ejemplos en los que inicialmente se deposita el precursor del PIL, basado en compuestos de imidazol, y luego se produce la cuaternización y la posterior metátesis aniónica.[421]

Un aspecto final a considerar es la necesidad de evaluar el impacto medio ambiental que tienen los procesos de fabricación de todo tipo de dispositivos.[422] Comprender los posibles efectos tanto positivos como negativos en la aplicación de nuevas tecnologías para la fabricación nuevos materiales, dispositivos y aplicaciones que los utilicen, requiere la aplicación de herramientas como el análisis del ciclo de vida,[423] y es clave para los procesos de toma de decisiones basados en la Química Verde y la sostenibilidad ambiental.

1.6. Materiales Conductores Iónicos

Los materiales conductores, en particular aquellos que son flexibles y estables y se adaptan a una amplia variedad de condiciones ambientales, se usan en una amplia variedad de aplicaciones como pantallas, dispositivos médicos implantables, paneles táctiles, mecanismos de detección y dispositivos de almacenamiento de energía portátil.[424] Este último campo representa un ejemplo paradigmático, ya que la rápida revolución de la electrónica portátil ha creado una demanda creciente de dispositivos de almacenamiento de energía más eficientes. En esta área, la batería recargable de iones de litio (ion-Li) ofrece

[421] Karjalainen, E.; Wales, D. J.; Gunasekera, D. H. A. T.; Dupont, J.; Licence, P.; Wildman, R. D.; Sans, V. Tunable Ionic Control of Polymeric Films for Inkjet Based 3D Printing. *ACS Sustainable Chem. Eng.* **2018**, *6* (3), 3984–3991.
[422] Cerdas, F.; Juraschek, M.; Thiede, S.; Herrmann, C. Life Cycle Assessment of 3D Printed Products in a Distributed Manufacturing System. *J. Ind. Ecol.* **2017**, *21* (S1), S80–S93.
[423] Maciel, V. G.; Wales, D. J.; Seferin, M.; Sans, V. Environmental Performance of 3D-Printing Polymerisable Ionic Liquids. *J. Clean. Prod.* **2019**, *214*, 29–40.
[424] Rong, Q.; Lei, W.; Liu, M. Conductive Hydrogels as Smart Materials for Flexible Electronic Devices. *Chem. Eur. J.* **2018**, *24* (64), 16930–16943.

ventajas sobre las baterías convencionales en términos de voltaje de operación, alta densidad de energía, largo tiempo de vida o flexibilidad en el diseño, entre otros.[425,426]

Hoy día el potencial de las baterías de ion-Li no se ha explotado en su totalidad y la mejora de propiedades como la densidad de energía /potencia para una mayor aplicabilidad en industrias como la automotriz, la exploración petrolera y la minería es un reto importante puesto que requieren condiciones ambientales especiales.[427] En la actualidad, se está trabajando con baterías de litio-azufre,[428] litio-oxígeno[429] y litio-aire[430] consideradas baterías de próxima generación.

Existen, sin embargo, en estas baterías, una serie de problemas que se deben de resolver para alcanzar una mayor seguridad en la batería y un mejor rendimiento electroquímico. Algunas de ellos se relacionan con los materiales de los electrodos, pero, además, muchos de los compuestos conductores utilizados son inflamables y altanamente volátiles por lo que las fugas representan un grave riesgo de seguridad y acortan la vida útil de la batería. La solución a estos desafíos depende en gran medida del desarrollo de nuevos materiales que sirvan como componentes novedosos para las baterías a base del ion litio.[427]

Las propiedades de los líquidos iónicos descritas en la sección 1.2.1, les otorgan grandes posibilidades en diversos procesos electroquímicos, entre los cuáles el

[425] Scrosati, B.; Garche, J. Lithium Batteries: Status, Prospects and Future. *J. Power Sources.* **2010**, *195* (9), 2419–2430.
[426] Goodenough, J. B.; Park, K.-S. The Li-Ion Rechargeable Battery: A Perspective. *J. Am. Chem. Soc.* **2013**, *135* (4), 1167–1176.
[427] Yang, Q.; Zhang, Z.; Sun, X.-G.; Hu, Y.-S.; Xing, H.; Dai, S. Ionic Liquids and Derived Materials for Lithium and Sodium Batteries. *Chem. Soc. Rev.* **2018**, *47* (6), 2020–2064.
[428] Yin, Y.-X.; Xin, S.; Guo, Y.-G.; Wan, L.-J. Lithium–Sulfur Batteries: Electrochemistry, Materials, and Prospects. *Angew. Chem. Int. Ed.* **2013**, *52* (50), 13186–13200.
[429] Kwak, W.-J.; Rosy; Sharon, D.; Xia, C.; Kim, H.; Johnson, L. R.; Bruce, P. G.; Nazar, L. F.; Sun, Y.-K.; Frimer, A. A.; Noked, M.; Freunberger, S. A.; Aurbach, D. Lithium–Oxygen Batteries and Related Systems: Potential, Status, and Future. *Chem. Rev.* **2020**. DOI: 10.1021/acs.chemrev.9b00609
[430] Grande, L.; Paillard, E.; Hassoun, J.; Park, J.-B.; Lee, Y.-J.; Sun, Y.-K.; Passerini, S.; Scrosati, B. The Lithium/Air Battery: Still an Emerging System or a Practical Reality? *Adv. Mater.* **2015**, *27* (5), 784–800.

almacenamiento de energía eléctrica es una de las áreas más prometedoras. Los líquidos iónicos han sido utilizados en diversas aplicaciones electroquímicas como resultado de su alta conductividad iónica y su amplio potencial electroquímico.[431] No obstante, desde el punto de su aplicación como electrolitos, cualquier electrolito líquido siempre tiene el riesgo potencial de fugas, aunque en el caso de los ILs las fugas por evaporación se minimicen.[432]

Para evitar estos inconvenientes se pueden utilizar materiales poliméricos basados o modificados con unidades de líquidos iónicos, como los SILLPs y los PILs. Como bien se ha descrito en secciones anteriores, estos materiales conservan la mayoría de las propiedades de los ILs, a la vez que están dotados de nuevas características. Debemos resaltar en esta sección que su uso proporciona una seguridad mejorada, reduciendo muy notablemente el riesgo de fugas, pero también una mayor flexibilidad mecánica y de diseño.[433] Además, dadas las posibilidades casi infinitas de combinación de cationes y aniones, es posible modular la estructura y comportamiento del SILLP o PIL para generar sistemas de electrolitos que, idealmente, proporcionen un rendimiento electroquímico indefinido.[434,435]

En este contexto, en el grupo de Química Sostenible y Supramolecular se han desarrollado de forma exitosa materiales iónicos conductores basados en la inmovilización de líquidos iónicos derivados de imidazolio en matrices

[431] Bideau, J. L.; Viau, L.; Vioux, A. Ionogels, Ionic Liquid Based Hybrid Materials. *Chem. Soc. Rev.* **2011**, *40* (2), 907–925.
[432] Maršavelski, A.; Smrečki, V.; Vianello, R.; Žinić, M.; Moguš-Milanković, A.; Šantić, A. Supramolecular Ionic-Liquid Gels with High Ionic Conductivity. *Chem. Eur. J.* **2015**, *21* (34), 12121–12128.
[433] Eshetu, G. G.; Mecerreyes, D.; Forsyth, M.; Zhang, H.; Armand, M. Polymeric Ionic Liquids for Lithium-Based Rechargeable Batteries. *Mol. Syst. Des. Eng.* **2019**, *4* (2), 294–309.
[434] Wang, A.; Liu, X.; Wang, S.; Chen, J.; Xu, H.; Xing, Q.; Zhang, L. Polymeric Ionic Liquid Enhanced All-Solid-State Electrolyte Membrane for High-Performance Lithium-Ion Batteries. *Electrochim. Acta.* **2018**, *276*, 184–193.
[435] Lu, F.; Gao, X.; Wu, A.; Sun, N.; Shi, L.; Zheng, L. Lithium-Containing Zwitterionic Poly(Ionic Liquid)s as Polymer Electrolytes for Lithium-Ion Batteries. *J. Phys. Chem. C.* **2017**, *121* (33), 17756–17763.

poliméricas mediante una unión covalente (SILLPs).[436,437] Estos materiales han mostrado tener la capacidad de conducir iones a través de una red polimérica altamente entrecruzada, pero al tratarse de sólidos la conductividad se reduce en comparación con los sistemas análogos es estado líquido. Desarrollar materiales sólidos o semisólidos a base de ILs que tengan una alta conductividad puede tener un impacto directo en el avance tecnológico de dispositivos electroquímicos,[432] capacitores,[438] celdas solares[439] y baterías de iones de litio.[440,441]

Una forma de conservar la alta conductividad de los ILs es mediante la formación de ionogeles. En este caso el IL se inmoviliza de tal forma que el componente líquido queda atrapado dentro de una matriz gelante.[432] El ionogel, también denominado gel iónico o gel de líquido iónico, es un material híbrido en el que el IL está confinado como fase dispersa o líquida en una fase sólida.[442,443]Los ionogeles se pueden preparar de diferentes formas mediante el uso de gelantes supramoleculares de bajo peso molecular, partículas inorgánicas o polímeros.[431] Los ILs incorporados en el ionogel actúan como plastificantes y como portadores de carga, por lo que mejoran la conductividad iónica, exhiben una alta

[436] Garcia-Bernabé, A.; Compañ, V.; Burguete, M. I.; García-Verdugo, E.; Karbass, N.; Luis, S. V.; Riande, E. Conductivity and Polarization Processes in Highly Cross-Linked Supported Ionic Liquid-Like Phases. *J. Phys. Chem. C.* **2010**, *114* (15), 7030–7037.
[437] García-Bernabé, A.; Rivera, A.; Granados, A.; Luis, S. V.; Compañ, V. Ionic Transport on Composite Polymers Containing Covalently Attached and Absorbed Ionic Liquid Fragments. *Electrochim. Acta.* **2016**, *213*, 887–897.
[438] Martins, V. L.; Torresi, R. M.; Rennie, A. J. R. Design Considerations for Ionic Liquid Based Electrochemical Double Layer Capacitors. *Electrochim. Acta.* **2018**, *270*, 453–460.
[439] Lee, C.-P.; Ho, K.-C. Poly(Ionic Liquid)s for Dye-Sensitized Solar Cells: A Mini-Review. *Eur. Polym. J.* **2018**, *108*, 420–428.
[440] Balducci, A. Ionic Liquids in Lithium-Ion Batteries. *Top. Curr. Chem. (Z).* **2017**, *375* (2), 20.
[441] Vélez, J. F.; Vazquez-Santos, M. B.; Amarilla, J. M.; Tartaj, P.; Herradón, B.; Mann, E.; del Río, C.; Morales, E. Asymmetrical Imidazolium-Trialkylammonium Room Temperature Dicationic Ionic Liquid Electrolytes for Li-Ion Batteries. *Electrochim. Acta.* **2018**, *280*, 171–180.
[442] Néouze, M.-A.; Le Bideau, J.; Gaveau, P.; Bellayer, S.; Vioux, A. Ionogels, New Materials Arising from the Confinement of Ionic Liquids within Silica-Derived Networks. *Chem. Mater.* **2006**, *18* (17), 3931–3936.
[443] Osada, I.; de Vries, H.; Scrosati, B.; Passerini, S. Ionic-Liquid-Based Polymer Electrolytes for Battery Applications. *Angew. Chem. Int. Ed.* **2016**, *55* (2), 500–513.

flexibilidad mecánica y proporcionan un mejor contacto entre electrodos y electrolitos respecto a sus homólogos completamente sólidos.[427,444]

En comparación a los electrolitos de gel convencionales que contienen disolventes orgánicos volátiles, estos ionogeles pueden usarse a temperaturas elevadas, debido a la baja presión de vapor, la no inflamabilidad y la alta estabilidad térmica de los ILs. Además, son menos viscosos que los ILs puros debido a la difusión del catión metálico (por ejemplo litio) a través de los canales del gel y su flexibilidad otorga más oportunidades de diseño de la celda.[427, 445]

[444] Marr, P. C.; Marr, A. C. Ionic Liquid Gel Materials: Applications in Green and Sustainable Chemistry. *Green Chem.* **2015**, *18* (1), 105–128

[445] Yoshizawa, M.; Narita, A.; Ohno, H. Design of Ionic Liquids for Electrochemical Applications. *Aust. J. Chem.* **2004**, *57* (2), 139–144.


R'
R''
+

CAPÍTULO II

Objetivos

Capítulo II. Objetivos

2.1. Objetivo General

El objetivo general de la presente tesis Doctoral es el diseño y aplicación, en diferentes campos de la Química e Ingeniería Sostenible, de materiales poliméricos avanzados multifuncionales. El diseño de éstos se enmarca bajo las siguientes consideraciones: i) los materiales están basados en polímeros entrecruzados que presenten en su estructura unidades moleculares similares a las de los líquidos iónicos como funcionalización principal y ii) las metodologías a desarrollar deben de ser sencillas, en la medida de lo posible, con el fin de que puedan ser desarrolladas, después de mi reincorporación, en la UNED de Costa Rica.

2.2. Objetivos Específicos

Para este trabajo los objetivos específicos propuestos son los siguientes:

1. Desarrollar metodologías que permitan la síntesis y evaluación de nuevos materiales avanzados que contengan diferentes unidades que puedan actuar como medio de transporte de iones libres mediante la síntesis de líquidos iónicos poliméricos de tipo ionogel derivados de estructuras de imidazolio con sales zwitterionicas sulfonadas e iones de litio confinados en la matriz polimérica.

2. Diseñar, obtener y caracterizar nuevos compuestos poliméricos que contengan la amino-homocisteína tiolactona como grupo funcional principal. La presencia de este grupo permite, a través de la reacción de aminólisis del anillo de tiolactona y la posterior funcionalización del -SH generado *in situ* mediante reacciones de tipo *click* tiol-eno, la obtención de materiales avanzados con

diferentes niveles de funcionalización y morfologías, que se pueden ajustar en función de las aplicaciones potenciales de dichos materiales.

3. Optimizar la generación de membranas poliméricas obtenidas a partir de PILs/PVP utilizando la técnica de electrohilado, así como el desarrollo de metodologías que permitan llevar a cabo post-modificaciones químicas de dichas membranas con el fin de evaluar los efectos de estas modificaciones en su morfología estructural y sus posibles aplicaciones.

4. Sintetizar y caracterizar líquidos iónicos soportados covalentemente, los cuales hemos denominado SILLPs (*Supported Ionic Liquid-like Phases*) sobre diferentes tipos de resinas poliméricas mediante la introducción de subunidades funcionales de grupos alquil-imidazolio.

5. Evaluar el potencial de las propiedades modulables en los SILLPs de dichas unidades, para gestionar la inmovilización y el comportamiento de diferentes unidades catalíticas. Esto debe permitir el obtener sistemas avanzados donde el soporte polimérico no sea "inocente", ejerciendo un papel activo a la hora de ajustar e incrementar la eficiencia catalítica de estos sistemas en términos de actividad, estabilidad y selectividad.

6. Implementar el uso de técnicas de fabricación aditivas como la impresión 3D para el diseño y preparación de materiales con arquitecturas tridimensionales complejas basados en SILLPs, con el fin de obtener materiales 3D que presenten a nivel molecular propiedades análogas a las de los líquidos iónicos en fase homogénea.

7. Desarrollar transformaciones catalíticas basadas en materiales funcionalizados para llevar a cabo procesos sintéticos sencillos que permitan obtener, de forma discontinua o continua, los productos puros con total recuperación y reutilización de todos los elementos del sistema.

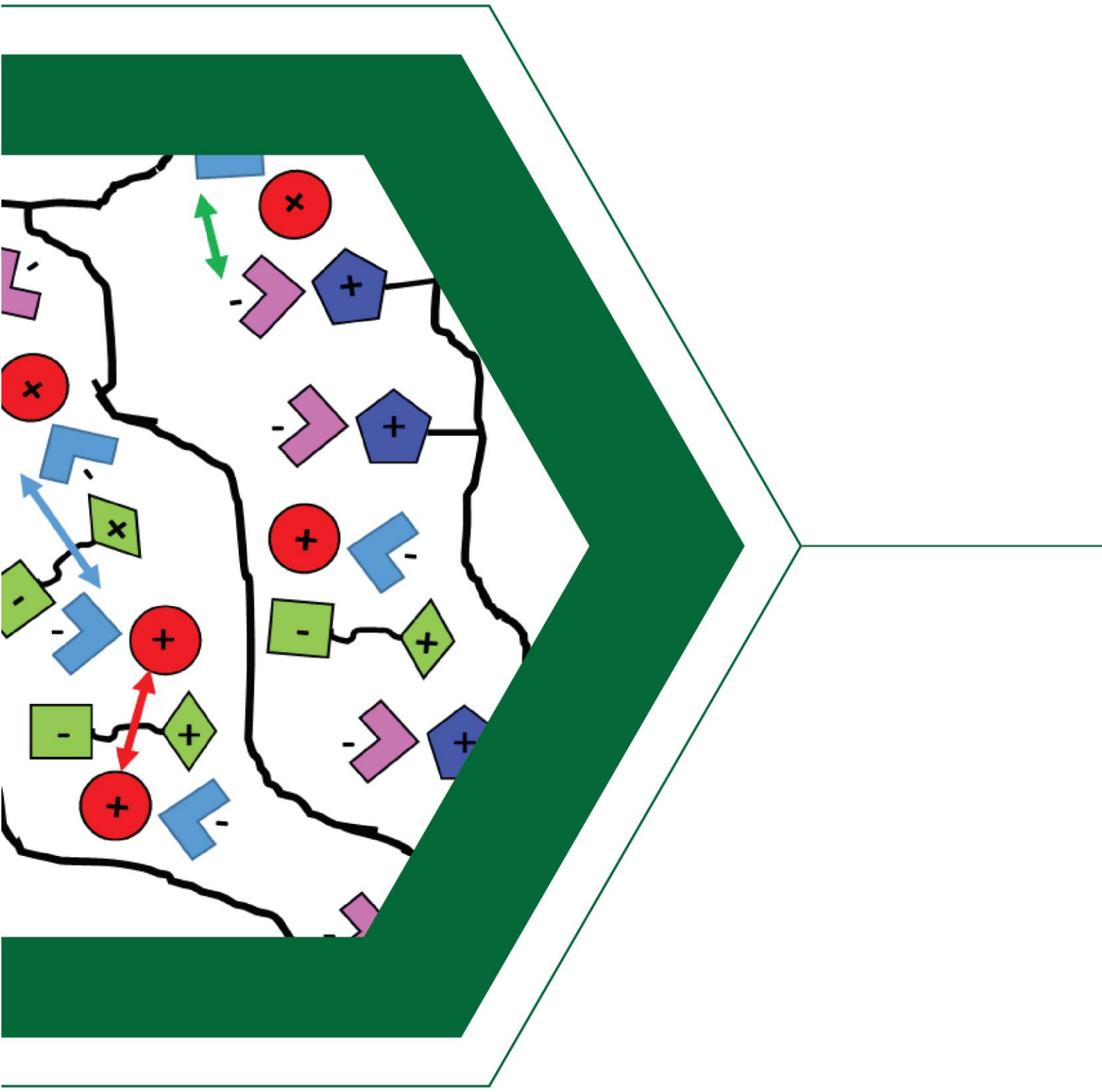

CAPÍTULO III

Difusividad de iones libres y concentración de carga en membranas de líquidos iónicos poliméricos entrecruzados tipo ionogel basados en sales zwitterionicas sulfonadas e iones Litio

Resumen. Las propiedades de una variedad de mezclas de líquidos iónicos zwiterionicos (**ZIs-1**) y $LiNTf_2$, incluyendo su conductividad, han sido estudiadas mostrando cómo se pueden ajustar a través de su composición molar. La conductividad tiende aumentar con el contenido de $LiNTf_2$, pero, sin embargo, presenta un mínimo en la región cercana al punto eutéctico. Estas mezclas también proporcionan excelentes propiedades para su uso como fases líquidas en la preparación de materiales compuestos basados en PILs entrecruzados. Las membranas preparadas muestran excelentes propiedades ajustables como materiales conductores, con conductivades que pueden ser mayores que 10^{-2} S cm^{-1} por encima de los 100 °C. Las composiciones poliméricas seleccionadas muestran muy buenas propiedades mecánicas y estabilidad térmica, incluso para bajos grados de entrecruzamiento, junto con una flexibilidad adecuada y buena transparencia. Las propiedades finales de las membranas se correlacionan con la composición monomérica utilizada y con la mezcla de **ZIs-1**:$LiNTf_2$.

Chapter III. Free ion diffusivity and charge concentration on cross-linked Polymeric Ionic Liquid iongels films based on sulfonated zwitterion salts and Lithium ions

Abstract. The properties of a variety mixtures of a zwitterionic ionic liquid (**ZIs-1**) and $LiNTf_2$, including their conductivity, have been studied showing how they can be adjusted through their molar composition. Conductivity tends to increase with the $LiNTf_2$ content although presents a minimum at the region close to the eutectic point. These mixtures also provide excellent features as liquid phases for the preparation of composite materials based on crosslinked PILs. The prepared films display excellent and tuneable properties as conducting materials, with conductivities that can be higher than 10^{-2} S cm^{-1} above 100 ^{o}C. The selected polymeric compositions show very good mechanical properties and thermal stability, even for low crosslinking degrees, along with a proper flexibility and good transparency. Final properties of the films correlate with the composition of the monomeric mixture used and with that of the **ZIs-1**:$LiNTf_2$ mixture.

Keywords: Zwitterionic ionic liquid sen conductivity • Polymeric Ionic Liquids • iongel.

3.1. Introduction

Lithium ion batteries have been considered as an attractive power source for a variety of wide applications such as consumer electronics, electric vehicles and energy storage systems.[1] Although these devices display good performance, polymer electrolytes are being explored as replacements for liquid electrolytes since they can maintain high ionic conductivities and good mechanical strengths without the risk of leakage and provide a larger operative temperature range.[2,3] Among these polymeric electrolytes, polymeric ionic liquids (PILs) have gained attention due to their interesting physical features in terms of their excellent thermal and chemical stability

[1] Etacheri, V.; Marom, R.; Elazari, R.; Salitra, G.; Aurbach, D. Challenges in the Development of Advanced Li-Ion Batteries: A Review. *Energy Environ. Sci.* **2011**, *4* (9), 3243–3262.
[2] Arya, A.; Sharma, A. L. Polymer Electrolytes for Lithium Ion Batteries: A Critical Study. *Ionics.* **2017**, *23* (3), 497–540.
[3] Kalhoff, J.; Eshetu, G. G.; Bresser, D.; Passerini, S. Safer Electrolytes for Lithium-Ion Batteries: State of the Art and Perspectives. *ChemSusChem.* **2015**, *8* (13), 2154–2175.

and ionic transport properties.[4] Nevertheless, the performance of PIL-based lithium ion batteries still needs to be improved in order to be fully competitive with those based on conventional systems.[5] In general, PILs show low conductivity values (~10^{-6} S cm^{-1}) as a result of the low mobility of the ionic moiety and have to be doped with ILs to form "ion-gels".[6] Since bulk ILs have high ion densities and high mobility of their component ions, they also provide a high ionic conductivity.[7,8] A particular class of ILs is that of *Zwitterionic ionic salts* (ZIs), having the cation and anion tethered in the same molecular structure.[9] ZIs do not display net charge and do not migrate even under a gradient of potential. ZIs can also interact with Li^+ or H^+ cations to obtain mixed molten salts. For instance, the addition of lithium bis(trifluoromethylsulfonyl)amide ($LiNTf_2$) or 1,1,1-trifluoro-N-(trifluoromethyl sulfonyl) methane sulfonamide ($HNTf_2$) to ZIs results in room temperature liquids due to the effects of the NTf_2^- anion.[10,11] Therefore, they are a good candidate to be used in combination with PILs to prepare advanced composite materials with potential applications in electrochemical devices such as lithium batteries or fuel cells

[4] Eftekhari, A.; Liu, Y.; Chen, P. Different Roles of Ionic Liquids in Lithium Batteries. *J. Power Sourc.* **2016**, *334*, 221–239.
[5] Osada, I.; de Vries, H.; Scrosati, B.; Passerini, S. Ionic-Liquid-Based Polymer Electrolytes for Battery Applications. *Angew. Chem. Int. Ed.* **2016**, *55* (2), 500–513.
[6] Shaplov, A. S.; Marcilla, R.; Mecerreyes, D. Recent Advances in Innovative Polymer Electrolytes Based on Poly(Ionic Liquid)s. *Electrochim. Acta* **2015**, *175*, 18–34.
[7] Yoshizawa, M.; Hirao, M.; Ito-Akita, K.; Ohno, H. Ion Conduction in Zwitterionic-Type Moltensalts and their Polymers. *J. Mater. Chem.* **2001**, *11* (4), 1057–1062.
[8] Watanabe, M.; Thomas, M. L.; Zhang, S.; Ueno, K.; Yasuda, T.; Dokko, K. Application of Ionic Liquids to Energy Storage and Conversion Materials and Devices. *Chem. Rev.* **2017**, *117* (10), 7190–7239.
[9] Yoshizawa, M.; Narita, A.; Ohno, H. Design of Ionic Liquids for Electrochemical Applications. *Aust. J. Chem.* **2004**, *57* (2), 139–144.
[10] Yoshizawa, M.; Ohno, H. Anhydrous Proton Transport System Based on Zwitterionic Liquid and HTFSI. *Chem. Commun.* **2004**, No. 16, 1828–1829.
[11] Yoshizawa-Fujita, M.; Tamura, T.; Takeoka, Y.; Rikukawa, M. Low-Melting Zwitterion: Effect of Oxyethylene Units on Thermal Properties and Conductivity. *Chem. Commun.* **2011**, *47* (8), 2345–2347.

In this paper, we demonstrated that different mixtures based on 3-(1-butyl-1H-imidazol-3-ium-3-yl)propane-1-sulfonate and $LiNTf_2$ mixtures can be used to develop stable "ion-gels" in PILs based on 1-methyl(-4-vynilbenzene)-3-butylimidazolium bis(trifluoromethylsulfonyl)imide (**IL-1**) and an appropriate crosslinking agent. The resulting films were analysed and characterised by impedance spectroscopy, DSC, TGA, ATR-FTIR and FT-Raman. The conductivity of the resulting films has been fully discussed and the free ion diffusivity and free ion charge density calculated and compared following two different procedures.

3.2. Results and Discussion

The zwitterionic salt **ZIs-1** (3-(1-butyl-1H-imidazol-3-ium-3-yl)propane-1-sulfonate) was obtained as previously reported by reaction of butylimidazole with 1,3-propanesultone as a white solid of high melting point (T_m = 170 ^oC, Figure SI.1).[7,9,10] Mixtures of this **ZIs-1** with different molar ratios of $LiNTf_2$ (Table 1) were obtained by solving both components in methanol, evaporation of the solvent and thorough vacuum drying or, better, they were prepared by mixing **ZIs-1** and $LiNTf_2$ in the solid state, in the ratios shown in Table 1, and heating the resulting mixture above the melting point of the . mixture. Both methods provided ZIs with identical properties, but the preparation in the absence of solvent was preferred, for simplicity, for large scale preparation, avoiding the need of removing residual solvent molecules. In any case, all the samples were thoroughly dried at high temperature (> 120 ^oC) at high vacuum. Properties discussed below correspond to mixtures prepared using this protocol. In all cases, the measures taken were fully reproducible for samples from the same or from different batches. Mixtures containing a larger molar mass of $LiNTf_2$ (x_{LiNTf2} ≥ 0.3, from **M-1a** to **M-1d** and **M-1g**) were liquid at r.t., while those rich in

the zwitterion salt ($x_{ZIs\text{-}1}$ > 0.7, **M-1e** and **M-1f**) were liquid-solid mixtures (Figure SI.2a).

Table 1. Composition of the mixtures based on **ZIs-1** and $LiNTf_2$.

Entry	M-1	Molar ratio[a]	$X_{ZIs\text{-}1}$	X_{LiNTf2}	State[b]	T_m [c]
1	**M-1a**	1:2	0.33	0.67	l	2
2	**M-1b**	1:3	0.25	0.75	l	9
3	**M-1c**	1:5	0.17	0.83	l	23
4	**M-1d**	2:1	0.67	0.33	l	16
5	**M-1e**	3:1	0.75	0.25	l-s	16
6	**M-1f**	5:1	0.83	0.17	l-s	16
7 [d]	**M-1g**	1:1	0.5	0.5	l	5

[a] Molar ratio **ZIs-1**:$LiNTf_2$. [b] Solid (s) or liquid (l) state observed after drying under high vacuum till constant weight. [c] Calculated from the second cycle in DSC. [d] For the preparation and study of this mixture see ref. 11.

These mixtures were also analysed by DSC and TGA (Figures SI.3 and SI.4). DSC analysis confirmed the formation of a molten salt domain due to the plastic effect of the NTf_2 anion, with melting temperatures lower than the ones for the individual components. Mixtures **M-1a, M-1b, M-1c**, **M-1d** and **M-1g** ($x_{LiNTf2} \geq 0.3$) showed melting temperatures lower than room temperature (Table 1 and Figure SI.3). Noteworthy the mixtures having a larger molar amount of **ZIs-1** and l-s original appearance (**M-1e** and **M-1f**) became also liquid at room temperature after heating at 240 °C. Indeed, the second DSC heating cycle of the mixtures showed only T_g values lower than 25 °C (Figure S3). TGA experiments also showed that **M-1e** and **M-1f** ($x_{ZIs\text{-}1}$ > 0.7) decomposed at similar temperatures than **ZIs-1** (*ca.* 320 °C), while mixtures with a larger amount of $LiNTf_2$ ($x_{LiNTf2} \geq 0.5$) were stable up to *ca.* 360 °C. Both DSC and TGA confirmed the absence of adsorbed water or solvent molecules.

The ^{1}H-NMR spectra of the mixtures in either CD_3OD or CD_3SOCD_3 did not show any significant shift for the signals characteristics of **ZIs-1** (Figure SI.2b) discarding the presence, in solution, of strong discrete interactions between the two components in solution. Noteworthy, however, the ATR-FTIR and Raman spectra of these mixtures provided important information on the nature of the interactions, in the pure mixtures, between **ZIs-1** and $LiNTf_2$.[12] Figure 1 shows some selected regions of the spectra for **ZIs-1** and different **ZIs-1**:$LiNTf_2$ mixtures. Additional ATR-FT-IR data for the as-prepared mixtures and for the equimolecular mixture (**M-1g**) and the individual compounds (**ZIs-1** and $LiNTf_2$) have been included in the ESI (Figures. SI.5, SI.15 and SI.16). The peak assignable to the S-N-S asymmetric and symmetric stretching of the NTf_2, which appeared at 747 cm^{-1} at the lithium salt, was shifted in the mixture to lower wavenumbers (up to 740 cm^{-1}) suggesting a weaker interaction of Li^+ with this anion due to its additional coordination with the zwitterion.

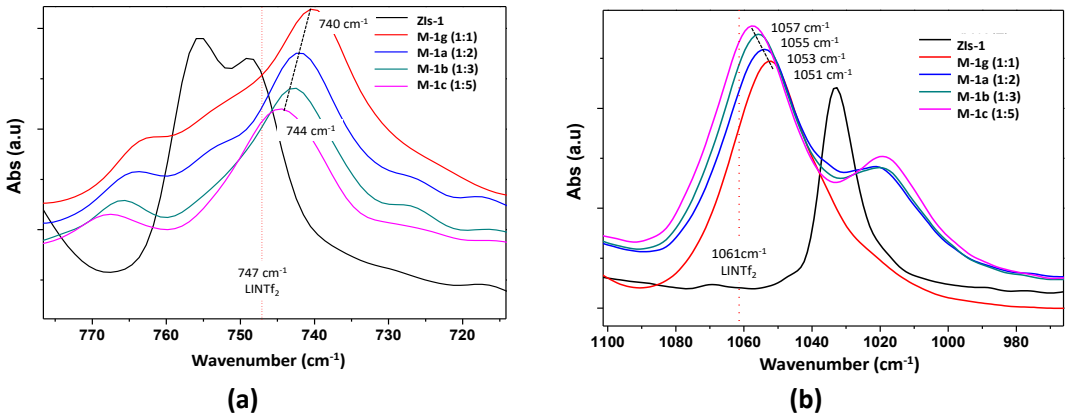

Figure 1. Selected regions of the ATR-FT-IR spectra of **ZIs-1** and **ZIs**:$LiNTf_2$ molar mixtures. The red line indicates the characteristic peak found for pure $LiNTf_2$.

[12] Paschoal, V. H.; Faria, L. F. O.; Ribeiro, M. C. C. Vibrational Spectroscopy of Ionic Liquids. *Chem. Rev.* **2017**, *117* (10), 7053–7112.

Indeed, the well-defined peaks assignable to the S-O stretching for **ZIs-1** at 755 and 749 cm^{-1} appeared in the mixture as broader signals shifted to higher frequencies. In a similar way, the strong band associated with the stretching vibration of the C-F group at 1061 cm^{-1} for $LiNTf_2$ was shifted to 1052 cm^{-1} in the mixture. The observed shifts are a function of the composition of the **ZIs-1**:$LiNTf_2$ mixture. Thus, for an increase from 0.5 to 0.83 in the molar fraction of $LiNTf_2$ the peak related to the S-N-S stretching shifts from 740 cm^{-1} to 744 cm^{-1} and the symmetrical stretching peak of the $–SO_2$-N-SO_2- from 1051 to 1057 cm^{-1}. Similar trends were found when the mixtures were analysed by Raman spectroscopy. The characteristic peak assignable to S-N-S stretching always appeared at lower wavenumbers in the mixtures, from 745 to 742 cm^{-1} as a function of the amount of **ZIs-1** (746 cm^{-1} for neat $LiNTf_2$, Figure SI.7). Changes were also observed for the bands of the imidazolium unit associated to the C(4)=C(5) and N(1)−C(2)−N(3) fragments, appearing in the Raman spectra of the mixtures at lower frequencies and as broader signals (*i.e.* 1445 cm^{-1} and 1419 cm^{-1} for **M-1a** in comparison with 1456 cm^{-1} and 1425 cm^{-1} for **ZIs-1**, see Figure SI.8). Similarly, the well-defined strong peak at 1561 cm^{-1} of **ZIs-1** shifts to 1565 cm^{-1} in **M-1a** experiencing a significant broadening and reduction of peak intensity. A related effect was also observed for the peaks appearing in the 1490-1380 cm^{-1} range, also attributed to imidazole ring vibrations. This clearly indicates a weakening of intramolecular interactions at the zwitterionic salt in the presence of $LiNTf_2$.[13]

A similar trend was also observed for the band at ~1250 cm^{-1} ascribed to the (S-O) stretching vibration (Figure SI.8). The peak shifts from 1242 cm^{-1} in bulk $LiNTf_2$ to lower frequencies with the presence of **ZIs-1** (1241, 1240 and 1239 cm^{-1} for **M-1c**, **M-1b** and **M-1a**, respectively). All these data

[13] Narita, A.; Shibayama, W.; Ohno, H. Structural Factors to Improve Physico-Chemical Properties of Zwitterions as Ion Conductive Matrices. *J. Mater. Chem.* **2006**, *16* (15), 1475–1482.

suggest that in the mixtures the lithium cation is less coordinated to the NTf_2 anions.

The ionic conductivity of mixtures **M-1a, M-1b, M-1c**, **M-1d** and **M-1g** ($x_{LiNTf2} \geq 0.33$) was measured (Figure 2). The measurement of the other mixtures was precluded as they were not fully liquid at room temperature. It is worth noting that the ionic conductivity of the pure zwitterionic salt (**ZIs-1**) was very low (below 10^{-8} S cm^{-2}),[14] while conductivities found for the mixtures were in the 10^{-2} to 10^{-6} S cm^{-1} range depending on the temperature and composition. The slightly convex curve observed in these plots for all the composites studied suggests that the ion conductive process can be expressed by the Vogel-Fulcher-Tamman (VFT) equation, describing the temperature dependence of viscosity in amorphous materials. Regarding the dependence with the composition (Figure SI.6), the equimolecular mixture (**M-1g**) led to the lowest conductivity, while the **ZIs-1**:$LiNTf_2$ mixture displaying a 1:5 molecular ratio (**M-1c**, $x_{LiNTf2} = 0.83$) provided the highest conductivities for the temperatures assayed (*e.g.* 1.6 10^{-3}, 1.4 10^{-2} and 2.3 10^{-2} at 20, 80 and 100 ^{o}C, respectively). As the **M-1d** mixture ($x_{LiNTf2} = 0.33$) displayed always a conductivity higher than **M-1g**, it is clear that the concentration of $LiNTf_2$ is not the only factor determining the conductivity.

[14] Ohno, H.; Yoshizawa-Fujita, M.; Kohno, Y. Design and Properties of Functional Zwitterions Derived from Ionic Liquids. *Phys. Chem. Chem. Phys.* **2018**, *20* (16), 10978–10991.

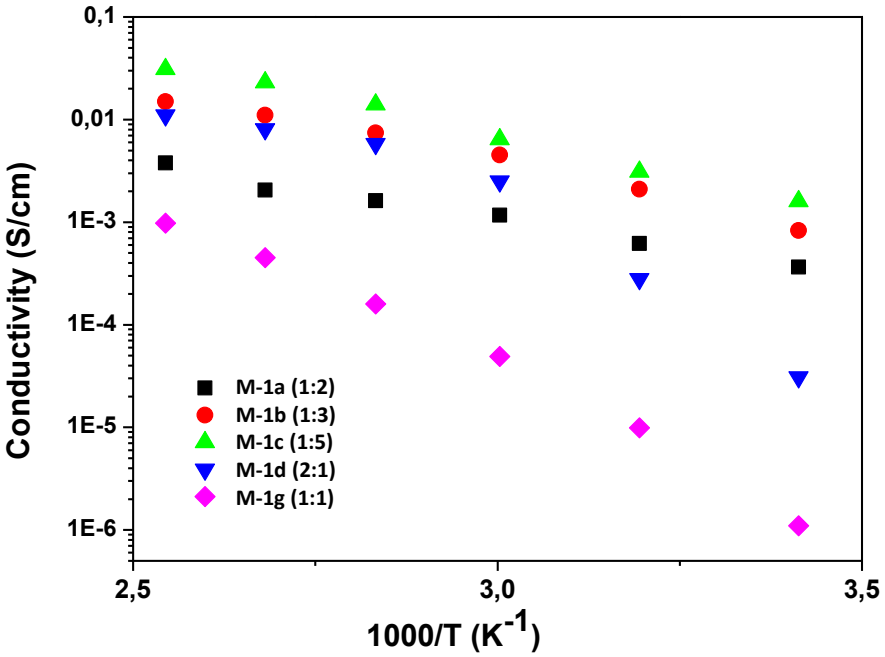

Figure 2. Ionic conductivity of the different **ZIs-1**:$LiNTf_2$ mixtures as a function of the temperature.

These differences on conductivity with the composition can be explained considering the concentration of the mobile ions and their mobility associated to the strength of the interactions between the species present in the mixtures and revealed by ATR-FTIR and Raman spectroscopy, as discussed above. In this context, physical properties like viscosity also relate to intermolecular and interionic interactions. At 25 ºC the viscosity increased with the $LiNTf_2$ content, except for the region close to the eutectic point for x_{LiNTf2} = 0.67, where a minimum in viscosity is detected, following the expected trend for a eutectic mixture (Figure SI.6b). The measured viscosities were 123, 500, 49, 1090 and 2955 Pa·s for **M-1d**, **M-1g**, **M-1a**, **M-1b** and **M-1c**, respectively. At 100 ºC variations in viscosity are minimal, displaying values characteristic of non-viscous fluids, with the minimum value reached again at the eutectic point. Data presented in Figure SI.6 show that conductivity also does not follow the expected trend of increasing conductivity when reducing viscosity. Instead, a constant

increase in conductivity is observed for the higher $LiNTf_2$ contents (above the eutectic point) as a function of the concentration of the carrier, suggesting that near the eutectic point specific intermolecular interactions are present developing discrete supramolecular clusters (neutral net charge) that reduce ion mobility in spite of a reduced viscosity.

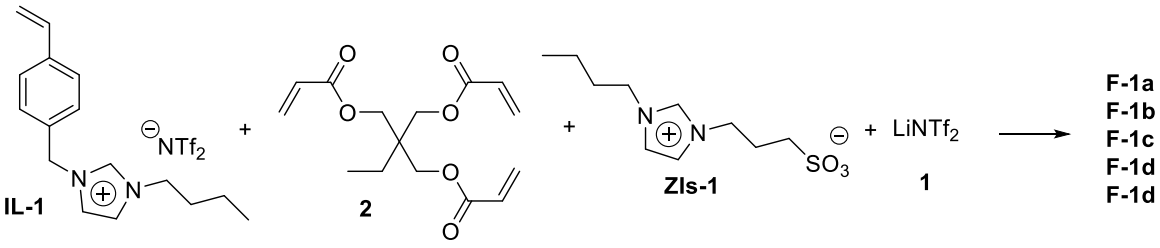

Scheme 1. Chemical composition of the films.

Cross-linked Polymeric Ionic Liquid ion-gel films

In the light of the excellent and tuneable conductivities achieved with the former mixtures composed by **ZIs-1** and $LiNTf_2$, a series of crosslinked polymeric films were prepared based on the mixtures displaying higher conductivities (and the equimolar mixture **M-1g**). This was carried out by polymerization of a crosslinking monomer (trimethylolpropane trimethacrylate, TMPTMA, **2**) and an ionic liquid monomer (**IL-1**) in the presence of the **ZIs-1**:$LiNTf_2$ mixtures (Scheme 1). Best results were obtained for the compositions shown in Table 2, providing mechanically stable and transparent films able to efficiently entrap the **ZIs-1**:$LiNTf_2$ mixtures inside the polymeric matrix without any sign of leaching even after several months of storage.[15,16] In these films, around 50% of the weight

[15] García-Bernabé, A.; Rivera, A.; Granados, A.; Luis, S. V.; Compañ, V. Ionic Transport on Composite Polymers Containing Covalently Attached and Absorbed Ionic Liquid Fragments. *Electrochim. Acta.* **2016**, *213*, 887–897.

[16] Altava, B.; Compañ, V.; Andrio, A.; del Castillo, L. F.; Mollá, S.; Burguete, M. I.; García-Verdugo, E.; Luis, S. V. Conductive Films Based on Composite Polymers Containing Ionic Liquids Absorbed on Crosslinked Polymeric Ionic-like Liquids (SILLPs). *Polymer.* **2015**, *72*, 69–81.

corresponds to the polymeric matrix and the other 50% to the **ZIs-1**:$LiNTf_2$ mixture.

The five transparent, flexible polymeric films could be easily cut into any desired size and shape or be bent with one pair of tweezers, even under dry conditions. In these materials, two different components can contribute to their final conductivity: the ionic liquid fragment attached to the polymeric backbone derived from **IL-1** and the respective **ZIs-1**:$LiNTf_2$ mixture.

Table 2. Films composition[a].

	PILs[a] (wt %)			Molar composition [c]		
Film	**TMPTMA**	**IL-1**	**ZIs-1:$LiNTf_2$ [b]**	X_{IL-1}	X_{ZIs-1}	X_{LiNtf2}
F-1g'	10	90	**M-1g**	0.338	0.357	0.306
F-1g	5	95	**M-1g**	0.339	0.356	0.305
F-1a	5	95	**M-1a**	0.343	0.242	0.415
F-1b	5	95	**M-1b**	0.345	0.183	0.472
F-1c	5	95	**M-1c**	0.349	0.123	0.528

[a] Weight percentage of each monomer in the monomeric mixture. [b] 1:1 weight ratio with the monomeric mixture; for the composition of the **ZIs-1**:$LiNTf_2$ mixtures see Table 1. [c] Molar composition of the final films.

Differential scanning calorimetry (DSC) was used to determine the thermal properties of the obtained films. In the thermograms obtained at 10 K/min, under a nitrogen atmosphere, for the −50 - 275 C range (ESI, Figure SI.9) the non-doped polymeric films did not show any detectable T_g values for this temperature range. In the doped films, the transitions observed at low temperatures (*ca*. 5-20 ^oC) correspond with those for the isolated **ZIs-1**:$LiNTf_2$ mixtures (Figure SI.3). The TGAs of the films revealed their stability up to 350 ^oC (Figure SI.10).

Regarding their conductivity, Figure 3 depicts the dependence of the dc-conductivity of the films doped with **ZIs-1**-$LiNTf_2$ mixtures with the temperature. Arrhenius behaviour was observed for the all composites. The activation energy follows the trend E_{act} (**F-1g'**) > E_{act} (**F-1g**)> E_{act} (**F-1a**) > E_{act} (**F-1b**) > E_{act} (**F-1c**) with the respective values being 22.8 ± 0.4, 21.3 ± 0.5, 19.8 ± 0.5, 19.7 ± 0.6 and 18.8 ± 0.7 kJ/mol.

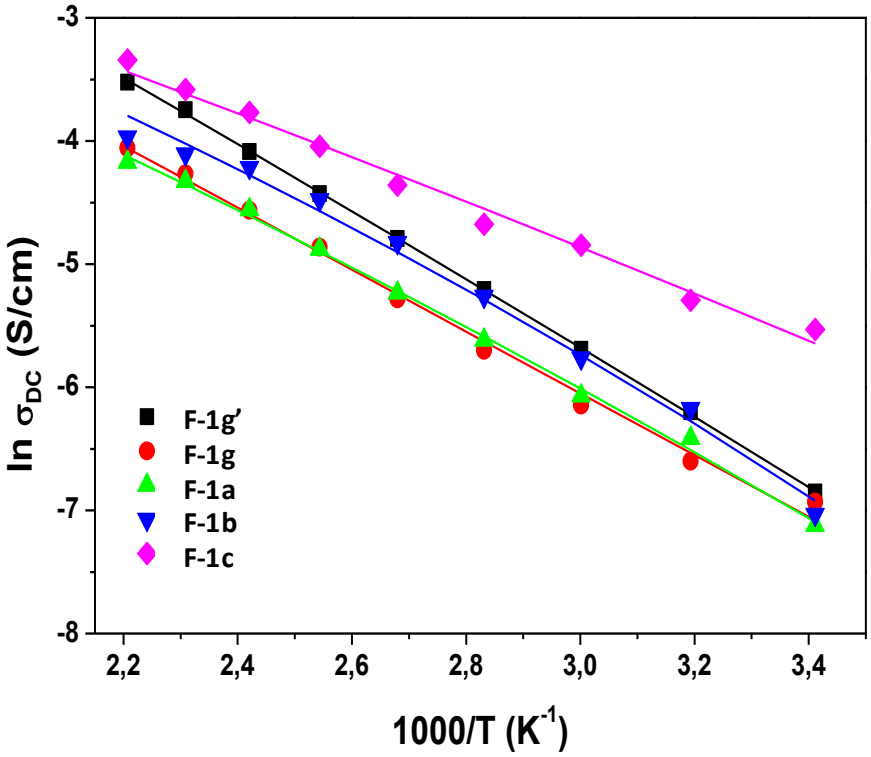

Figure 3. Temperature dependence of the dc-conductivity for the doped films.

The lower activation energy of **F-1g** in comparison with **F-1g'** can be correlated with the higher crosslinking degree of **F-1g'** (10% *vs* 5% of **2**). This is associated simultaneously to a reduced mobility of the polymeric chain and to a decrease in the loading of IL-like fragments covalently attached to the polymeric matrix. For the other films, having the same crosslinking degree, the E_{act} follows a lineal trend with the amount of $LiNTf_2$ (X_{LiNTf2}) present (Figure SI.11). Thus, the conductivity increases

with X_{LiNTf2} following the trend observed in related **ZIs-1**:$LiNTf_2$ mixtures: $\sigma_{(F\text{-}1g)} \approx \sigma_{(F\text{-}1a)} < \sigma_{(F\text{-}1b)} < \sigma_{(F\text{-}1c)}$. The main contribution to the conductivity corresponds to the **ZIs-1**:$LiNTf_2$ mixtures, as the non-doped cross-linked films presented conductivities in the 10^{-5} to 10^{-10} range (**F-2** in Figure SI.12). The conductivity values obtained for the doped films were higher than those reported for related "ion-gel" cross-linked PILs containing either [BMIM][NTf_2] or [BMIM][Cl] (**F-3** and **F-4** in Figure SI.12). Thus, at 80ºC the conductivities were 4.8 x 10^{-3}, 5.1 x 10^{-3}, 7.2 x 10^{-3} and 9.8 x 10^{-3} S/cm for **F-1g**, **F-1a**, **F-1b** and **F-1c** (5.1 × 10^{-4} and 9.0 × 10^{-4} S/cm reported at the same temperature for **F-3** and **F-4**).[16]

ATR-FTIR and Raman spectroscopy provided again valuable information regarding the interaction of the charged ions in the composite materials, displaying similar trends to those observed in the related **ZIs-1**:$LiNTf_2$ mixtures. Thus, in the ATR-FTIR of the films, the symmetrical stretching peaks of the $–SO_2$ and the $–SO_2–N–SO_2–$ groups appearing at 1198 cm^{-1} and 1060 cm^{-1} in neat $LiNTf_2$ were shifted to lower wavenumbers in the films (Figure SI.13). The shift was proportional to the **ZIs-1** content, reaching a frequency of 1178 cm^{-1} for **F-1g**. The characteristic Raman peaks for the NTf_2^- anion, at 1241 and 746 cm^{-1} in the lithium salt, also appeared shifted to lower wavenumbers in the films (Figure SI.14) as a function of the **ZIs-1** content. Overall, the film **F-1c** having the larger loading of $LiNTf_2$ but still less associated ions than $LiNTf_2$ has the higher conductivity.

Diffusivity and ionic charge density

In order to get information about the behaviour of the ionic conductivity and diffusion processes for mobile carriers, electrochemical impedance spectroscopy measurements were performed on the different films.

The electrode polarization (EP) is a phenomenon which takes place always that a conductive sample is sandwiched between two electrodes. It is a consequence of the two interfaces formed between the two faces of the sample and the metallic phase of the electrodes. The polymeric film is a neutral matrix with a permittivity ε and thickness L sandwiched within two parallel plates of equal area. In the presence of an electric field, the free cation tends to accumulate near the negative electrode. The accumulation is limited by the concentration gradient and opposed to the electric force. In the time-dependent ac field, the ions at the interfaces depend on the time constant of the ac field. The application of an alternate electric field with angular frequency ω to a neutral matrix, produces a distribution of the charge into the polymeric matrix with an electrostatic double layer or Debye length LD, given by the expression

$$L_D = \frac{1}{q}\left(\frac{\varepsilon \cdot k_B \cdot T}{n}\right)^{\frac{1}{2}}$$

where n is the charge concentration, kB is the Boltzmann constant, ε the dielectric permittivity of the material and q the charge of a monovalent cation. Following the Coelho model, EP is found to be represented by a Debye relaxation for the characterization of the dielectric permittivity (ε*).[17] When the maximum in ε" corresponding to EP is difficult to separate from the conductivity, the procedure is to obtain the real and imaginary parts of the permittivity and the result is a simple equation for tan δ.[18] The application of the Cole-Cole relaxation for the description of electrode polarization given by eq. (1) can be used.

[17] Coelho, R. On the Static Permittivity of Dipolar and Conductive Media — an Educational Approach. *Non-Cryst. Solids.* **1991**, *131–133*, 1136–1139.

[18] Klein, R. J.; Zhang, S.; Dou, S.; Jones, B. H.; Colby, R. H.; Runt, J. Modeling Electrode Polarization in Dielectric Spectroscopy: Ion Mobility and Mobile Ion Concentration of Single-Ion Polymer Electrolytes. *J. Chem. Phys.* **2006**, *124* (14), 144903.

$$\varepsilon^*_{EP}(\omega) = \varepsilon_\infty + \frac{\Delta\varepsilon_{EP}}{1 + (i\omega\tau_{EP})^\alpha} \quad (1)$$

Where

$$\Delta\varepsilon_{EP} = \varepsilon_{EP,S} - \varepsilon_\infty$$

is the strength of the relaxation, with the static permittivity in the presence of electrode polarization being

$$\varepsilon_{EP,S} = M\varepsilon_\infty,$$

α is a parameter related to the shape of the Cole-Cole relaxation and τ_{EP} is the electrode polarization time relaxation defined as

$$\tau_{EP} = M\tau = \frac{L}{2\mu}\left(\frac{\varepsilon}{nk_BT}\right)^{\frac{1}{2}} \quad (2)$$

being τ the relaxation time defined by

$$\tau = \frac{\varepsilon}{\sigma_{dc}}$$

and M the ratio of the sample thickness to twice the Debye length,

$$M = \frac{L}{2L_D} = \frac{qL}{2}\left(\frac{n}{\varepsilon k_BT}\right)^{1/2}$$

The real and imaginary parts of the Cole-Cole relaxation are respectively

$$\varepsilon'_{EP}(\omega) = \varepsilon_\infty + \frac{\Delta\varepsilon_{EP}\left[1+(\omega\tau_{EP})^\alpha \sin\left[\frac{\pi}{2}(1-\alpha)\right]\right]}{1+(\omega\tau_{EP})^{2\alpha}+2(\omega\tau_{EP})^\alpha \sin\left[\frac{\pi}{2}(1-\alpha)\right]}$$

$$\varepsilon''_{EP}(\omega) = \frac{\Delta\varepsilon_{EP}(\omega\tau_{EP})^\alpha \cos\left[\frac{\pi}{2}(1-\alpha)\right]}{1+(\omega\tau_{EP})^{2\alpha}+2(\omega\tau_{EP})^\alpha \sin\left[\frac{\pi}{2}(1-\alpha)\right]} \qquad (3)$$

These equations can be fitted to the experimental data to provide values for ε, $\Delta\varepsilon_{EP}$, τ_{EP} and α, when the imaginary part shows a peak or shoulder with maximum at $f_{Ep}=1/(2\,\pi\tau_{EP})$.

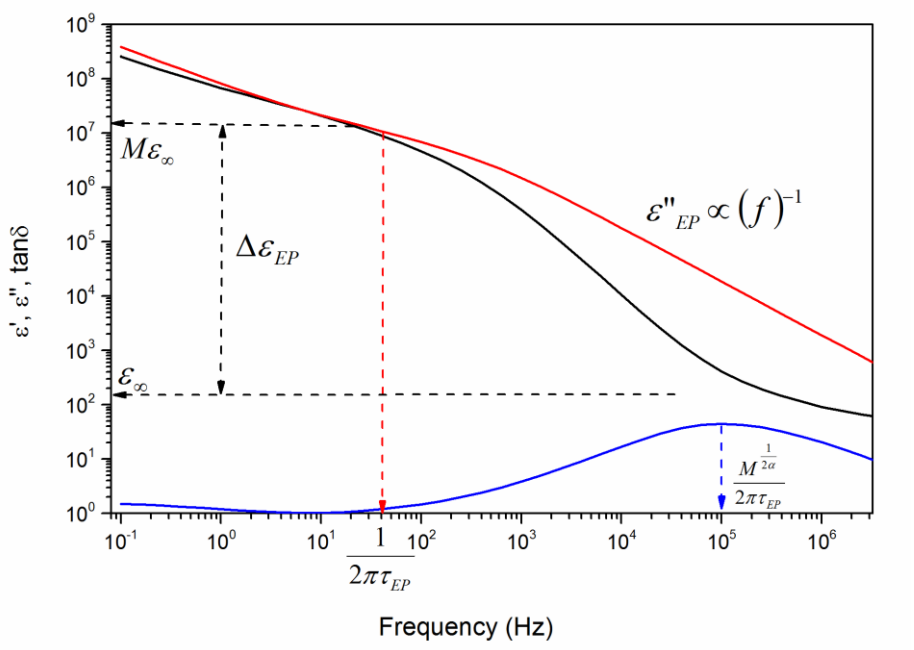

Figure 4. Dielectric permittivity (black), loss permittivity (red) and tan δ (blue) as a function of frequency for **F-1g'** at 20 °C.

When the conductivity term is very important, the imaginary part decreases with frequency increase with a slope close to minus one (-1), and the peak maximum is absent as can be observed in Figure 4 for **F-1g'**. In

these cases, it is advisable to use eq. (3) adding the conductivity term $\sigma_{dc}/(\varepsilon_0\omega)$, in terms of

$$\tan\delta = \frac{\varepsilon''}{\varepsilon'} = \frac{\Delta\varepsilon_{EP}(\omega\tau_{EP})^{\alpha}\cos\left[\frac{\pi}{2}(1-\alpha)\right] + \frac{\sigma_{DC}}{\varepsilon_{vac}\omega}\left\{1+(\omega\tau_{EP})^{2\alpha}+2(\omega\tau_{EP})^{\alpha}\sin\left[\frac{\pi}{2}(1-\alpha)\right]\right\}}{\varepsilon_{\infty}\left\{1+(\omega\tau_{EP})^{2\alpha}+2(\omega\tau_{EP})^{\alpha}\sin\left[\frac{\pi}{2}(1-\alpha)\right]\right\}+\Delta\varepsilon_{EP}\left[1+(\omega\tau_{EP})^{\alpha}\sin\left[\frac{\pi}{2}(1-\alpha)\right]\right]} \quad (4)$$

The contribution of σ_{dc} can be removed for low conductivity values (< 10^{-5} S /cm) and when the maximum peak in tan δ is bigger than 100 Hz.[18] The simplification can be used for very large values of M (M >>1). Under these conditions eq. (4) can be simplified to obtain

$$tan\,\delta = \frac{(\omega\tau_{EP})^{\alpha}\,cos\left[\frac{\pi}{2}(1-\alpha)\right]}{1+\frac{(\omega\tau_{EP})^{2\alpha}}{M}} \quad (5)$$

where the maximum in tan δ is verified for

$$\omega_{max}^{tan\,\delta} = \frac{M^{\frac{1}{2\alpha}}}{\tau_{EP}} = \frac{1}{\tau_m} \quad (6)$$

Where τ_m is the relaxation time associated to the conductivity. It is related with the frequency where tan δ shows a maximum. Notice that If α=1, then eqn (1) is reduced to Coelho model, where EP behavior is represented by a single Debye relaxation, and the eq.(6) is simplified to $\tau_{EP} = \tau_m\sqrt{M}$.

The difference between the Cole-Cole and Debye descriptions is essentially the exponent α, that describes subdiffusion when $\alpha < 1$. This exponent is the manifestation of cumulative processes in the system that are due to interactions among charge carriers. When $\alpha \ll 1$ the interactions are strong, and when $\alpha \lesssim 1$ the interactions do not dominate the transport process.

Taking into account the expression (2) together with M, the ionic mobility can be obtained as

$$\mu = \frac{qL^2}{4M^{1+\frac{1}{2\alpha}}\tau_m k_B T} \qquad (7)$$

Knowing the mobility, the charge concentration is obtained from

$$n = \frac{\sigma_{dc}}{q\mu} = \frac{\sigma_{dc} 4M^{1+\frac{1}{2\alpha}}\tau_m k_B T}{(qL)^2} \qquad (8)$$

And the diffusivity considering to be related to mobility by means of the Nernst-Einstein equation,[19] will be

$$D = \frac{L^2}{4M^{1+\frac{1}{2\alpha}}\tau_m} \qquad (9)$$

We can observe that eq(9) can be also easily obtained from the Macdonald-Trukhan model assuming identical diffusion coefficients for the anion, Da, and cation, Dc, (Da=Dc) where the average free ion diffusivity, D, can be estimated as[19,23,20,24]

$$D = \frac{2\pi}{32} \frac{f_{max}^{tan\,\delta^2} \cdot L^2}{[(tan\,\delta)_{max}]^3} \qquad (10)$$

Finally, the static dielectric permittivity can be easily obtained to give

[19] Bandara, T. M. W. J.; Dissanayake, M. A. K. L.; Albinsson, I.; Mellander, B.-E. Mobile charge carrier concentration and mobility of a polymer electrolyte containing PEO and $Pr_4N^+I^-$ using electrical and dielectric measurements. *Solid State Ionics.* **2011**, *189* (1), 63–68.
[20] Sørensen, T. S.; Compañ, V. Complex Permittivity of a Conducting, Dielectric Layer Containing Arbitrary Binary Nernst–Planck Electrolytes with Applications to Polymer Films and Cellulose Acetate Membranes. *J. Chem. Soc., Faraday Trans.* **1995**, *91* (23), 4235–4250.

$$\varepsilon_{\infty} = \frac{\sigma_{dc}\tau_m}{M^{1-\frac{1}{2\alpha}}\varepsilon_{vac}} \quad (11)$$

Dielectric spectra results

The dielectric analysis of the composite materials considered can be illustrated using the complex permittivity, ε*(ω,T) = ε′ (ω,T) - jε″(ω,T) where ε′ (ω) and ε″(ω) are the real and imaginary parts of the frequency dependent permittivity due to the applied electric field, and j the imaginary unity (j^2 = -1). The relation between the complex dielectric permittivity ε*(ω,T) and the complex conductivity, σ*(ω,T), is given by:

$$\sigma^*(\omega,T) = j\varepsilon_0\omega\varepsilon^*(\omega,T) \quad (12)$$

which can be decomposed in the real and imaginary parts as follows:

$$\sigma' = \varepsilon_0\omega\varepsilon'' \quad (13)$$

$$\sigma'' = \varepsilon_0\omega\varepsilon' \quad (14)$$

where ε_0 represents the vacuum permittivity and ω the angular frequency of the applied electric field ($\omega = 2\pi f$). The conductivity σ´ is characterized by a plateau regime that directly yields the dc conductivity. In this regime σ′(ω) is identical to the bulk dc conductivity σ_{dc} (*i.e.* σ_0). Typical curves showing the variation of the real part of conductivity for the films at different temperatures are shown in Figure 5.

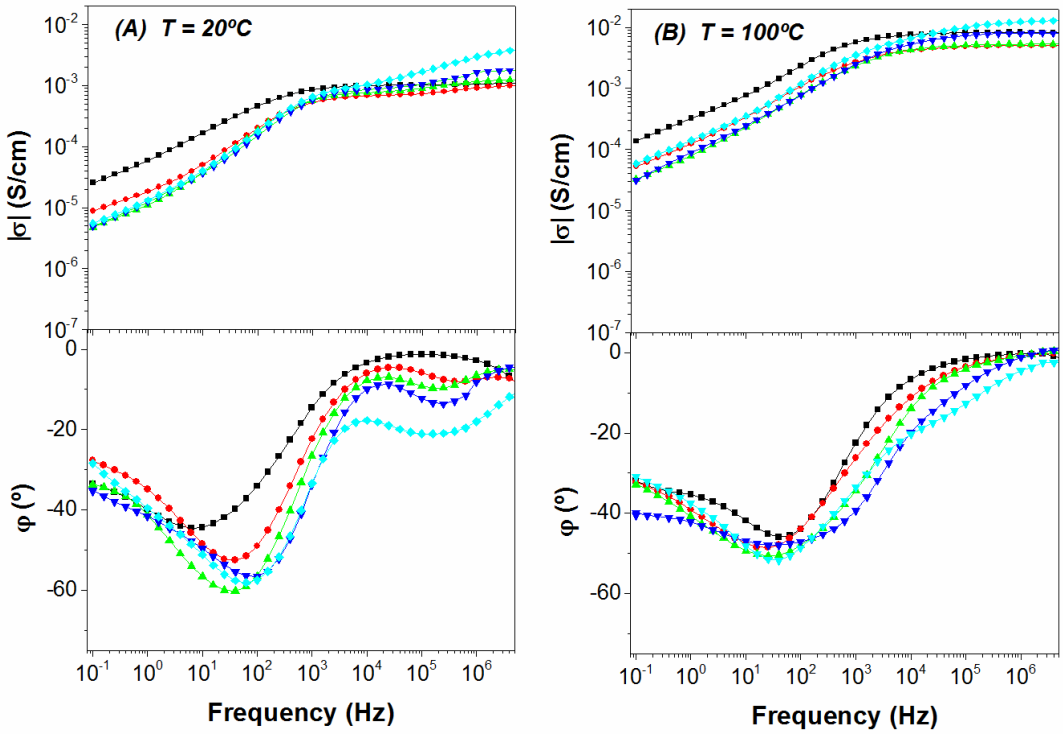

Figure 5. Bode diagrams for films **F-1g'** (black, squares), **F-1g** (red, circles) **F-1a** (green, up triangles), **F-1b** (blue, down triangles), **F-1c** (cyan, diamonds), at 20 and 100 ºC. The conductivity and phase angle scales are the same in both temperatures for better comparison.

In these graphics three different regions can be identified. The region at low frequencies, where the electrode polarization (EP) effect produced by mobile charge accumulation from blocking electrodes is present,[21,22,23,24,25] the region where the dc-conductivity is dominant and will be determined

[21] Choi, U. H.; Mittal, A.; Price, T. L.; Gibson, H. W.; Runt, J.; Colby, R. H. Polymerized Ionic Liquids with Enhanced Static Dielectric Constants. *Macromolecules*. **2013**, *46* (3), 1175–1186.
[22] Serghei, A.; Tress, M.; Sangoro, J. R.; Kremer, F. Electrode Polarization and Charge Transport at Solid Interfaces. *Phys. Rev. B* **2009**, *80* (18), 184301.
[23] Sørensen, T. S.; Compañ, V.; Diaz-Calleja, R. Complex Permittivity of a Film of Poly[4-(Acryloxy)Phenyl-(4-Chlorophenyl)Methanone] Containing Free Ion Impurities and the Separation of the Contributions from Interfacial Polarization, Maxwell–Wagner–Sillars Effects and Dielectric Relaxations of the Polymer Chains. *J. Chem. Soc., Faraday Trans.* **1996**, *92* (11), 1947–1957.
[24] Wang, Y.; Fan, F.; Agapov, A. L.; Saito, T.; Yang, J.; Yu, X.; Hong, K.; Mays, J.; Sokolov, A. P. Examination of the Fundamental Relation between Ionic Transport and Segmental Relaxation in Polymer Electrolytes. . **2014**, *55* (16), 4067–4076.
[25] Fragiadakis, D.; Dou, S.; Colby, R. H.; Runt, J. Molecular Mobility and Li^+ Conduction in Polyester Copolymer Ionomers Based on Poly(Ethylene Oxide). *J. Chem. Phys.* **2009**, *130* (6), 064907.

by σ_{dc}, and the region at high frequencies where a subdiffusive conductivity (SD) is present, which may be due to the reorientation motion of dipoles and specifically to the motion of the localized charges, which dominates over the dc-conductivity.[18,22,26,27,28]

Figures 5a and 5b show the Bode diagrams for the different films at 20 and 100 ^{o}C, respectively. The top graphic represents the modulus of conductivity, $|\sigma|$, which increases with the frequency and tends to reach a constant value when the phase angle, φ (lower graphic), reaches a maximum or tend to a zero value for each temperature. It must be noted that the scales of conductivity are the same for both temperatures, which facilitates visualizing the variation of conductivity with temperature. As can be seen, all Bode diagrams showed a plateau when plotting $|\sigma|$ *vs* frequency in the region of high frequencies (10^3 Hz at 20 ^{o}C and 10^5 Hz at 100 ^{0}C), coexisting with the peak of the phase angles tending to zero values. On the other hand, in the region of high frequencies (10^4 Hz-10^7Hz at low temperatures, *i.e.* 20 ^{o}C), a second plateau was observed for the conductivity of all samples except for the sample **F-1g'** at the region where the phase angle reaches a pronounced maximum around -10°.

[26] Leys, J.; Wübbenhorst, M.; Preethy Menon, C.; Rajesh, R.; Thoen, J.; Glorieux, C.; Nockemann, P.; Thijs, B.; Binnemans, K.; Longuemart, S. Temperature Dependence of the Electrical Conductivity of Imidazolium Ionic Liquids. *J. Chem. Phys.* **2008**, *128* (6), 064509.
[27] Sangoro, J. R.; Serghei, A.; Naumov, S.; Galvosas, P.; Kärger, J.; Wespe, C.; Bordusa, F.; Kremer, F. Charge Transport and Mass Transport in Imidazolium-Based Ionic Liquids. *Phys. Rev. E.* **2008**, *77* (5), 051202.
[28] Munar, A.; Andrio, A.; Iserte, R.; Compañ, V. Ionic Conductivity and Diffusion Coefficients of Lithium Salt Polymer Electrolytes Measured with Dielectric Spectroscopy. *J. Non-Cryst Solids.* **2011**, *357* (16), 3064–3069.

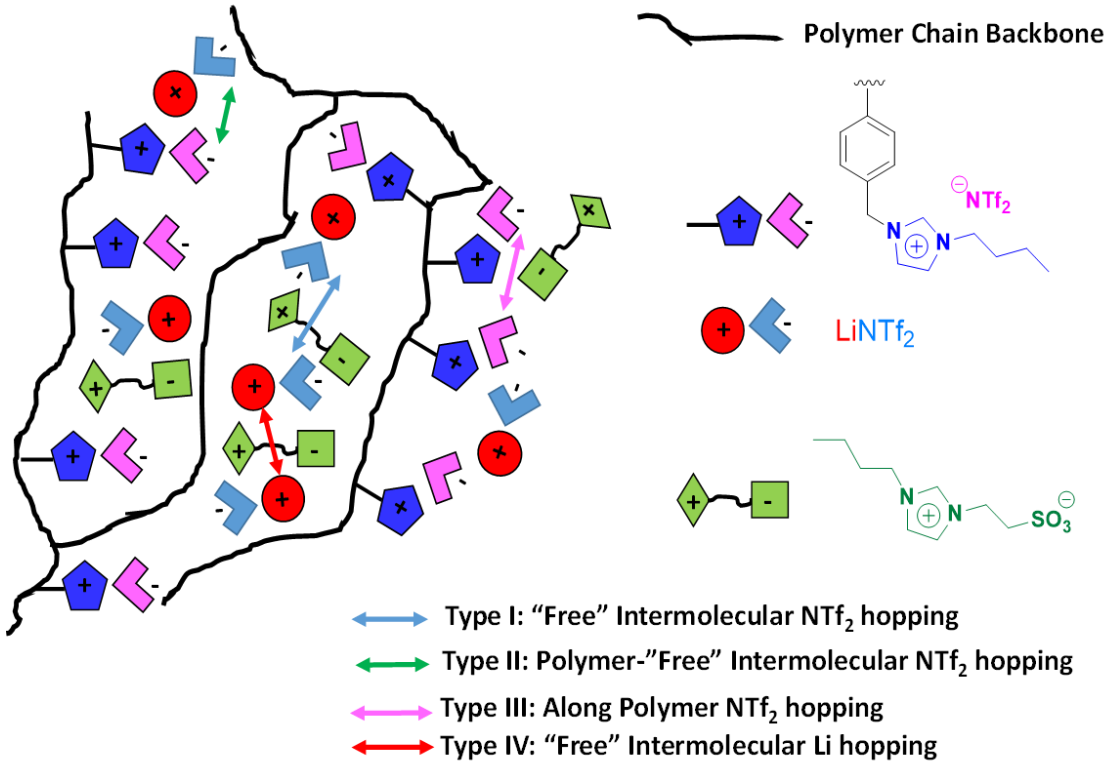

Scheme **2.** Schematic representation of mobility events in the film.

The presence of these two conductivities can be assigned to different processes related with the nature of the ions present in the polymeric matrix. Each ion can contribute in diverse ways to the motions within the material, depending on its shape, size and interaction with the polymeric matrix, providing different mobility and diffusion coefficients. It is important to bear in mind that the considered "ion-gels" have two different types of NTf_2^- anions, namely the counter ion of the polymeric ionic liquid-like imidazolium fragments and the NTf_2^- from $LiNTf_2$. On the other hand, the lithium cation (Li^+) can also contribute to the conductivity. It is likely that at least four possible transport events can add to the conductivity, all of them related with the mobility of the ions involving formation and breaking of ion-associations in the presence of an electric field (Scheme 2). The first one is related with the "free" intermolecular NTf_2^- hopping in the

"ion-gel" phase. A second one should be the NTf_2^- hopping from the polymer to the liquid phase and vice versa. The third one is associated with the NTf_2^- hopping events along the polymeric chain. This one seems to be less important at the view of the low conductivity of the films in the absence of **ZIs-1** : $LiNTf_2$ mixtures. Finally, the events related with the mobility of "free" Li cations in the medium can also be considered, although the presence of the sulfonic groups in **ZIs-1** may constrain Li^+ mobility by complexation.

In the different films considered, the NTf_2^- anion has two different origins, $LiNTf_2$ and the IL-like fragments from the polymerization of **IL-1**. In the last case, the mobility of the imidazolium cation is reduced as corresponds to its attachment to the polymeric backbone. The ratio between both anions changes systematically in the films. For instance, for **F-1g** the molar fraction of **IL-1** is very similar to the one of $LiNTf_2$ (0.339 and 0.305, respectively) leading to a total NTf_2^- : Li^+ ratio of 0.644 : 0.356. The progressive substitution in the mixtures of **ZIs-1** by the corresponding Li salt provides an increase in the molar fraction of $LiNTf_2$ that reaches, in the case of **F-1c**, a maximum value of 0.528. As the molar fraction of NTf_2^- in **F-1c** coming from **IL-1** in is 0.394, the overall NTf_2^- : Li^+ ratio is 0.877 : 0.528 in this film. This makes the total concentration of the NTf_2^- anion higher than the one for the Li^+ cation in all the films studied. Thus, the contribution to conductivity of the NTf_2^- anion is expected to be more pronounced than the one of Li^+. Previous studies carried out with films based on highly cross-

linked PILs have also revealed the important contribution of the mobility of the anion to the measured conductivity.[15,16,29,30,31]

Table 3. Parameters M, τ_{EP} and α described in equation (5) at 20, 60 and 100 °C, obtained from fitting the experimental data of tan δ.

	T=20 °C			T=60 °C			T=100 °C		
Sample	**M**	**τ_{EP} [s]**	**α**	**M**	**τ_{EP} [s]**	**α**	**M**	**τ_{EP} [s]**	**α**
F-1g'	45000	3.5×10^{-4}	0.992	75000	1.2×10^{-4}	0.9975	100000	5.0×10^{-5}	0.9995
F-1g	5000	4.0×10^{-4}	0.970	11000	3.5×10^{-5}	1	300000	1.8×10^{-5}	1
F-1a	3000	3.8×10^{-4}	0.951	11000	2.5×10^{-5}	0.9999	-	-	-
F-1b	3000	4.0×10^{-4}	0.930	9000	1.4×10^{-5}	0.9990	-	-	-
F-1c	3300	7.0×10^{-4}	0.835	10000	6.5×10^{-6}	0.9920	-	-	-

Free ion diffusivity and charge concentration

The most important parameters to estimate the ionic transport in materials are the mobility and concentration of charge carriers and there are a great

[29] Garcia-Bernabé, A.; Compañ, V.; Burguete, M. I.; García-Verdugo, E.; Karbass, N.; Luis, S. V.; Riande, E. Conductivity and Polarization Processes in Highly Cross-Linked Supported Ionic Liquid-Like Phases. *J. Phys. Chem. C.* **2010**, *114* (15), 7030–7037.

[30] Compañ, V.; Molla, S.; García Verdugo, E.; Luis, S. V.; Burguete, M. I. Synthesis and Characterization of the Conductivity and Polarization Processes in Supported Ionic Liquid-like Phases (SILLPs). *J. Non-Cryst Solids.* **2012**, *358* (9), 1228–1237.

[31] Huber, B.; Rossrucker, L.; Sundermeyer, J.; Roling, B. Ion Transport Properties of Ionic Liquid-Based Polyelectrolytes. *Solid State Ionics* **2013**, *247–248*, 15–21.

number of alternative approaches for determining these parameters under the application of an electric field.[6,18,19,32,33,34,35,36]

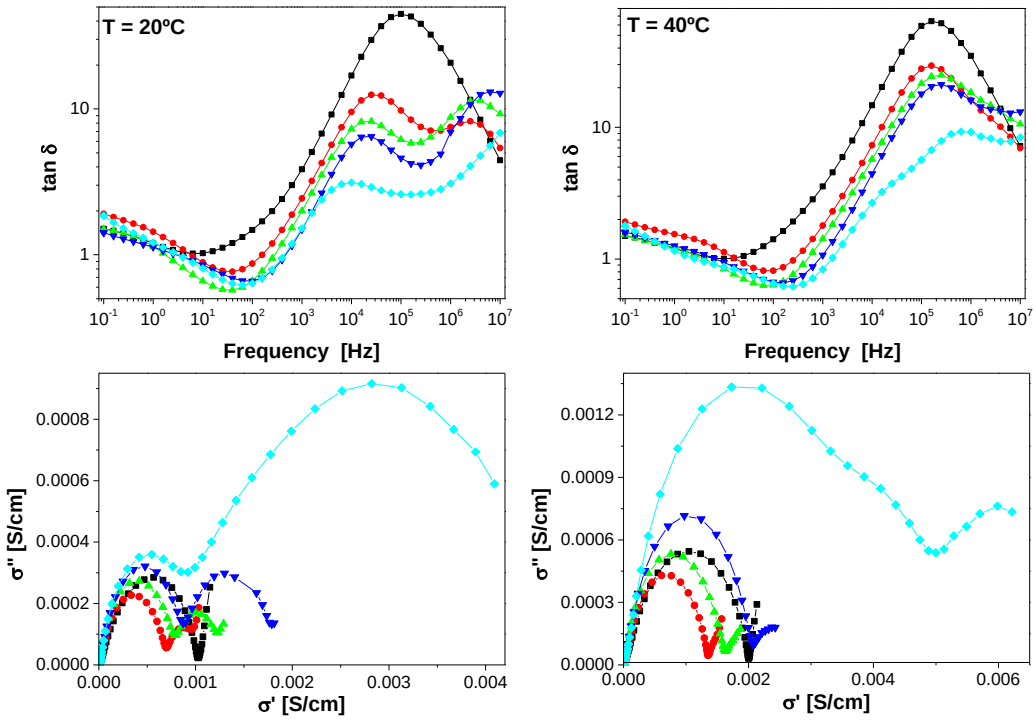

Figure 6. Tan δ as a function of frequencies (up) and Nyquist plots (bottom) at 20 °C (left) and 40 °C (right). **F-1g'** (■), **F-1g** (●), **F-1a** (▲), **F-1b** (▼), **F-1c** (◆).

Figure 6 shows the experimental values of *tan δ* for all samples at 20 and 40 °C obtained using a modification of the approach reported Klein *et al*.[15,16,18,20,23,29] As can be seen, the doped films, except **F-1g'** presenting a

[32] Wang, Y.; Sun, C.-N.; Fan, F.; Sangoro, J. R.; Berman, M. B.; Greenbaum, S. G.; Zawodzinski, T. A.; Sokolov, A. P. Examination of Methods to Determine Free-Ion Diffusivity and Number Density from Analysis of Electrode Polarization. *Phys. Rev. E.* **2013**, *87* (4), 042308.
[33] Dudowicz, J.; Freed, K. F.; Douglas, J. F. The Glass Transition Temperature of Polymer Melts. *J. Phys. Chem. B* **2005**, *109* (45), 21285–21292.
[34] Leys, J.; Rajesh, R. N.; Menon, P. C.; Glorieux, C.; Longuemart, S.; Nockemann, P.; Pellens, M.; Binnemans, K. Influence of the Anion on the Electrical Conductivity and Glass Formation of 1-Butyl-3-Methylimidazolium Ionic Liquids. *J. Chem. Phys.* **2010**, *133* (3), 034503.
[35] Niklasson, G. A.; Jonsson, A. K.; Stromme, M.; Barsoukova, Y.; MacDonald, J. R.; (Eds) In *Impedance Spectroscopy* 2nd ed., Wiley, New York, 2005, pp 302-326.
[36] Schütt, H. J. Determination of the Free Ionic Carrier Concentration: A Discussion of Different Methods. *Solid State Ionics*. **1994**, *70–71*, 505–510.

higher crosslinking degree, present two clear peaks around 10^4 Hz and between 10^6-10^7 Hz, respectively, at 20 ^oC. The peak at moderate frequencies (10^4 Hz to 10^5Hz) is shifted towards higher frequencies as the temperature increased bringing both peaks together. Similarly, the same behaviour is observed from the Nyquist diagrams showed in Figure 6 (bottom) where at 20^oC two semicircles are present due presumable to two types of mobilities and conductivities also observed in the Bode diagrams.

In a first approach, the tan δ values for the detected maxima in Figure 6 were fitted to eq. (5). This provided an estimation for M, τ_{EP} and α, and also allowed calculating the free ion diffusivity. Values obtained for α were close to unity, indicating a limit value in the Cole-Cole model corresponding to a Debye behaviour. A dependence on the temperature of the electrode polarization relaxation time τ_{EP} and the parameter M, was also observed.

The curves shown in Figure 7 display the peaks corresponding to the maximum in tan δ (Eq. (5)) and are associated with the plateau of the real part of the conductivity observed in the Bode diagrams (Figure 5). Their corresponding values in frequency are related with the parameters M, α and τ_m, which permits to calculate the mobility, the ionic diffusion coefficient and the density of free charge into the polymeric matrix applying eqs. (7), (8) and (9), respectively.

Figure 7 also shows the dielectric permittivity and the temperature dependence of τ_{EP} is presented in the inset. A dielectric α-relaxation effect can be observed in tan δ spectra with an excess wing at higher frequencies and as a jump in dielectric spectra. After EP relaxation, a decrease in dielectric permittivity appears in dielectric spectra until reaching constant value in the range of high frequencies, although for some samples the expected plateau is not still visible at the experimental frequencies used.

Table 3 summarizes the parameters for the analysis of eq. (5) at 20, 60 and 100 °C, respectively. A close inspection of Table 3 shows that parameters M and τ_{EP} decrease as the amount of $LiNTf_2$ increase in the film, with the highest value being always obtained for **F-1g'** with a higher crosslinking degree.

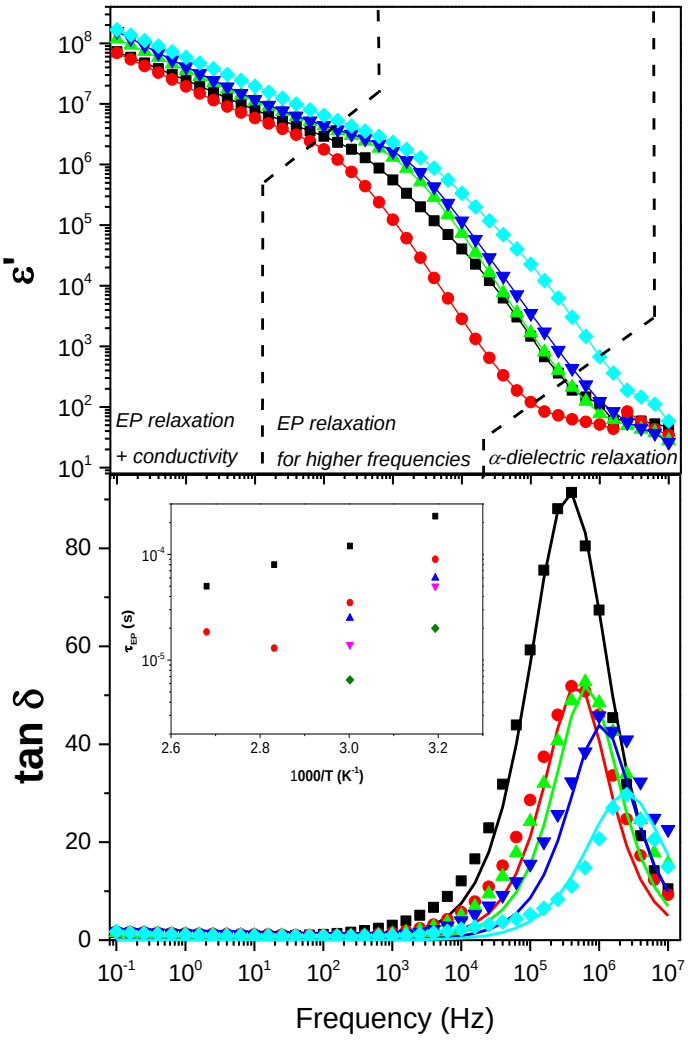

Figure 7. Dielectric permittivity (top) and *tan δ* (bottom) as a function of frequencies at 60 °C. **F-1g'** (■), **F-1g** (●), **F-1a** (▲), **F-1b** (▼) and **F-1c** (◆). The solid line indicates the convolution of equation 11 in the peak of *tan δ* at higher frequencies. The insert displays is the temperature dependence of τ_{EP}.

The temperature dependence of τ_{EP} exhibits an essentially linear behaviour for the range of temperatures analysed. Diffusion coefficients, dielectric permittivity (static permittivity) and mobile charge concentration were

calculated using eqs. (7)-(10) and are shown in Figure 8. The values for the diffusion coefficients are reasonably similar to those for other related systems,[15,16,31,,37] and increase with temperature increase. A close inspection of the variation of the values represented in the activation plot of Figure 8 allows indicates the excellent ion mobilities that can be obtained with these films. The comparison between them reveals that a decrease in the crosslinking degree **F-1g'** and **F-1g** associated with practically the same amount of IL produce a decreasing of the diffusion coefficient between one or two order of magnitude depending of the temperature. For the others films the diffusivity increase with the amount of NTf_2^-.

The calculated charge concentration increases with temperature and varies for the five films, being higher, rather surprisingly, for **F-1g'** and lower for the other films, correlating with the amount of ZIs-1 present in the film.

On the other hand, the values of the mobile ion concentration are higher than those from stoichiometric calculations providing a total concentration of ions (n_{tot}) around 10^{27} m^{-3} at room temperature. This yields a dissociation degree of roughly 10^{-2} at 20 ºC. These values are quite similar to those found for other polyelectrolytes like a Li^+ poly(ethyleneoxide)-based sulfonated ionomer.[18] Thus, it seems that the analysis based on electrode polarization subestimates ion diffusivity respect the estimation from Einstein relation, (D^*), considering the stoichiometric free-ion number density, where $D^*=\sigma_{dc}$ k_BT/n q^2. It is due because in Einstein equation the number density of free ions, (n_{tot}), is considered complete and then it is constant for any temperature. However, the dissociation-association dynamics should be assumed to be much faster than the macroscopic electrode polarization and increasing with the temperature.

[37] Macdonald, J. R. Utility of Continuum Diffusion Models for Analyzing Mobile-Ion Immittance Data: Electrode Polarization, Bulk, and Generation–Recombination Effects. *J. Phys.: Condens. Matter* **2010**, *22* (49), 495101.

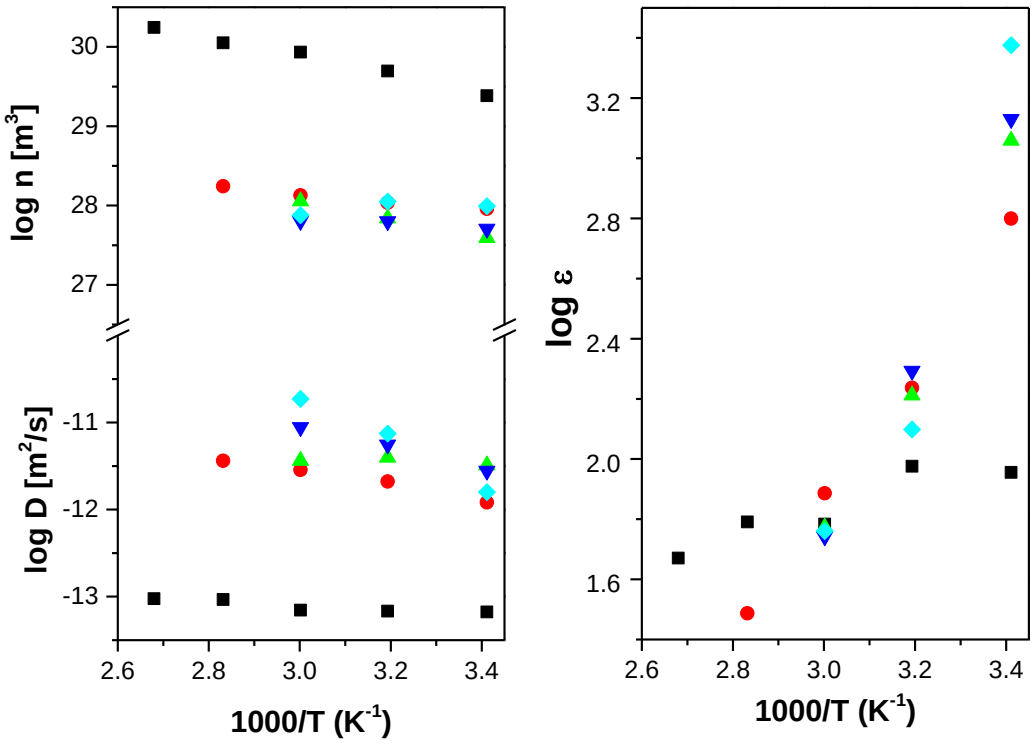

Figure 8. (Left) Temperature dependence of free ion diffusion (D) and charge concentration (n), (Right) dielectric permittivity (ε) for the films. **F-1g'** (■), **F-1g** (●), **F-1a** (▲), **F-1b** (▼), **F-1c** (◆).

In general, the free ion concentration can be described by the Arrhenius equation

$$n=n_0 \exp(-E_{dis}/k_BT)$$

where E_{dis} is the dissociation energy and n_0 the number density in the high temperature limit at which a complete dissociation can be assumed. The values found for the dissociation energy of the different samples were E_{dis} (**F-1g'**) = 9.5 kJ/mol > E_{dis} (**F-1a**) = 9.4 kJ/mol > E_{dis} (**F-1g**)= 4.0 kJ/mol > E_{dis} (**F-1c**)= 2.2 kJ/mol > E_{dis} (**F-1b**)= 2.0 kJ/mol. This energy increases with the value of X_{ZIs}. As it is known, the electrode polarization model is based on the Debye-Hückel theory and therefore can be expected that this model fails in the case of high ionic concentrations.

A comparison between the values of the diffusion coefficients obtained from EP model and using the Einstein relation suggests a possible correlation between the conductivity and the increase in free charge carrier density. This can be due to structural and morphological changes occurring at the ILs phase and at the polymeric matrix. Figures. 8 and 9 show that in general the diffusivity (*i.e.* mobility) increase with increasing temperatures that can also contribute to increase the concentration of charge carriers and/or the conductivity. This trends can be associated with the variations in interionic interactions that will be higher with an increase in loading of functional groups in the polymer, with an increase in the concentration of IL-phase that could facilitate such interactions, most likely through an array of polar species, and with an increase in temperature that will favour the mobility of the polymer chains bearing the functional sites. In this regard, an increase in the amount of crosslinker (TMPTMA) decreases the diffusivity as it reduces polymer chain mobility and accordingly interactions between ions in the liquid phase and those covalently attached to the polymer matrix. This is illustrated in Figure 9 by the comparison between **F-1g** and **F-1g'**. Interestingly, the same figure shows that these two films prepared with a 1:1 **ZIs-1**:$LiNTf_2$ mixture (in the region of the eutectic point) are the only ones displaying a diffusivity that increases with temperature as corresponds with the presence of discrete clusters in the eutectic and a limited number of long-range cluster-cluster interactions in the eutectic. It is known that ionic mobility is associated and coupled to structural relaxation and high ionic conductivity is possible due to very short structural relaxation time such is happen in our samples, $\tau \approx 10^{-6}$ s, where the polymer have relatively rigid structures and then the ionic transport can be strongly decoupled from the structural relaxation.

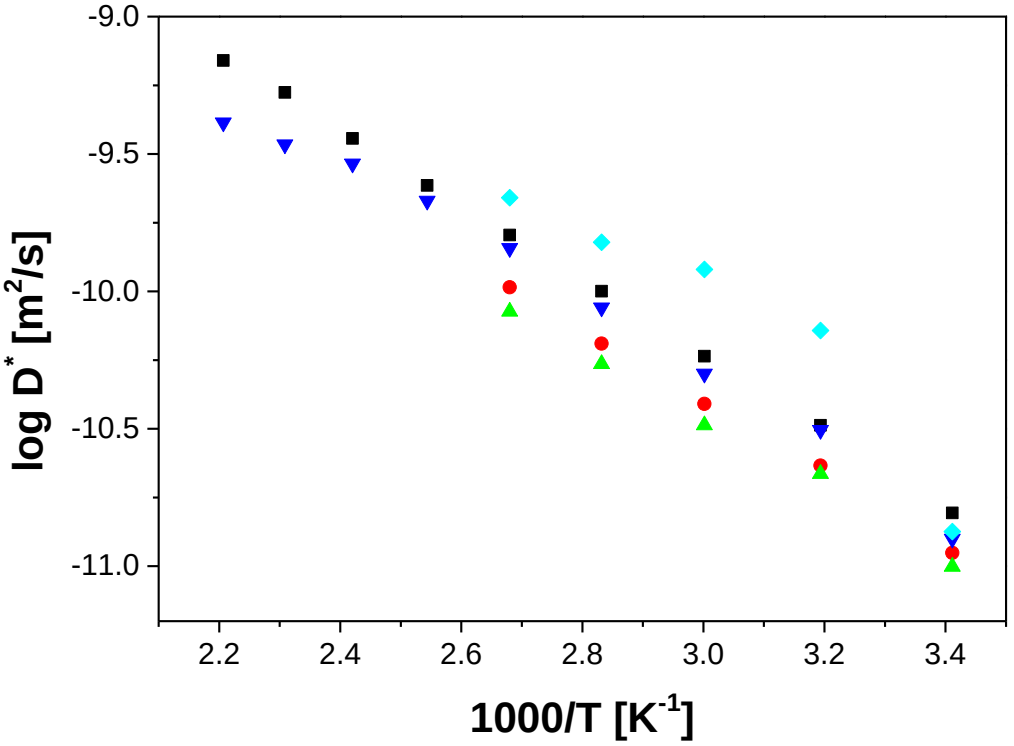

Figure 9. Temperature dependence of the corrected diffusion coefficient of the free ions for all the samples. **F-1g'** (■), **F-1g** (●), **F-1a** (▲), **F-1b** (▼), **F-1c** (◆).

3.3. Conclusions

The results presented here show that the properties of the mixtures of the zwitterionic imidazolium salt **ZIs-1** with $LiNTf_2$ can be tuned through a proper selection of the molar fraction of both components. Changes in the composition define not only the concentration of mobile ions but also the strength of the interactions between anions and cations that affect their mobility and macroscopic properties like viscosity and finally conductivity, which is affected by a balance between all those factors. Thus, mixtures in the eutectic point show the lower conductivities that increase significantly for the higher contents in $LiNTf_2$. The incorporation of those mixtures into crosslinked polymeric matrices allows obtaining composite materials with excellent properties and potential for devices requiring conductive

membranes, with no leaching of the liquid phase observed after long term experiments. The conductivity of the different films prepared increases with temperature and with the content in $LiNTf_2$, reaching maximum values for **F-1c** (i.e. $2.0x10^{-2}$ S cm^{-1} at 140 °C). These conductivity values indicate that such composite materials represent a promising alternative for application in different energy devices. It must be noted that **F-1c** presents an excellent mechanical and thermal stability, even for small crosslinking degrees, while being flexible and transparent. A further increase in the amount of $LiNTf_2$, however, did not allow obtaining films with the required properties. The comparison of **F-1g** and **F-1g'** shows that a moderate increase in crosslinking (from 5 to 10% of TMPTMA) is accompanied in this case by a slight increase in conductivity (i.e. $9.7x10^{-3}$. *vs*. $1.6x10^{-2}$ S cm^{-1} for **F-1g** and **F-1g'** respectively) with activation energies associated of 22.8 and 21.3 kJ/mol, respectively

Although the study of free ion diffusivity and number density from the EP model gives reasonable estimates, the direct quantitative data need to be handle with some caution. Our results indicate that this approach tend to overestimate the values of mobile charge density (n) and, therefore, to underestimate the values of the diffusion coefficients (D). This can be solved, using the same line of reasoning developed by Wang *et al.*,[24,37] through the use of the corrected diffusion coefficient (D^*) calculated using the ratio between the stoichiometric charge density and the one calculated using the EP model

$$N = \frac{n_{tot}}{n_0}.$$

This means that overestimation of ion of mobile charge density is a generic problem in electrode polarization analysis, which may be originated from the estimation of the ionic carriers density, from the definition of conductivity and the Eisntein relation, because in such consideration the

free ion number density should be considered constant with temperature, although this parameter (n) can increase by about 10^3-10^4 with the temperature. Consequently, the diffusion coefficient obtained from EP model decreases with temperature in comparison with that obtained directly by means of the Einstein relation considered constant to the number of ionic carriers.

3.4. Experimental Section

Materials

All reagents were purchased from Sigma-Aldrich and used without further purification. ^{1}H and ^{13}C NMR experiments were carried out using a Varian INOVA 500 (^{1}H, 500 MHz and ^{13}C, 125 MHz) spectrometer. The chemical shifts are given in delta (δ) values and the coupling constants (J) in Hertzs (Hz).

General characterization protocols

Impedance measurements

Impedance measurements were carried out on samples at several temperatures lying in the range 393 K (20ºC) to 453 K (180ºC) and frequency window $10^{-1} < f < 10^7$ Hz. The temperature was firstly and gradually raised and lowered from 20ºC to 180ºC in steps of 20ºC. To ensure the measurements reproducibility the values considered in this work were obtained from the third cycle of temperature scan. The experiments were performed with 100 mV amplitude, using a Novocontrol broadband dielectric spectrometer (Hundsangen, Germany) integrated by a SR 830 lock-in amplifier with an Alpha dielectric interface. The amplitude of 100 mV

was chosen in order to get a linear regime. The membranes were placed between two gold electrodes of 20 mm of diameter coupled to the impedance spectrometer acting as blocking electrodes in a liquid parallel plate cell coupled to the spectrometer and deionized water was incorporated to ensure a fully hydrated state of the samples below 100 °C and in equilibrium with its vapor above 100 °C. The membranes thickness was measured afterwards using a digital micrometer, taking the average of ten measurements at different parts of the surface. During the conductivity measurements, the temperature was kept constant or changed stepwise in all the range of temperatures controlled by a nitrogen jet (QUATRO from Novocontrol) with a temperature error of 0.1 ^{o}C, during every single sweep in frequency.

Differential scanning calorimetry

Glass-transition temperatures and melting points were measured by using a Mettler–Toledo differential scanning calorimeter (DSC), model DSC822e. The instrument was calibrated for temperature and heat flow with zinc and indium reference samples provided by Mettler-Toledo. The samples were placed in a 40-μL hermetically sealed aluminum pan with a pinhole in the top. An empty aluminum pan was used as the reference. Samples were exposed to a flowing N_2 atmosphere. Before the DSC test, each sample was dried at 90–100 ^{o}C and 10^{-2}-10^{-3} mbar for 4 h, and further *in situ* dried in the differential scanning calorimeter by holding the sample at 130 ^{o}C for 120 min as the presence of volatiles, especially water, can affect the glass transition and melting temperatures. Melting transition temperatures were determined by multiple cycles (typically three) involving heating the sample from -50 to 250 ^{o}C, followed by cooling from 250 to -50 ^{o}C, both at a rate of 5 ^{o}C min^{-1}. The melting temperatures were determined at the onset of the transition.

Spectroscopic studies

FT-IR-ATR spectra were acquired with a MIRacle single-reflection ATR diamond/ZnSe accessory in a JASCO FT/IR-6200 instrument. Raman spectra were obtained in a NRS-3100 equipment (Jasco) with optic microscope and a CCD detector. Samples were exposed to a flowing N_2 atmosphere. Before the spectra were recorded, each sample was dried at 90–100 ^oC and 10^{-2}-10^{-3} mbar for 4 h to remove traces of residual solvent and water.

Thermogravimetric analysis (TGA)

The data were recorder in a TG-STDA Mettler Toledo model TGA/SDTA851e/LF/1600 using the following heating program: 1. Heating from 25 ^oC to a 120 ^oC at 10 ^oC/min under N_2 and holding the sample at this temperature for 25 min. 2. Cooling from 120^oC to 25^o, at 10 ^oC/min. 3. Measuring the weight loss from 25^oC a 700^oC at 10 ^oC/min under N_2.

Viscosity

It was determined with a rotating viscometer (Brookfield R/S-CPS+ Rheometer, USA). Before data were recorded, each sample was dried at 90–100 ^oC and 10^{-2}-10^{-3} mbar for 4 h to remove traces of residual solvent and water.

Synthetic protocols

Preparation of ZIs:$LiNTF_2$ mixtures (melting protocol)

Mixtures of ZIs and $LiNTF_2$ were prepared the ratios indicated in Table 1. For this purpose, $LiNTF_2$ and ZIs-1 were mixed together in a mortar till forming a homogeneous solid paste. The resulting mixture was introduced into a glass vial and heated-up to 150 - 160 ^oC to obtain a melted mixture. Nitrogen was bubbled for 10 min to eliminate dissolved oxygen. The samples were then heated in vacuum at 130-140 ^oC under high vacuum to eliminate any residual water present.

General procedure for film fabrication

The cross-linked films used in this study were prepared by thermal copolymerisation of the monomeric mixture containing the **ZIs-1**-$LiNTf_2$ mixtures following the composition indicated in Table 2. A typical procedure for the preparation of the samples is described as follows: AIBN was added to a solution formed by the monomeric mixture and the **ZIs-1**-$LiNTf_2$ mixture. Nitrogen was bubbled for 10 min to eliminate dissolved oxygen. A small part of this solution was pipetted into the narrow space formed between two glass microscopy plates separated by means of two thin lamellas at the ends. The system was introduced into an oven at 65 ^oC for 24 hours. After polymerization, the two glasses were separated and the film removed and stored in a desiccator. The measured film thickness was very homogeneous even in different points of large samples and from sample to sample.

3.5. Supplementary Information

Free ion diffusivity and charge concentration on cross-linked Polymeric Ionic Liquid films doped with sulfonated zwitterion salts and Lithium ions

Table of Contents.

Figure SI.8. Selected region of the Raman spectra of the different **ZIs-1**:$LiNTf_2$ molar mixtures in comparison with $LiNTf_2$ and **ZIs-1**.

Figure SI.9. DSC for the films prepared.

Figure SI.10. TGA of all films prepared in comparison with **ZIs-1**.

Figure SI.11. Activation Energy vs composition of the mixture used.

Figure SI.12. A comparative study of conductivity versus temperature for different PILs.

Figure SI.13. Selected region of the ATR-FT-IR of the some of the films doped with different **ZIs-1:**$LiNTf_2$ mixtures in comparison with **F-2.**

Figure SI.14. Selected region of the Raman spectra of the some of the films doped with different **ZIs-1:**$LiNTf_2$ mixtures.

Figure SI.15. Comparison of ATR-FT-IR spectra of the different **ZIs-1**:$LiNTf_2$ molar mixtures as prepared using the melting protocol.

Figure SI.16. Comparison of ATR-FT-IR spectra of **ZIs-1**:$LiNTf_2$ 1:2 molar mixtures as prepared using the dissolution protocol (black line) and the melting protocol (red line) as well as a sample after thorough vacuum drying (> 120 ^{o}C).

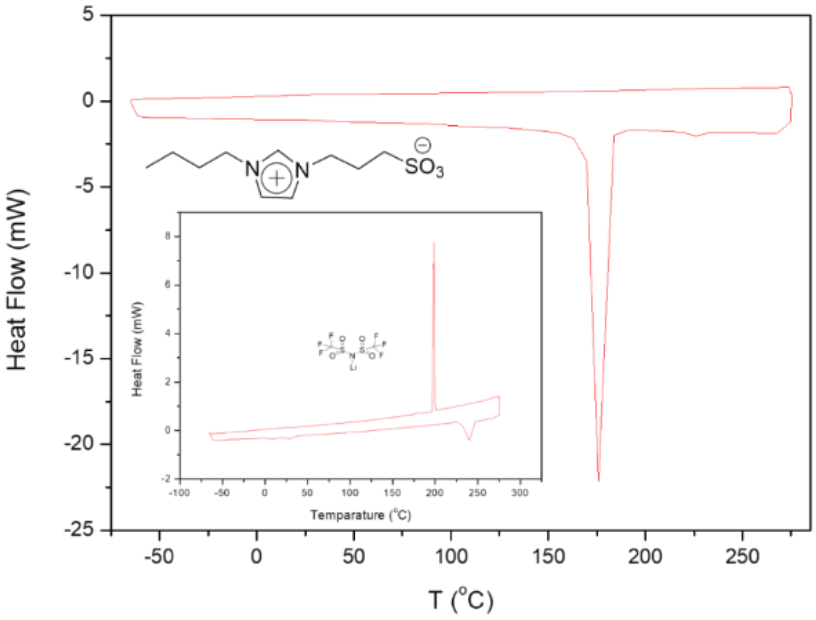

Figure SI.1. DSC of the zwitterionic salt (3-(1-butyl-1H-imidazol-3-ium-3-yl)propane-1-sulfonate **ZIs-1**. Insert: DSC of $LiNTf_2$. Conditions: 10 K/min under a nitrogen atmosphere.

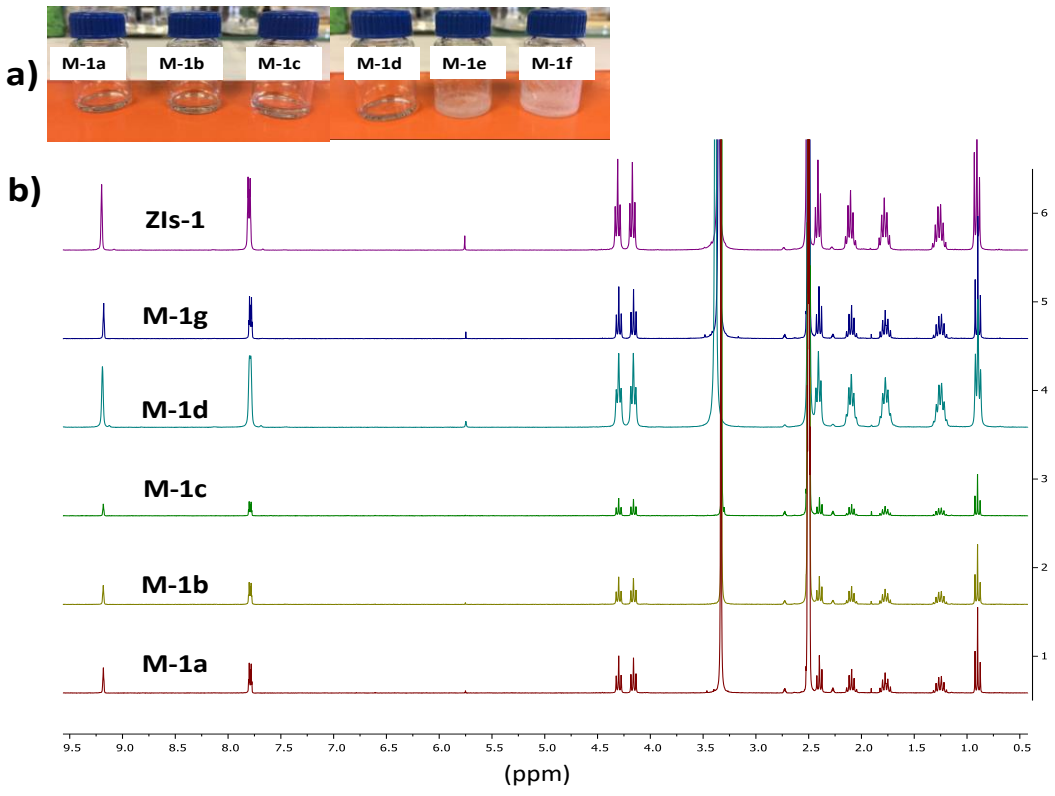

Figure SI.2. **(a)** Pictures for the different mixtures obtained by mixing **ZIs-1** and $LiNTf_2$ at different molar ratios (see Table 1 in the main text for composition). **(b)** ^{1}H-NMR (CD_3SOCD_3) of the some of these mixtures in comparison with pure **ZIs-1**.

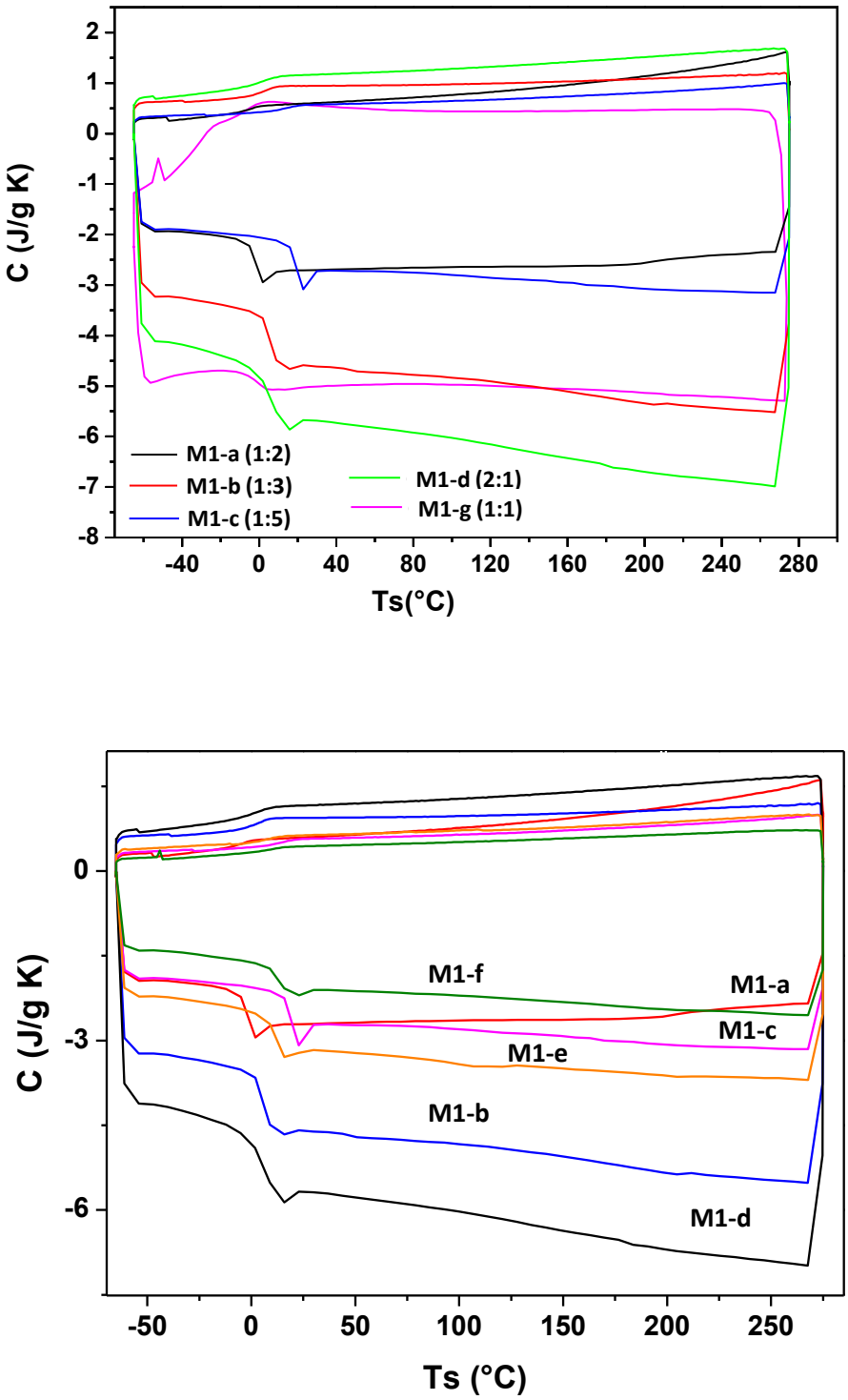

Figure SI.3. Top: DSC of the different r.t. liquid mixtures obtained by mixing **ZIs-1** and $LiNTf_2$ at different molar ratios (see Table 1 in the main text for composition). Bottom: DSC of all the mixtures obtained by mixing **ZIs-1** and $LiNTf_2$ at different molar ratios (see Table 1 in the main text for composition) after being heated to >200 °C. Curves correspond to the second cycle. Obtained at 10 K/min under a nitrogen atmosphere.

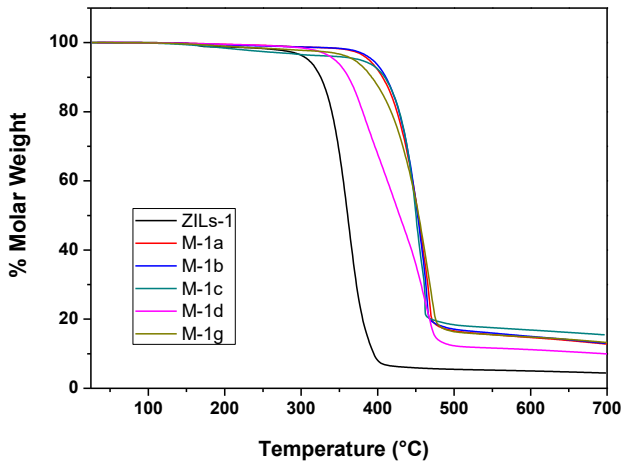

Figure SI.4. TGA of the mixtures obtained by mixing **ZIs-1** and $LiNTf_2$ at different molar ratios (see Table 1 in the main text for composition).

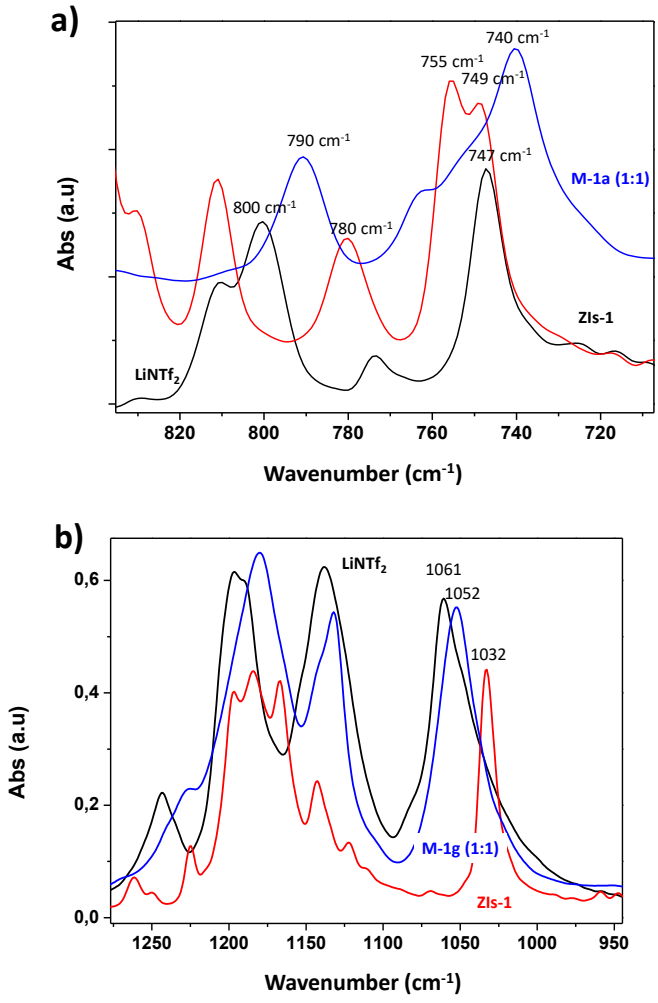

Figure SI.5. Selected region of the ATR-FT-IR of $LiNTf_2$, **ZIs-1** and **M-1g** (equimolecular mixture of $LiNTf_2$ and **ZIs-1**).

a)

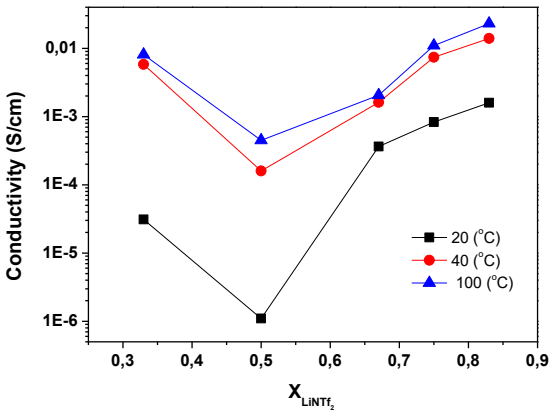

b) T=25

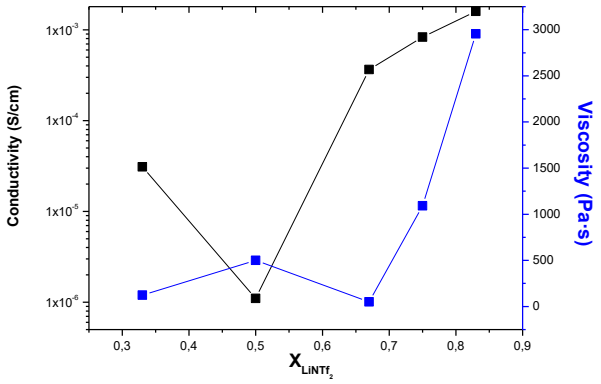

T= 100

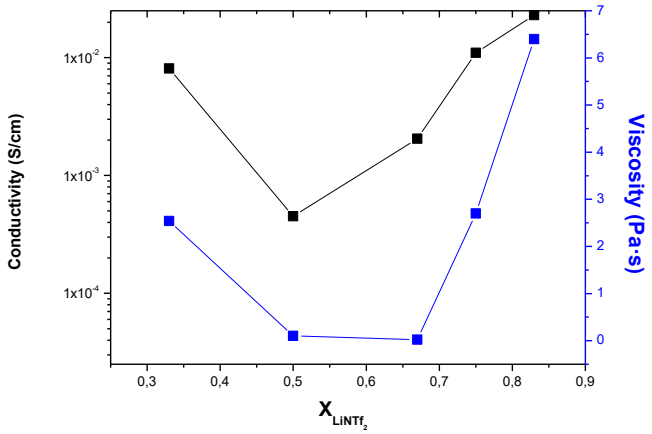

Figure SI.6. **(a)** Effect of the mole fraction of $LiNTf_2$ on the ionic conductivity at 20, 40 and 100 °C for the different molar mixtures **ZIs-1**:$LiNTf_2$. **(b)** Comparison of conductivity and viscosity at 25 and 100 °C for the different molar mixtures **ZIs-1**:$LiNTf_2$.

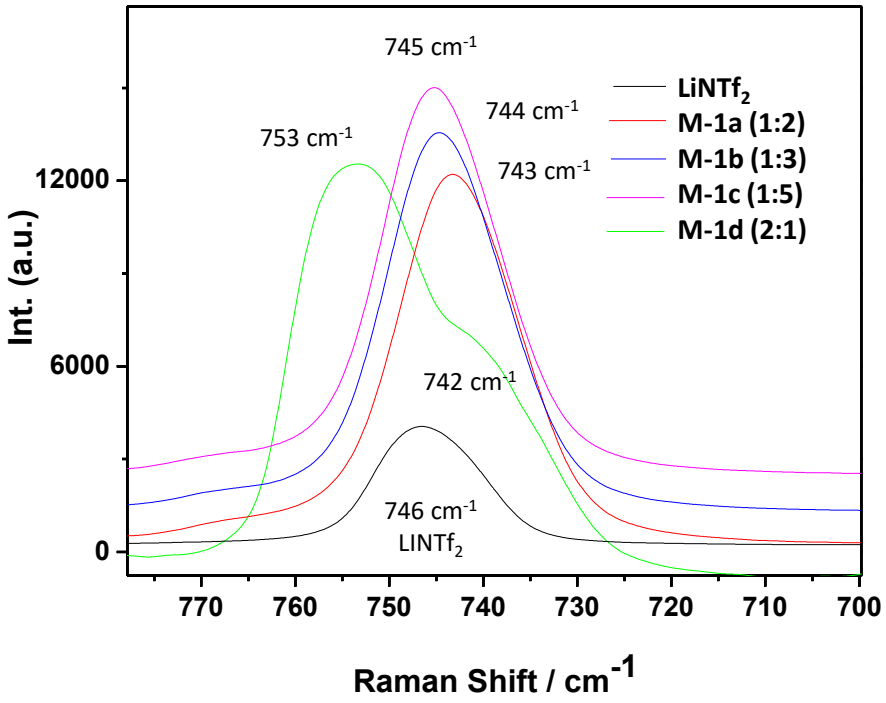

Figure SI.7. Selected region of the Raman spectra of the different **ZIs-1**:$LiNTf_2$ molar mixtures in comparison with $LiNTf_2$.

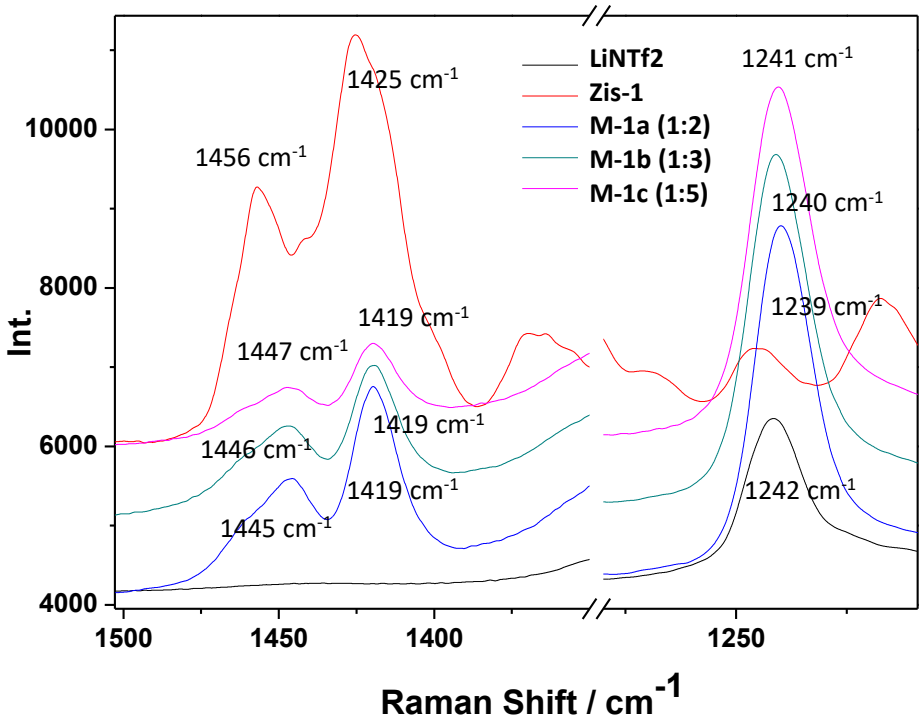

Figure SI.8. Selected region of the Raman spectra of the different **ZIs-1**:$LiNTf_2$ molar mixtures in comparison with $LiNTf_2$ and **ZIs-1**.

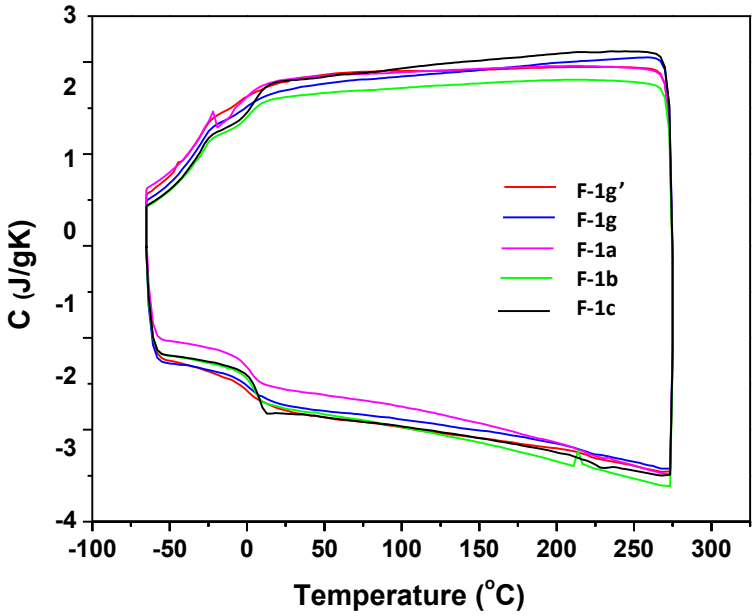

Figure SI.9. DSC for the films prepared (see Table 2 in the main text for composition). Cycle 2. Obtained at 10 K/min under a nitrogen atmosphere.

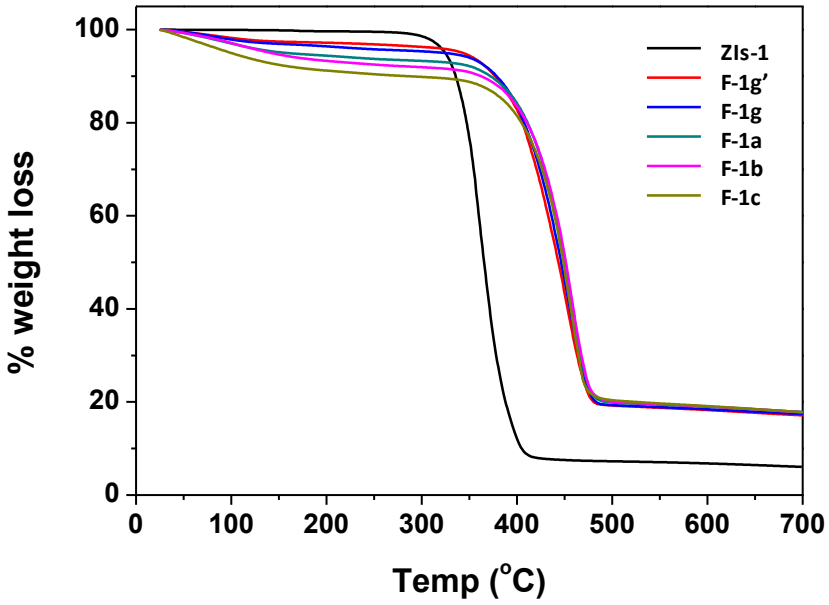

Figure SI.10. TGA of all films prepared in comparison with **ZIs-1** (see Table 2 in the main text for composition).

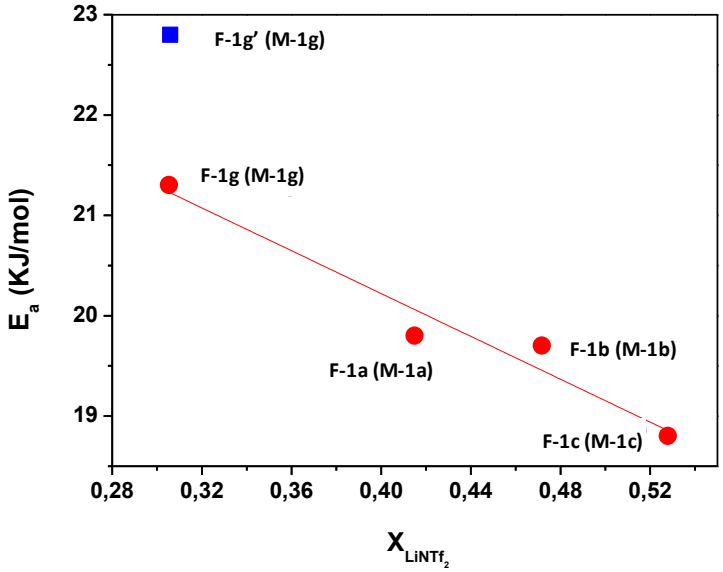

Figure SI.11. Activation Energy vs composition of the mixture used (see Table 2 in the main text for composition).

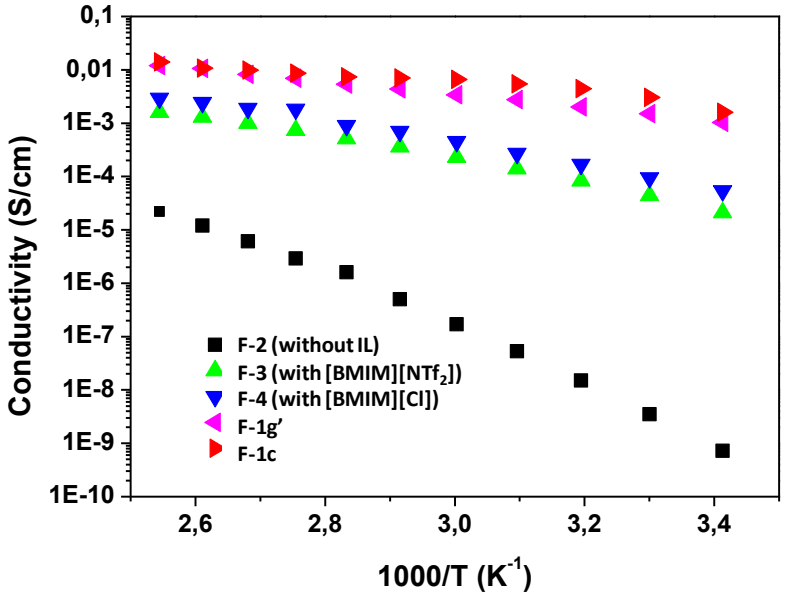

Figure SI.12. A comparative study of conductivity versus temperature for different PILs with similar crosslinking and doped with either [BMIM][Cl] or [BMIM][NTf_2] (B. Altava, V. Compañ, A. Andrio, L. F. del Castillo, S. Mollá, M. I. Burguete, E. García-Verdugo and S. V. Luis, *Polymer*, 2015, **72**, 69 and A. Garcia-Bernabé, A. Rivera, A. Granados, S. V. Luis and V. Compañ, *Electrochim. Acta,* 2016, **213**, 887) and "ion gels" **F-1g'** and **F-1c** from this work. **F-2**: *ca*. 90 % wt of **IL-1** and 10 % wt TMPTMA in the monomeric mixture (without IL). **F-3**: *ca*. 90 % wt of **IL-1**, 10 % wt TMPTMA in the monomeric mixture, *ca*. 50 % [BMIM][NTf_2] in the film; **F-4:** *ca*. 90 % wt of **IL-1** and 10 wt % TMPTMA in the monomeric mixture, *ca*. 50 % [BMIM][NTf_2] in the film.

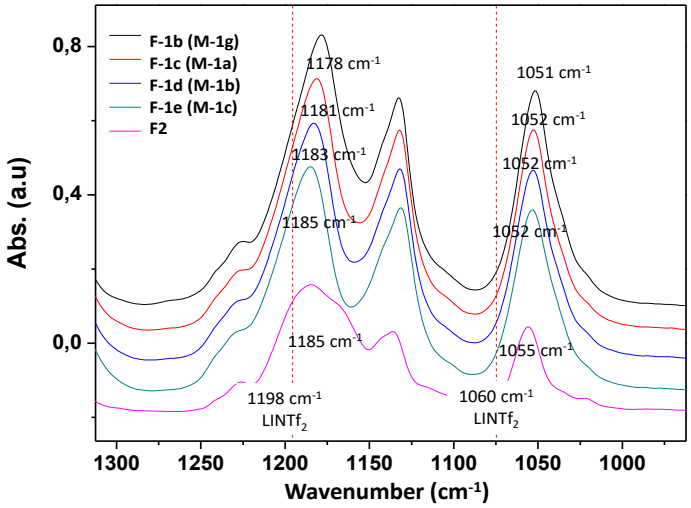

Figure SI.13. Selected region of the ATR-FT-IR of the some of the films doped with different **ZIs-1:**$LiNTf_2$ mixtures (see Table 2 in the main text for composition) in comparison with **F-2** (film without doping).

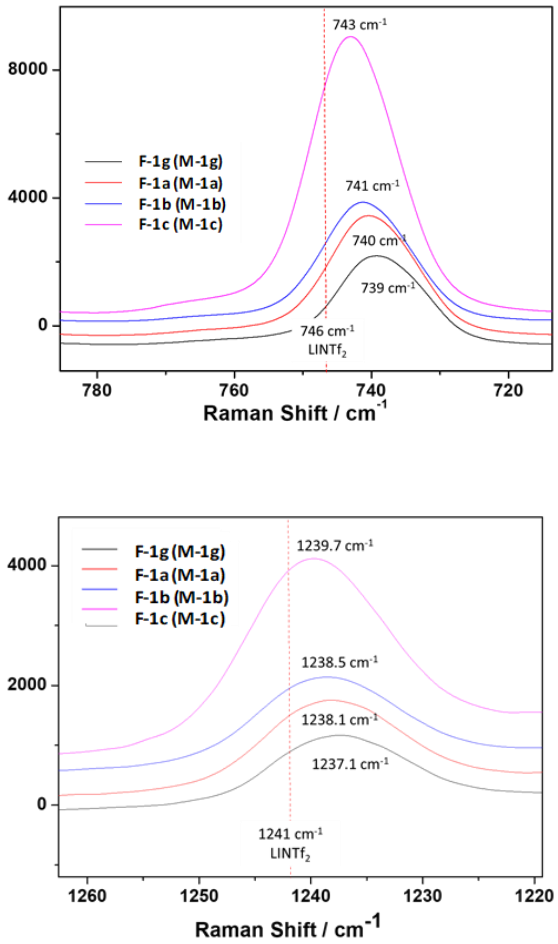

Figure SI.14. Selected region of the Raman spectra of the some of the films doped with different **ZIs-1:**$LiNTf_2$ mixtures (see Table 2 in the main text for composition).

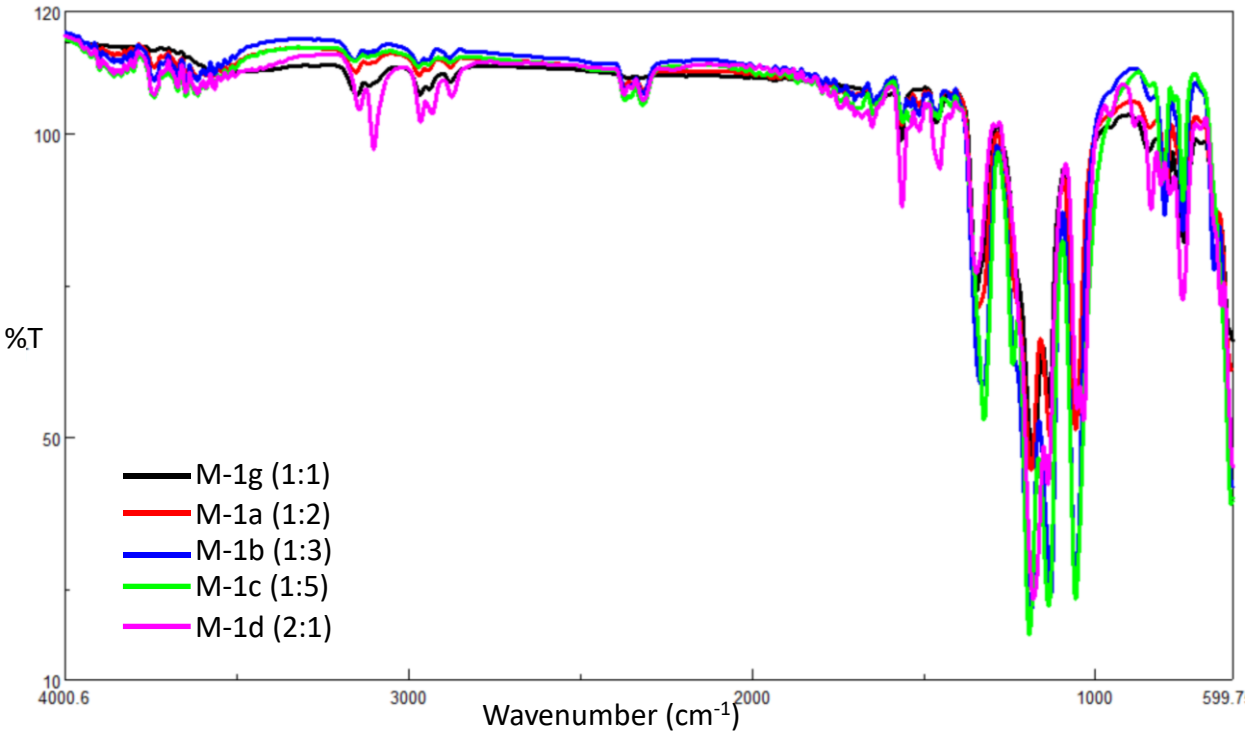

Figure SI.15. Comparison of ATR-FT-IR spectra of the different **ZIs-1**:$LiNTf_2$ molar mixtures as prepared using the melting protocol.

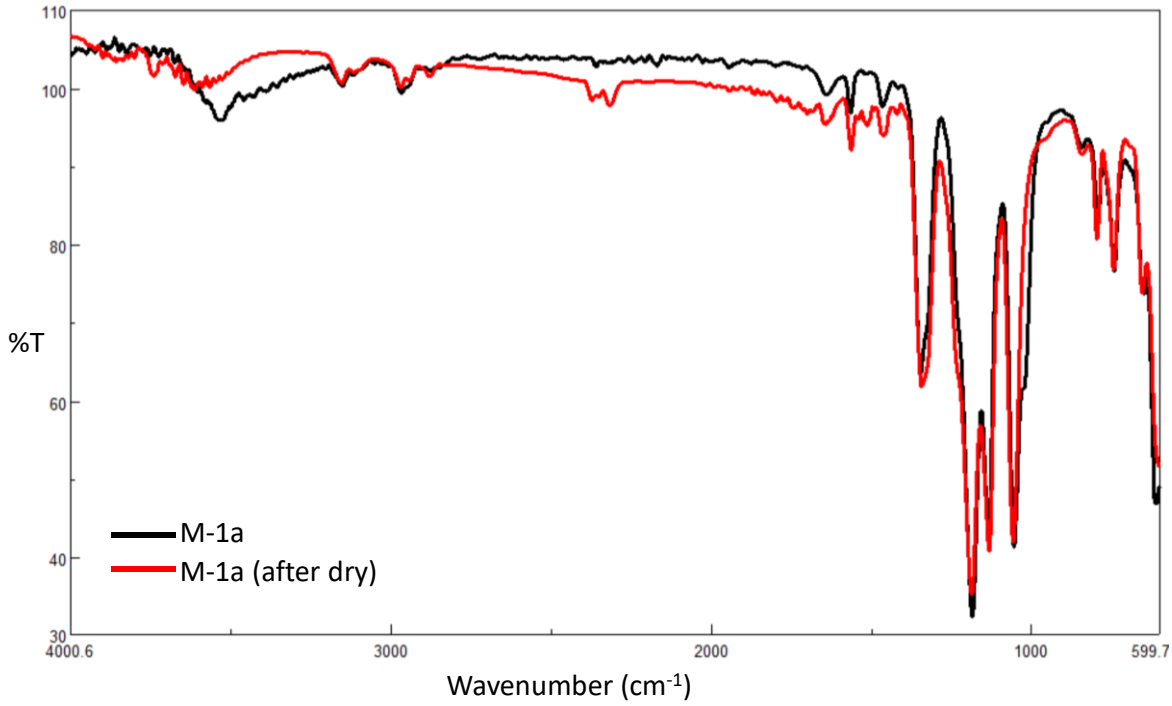

Figure SI.16. Comparison of ATR-FT-IR spectra of **ZIs-1**:$LiNTf_2$ 1:2 molar mixtures as prepared using the dissolution protocol (black line) and the melting protocol (red line) as well as a sample after thorough vacuum drying (> 120 ^{o}C).

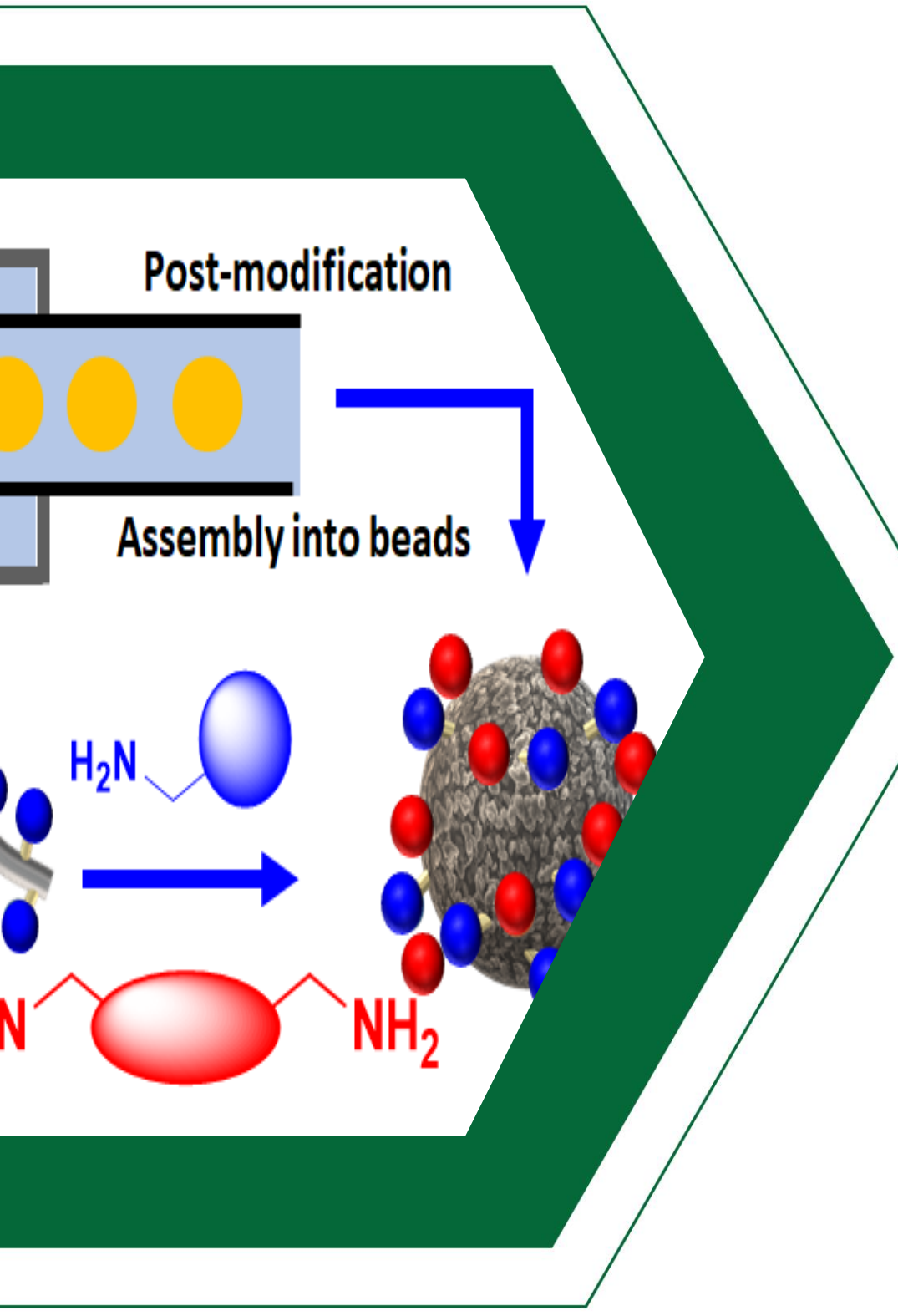
Post-modification
Assembly into beads
H_2N
N
NH_2

CAPÍTULO IV

Sistemas en flujo continuo para la preparación simple de polímeros esféricos funcionalizados derivados del Poli(acrilamida-tiolactona)

Resumen. Aquí reportamos acerca de un sistema simple y robusto basado en sistemas de flujo cotinuo para preparar polímeros esféricos funcionalizados en 6 minutos. La presencia de los grupos de tiolactona permite la incoroporación de dos grupos funiconales. La poli(tiolactona) soluble es transformada en presencia de una amina y un agente entrecruzante en las correspondientes esferas poliméricas a través de la generación continua de gotas y la gelificación y entrecruzamiento *in situ*. Se evaluaron y optimizaron las variables para la preparación de polímeros esféricos funcionalizados. Las esferas funcionalizadas fueron probadas en aplicaciones catalíticas.

Chapter IV. Continuous flow system for the simple preparation of functionalized polymeric beads derived from Poly(acrylamide-thiolactone)

Abstract. Here we report on a simple and robust approach based on continuous flow devices to fabricate functional spherical polymers in 6 minutes. The presence of thiolactone groups allow the introduction of two functionalization levels. The soluble poly(acrylamide-thiolactone) is converted in the presence of an amine and a crosslinker in the corresponding spheres via continuous droplets generation and an *in-situ* gelation and cross-linking process. The key experimental variables for the preparation of functional spherical polymers were evaluated and optimised. The functionalized beads were modified and preliminary tested in catalytic applications.

Keywords: Continous flow • functional polymers • poly(acrylamide-thiolactone).

4.1. Introduction

Poly(acrylamide-thiolactone) derivatives have been identified as suitable polymeric scaffolds to build-up hierarchic functional polymers by post-modification procedures.[1] The high flexibility of this multi-component platform provides unique opportunities for the incorporation onto a polymer different functional moieties by post-polymerization modification.[2] Indeed, these methodologies allow the preparation of a large variety of functional polymeric structures through the synthetic manipulation of a reduced number of common simple intermediates.[3] Thus, this polymeric synthetic platform has been exploited, according to the required needs, to introduce active elements (i.e. catalytic moieties),

[1] Frank, D.; Espeel, P.; Claessens, S.; Mes, E.; Du Prez, F. E. Synthesis of Thiolactone Building Blocks as Potential Precursors for Sustainable Functional Materials. *Tetrahedron.* **2016**, *72* (42), 6616–6625.

[2] Kubo, T.; Easterling, C. P.; Olson, R. A.; Sumerlin, B. S. Synthesis of Multifunctional Homopolymers via Sequential Post-Polymerization Reactions. *Polym. Chem.* **2018**, *9* (37), 4605–4610.

[3] Espeel, P.; Du Prez, F. E. One-Pot Multi-Step Reactions Based on Thiolactone Chemistry: A Powerful Synthetic Tool in Polymer Science. *Eur. Pol. J.* **2015**, *62*, 247–272.

hydrophobic / hydrophilic residues, additional functional groups (i.e OH, NR_3, imidazolium, SO_3H, etc), ligands (i.e. N or O chelators), or even cross-linking units. At the view of the high versatility of the poly-(acrylamide-thiolactone) as a synthetic platform, here we propose to adopt a continuous flow approach for the simple, fast and robust preparation of new functional polymers derived from it. A liquid–liquid multiphase plug-play flow platform allows the synthesis of cross-linked functional polymer beads by post-modification of poly(acrylamide-thiolactone) in a higher controlled fashion. The optimal parameters (concentration, crosslinking, flow rates, residence time, etc.) led to simple and reproducible conditions for the preparation of functional spherical cross-linked polymers. The variation of the relative proportions of the building blocks and the conditions used define not only the polymer functionalization but also the morphological and mechanical properties of the resulting polymeric beads. The functional polymeric beads prepared by this methodology were initially assayed in different applications.

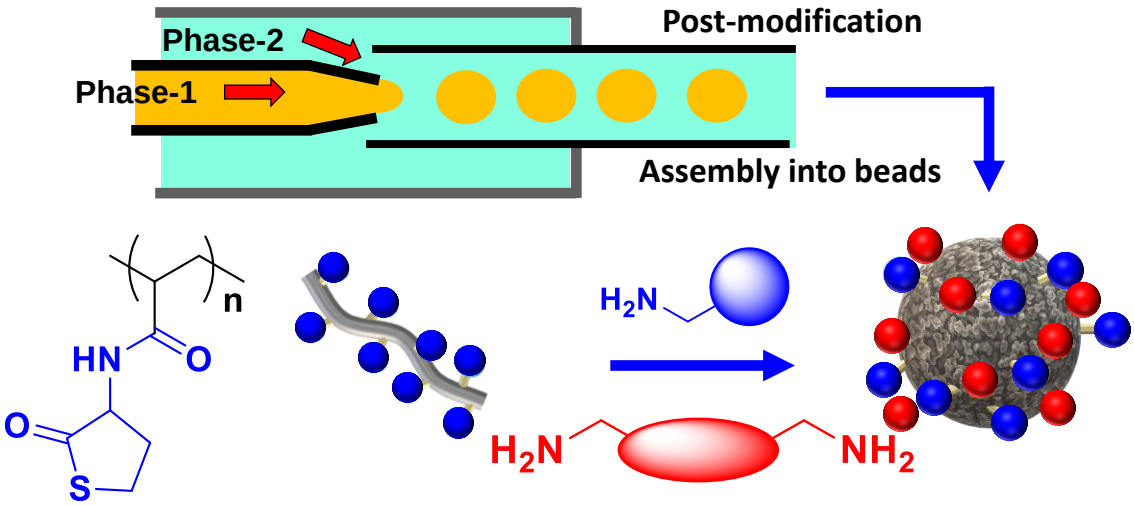

Figure. 1. Schematic illustration of the preparation of the functionalized beads by postmodification of poly(acrylamide-thiolactone) with a modifier and a crosslinker.

4.2. Results and discussion

Plug and play continuous flow platform for droplets generation

A large amount of research efforts has been devoted to development of microfluidic continuous-flow systems for the synthesis of materials.[4,5,6] These systems can provide a precise control reaction conditions including rapid heat and mass transfer, high mixing efficacy, large reaction interfaces, and compatibility with online analysis.[7] In particular, droplet-based microfluids are a suitable technology for the preparation of polymeric beads materials.[8] Taking into account these antecedents, the first goal of this work was to build-up a plug-and-play system enabling the synthesis of functional polymers under continuous flow conditions.[9]

The reactor design was based on a needle-like droplets generator (Figure 2). The droplet generator was built using a PTFE body three-way connector valve, which was drilled to accommodate a stainless-steal cannula (43 mm length and 0.5 mm OD) passing through it.

[4] Ma, J.; Lee, S. M.-Y.; Yi, C.; Li, C.-W. Controllable Synthesis of Functional Nanoparticles by Microfluidic Platforms for Biomedical Applications – a Review. *Lab Chip.* **2017**, *17* (2), 209–226.
[5] Dendukuri, D.; Doyle, P. S. The Synthesis and Assembly of Polymeric Microparticles using Microfluidics. *Adv. Mater.* **2009**, *21* (41), 4071–4086.
[6] *Flow Chemistry: Integrated Approaches for Practical Applications*; Luis, S. V., Garcia-Verdugo, E., Eds.; Green Chemistry; Royal Society of Chemistry: London. United Kingdom, 2020.
[7] Luo, G.; Du, L.; Wang, Y.; Wang, K. Recent Developments in Microfluidic Device-Based Preparation, Functionalization, and Manipulation of Nano- and Micro-Materials. *Particuology*. **2019**, *45*, 1–19.
[8] Shang, L.; Cheng, Y.; Zhao, Y. Emerging Droplet Microfluidics. *Chem. Rev.* **2017**, *117* (12), 7964–8040.
[9] Bédard, A.-C.; Adamo, A.; Aroh, K. C.; Russell, M. G.; Bedermann, A. A.; Torosian, J.; Yue, B.; Jensen, K. F.; Jamison, T. F. Reconfigurable System for Automated Optimization of Diverse Chemical Reactions. *Science.* **2018**, *361* (6408), 1220–1225.

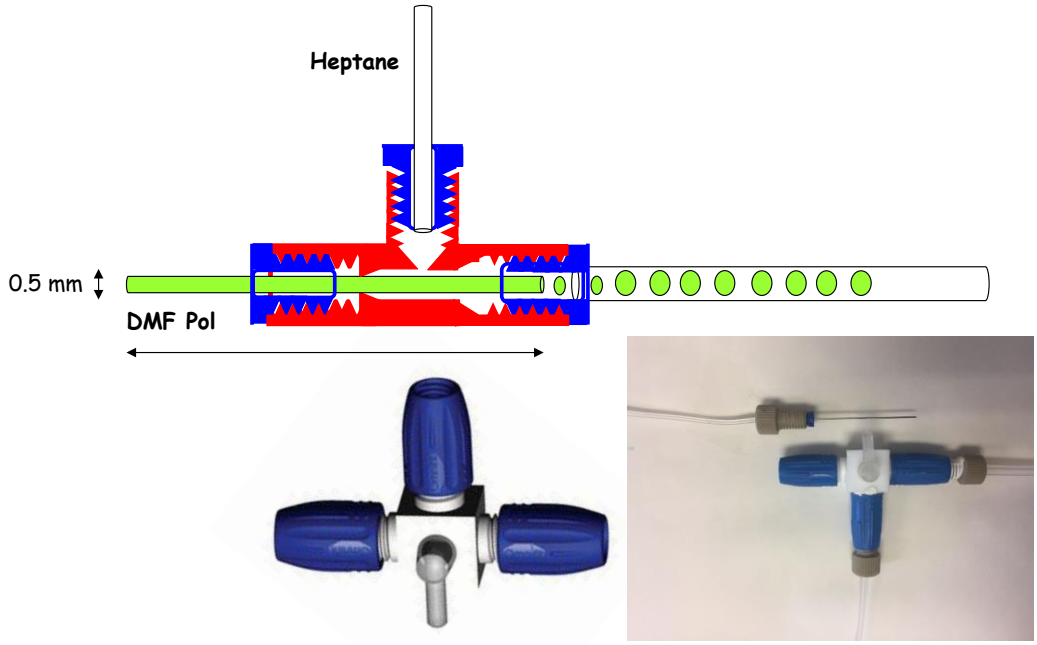

Figure 2. Droplet generator. 1/8 in. (1.5mm) Teflon tee-piece fitting with a needle though (0.5 mm i.d.).

This simple device produces drops when two immiscible fluids (DMF and heptane) meet at the exit of the needle breaking up into droplets of DMF (blue colored in Figure 3, color provided by a dye soluble in DMF but not in the heptane) dispensed in a surrounding immiscible fluid (heptane, Figure 3, Figure SI.1). In all the cases, together with the formation of the droplet, the generation of a gas slug, in this case air, was observed (Figure 3b and 3c). The droplet generator was connected to a PTFE tube (678 cm of length and 0.16 cm ID) corresponding with a volume of 13.62 mL, to provide the required residence time for the modification and the cross-linking of a DMF soluble poly(acrylamide-thiolactone) linear polymer to afford the corresponding functionalized insoluble polymeric beads (Figure 3b, see also in the available video SI.V1-2).

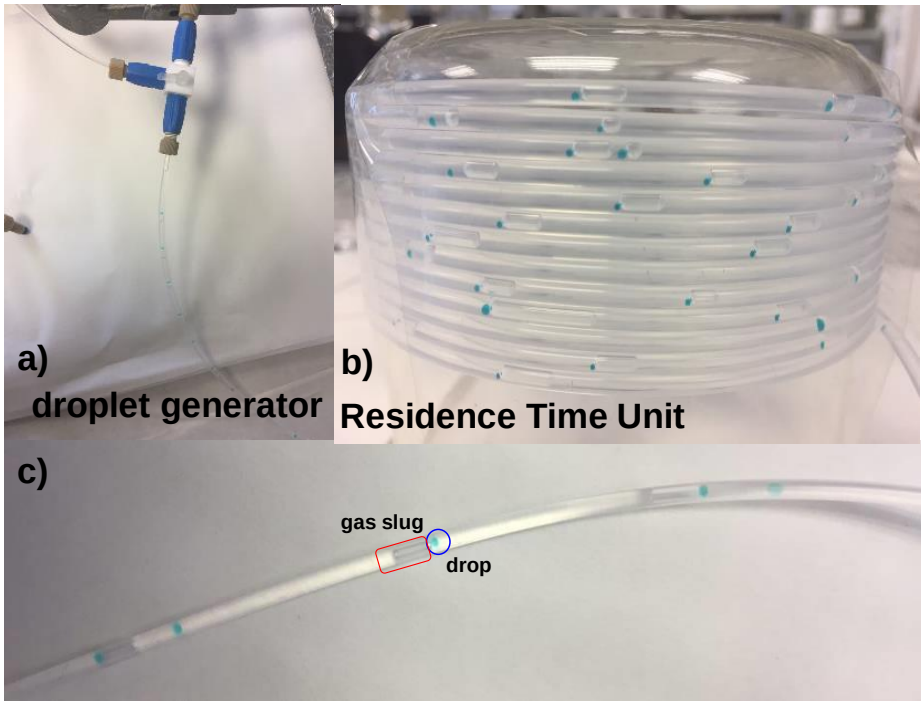

Figure 3. Droplets generated by the phase-phase system. Flow rates: phase 1 0.075 mL/min of DMF dyed with Malachite Green and 5 mL/min of heptane.

Gelation Studies

The starting poly(acrylamide-thiolactone) linear polymer (**1**) was prepared by RAFT polymerization as already reported.[10] A simple three-component sequential reaction enables the bi-functionalization of the polymer **1** and the simultaneous crosslinking of the polymeric chains into the corresponding modified polymer **4** (Scheme 1). 3-(Di-methylamino)-1-propylamine (**2**) was selected as an *n*-alkyl-amine to introduce a basic tertiary amine functional group (first level of functionalization, Scheme 1), while 1,5-di-amino-heptane (**3**) was used as the cross-linker. The amylolysis reaction produces *in-situ* thiol groups, which may also contribute, in the absence of any additional modifier, to a dynamic

[10] Montolio, S.; Zagorodko, O.; Porcar, R.; Burguete, M. I.; Luis, S. V.; Tenhu, H.; García-Verdugo, E. Poly(Acrylamide-Homocysteine Thiolactone) as a Synthetic Platform for the Preparation of Polymeric Ionic Liquids by Post Ring-Opening-Orthogonal Modifications. *Polym. Chem.* **2017**, *8* (33), 4789–4797.

crosslinking of the polymer chains by the formation of sulfur bridges (R-S-S-R). These two crosslinking reactions (covalent and dynamic) led to the gelation of the polymer solution.[10]

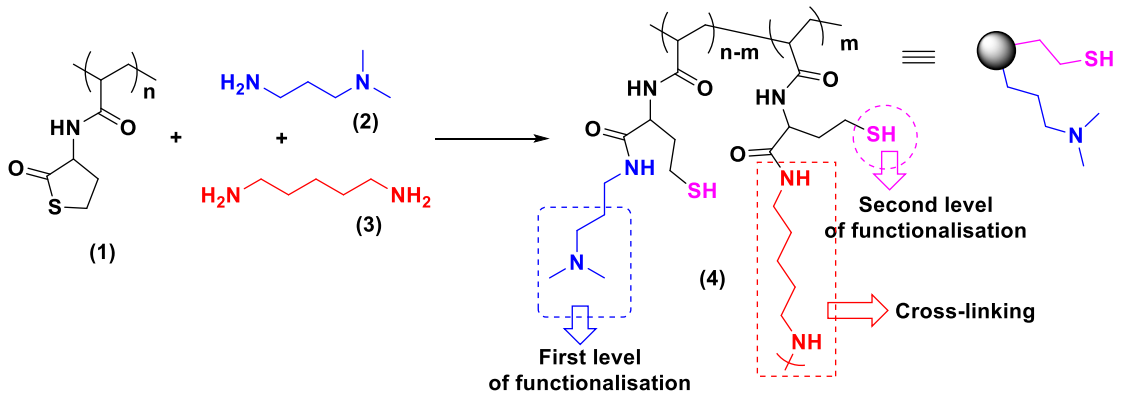

Scheme 1. Modification of poly(acrylamide-thiolactone) (**1**) with 3-(di-methylamino)-1-propylamine (**2**) and 1,5-di-amino-pentane (**3**).

Under continuous flow conditions, the modification of the polymer and its gelation in the droplets, can freeze the shape of the resulting crosslinked polymers leading to beads formation. However, it should be noted that if the gelation is too fast and takes place before droplet formation the reactor can be blocked. Thus, the gelation rate was initially screened in HPLC vials using the stable-to-inversion test.[11,12] Table SI.1 shows the results obtained for these experiments. The tests were carried out using a 1:1.5:0.2 molar ratio for the polymer, *n*-alkyl-amine **2** and *n*-alkyl-di-amine **3**. The gelation time was highly dependent of the polymer concentration. Indeed, a decrease in the polymer concentration produced an increase in the gelation

[11] After a given period time, the vial containing the polymeric solution with the reactants was inverted and if no flow downwards of the polymeric material was observed the sample was considered a gel. The gelation time was defined as the minimum time at which the polymer solution does not flow under its own weight when the vial was turn upside-down.

[12] Raghavan, S. R.; Cipriano, B. H. Gel Formation: Phase Diagrams Using Tabletop Rheology and Calorimetry. In *Molecular Gels: Materials with Self-Assembled Fibrillar Networks*; Weiss, R. G., Terech, P., Eds.; Springer Netherlands: Dordrecht, 2006; pp 241–252.

time, with gelation times going from 20 to 50 min with the decrease of the concentration from 1.114 to 0.826 M.

An additional factor having a strong influence on the gelation time was the amount of crosslinking agent used, in this case the polymer to *n*-alkyl-di-amine ratio. Table SI.2 summarizes the results obtained in an initial screening for the influence of this parameter. As expected, in the absence of diamine **6**, the gelation did not take place, as no covalent crosslinking occurred (Entry 1, Table SI.2). For crosslinking degrees lower than 20%, gelation was not observed even after 24 h in the absence of air (Entries 2 and 3, Table SI.2). The use of a large excess of the crosslinking agent (Entry 4, Table SI.2) led to the instantaneous gelation of the polymeric solution. Efficient gelation took place, in the absence of air, for nominal crosslinking degrees higher than 40%. The gelation time, under these conditions, could be controlled with the amount of crosslinking, increasing from 2 to 10 min when the nominal crosslinking changed from 100% to 40% (Entries 5-7, Table SI.2).

Synthesis of modified PAHT under flow conditions

Once proved the gelation feasibility of the polymeric solution with the suitable concentration and crosslinking degree, the formation of the polymeric cross-linked beads under flow conditions was evaluated. Two different DMF solutions (A and B) were pumped into the droplet generation device using syringe pumps. Solution A contained the poly(acrylamide-thiolactone), while the polymer modifiers were enclosed in solution B. The second immiscible phase (heptane), requiring higher flow rates for the formation of stable and well-formed droplets, was pumped using a HPLC pump (Figure SI.1). All the pumps and elements of the reactor were connected using a 1/8 inch PTFE tubing.

Table 1. Synthesis of functional crosslinked polymers from **4**.[a]

Entry	Phase 1		Phase 2	Sol. A	Sol. B			Ratio		Res. Time (min)
	Flow A (mL/min)	Flow B (mL/min)	Heptane (mL/min)	**4**[b] (M)	**5**[c] (M)	**6**[d] (M)	Et_3N[e] (M)	5+6:4:	4:6	
1	0.075	0.109	4	2.34	2.39	0.32	4.77	1.88	5.0	3.25
2	0.075	1.500	5	2.34	1.92	0.26	3.83	20.85	0.5	2.07
3	0.050	0.067	2	2.34	1.58	0.21	3.20	1.15	8.3	1.35
4	0.050	0.067	10	1.75	1.58	0.21	3.20	1.53	6.2	6.38
5	0.050	0.083	2	1.17	1.19	0.16	2.39	2.14	4.4	2.66
6	0.050	0.067	5	1.17	1.58	0.21	3.20	2.29	4.2	6.43

[a] Phase 1: Solution formed by mixing Sol A (**1** in DMF) with Sol B (**5**+**6**+Et_3N in DMF) and Phase 2: Heptane; [b] Concentration of **4** in DMF before the mixing point; [c] concentration of 3-(di-methylamino)-1-propylamine (DMAPA, **5**) in DMF before the mixing point; [d] concentration of 1,5-diamino-pentane (**6**) before the mixing point; [e] concentration of Et_3N before the mixing point.

All the experiments were performed at room temperature, and the effect of different experimental parameters like the residence time, concentration of the homopolymer and the ratio of *n*-alkyl-amine **5** and *n*-alkyl-di-amine **6** relative to the homopolymer was analyzed. Table 1 summarizes the conditions tested. The initial experiments were performed with a polymer solution (Sol A) of 2.34 M in DMF (Entries 1-3, Table 1). This solution was pumped at two different flow rates (0.075 mL/min and 0.050 mL/min, flow A) and diluted in the T-piece connection (b in Figure SI.1) with a second solution (Sol. B). Solution B presented a variable concentration of Et_3N, **5** and **6** (Table 3, Entries 1-3). The final concentration of all of reactants at the mixing point depended of the flow rates used (flow A and B). Under the conditions reported in Entry 1, a blockage of the needle of the droplet generator was observed. The blockage is likely to be due to a fast reaction between the polymer **4** and the amines (**5** and **6**). Similar results were observed when the conditions of the Entry 2 were assayed, although this time the blockage was located directly in the T-piece where solution A and solution B met. In this case, a larger flow rate of B (1.5 mL/min) was used to try to reduce the concentration of the polymer (0.11 M) avoiding the clogging. However, such conditions involve of large amounts of the amines, which can induce a fast crosslinking and precipitation of the modified polymer. Finally, reducing the flow rates of solution A and B to 0.050 and 0.065 mL/min (Table 3, Entry 3) the formation of droplets was achieved. Under these conditions, the concentration of the polymer after the mixing point was 1 M in DMF and a nominal crosslinking of *ca*. 25 % was expected. Unfortunately, the droplets of polymer formed in the droplet generator tended to fuse together in the residential unit to form an insoluble filament, which can be collected at the exit of the reactor (Figure SI.2a). The residence time was also reduced by increasing the heptane (phase 2) flow rate from 2 to 10 mL/min in order to avoid the fusion of the droplets, but the same effect was found.

In the light of those initial results, we decided to use similar conditions than those of used in the Entry 3, keeping the flow rates for solutions A and B at 0.050 and 0.065 mL/min (Table 3, Entry 4) but reducing the initial concentration of the polymer from 2.34 to 1.75 M. The flow rate of the second phase (heptane) was set to a high flow rate value (10 mL/min). Furthermore, the reactor was introduced in an ultrasonic bath in order to avoid the possible fusion of the polymeric droplets formed. In this case, the concentration of the polymer **4** after the mixing was 0.75 M and a nominal crosslinking of *ca*. 30% was expected. Under these conditions, the droplets were formed and individual spherical particles were obtained and collected but most of the polymer was obtained as an insoluble pearl necklace type system (Figure SI.2b) resulting from the partial fusion of the polymeric droplets inside of the reactor unit.

In order to address this issue, the concentration of the polymer after the mixing point was further reduced from 0.75 to 0.44 M (Table 3, Entry 5) by increasing the flow rate of the solution B that simultaneously afforded an increase of the nominal crosslinking to *ca*. 47%. The heptane flow rate was reduced to 2 mL/min. Under these conditions a soluble polymer was obtained, the gelation and crosslinking did not take place under the concentration assayed. Finally, the concentration of the polymer **4** was slightly reduced in comparison with the conditions reported in Entry 4 from 0.75 to 0.50 M but the same flow rates of the sol. A and B were used (Table 3, Entry 6). Under these conditions, the system achieved a continuous production of polymeric spherical particles with a nominal crosslinking of *ca*. 47%. Under these experimental conditions, the functional polymer yield obtained after filtration, washing and drying was *ca*. 62 % (Figure SI.2c). The post-modification and crosslinking of the polymer **1** was repeated several times achieving comparable results, which

showed the robustness of the methodology to produce the functional polymers in beads form.

Characterization of cross-linked functionalized beads

The polymeric beads were analyzed to verify their nature and properties. Thus, initially, the beads were characterized by FT-IR-ATR. Figure 4 compares the spectra of the obtained polymeric beads (**4**) and the unmodified polymer (**1**). The aminolysis reaction was confirmed by the disappearance of the signals at 1696 cm^{-1} and 919 cm^{-1} assignable to the C=O and the C-S bonds of the thiolactone, suggesting the complete aminolysis of the thiolactone groups.[10] Furthermore, the bands for $C{=}O_{amide}$ and $N{-}H_{amide}$ shifted to 1652 cm^{-1} and 3325 cm^{-1} from the initial position in **1** at 1642 cm^{-1} and 3273 cm^{-1}. The modified polymer also showed new signals at 2817 cm^{-1} and 2862 cm^{-1} corresponding to the $C{-}H_{st}$ band of the methyl group from 3-(dimethylamino)-1-propylamine and at 2776 cm^{-1} assignable to the thiol group. Indeed, the presence of free thiol groups was confirmed by a positive Ellman's test, which consists on the development of an orange color on the polymers caused by the reaction of the –SH groups with Ellman's reagent (Figure 4, insert).[13,14] The elemental analysis of the resulting polymer revealed a loading of 2.65 meq of SH / g polymer The Raman analysis of the polymeric beads also provided additional information.

[13] Ellman, G. L. A Colorimetric Method for Determining Low Concentrations of Mercaptans. *Arch. Biochem. Biophys.* **1958**, *74* (2), 443–450.
[14] Gaggini, F.; Porcheddu, A.; Reginato, G.; Rodriquez, M.; Taddei, M. Colorimetric Tools for Solid-Phase Organic Synthesis. *J. Comb. Chem.* **2004**, *6* (5), 805–810.

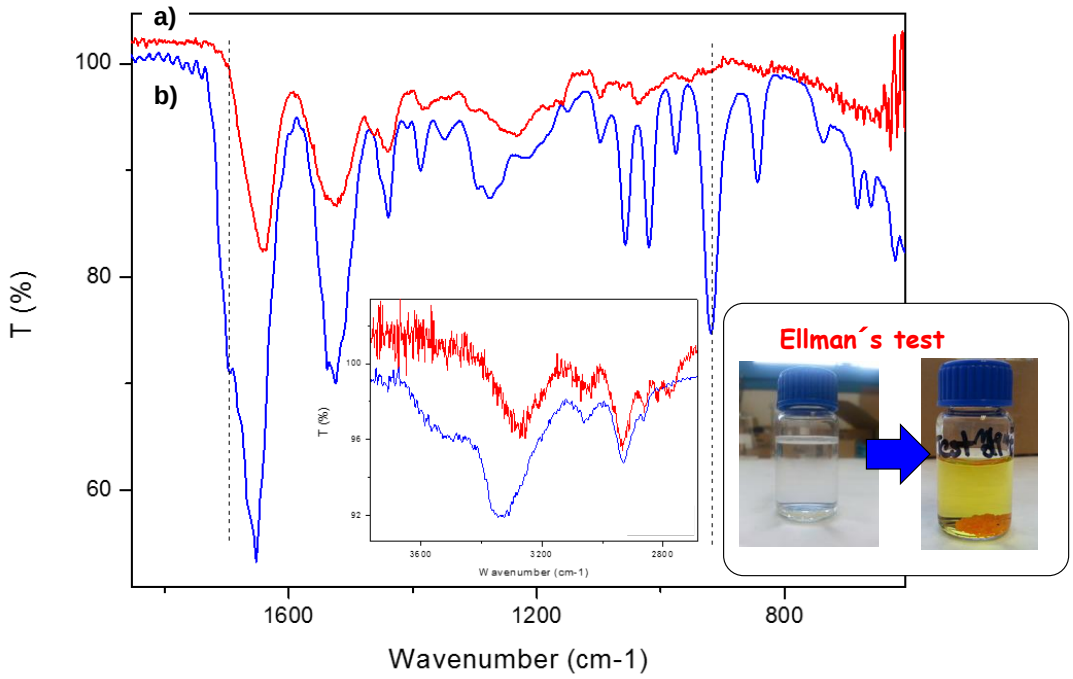

Figure 4. FT-IR-ATR **(a) 1** and **(b) 4.** Insert: Ellman test.

Altogether, the FT-IR-ATR and the Ellman´s test suggests a successful conversion of the homocysteine thiolactone groups of the initial polymer by aminolysis with the amines **5** and **6**. The mean size of the particles was determined using a Coulter counter system and showed a bimodal size distribution, where *ca*. 20% of the particles displayed sizes centered at 829 µm and *ca*. 80% at 1426 µm sizes around 1345 µm (Figure SI.3). It seems that the particle size is mainly determined by the internal diameter of the tubing used to build the reactor (0.16 cm ID).

Swelling experiments are a simple and relevant methodology to characterize the nature of a polymeric network.[15] No appreciable swelling was observed for the polymer beads in dichloromethane, while in polar

[15] Santini, R.; Griffith, M. C.; Qi, M. A Measure of Solvent Effects on Swelling of Resins for Solid Phase Organic Synthesis. *Tetrahedron Lett.* **1998**, *39* (49), 8951–8954.

solvents a good swelling was observed with a *ca*. 50% increase in volume for the swollen beads, in agreement with the polar nature of the polymeric backbone.

Chemical modification of the beads

The thiol group is a versatile fragment able to react with different reagents to facilitate the introduction of a second level of functionality. Thus, the polymeric beads **4** obtained by post-polymerization modification of **1** could be further modified to obtain materials with orthogonal functionality. Scheme 2 depicts the two different modifications assayed to introduce new functional groups in the polymer.

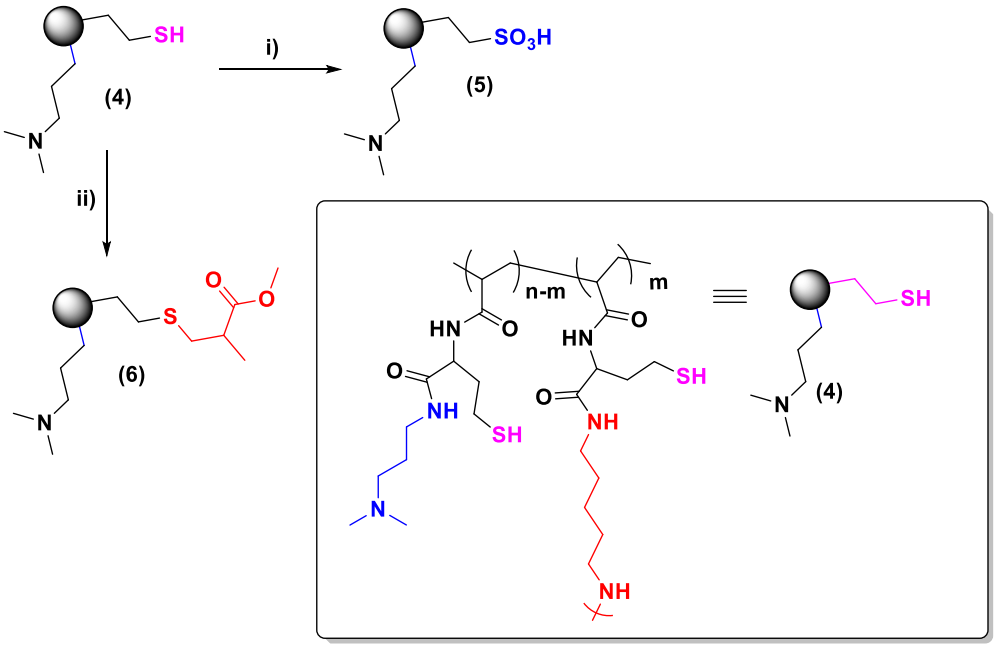

Scheme 2. Chemical modification of the polymeric beads (**4**) based on the thiol grups present. i) MeOH, H_2O_2 (32%), r.t., 2 h. ii) (a) 1,4-dioxane, PPh_3, r.t., 4 h., N_2, (b) DMF, methyl methacrylate, 80 ^oC, 24 h., N_2.

Oxidation of the thiol group to sulfonic acid groups

The oxidation of the -SH groups of **4** to -SO_3H is highly attractive as it can lead to bifunctional heterogeneous catalysis with the coexistence of incompatible catalytic species, such as acid and base, nearby on a same solid particle surface (Scheme 2). The thiol group can be transformed into the corresponding -SO_3H groups by oxidation with hydrogen peroxide. The dropwise addition of the oxidant to a suspension of the polymer at 0 ºC using a 1:2 SH: H_2O_2 molar ratio led to the oxidation of the –SH groups as confirmed by IR spectra (Figure SI. 5) The appearance of new peaks at 1037 cm^{-1}, 1175 cm^{-1} and 1203 cm^{-1} confirmed the oxidation of the SH groups into the corresponding -SO_3H groups.

Thiol-ene reaction

Thiol groups allow the introduction of new moieties by thiol-ene reactions with alkenes to form alkyl sulfides. This is a classical click reaction given its high yield, stereoselectivity, high rate, and thermodynamic driving force, and facilitates a simple modification of polymers.[16] In this context, the reaction between the thiol groups present in the polymeric beads of **4** and methyl methacrylate was evaluated (Scheme 2). Polymer **4** was initially treated with triphenylphosphine as a reducing agent able to cleave the possible sulfur bridges (-S-S-) developed. Then, the beads were reacted with methyl methacrylate under an inert atmosphere and at 80 ºC for 24 h. After filtering, washing and drying, the FT-IR-ATR of the resulting beads showed the presence of a new carbonyl band assignable to the ester groups of the acrylate fragments at 1733 cm^{-1} (Figure SI.6) suggesting the successful modification of the beads and the transformation of polymer **4** into

[16] Lowe, A. B. Thiol-Ene "Click" Reactions and Recent Applications in Polymer and Materials Synthesis. *Polym. Chem.* **2010**, *1* (1), 17–36.

polymer **6**. This demonstrates that the –SH groups are easily accessible for different orthogonal modifications, opening the possibility to design materials with two levels of functionalization.

Catalytic application

The obtained multifunctional beads could be exploited for catalytic purposes. Polymer **6** presents in their structure a basic group (-$N(CH_3)_2$) able, in principle, to catalyze the Knoevenagel condensation between *p*-nitro-benzaldehyde (**7**) and ethyl 2-cyanoacetate (**8**, Scheme 3) and the Henry reaction between *p*-nitro-benzaldehyde (**7**) and nitromethane (**10**). The tests were carried out using dimethyl carbonate (DMC) as the solvent. Under the same conditions, the reactions did not proceed in the absence of polymer **6**. With polymer **6** as the catalyst yields obtained were 82% for the Knoevenagel condensation, and 72% for the Henry reaction showing the catalytic effect of the basic units (-NR_3) presented in the polymer **6**.

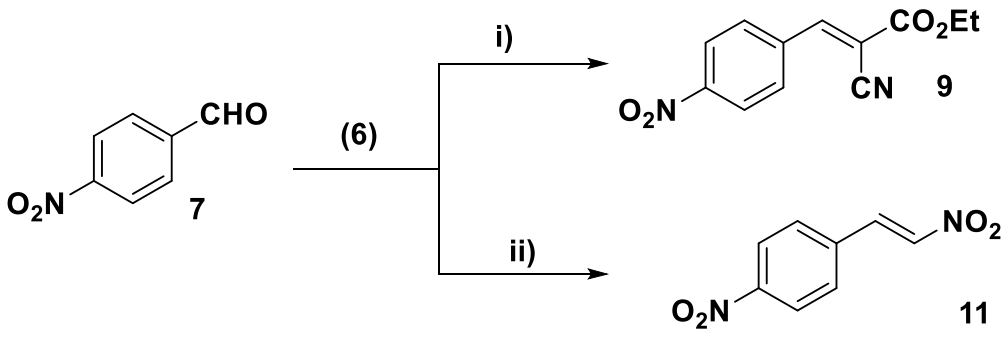

Scheme 3. Evaluation of the catalytic properties of 6. i) ethyl 2-cyanoacetate (8) in DCM (750 µL, 1:1 molar ration of **7**:**8**) 40 °C, 24 hours,. ii) Nitromethane(10) in DCM (750 µL, 1:4 molar ration of 7:10) 80 °C, 24 hours.

4.3. Conclusions

We have demonstrated that crosslinked functional spherical polymers (beads) can be obtained by post-modification of poly(acrylamide-thiolactone) by a simple and robust approach using a simple continuous flow setup. The soluble linear poly(thiolactone) was converted in the presence of an amine and a crosslinker in the corresponding spheres via continuous droplets generation and *in-situ* gelation and crosslinking. The adjustment of the experimental conditions (i.e. polymer concentration, crosslinking, flow rates, etc) allows to obtain beads after only six minutes of residence time. The presence of the thiol groups allows the introduction of additional functionalities. Initial studies suggest that these new functional resins may find applications in catalysis but also in other areas such as SPPS, SPOS, scavenging, immobilization of enzymes, etc.

4.4. Experimental Section

Materials

All the reagents and solvents used were commercially available. DL-homocysteine thiolactone hydrochloride, acryloyl chloride, cyanomethyl dodecyl trithiocarbonate (CMDTTC), triethylamine, 3-(dimethylamino)-1-propylamine, 1,5-diaminopentane, azobisisobutyronitrile (AIBN), hydrogen peroxide, acetic acid, methyl methacrylate, triphenylphosphine, chloroauric acid, sodium borohydride, 4-nitro-benzaldehyde, ethyl cyanoacetate, 1,4-dioxane, N,N-dimethylformamide (DMF), dimethyl sulfoxide (DMSO), diethyl ether, dimethylcarbonate (DMC), 2-methyl tetrahydrofuran (2-MeTHF) were purchased from Sigma Aldrich and used without further purification. Sodium hydrocarbonate was purchased from Riedel-de-Haën (Seelze, Germany) and used without further purification.

General characterization protocols

FT-IR-ATR spectra were obtained using a spectrometer (JASCO FT/IR-6200) equipped with an ATR (MIRacle single-reflection ATR diamond/ZnSe) accessory at 4 cm^{-1} resolution (4000-600 cm^{-1} spectral range). Raman spectra were obtained with a NRS-3100 (Jasco) dispersive Raman spectrometer equipped with an optical microscope and an air-cooled CCD detector (-65 ^{o}C) using the following conditions: 785 nm laser with a single monochromator, 600 l/mm grating, 0.2 mm slit, 12.75 cm^{-1} resolution; with a center wavenumber of 1200 cm^{-1}, a laser power of 90.1 mW and 10 accumulations of 5 s. Elemental analyses were obtained with a CHN Euro EA 3000 instrument. ^{1}H-NMR experiments were carried out using a Varian INOVA 500 (^{1}H-NMR, 500 MHz) and Bruker 400 MHz spectrometer. Chemical shifts are given in delta (δ) values relative to TMS and the coupling constants (*J*) in Hertz (Hz). Distribution dimension was obtained with a LS particle size analyzer Beckman Coulter.

^{1}H-NMR experiments were carried out using a Varian INOVA 500 (^{1}H-NMR, 500 MHz) spectrometer. Chemical shifts are given in delta (δ) values relative to TMS and the coupling constants (*J*) in Hertz (Hz). IR spectroscopy was used to monitor the synthesis of the monomers and polymers. The FT-IR-ATR spectra were obtained at 4 cm^{-1} resolution for the 4000 to 600 cm^{-1} spectral range using a spectrometer (JASCO FT/IR-6200) equipped with an ATR (MIRacle singlereflection ATR diamond/ZnSe). Elemental analyses were obtained with a CHN Euro EA 3000 instrument. Distribution dimension was obtained with a LS particle size analyzer Beckman Coulter.

Modular plug-play flow platform

A schematic representation of the reactor can be found in Figure SI.1. The reactive solutions were loaded in two different glass Hamilton syringes (5 and 10 mL) and

inserted in two syringe pumps Model 100 Series of KD Scientific Inc. (USA). All of components are made of PEEK, while a PTFE tubing was used.

Synthesis of poly (acrylamide-thiolactone) (1)

Acryloyl homocysteine thiolactone (171 mg, 1 mmol), CMDTTC (2.12 mg, 6.6 µmol) and AIBN (0.1 mg, 0.6µmol) were dissolved in DMF. The mixture was degassed through 3 freeze-thaw cycles. The reaction was allowed to proceed for 24 h at 110 ^{o}C. The polymerisation was stopped by freezing the mixture in liquid nitrogen. The product was precipitated in methanol, purified by reprecipitation from DMF to methanol and washed with diethyl ether. Yield of crude product: 85-90 %.^{1}H NMR (DMSO-d_6,500 MHz), δ (ppm): 7.21-8.25 (br. m, 1H), 7.58 (br. d, 1H), 3.40 (br. d, 2H), 2.47 (br. s,1H), 2.11 (br. s, 2H), 1.52 (br. d, 2H). ^{13}C NMR (DMSO-d_6, 101 MHz), δ (ppm): 206.4, 174.3, 58.9, 41.5, 36.0, 30.3, 27.2.

Preparation of polymer beads of polymer 4 by post-modification of 1 with a plug-play flow platform

Poly (acryloyl homocysteine thiolactone) (3 g, 1.17 mmol) was dissolved in 15 mL of DMF. Triethylamine (8.7 mL, 62.46 mmol), 3-(dimethylamino)-1-propylamine (3.9 mL, 31.23 mmol) and 1,5-diaminopentane (490 µL, 4.16 mmol) were dissolved in 6.5 mL of DMF. The flow conditions were adjusted as reported in the Entry 6 of Table 1.

Synthesis of polymer 5 by oxidation of 4 with hydrogen peroxide

A suspension of the polymer **4** (50 mg), in methanol (5 mL) was oxidized employing an excess of H_2O_2 (21.32 µL of H_2O_2 at 32 %) at room temperature for

2 h. Then, the beads were filtered, washed with water and acetone (3 x 15 mL), and dried until constant weight.

Synthesis of polymer 6 by modification of 4 by a thiol-ene reaction

Polymeric beads of **4** (50 mg) were suspended in 1,4-dioxane (30 mL) and triphenylphosphine (228.2 mg, 0.87 mmol) was added. The suspension was stirred for 4 h, at rt and under an inert atmosphere (N_2). Then, the polymer beads were filtered and suspended again in dry DMF (5 mL) and then methyl methacrylate (155µL, 1.45 mmol) was added. The suspension was stirred for 24 h at 80 ºC and under an inert atmosphere (N_2). Then, the polymer was filtered, washed with acetone and methanol (3x), and dried dry until constant weight.

Catalysis test

All the reactions were carried out under the same conditions: **7** (50 mg, 0.29 mmol), 4-nitrobenzaldehyde (22.3 mg, 0.15 mmol), ethyl cyanoacetate (15.5 µL, 0.15 mmol) or nitromethane (33 µL, 0.62 mmol), solvent (725 µL): dimethyl carbonate, 2-methyl tetrahydrofuran , ultra-pure water. The solutions were stirred with orbital stirring at 40 ºC and 180 rpm for 24 h.

4.5. Supplementary Information

Continuous flow system for the simple preparation of functionalized polymeric beads derived from Poly(acrylamide-thiolactone)

Table of Contents

Table SI.1. Effect of the concentration on the gelation time.

Entry	DMF[a] [µL]	1 [mol L^{-1}]	Inversion test[b] (time/ min)		
1	92	1.114	L (0)	L (10)	G (20)
2	137	1.026	L (0)	L (10)	G (25)
3	229	0.884	L (0)	L (10)	G (45)
4	275	0.826	L (0)	L (10)	G (50)

[a] 0.25 mL of a polymer solution of 2.34 mmol mL^{-1} (400 mg mL^{-1}) in DMF was added to different volumes of DMF containing the same amount of trimethylamine (121 µL, PAHT (**4**) : Et_3N, 1 : 1.5 molar ratio), 3-(dimethylamino)-1-propylamine (DMAPA, **5,** 55 µL, PAHT : **5 ,** 1 : 1.34 molar ratio) and 1,5-diaminopentane (**6**, 7 µL, PAHT : **6.** 5 : 1 molar ratio). 40 % mol crosslinking. [b] vial inversion test L: liquid, G: gel, the time for each vial inversion test if provided in brackets.

Table SI.2. Effect of the amount of crosslinking agent on the gelation time.[a]

Entry	5+6:1	1:6	Molar ratio crosslinking	1 [M]	Inversion test[b] (time/ min)		
1	1.49	0.00	0	0.69	L (0)	L (0)	L (24 h)
2	1.64	13.76	15	0.69	L (0)	L (10)	G (24 h)
3	1.69	10.12	20	0.69	L (0)	L (10)	G (24 h)
4	4.49	0.67	299	0.69	G (0)	-	-
5	2.49	2.00	100	0.69	L (0)	G (2)	/
6	2.09	3.34	60	0.69	L (0)	G (3)	/
7	1.90	4.98	40	0.69	L (0)	G (10)	/

[a]To 0.25 mL of a polymer solution of 1.17 mmol mL^{-1} (200 mg mL^{-1}) in DMF was added the same amount of trimethylamine (121 µL, PAHT (**4**) : Et_3N, 1 : 3 molar ratio), 3-(dimethylamino)-1-propylamine (DMAPA, **5,** 55 µL, PAHT (**4**) : **5,** 1 : 1.5 molar ratio) and a variable volume of 1,5-diaminopentane (**6**). [b] using the vial inversion test L: liquid, G: gel.

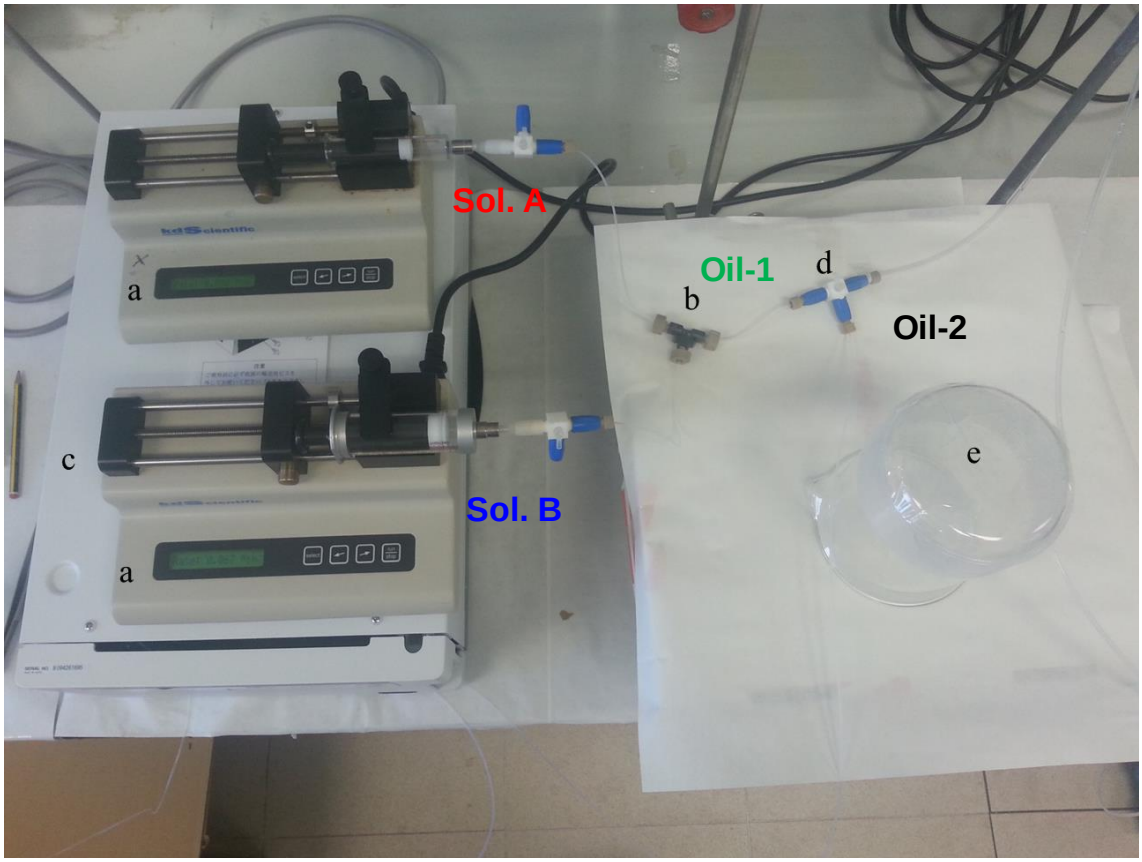

Figure SI.1. General scheme of reactor for the post-polymerization modification of **1** to obtain beads of polymer **4** in flow. **a:** syringe pumps, **b:** T-piece connection to mix solution A (polymer solution) Solution B (modifiers solutions), **c:** HPLC pump, **d:** generator droplets, **e:** residence unit (reactor).

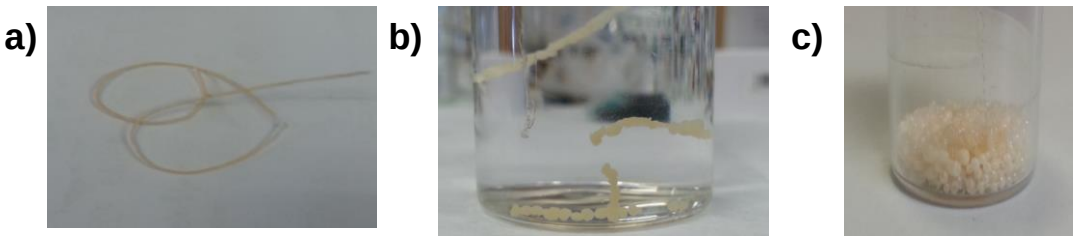

Figure SI.2. Functional insoluble polymers obtained by post-polymerization modification of **1**. **(a)** Obtained with the conditions reported in Table 1, Entry 3. **(b)** Obtained with the conditions reported in Table 1, Entry 4. **(c)** Obtained with the conditions reported in Table 1, Entry 6.

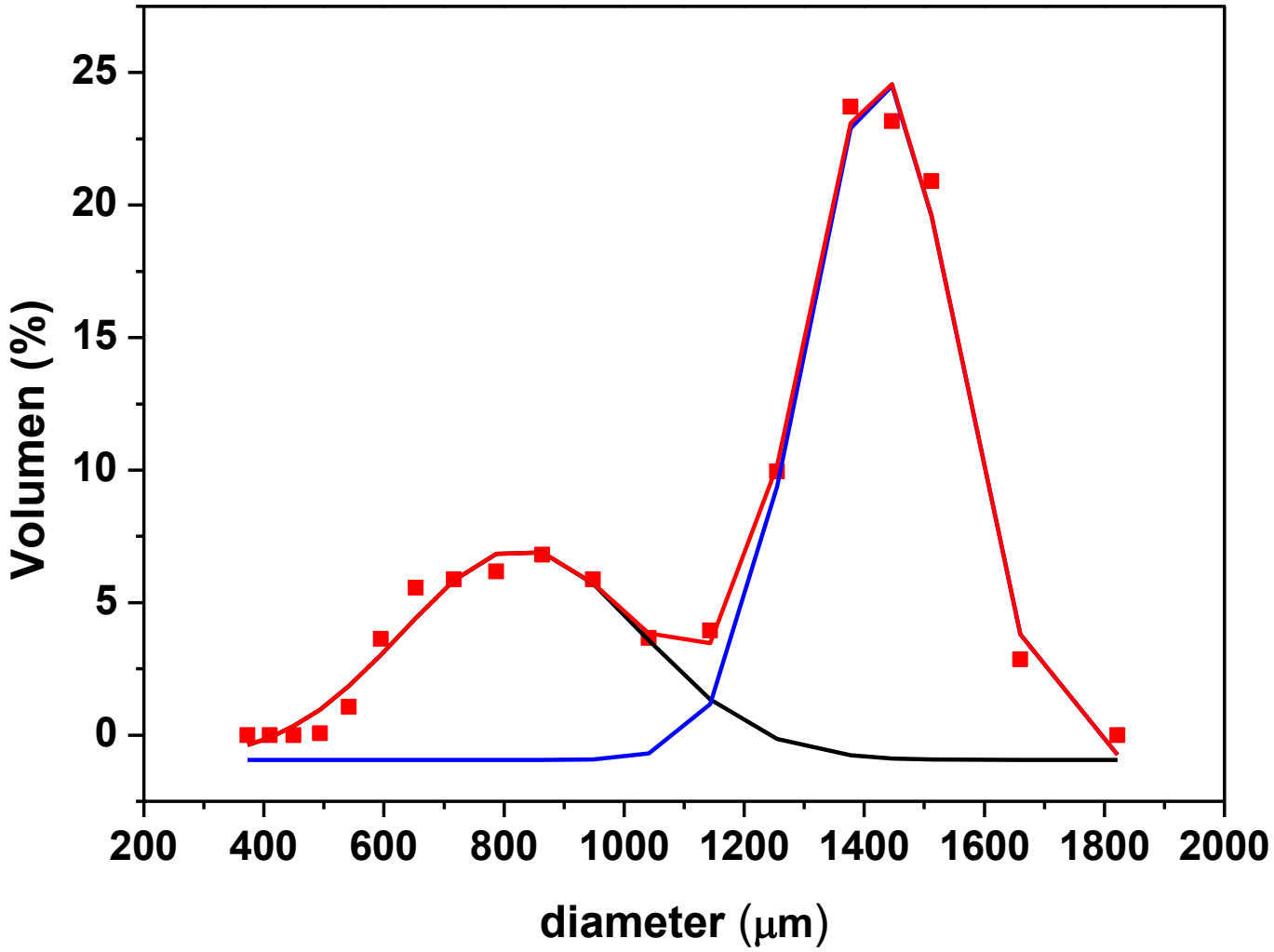

Figure SI.3. Size distribution of the polymer **4** obtained using a Coulter counter system.

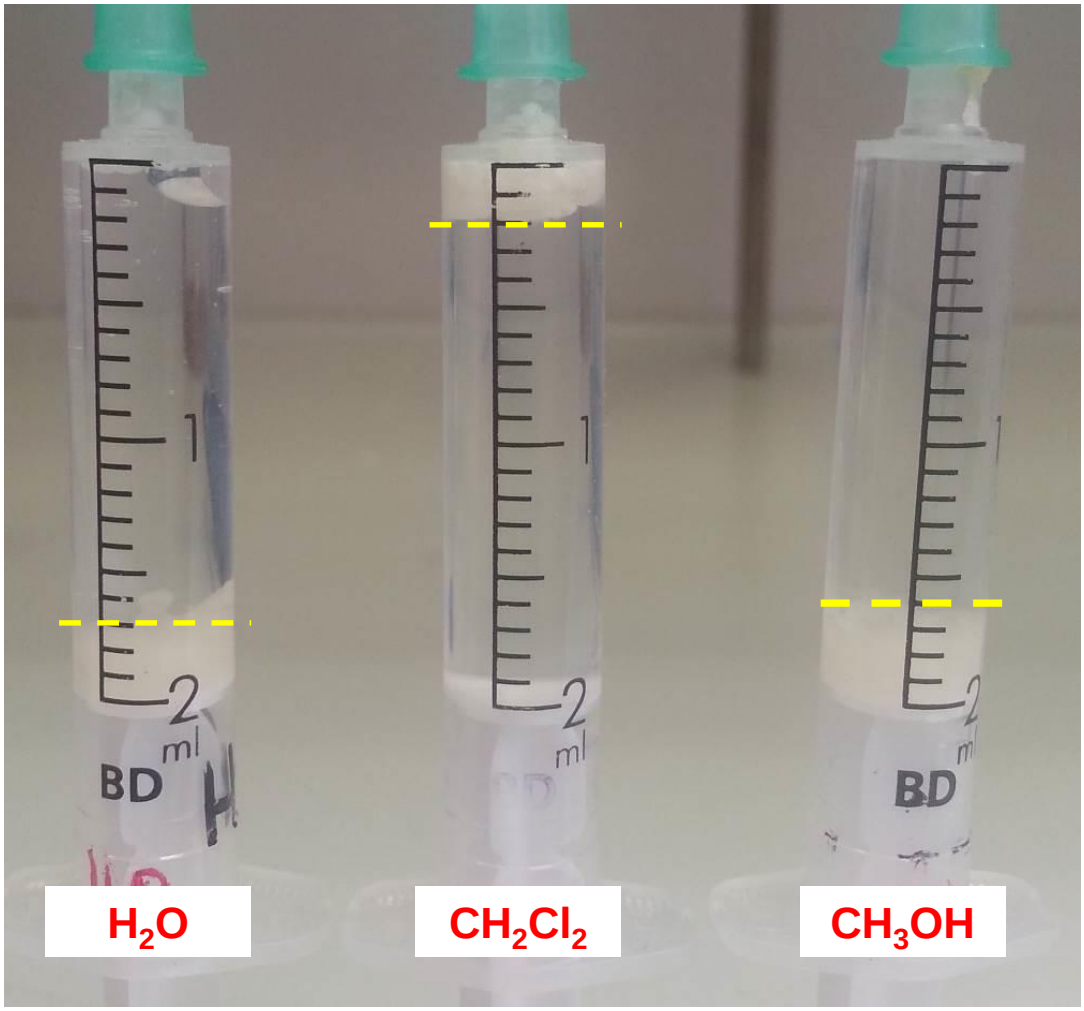

Figure SI.4. Swelling of the resin **4** in three different solvents.

Syringe method for the swelling test

The swelling properties of the polymers were measured by the syringe method. A syringe was loaded with a known amount (typically 100 mg) of the polymer, and the volume of the dry polymer was recorded (*b* mL). H_2O, MeOH or CH_2Cl_2 was added to the syringe, and the mixture was let to stand at room temperature to reach equilibrium. The extra solvent was removed from the syringe by using a plunger, and the volume of the swollen polymer was recorded (*c* mL). The swelling volume (mL g^{-1}) was estimated as the volume of solvent in the swollen polymer (*c*–*b* mL) divided by the weight of the used polymer.

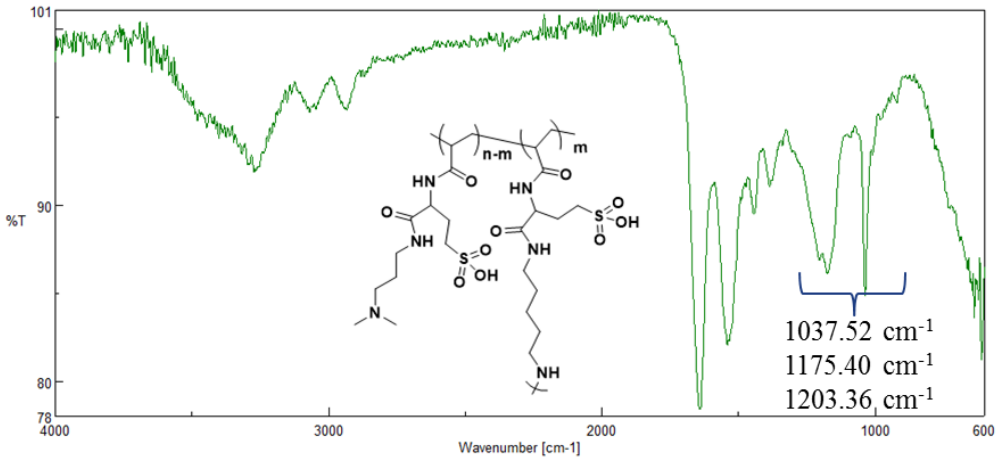

Figure SI.5. FT-IR-ATR of the polymer **5** obtained by chemical modification of **4.**

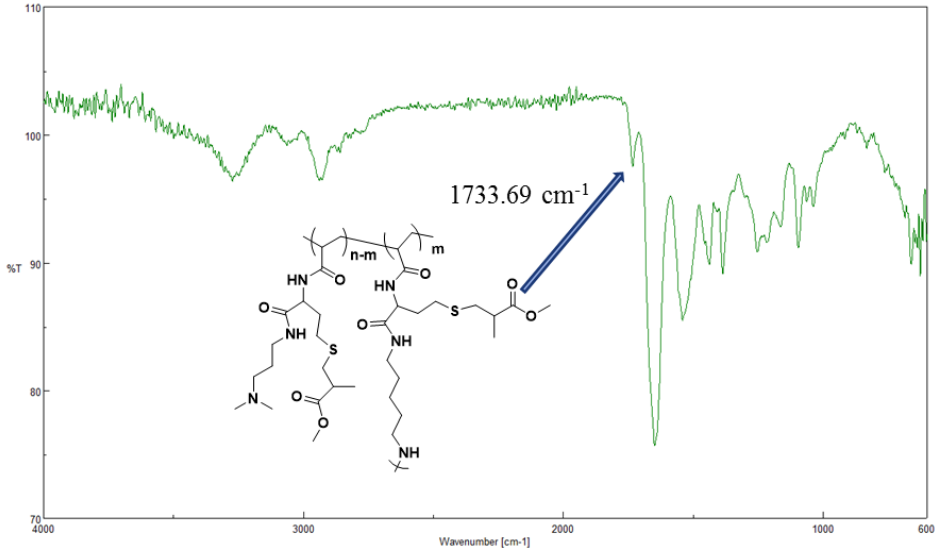

Figure SI.6. FT-IR-ATR of the polymer **6** obtained by chemical modification of **4.**

Video_SI.V1.mp4

Video_SI.V2.mp4

Video SI.V1 and S1.V2. Droplet generator to afford the corresponding functionalized insoluble polymeric beads (**4**). Droplets generated by the phase-phase system.

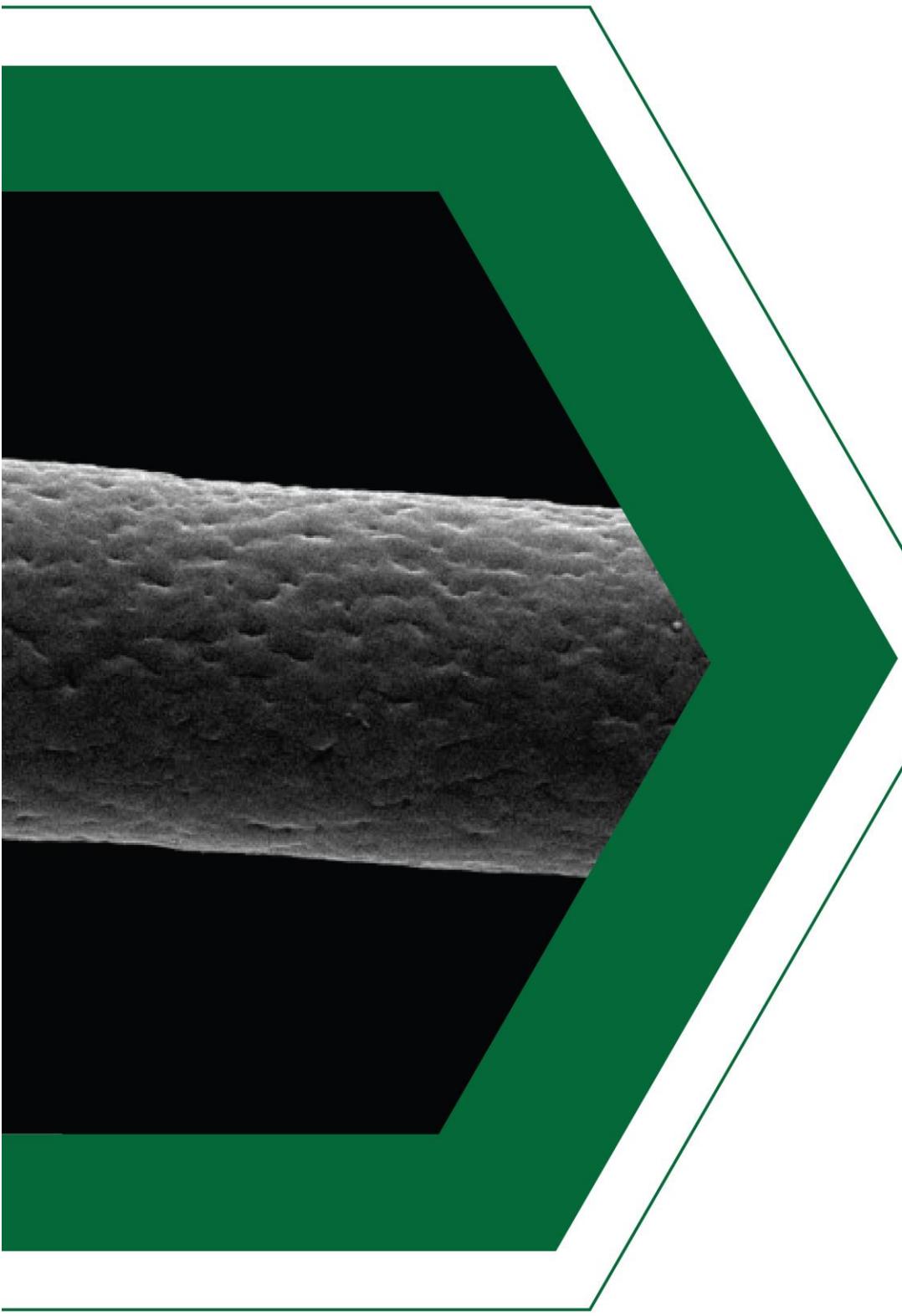

CAPÍTULO V

Preparación y aplicación de tejidos de nanofibras derivadas de Líquidos Iónicos Poliméricos

Resumen. Las mezclas de un líquido iónico polimérico derivado de la poli(homocisteína tiolactona) con poli(vinilpirrolidona) permiten la preparación de tejidos de nanofibras por electrohilado. Estos tejidos pueden ser modificados para obtener materiales con diferentes grados de funcionalización, entrecruzamiento, propiedades y morfología. El desarrollo de esta metología abre la posibilidad de obtener materiales nanoestructurados con potenciales aplicaciones en diferentes campos, como muestran los estudios preliminares realizados para aplicaciones como detección de aminas y transformacion catalitica del CO_2.

Chapter V. Preparation and application of Nanofibers mats derived from a Task Specific Polymeric Ionic Liquid

Abstract. Poly(homocysteine thiolactone) ionic-liquids / poly(vinylpyrrolidone) blends allowed the preparation of nanofiber mats by electrospinning. These mats can be modified to obtain materials with different functionality, crosslinking, properties and morphologies. The developed methodology opens the possibility to obtain nanostructured materials with potential applications in different fields as highlighted by the promising results obtained for preliminary sensing and catalytic applications.

Keywords: Poly(homocysteine thiolactone) • nanofibers • electrospinning •sensing • catalysis.

5.1. Introduction

Electrospinning techniques combine simplicity, versatility and low cost with superior capabilities to elaborate scalable ordered and complex nanofiber (NFs) assemblies.[1] NFs mats present advantages over other nanostructured materials due to their high porosity, high surface-area-to-volume ratio, interconnectivity, and ease preparation.[2] These have demonstrated their potential application in different fields such as filter

[1] Xue, J.; Wu, T.; Dai, Y.; Xia, Y. Electrospinning and Electrospun Nanofibers: Methods, Materials, and Applications. *Chem. Rev.* **2019**, *119* (8), 5298–5415.
[2] Ibrahim, H. M.; Klingner, A. A Review on Electrospun Polymeric Nanofibers: Production Parameters and Potential Applications. *Polym. Test.* **2020**, *90*, 106647.

media,[3] oil/water separation,[4] energy,[5] drug delivery,[6] sensors,[7,8] food packaging,[9] tissue engineering,[10] catalysis, [11] etc.

Polymeric Ionic Liquids (PILs) merge the unique properties of the Ionic Liquids (ILs) with those of advanced materials.[12,13] PILs with different architectures and properties can be designed according to the desired specific application.[14,15,16] Different methodologies have been assayed for

[3] Ma, Q.; Cheng, H.; Fane, A. G.; Wang, R.; Zhang, H. Recent Development of Advanced Materials with Special Wettability for Selective Oil/Water Separation. *Small.* **2016**, *12* (16), 2186–2202.
[4] Ma, W.; Zhang, Q.; Hua, D.; Xiong, R.; Zhao, J.; Rao, W.; Huang, S.; Zhan, X.; Chen, F.; Huang, C. Electrospun Fibers for Oil–Water Separation. *RSC Adv.* **2016**, *6* (16), 12868–12884.
[5] Cavaliere, S.; Subianto, S.; Savych, I.; Jones, D. J.; Rozière, J. Electrospinning: Designed Architectures for Energy Conversion and Storage Devices. *Energy Environ. Sci.* **2011**, *4* (12), 4761–4785.
[6] Sebe, I.; Szabó, P.; Kállai-Szabó, B.; Zelkó, R. Incorporating Small Molecules or Biologics into Nanofibers for Optimized Drug Release: A Review. *Int. J. Pharm.* **2015**, *494* (1), 516–530.
[7] Liu, Y.; Hao, M.; Chen, Z.; Liu, L.; Liu, Y.; Yang, W.; Ramakrishna, S. A Review on Recent Advances in Application of Electrospun Nanofiber Materials as Biosensors. *Curr. Opin. Biomed. Eng.* **2020**, *13*, 174–189.
[8] A. E. Zampetti and E. Kny Electrospinning for High Performance Sensors, Springer International Publishing Switzerland 2015
[9] Mohammadi, M. A.; Hosseini, S. M.; Yousefi, M. Application of Electrospinning Technique in Development of Intelligent Food Packaging: A Short Review of Recent Trends. *Food Sci Nutr.* **2020**, *8* (9), 4656–4665.
[10] Pham, Q. P.; Sharma, U.; Mikos, A. G. Electrospinning of Polymeric Nanofibers for Tissue Engineering Applications: A Review. *Tissue Eng.* **2006**, *12* (5), 1197–1211.
[11] Huang, Z.-M.; Zhang, Y.-Z.; Kotaki, M.; Ramakrishna, S. A Review on Polymer Nanofibers by Electrospinning and Their Applications in Nanocomposites. *Compos. Sci. Technol.* **2003**, *63* (15), 2223–2253.
[12] Zhang, S.-Y.; Zhuang, Q.; Zhang, M.; Wang, H.; Gao, Z.; Sun, J.-K.; Yuan, J. Poly(Ionic Liquid) Composites. *Chem. Soc. Rev.* **2020**, *49* (6), 1726–1755.
[13] Qian, W.; Texter, J.; Yan, F. Frontiers in Poly(Ionic Liquid)s: Syntheses and Applications. *Chem. Soc. Rev.* **2017**, *46* (4), 1124–1159.
[14] Lin, H.; Zhang, S.; Sun, J.-K.; Antonietti, M.; Yuan, J. Poly(Ionic Liquid)s with Engineered Nanopores for Energy and Environmental Applications. *Polymer* **2020**, *202*, 122640.
[15] Minami, H. Preparation and Morphology Control of Poly(Ionic Liquid) Particles. *Langmuir* **2020**, *36* (30), 8668–8679.
[16] Montolio, S.; Altava, B.; García-Verdugo, E.; Luis, S. V. Supported ILs and Materials Based on ILs for the Development of Green Synthetic Processes and Procedures. In *Green Synthetic Processes and Procedures*; 2019; pp 289–318.

the preparation of PILs, however there are only few examples of the preparation of NFs derived from PILs.[17,18,19,20]

Here, we report on the use of functionalized PILs with amide-thiolactone moieties as a unique platform for the development of NFs mats by electrospinning. The presence of the thiolactone unit allows the orthogonal post-functionalization of these NFs mats through its aminolysis in the presence of an amine (first level of functionalization) followed by the so-called thiol–alkene "click" reaction of the generated –SH groups in the presence of an alkene (second level of functionalization).

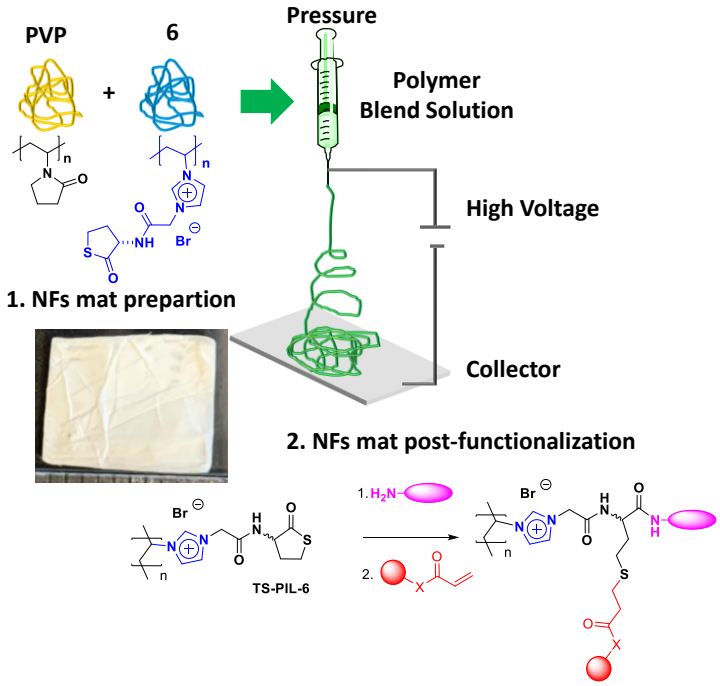

Figure 1. Preparation and post-functionalization of NFs mats derived from TS-PIL **6**.

[17] Josef, E.; Guterman, R. Designing Solutions for Electrospinning of Poly(Ionic Liquid)s. *Macromolecules*. **2019**, *52* (14), 5223–5230.
[18] Montolio, S.; Abarca, G.; Porcar, R.; Dupont, J.; Burguete, M. I.; García-Verdugo, E.; Luis, S. V. Hierarchically Structured Polymeric Ionic Liquids and Polyvinylpyrrolidone Mat-Fibers Fabricated by Electrospinning. *J. Mater. Chem. A*. **2017**, *5* (20), 9733–9744.
[19] Thomas, M.; Rajiv, S. Grafted PEO Polymeric Ionic Liquid Nanocomposite Electrospun Membrane for Efficient and Stable Dye Sensitized Solar Cell. *Electrochim. Acta.* **2020**, *341*, 136040.
[20] Pang, H.-W.; Yu, H.-F.; Huang, Y.-J.; Li, C.-T.; Ho, K.-C. Electrospun Membranes of Imidazole-Grafted PVDF-HFP Polymeric Ionic Liquids for Highly Efficient Quasi-Solid-State Dye-Sensitized Solar Cells. *J. Mater. Chem. A* **2018**, *6* (29), 14215–14223.

The high flexibility of this post-modification protocol permits obtaining a large variety of TS-PILs through the synthetic manipulation of a reduced number of common simple intermediates, easily available even in large scale. The methodology here reported not only allows introducing orthogonal functionalities but also provides a simple strategy for crosslinking the NFs without losing their NFs morphology. The simple preparation and post-medication procedures here developed allows exploiting these NFs mats as advanced materials for sensing and catalytic applications.

5.2. Results and discussion

Synthesis and characterization of a Task Specific PIL containing thiolactone fragments

The desired functionalized PIL containing amino-homocysteine thiolactone units was obtained as depicted in Scheme 1. TS-PILs **6** was synthesized by alkylation of poly(1-vinylimidazole) (**5**) with the 2-bromoacetamide of the amino-homocysteine thiolactone **3** in DMF. Poly(1-vinylimidazole) (**5**) was prepared following the methodology reported by Yuan and co-workers.[21] The alkylating agent could be synthetized in multi-gram scale by reaction of DL-homocysteine thiolactone hydrochloride (**1**) with 2-bromoacetyl bromide (**2**). This methodology allows for the synthesis of functionalized PILs with high molecular weight, which are difficult to access by direct polymerization of the corresponding functionalized IL-monomers. Indeed, it should be mentioned that all attempts to obtain the

[21] Yuan, J.; Márquez, A. G.; Reinacher, J.; Giordano, C.; Janek, J.; Antonietti, M. Nitrogen-Doped Carbon Fibers and Membranes by Carbonization of Electrospun Poly(Ionic Liquid)s. *Polym. Chem.* **2011**, *2* (8), 1654–1657.

polymer **6** by direct polymerization of the IL-monomer resulting from the alkylation of vinyl imidazole with **3** were unsuccessful.

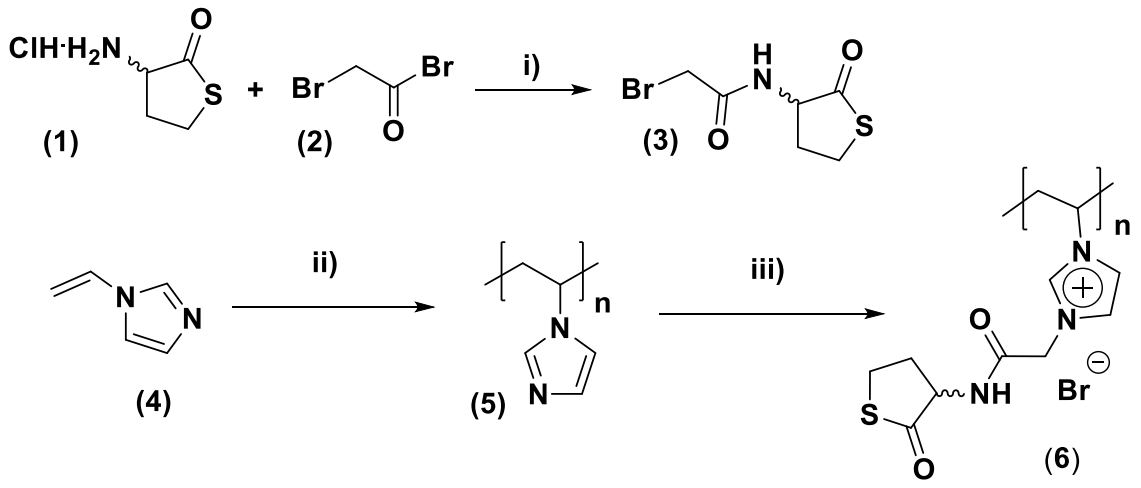

Scheme 1. Synthesis of PIL **6**. i) K_2CO_3, H_2O/CH_2Cl_2 0 °C, then rt. ii) AIBN, 100 °C, 24 h DMF. iii) DMF, 80 °C, 24 h.

The chemical modification of the polymer **5** was confirmed by FT-IR-ATR and NMR analysis. Figure 2a shows the C=C/C=N stretching bands at 1484 cm^{-1} and 1440 cm^{-1} assignable to the presence of the imidazole rings in polymer **5**. The disappearance of these bands suggests the complete conversion of these imidazole rings into the corresponding imidazolium salts (Figure 2b).

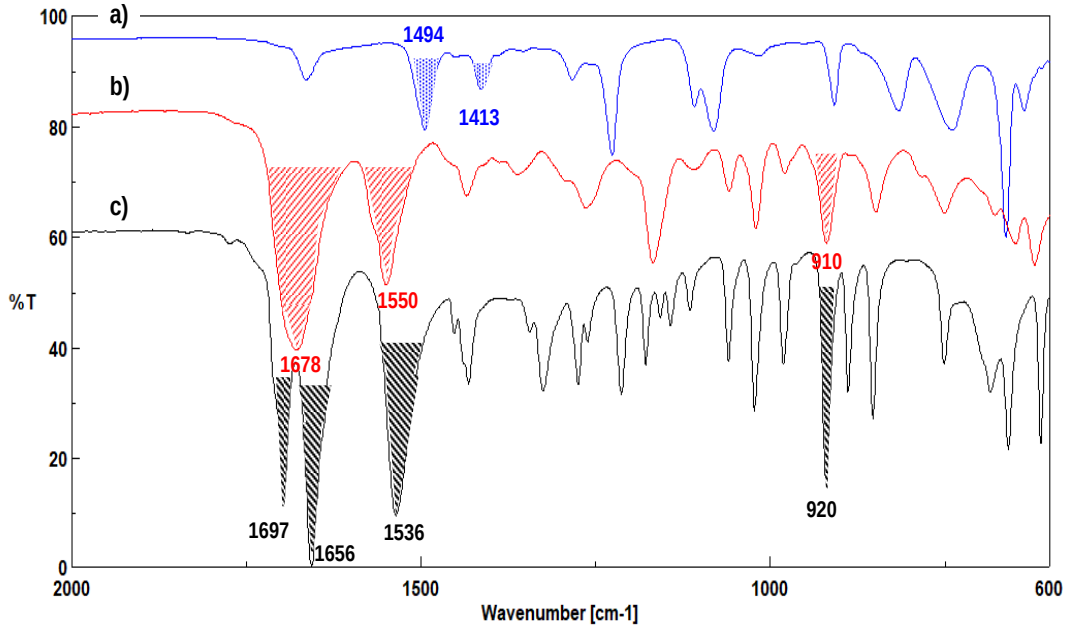

Figure 2. Synthesis of the polymer **6** monitored by FT-IR-ATR. **(a)** Polymer **5**, **(b)** Polymer TS-PIL **6** and **(c)** alkylating agent containing amino-thiolactone units (**3**).

The IR-spectra of the polymer **6** also showed the appearance of a broad band at 1650-1720 cm^{-1} associated to the C=O stretching of both thiolactone and amide carbonyl groups, appearing as two different bands for **3** (1697 cm^{-1} and 1656 cm^{-1} respectively). The polymer **6** also showed an intense peak at 910 cm^{-1} assignable to the C-S stretching of the thiolactone ring.

The ^{1}H-NMR of polymers **5** and **6** confirmed a quantitative quaternization of the imidazole rings (Figure 3). The proton signals of the imidazole ring in **5** (6.4–7.5 ppm) disappeared after the alkylation and shifted to 7.5-9.5 ppm in good agreement with the position expected for imidazolium signals.[21] A series of new signals corresponding to the protons of the -CH_2- and –CH groups in the thiolactone units appeared at 4.7-5.4 ppm. The integrals for the thiolactone proton signals at 4.7-5.4 ppm and the imidazolium and amide proton signals (7.5-9.5 ppm) displayed the expected ratio of 4.0/3.0. The presence of the peak at 209 ppm associated with C=O of thiolactone and the peak at 166 ppm assignable to the C=O of

the amide on the ^{13}C-NMR of polymer **6** confirmed successful alkylation of the polymeric imidazole (Figure SI. 14).

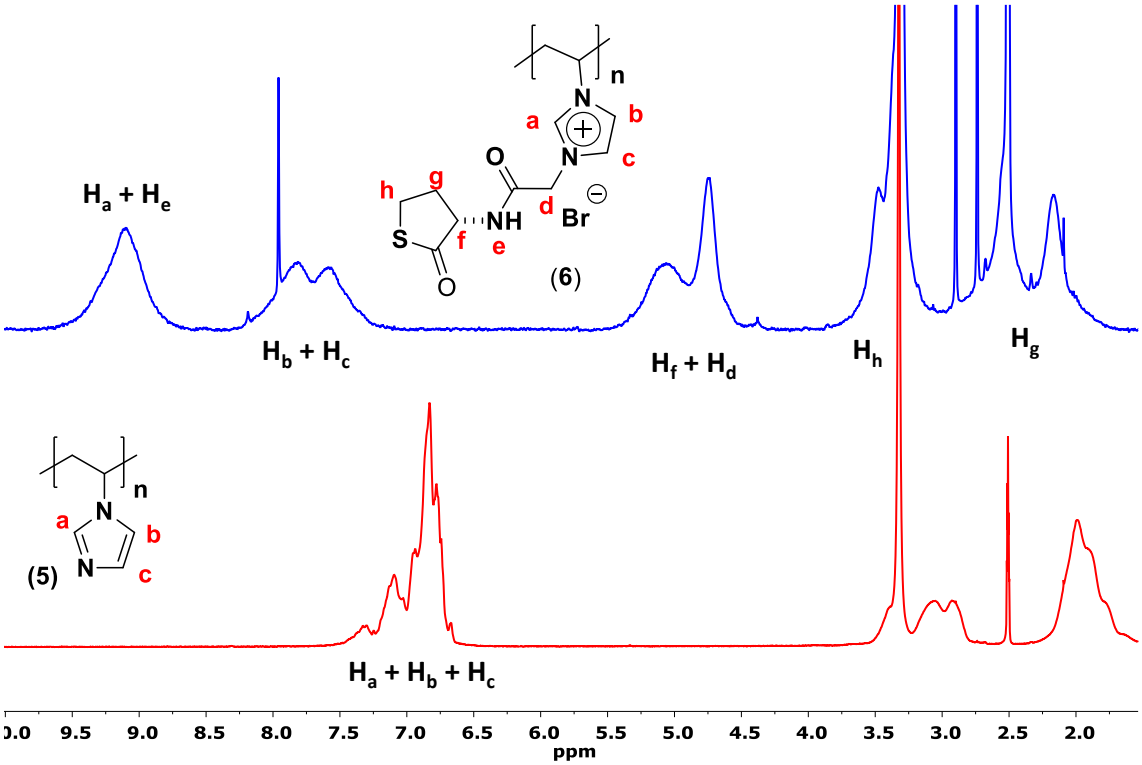

Figure 3. ^{1}H-NMR (D_2O) spectra of **5** (poly(1-vinylimidazolium bromide)) and **6** (3-acetamide- DL-homocysteine thiolactone-1-vinylimidazolium bromide).

Synthesis of NFs mats by electrospinning

The preparation of NFs mats was evaluated using different electrospinning parameters, which could be adjusted during the process by collecting small samples *in-situ* and analyzing their morphology by optical microscope. The Table SI.1 summarizes the conditions evaluated to achieve NFs formation by electrospinning. Negative voltages were applied to the collector in order to direct the electrospinning jet towards the collector. Once stabilized the efficient electrospinning conditions, NFs mats were collected over aluminum foil as membranes of *ca.* 20 x 15 cm^2. The mats were dried under

vacuum at 50 ºC and their morphology analyzed by scanning electron microscopy (SEM).

Initially, electrospinning of a 65% w/v solution of polymer **6** in DMF was assayed. The material collected under these conditions was basically composed by beads mixed with some fibers (Figure SI.1). At the view of these initial results, a 50% weight/volume polymer blend solution formed by polyvinylpyrrolidone (PVP, Mw = 1300000 g/mol) and the polymer **6** in a 1:1 weight ratio in DMF was assayed. It has been reported that PVP-PILs blends can enable the production of NFs by electrospinning.[18] Using this solution and the conditions summarized in table SI.1 the collection of NFs mats (NFm-**6**) was possible. Figure 4 shows some representative images of the morphologies observed for these electrospun mats. The PVP/**6** blend afforded a dense entanglement of bead-free fibers in most cases displaying a cylindrical form and with an average diameter of 474 nm (Figure 4a and c). The presence of some micro-ribbons instead of cylindrical fibers was also detected (Figure 4b). The width of these micro-ribbons was in the micrometer range (*ca*. 2.4 μm). The presence of these ribbons can be attributed to the association of some of the fibers.[1] The mat shows a large number of interconnected NFs crossing in different direction defining a clear open porosity. The section of the NFs mat showed a thickness of *ca*. of 92 μm (Figure 4d).

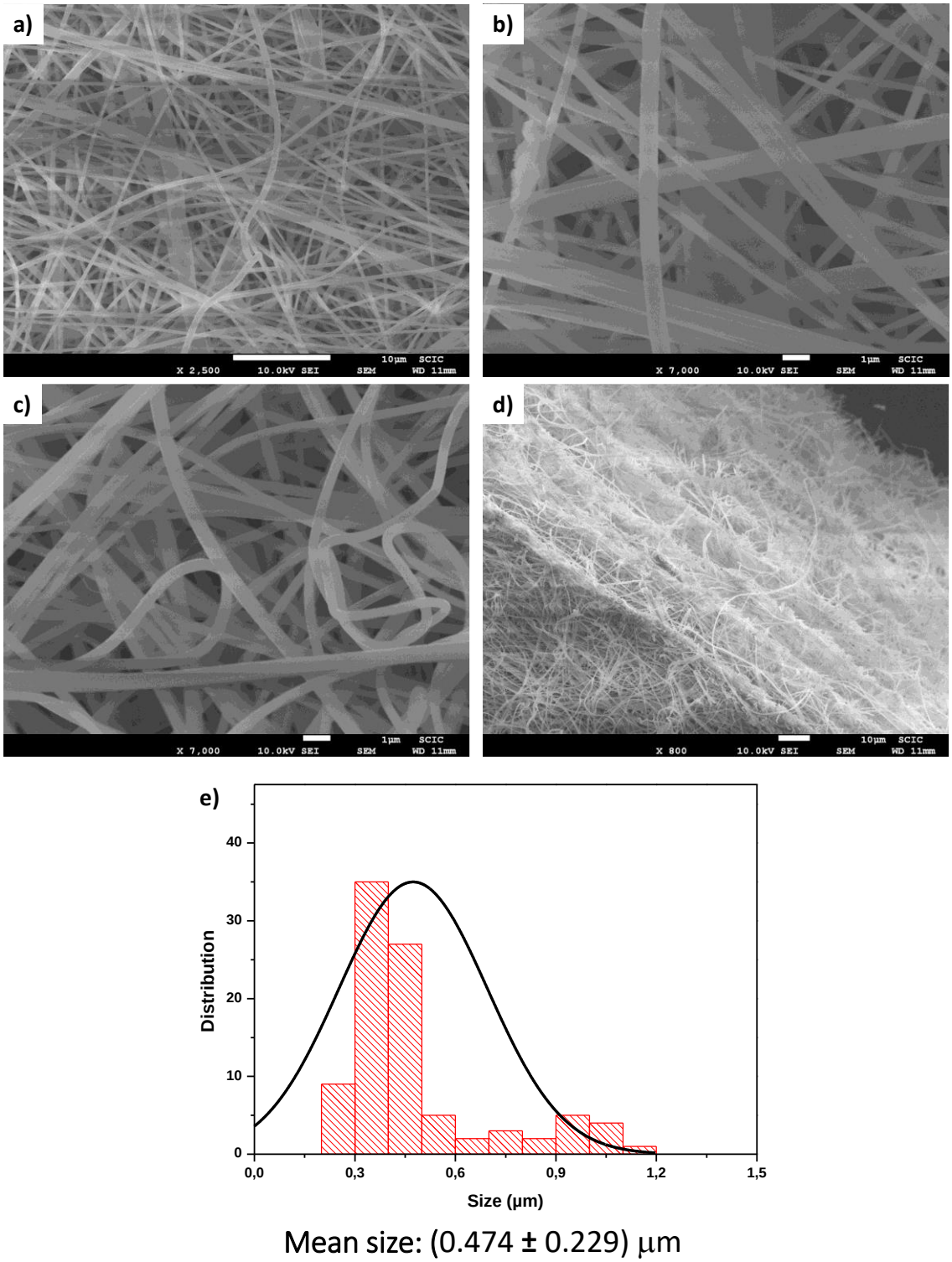

Figure 4. SEM images for the electrospun mat (NFm-**6**) formed from polymer blends PVP/TS-PIL **6** at different magnification. Surface view **(a-c)** and section view **(d)**. Scale bar represent 10 µm **(a, d)** and 1 µm (**b, c**). **(e)** NFs size distribution.

The obtained NFm-**6** was also analyzed by FT-IR-ATR showing the characteristics bands corresponding to both PVP and **6**. A complex broad band at 1750-1600 cm^{-1} was observed for the NFm-**6**, resulting from the overlapping of the individual bands corresponding to the carbonyl groups of the thiolactone and the amide fragments present in **6** and the amide group from PVP. The mat also showed the peak assignable to the amide II of **6**, which appeared red shifted (1553 cm^{-1} *vs* 1550 cm^{-1} for **6** alone). The thiolactone C-S_{str} band at 920 cm^{-1} also confirmed the presence of **6** in NFm-**6**. The skeletal symmetric stretching of the imidazolium ring along with components assigned to CH_2(N) stretching appeared in the mat at 1169 cm^{-1}, while peaks at 1157 cm^{-1} and 1167 cm^{-1} were found for the corresponding original PILs. The peak for the -CH- wagging ν(C–N) of PVP for NFm-**6** mat also showed a shift to 1289 cm^{-1} from the value of 1287 cm^{-1} for pure PVP. All these red shifts suggest an interaction between PVP and **6** leading to an intimate blending through electrospinning. This interaction justifies the morphology of the NFs observed by SEM, where no signals of phase separation was appreciated.[22]

Post-functionalization of the NFs mat

Once demonstrated the suitability of polymer **6** blended with PVP for the preparation of NFs mats, their solubility and the effect of different solvents was evaluated. The results obtained are summarized on Table SI.2. The mat was soluble in polar solvents (water and methanol) while being insoluble in apolar media such as toluene, hexane or diethyl ether. In these solvents, the material maintained their shape (1 x 1 cm mat pieces) once dried.

[22] Bahadur, I.; Momin, M. I. K.; Koorbanally, N. A.; Sattari, M.; Ebenso, E. E.; Katata-Seru, L. M.; Singh, S.; Ramjugernath, D. Interactions of Polyvinylpyrrolidone with Imidazolium Based Ionic Liquids: Spectroscopic and Density Functional Theory Studies. *J. Mol. Liq.* **2016**, *213*, 13–16.

However, when dichloromethane was tested the size of the mat was reduced from 1 x 1 cm to 0.3 x 0.2 cm also increasing its rigidity. Thus, apolar solvents such as toluene and diethyl ether were suitable solvent media for the modification and washing of these mats. Thus, the post-functionalization of **6** with different amines and acrylates and acrylamides was assayed as highlighted in Figure 1. In a first experiment, the modification of NFm-**6** was performed in the presence of an amine by suspending the mats in the corresponding liquid amine at 60 ºC for 20 h. The film was then rinsed with toluene and the excess solvent evaporated at 50 ºC until constant weight.

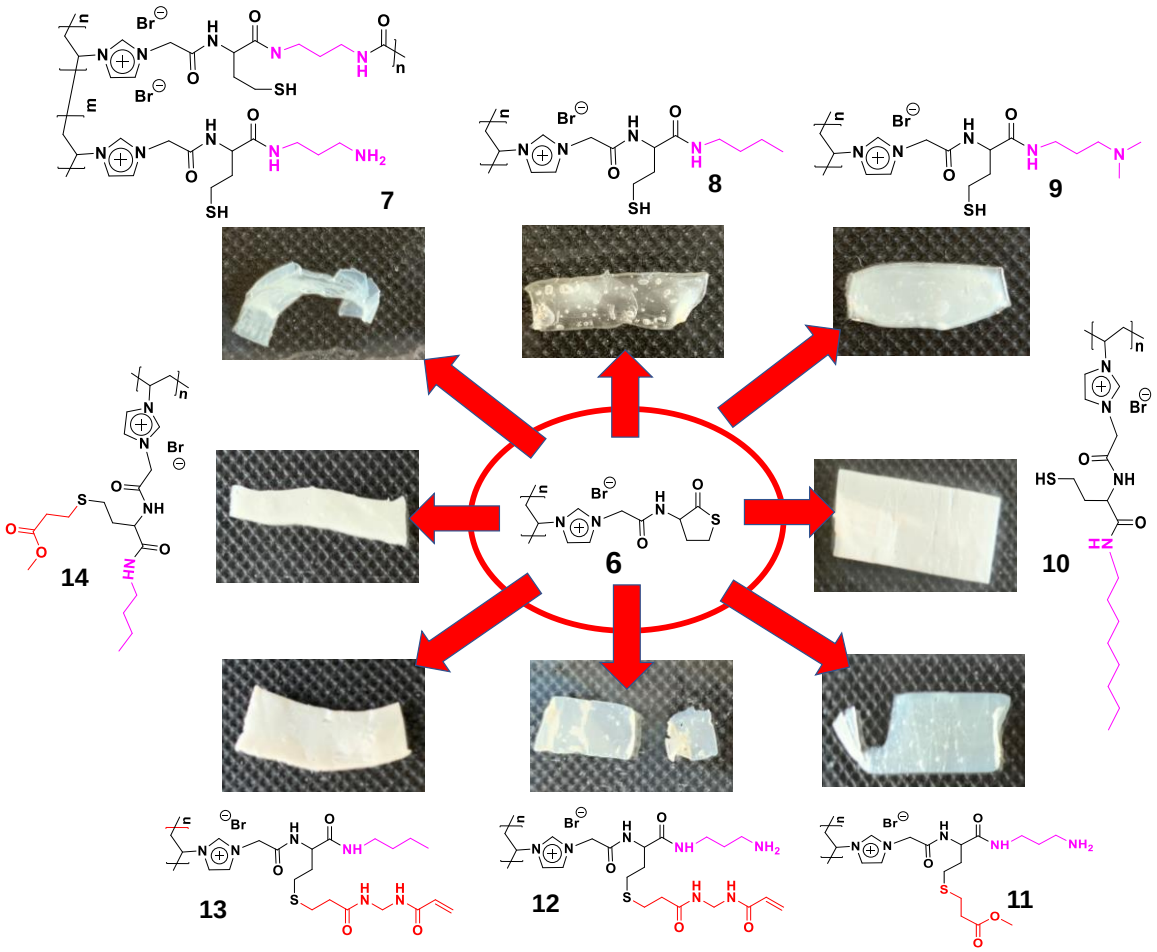

Figure 5. Post-modification of NFm-**6** using different reagents (amines and diamines). Pictures show the appearance of the mat after modification.

Mat **7** was obtained by modification of NFm-**6** with 1,3-diaminopropane (Figure 5). The modification was confirmed by FT-IR-ATR (Figure SI.3a) showing the disappearance of the peak at 920 cm^{-1} assignable to the C-S stretching of the thiolactone ring together with the presence of a strong band at 1557 cm^{-1} (amide II) assignable to the formation of new amide groups. The SEM pictures (Figure SI.3c) for mat **7** suggest that the post-modification of the membrane induced important changes on the morphology. The modified mat showed a complete porosity loss (Figure SI.3c *vs* Figure 4). The di-topic nature of the amine can yield not only the aminolysis of the thiolactone but also the crosslinking of the polymeric NFs. An additional crosslinking of the NFs via S-S bridges, it is also possible. Thus, this double crosslinking mechanism by diamide and disulfide bridges led to strong NFs fusion inducing a complete loss of the initial structure. Similarly, the FT-IR-ATR of the mat **8** confirmed the post-functionalization with butylamine (Figure SI.4c). SEM pictures also showed the fusion of NFs and the loss of the porosity. In this case, the change on morphology can be only due to the dynamic crosslinking and fusion of the NFs via S-S bridges (Figure SI.4c). Noteworthy the mats modified under these conditions changed their solubility properties, becoming insoluble in DMF.

FT-IR-ATR spectra also demonstrated the successful modification of NFm-**6** with octylamine and 3-(dimethylamine)-1-propylamine affording mats **9** and **10** (Figure SI.5a and Figure SI.6a). However, in this case, after the post-functionalization, the open porosity defined by the NFs in NFm-**6** was preserved (Figure SI.5c and SI.6 vs Figure 3). The modification with 3-(dimethylamine)-1-propylamine produced an increase of the average diameter of the NFs from 474 nm (NFm-**6**) to 644 nm (Figure SI.5b). Similar results were also found for the mat modified with octylamine, although in this case with a slightly lower NFs size increase (545 nm, Figure SI.6b). Mats

9 and **10** were insoluble in DMF confirming the crosslinking of the NFs via S-S bridging of the thiols generated *in-situ* by the aminolysis of the thiolactone moieties. In comparison with the mat **8**, the larger hindrance introduce by the amine, can preclude, at some extent, the crosslinking via S-S bridge decreasing the deformation of the NFs and the loss of the open pore nanostructure of the mat.

NFm-**6** could also be modified sequentially with 1,3-diaminopropane and methacrylate, which can react with the thiols obtained *in-situ* by aminolysis of the thiolactone group and avoiding additional crosslinking via S-S bridges and leading to two different levels of functionalization. The disappearance of the band at 920 cm^{-1} and the presence, among others, of a stronger amide II band at 1556 cm^{-1} confirmed the aminolysis, while the strong peak corresponding to the C=O of the ester at 1730 cm^{-1} suggested the success functionalization of the thiol (Figure SI.7a). SEM pictures of the modified mat showed that the NFs were fused and entangled together due to crosslinking induced by the diamine. Indeed, the NFs average size increased from 474 nm for the unmodified NFm-**6** to 922 nm. However, in this case, the addition of the acrylate avoided the crosslinking via S-S bridges allowing to keep the nanostructure of open pores of the mat (Figure SI.7a *vs* Figure SI.2), although the porosity was greatly reduced in comparison with the unmodified NFm-**6**.

In the search of the additional methodologies allowing the simultaneous modification and crosslinking of the NFs while maintaining the nanostructure and open porosity the second level modification with *N*,*N*'-methylenebis(acrylamide) was evaluated. The bis-acrylamide, in principle, can react through a Michael reaction with the generated thiol groups providing an additional possibility for crosslinking. Two different amines, 1,3-diaminopropane and butyl amine, were assayed for the first level of functionalization. The first combination can lead to crosslinking both

through the aminolysis and through thiol modification, while in the case of butyl amine the crosslinking would be only due to the thiol-ene click reactions. The modification was followed by FT-IR-ATR and afforded the modified mats **12** and **13** (Figure SI.8a and SI.9a). The mat modified with 1,3-diaminopropane and bisacrylamide showed an almost completely loss of the porosity (Figure SI.8b). However, thick fused cylindrical NFs were still observable. This change in the morphology can be attributed to the extensive crosslinking provided by the bifunctional modifiers. When the modification was performed with butyl amine, instead of 1,3-diaminopropane, a complete loss of the NFs morphology was appreciated (Figure SI.9b). This reveals that S-S bridging represents a more efficient mechanism for NFs fusion with the corresponding loss of the original nanostructure.

Finally, the modification of NFm-**6** was performed with butyl amine and methyl methacrylate in order to minimize the crosslinking of the fibers. The modification was successfully achieved as the FT-IR-ATR showed again the band for the ester group at 1738 cm^{-1} and a strong amide II band at 1557 cm^{-1} along with the total disappearance of the C-S peak of the thiolactone group (Figure SI.10a). The mat after the modification showed entangled cylindrical NFs with an average size of 710 nm, thus preserving the essential nanostructure but achieving a reduction in the porosity in comparison with the morphology observed for unmodified NFm-**6**.

In summary, the presence of the thiolactone unit allows the chemical post-modification of the NFs, although the resulting nanostructure of mats obtained was highly dependent of the nature of the modifiers.

Application of the NFs mat to sensing

In the search of possible applications for the materials here prepared, a series of proof-of-concept studies were carried out. Materials composed by NFs mats have found promising applications as sensing devices,[23] for instance, for a fast and low cost detection of volatile amines.[24] Natural volatile amines, which are often toxic, can be present in our daily life (i.e. chemical manufacturing, agriculture and farming, release by rotten food or exhalation under certain medical conditions or diseases, etc).[25,26] In the same way, ILs and related materials have shown to be of interest in optical sensing technologies.[27,28] Different sensing principles have been reported for volatile amines detection. Among them, the use of pH colorimetric sensors, which change their color upon contact to the volatile amine, represents a facile, cost-effective, and non-power operated material for gas amine detection.[29]

[23] Schoolaert, E.; Hoogenboom, R.; Clerck, K. D. Colorimetric Nanofibers as Optical Sensors. *Adv. Funct. Mater.* **2017**, *27* (38), 1702646.
[24] Jornet-Martínez, N.; Moliner-Martínez, Y.; Herráez-Hernández, R.; Molins-Legua, C.; Verdú-Andrés, J.; Campíns-Falcó, P. Designing Solid Optical Sensors for in Situ Passive Discrimination of Volatile Amines Based on a New One-Step Hydrophilic PDMS Preparation. *Sens. Actuators, B.* **2016**, *223*, 333–342.
[25] Askim, J. R.; Mahmoudi, M.; Suslick, K. S. Optical Sensor Arrays for Chemical Sensing: The Optoelectronic Nose. *Chem. Soc. Rev.* **2013**, *42* (22), 8649–8682.
[26] Li, Z.; Askim, J. R.; Suslick, K. S. The Optoelectronic Nose: Colorimetric and Fluorometric Sensor Arrays. *Chem. Rev.* **2019**, *119* (1), 231–292.
[27] Muginova, S. V.; Myasnikova, D. A.; Kazarian, S. G.; Shekhovtsova, T. N. Applications of Ionic Liquids for the Development of Optical Chemical Sensors and Biosensors. *Anal. Sci.* **2017**, *33* (3), 261–274.
[28] Guterman, R.; Ambrogi, M.; Yuan, J. Harnessing Poly(Ionic Liquid)s for Sensing Applications. *Macromol. Rapid Commun.* **2016**, *37* (14), 1106–1115.
[29] Ruiz-Capillas, C.; Jiménez-Colmenero, F. Biogenic Amines in Meat and Meat Products. *Crit. Rev. Food Sci. Nutr.* **2005**, *44* (7–8), 489–599.

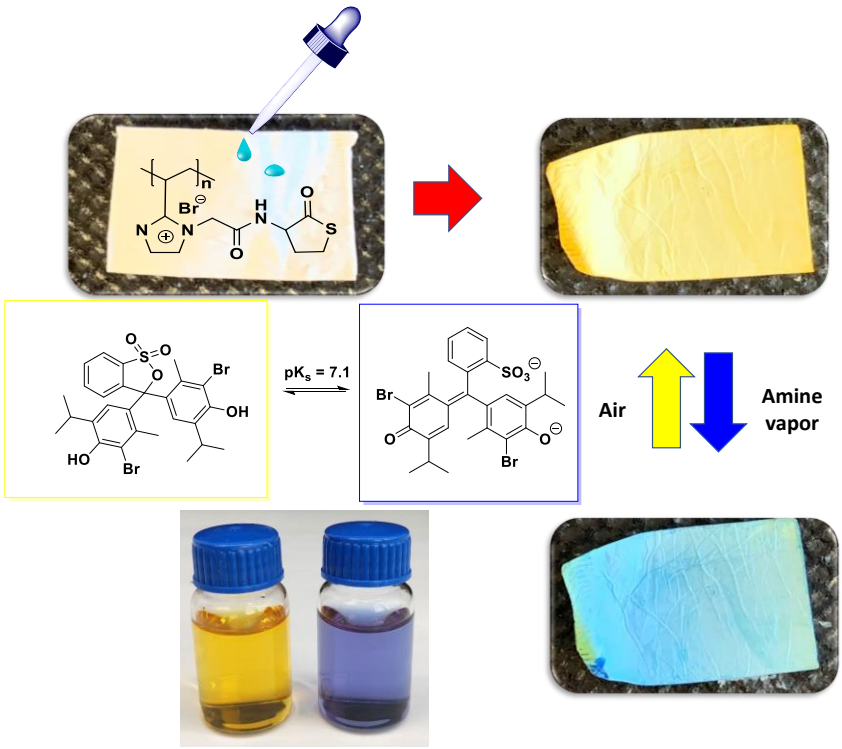

Figure 6. Naked-eye detection of a volatile amine (NH_3) using NFm-**6** doped with bromothymol blue (BTB).

For this purpose, NFm-**6** films were impregnated with a solution of bromothymol blue (BTB) in toluene (2 mg in 10 mL). The films were dried under vacuum until constant weight showing a yellow color due to the presence of the BTB in its acid form (Figure 6). To evaluate the ability of these mats as volatile amine sensor, they were exposed to the vapors of different amines (NH_3, methylamine, butylamine, *iso*-propylamine and piperidine). In all the cases, the NFs mats experimented, independently of the amine nature, a color change from yellow to blue in less than a few seconds, easily observable by the naked eye (see videos SI). The change agrees with those for aqueous solutions of BDB thar are yellow at pH < 7, green under neutral pH and blue at pH> 7. The color change was reversible, and the mats could be used in consecutives cycles of air-amine exposure (see video SI). Noteworthy, the films also responded to the presence of acid gases (HCl) experimenting film shrinking and a color change to violet. The

change in size can be explained through an increase in the ionic interactions in the fibers.

The colorimetric behavior of NFm-**6** was compared, under the same conditions, with that of films prepared by casting from and identical polymeric blend. The sensor obtained by electrospinning, when exposed to the volatile amine, showed a faster and more intense color change than the mat prepared by casting (Figure SI.11 and video SI.V1-V3). Thus, NFm-**6** is able to break the so-called "trade-off" rule in sensing harnessing high sensitivity and fast response simultaneously in comparison with the membrane obtained by casting. The good response relies on the open and well-defined porous structure defined by the NFs (Figure 3) allowing a fast diffusion of the target analyte into the membrane and enhancing its interaction with the sensing unit.

These initial results demonstrated that NFs mats obtained from TS-PILs **6** are a suitable platform for sensing application as: i) the TS-PIL units do not react or interfere with the sensing dye, ii) the polymer provides a uniform background not interfering in the color change iii) the mats present good surface properties, allowing the colorimetric sensor to spread uniformly, which is reflected in the uniform mat color and iv) the NFs structure obtained by electrospinning render a microstructure with high surface area enhancing the diffusion of the analyte to the sensing unit and leading to a fast response.

Application of the fiber-mats for catalysis

Electrospun NFs presenting catalytic units have demonstrated great potential in a variety of catalytic application.[30] The large surface area and optimal surface chemistry of electrospun nanofibers greatly enhance the catalyst–support interaction and can improve their activity, selectivity, stability, and reusability. Although NFs mats obtained by electrospinning offers very attractive properties for the development of catalytic systems, there is not a single application, as far as we know, of electrospun NFs mats based on PILs and used in catalysis.

Advanced materials based on PILs have been used as efficient systems for the capture, activation and conversion of CO_2.[31] For instance, different polymers containing IL-like moieties have been reported as efficient catalysts for the cycloaddition reaction of CO_2 with various epoxides to generate cyclic carbonates, which is one of the most promising and efficient approaches for CO_2 fixation.[32] In this context, the modified mat **14** was studied for the catalytic reaction of styrene oxide with CO_2. In general, this process requires harsh experimental conditions (temperature >130 ^oC and pressure > 10 bars) to lead to the corresponding carbonates. When the mat **14** was tested as heterogeneous catalyst for this reaction (Scheme 2) 44 % of conversion of the epoxide was observed with full selectivity to the corresponding carbonate at 120 ^oC and 10 bar after 24 hours. This is a remarkable result if we consider the bromide content, as this is expected to

[30] Lu, P.; Murray, S.; Zhu, M. Electrospun Nanofibers for Catalysts. In *Electrospinning: Nanofabrication and Applications*; Ding, B., Wang, X., Yu, J., Eds.; Micro and Nano Technologies; William Andrew Publishing, 2019; pp 695–717.
[31] Zhou, X.; Weber, J.; Yuan, J. Poly(Ionic Liquid)s: Platform for CO_2 Capture and Catalysis. *Curr. Opin. Green Sustain. Chem.* **2019**, *16*, 39–46.
[32] Luo, R.; Liu, X.; Chen, M.; Liu, B.; Fang, Y. Recent Advances on Imidazolium-Functionalized Organic Cationic Polymers for CO_2 Adsorption and Simultaneous Conversion into Cyclic Carbonates. *ChemSusChem.* **2020**, *13* (16), 3945–3966.

be the nucleophilic anion catalyzing the reaction, which was only 0.03% mol Br/substrate. This represents a notable TON of 1244.

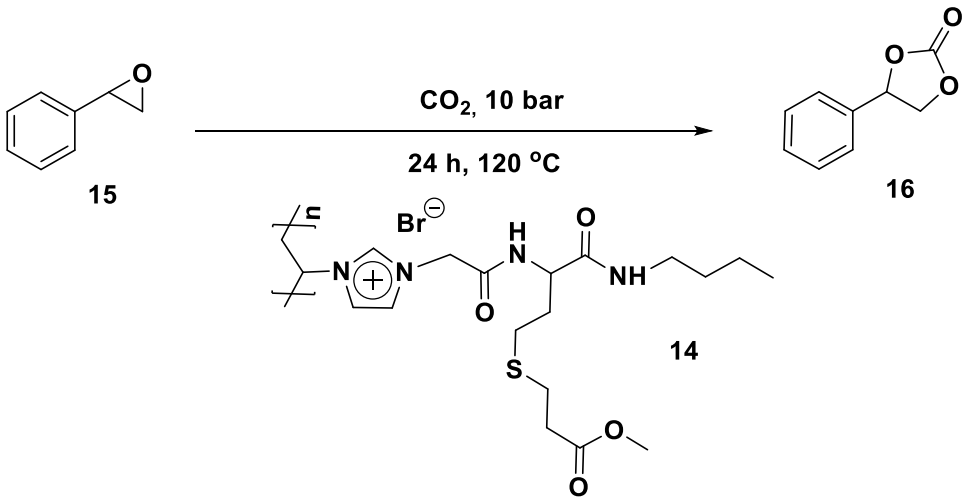

Scheme **2.** Cycloaddition reaction of CO_2 to styrene epoxide catalyzed by **14**.

5.3. Conclusions

We have demonstrated that NFs mats derived from the TS-PILs based on homocysteine thiolactone can be obtained by electrospinning as blends with PVP. The presence of this functional moiety allowed the post-functionalization of these mats through the aminolysis of the thiolactone ring in the presence of an amine that can be followed by a thiol–alkene "click" reaction. Under controlled experimental conditions the modification can be performed introducing different functionalization and crosslinking of the NFs. The morphology of the modified mats was highly dependent of nature of the modifiers. Different conditions were stabilized for the modification of the mat while maintaining the nanostructure obtained by the electrospinning. Initial studies suggest that the NFs based

on these Functionalized PILs can be used in both sensing and catalytic applications.

5.4. Experimental Section

Materials

All the reagents and solvents used were commercially available. K_2CO_3 (Scharlau extra pure), DL-homocysteine thiolactone hydrochloride (Aldrich 99%), bromoacetyl bromide (Aldrich 98%), citric acid (Aldrich 99%), anhydrous $MgSO_4$ (Scharlau extra pure), 4,4'-azobis(2-methylpropionitrile) (Aldrich 98 %), poly(4-vinylpyridine) (Aldrich, average *M*w ~ 160,000 g/mol) and were used as received. 1-vinylimidazole (Aldrich 99 %) was purified by vacuum distillation. All solvents used were of analytic degree.

General characterization protocols

FT-IR-ATR spectra were obtained using a spectrometer (JASCO FT/IR-6200) equipped with an ATR (MIRacle single-reflection ATR diamond/ZnSe) accessory at 4 cm^{-1} resolution (4000-600 cm^{-1} spectral range). Raman spectra were obtained with a NRS-3100 (Jasco) dispersive Raman spectrometer equipped with an optical microscope and an air-cooled CCD detector (-65 ^{o}C) using the following conditions: 785 nm laser with a single monochromator, 600 l/mm grating, 0.2 mm slit, 12.75 cm^{-1} resolution; with a center wavenumber of 1200 cm^{-1}, a laser power of 90.1 mW and 10 accumulations of 5 s. ^{1}H-NMR experiments were carried out using a Varian INOVA 500 (^{1}H-NMR, 500 MHz, ^{13}C, 125 MHz) and Bruker (^{1}H-NMR, 400 MHz) spectrometer.

Synthetic protocols

Synthesis of thiolactone derivative (3).

DL-homocysteine thiolactone hydrochloride (9.2 g, 60 mmol) was dissolved in milli-Q H_2O (20 mL) in round-bottom flask equipped with a stir bar an ice-cooled (0 °C), then K_2CO_3 (25,7 g, 186 mmol) was slowly added. The resulting mixture was stirred for 5 min and CH_2Cl_2 (200 mL) was added. After this, bromoacetyl bromide (10,5 mL, 120 mmol), dissolved in CH_2Cl_2 (40 mL), was added dropwise during 1 h. After the addition, the reaction mixture was allowed to react for 30 min at 0 °C and then and then 1 h when the reaction reached rt. A 5% solution of citric acid (2 x 40 mL) was added afterwards to the reaction mixture. The organic phase was decanted, washed with milli-Q® H_2O (2x40 mL), dried over anhyd. $MgSO_4$, filtered and concentrated providing a white solid used without further purification. Yield: 70 %. ^{1}H NMR (CD_3CN, 400 MHz): δ (ppm): 7.03 (s, 1H), 4.65 – 4.48 (m, 1H), 3.85 (s, 2H), 3.45 – 3.21 (m, 2H), 2.58 (dddd, 1H), 2.24 – 2.06 (m, 1H). ^{13}C NMR (CD_3CN, 101 MHz): δ (ppm): 205.7, 167.4, 59.9, 31.1, 29.4, 27.9.

Synthesis of poly(1-vinylimidazole) (5)

Compound **5** was obtained as shown in Scheme 1 according to methods already reported in the literature. Characterization data were consistent with published values.[21]

Quaternization of poly(1-vinylimidazole) (5) to produce (6)

Poly(-1-vivylimidazole) (**5**) (5.9 g, 5.88 mmol) was dissolved in dry DMF (15 mL). The solution was heated to 85 ^{o}C, and **3** (2,1 g, 8.82 mmol) dissolved in dry DMF (15 mL) was added dropwise. The reaction mixture was bubbled by N_2 and was allowed to react for 24 h, to 85 ^{o}C with stirring keeping N_2 atmosphere. After cooling down to room temperature the polymer was precipitated in to 1L of

diethyl ether and the mixture was left stirring for 30 min. Finally, the diethyl ether was decanted and the solid was washed with diethyl ether (4 x 20 mL) and dried under high vacuum. The solid was purified by dialysis in water and lyophilized, obtaining a brown solid. Yield: 40%. ^{1}H NMR (400 MHz, D_2O) δ (ppm): 7.58 (d, 1H), 5.11 (s, 1H), 4.36 (s, 1H), 3.51 (d, 1H), 2.55 (d, 2H). ^{13}C NMR (101 MHz, D_2O) δ (ppm): 209.93, 166.27, 137.02, 136.21, 126.40, 119.17, 59.70, 51.16, 39.50, 29.70, 27.84.

5.5. Supplementary Information

Preparation and application of Nanofibers mats derived from a Task Specific Polymeric Ionic Liquid

Table of Contents.

Figure SI.8. (a) Comparison of the FT-IR-ATR for the NFm**6** and **12**. **(b)** Optical imagine of the mat **12** after modification. **(c)** SEM of the polymeric mat **12**.

Figure SI.9. (a) Comparison of the FT-IR-ATR for the NFm**6** and mat **13**. **(b)** Optical imagine of the mat **13** after modification. **(c)** SEM of the polymeric mat **13**.

Figure SI.10. (a) Comparison of the FT-IR-ATR for the NFm**6** and mat **14**. **(b)** Optical imagine of the mat **14** after modification. **(c)** SEM of the polymeric mat **14**. **(d)** NFs size distribution

Figure SI.11. Comparison of color changing of the polymer blend PVP/TS-PIL **6** obtained by electrospinning **(a)** or by casting **(b)** in presence of the NH_3 vapor.

Figure SI.12. Spectrum of compound **3**. **(a)** ^{1}H NMR spectra in CD_3CN and **(b)** ^{13}C NMR Spectra in CD_3CN.

Figure SI.13. Spectrum of polymer **5. (a)** ^{1}H NMR spectra in D_2O and **(b)** ^{13}C NMR Spectra in D_2O.

Figure SI.14. Spectrum of polymer **6. (a)** ^{1}H NMR spectra in D_2O and **(b)** ^{13}C NMR Spectra in D_2O.

Video SI.V1. Colorimetric changes of NFm-**6** with butylamine.

Video SI.V2. Colorimetric changes of NFm-**6** with different amines.

Video SI.V3. Colorimetric changes of NFm-**6** with ammonia.

Table SI.1. Electrospinning parameters used to fabricate NFs mats.

Entry	Pol. Mix.	Voltage (kV)	Fiber morphology	Size[c]
1	**6** [a] (65%)	+20.5, -14.7	-	-
2	**6**:PVP [b] (50%)	+19.5, -14.7[d]	fibers	474 ± 222 nm

[a] Distance: x: 145 mm, y: 155mm, z: 200mm, Solvent: DMF, flow rate 300 µL/min, humidity: 30-40%. [b] Distance: x: 155 mm, y: 155mm, z: 200mm Solvent: DMF, flow rate 1500 µL/min, humidity: 39-41%. [c] Diameter and thickness determined by SEM analysis.

Table SI.2. Solubility evaluation of the NFs mat obtained by PVP/TS-PIL **6**.[a]

Solvent	Solubility[b]	Initial size [cm]	Final Size [cm]
DMSO	S	1x1	-
DMF	S	1x1	-
H_2O	S	1x1	-
MeOH	S	1x1	-
CH_2Cl_2	P	1x1 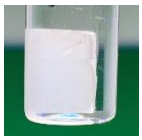	0,3x0,2 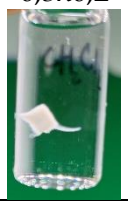
Toluene	I	1x1 	1x1 
Hexane	I	1x1 	1x1 
Diethyl ether	I	1x1 	1x1 

[a] The mat 1 x1 cm was submerged in the corresponding solvent and left to stand for 24 hours at room temperature. [b] **S**: Soluble, **I**: Insoluble, **P**: Partially.

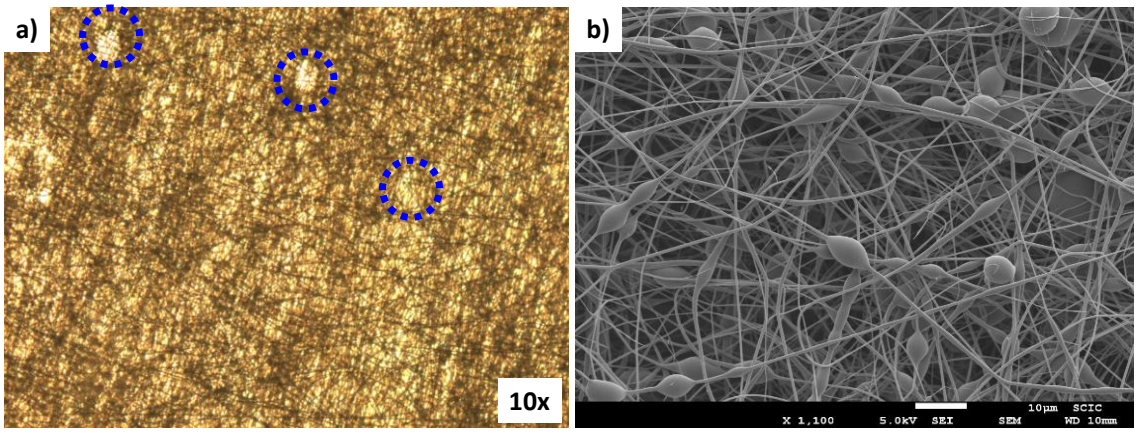

Figure SI.1. Images of fibers with the formation of beads obtained by electrospinning of polymer **6** (65 % w/v). **(a)** Optical microscope imagen, 10 x / 0,25 mm. **(b)** SEM imagen, scale bar represent 10 µm.

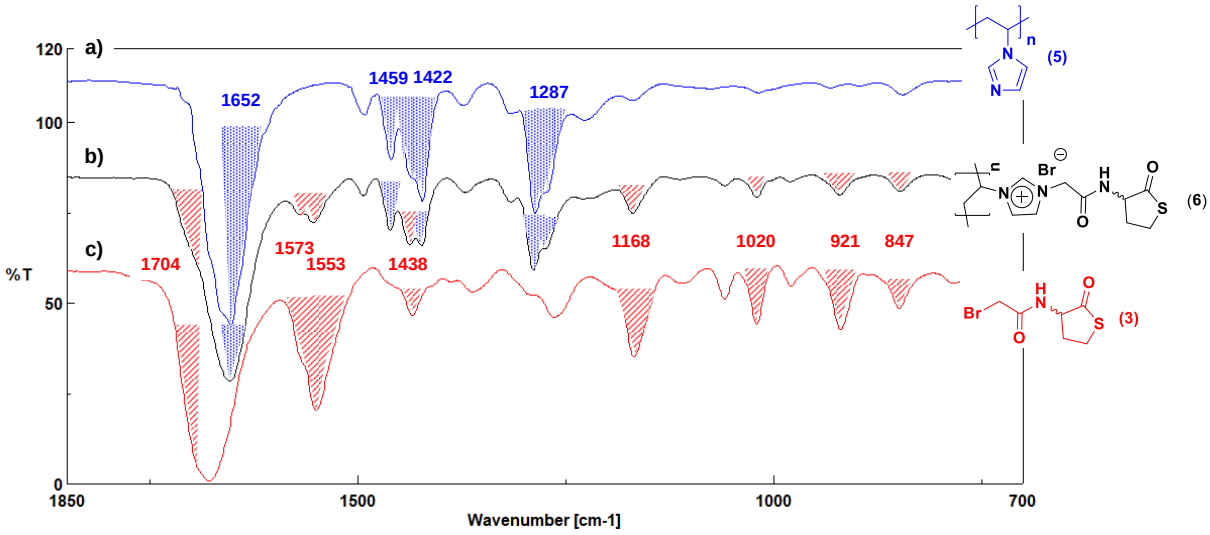

Figure SI.2. Synthesis of the polymer **6** monitored by FT-IR-ATR. **(a) 5**, **(b) 6** and **(c) 3**.

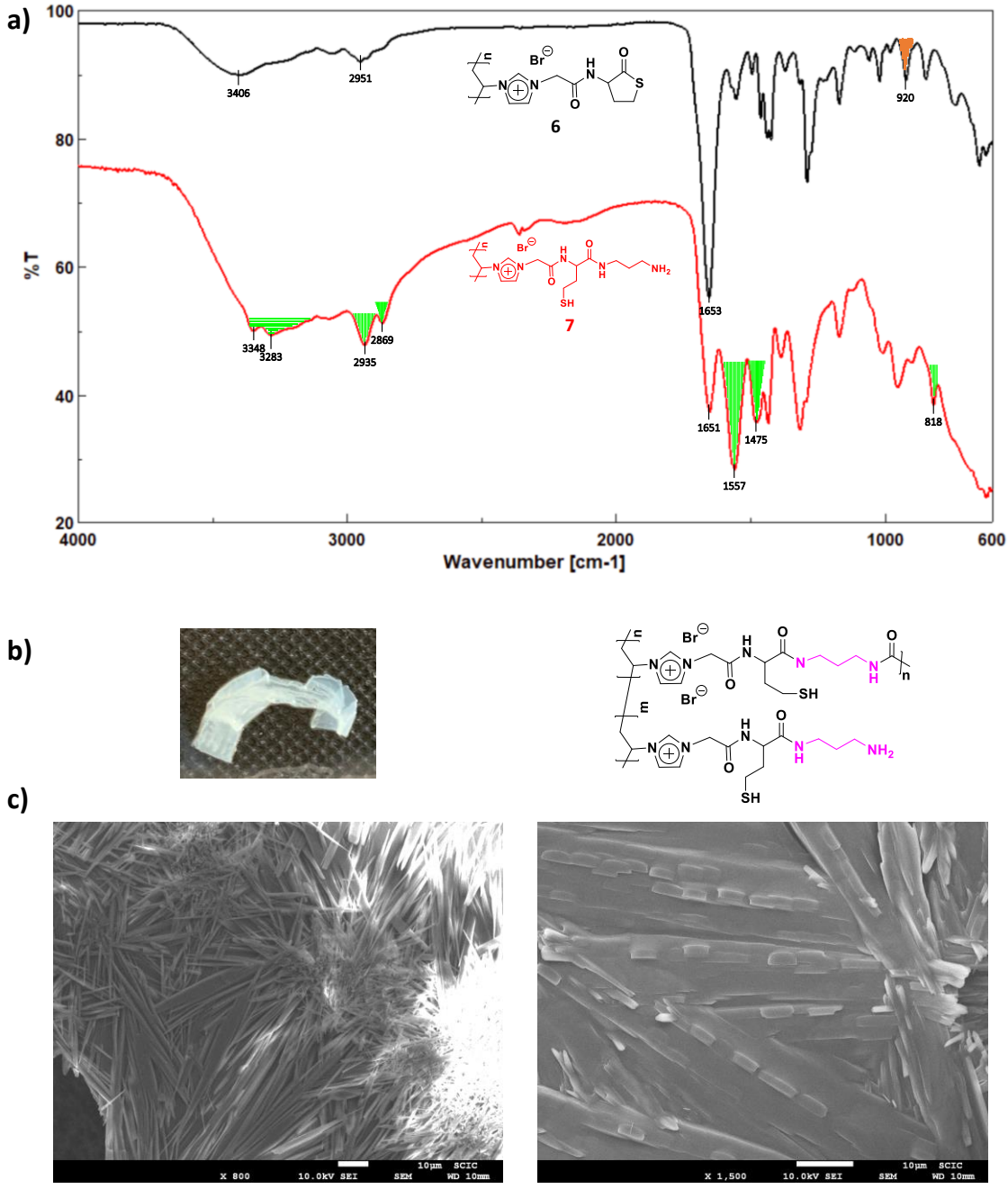

Figure SI.3. **(a)** Comparison of the FT-IR-ATR spectra for NFm-**6** and **7**. **(b)** Optical images for mat **7** after modification. and structure **(c)** SEM pictures for the polymeric mat **7**, scale bars correspond to 10µm.

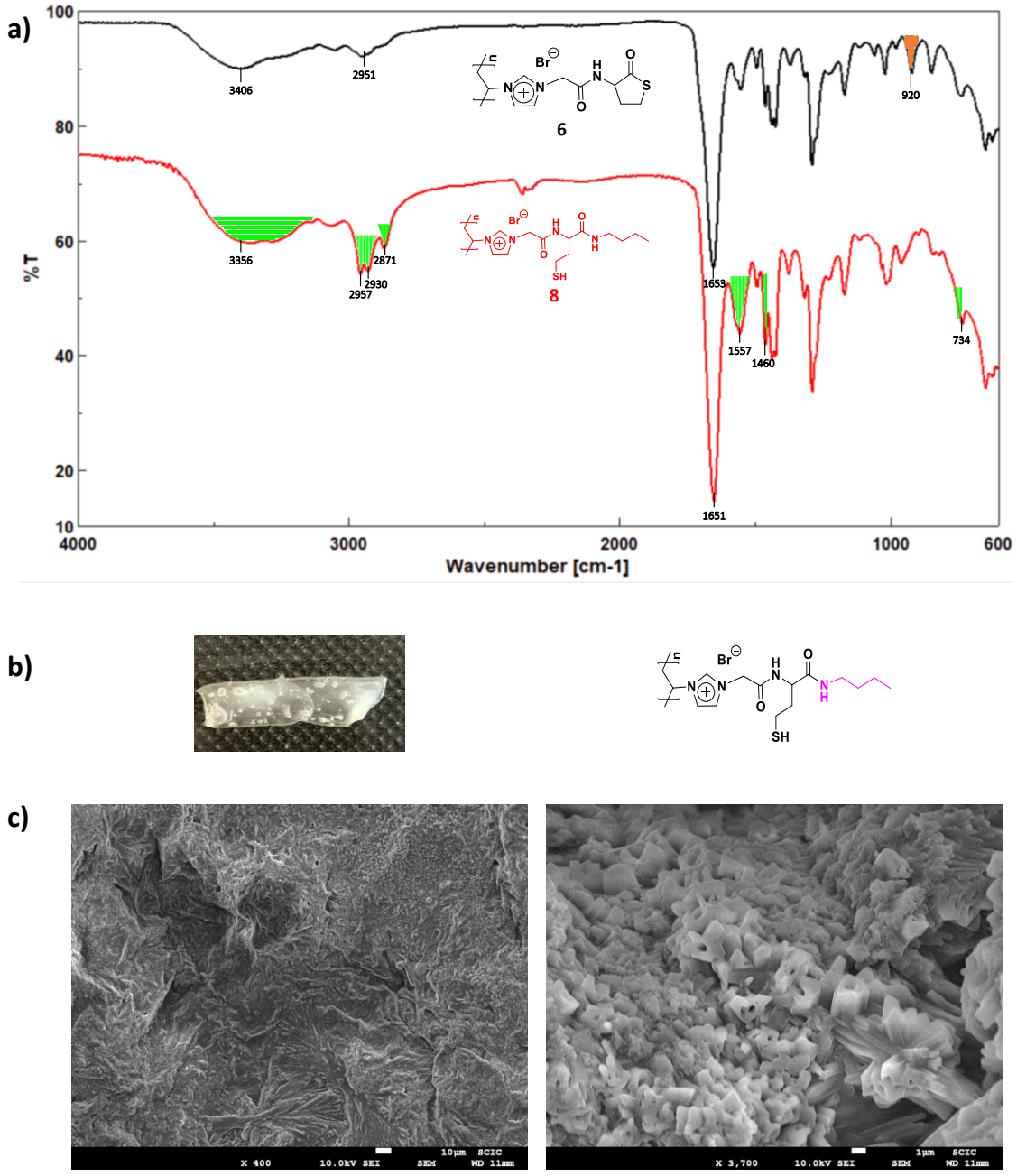

Figure SI.4. **(a)** Comparison of the FT-IR-ATR for the NFs mat **6** and **8**. **(b)** Optical imagine of the mat **8** after modification and structure **(c)** SEM of the polymeric mat **8**, scale bars correspond to left: 10µm, right: 1µm.

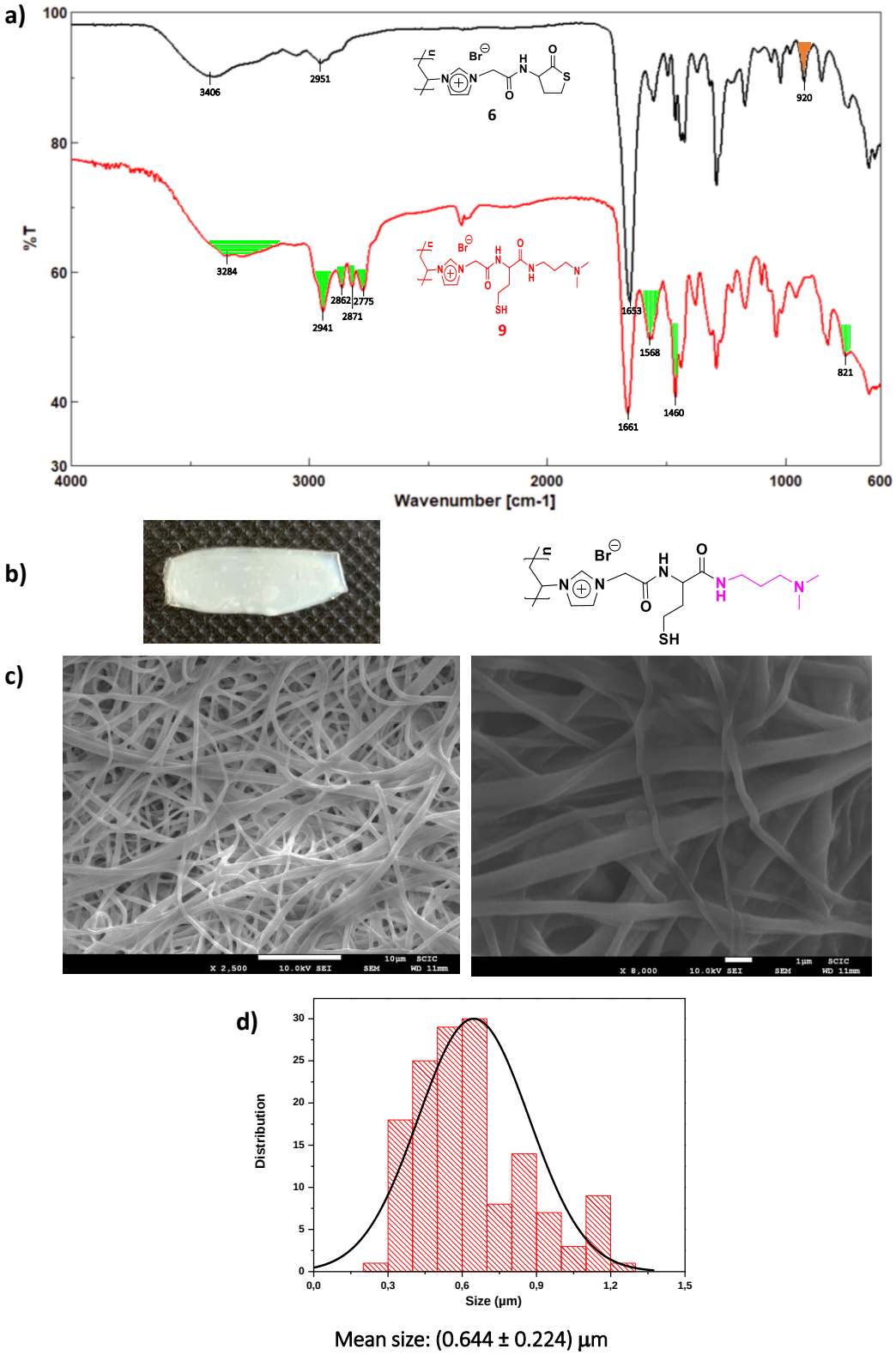

Figure SI.5. **(a)** Comparison of the FT-IR-ATR for the NFs mat **6** and **9**. **(b)** Optical imagine of the mat **9** after modification and structure. **(c)** SEM of the polymeric mat **9**, scale bars correspond to left: 10µm, right: 1µm. **(d)** NFs size distribution.

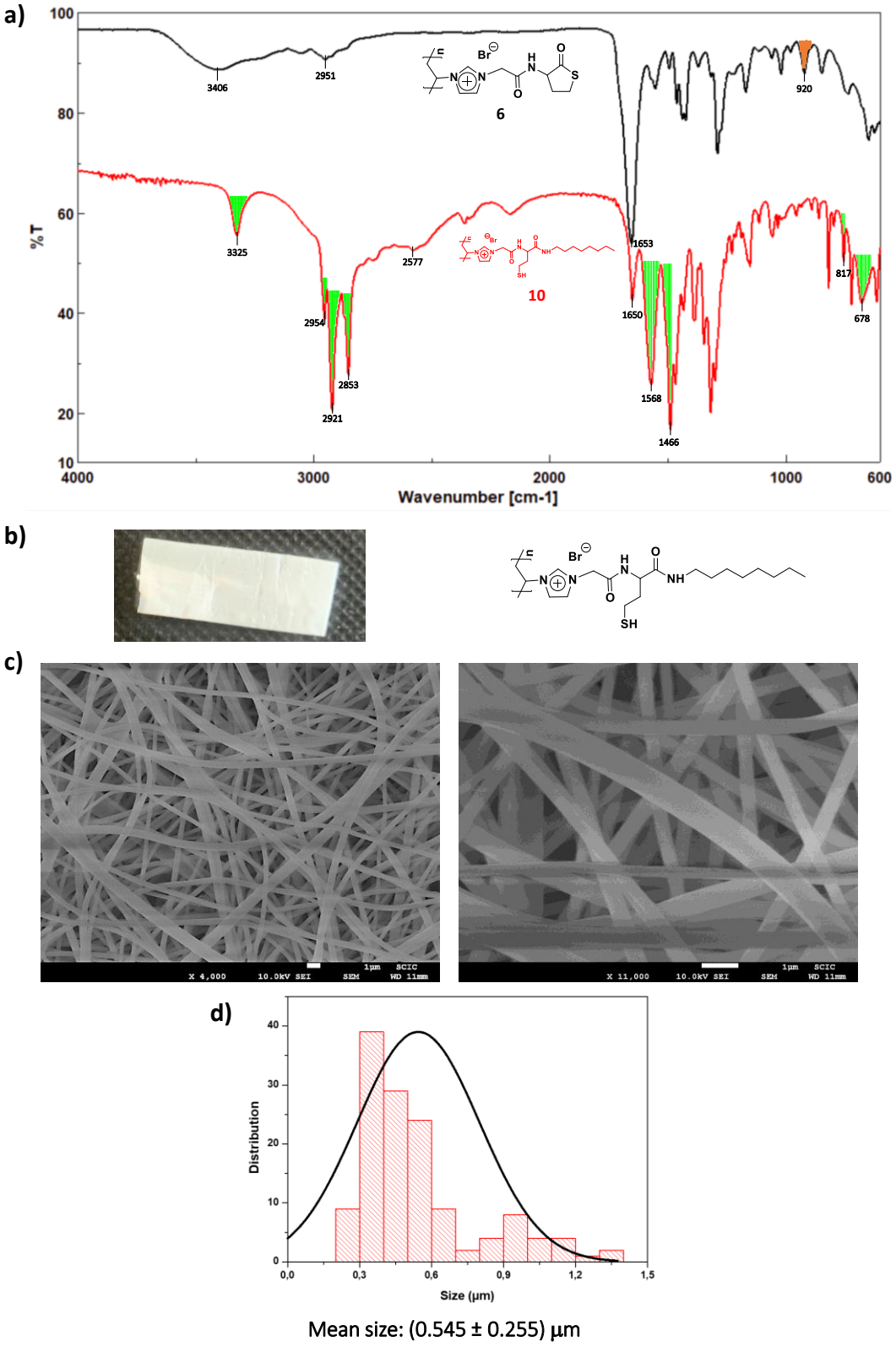

Figure SI.6. **(a)** Comparison of the FT-IR-ATR for the NFs mat **6** and **10**. **(b)** Optical imagine of the mat **10** after modification and structure. **(c)** SEM of the polymeric mat **10**, scale bars correspond to 1µm **(d)** NFs size distribution.

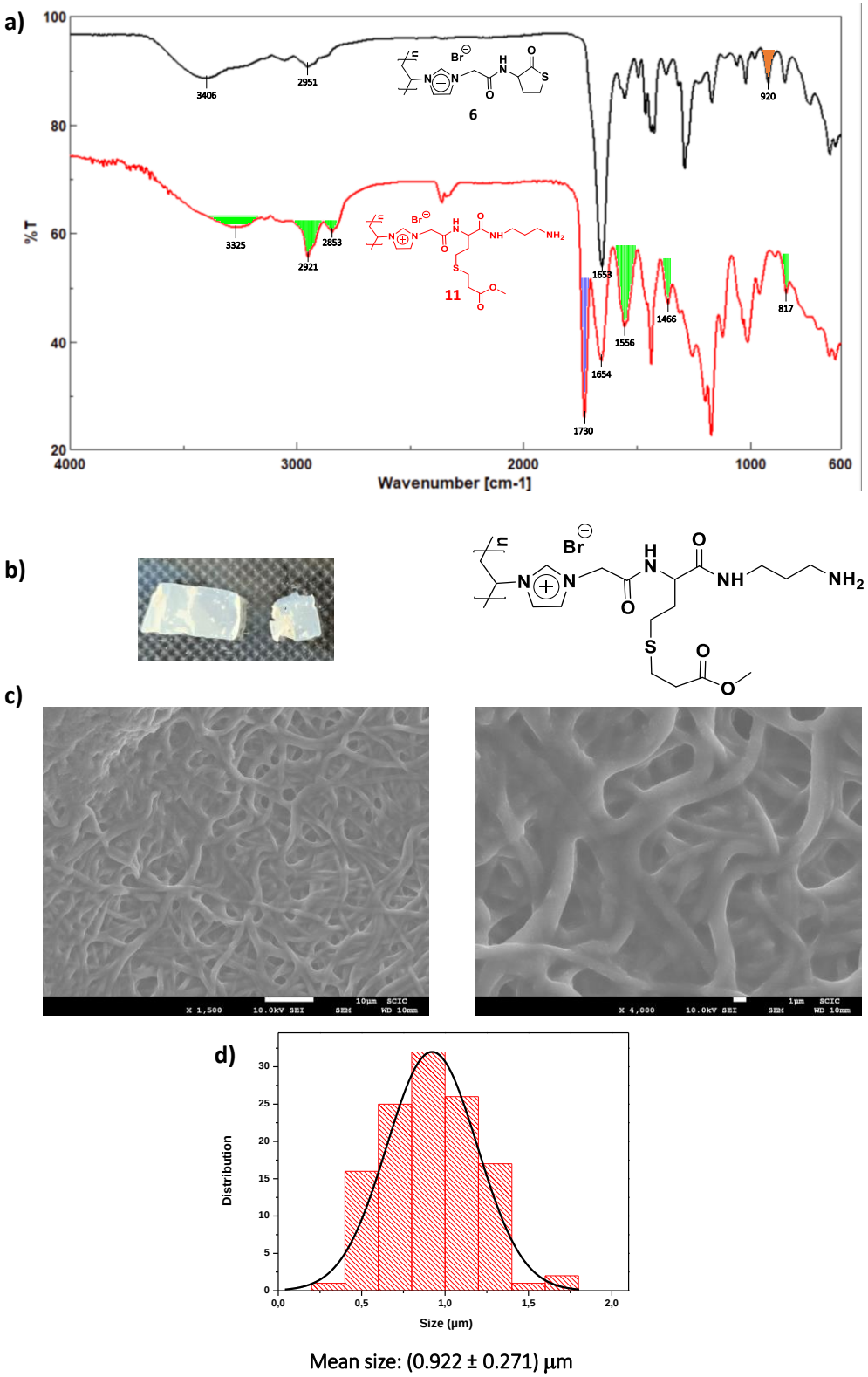

Figure SI.7. **(a)** Comparison of the FT-IR-ATR for the NFs mat **6** and **11**. **(b)** Optical imagine of the mat **11** after modification and structure. **(c)** SEM of the polymeric mat **11**, scale bars correspond to left: 10µm, right: 1µm. **(d)** NFs size distribution.

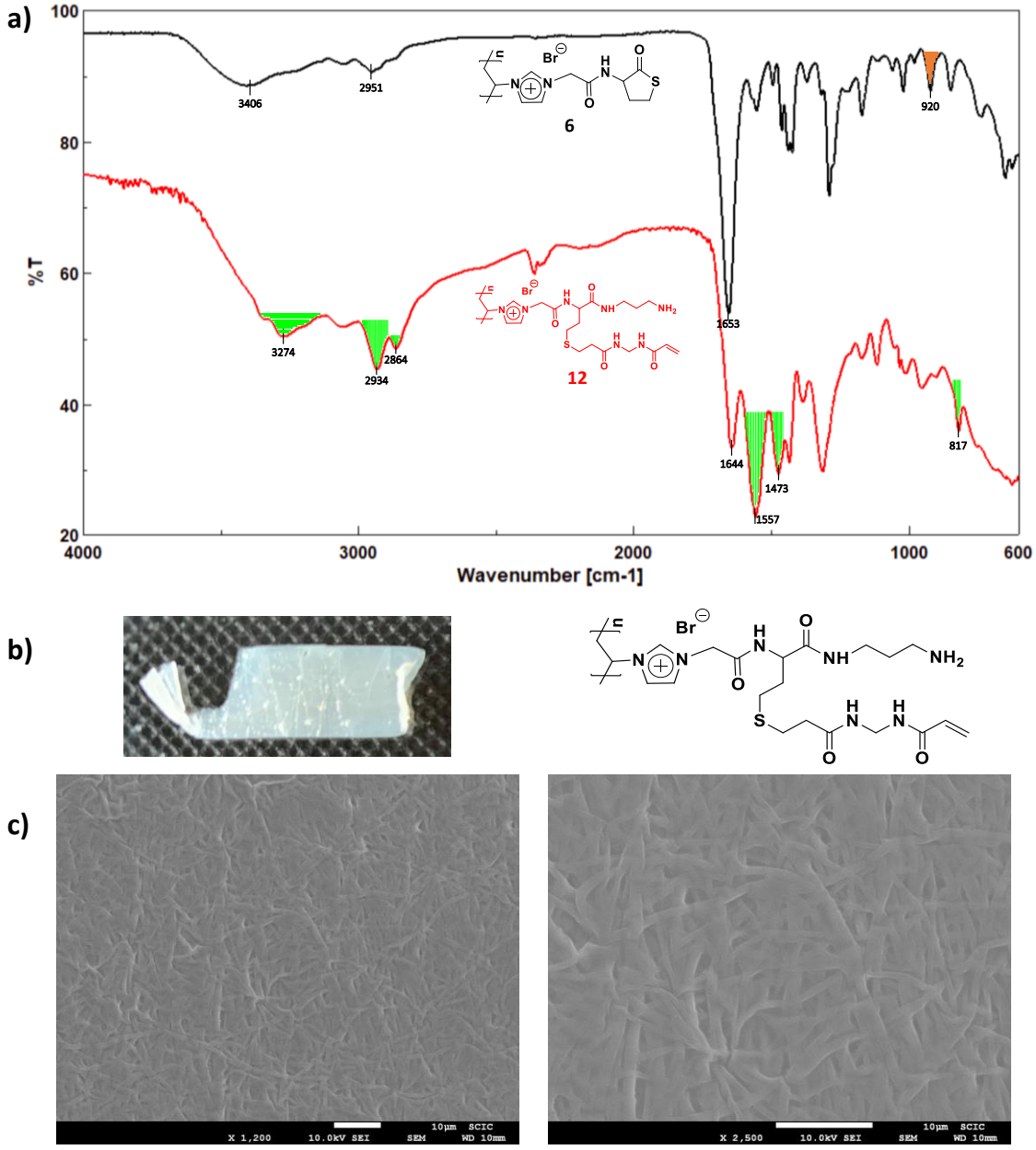

Figure SI.8. **(a)** Comparison of the FT-IR-ATR for the NFs mat **6** and **12**. **(b)** Optical imagine of the mat **12** after modification and structure. **(c)** SEM of the polymeric mat **12**, scale bars correspond to 10µm.

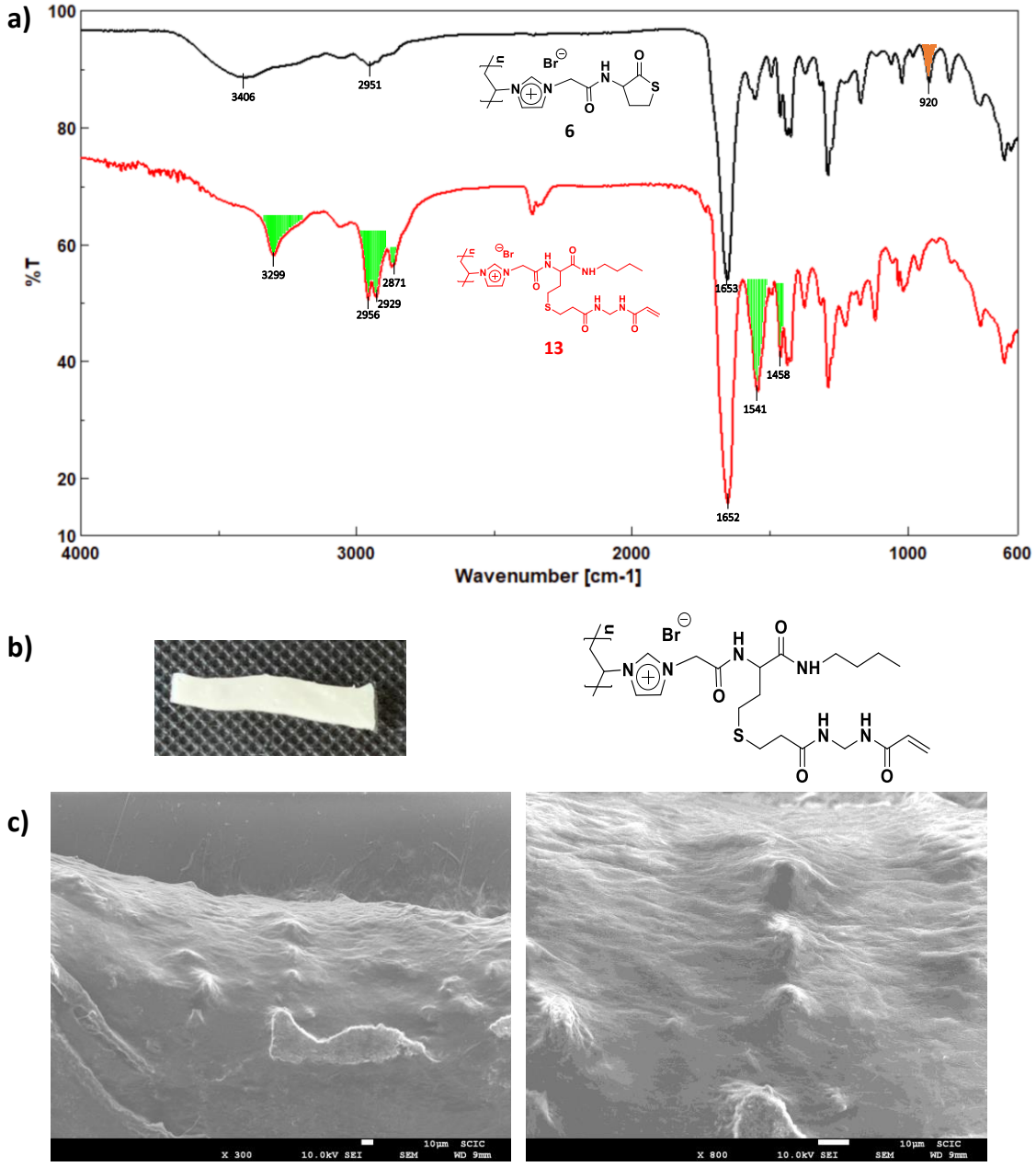

Figure SI.9. **(a)** Comparison of the FT-IR-ATR for the NFs mat **6** and **13**. **(b)** Optical imagine of the mat **13** after modification and structure. **(c)** SEM of the polymeric mat **13**, scale bars correspond to10µm.

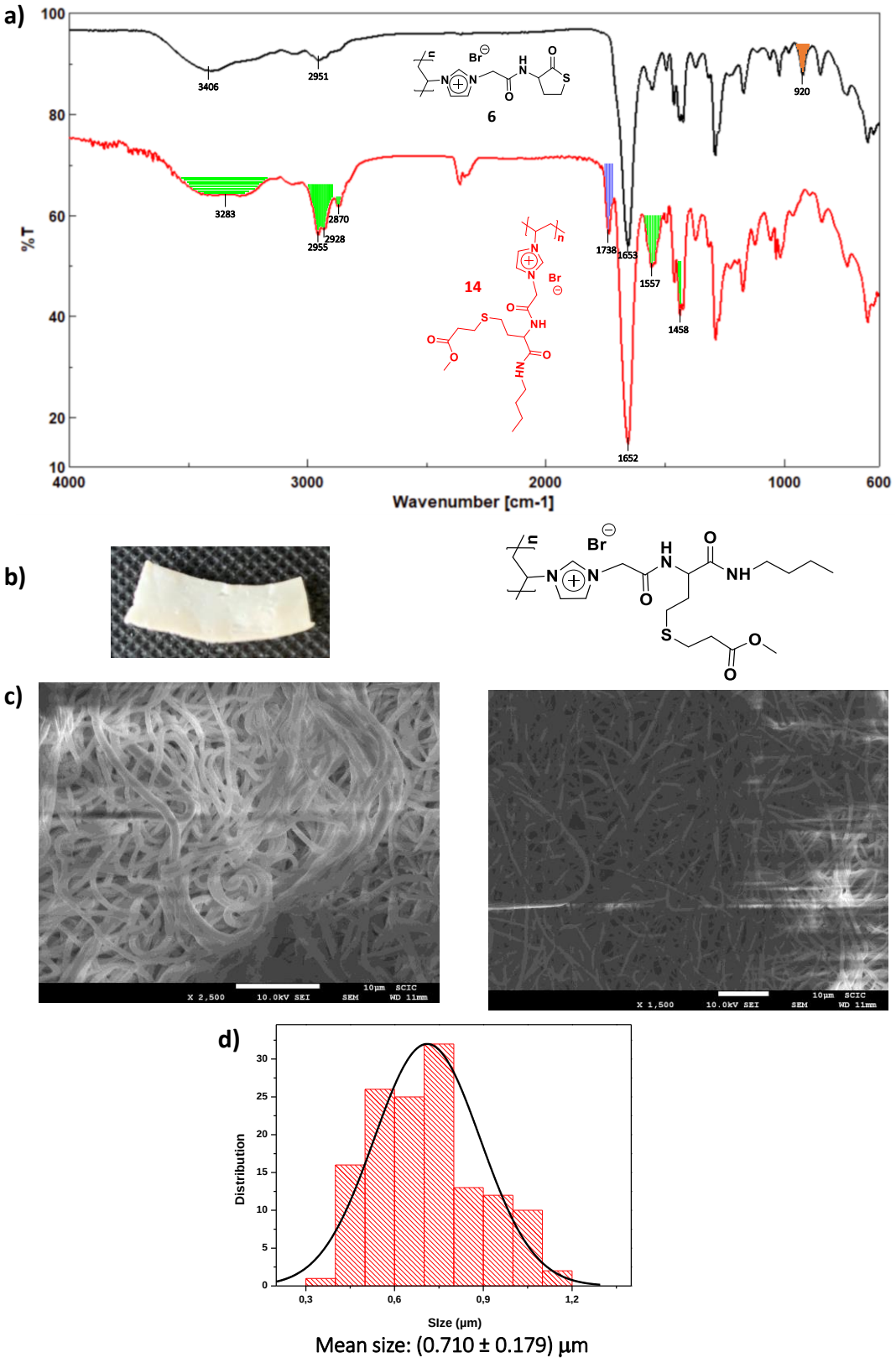

Figure SI.10. **(a)** Comparison of the FT-IR-ATR for the NFs mat **6** and **14**. **(b)** Optical imagine of the mat **14** after modification and structure. **(c)** SEM of the polymeric mat **14,** scale bars correspond to 10µm **(d)** NFs size distribution.

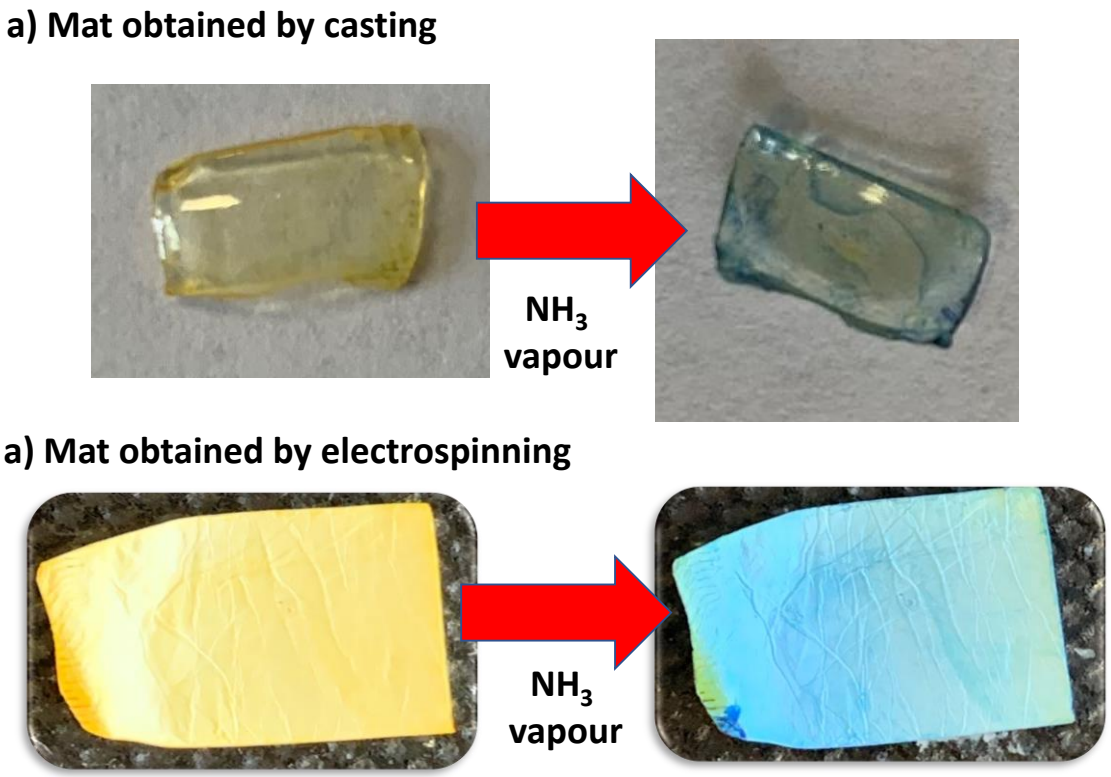

Figure SI.11. Comparison of color changing of the polymer blend PVP/TS-PIL **6** obtained by **(a)** casting or by **(b)** electrospinning in presence of the NH_3 vapor.

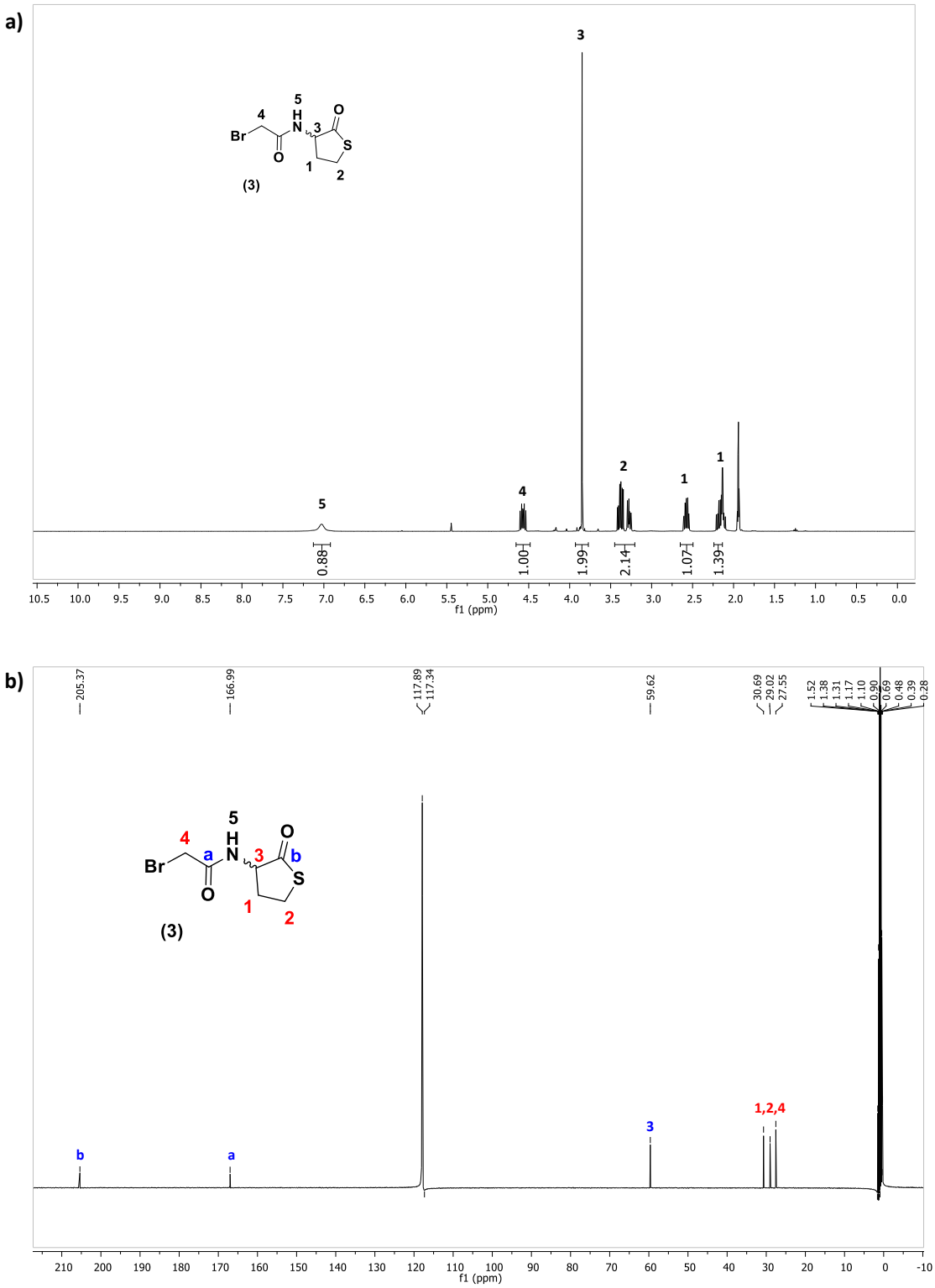

Figure SI.12. Spectrum of compound **3**. **(a)** ^{1}H NMR spectra in CD_3CN and **(b)** ^{13}C NMR Spectra in CD_3CN.

a)

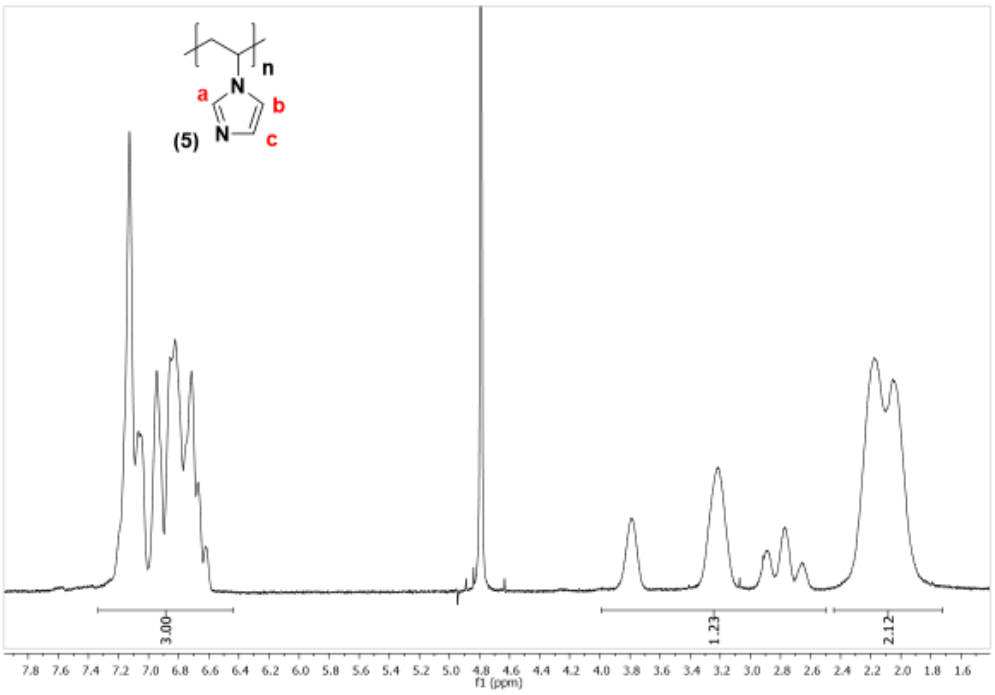

b)

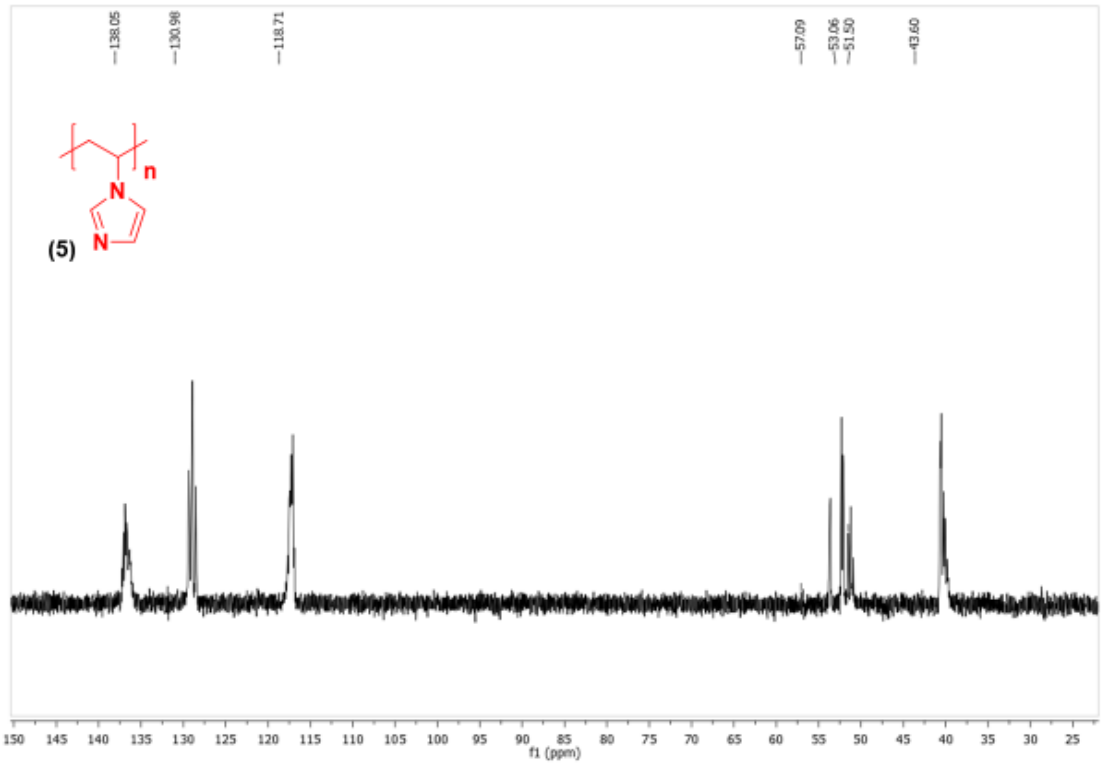

Figure SI.13. Spectrum of polymer **5**. **(a)** ^{1}H NMR spectra in D_2O and **(b)** ^{13}C NMR Spectra in D_2O.

a)

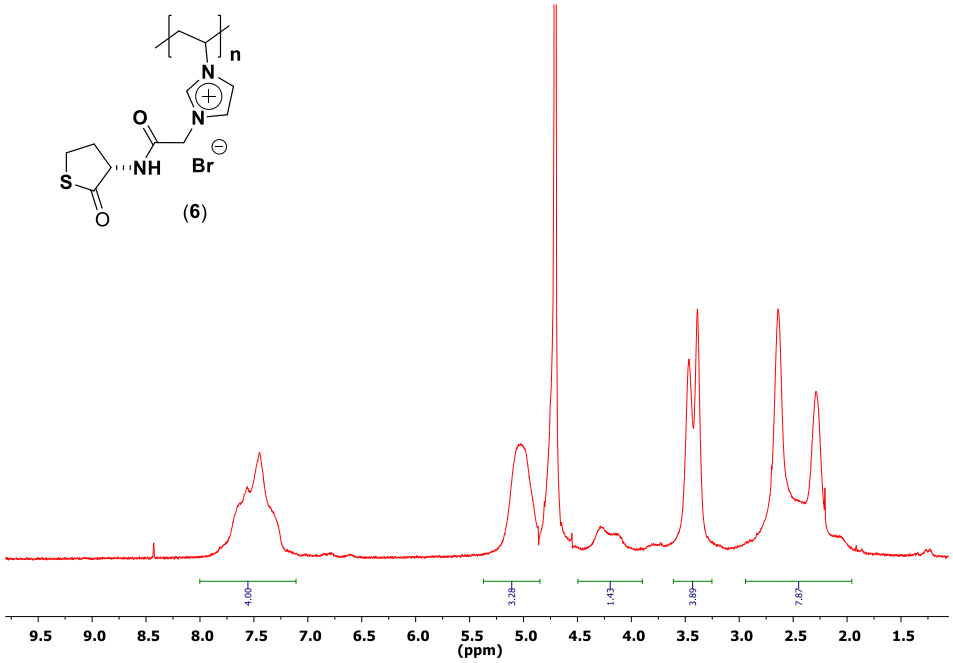

b)

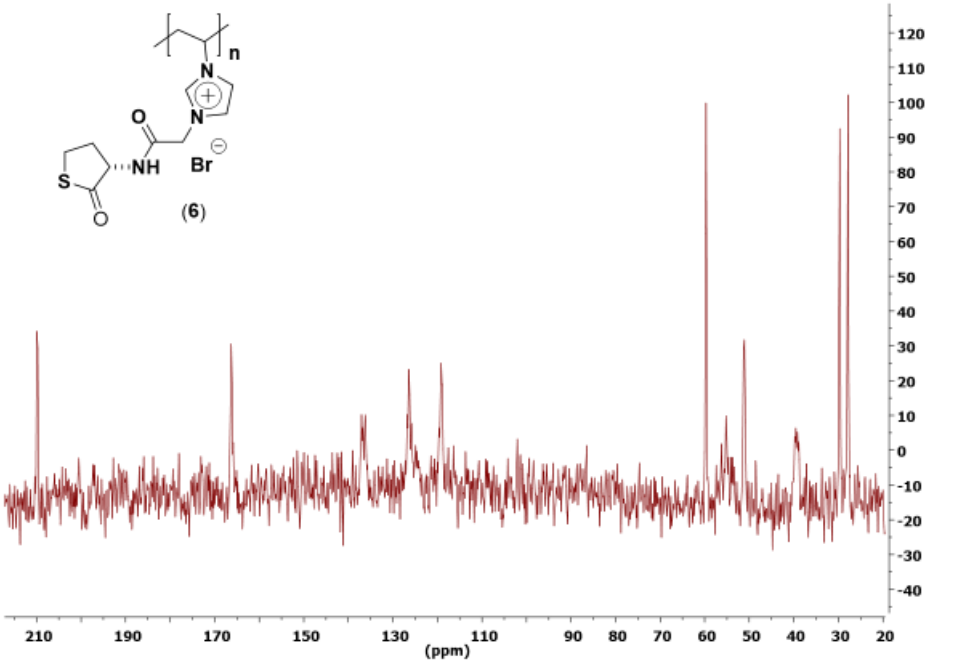

Figure SI.14. Spectrum of polymer **6**. **(a)** ^{1}H NMR spectra in D_2O and **(b)** ^{13}C NMR Spectra in D_2O.

a.Butylamine-mat NFm-6-ES.mp4 **(a)**

b.Butylamine-mat NFm-6-casting.mp4 **(b)**

c.Butylamine-mat NFm6-N2.mp4 **(c)**

d.Butylamine-mat NFm-6 comparison.n **(d)**

Video SI.V1. Colorimetric changes of NFm-**6** with butylamine. Mats prepared by **(a)** electrospinning and **(b)** casting. **(c)** Reversible change exposing to N_2. **(d)** Comparison of color before (yellow) and after (blue) sensing (see in electronic annexes, videos SI. CAP. V).

a.Methylamine-mat NFm6-Es.mp4 **(a)**

b.Isopropylamine-mat NFm6-Es.mp4 **(b)**

c.Piperidine-mat NFm6-Es.mp4 **(c)**

Video SI.V2. Colorimetric changes of NFm-**6** with different amines. **(a)** Methylamine **(b)** Isopropylamine. **(c)** Piperidine (see in electronic annexes, videos SI. CAP. V).

a.NH3-mat NFm-6-ES.mp4 **(a)**

b.NH3-mat NFm-6-casting.mp4 **(b)**

Video SI.V3. Colorimetric changes of NFm-**6** with ammonia. Mats prepared by **(a)** electrospinning and **(b)** casting (see in electronic annexes, videos SI. CAP. V).

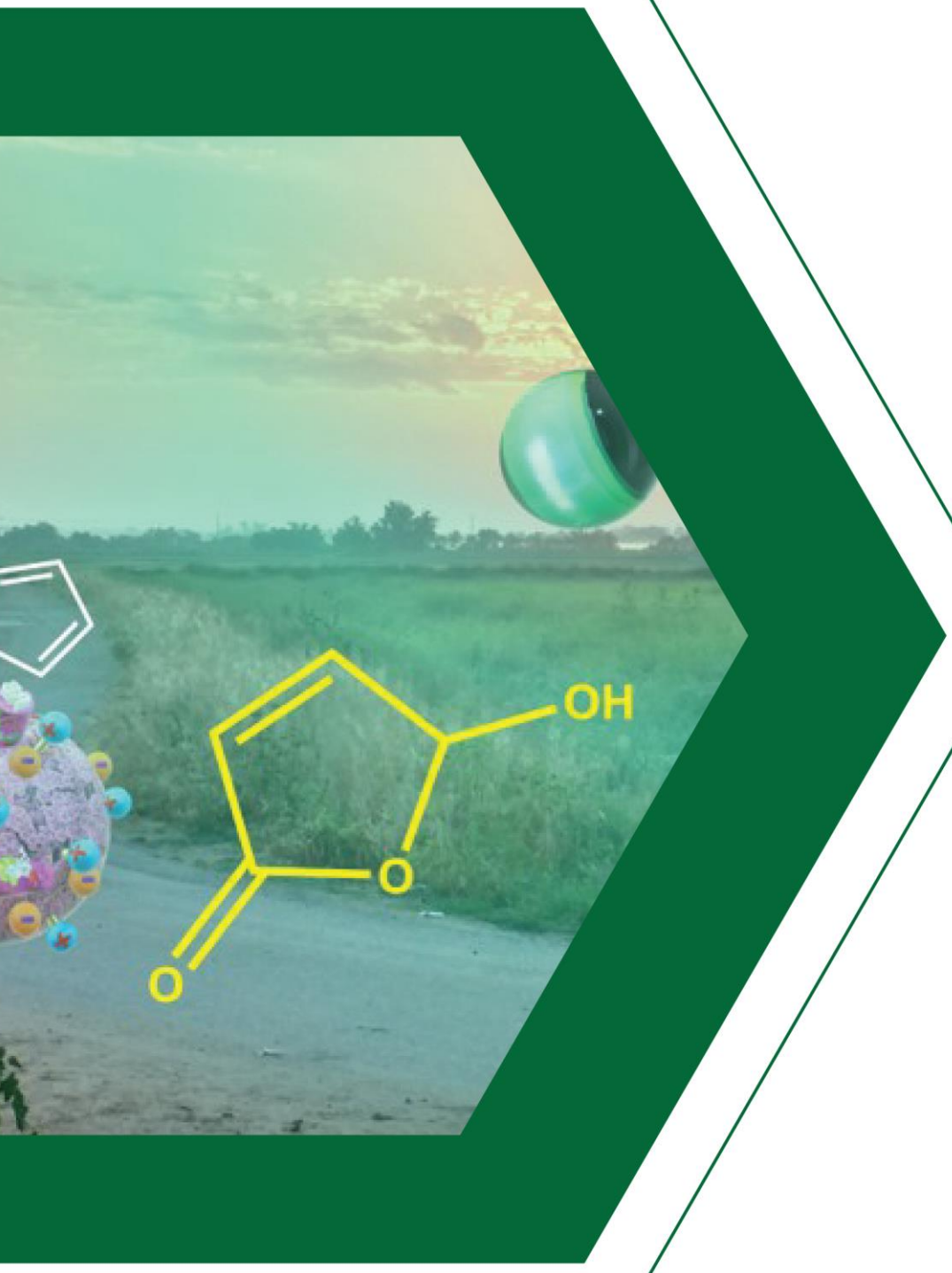
OH
O
O

CAPÍTULO VI

Rosa de Bengala inmovilizado sobre "Fases Soportadas relacionadas con los Líquidos Iónicos": Un fotocatalizador eficiente para procesos en discontinuo y en flujo continuo

Resumen. La actividad catalítica del Rosa de Bengala (RB) inmovilizado sobre materiales conteniendo fases soportadas relacionadas con los líquidos iónicos se evaluó desde la perspectiva de un fotocatalizador soportado sobre un polímero. En estos sistemas, el polímero fue diseñado para desempeñar un papel fundamental. La estructura polimérica adecuadamente modificada con unidades relacionadas con los ILs (líquidos iónicos soportados covalentemente, SILLPs) no solamente es un soporte inerte para el RB, sino que también controla la accesibilidad de los reactivos / sustratos a los centros activos, y proporciona un microambiente específico para la reacción. Las estructuras de los SILLPs pueden ser modificadas para ajustar la eficiencia catalítica de los compuestos de RB-SILLP, obteniendo sistemas mas activos y estables que sistemas semejantes que no poseen las unidades de IL.

Chapter VI. Rose Bengal immobilized onto Supported Ionic Liquid-like Phases: An Efficient photocatalyst for batch and flow processes

Abstract. The catalytic activity of Rose Bengal (RB) immobilized onto supported ionic liquid (IL)-like phases was evaluated as a polymer supported photocatalyst. In these systems, the polymer was designed to play a pivotal role. The polymeric backbone adequately modified with IL-like moieties (Supported IL-Like Phases, SILLPs) was not just an inert support for the dye but controlled the accessibility of reagents/substrates to the active sites and provides specific microenvironments for the reaction. The structure of SILLPs can be finetuned to adjust the catalytic efficiency of the RB−SILLP composites, achieving systems that were more active and stable than the related systems in absence of IL-like units.

Keywords: photocatalysis • Ionic Liquids • Supported Ionic Liquids • Rose Bengal • Flow Chemistry

6.1. Introduction

Singlet oxygen is a powerful and versatile reagent that has been applied for a wide range reaction of sequences in order to synthetize molecules with a certain degree of complexity.[1] It can be considered as a green reagent, being generated *in situ* from oxygen through irradiation with visible light of a photosensitizer.[2] The use of singlet oxygen does not produce any waste or residue, other than the photocatalyst, at the end of the process.[3] In this context, different approaches have designed for the immobilization of photosensitizers into a different phase than reactants and products, facilitating its recovery and reuse for further

[1] Ghogare, A. A.; Greer, A. Using Singlet Oxygen to Synthesize Natural Products and Drugs. *Chem. Rev.* **2016**, *116* (17), 9994–10034.
[2] Albini, A.; Fagnoni, M. Green Chemistry and Photochemistry were Born at the Same Time. *Green Chem.* **2004**, *6* (1), 1–6.
[3] Pibiri, I.; Buscemi, S.; Palumbo, A. P.; Pace, A. Photochemically Produced Singlet Oxygen: Applications and Perspectives. *ChemPhotoChem.* **2018**, *2* (7), 535–547.

catalytic cycles.[4,5] However, in some cases, this immobilization can lead to a reduction of the photocatalytic efficiency through the quenching of the excited states by the polymeric matrix or by shortening the lifetime of the reactive species. Therefore, an efficient support should provide a suitable environment for the photocatalyst, providing site isolation to prevent dye oligomerization and self-quenching, enhancing quantum yields for singlet oxygen formation and dye photostability.[6,7,8] he support should also facilitate the accessibility to the immobilized species of the reagents and substrates used in the selected solvents.[9]

Traditionally polymeric supported photocatalysts have been based on hydrophobic matrices, which are hardly compatible with polar or aqueous environments,[10,11] thus limiting their application to processes performed in organic solvents like chloroform or dichloromethane. To avoid the use of such non-polar VOC solvents, the hydrophilic/hydrophobic balance of the support should be fine-tuned increasing their compatibility with polar solvents like water and alcohols.

[4] Wahlen, J.; De Vos, D. E.; Jacobs, P. A.; Alsters, P. L. Solid Materials as Sources for Synthetically Useful Singlet Oxygen. *Adv. Synth. Catal.* **2004**, *346* (2–3), 152–164.
[5] Friedmann, D.; Hakki, A.; Kim, H.; Choi, W.; Bahnemann, D. Heterogeneous Photocatalytic Organic Synthesis: State-of-the-Art and Future Perspectives. *Green Chem.* **2016**, *18* (20), 5391–5411.
[6] Xie, Z.; Wang, C.; deKrafft, K. E.; Lin, W. Highly Stable and Porous Cross-Linked Polymers for Efficient Photocatalysis. *J. Am. Chem. Soc.* **2011**, *133* (7), 2056–2059.
[7] Lacombe, S.; Pigot, T. Materials for Selective Photo-Oxygenation vs. Photocatalysis: Preparation, Properties and Applications in Environmental and Health Fields. *Catal. Sci. Technol.* **2016**, *6* (6), 1571–1592.
[8] Petrizza, L.; Bechec, M. L.; Decompte, E.; Hadri, H. E.; Lacombe, S.; Save, M. Tuning Photosensitized Singlet Oxygen Production from Microgels Synthesized by Polymerization in Aqueous Dispersed Media. *Polym. Chem.* **2019**, *10* (23), 3170–3179.
[9] (a) Altava, B.; Burguete, M. I.; García-Verdugo, E.; Luis, S. V. Chiral Catalysts Immobilized on Achiral Polymers: Effect of the Polymer Support on the Performance of the Catalyst. *Chem. Soc. Rev.* **2018**, *47* (8), 2722–2771. (b) Altava, B.; Burguete, M. I.; García-Verdugo, E.; Luis, S. V.; Vicent, M. J.; Mayoral, J. A. Supported Chiral Catalysts: The Role of the Polymeric Network. *React. Funct. Polym.* **2001**, *48* (1), 25–35.
[10] Paczkowski, J.; Neckers, D. C. Polymer-Based Sensitizers for the Formation of Singlet Oxygen: New Studies of Polymeric Derivatives of Rose Bengal. *Macromolecules.* **1985**, *18* (6), 1245–1253.
[11] Suzuki, M.; Ohta, Y.; Nagae, H.; Ichinohe, T.; Kimura, M.; Hanabusa, K.; Shirai, H.; Wöhrle, D. Synthesis, Characterization and Application of a Novel Polymer Solid Photosensitizer. *Chem. Commun.* **2000**, No. 3, 213–214.

Ionic Liquids (ILs) have been evaluated as alternative reaction media for a wide range of catalytic processes,[12,13,14] and also represent a simple and tunable alternative for the immobilization and stabilization of photosensitizers, opening new avenues for photocatalytic synthetic processes.[15,16,17,18,19,20,21,22,23] However, processes involving homogenous ILs require the full recovery of the IL-phase and the photosensitizer in a further step, which is not always a simple task. The simplest solution is represented by the use of supported ionic liquids (SILs).[24] In the case of polymers bearing IL-like fragments colantly atttached (Supported Ioinic Liquid-Like Phases: SILLPs) the nature and loading of the IL-like units influence the macroscopic properties of the material,[25] but also plays an

[12] Hallett, J. P.; Welton, T. Room-Temperature Ionic Liquids: Solvents for Synthesis and Catalysis. 2. *Chem. Rev.* **2011**, *111* (5), 3508–3576.
[13] Welton, T. Ionic Liquids: A Brief History. *Biophys Rev.* **2018**, *10* (3), 691–706.
[14] Qiao, Y.; Ma, W.; Theyssen, N.; Chen, C.; Hou, Z. Temperature-Responsive Ionic Liquids: Fundamental Behaviors and Catalytic Applications. *Chem. Rev.* **2017**, *117* (10), 6881–6928.
[15] Qadir, M. I.; Zanatta, M.; Gil, E. S.; Stassen, H. K.; Gonçalves, P.; Neto, B. A. D.; de Souza, P. E. N.; Dupont, J. Photocatalytic Reverse Semi-Combustion Driven by Ionic Liquids. *ChemSusChem.* **2019**, *12* (5), 1011–1016.
[16] Murphy, B.; Goodrich, P.; Hardacre, C.; Oelgemöller, M. Green Photochemistry: Photo-Friedel–Crafts Acylations of 1,4-Naphthoquinone in Room Temperature Ionic Liquids. *Green Chem.* **2009**, *11* (11), 1867–1870.
[17] Garcia, H.; Navalon, S. Photochemistry in Ionic Liquids. In *Catalysis in Ionic Liquids*; Hardacre, C.; Parvulescu, V., Eds.; RSC, Cambridge, 2014; pp 474–507.
[18] Shimakoshi, H.; Houfuku, N.; Chen, L.; Hisaeda, Y. Redox Active Ionic Liquid as Efficient Mediator and Solvent for Visible Light-Driven B12 Catalytic Reactions. *Green Energy and Env.* **2019**, *4* (2), 116–120.
[19] Fabry, D. C.; Ronge, M. A.; Rueping, M. Immobilization and Continuous Recycling of Photoredox Catalysts in Ionic Liquids for Applications in Batch Reactions and Flow Systems: Catalytic Alkene Isomerization by Using Visible Light. *Chem. Eur. J.* **2015**, *21* (14), 5350–5354.
[20] Zhang, W.; Shimakoshi, H.; Houfuku, N.; Song, X. M.; Hisaeda, Y. A Polymerized Ionic Liquid-Supported B_{12} Catalyst with a Ruthenium Trisbipyridine Photosensitizer for Photocatalytic Dechlorination in Ionic Liquids. *Dalton Trans.* **2014**, *43* (37), 13972–13978.
[21] Xu, D.; Zhang, H.; Chen, X.; Yan, F. Imidazolium Functionalized Cobalt Tris(Bipyridyl) Complex Redox Shuttles for High Efficiency Ionic Liquid Electrolyte Dye-Sensitized Solar Cells. *J. Mater. Chem. A.* **2013**, *1* (38), 11933–11941.
[22] Rosspeintner, A.; Koch, M.; Angulo, G.; Vauthey, E. Salt Effect in Ion-Pair Dynamics after Bimolecular Photoinduced Electron Transfer in a Room-Temperature Ionic Liquid. *J. Phys. Chem. Lett.* **2018**, *9* (24), 7015–7020.
[23] Aster, A.; Vauthey, E. More than a Solvent: Donor–Acceptor Complexes of Ionic Liquids and Electron Acceptors. *J. Phys. Chem. B.* **2018**, *122* (9), 2646–2654.
[24] Giacalone, F.; Gruttadauria, M. Covalently Supported Ionic Liquid Phases: An Advanced Class of Recyclable Catalytic Systems. *ChemCatChem.* **2016**, *8* (4), 664–684.
[25] (a) Burguete, M. I.; Galindo, F.; García-Verdugo, E.; Karbass, N.; Luis, S. V. Polymer Supported Ionic Liquid Phases (SILPs) versus Ionic Liquids (ILs): How Much Do They Look Alike. *Chem.*

important role on the activity and stability of the immobilized catalytic species. Indeed, both the polymer nature and the structural features of the IL-like units can be used to fine-tune their catalytic efficiency.[26] Furthermore, SILPs based on solid-insoluble crosslinked polymers allow their straightforward application for the development of continuous flow processes.[27] In the search of new applications of SILLPs, here we report the synthesis of polymeric materials modified with IL-like units as suitable supports and solid media for photocatalytic processes. The use of supported Rose Bengal (RB), immobilized on a variety of SILLPs, has been evaluated as a photosensitizer for the photooxygenation of furoic acid as a well-established benchmark reaction.

6.2. Results and Discussion

IL-like polymeric materials (PILs) were easily prepared by the polymerization of monomers containing imidazolium fragments (Scheme 1).[28,29,30] Different di-styrenic bisimidazolium monomers were obtained by alkylation of 1-(4-vinylbenzyl)-1*H*-imidazole with different α,ω-bisbromoalkanes (*n*= 2, 4 and 6 for **1**-**3** respectively, Scheme SI.1). These crosslinking monomers were co-polymerized with 2-hydroxyethyl methacrylate (**4**, HEMA) using a 4:6 weight

Commun. **2007**, No. 29, 3086–3088. (b) ans, V.; Karbass, N.; Burguete, M. I.; Compañ, V.; García-Verdugo, E.; Luis, S. V.; Pawlak, M. Polymer-Supported Ionic-Liquid-Like Phases (SILLPs): Transferring Ionic Liquid Properties to Polymeric Matrices. *Chem. Eur. J.* **2011**, *17* (6), 1894–1906.

[26] Montolio, S.; Altava, B.; García-Verdugo, E.; Luis, S. V. Supported ILs and Materials Based on ILs for the Development of Green Synthetic Processes and Procedures. In *Green Synthetic Processes and Procedures*; Ballini, R., Ed.; Green Chemistry Series; Royal Society of Chemistry.: United Kingdom, 2019; pp 289–318.

[27] García-Verdugo, E.; Altava, B.; Burguete, M. I.; Lozano, P.; Luis, S. V. Ionic Liquids and Continuous Flow Processes: A Good Marriage to Design Sustainable Processes. *Green Chem.* **2015**, *17* (5), 2693–2713.

[28] Mecerreyes, D. Polymeric Ionic Liquids: Broadening the Properties and Applications of Polyelectrolytes. *Prog. Polym. Sci.* **2011**, *36* (12), 1629–1648.

[29] Andrzejewska, E. Photoinitiated Polymerization in Ionic Liquids and Its Application. *Polym. Int.* **2017**, *66* (3), 366–381.

[30] Qian, W.; Texter, J.; Yan, F. Frontiers in Poly(Ionic Liquid)s: Syntheses and Applications. *Chem. Soc. Rev.* **2017**, *46* (4), 1124–1159.

ratio, in presence of porogenic agents, leading to a series of monolithic polymers (**5-7**). Materials containing different monomer **2** / HEMA ratios were also prepared (**6a-c**). Additionally, the imidazolium monomer **8**, obtained by alkylation of N-butylimidazole with *p*-chloromethyl styrene, was co-polymerized with three different crosslinkers, the divinylic momomer **2**, trimethylolpropane trimethacrylate (**9**) and N,N′-methylene-bis-acrylamide (**10**). Table 1 summarizes the polymerization mixtures used for preparing all these materials.[31] All of them were obtained in excellent yields (> 95 %) and showed a good compatibility with polar solvents such as water and methanol. Thus, for instance, polymer **11** was able to absorb 45.9 g_{water} $g_{polymer}^{-1}$ and 24.6 g_{MeOH} $g_{polymer}^{-1}$, while polymers **12** and **13**, with higher crosslinking degrees, showed lower absorption capacities (4.8 g_{water} g and 3.4 g_{MeOH} $g_{polymer}^{-1}$ **12** or 5.7 g_{water} $g_{polymer}^{-1}$ and 3.9 g_{MeOH} $g_{polymer}^{-1}$ for **13**.

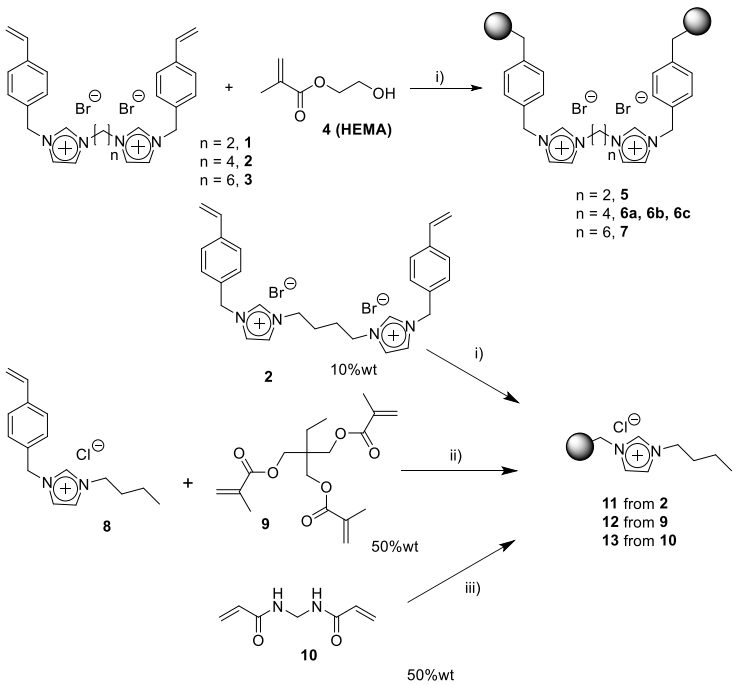

Scheme 1. Synthesis of PILs by polymerization. i) 65 ºC, H_2O, 1% AIBN. ii) 65 ºC, MeOH/H_2O (4:1), 1% AIBN. iii) 70 ºC, MeOH/H_2O (5:1), 1% AIBN.

[31] Lozano, P.; García-Verdugo, E.; Piamtongkam, R.; Karbass, N.; Diego, T. D.; Burguete, M. I.; Luis, S. V.; Iborra, J. L. Bioreactors Based on Monolith-Supported Ionic Liquid Phase for Enzyme Catalysis in Supercritical Carbon Dioxide. *Adv. Synth. Catal.* **2007**, *349* (7), 1077–1084.

Table 1. Polymerization mixtures.

Entry	SILLP[a]	IL monomer (w/w)	Co-monomer (w/w)	Loading[b] [mmol g^{-1}]	IL[c] [%]
1	**5**	**1** (0.4)	**4** (0.6)	1.24	68.9
2	**6a**	**2** (0.8)	**4** (0.2)	1.58	92.3
3	**6b**	**2** (0.5)	**4** (0.5)	1.38	80.6
4	**6c**	**2** (0.4)	**4** (0.6)	1.25	73.0
5	**7**	**3** (0.4)	**4** (0.6)	1.21	74.1
6	**11**	**8** + **2**(1)	**2** (0.1)	3.17	100
7	**12**	**8** (0.5)	**9** (0.5)	1,27	35.1
8	**13**	**8** (0.5)	**10** (0.5)	2.27	62.0

[a] AIBN 1% by wt% of the polymerization mixture, porogen: H_2O/diethylenglycol (1:1, *w/w*) for **5**, **6** and **7** with a porogen/monomeric mixture ratio of 75:40 (*w/w*). Porogen for **11**: H_2O, porogen for **12**: MeOH H_2O (4:1), porogen for **13**: MeOH H_2O (5:1) with a porogen/momeric mixture ratio of 4.5:1 (*w/w*) for **11**, 2.5:1 (*w/w*) for **12** and 6.5:1(*w/w*) for **13**. [b] Imidazolium unit loading calculated by elemental analysis. [c] Percentage by weight of the IL-like units calculated as IL [%] = ($mmol_{imidazolium\ unit}\ g_{polymer}^{-1}$) x *M* x 10^{-1}. *M* = molecular weight of the imidazolium salt fragment in the corresponding polymer.

The immobilization of Rose Bengal (RB) was performed by suspending the polymeric matrices (**5-7** and **11-13**) in a methanolic solution of RB. Eight different SILLPs, all of them loaded with 3.92 x 10^{-2} $mmol_{RB}\ g_{polymer}^{-1}$, were obtained (**15-22**, Scheme 2). The total absence color of the solution indicated the quantitative absorption of RB onto the polymeric matrix. Furthermore, during the polymer washing no color loss was detected and the analysis by UV-Vis at 557 nm of the MeOH used did not show any trace of leached RB in the washing solution.

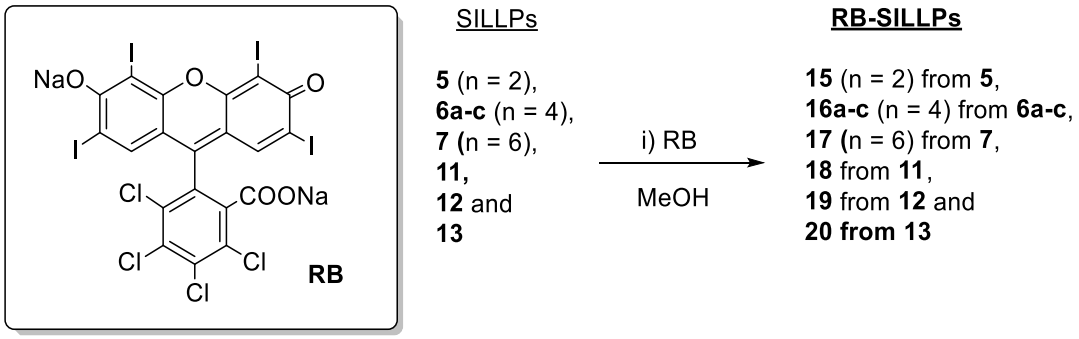

Scheme 2. Immobilisation of RB on SILLPs. i) 1 mL of a 1000 ppm solution of RB in MeOH for each 25 mg of polymer. RB loading 39.36 μmol_{RB} $g^{<M<1}$.

To evaluate the photocatalytic efficiency of those RB-SILLPs, the photooxygenation of 2-furoic acid **21** to butenolide **22** (5-hydroxy-5H-furan-2-one) reaction (Scheme 3). A long list of applications of **22** can be found in the literature, because it is an important starting substrate for the synthesis of insecticides, prostanoids, alkaloids, and so on.[32,33] The oxidation of **21** to **22** was performed by irradiating (125 W Hg vapor lamp) a suspension of the corresponding supported photocatalyst in a solution of **21**. The reactions were monitored by UV–vis following the bleaching of the characteristic absorption band of **21** at 247 nm. Both conversions and rate constants were used to analyze the efficiency of the different polymeric photosensitizers.

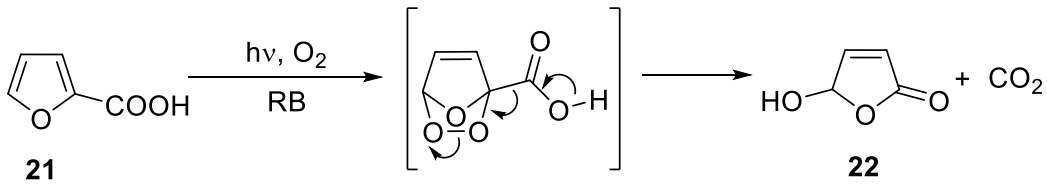

Scheme 3. Photocatalytic benchmark reaction: 50:1 substrate/photocatalyst molar ratio (2% mol), RT. Irradiation: 125 W medium-pressure Hg vapor lamp for 120 min in open test tubes equilibrated with air. [**21**] = 9.6 mM in MeOH.

[32] Vassilikogiannakis, G.; Stratakis, M. Biomimetic Total Synthesis of Litseaverticillols A, C, D, F, and G: Singlet-Oxygen-Initiated Cascades. *Angew. Chem., Int. Ed.* **2003**, *42* (44), 5465–5468.
[33] Ioannou, G. I.; Montagnon, T.; Kalaitzakis, D.; Pergantis, S. A.; Vassilikogiannakis, G. Synthesis of Cyclopent-2-Enones from Furans Using a Nebulizer-Based Continuous Flow Photoreactor. *Org. Biomol. Chem.* **2017**, *15* (48), 10151–10155.

Under these conditions, all the supported photocatalysts yielded > 90 % conversions after 120 minutes. Essentially, a quantitative selectivity for the transformation of **21** into **22** was observed in all cases. It should be noted that no loss of the characteristic coloration of the Rose Bengal was observed at the end of the reaction in any of the cases studied. Small differences were observed for the kinetic profiles of the tested systems showing, regardless of loading and type of IL-like moieties, similar catalytic efficiencies (Table 2, Figure SI.1). In the same way, the percentage and type of the crosslinker seems to have little influence. Noteworthy, faster kinetics were observed for the immobilized RB-SILLPs than for an RB solution and conversions achieved after 120 min were always better than those for the control experiment catalyzed by the disodium salt of RB (95-99% *vs.* 65-70%). The reuse of the photosensitizer **16c** in consecutive reaction cycles was also studied. This RB-SILLP system was very stable, being reused for eight reaction cycles without any decay in its photocatalytic activity (see Figure SI.2 in the Supporting Information).

Table 2. Photooxidation of **21** by different RB-SILLPs obtained by polymerization.

Entry	RB-SILLP	Loading[a] [mmol g^{-1}]	IL[b] [%]	Conv.[c] [%]	k [d] [10^{-4} x s^{-1}]
1	**15**	1.24	68.9	99	4.51 ± 0.18
2	**16a**	1.58	92.3	97	3.81 ± 0.06
3	**16b**	1.38	80.6	90	3.29 ± 0.10
4	**16c**	1.25	73.0	98	4.43 ± 0.09
5	**17**	1.21	74.1	99	4.2 ± 0.8
6	**18**	3.17	100	98	5.4 ± 0.3
7	**19**	1.27	35.1	99	5.3 ± 0.3
8	**20**	2.27	62.0	98	5.5 ± 0.19
9	**RB**	-	-	70	3.25 ± 0.11

[a] Imidazolium units loading calculated by elemental analysis. [b] Percentage by weight of the IL-like units calculated as IL [%] = ($mmol_{imidazolium\ unit}$ $g_{polymer}^{-1}$) x M x 10^{-1}. M = molecular weight of the imidazolium salt fragment in the corresponding polymer. [c] Conversion for the photooxidation of **21**. [d] Rate constants for the photooxidation of **21** calculated as the first-order rate constant for the initial period of the reaction.

Table 3. Effect of the RB loading onto SILLP **6c**.

Entry	RB-SILLP	RB [μmol g^{-1}]	k 10[a] [10^{-4} x s^{-1}]	TON[b]	TOF_{50}[c] [h^{-1}]
1	**16c**	39.36	4.43 ± 0.09	26	57
2	**23a**	19.84	4.65 ± 0.11	57	114
3	**23b**	0.40	4.95 ± 0.07	289	527
4	**23c**	0.20	1.93 ± 0.012	2867	5213

[a] Rate constant for the photooxidation of **21** calculated as the first-order rate constant for the initial period of the reaction. [b] TON calculated at 30 min. [c] TOF calculated at 50% of conversion.

Encouraged by these results, the effect of different variables was evaluated in order to optimize the efficiency of the immobilized system. In this way, the influence of the RB loading on the SILLP was firstly examined. Variable amounts of RB were absorbed onto the polymer **6c** (39.36 to 0.20 $\mu mol_{RB}\ g_{SILLP}^{-1}$, polymers **16c** and **23a-c**). The results obtained are summarized in Table 3 and Figure SI.3 (Supporting Information). A complete conversion of **21** was observed after 60 min of reaction for the catalyst with the higher RB loading (**16c**), whereas an irradiation time of 180 minutes was required for the photocatalyst with the lowest RB-loading (**23c**). The photocatalysts with intermediate loadings (**23a** and **23b**) showed similar profiles of yield *vs* time (Figure SI.3 in the Supporting Information) as **16c**, althought their RB loadings were 2 and 10 times lower, respectively. Thus, the highest turnover number (TON) and frequency (TOF_{50} at 50% conversion) values were obtained for **23c**, a polymer with a very low RB loading (0.2 μmol g^{-1}) with TON = 2867 (30 min) and TOF_{50} = 5213 h^{-1}. These results suggest that for the polymeric photosensitizer **16c** (with the highest loading, 39.36 $\mu mol_{RB}\ g_{SILLP}^{-1}$) RB groups located near the surface of the polymer can act as a filter, absorbing the incident radiation and preventing it from reaching the dye groups located in more hindered sites ("screen effect"). This effect decreases upon the reduction of the RB loading, increasing the catalytic efficiency per dye unit. All the systems presented so far are based in SILLPs obtained by copolymerization of the corresponding IL-monomers (Scheme 1). To

stablish the effect of the polymer matrix on the behavior of the photosensitizers, a new series of gel-type SILLPs were synthesized (Scheme 4) by grafting IL-like units onto already preformed polystyrene-di-vinylbenzene polymeric matrices (PS-DVB, Merrifield gel-type resins). Three different SILLPs (**25a-c**) were synthetized by modification of PS-DVB resins with different loadings (1.1, 2.1 and 4.1 meq_{Cl} g^{-1}, **24a-c**, 1% DVB, gel-type, 200-400 mesh).

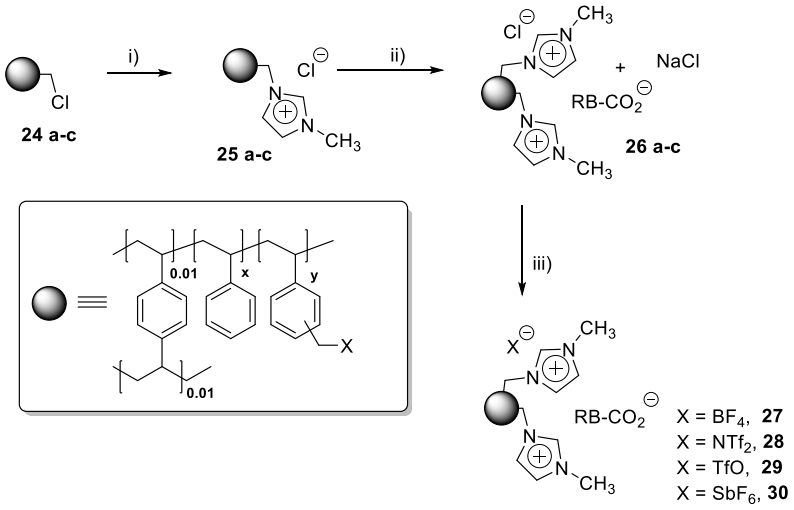

Scheme 4. Synthesis of gel-type SILLPs and the corresponding RB photocatalysts i) methylimidazole in DMF, 80 °C, 14 h. ii) 1 mL of a 1000 ppm solution of RB in MeOH for each 25 mg of polymer. RB loading 39.36 μmol_{RB} g^{-1}. iii) Anion metathesis with the corresponding salt in MeOH.

The modification with methylimidazole took place quantitatively with a significant change on the resin polarity. SILLPs **25a-c**, although based on a PS-DVB hydrophobic polymeric backbone, showed a significant swelling in a polar solvent such as MeOH, with swellings of 40, 59 and 84% (percentage of diameter increase in MeOH) for **25a**, **25b** and **25c** respectively. RB was quantitatively absorbed on polymers **25a-c** and the resulting RB-SILLPs (**26a-c**) were assayed for the model photooxidation of **21**. The results are summarized in Table 4 and Figure SI.4 (Supporting Information). The different kinetic profiles observed for these systems suggest that the amount of IL-like units can be used to finetune the

catalytic behavior of the RB-SILLPs. For the polymers with a low loading of IL-like moieties (**26a**), the limited swelling in MeOH can provide a less effective diffusion of reagents and oxygen through the polymer beads. In this regard, a good diffusion is essential because $^1O_2$ is a short-lived species, which can be quenched by the protic solvent before meeting the substrate. In addition, a lower swelling can also produce local photocatalyst aggregates (higher local concentration), which would decrease the photochemical activity.

Table 4. Effect of the amount of IL-like units on the SILLPs.

Entry	Catalyst	Loading[a] [mmol g^{-1}]	IL[b] [%]	k [c] [10^{-4} x s^{-1}]
1	**26a**	0.89	23	2.99 ± 0.03
2	**26b**	1.92	45	7.90 ± 0.40
3	**26c**	2.99	70	5.13 ± 0.08

[a] Imidazolium units loading calculated by elemental analysis. [b] Percentage by weight of the IL-like units calculated as IL [%] = ($mmol_{imidazolium\ unit}$ $g_{polymer}^{-1}$) x M x 10^{-1}. M = molecular weight of the imidazolium salt fragment in the corresponding polymer. [c] Rate constants for the photooxidation of **21** calculated as the first-order rate constant for the initial period of the reaction.

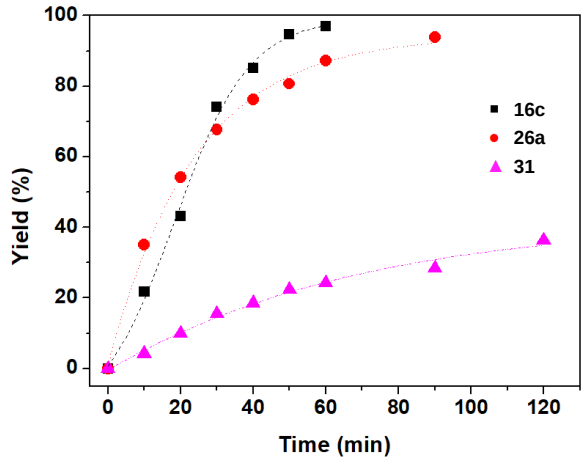

Figure 1. Comparison of yield versus time profiles obtained for the oxidation of **21** with singlet oxygen in the presence of RB-SILLPs **16c** and **26a** and in the presence of commercial RB-PS-DVB **31**. 50:1 substrate/photocatalyst molar ratio (2 mol %), RT. Irradiation: 125W medium-pressure Hg vapor lamp for 120 min in open test tubes equilibrated with air. [**21**] = 9.6 mM in MeOH. Squares: **16c**. Dots: **26a**. Triangles: **31** (Necker´s catalyst). Initial reaction rates: (6.19 ± 0.12) x 10^{-4} s^{-1} for **16c**; (6.40 ± 0.14) x 10^{-4} s^{-1} for **26a**; (0.82 ± 0.02) x 10^{-4} s^{-1} for **31**.

The photocatalytic activity was clearly improved by the enhanced swelling in MeOH for **26b**. However, the further increase in swelling for **26c** was accompanied by some decrease in activity. The much larger diameter of the polymeric beads for **26c** when swollen, can hamper the efficient radiation absorption by the RB units at the core of the particles. Accordingly, a compromise between the loadings of both the photocatalyst and the IL-like units must be reached to achieve the best catalytic performance.

These results suggest that the IL-like units in the support allow a fine-tuning of the photocatalytic efficiency of RB. This is highlighted in Figure 1, which shows a comparison of the RB-SILLPs **16c** and **26a** with the commercially available RB grafted onto PS-DVB (1% crosslinking, 0.1 $mmol_{RB}$ g^{-1}, 200-400 mesh, **31**). RB immobilized on polymers containing IL-like units (SILLPs) were clearly more active systems that those supported on a polymer lacking such units, with an approximately. 7.5 times higher initial reaction for RB-SILLPs.

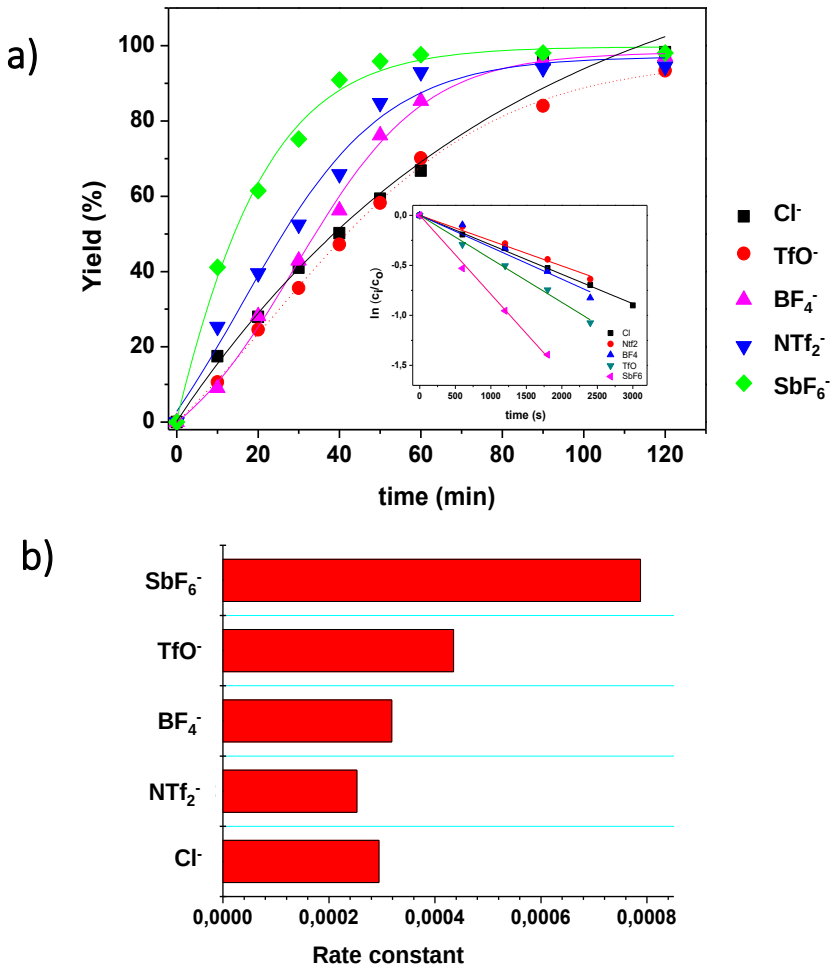

Figure 2. **(a)** Yield *vs* time profiles obtained for RB-SILLPs derived from **26a** by anion metathesis (**27a-30a**) for the oxidation of **21** with singlet oxygen. Inset: $\ln(C_t/C_0)=kt$ for the initial period of the reaction, in which C_t and C_0 are the concentrations of **21** at a certain time (t) and at t = 0, respectively and k is the rate constant. Conditions: 50:1 substrate/photocatalyst molar ratio (2% mol), RT. Irradiation: 125W medium-pressure Hg vapor lamp for 120 min in open test tubes equilibrated with air. [**21**] = 9.6 mM in MeOH. **(b)** Effect of the IL-like moieties counteranion on the rate constants.

The nature of the anion can also be used to tune the properties of catalytic units immobilized onto SILs.[34,35,36] Therefore, the effect of the anion was evaluated by exchanging the Cl^- anion of the RB-SILLP **26a** by BF_4^-, NTf_2^-, TfO^- and SbF_6^- (RB-SILLPs **27a**-**30a**, Scheme 4). Attenuated total reflection Fourier-transform IR (ATR-FTIR) and Raman spectroscopy were used to follow the corresponding anion exchange,[25] whereas diffuse reflectance UV/Vis spectroscopy was used to analyze the presence of RB. It has been reported that RB grafted onto Merrifield resins display two high-intensity absorption bands located between 571 and 560 nm.[37] The presence of a shoulder at shorter wavelengths (≈ 530 nm) has been associated with the formation dimers or aggregates in homogeneous and supported RB esters.[38,39] RB-SILLPs displayed two broad bands at (566±3) and (523±4) nm, affected in position and intensity by the counteranion present (Figure SI.5 and Table SI.1in the Supporting Information) along with a small shoulder below 500 nm. These changes highlight the very different environments for the dye present in RB-SILLPs, which is also affected by the nature of the counteranion of the IL-like fragments. Independently of the anion present, most photosensitizers showed a similar activity (Figure 2). Only **30a**, bearing SbF_6^- as the anion, showed an increased reactivity in comparison with the photosensitizers containing Cl^-, TfO^-, NTf_2^- and BF_4^-, which can be related to the

[34] Martín, S.; Porcar, R.; Peris, E.; Burguete, M. I.; García-Verdugo, E.; Luis, S. V. Supported Ionic Liquid-like Phases as Organocatalysts for the Solvent-Free Cyanosilylation of Carbonyl Compounds: From Batch to Continuous Flow Process. *Green Chem.* **2014**, *16* (3), 1639–1647.
[35] Porcar, R.; Lozano, P.; Burguete, M. I.; Garcia-Verdugo, E.; Luis, S. V. Dimethyl Carbonate as a Non-Innocent Benign Solvent for the Multistep Continuous Flow Synthesis of Amino Alcohols. *React. Chem. Eng.* **2018**, *3* (4), 572–578.
[36] Restrepo, J.; Lozano, P.; Burguete, M. I.; García-Verdugo, E.; Luis, S. V. Gold Nanoparticles Immobilized onto Supported Ionic Liquid-like Phases for Microwave Phenylethanol Oxidation in Water. *Catal. Today.* **2015**, *255*, 97–101.
[37] Neckers, D. C.; Paczkowski, Jerzy. Microheterogeneous Photooxidation. *J. Am. Chem. Soc.* **1986**, *108* (2), 291–292.
[38] Nowakowska, M.; Kępczyński, M.; Dąbrowska, M. Polymeric Photosensitizers, 5. Synthesis and Photochemical Properties of Poly[(N-Isopropylacrylamide)-Co-(Vinylbenzyl Chloride)] Containing Covalently Bound Rose Bengal Chromophores. *Macromol. Chem. Phys.* **2001**, *202* (9), 1679–1688.
[39] Valdes-Aguilera, O.; Neckers, D. C. Rose Bengal Ethyl Ester Aggregation in Aqueous Solution. *J. Phys. Chem.* **1988**, *92* (15), 4286–4289.

low coordinating ability of this anion facilitating a tighter interaction of RB with the IL-fragments.

All the above reactions were assayed with high-pressure Hg lamps, which can be considered as the standard light source for UV photochemical reactions. However, for this type of light source, there is some mismatch between the light emitted and the absorption frequency of the target molecular dye, which can lead to reduction in efficiency, photocatalyst deactivation, degradation of products and less selective processes. Therefore, the use of using simple LEDs, instead of the Hg lamp, was also evaluated. UV-LEDs allow energy efficient, reliable, and simple generation of almost monochromatic near-UV light, and allow a straightforward building of cheap photochemical reactors. Figure SI.6 (Supporting Information) shows the comparison of the results obtained from RB in solution as well as with the RB-SILLP **27a**, by using the Hg lamp and green UV-LEDs, for the photooxidation of **21**. Comparable results were obtained, especially regarding the initial rates, although the Hg lamp, with a higher power, achieved slightly higher final yields.

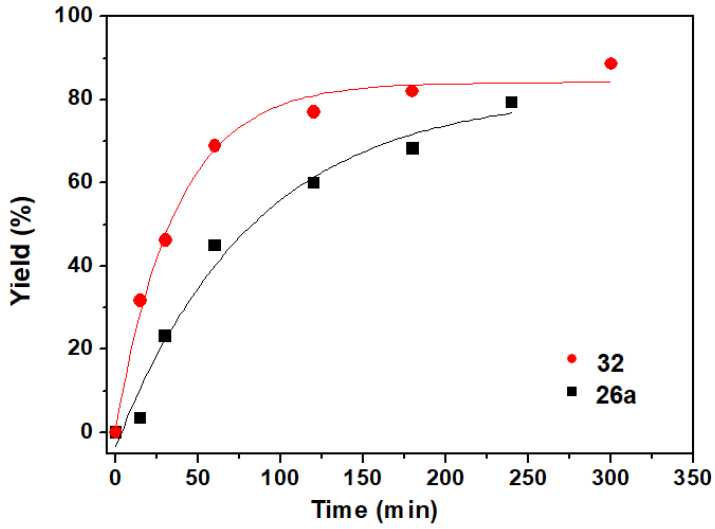

Figure 3. Yield *vs* time profiles obtained for the oxidation of **21** with singlet oxygen. Conditions: 50:1 substrate/photocatalyst molar ratio (2 mol %), R.T. Irradiation: Blue LED for 300 mim in open test tubes equilibrated with air. [**21**] = 9.6 mM in MeOH. Squares: **26a**. Dots: **32** (QDs-RB-SILLP). Initial reaction rates: (1.32 ± 0.09) x 10^{-4} s^{-1} for **26a**; (4.05 ± 0.08) x 10^{-4} s^{-1} for **32**.

Additionally, the use of LEDs can open new avenues in the search for more efficient photocatalytic processes. This is illustrated by the combination of RB-SILLPs with a semiconductor quantum dot (QD, that is, CdSe), acting as a "light antenna" to capture energy at a wavelength not usable directly usable by the photosensitizer.[40,41] Thus, a QDs-SILLP (**31**) composite was easily obtained by exposing SILLP **25a** to solution of core–shell CdSe/ZnS QDs (50 μg mL^{-1} in toluene). UV-Vis data indicated a quantitative immobilization of the QDs in the SILLP. Then, RB was supported on the QDs-SILLP, affording the QDs-RB-SILLP composite (**32**) with a loading of 60 $\mu g_{QDs}\ g^{-1}$ and 39.36 $\mu mol_{RB}\ g_{composite}^{-1}$. As seen in Figure 3, the use of the composite **32** allowed the photooxidation to occur efficiently upon irradiation with blue UV-LEDs. Thus, at 15 minutes, a 32% conversion was obtained for **32**, whereas only a 5 % yield was achieved with the related RB-SILLP **26a**. This suggests the existence of an effective Förster's Resonance Energy Transfer (FRET) process leading to the indirect excitation of the RB moiety when exciting the QD nanoparticle. The overlapping between the emission of QDs and the absorption of RB at the SILLP leads to population of the RB triplet state and concomitantly to the efficient generation of singlet oxygen. Nevertheless, the process was less efficient that when irradiating directly **26a** with green UV-LEDs (Figure 3) even if the initial rates were comparable.

[40] Hildebrandt, N.; Spillmann, C. M.; Algar, W. R.; Pons, T.; Stewart, M. H.; Oh, E.; Susumu, K.; Díaz, S. A.; Delehanty, J. B.; Medintz, I. L. Energy Transfer with Semiconductor Quantum Dot Bioconjugates: A Versatile Platform for Biosensing, Energy Harvesting, and Other Developing Applications. *Chem. Rev.* **2017**, *117* (2), 536–711.

[41] Fabregat, V.; Burguete, M. I.; Luis, S. V.; Galindo, F. Improving Photocatalytic Oxygenation Mediated by Polymer Supported Photosensitizers Using Semiconductor Quantum Dots as 'Light Antennas.' *RSC Adv.* **2017**, *7* (56), 35154–35158.

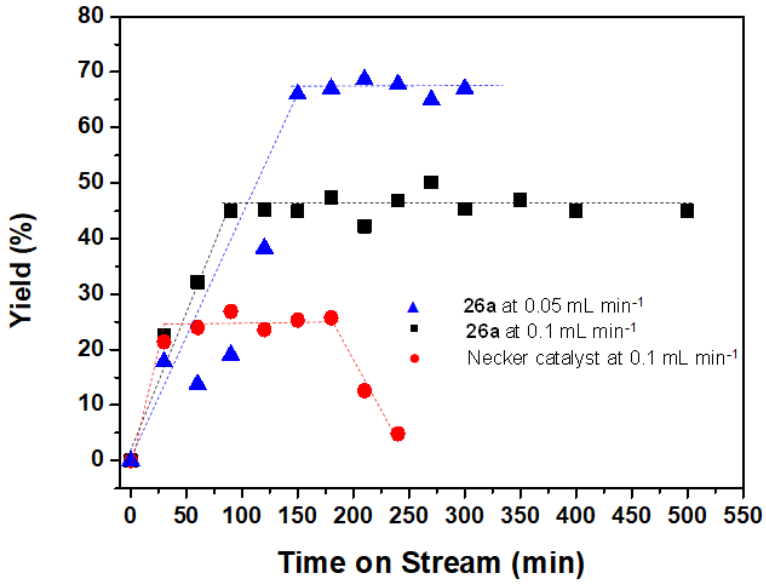

Figure 4. Yield versus time on stream obtained for the photooxidation of **21**. Dots: Necker catalyst at 0.1 mL min^{-1}. Squares: **26a** at 0.1 mL min^{-1}. Triangles: **26a** at 0.05 mL min^{-1}.

Continuous flow processes can help to increase the sustainability of photocatalytic reactions because they present some distinct advantages such as the easy separation of products and the continuous reutilization of the photocatalyst in consecutive cycles, avoiding downtime, and the consequent loss of productivity.[42] Figure SI.7 shows a schematic representation of the continuous flow reactor used to perform the photooxidation of furoic acid. The system consists in a HPLC pump that feeds the substrate to the reactor, which is a fluid-bed reactor loaded with RB-SILLP. A Hg lamp was used as the light source. The behavior of **26a** was compared with that of the commercially available Necker catalyst (RB-PS-DVB).[10] Figure 4 summarizes the results obtained. When using an initial flow rate of 0.1 mL min^{-1}, the commercial catalyst provided a yield of approximately 25 %, which was lower than the one achieved with **26a** (≈ 45% yield). Furthermore, the commercial catalyst showed a strong deactivation after 200 min on continuous use, whereas the performance of the RB-SILLP remained

[42] Cambié, D.; Bottecchia, C.; Straathof, N. J. W.; Hessel, V.; Noël, T. Applications of Continuous-Flow Photochemistry in Organic Synthesis, Material Science, and Water Treatment. *Chem. Rev.* **2016**, *116* (17), 10276–10341.

constant during at least 8 hours. The yield with **26a** could be further improved until approximately 70% by increasing the residence time through reducing the flow rate to 0.05 mL min^{-1}. These results suggest that the continuous-flow photochemical generation of singlet oxygen can be achieved by the simple immobilization RB onto SILLPs providing a scalable, selective and high-yielding platform, where the oxidation proceeds using only light, air and catalytic amounts of supported RB.

6.3. Conclusions

Rose Bengal (RB) immobilized on supported ionic liquids (SILs) prepared by direct copolymerization of imidazolium monomers or by grafting imidazolium units on already performed polymers efficiently promotes the photooxidation of furoic acid by generation of singlet oxygen. The supported photocatalysts are equally active under irradiation using an Hg lamp or, alternatively, under UV-LEDs irradiation. The chemical and structural parameters of the supported IL-like phases (SILLPs) can be easily fine-tuned to optimize the catalytic efficiency of the RB-SILLPs. Adjusting the IL-like units loading as well as the nature of the IL-counteranion results in supported catalysts that are significantly more active than related systems lacking the IL-like units, including commercially available polystyrene-divinylbenzene (RB-PS-DVB) systems. Furthermore, the presence of these IL-like units facilitates the immobilization and stabilization of QDs working as light antennas to increase the light harvesting capacity as wavelengths not corresponding to the optimal absorption of RB. Optimized RB-SILLPs showed a remarkable stability and this has been used for developing an efficient continuous mini-flow photocatalytic process implemented for the photooxidation of furoic acid, which demonstrated to be a more active and stable system than the related one using the commercial polymer where the photosensitizer is grafted to a PS-DVB backbone in the absence of IL-like units.

These results open a new avenue for the combination of advanced materials based on polymeric ILs with organic photodyes to develop more efficient and easier to use photocatalytic systems.

6.4. Experimental Section

Materials

All the reagents and solvents used were commercially available. 4-Vinylbenzyl chloride (p-chloromethylstyrene, 90%, Aldrich) was purified over a column of basic aluminium oxide. 2,2′-Azobis(2-methylpropionitrile) used as free radical initiator (AIBN, >98%, Aldrich), N,N-dimethylformamide (DMF, 99.5%, Scharlau), 1-methylimidazole (99%, Aldrich), 1-butylimidazole (98%, Aldrich), 1-decyl-2-methylimidazole (97% Aldrich), trimethylolpropane trimethacrylate (technical grade, TMPTMA Aldrich), N,N′-methylenebis(acrylamide) (99% Aldrich), 4,5,6,7-tetrachloro-2,4,5,7′-tetraiodofluorescein disodium salt, Acid Red 94, Rose Bengal B sodium salt (Rose Bengal sodium salt, 95%, Aldrich), polystyrene-bound Rose Bengal B (200-400 mesh, ≈0.1 mmol g^{-1}, Aldrich), chloromethylated stryene/divinylbenzene copolymer resins (Merrifield peptide resin, 200-400 mesh, 1.2, 2.1 or 4.3 $mmol_{Cl}$ g^{-1} loading, 2 % cross-linked), methanol (MeOH, 99.9%, Scharlau), bis(trifluoromethane) sulfonimide lithium salt ($LiNTf_2$, 99%, Aldrich), acetone HPLC (99.9%, Scharlau) and other salts and solvents were used as received.

General characterization protocols

FT-IR-ATR spectra were obtained using a spectrometer (JASCO FT/IR-6200) equipped with an ATR (MIRacle single-reflection ATR diamond/ZnSe) accessory at 4 cm^{-1} resolution (4000-600 cm^{-1} spectral range). Raman spectra were

obtained with a NRS-3100 (Jasco) dispersive Raman spectrometer equipped with an optical microscope and an air-cooled CCD detector (-65 ^{o}C) using the following conditions: 785 nm laser with a single monochromator, 600 l/mm grating, 0.2 mm slit, 12.75 cm^{-1} resolution; with a center wavenumber of 1200 cm^{-1}, a laser power of 90.1 mW and 10 accumulations of 5 s. Elemental analyses were obtained with a CHN Euro EA 3000 instrument. ^{1}H-NMR experiments were carried out using a Varian INOVA 500 (^{1}H-NMR, 500 MHz) spectrometer. Chemical shifts are given in delta (δ) values relative to TMS and the coupling constants (*J*) in Hertz (Hz). UV-Vis spectroscopy measurements were performed in a Shimadzu UV2450 spectrophotometer (diffuse reflectance mode for polymers) using an integrated sphere accessory and a light wavelength range between 200 and 800 nm.

Synthetic protocols

Monomers **1-3** and **8** were obtained as shown in Scheme SI.1(Supporting Information) according to methods already reported in the literature.[43]

Synthesis of 1-(4-vinylbenzyl)-1H-imidazole

$NaHCO_3$ (5.25 g, 62.4 mmol, 1.25 eq) was added to a mixture of imidazole (13.61 g, 199 mmol, 4 eq) in CH_3CN, then 1-(chloromethyl)-4-vinylbenzene (7.1 mL, 49.8 mmol, 1 eq) was added dropwise at RT. After the addition, the reaction mixture was heated to 50 ^{o}C and stirred for 20 h. The solvent was removed in vacuum, and the remaining solution was extracted with Et_2O (3x20mL). The organic phase was washed with 2 M HCl (final pH = 4-5) 4 M NaOH was then added to the

[43] Tang, J.; Tang, H.; Sun, W.; Roadosz, M.; Shen, Y. *J. Polym. Sci., Part A: Polym. Chem.* **2005**, *43* (22), 5477–5489.

resulting aqueous phase until pH = 7-8 (cloudy solution), and this solution was extracted with Et_2O (3x20mL). The obtained organic phase was dried over Na_2SO_4 and the solvent was removed in vacuum to afford the desired 1-(4-vinylbenzyl)-1H-imidazole (6.55 g, 71 % yield). FT-IR-ATR (cm^{-1}): 3005; 1570; 1505; 1408; 1320; 1285; 1231; 1017; 825; 745; 622. Raman (cm^{-1}): 3059; 1622; 1571; 1409; 1347; 1205; 1182; 1075; 831; 639. ^1H NMR (CD_3OD, 500 MHz), δ (ppm): 5.08 (s, 2H), 5.27 (d, *J* = 10.9 Hz, 1H), 5.75, (d, *J* = 17.9 Hz, 1H), 6.66-6.71 (m, 1H), 6.88 (d, *J* =17.7 Hz, 2H), 7.08 (d, *J* = 9.5 Hz, 2H), 7.36 (d, *J* = 8.1 Hz, 2H), 7.53 (s, 1H). ^{13}C NMR (CD_3OD, 300 MHz) δ (ppm) 49.9, 115.2, 120.9, 127.1, 128.4, 129.4, 136.8, 137.3, 138.1. ESI/MS (m/z). [M+H] = 185.2.

General procedure for the synthesis of ionic monomers 1-3

1-(4-vinylbenzyl)-1H-imidazole (4.2 mmol), the appropriate dibromo-alkyl spacer (2 mmol), and CH_3CN (10 mL) were loaded into a 25 mL two-necked flask. The mixture was heated to 80 °C for 24 h. The reaction mixture was cooled down to RT and transferred to a 100 mL round-bottomed flask. The product was precipitated with Et_2O (50 mL) and sonicated for 10 min, and the white solid was then left to settle. The liquid phase was removed carefully, and the washing procedure was repeated twice with Et_2O (2×50 mL). Finally, the white solid product was dried under vacuum overnight.

3,3′-(Ethane-1,2-diyl)bis(1-(4-vinylbenzyl)-1 H-imidazol-3-ium) chloride (1)

Obtained as a white solid in 60% yield using the former standard procedure. FT-IR (cm^{-1}): 3053; 1558; 1416; 1341; 1156; 988; 908; 857; 795; 623. Raman (cm^{-1}): 1620, 1601, 1414, 1316, 1195, 1174, 1016, 828, 629, 291. ^1H-NMR (CD_3OD, 500 MHz) δ

(ppm) 4.74 (s, 4H), 5.28 (d, *J* = 10.9 Hz, 2H), 5.41 (s, 4H), 5.84 (d, *J* = 17.7 Hz, 2H), 6.70-6.76 (m, 2H), 7.35 (d, *J* = 18.1 Hz, 4H), 7.49 (d, *J* = 8.1 Hz, 4H), 7.72 (d, *J* = 7.9 Hz, 2H), 7.82 (d, *J* = 7.9 Hz, 2H), 9.32 (s, 2H). ^{13}C RMN (CD_3OD, 300 MHz) δ (ppm), 35.5, 53.0, 114.5, 122.9, 123.3, 127.0, 129.1, 133.5, 136.0, 139.1. ESI/MS (m/z) [M^{2+}-2Br/2] = 198.2.

3,3′-(Butane-1,4-diyl)bis(1-(4-vinylbenzyl)-1 H-imidazol-3-ium) chloride (2)

Obtained as a white solid with 83% yield using the former standard procedure. FT-IR (cm^{-1}): 3143, 1561, 1459, 1156, 1009, 929, 860, 744, 627. Raman (cm^{-1}): 1620, 1598, 1408, 1317, 1195, 1176, 1011, 825, 627, 315. ^{1}H-NMR (CD_3OD, 500 MHz) δ (ppm) 1.95 (s, 4H), 4.30 (s, 4H), 5.28 (d, *J* = 10.2 Hz, 2H), 5.30 (s, 4H), 5.82, (d, *J* =15.3 Hz, 2H), 6.70-6.75 (m, 2H), 7.39 (d, *J* = 16.3 Hz, 4H), 7.48 (d, *J* = 7.6, 4H), 7.62 (d, *J* = 7.6 Hz, 2H), 7.68 (d, *J* = 7.6 Hz, 2H), 9.28 (s, 2H). ^{13}C RMN (CD_3OD, 300 MHz) δ (ppm) 26.8, 30.1, 48.9, 52.4, 116.0, 123.3, 123.5, 127.4, 129.4, 134.9, 136.6, 138.3. ESI/MS (m/z) [M^{2+}-2Br/2] = 212.3.

3,3′-(Hexane-1,6-diyl)bis(1-(4-vinylbenzyl)-1 H-imidazol-3-ium) chloride (3)

Obtained as a white solid with 78% yield using the former standard procedure. FT-IR (cm^{-1}): 3053, 1557, 1451, 1153, 922, 829, 740, 639. Raman (cm^{-1}): 1615, 1598, 1398, 1301, 1192, 1013, 818, 629, 599, 323. ^{1}H-NMR (CD_3OD, 500 MHz) δ (ppm) 1.41 (s, 4H), 1.92 (s, 4H), 4.24 (s, 4H), 5.28 (d, *J* = 10.1 Hz, 2H), 5.42 (s, 4H), 5.79 (d, *J* = 15.6 Hz, 2H), 6.71-6.75 (m, 2H), 7, 41 (d, *J* = 17.0 Hz, 4H), 7.50 (d, *J* = 8.2, 4H), 7.63 (d, *J* = 7.9 Hz, 2H), 7.68 (d, *J* =7.8 Hz, 2H), 9.18 (s, 2H). ^{13}C RMN (CD_3OD, 500

MHz) δ (ppm) 25.8, 48.5, 112.1, 119.3, 119.6, 123.4, 123.5, 131.1, 132.7, 132.9, 136.8, 138.3. ESI/MS (m/z) [M^{2+}-2Br/2] = 226.3.

Synthesis of 1-[(4-Ethenylphenyl)methyl]-3-butyl-imidazolium chloride (8)

1-butylimidazole (125 mmol) was dissolved in CH_3CN (30 mL) in a 100 mL round-bottom flask equipped with a stir bar. 4-Chloromethylstyrene (19.5 mL, 139 mmol) was then added, and the reaction was heated at 50 °C while stirring overnight. The reaction was stopped after this time, and the reaction mixture was poured into Et_2O (250 mL). The ionic product precipitated, and the mixture was placed in a freezer for several hours. The Et_2O phase was decanted and the resulting solid dried under vacuum lines at 40 °C overnight. Yield = 53.73 g, 82%. Characterization data were consistent with published values.[43]

General procedure for the preparation of the polymers 5-7 and 11-13 by bulk polymerization.

The polymerization mixture was prepared using the corresponding composition of the monomeric mixture as shown in Table 1 and different weight percentages of the solvent mixture used as the porogen an reported in the same table. The initiator, AIBN, was 1% of the mass of the monomers. The mixture was vortexed, sonicated and degassed until homogenous, then poured into a test tube and placed in a hot bath at 70 °C for 24 hours. The resulting polymers were washed in a Soxhlet extractor (MeOH, 300mL, 24h) to remove the unreacted starting materials. The polymerization took place in all the cases with > 95% yield.

Polymer 5: FT-IR (cm^{-1}): 2943, 1721, 1563, 1456, 1392, 1271, 1157, 1078, 1025, 848, 757. Raman (cm^{-1}): 1603, 1440, 1267, 1179, 1015, 956, 820, 593, 306. CHN analysis

(%): N (found): 3.4, loading 1.24 mmol IL-like units per gram of polymer. N (calcd): 3.73 for 1.33 mmol IL-like units per gram of polymer.

Polymer 6a: FT-IR (cm^{-1}): 2945, 1720, 1564, 1457, 1389, 1155, 845, 760, 623. Raman (cm^{-1}): 1603, 1440, 1179, 1014, 957, 821, 631, 594, 306. CHN analysis (%): N (found): 4.4 loading 1.58 mmol IL-like units per gram of polymer. N (calcd): 4.54 for 1.62 mmol IL-like units per g of polymer.

Polymer 6b: CHN analysis (%): N (found): 3.9, loading 1.38 mmol IL-like units per gram of polymer. N (calcd): 3.90 for 1.4 mmol IL-like units per gram of polymer.

Polymer 6c: CHN analysis (%): N (found): 3.5, loading 1.25 mmol IL-like units per gram of polymer. N (calcd): 3.59% for 1.28 mmol IL-like units per fram of polymer.

Polymer 7: FT-IR (cm^{-1}): 2946, 1721, 1562, 1455, 1392, 1273, 1157, 1076, 1022, 847, 757. Raman (cm^{-1}): 1604, 1440, 1411, 1322, 1179, 1015, 822, 632, 595, 307. CHN analysis (%): N (found): 3.4, loading 1.21 mmol IL-like units per gram of polymer. N (calcd): 3.47 for 1.24 mmol IL-like unitsper gram of polymer.

Polymer 11. FT-IR (cm^{-1}): 3382, 3133, 3058, 2959, 2928, 2870, 1630, 1613, 1560, 1513, 1453, 1425, 1359, 1326, 1155, 1117, 1020, 850, 825. CHN analysis (%): N (found): 8.9, loading 3.17 mmol IL-like units per gram of polymer. N (calcd): 9,10 for 3.25 mmol IL-like units per gram of polymer.

Polymer 12. FT-IR (cm^{-1}): 3375, 2959, 2940, 2877, 1720, 1634, 1560, 1459, 1387, 1266, 1148, 1013, 973, 817, 756. CHN analysis (%): N (found): 3.6 loading 1.27 mmol IL-like units per gram of polymer. N (calcd): 3.64 for 1.30 mmol IL-like units per gram of polymer.

Polymer 13. FT-IR (cm^{-1}): 3272, 3057, 2959, 2933, 2872, 1644, 1515, 1381, 1213, 1113, 816. CHN analysis (%): N (found): 6.4, loading 2.27 mmol IL-like units per gram of polymer. N (calcd): 6.44for 2.3 mmol IL-like units per gram of polymer.

Standard procedure for the preparation of polymers 15-20

500 mg of the corresponding SILLP (**5-7** and **11-13**) was suspended in 20 mL of a solution of RB (1000 ppm in MeOH) and left under stirring for 24 h. Then the polymer was filtered, washed with MeOH and dried in a vacuum oven at 45 ºC. The absorption for RB at 557 nm was measured in the mother liquor and in the washing liquid. In all cases the absorption corresponded with a quantitative uptake. RB loading: $3.98.10^{-3}$ $mmol_{RB}$ $g_{polymer}^{-1}$.

General synthesis of polymers 25a-c.

The synthesis was performed as already reported.[44] A Merrifield resin (10 g, **24a-c**) was introduced in a round-bottomed flask (250 mL) then, the alkylimidazole (6 eq.) was dissolved in DMF (100 mL) and introduced in the flask and the suspension was refluxed for 14 hours. The NBP test was negative at the end of this period confirming full conversion of chloromethyl groups.[45] he reaction was then filtered and the polymer was washed with DMF, DMF : H_2O (1:1), THF and CH_2Cl_2 and dried in a vacuum oven at 60 ºC.

Polymer 25a: FT-IR (cm^{-1}): 3419, 3141, 3060, 2922, 2848, 1567, 1616, 1510, 1449, 1332, 1159, 1022, 823, 761, 706, 661, 619. Raman (cm^{-1}): 1612, 1579, 1450, 1413, 1385,

[44] Burguete, M. I.; García-Verdugo, E.; Luis, S. V.; Restrepo, J. A. Preparation of Polymer-Supported Gold Nanoparticles Based on Resins Containing Ionic Liquid-like Fragments: Easy Control of Size and Stability. *Phys. Chem. Chem. Phys.* **2011**, *13* (33), 14831–14838.
[45] Galindo, F.; Altava, B.; Burguete, M. I.; Gavara, R.; Luis, S. V. A Sensitive Colorimetric Method for the Study of Polystyrene Merrifield Resins and Chloromethylated Macroporous Monolithic Polymers. *J. Comb. Chem.* **2004**, *6* (6), 859–861.

1331, 1188, 1160, 1091, 1022, 1001, 831, 765, 716, 664, 642, 620, 411, 332. CHN analysis (%):N (found): 2.5 loading 0.89 mmol IL-like units per gram of polymer. N (calcd): 2.6 for 0.93 mmol IL-like units per gram of polymer.

Polymer 25b: FT-IR (cm^{-1}): 3023, 2924, 1561, 1450, 1160, 824, 762, 703, 661.4, 619, 548. Raman (cm^{-1}): 1605, 1406, 1325, 1181, 1015, 995, 824, 636, 614. CHN analysis (%): N (found): 5.4, loading 1.92 mmol IL-like units per gram of polymer. N (calcd): 5.9 for 2.1 mmol IL-like units per gram of polymer.

Polymer 25c: FT-IR (cm^{-1}): 3931, 3891, 3830, 3738, 3386, 3147, 3086, 2925, 1644, 1566, 1515, 1451, 1334, 1159, 824, 761, 706, 616. Raman (cm^{-1}): 1615, 1455, 1415, 1387, 1332, 1192, 1092, 1024, 1004, 836, 769, 669, 646, 624, 414, 358, 270, 149. CHN analysis (%): N (found): 10.6, loading 3.79 mmol IL-like units per gram of polymer. N (calcd): 10.44 for 3.73 mmol IL-like units per gram of polymer.

General procedure for the preparation of polymers 26a-c

500 mg of the corresponding SILLP (**25a-c**) was suspended in 20 mL of a solution of RB (1000 ppm in MeOH) and left under stirring for 24 h. Then the polymer was filtered, washed with MeOH and dried in a vacuum oven at 45 °C. The absorption for RB at 557 nm was measured in the mother liquors and in the washing liquid. In all cases the absorption corresponded with a quantitative uptake. RB loading $3.98.10^{-3}$ $mmol_{RB}$ $g_{polymer}^{-1}$.

General procedure for the preparation of polymers 27-30.

100 mg of the corresponding SILLP (**26a**) was suspended in 12 mL of a MeOH : H_2O mixture (10:1 v/v) containing an excess of the corresponding YX salt and

left under stirring for 24 h. Then the polymer was filtered, washed with MeOH and dried in a vacuum oven at 45 ºC.

Polymer 27: YX = $NaBF_4$. FT-IR (cm^{-1}): 3026, 2922, 1596, 1496, 1448, 1350, 1194, 1057, 756, 700, 613. Raman (cm^{-1}): 1592, 1439, 1317, 1174, 1145, 1020, 990, 784, 610, 397. CHN analysis (%):N (found): 2.2, loading 0.77 mmol IL-like units per gram of polymer. N (calcd): 2.25 for 0.80 mmol IL-like units per gram of polymer.

Polymer 28. YX = $LiNTf_2$. FT-IR (cm^{-1}): 3026, 2922, 1596, 1496, 1448, 1350, 1194, 1057, 756, 700, 613. Raman (cm^{-1}): 1591, 1438 1317, 1172, 1144, 1019, 990, 782, 730, 610, 395. CHN analysis (%): N (found): 2.5, loading 0.60 mmol IL-like units per gram of polymer. N (calcd): 2.92 for 0.69 mmol IL-like units per gram of polymer.

Polymer 29. YX = KTfO. FT-IR (cm^{-1}): 3026, 2922, 1596, 1452, 1267, 1159, 1026, 757, 700, 632, 544. Raman (cm^{-1}): 1592, 1483, 1174, 1145, 1020, 991, 783, 747, 611. CHN analysis (%): N (found): 2.04, loading 0.73 mmol IL-like units per gram of polymer. N (calcd): 2.14 for 0.76 mmol IL-like units per gram of polymer.

Polymer 30. YX = $KSbF_6$. FT-IR (cm^{-1}): 3026, 2922, 1596, 1487, 1450, 1159, 757, 700, 653, 626, 545. Raman (cm^{-1}): 1591, 1439, 1317, 1174, 1145, 1020, 991, 784, 611, 399. CHN analysis (%): N (found): 2.0, loading 0.70 mmol IL-like units per gram of polymer. N (calcd): 2.01 for 0.72 mmol IL-like units per gram of polymer.

Synthesis of polymer 32: To a suspension of SILLP **25a** (250 mg) in DMF (5 mL), 1.5 mL of a QDs solution in toluene (CdSe/ZnS, 510nm, 50 µg / mL) was added and the mixture left under stirring (300 rpm) and protected from the light during 24 h. Then, the polymer was filtered, washed with DMF : H_2O (1:1), H_2O, CH_2Cl_2 and MeOH (5x5 mL) and dried under vacuum at 45 ºC. QDs loading: 0.3 mg_{QDs} $g_{polymer}^{-1}$.

100 mg of this resin (**31**) were suspended in a 1000 ppm solution of RB in MeOH (4 mL) and left under stirring (300 rpm) and protected from the light for 24 h. Afterwards, the polymer was filtered, washed with DMF : H_2O (1:1), H_2O,

CH_2Cl_2 and MeOH (5x5 mL) and vacuum dried at 45 °C. RB loading: $3.98.10^{-3}$ $mmol_{RB}$ $g_{polymer}^{-1}$.

Standard protocol for the photooxidation of 21 to 22.

The corresponding photosensitizer was added to 10 mL of a methanolic solution of 2-furoic acid (9.6 mM) in a test tube. The heterogeneous mixture was kept under stirring and in equilibrium with air. These test tubes were placed at 2 cm of a 0.1 M aqueous solution of $FeCl_3$ used as a filter for wavelengths lower than 450 nm and irradiated with a 125-W medium-pressure Hg vapor lamp for at least 6 h. The same experimental conditions were used in the dark in order to evaluate a possible adsorption of the substrate into the polymer. Moreover, the following control experiments were carried out: (a) irradiation in the absence of polymer and (b) irradiation of 2-furoic acid with free Rose Bengal in solution (5 μM) as the photosensitizer. The decreasing absorbance of 2-furoic acid was monitored by means of UV–vis spectroscopy at 246 nm. For each measurement, 80 μL aliquots were removed from the reaction mixture and diluted in 25 mL of the appropriate solvent. The initial rate constants for each oxidation reaction were calculated as first-order rate constants (*k*) as reported in the literature.[41] At the end of the irradiation period the solutions were filtered, concentrated, and the product obtained in these irradiations was identified as pure butenolide **22** by ^{1}H-NMR, ^{13}C-NMR and MS. The ability of the photosensitizer to generate singlet oxygen was demonstrated using the RB-SILLPs as photocatalysts for the chemical oxidation of 9,10-diphenylanthracene (DPA) to its endocyclic endoperoxide.[46,47]

[46] Burguete, M. I.; Galindo, F.; Gavara, R.; Luis, S. V.; Moreno, M.; Thomas, P.; Russell, D. A. Singlet Oxygen Generation Using a Porous Monolithic Polymer Supported Photosensitizer: Potential Application to the Photodynamic Destruction of Melanoma Cells. *Photochem. Photobiol. Sci.* **2009**, *8* (1), 37–44.

[47] Fudickar, W.; Linker, T. Remote Substituent Effects on the Photooxygenation of 9,10-Diarylanthracenes: Strong Evidence for Polar Intermediates. *Chem. Commun.* **2008**, No. 15, 1771–1773.

Continuous flow photooxidation of 21.

A solution of 2-furoic acid (9.6 mM) in MeOH was passed continuously through a fluid-bed reactor using a Jasco HPLC pump at a rate of 0.100 mL/min. The reactor was a 5 mL Onmifit® column, where the corresponding photocatalyst was swelled and suspended under stirring. The reactor used a medium-pressure Hg lamp (lamp power 75%, approximately 112.5 W), and all the required connections were made with FEP coil. A quartz glass was used as filter. The flow stream was passed through an 8-bar back pressure valve. The reaction stream of crude product was collected into a round-bottom flask, and the samples taken analyzed by UV-Visible to determine the conversion and yield.

6.5. Supplementary Information

Rose Bengal immobilized onto Supported Ionic Liquid-like Phases: Efficient photocatalyst for batch and flow processes

Table of Contents

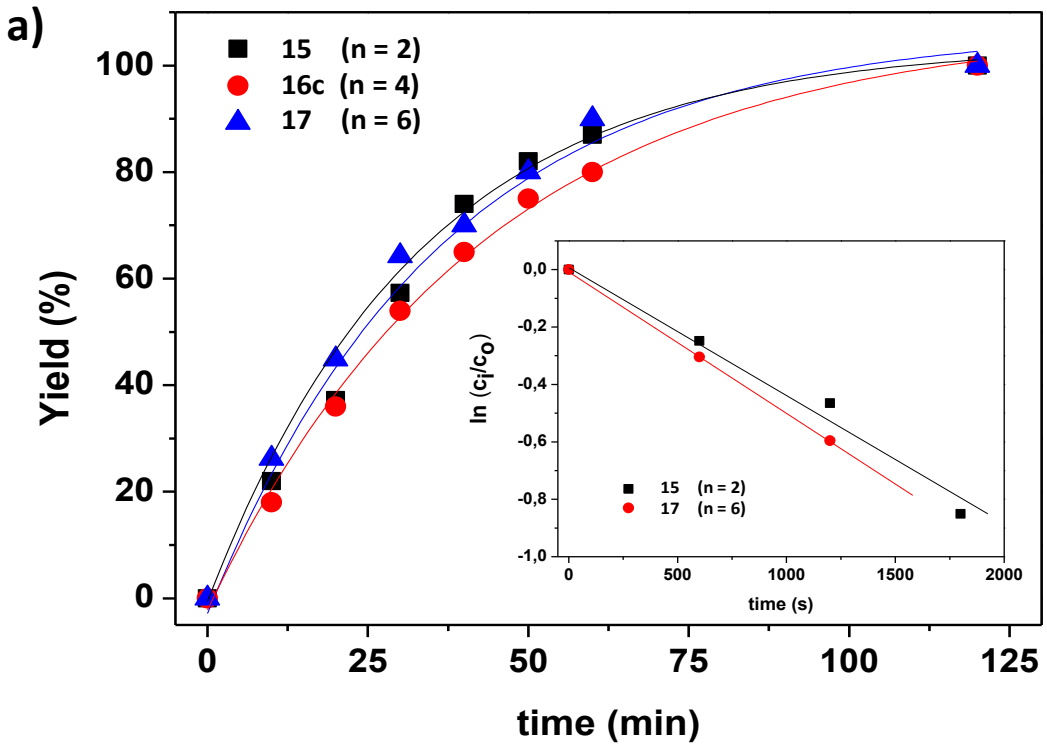
a)
15 (n = 2)
16c (n = 4)
17 (n = 6)
Yield (%)
time (min)
ln (c_i/c_0)
time (s)
15 (n = 2)
17 (n = 6)

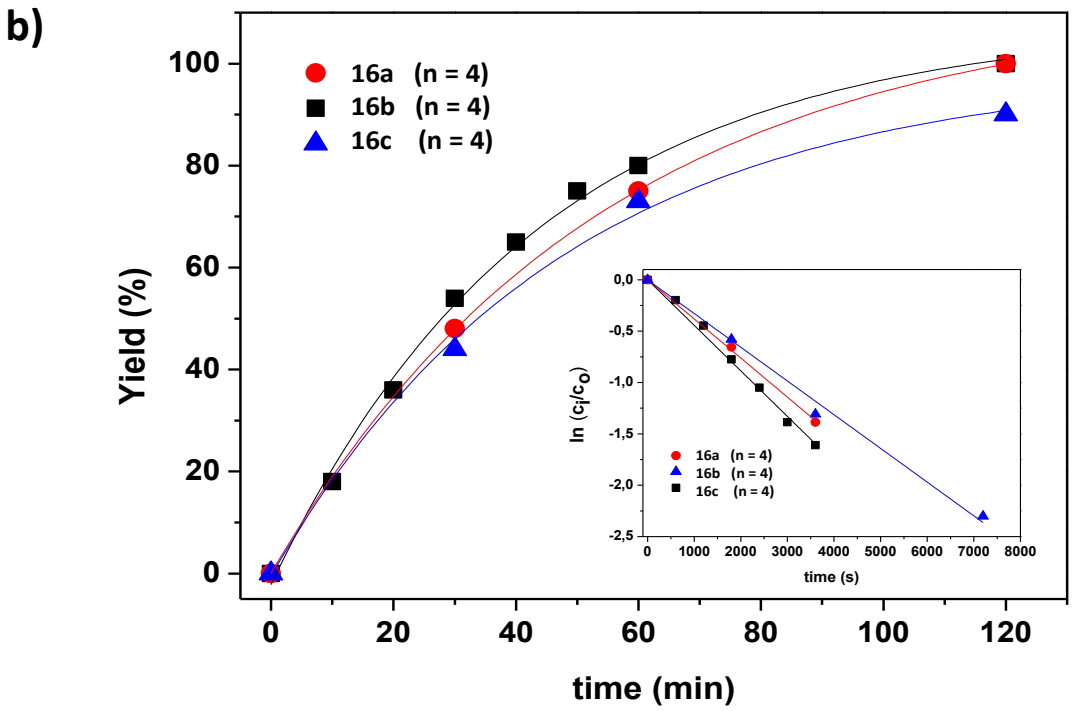
b)
16a (n = 4)
16b (n = 4)
16c (n = 4)
Yield (%)
time (min)
ln (c_i/c_0)
time (s)
16a (n = 4)
16b (n = 4)
16c (n = 4)

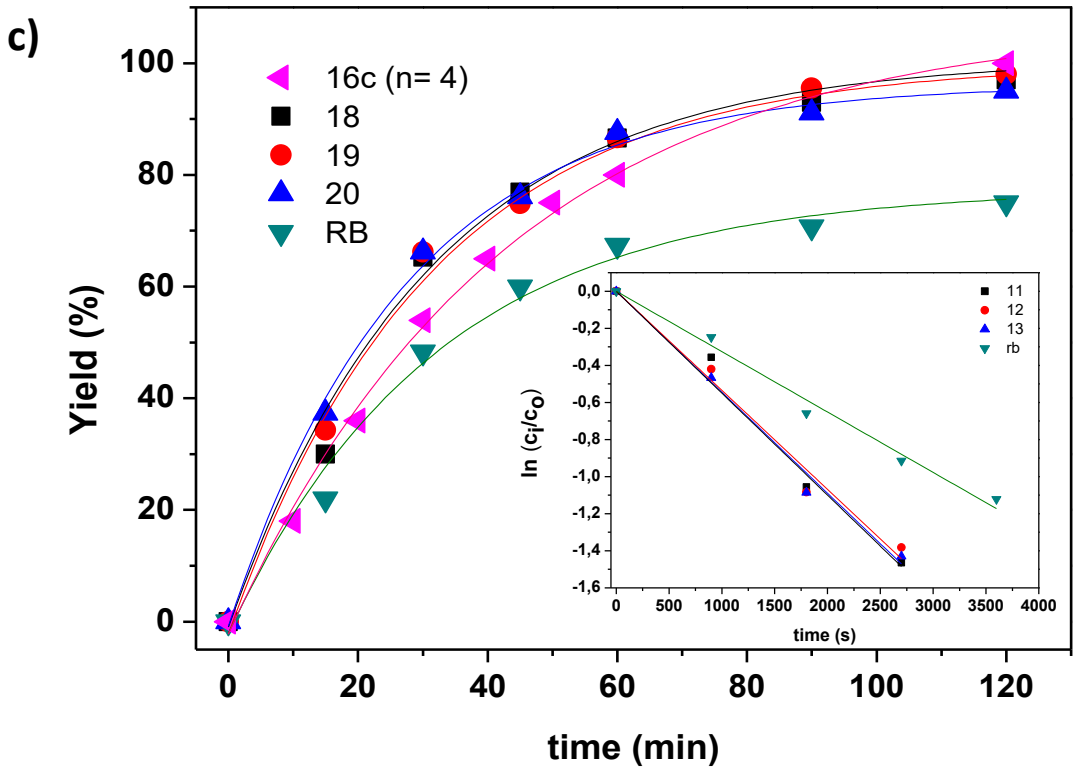

Figure SI.1. Effect of the polymer composition. Yield *vs* time profiles obtained for different RB-SILLPs used as photocatalyst for the oxidation of 2-furoic acid with singlet oxygen ($^1O_2$). Inset: $\ln(C_i/C_0)=kt$ for the initial period of the reaction, where C_i and C_0 are the concentrations of **21** at a certain time (t) and at $t = 0$, respectively. **(a)** Effect of the monomer nature; **(b)** effect of the molar composition; **(c)** effect of the spacer length for the divinylic bisimidazolium monomer. Conditions: 50:1 substrate : photocatalyst molar ratio (2% molar), room temperature. Irradiation: 125W medium pressure Hg vapor lamp for 120 min in open reaction test tubes equilibrated with air. [**21**] = 9.6 mM in MeOH.

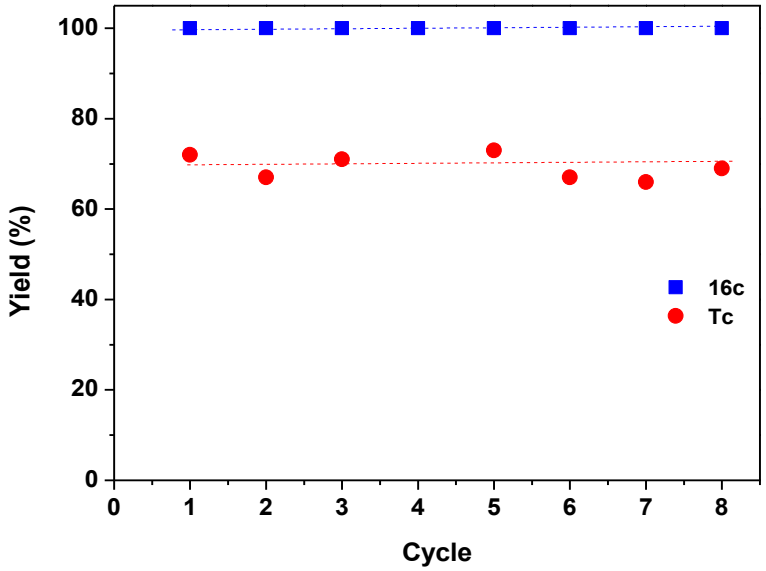

Figure SI.2. Recycling under batch conditions of RB-SILLP **16c** for the photooxidation of 2-furoic acid. Squares: **16c**, Circles: Test control using as the photocatalyst a solution of the disodium salt of RB.

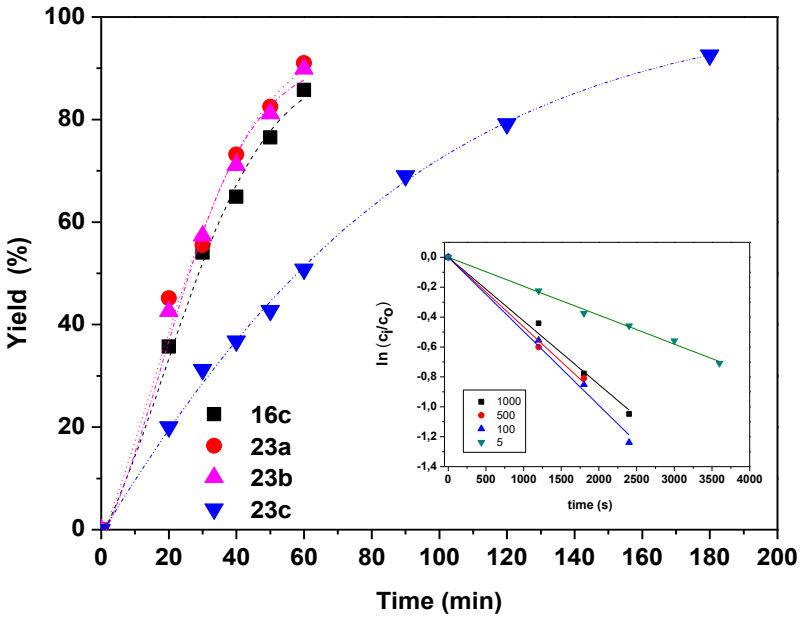

Figure SI.3. Effect of the RB loading. Yield *vs* time profiles obtained for different RB- SILLPs used as photocatalysts for the oxidation 2-furoic acid with singlet oxygen ($^1O_2$). Inset: $\ln(C_i/C_0)=kt$ for the initial period of the reaction, where C_i and C_0 are the concentrations of **21** at a certain time (t) and at t = 0, respectively. Polymeric photocatalysts: **16c** (39.36 µmol of RB / g), **23a** (19.84 µmol of RB / g), **23b** (0.40 µmol of RB / g) and **23c** (0.20 µmol of RB / g); 50:1 substate : phothocatalyst molar ratio (2% molar), room temperature. Irradiation: 125W medium pressure Hg vapor lamp for 120 min in open reaction test tubes equilibrated with air. [**21**] = 9.6 mM in MeOH.

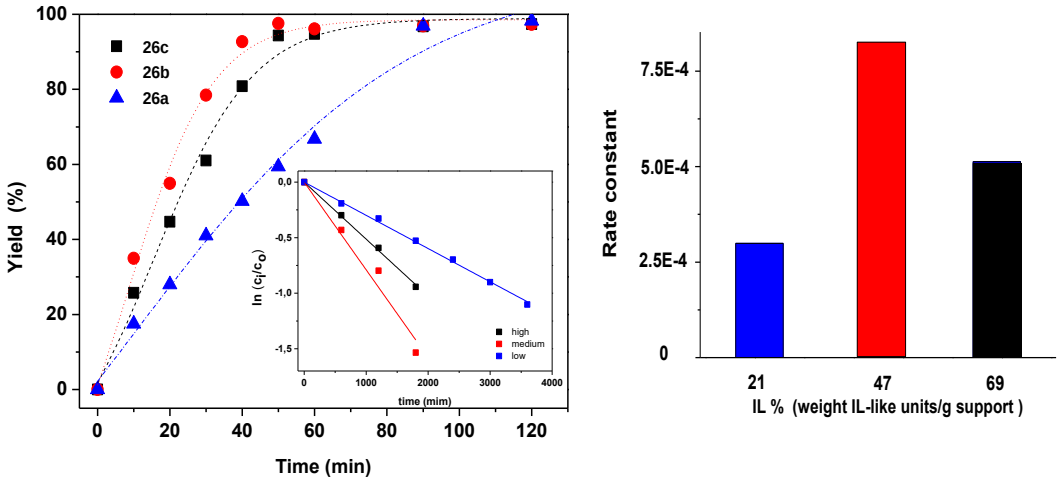

Figure SI.4. Effect of the IL-like moieties loading on RB-SILLPs. Yield *vs* time profiles obtained for different RB- SILLPs used as photo catalyst for the oxidation 2-furoic acid with singlet oxygen ($^1O_2$). Inset: $\ln(C_i/C_0)=kt$ for the initial period of the reaction, where C_i and C_0 are the concentrations of **21** at a certain time (t) and at $t = 0$, respectively. Polymers: **26a** (21% weight of IL-like units / g SILLP), **26b** (47% weight of IL-like units / g SILLP), **26c** (69% weight of IL-like units / g SILLP); 50:1 substrate : photocatalyst molar ratio (2% molar), room temperature. Irradiation: 125W medium pressure Hg vapor lamp for 120 min in open reaction test tubes equilibrated with air. [**21**] = 9.6 mM in MeOH.

Table SI.1. λ_{max} values for the different RB-SILLPs derived from **26a** through anion metathesis

RB-SILLP	Anion	λ_{max} (nm)
25a	Cl^-	523, 563
27	BF_4^-	523, 567
28	NTf_2^-	524, 567
29	TfO^-	519, 566
30	SbF_6^-	527, 568

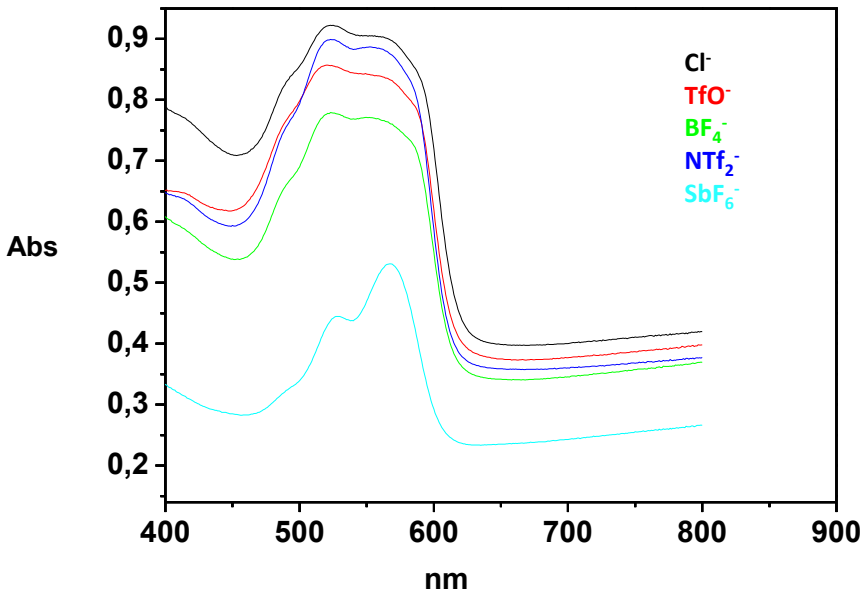

Figure SI.5. Diffuse reflectance UV-Vis spectra obtained for the different RB-SILLPs derived from **26a** through anion metathesis.

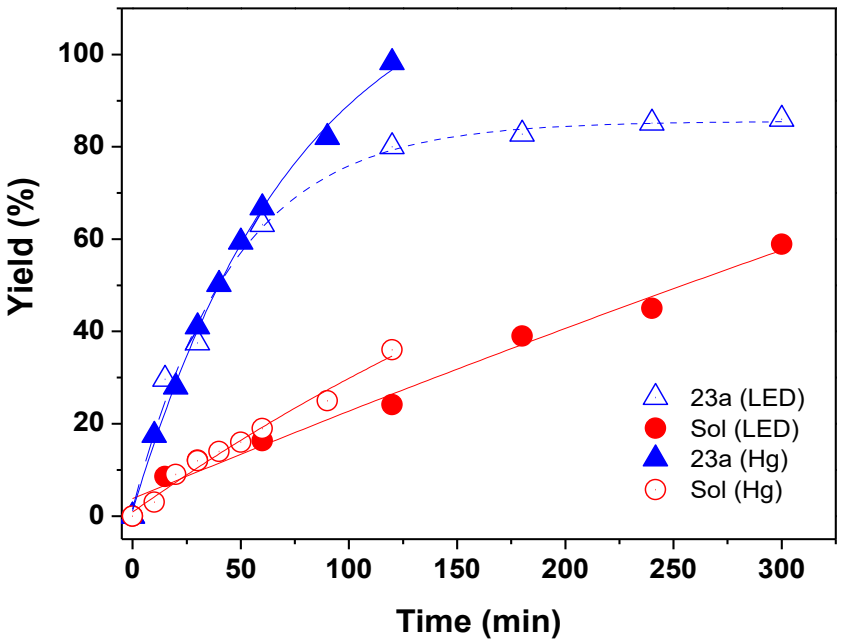

Figure SI.6. Effect of irradiation source. Yield *vs* time profiles obtained for the oxidation 2-furoic acid with singlet oxygen ($^1O_2$) catalyzed with RB disodium salt or RB-SILLP **23** under irradiation with a 125W medium pressure Hg vapor lamp or with green LEDs (530 nm). 50:1 substrate : photocatalyst molar ratio (2% molar), room temperature, in open reaction test tubes equilibrated with air. [**21**] = 9.6 mM in MeOH.

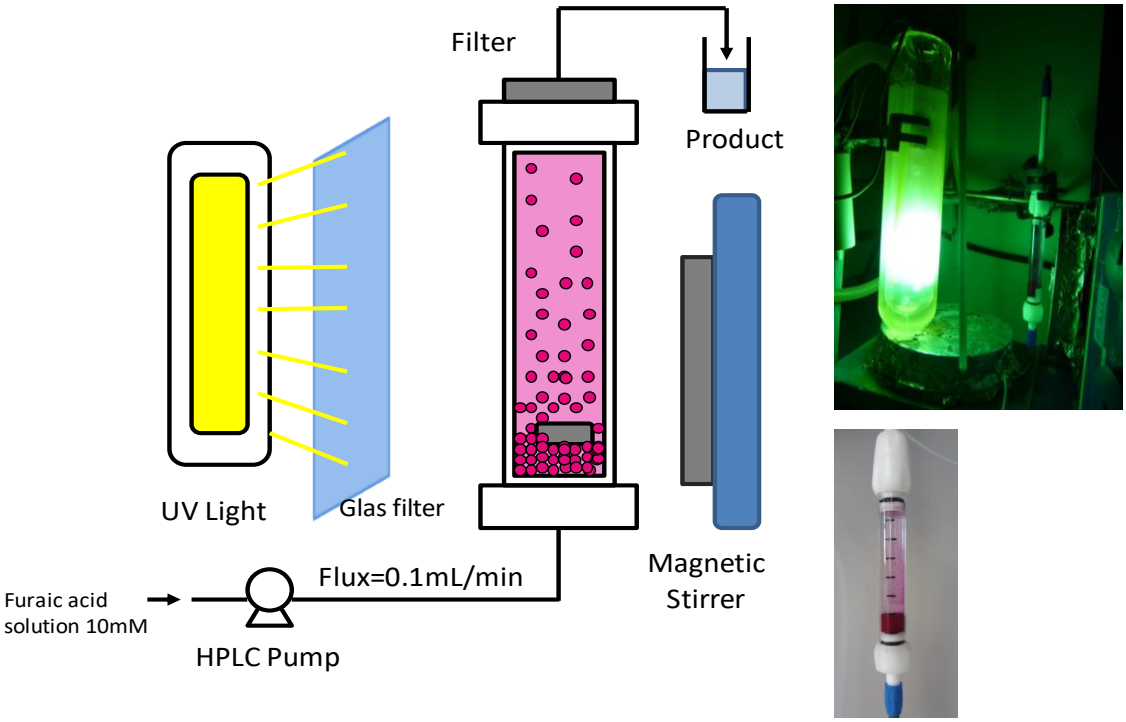

Figure SI.7. Schematic representation of the continuous flow reactor for photooxidation

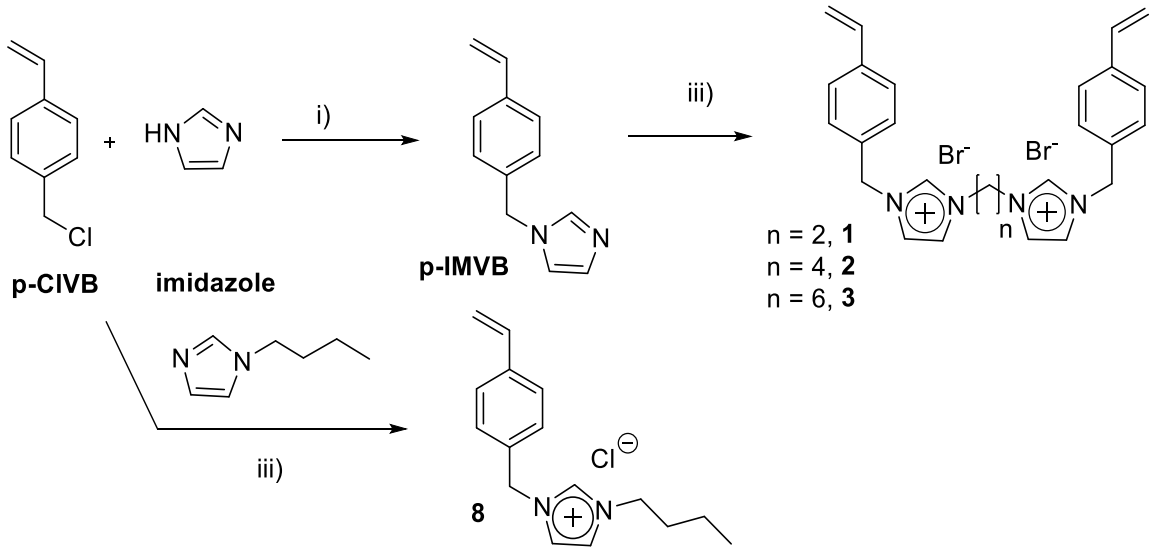

Scheme SI.1. Synthesis of imidazolium monomers.

CAPÍTULO VII

Polímeros Multifuncionales basados en líquidos iónicos y fragmentos de Rosa de Bengala para la conversión de CO_2 a carbonatos

Resumen. Se han utilizado materiales poliméricos conteniendo fases soportadas relacionadas con los líquidos iónicos y que contienen unidades de Rosa de Bengala para desarrollar sistemas organocatalíticos para la cicloadición de CO_2 a epóxidos. La actividad de los fragmentos de RB soportados se pueden ajustar controlando la naturaleza del SILLP (por ejemplo la sustitución en el anillo de imidazolio, el grado de entrecruzameinto de la matriz polimérica, carga, etc.). Un sistema catalítico de este tipo preparado a partir de componentes económicos, simples y disponibles comercialmente proporciona una alta actividad y estabilidad sin que se observe una disminución de la actividad catalítica durante al menos diez días de uso en condiciones de flujo continuo.

Chapter VII. Multifunctional polymers based on ionic liquid and Rose Bengal fragments for the conversion of CO_2 to carbonates

Abstract. Supported ionic liquid-like phases containing Rose Bengal units are used to develop organocatalytic systems for the cycloaddition of CO_2 to epoxides. The activity of the supported RB fragments can be fine-tuned by controlling the nature of the SILLPs (i.e. substitution at the imidazolium ring, crosslinking degree of the polymeric matrix, loading, etc). Such a catalytic system prepared from cheap, simple and commercially available components provides high activity and stability, with no decay in activity for at least ten days of continuous use under flow conditions.

Keywords: flow chemistry • supported ionic liquids • CO_2 conversion • catalysis • Rose Bengal.

7.1. Introduction

Cyclic carbonates have emerged as compounds of interest for many applications including their use as electrolytes in Li-ion batteries, as polar aprotic solvents for the synthesis of fine chemicals, or as monomers in the preparation of polycarbonates and polyurethanes.[1,2,3,4] Thus, enormous progress has been made in the past few years to improve their synthetic access. In this context, a wide

[1] Dibenedetto, A.; Angelini, A. Synthesis of Organic Carbonates. In *Advances in Inorganic Chemistry*; Aresta, M., van Eldik, R., Eds.; CO_2 Chemistry; Academic Press: USA, 2014; Vol. 66, pp 25–81.
[2] Zhang, X.; Fevre, M.; Jones, G. O.; Waymouth, R. M. Catalysis as an Enabling Science for Sustainable Polymers. *Chem. Rev.* **2018**, *118* (2), 839–885.
[3] Yadav, N.; Seidi, F.; Crespy, D.; D'Elia, V. Polymers Based on Cyclic Carbonates as Trait d'Union Between Polymer Chemistry and Sustainable CO_2 Utilization. *ChemSusChem.* **2019**, *12* (4), 724–754.
[4] Dabral, S.; Schaub, T. The Use of Carbon Dioxide (CO_2) as a Building Block in Organic Synthesis from an Industrial Perspective. *Adv. Synth. Catal.* **2019**, *361* (2), 223–246.

range of catalysts, both homogeneous[5,6] and heterogeneous,[7,8] have been developed to carry out their preparation from the CO_2/epoxide ring expansion reaction, through a low carbon footprint process.[9,10]

Cost-effective CO_2 capture and conversion need to increase as much as possible the CO_2 concentration available to the catalysts in the reaction mixture, even at reduced pressure (0.1 MPa). This facilitates achieving more efficient catalytic processes. In this regard, Ionic Liquids (ILs) can provide a larger CO_2 solubility than other molecular solvents.[11] Furthermore, the unique properties of ILs, besides, have been used to fine tune the catalytic behavior of a variety of catalytic systems including enzymes, organocatalysts or metal complexes, also for CO_2 conversion.[12] In order to mitigate some of the limitations for ILs (*i.e.* ecotoxicity, separation and recovery issues, etc.) Supported Ionic Liquid Phases (SILPs) and

[5] Shaikh, R. R.; Pornpraprom, S.; D'Elia, V. Catalytic Strategies for the Cycloaddition of Pure, Diluted, and Waste CO_2 to Epoxides under Ambient Conditions. *ACS Catal.* **2018**, *8* (1), 419–450.
[6] Alves, M.; Grignard, B.; Mereau, R.; Jerome, C.; Tassaing, T.; Detrembleur, C. Organocatalyzed Coupling of Carbon Dioxide with Epoxides for the Synthesis of Cyclic Carbonates: Catalyst Design and Mechanistic Studies. *Catal. Sci. Technol.* **2017**, *7* (13), 2651–2684.
[7] Huang, K.; Zhang, J.-Y.; Liu, F.; Dai, S. Synthesis of Porous Polymeric Catalysts for the Conversion of Carbon Dioxide. *ACS Catal.* **2018**, *8* (10), 9079–9102.
[8] Marciniak, A. A.; Lamb, K. J.; Ozorio, L. P.; Mota, C. J. A.; North, M. Heterogeneous Catalysts for Cyclic Carbonate Synthesis from Carbon Dioxide and Epoxides. *Curr. Opin. Green Sustain. Chem.* **2020**, *26*, 100365.
[9] North, M.; Pasquale, R.; Young, C. Synthesis of Cyclic Carbonates from Epoxides and CO_2. *Green Chem.* **2010**, *12* (9), 1514–1539.
[10] Kamphuis, A. J.; Picchioni, F.; Pescarmona, P. P. CO_2-Fixation into Cyclic and Polymeric Carbonates: Principles and Applications. *Green Chem.* **2019**, *21* (3), 406–448.
[11] Chen, Y.; Mu, T. Conversion of CO_2 to Value-Added Products Mediated by Ionic Liquids. *Green Chem.* **2019**, *21* (10), 2544–2574.
[12] Chaugule, A. A.; Tamboli, A. H.; Kim, H. Ionic Liquid as a Catalyst for Utilization of Carbon Dioxide to Production of Linear and Cyclic Carbonate. *Fuel* **2017**, *200*, 316–332.

related polymeric ionic liquids (PILs), have been explored,[13] and some examples of their use for CO_2 transformations have been reported.[14, 15]

The topology and porosity of materials based on supported or polymeric ILs can be also tailored by varying the connectivity, size, and geometry of the building blocks by a bottom-up approach to enhance the control of the reaction.[13] Thus, the design of catalysts supported on materials containing a high density of IL-like fragments and crosslinking degrees (hyper-crosslinked porous materials)[16] may lead to high specific surface areas with a simultaneous enhancement of CO_2 adsorption and catalytic activity. The more efficient concentration of CO_2 and the presence of dual catalytic units may reduce the conditions of temperature and pressure required for its capture and conversion.[17, 18, 19] However, the development of IL-based catalysts able to facilitate the conversion of epoxides at low CO_2 concentrations and pressures (preferably at 0.1 MPa, namely simple air) remains challenging. The reported catalysts require high CO_2 pressures, usually 5–80 bar, and/or long reaction times to obtain high conversions of cyclic carbonates. Furthermore, despite the heterogeneous nature of these systems,

[13] Montolio, S.; Altava, B.; García-Verdugo, E.; Luis, S. V. Supported ILs and Materials Based on ILs for the Development of Green Synthetic Processes and Procedures. In *Green Synthetic Processes and Procedures*; Ballini, R., Ed.; Green Chemistry Series; Royal Society of Chemistry.: United Kingdom, 2019; pp 289–318.

[14] Bobbink, F. D.; Dyson, P. J. Synthesis of Carbonates and Related Compounds Incorporating CO_2 Using Ionic Liquid-Type Catalysts: State-of-the-Art and Beyond. *J. Catal.* **2016**, *343*, 52–61.

[15] Luo, R.; Liu, X.; Chen, M.; Liu, B.; Fang, Y. Recent Advances on Imidazolium-Functionalized Organic Cationic Polymers for CO_2 Adsorption and Simultaneous Conversion into Cyclic Carbonates. *ChemSusChem.* **2020**, *13* (16), 3945–3966.

[16] Tan, L.; Tan, B. Hypercrosslinked Porous Polymer Materials: Design, Synthesis, and Applications. *Chem. Soc. Rev.* **2017**, *46* (11), 3322–3356.

[17] Babu, R.; Kurisingal, J. F.; Chang, J.-S.; Park, D.-W. Bifunctional Pyridinium-Based Ionic-Liquid-Immobilized Diindium Tris(Diphenic Acid) Bis(1,10-Phenanthroline) for CO_2 Fixation. *ChemSusChem.* **2018**, *11* (5), 924–932.

[18] Yue, S.; Wang, P.; Hao, X. Synthesis of Cyclic Carbonate from CO_2 and Epoxide using Bifunctional Imidazolium Ionic Liquid under Mild Conditions. *Fuel.* **2019**, *251*, 233–241.

[19] Ziaee, M. A.; Tang, Y.; Zhong, H.; Tian, D.; Wang, R. Urea-Functionalized Imidazolium-Based Ionic Polymer for Chemical Conversion of CO_2 into Organic Carbonates. *ACS Sustainable Chem. Eng.* **2019**, *7* (2), 2380–2387.

their application under flow conditions is still limited and in many cases the systems showed either low activities or significant catalyst leaching.[20]

Here we report how a simple organocatalyst based on Rose Bengal (RB) immobilized onto Supported Ionic Liquid Like Phases (SILLPs) can be used to efficiently transform epoxides into the corresponding cyclic carbonates in the presence of CO_2 with relevant TON and TOF values. The results demonstrate the presence of a cooperative effect between RB and residual water molecules on the SILLPs, allowing to increase the activity of the catalytic system. The use of a crosslinked SILLP with the appropriate porosity has allowed the development of a continuous flow system highly active and stable.

7.2. Results and Discussion

Initial screening

The polymeric Supported Ionic Liquid-like Phases (SILLPs) considered in this work were prepared from commercially available Merrifield resins. Initially, both gel-type (**1**) and macroporous (**2**) chloromethylated polystyrene-divinylbenzene (PS-DVB, Scheme 1) resins in the form of beads and with low (1.1 meq/g, **1a**-**2a**) or high (4.4 meq/g, **1b**; 5.2 meq/g, **2b**) chloride loadings were used. The synthetic protocol for the preparation of SILLPs has been already described in detail allowing a quantitative transformation of the chloromethyl fragments into alkyl benzyl imidazolium groups (Scheme 1 and Table SI.1).[21,22]

[20] Seo, H.; Nguyen, L. V.; Jamison, T. F. Using Carbon Dioxide as a Building Block in Continuous Flow Synthesis. *Adv.Synth. Catal.* **2019**, *361* (2), 247–264.
[21] Burguete, M. I.; García-Verdugo, E.; Luis, S. V.; Restrepo, J. A. Preparation of Polymer-Supported Gold Nanoparticles Based on Resins Containing Ionic Liquid-like Fragments: Easy Control of Size and Stability. *Phys. Chem. Chem. Phys.* **2011**, *13* (33), 14831–14838.
[22] Burguete, M. I.; Erythropel, H.; Garcia-Verdugo, E.; Luis, S. V.; Sans, V. Base Supported Ionic Liquid-like Phases as Catalysts for the Batch and Continuous-Flow Henry Reaction. *Green Chem.* **2008**, *10* (4), 401–407.

Different PS-DVB materials bearing alkyl imidazolium moieties have been tested as catalysts for the addition of CO_2 to epoxides.[8,15,23,24] In general, such materials required harsh experimental conditions (temperature >130 °C and pressure > 10 bars) to lead to the corresponding carbonates. Indeed, when the SILLP **7a** was tested as heterogeneous catalyst for the reaction between styrene oxide and CO_2 (see reaction in Scheme 2) only a modest level of conversion (39 %) was achieved at 100 °C and 10 bar (Entry 1 from Table 1).

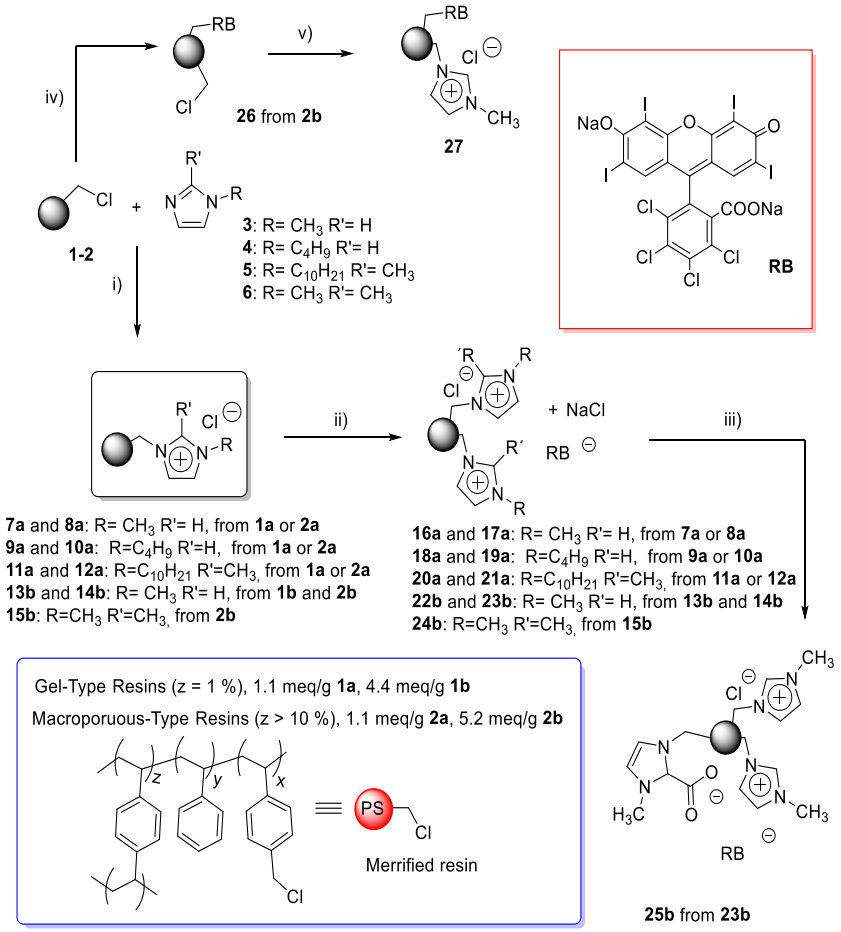

Scheme 1. Synthesis of supported catalysts. i) 80 °C, 150 rpm, 24 h. ii) RB (C:1000 ppm), 150 rpm, 12 h, rt. iii) KHMDS (1,05 eq.), N_2, dry THF, in dark, CO_2 balloon, 80 °C, 4 h. iv) RB : **1-2** (0.15:1 mmol), 60 °C, 150 rpm, 48 h. v) 60 °C, 150 rpm, 24 h (see Table SI.1).

[23] Xie, Y.; Zhang, Z.; Jiang, T.; He, J.; Han, B.; Wu, T.; Ding, K. CO_2 Cycloaddition Reactions Catalyzed by an Ionic Liquid Grafted onto a Highly Cross-Linked Polymer Matrix. *Angew. Chem. Int. Ed.* **2007**, *46* (38), 7255–7258.

[24] Wang, T.; Wang, W.; Lyu, Y.; Chen, X.; Li, C.; Zhang, Y.; Song, X.; Ding, Y. Highly Recyclable Polymer Supported Ionic Liquids as Efficient Heterogeneous Catalysts for Batch and Flow Conversion of CO_2 to Cyclic Carbonates. *RSC Adv.* **2017**, *7* (5), 2836–2841.

Two different strategies have been envisioned to enhance the efficiency of these supported ILs. The first one relays on the improvements of the morphological properties of the material increasing for instance the surface area, accessibility of the functional sites, crosslinking, etc.[14,15] The second approach is based in the introduction of additional catalytic moieties (i.e. HBD, metal sites, etc) to provide an acid-base or electrophile-nucleophile double activation mechanisms, that have been shown to be very efficient in a variety of catalytic systems.[6,7,8,9,10]

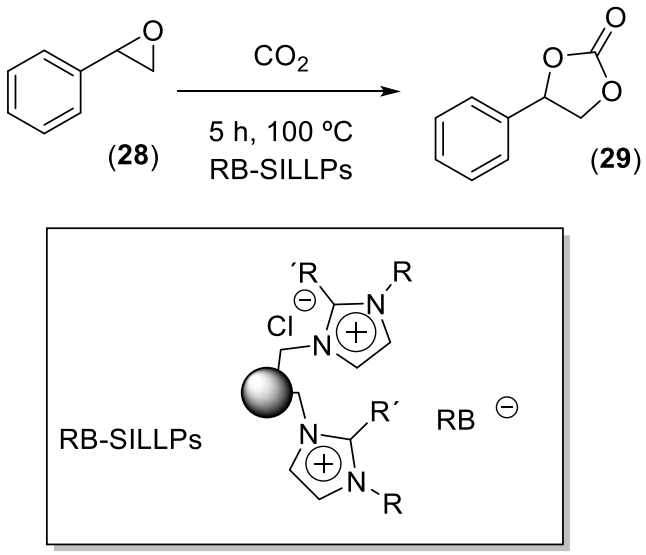

Scheme 2. Cycloaddition reaction of CO_2 to styrene epoxide catalyzed by Rose Bengal immobilized onto Supported Ionic Liquid Like Phases (RB-SILLPs).

The combination of an organocatalyst with the ionic liquid-like phase of SILLPs was considered and Rose Bengal (RB) was initially selected. RB can be easily immobilized onto SILLPs by covalent anchoring (ester formation) or by ionic exchange, just by exposing the corresponding SILLPs to a solution of RB,[25] and Zhang, Zhou and coworkers have exploited Rhodamine B (RhB) and Rhodamine 6G (Rh6G) in the presence of a base (Et_3N) as organocatalytic systems for the

[25] Valverde, D.; Porcar, R.; Izquierdo, D.; Burguete, M. I.; Garcia-Verdugo, E.; Luis, S. V. Rose Bengal Immobilized on Supported Ionic-Liquid-like Phases: An Efficient Photocatalyst for Batch and Flow Processes. *ChemSusChem.* **2019**, *12* (17), 3996–4004.

cycloaddition of CO_2 with epoxides.[26] RhB and Rh6G are xanthene dyes from the same family of Rose Bengal, which encouraged the study of the cheap and easily prepared polymeric composites RB-SILLPs for this process. In line with those expectations, the RB-SILLP **16a** containing 3.92 x 10^{-2} μmol RB / g of polymer provided a conversion of 63% instead of the 39% achieved with the same SILLP in the absence of RB (Entries 1 *vs* 2, Table 1). This represents a TON of 3860 attending to the RB loading. The conversion could be increased further (up to 96%) doubling the amount of immobilized catalyst used (Entry 3, Table 1).

Table 1. Screening of RB-SILLPs as catalysts in the reaction between styrene oxide (**28**) and CO_2 to afford **29**.[a]

Entry	SILLP	IL Loading[b] [mmol g^{-1}]	Co-catalyst[c]	R	R´	X⁻	Yield[d]	TON [f]
1	**7a**	1.01	-	CH_3	H	Cl	39	78 [i]
2	**16a**	1.01	yes	CH_3	H	Cl	63	3860
3	**16a**	1.01	yes	CH_3	H	Cl	96 [e]	1940
4	**22b**	3.18	yes	CH_3	H	Cl	76 [g]	4657
5	**18a**	0.97	yes	$CH_3(CH_2)_3$	H	Cl	31	1899
6	**20a**	0.88	yes	$CH_3(CH_2)_9$	CH_3	Cl	9	551
7	**30a** [h]	0.76	yes	CH_3	H	NTf_2	0	-
8	-	-	-	Necker catalyst			0	-

[a] solventless, 5 h, 100 °C, 10 bar CO_2, 1 mL epoxide, 36.7 mg supported cat. Gel type resin. [b] Imidazolium unit loading calculated by elemental analysis. [c] RB loading 3.92 x 10^{-2} μmol RB / g of polymer. [d] Calculated by ^{1}H-NMR. Selectivity > 99.9%. [e] 111.25 mg of RB-SILLP. [f] TON calculated related to RB loading. [g] macroporuous type resin. [h] Catalyst prepared from **7a** by anion exchange with $LiNTf_2$. [i] TON calculated related to RB loading.

[26] Gong, Q.; Luo, H.; Cao, D.; Zhang, H.; Wang, W.; Zhou, X. Efficient Cycloaddition Reaction of Carbon Dioxide with Epoxide by Rhodamine Based Catalyst Under 1 atm Pressure. *Bull. Korean Chem. Soc.* **2012**, *33* (6), 1945–1948.

Encouraged by these results, the effect of different variables were evaluated in order to optimize the efficiency of the immobilized system. An increase on the amount of the IL-like units in the polymeric RB-SILLPs from 12% (1.01 meq / g) to 37% by weight (3.18 meq / g) rendered an increase of conversion from 63% to 76% (Entries 2 *vs* 4, Table 1). On the contrary, the exchange of the Cl^- counteranion by a less basic and more hydrophobic anion such as NTf_2^- led to an inactive system (Entry 7, Table 1). It should also be noted that the commercially available RB covalently immobilized onto a PS-DVB support did not provide any catalytic activity under the same experimental conditions (Entry 8, Table 1). This result highlights the synergy existing between the RB fragments and the IL-like units of the SILLPs.

Effect of polymer

The morphology of the polymeric backbone can strongly influence the catalytic activity of polymer supported systems.[27] The initial SILLPs tested were based on gel-type polymers, which are the most classical example PS-DVB resins originally used for solid phase peptide synthesis.[28] For those microporous gel-type polymers, the accessibility of the functional sites, and accordingly the reactivity, are dramatically dependent on swelling and, therefore, on the nature of the solvent used. In this regard, it must be noted that the substitution pattern of the imidazolium units induces significant changes in the swelling properties of gel-

[27] Altava, B.; Burguete, M. I.; García-Verdugo, E.; Luis, S. V. Chiral Catalysts Immobilized on Achiral Polymers: Effect of the Polymer Support on the Performance of the Catalyst. *Chem. Soc. Rev.* **2018**, *47* (8), 2722–2771.
[28] (a) Seneci, P. *Solid-Phase Synthesis and Combinatorial Technology*, 1st.; John Wiley & Sons, New York, **2000**. (b) Dörwald, F. Z. *Organic Synthesis on Solid Phase: Supports, Linkers, Reactions*, Wiley-VCH, Weinheim, **2002**.

type SILLPs resins and can be used to tune their catalytic activity.[14,20, 29 , 30] Although, the cycloaddition reaction is performed under solventless conditions, the physico-chemical properties of the epoxide (*i.e.* styrene oxide) will determine the swelling and consequently the accessibility of the catalytic sites on the polymer. When the swelling for these gel-type resins with low loading of IL-like units was measured in styrene oxide (SO), it followed the trend CH_3- (56%) < CH_3-$(CH_2)_3$- (69%) < CH_3-$(CH_2)_9$- (81%). Surprisingly, the swelling did not match the reactivity order. In this case, the use of hydrophobic alkyl residues in the imidazolium fragments produced a significant decay on the activity: CH_3- (63%) > CH_3-$(CH_2)_3$- (31%) > CH_3-$(CH_2)_9$- (9%) (Entries 2, 5 and 6, Table 1, see also Figure 1) indicating that a more complex mechanism is acting.

To gain additional information on morphology effects, a second family of RB-SILLPs (**17a**, **19a** and **21a**) obtained from the macroporous resin **2a** was also assayed for the model reaction. For these resins, displaying a higher crosslinking degree (> 10 DVB, **2a**), the swelling is a less critical parameter as they present a permanent porosity even in the dry state.[31] Results obtained with these resins for the cycloaddition reaction between SO and CO_2 at 10 bar are compared with those for their analogous gel-type resins in Figure 1. In both cases, RB supported in SILLPs bearing methyl imidazolium units led to the highest conversion independently of the morphology (76% for RB-SILLP **16a** gel-type and 85 % for the macroporous RB-SILLP **17a**). As before, the introduction of hydrophobic chains reduced the activity, although this effect was significantly more important for gel-type resins. Thus, the macroporuous resins led to 86 % and 38% of

[29] Zhang, Y.; Zhang, Y.; Chen, B.; Qin, L.; Gao, G. Swelling Poly (Ionic Liquid)s: Heterogeneous Catalysts that are Superior than Homogeneous Catalyst for Ethylene Carbonate Transformation. *ChemistrySelect* **2017**, *2* (29), 9443–9449

[30] Zhang, Y.; Wang, B.; Elageed, E. H. M.; Qin, L.; Ni, B.; Liu, X.; Gao, G. Swelling Poly(Ionic Liquid)s: Synthesis and Application as Quasi-Homogeneous Catalysts in the Reaction of Ethylene Carbonate with Aniline. *ACS Macro Lett.* **2016**, *5* (4), 435–438.

[31] Sherrington, D. C. Preparation, Structure and Morphology of Polymer Supports. *Chem. Commun.* **1998**, No. 21, 2275–2286.

conversion for butyl and methyl decyl imidazolium respectively, while the gel type only achieved 31 % and 9 % respectively.

Zhang and coworkers have reported that for homogeneous ILs the conversion of epoxides into cyclic carbonates was faster as the alkyl chain on the imidazolium ring became longer.[32] This was related with an increase in the solubility of CO_2 and the epoxide in the IL phase.[33] As mentioned above, though changes in swelling for gel type SILLPs agree well with this, the activity trends observed for both families of SILLPs deviate from the results observed for the homogenous ILs.

Effect of the residual water

In the search of an alternative explanation, the presence of residual water molecules associated to the Ionic Liquid-like fragments must be considered. ILs are hygroscopic and can absorb significant amounts of water from the atmosphere even when they present hydrophobic structural elements.[34] Their hygroscopicity depends on both anion and cation structure, the relative humidity and the temperature.[35] This is a key factor as the presence of 1 wt% water in a IL

[32] Byun, J.; Zhang, K. A. I. Controllable Homogeneity/Heterogeneity Switch of Imidazolium Ionic Liquids for CO_2 Utilization. *ChemCatChem* **2018**, *10* (20), 4610–4616.
[33] Kawanami, H.; Sasaki, A.; Matsui, K.; Ikushima, Y. A Rapid and Effective Synthesis of Propylene Carbonate Using a Supercritical CO_2–Ionic Liquid System. *Chem. Commun.* **2003**, No. 7, 896–897.
[34] Dahi, A.; Fatyeyeva, K.; Chappey, C.; Langevin, D.; Rogalsky, S. P.; Tarasyuk, O. P.; Marais, S. Water Sorption Properties of Room-Temperature Ionic Liquids over the Whole Range of Water Activity and Molecular States of Water in These Media. *RSC Adv.* **2015**, *5* (94), 76927–76938.
[35] Cammarata, L.; Kazarian, S. G.; Salter, P. A.; Welton, T. Molecular States of Water in Room Temperature Ionic Liquids. *Phys. Chem. Chem. Phys.* **2001**, *3* (23), 5192–5200.

can enhance their CO_2 absorption capacity from 1:2 to 1:1 mol CO_2/IL,[36] but also modify the activity of a given catalyst in homogeneous ILs.[37,38]

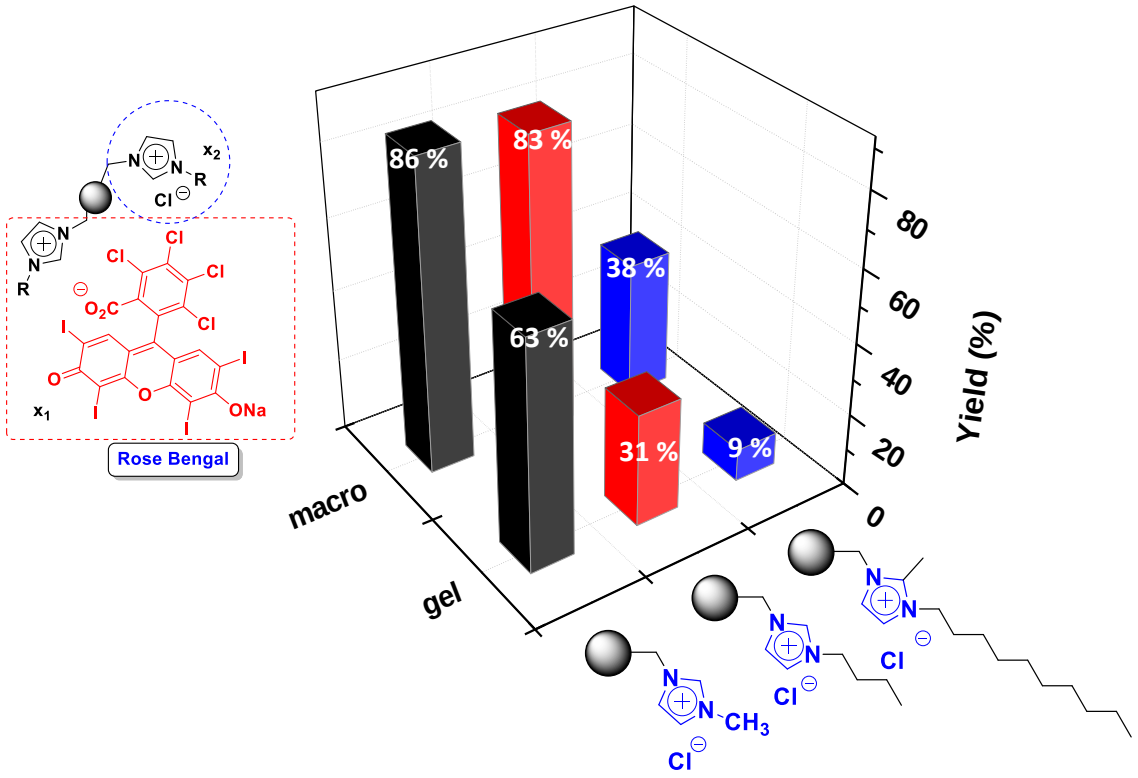

Figure 1. Effect of the support on the efficiency of RB-SILLPs as catalysts in the reaction between styrene oxide (**28**) and CO_2 to afford **29**.[a] Conversion determined by ^{1}H NMR. Selectivity > 99.9%.

In this regard, the analysis of RB-SILLPs by FT-IR-ATR clearly indicated the presence of residual water, with bands at *ca.* 3360 cm^{-1} and 1613 cm^{-1}. Their intensity was affected by the substitution of the imidazolium ring and the type of PS-DBV used (ESI, Figures. SI2 and SI3), decreasing for hydrophobic alkyl

[36] Zhang, J.; Zhang, S.; Dong, K.; Zhang, Y.; Shen, Y.; Lv, X. Supported Absorption of CO_2 by Tetrabutylphosphonium Amino Acid Ionic Liquids. *Chem. Eur. J.* **2006**, *12* (15), 4021–4026.
[37] Yoon, B.; Yen, C. H.; Mekki, S.; Wherland, S.; Wai, C. M. Effect of Water on the Heck Reactions Catalyzed by Recyclable Palladium Chloride in Ionic Liquids Coupled with Supercritical CO_2 Extraction. *Ind. Eng. Chem. Res.* **2006**, *45* (12), 4433–4435.
[38] Brown, R. A.; Pollet, P.; McKoon, E.; Eckert, C. A.; Liotta, C. L.; Jessop, P. G. Asymmetric Hydrogenation and Catalyst Recycling Using Ionic Liquid and Supercritical Carbon Dioxide. *J. Am. Chem. Soc.* **2001**, *123* (6), 1254–1255.

residues in the IL-like units following the trend CH_3- > CH_3-$(CH_2)_3$- > CH_3-$(CH_2)_9$-. On the other hand, the intensity was higher for macroporous than for gel-type resins. Finally, the FT-IR-ATR of the resins with a higher loading of IL-like moieties revealed also the presence of a larger amount of residual water (ESI, Figure SI.4).

This residual water content was determined by TGA of the different RB-SILLPs (Table SI.1).[39] Thus, RB-SILLP **16a** (R = CH_3, R´ = H) showed a water content of *ca*. 2.01%, while for the most hydrophobic one (RB-SILLP **20a**, R = CH_3-$(CH_2)_3$, R´ = CH_3) the water content fell to *ca*. 1.17%. Noteworthy, macroporous RB-SILLPs revealed a larger water content, ranging from *ca*. 3.5% for **17a** (R = CH_3, R´ = H), and 2.6% for **19a** (R = CH_3-$(CH_2)_3$-, R´ = H) to 2.1% for **21a** R = CH_3-$(CH_2)_3$, R´ = CH_3). The loading of IL-like units also affects the amount of residual water. For gel type resins this amount changed from 1.81 % to *ca*. 11.35% with the increase of the IL-like loading (RB-SILLPs **16a** *vs* **22b**), while for macroporuous resins it changed from 3.46% to 15.14 % (RB-SILLPs **17a** *vs* **23b**).

Thus, these variations in residual water can be associated to the observed activity changes, as it can contribute as co-catalyst to enhance the activity. It has been demonstrated that the addition of water as hydrogen bond donor (HBD) acts as very efficient co-catalyst for the cycloaddition of CO_2 to epoxides.[40] Indeed, the right amount of water can lead to a significant increase in activity.[41] This is clearly observed in the present case when the yields obtained were represented as a function of the molar ratio residual water : epoxide (Figure 2). For both series of RB-SILLPs, gel type and macroporous, yields increase with the water content and for a given loading and substitution pattern at the imidazolium ring the yield is

[39] Water loss measures the weight loss up to 100 ^oC after the different SILLPs weren left in contact with the air, under the same conditions, for 24 h.
[40] Alassmy, Y. A.; Pescarmona, P. P. The Role of Water Revisited and Enhanced: A Sustainable Catalytic System for the Conversion of CO_2 into Cyclic Carbonates under Mild Conditions. *ChemSusChem*. **2019**, *12* (16), 3856–3863.
[41] Sun, J.; Ren, J.; Zhang, S.; Cheng, W. Water as an Efficient Medium for the Synthesis of Cyclic Carbonate. *Tetrahedron Lett*. **2009**, *50* (4), 423–426.

always higher for the macroporous polymer displaying a higher residual water content.

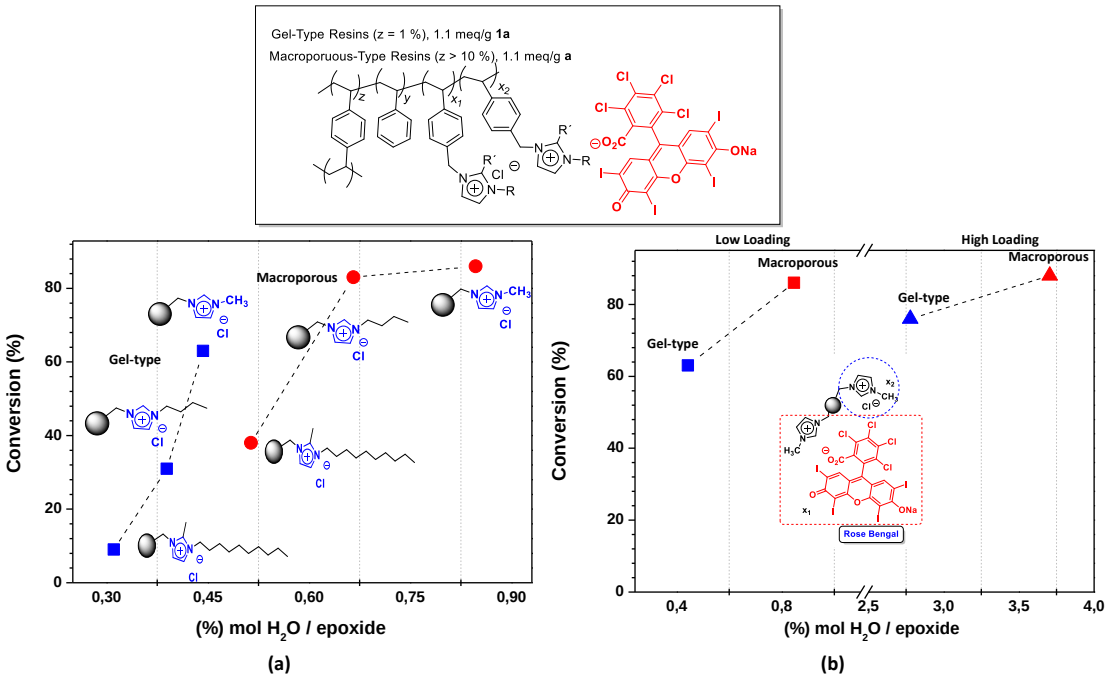

Figure 2. Effect of the residual water on the RB-SILLP on the synthesis of styrene carbonate (**29**). Conversion *vs* molar ratio of the residual water in the RB-SILLP with respect to the epoxide. Conversion determined by ^{1}H NMR. Selectivity > 99.9%. Reaction conditions: styrene oxide (1 mL), RB-SILLP (36.7 mg), 10 bar, 100 °C, 5 h. **(a)** Effect of imidazolium substitution. **(b)** Effect of the loading.

These findings follow a trend similar to that reported by Zhang and coworkers, who evaluated the effect H_2O/epoxide molar ratio from 0 to 2.[41] In the low-ratio region (from 0.3 to 0.9), they found how an increase in ratio resulted in a remarkable increase of conversion. Thus, Figure 2a shows how for gel type resins the conversion increased from 9% to 63% when the water content increases from 0.31 to 0.44. As found by Zhang, yield enhancements are smaller for higher H_2O/epoxide molar ratios. Thus, a change in this ratio from 0.44 to 2.7 (from low to high loading) just provided an enhancement from 63% to 76% (Figure 2b). Macroporous resins, having higher water contents displayed less pronounced

changes. This enhancement of the catalytic performance associated to the presence of water can be related with the effect of *essential water* on some natural enzymes used in organic media and in organocatalytic systems.[42] In some immobilized organocatalysts, the residual water has been observed to play an essential role.[43]

Effect of the pressure

Noteworthy, the reaction could be also performed at atmospheric pressure (CO_2 balloon, Table 2) although, as expected, yields were lower. The gel type resin RB-SILLP **16a** led to a conversion of 46 %, which is lower than the obtained at 10 bar keeping constant other conditions (Entry 1, Table 2 *vs* Entry 2, Table 1). The conversion could be increased to the same level achieved at 10 bar by increasing the amount of catalyst by *ca*. 1.5 and the reaction time from 5 to 14 h (Entry 2, Table 2). However, the observed activity trends were reversed at this pressure. Gel-type resins provided better conversions than the analogous macroporous resins: while 46% conversion was obtained for the gel-type resin **16a**, the macroporous analogue **17a** achieved a 29% conversion (Entries 1 *vs* 3, Table 2). This is likely to be related with the diffusion and concentration of CO_2 achieved under these two conditions (10 bars and atmospheric pressure). Tassaing has shown that in a mixture of CO_2 and SO at 100 ^oC and 10 bars, the liquid phase is rich in CO_2. The CO_2 exhibits a significant solubility in SO that increases with pressure at constant temperature and, therefore, the concentration of CO_2 in the epoxide is reduced at atmospheric pressure.[44] Under these conditions, CO_2

[42] Zaks, A.; Klibanov, A. M. Enzymatic Catalysis in Nonaqueous Solvents. *J. Biol. Chem.* **1988**, *263* (7), 3194–3201.
[43] (a) Jimeno, C. Water in Asymmetric Organocatalytic Systems: A Global Perspective. *Org. Biomol. Chem.* **2016**, *14* (26), 6147–6164. (b) Font, D.; Sayalero, S.; Bastero, A.; Jimeno, C.; Pericàs, M. A. Toward an Artificial Aldolase. *Org. Lett.* **2008**, *10* (2), 337–340.
[44] Foltran, S.; Cloutet, E.; Cramail, H.; Tassaing, T. In Situ FTIR Investigation of the Solubility and Swelling of Model Epoxides in Supercritical CO_2. *J. Supercrit. Fluids* **2012**, *63*, 52–58.

diffusion can become the limiting factor. Gel type resins display an excellent swelling in SO that facilitates the accessibility to the catalytic sites presenting reduced diffusional limitations. However, swelling is not relevant in macroporous polymers and the diffusion within the porous structure can be a relevant kinetic factor for low concentrations of CO_2 in SO.

Table 2. Reaction between styrene oxide (**28**) and CO_2 to afford **29** at atmospheric pressure.[a]

Entry	SILLP	IL Loading[b] [mmol g^{-1}]	Conversion[c]	TON[e]
1	**16a**	1.2	46	2819
2	**16a**	1.2	65[d]	2740
3	**17a**	1.2	29	1808

[a] solventless, 5 h, 100 ^{o}C, CO_2 balloon, 1 mL epoxide, 36.7 mg supported catalyst. [b] Imidazolium unit loading calculated by elemental analysis. [c] Calculated by ^{1}H-NMR. Selectivity > 99%. [d] 51.7 mg of RB-SILLP **16a** and 14 h. [e] TON calculated related to RB contain.

Effect of the catalyst loading

The use of lower loadings of RB-SILLPs was also investigated (Table 3). Interestingly, the high loading macroporous catalyst RB-SILLP **23b** provided considerable levels of activity even at low loadings. At a loading of 0.016% mol of RB with respect to SO a TOF of 1042 h^{-1} per mol of RB was obtained that was reduced to ca. 500 h^{-1} when the loading was further decreased (Entry 1 *vs* Entries 2, 3 and 4, Table 3). The TON, however, was significantly improved at very low loadings, reaching values of up to 83041 (Entry 4, Table 3). This value is in line with those for systems reported in the literature based on a dual activation involving metal catalysts, but higher than those for metal-free systems, It must

be noted, besides, that the present catalysts are prepared from simple and cheap commercially available resins and modifiers.

Table 3. Effect of the catalyst loading on TOF and TON values for the synthesis of organic carbonate **29** from SO and CO_2 catalyzed by RB-SILLP **23b**.[a]

Entry	cat % mol[b]	Conversion[c]	TOF[d]	TON[d]
1	0.01632	85	1042	5208
2	0.00328	93	591	28388
3	0.00164	60	509	36634
4	0.00082	68	494	83041

[a] solventless, 5 h, 100 ^{o}C, 10 bar CO_2, 1, 5, 10 and 20 mL SO, 36.7 mg of RB-SILLP **23b**. [b] mol of RB with respect to SO. [c] Calculated by ^{1}H-NMR. Selectivity > 99%. [d] TOF (h^{-1}) and TON calculated relative to RB loading.

Mechanistic Insights

To understand the role played by RB units, we analyzed the catalyst before and after the reaction by FT-IR-ATR. 1,3-Dialkylimidazolium cations paired with basic anions have been found to be good absorbents for CO_2, since they can react with CO_2 to form zwitterionic NHC−CO_2 adducts.[45] Both homogeneous and heterogeneous NHC-CO_2 adducts has been used as catalysts for the coupling reaction of CO_2 with epoxides to afford the corresponding carbonates with high efficiency. In RB-SILLPs, RB carboxylate and phenolate groups can enable, in the absence of any additional base, the formation of the carbene that in presence of CO_2 leads to the NHC-CO_2 adduct. The FT-IR-ATR spectrum of RB-SILLP **23b** after the reaction confirmed the formation of this adduct (**25b**, Figure SI.5). The spectrum showed a band at 1665 cm^{-1} assignable to the asymmetric $\nu(CO_2)$

[45] Wang, Z.; Wang, F.; Xue, X.-S.; Ji, P. Acidity Scale of N-Heterocyclic Carbene Precursors: Can We Predict the Stability of NHC–CO_2 Adducts? *Org. Lett.* **2018**, *20* (19), 6041–6045.

vibrations of N–COO^- as well as the disappearance of the bands at 1571 cm^{-1} for the asymmetric stretching of the $CH_2(N)/CH_3(N)CN$, at 1559 cm^{-1} for ν(N=C) and at 1159 cm^{-1} for C-C stretching and δ(CH), all of then characteristic of the imidazolium ring (Figure SI.5).

At the view of these results, the preparation of the zwitterionic NHC−CO_2 polymer (**31**) was assayed following already reported synthetic methods involving deprotonation of the C2 acid proton of the imidazolium in the presence of a base followed by reaction with CO_2.[46] This resin (**31**) provided the cyclic adduct **29** with a conversion of *ca*. 80%, slightly lower than the one found for the RB-SILLP **23b** (85%). The FT-IR-ATR of this resin before and after reaction showed a band at 1669 cm^{-1} assignable to the zwitterionic NHC−CO_2 (Figure SI.6). The spectra for **25b** and **31** (Figure SI.8) are comparable demonstrating the formation of the zwitterionic NHC-CO_2 adduct in the catalyst process. It must be mentioned that SILLP **8a**, structurally identical to **17a** but lacking the RB units, did not show significant changes in the FT-IR spectrum after its use as catalyst. The lack of the band at 1665-1669 cm^{-1} (Figure SI.7) indicates that, in the absence of RB, the NHC-CO_2 adduct was not formed. Altogether, the data suggest that the zwitterionic NHC-CO_2 adduct can be an active species in the catalytic process.

In addition to the use of these multifunctional resins, some polymer cocktails using two different monofunctional resins, were also assayed.[47] In the first one, the macroporous SILLP **8a** was mixed with a gel type resin containing covalently immobilized RB (Neckers catalyst) keeping the same RB:IL-like units molar ratio as in previous experiments. In the second one, two gel type resins were employed with the use of SILLP **7a**. Figure 3 summarizes the results obtained. Remarkably, the Neckers catalyst was not able to catalyze the model reaction. For the polymer

[46] Zhou, H.; Zhang, W.-Z.; Liu, C.-H.; Qu, J.-P.; Lu, X.-B. CO_2 Adducts of N-Heterocyclic Carbenes: Thermal Stability and Catalytic Activity toward the Coupling of CO_2 with Epoxides. *J. Org. Chem.* **2008**, *73* (20), 8039–8044.

[47] Sans, V.; Gelat, F.; Karbass, N.; Burguete, M. I.; García-Verdugo, E.; Luis, S. V. Polymer Cocktail: A Multitask Supported Ionic Liquid-Like Species to Facilitate Multiple and Consecutive C-C Coupling Reactions. *Adv. Synth. Catal.* **2010**, *352* (17), 3013–3021.

cocktails, the one formed involving the macroporous SILLP and the gel-type Neckers catalyst rendered a 64% yield of the carbonate, while the conversion was enhanced for the cocktail formed by the two gel-type resins (83%). Thus, the functionalities present in both the IL-like units and the RB fragments contribute to enhance the reaction of CO_2 and SO. However, the direct interaction between functional groups in two different solid phases is not possible,[48] and the involvement of both fragments requires the participation of a species transported between both phases.[49] Residual water can play this role of facilitating the interaction between RB and IL-like fragments, which is also in agreement with the fact that best results are observed with the cocktail involving two gel type resins for which the excellent swelling in SO facilitates the transport from one resin to the other.

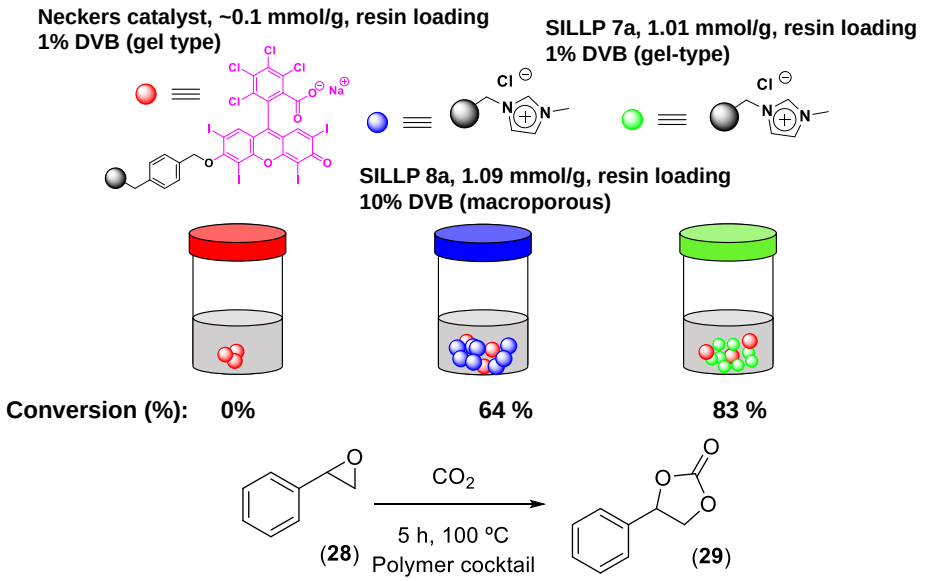

Figure 3. Synergistic effect between of RB and IL-like moieties supported onto polymeric cocktails.

[48] Rebek, J.; Gavina, F. Three-Phase Test for Reactive Intermediates. Cyclobutadiene. *J. Am. Chem. Soc.* **1974**, *96* (22), 7112–7114.
[49] Rebek, J.; Costello, T.; Marshall, L.; Wattley, R.; Gadwood, R. C.; Onan, K. Allosteric Effects in Organic Chemistry: Binding Cooperativity in a Model for Subunit Interactions. *J. Am. Chem. Soc.* **1985**, *107* (25), 7481–7487.

Figure 4 presents a plausible mechanism in agreement with the experimental data. Imidazolium units can produce NHC fragments with the simultaneous involvement of RB fragments and residual water. Reaction of CO_2 with this NHC forms the zwitterionic NHC−CO_2 (step 1). Both, residual water and the imidazolium hydrogen atoms can then act as potential HBD for the activation of the epoxide through hydrogen-bond interactions (step 2). This facilitates the epoxide ring opening by the zwitterionic NHC−CO_2 adduct (step 3). Then, insertion of CO_2 occurs by nucleophilic attack of the alkoxide formed in the ring opening (step 4), creating a carbonate ion intermediate, which undergoes intramolecular ring closure leading to the cyclic carbonate product and restoring the zwitterionic NHC−CO_2 fragment (step 5).

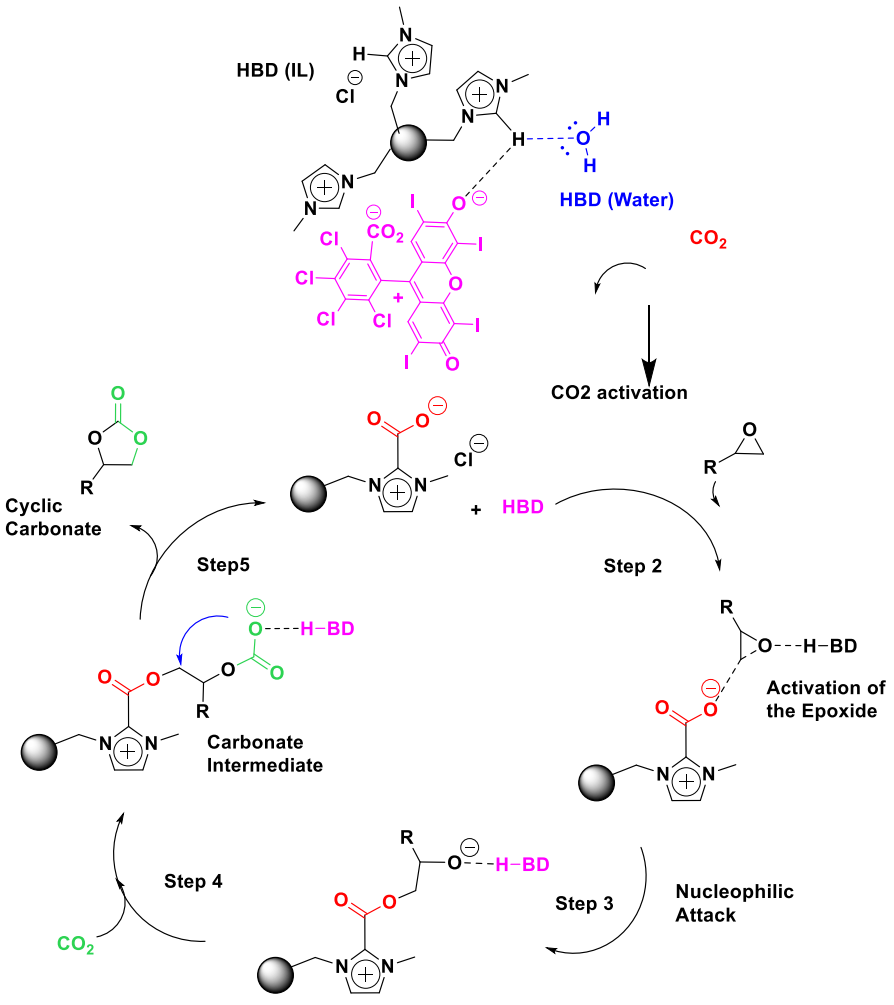

Figure 4. Proposed Mechanism for the cycloaddition of CO_2 to epoxides.

Stability study

To evaluate the stability of the catalyst, a set-up to work under flow conditions represents an optimal system. Thus, a continuous flow reactor, as illustrated in Figure 5, was built formed by two pumps to deliver CO_2 and the epoxide, forming a homogeneous mixture in a mixer and passing through a preheater to reach the reaction temperature before entering in contact with the supported catalyst. Preliminary experiments revealed that higher CO_2 pressures than for batch experiments due to experimental limitation of the continuous set-up. Thus, two reactors in-line packed with the corresponding catalyst were used. Initially, the SILLP **14b,** in the absence of RB was tested at a total flow rate of 55 μL/min, an oven temperature of 150 ^{o}C and a pressure of 140 bars. This system showed an average conversion of *ca*. 20% corresponding with a productivity of 0.46 g x g^{-1} x h^{-1}. The stability was very good. The catalyst was stable at least during the 55 hours tested. The results obtained for the catalyst RB-SILLP **23b** bearing RB units confirmed the synergetic effect between RB fragments, water molecules and IL-like units, providing a more active catalyst and reaching up to 80% conversion for the first few hours of operation. However, after five hours of continuous use the activity dropped to *ca*. 60% conversion. This new level of activity was kept constant till reaching 40 hours of operation. After this time, a new drop in activity was again observed (to *ca*. 50% conversion). This decay in activity can be correlated with the presence of some RB leaching, as the samples at the outlet of the reactor has a slight red coloration. The non-covalent attachment of RB fragments can favor this leaching.

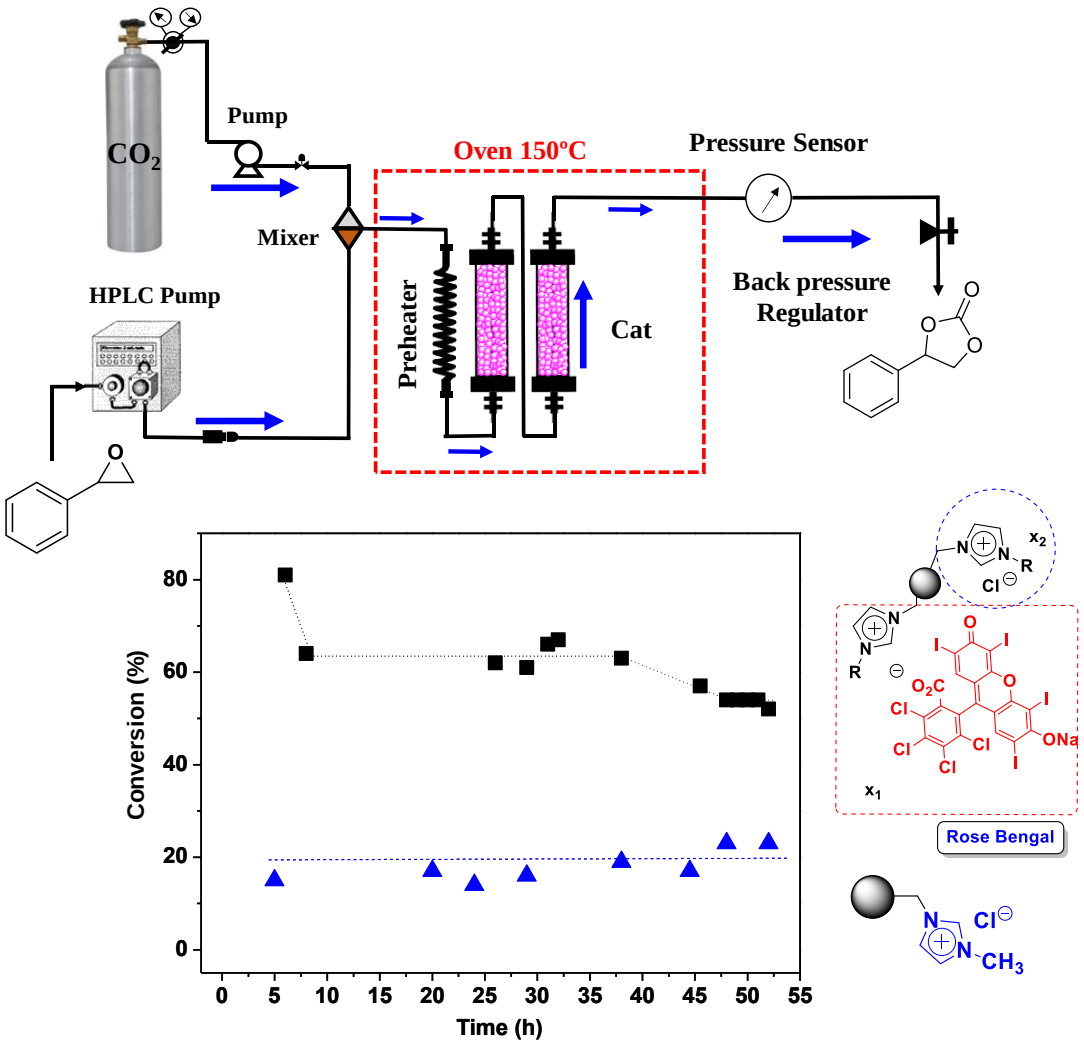

Figure 5. Schematic representation of the set-up for the continuous flow reactor. Conversion of SO *vs* time on stream obtained for the continuous flow reaction between SO and CO_2 at 150 °C and 140 bars. Triangle: 1.892 g of SILLP **14b** without RB. Squares: 2.266 g of RB-SILLP **23b**. Conversion calculated by ^{1}H-NMR. Selectivity > 99%.

The RB leaching can be avoided by using a covalent grafting of both the RB and imidazolium units to the polymeric support. For this, a sub-stoichiometric amount of RB was reacted with the chloromethylated resin to obtain a polymer (**26**) containing RB units and free -CH_2-Cl groups that were further modified to introduce methylimidazolium moieties (catalyst **27**, Scheme 1).[50] The process

[50] Sans, V.; Gelat, F.; Burguete, M. I.; Garcia-Verdugo, E.; Luis, S. V. Polymer-Supported Pd–NHC Complexes: Strategies for the Development of Multifunctional Systems. *Catal. Today*. **2012**, *196* (1), 137–147.

could be followed by FT-IR-ATR spectroscopy (Figure SI.9). In resin **26**, the introduction of RB units was confirmed by the appearance of characteristics bands at 1731, 1546 and 1263 cm^{-1} and the partial disappearance of the -CH_2-Cl band at 1267 cm^{-1}. The introduction of the imidazolium fragments was followed by the complete disappearance of the band at 1267 cm^{-1} and the appearance of bands at 1550 cm^{-1} and 1120 cm^{-1} assignable to the imidazolium units. Elemental analysis allowed to calculate a loading of 1.56 meq of RB/ g of polymer and 2.23 meq of IL-like unit / g of polymer in resin **27**.

The reaction between SO and CO_2 was then tested in batch with this new catalyst. After 5 h at 100 ºC and 10 bars the product **29** was obtained with a conversion of 70%. When catalyst **27** was tested under flow conditions, under the same experimental conditions used for the previous catalysts, the system showed a very stable behavior. An average conversion of 53% was achieved for ten days of continuous production of the corresponding carbonate.

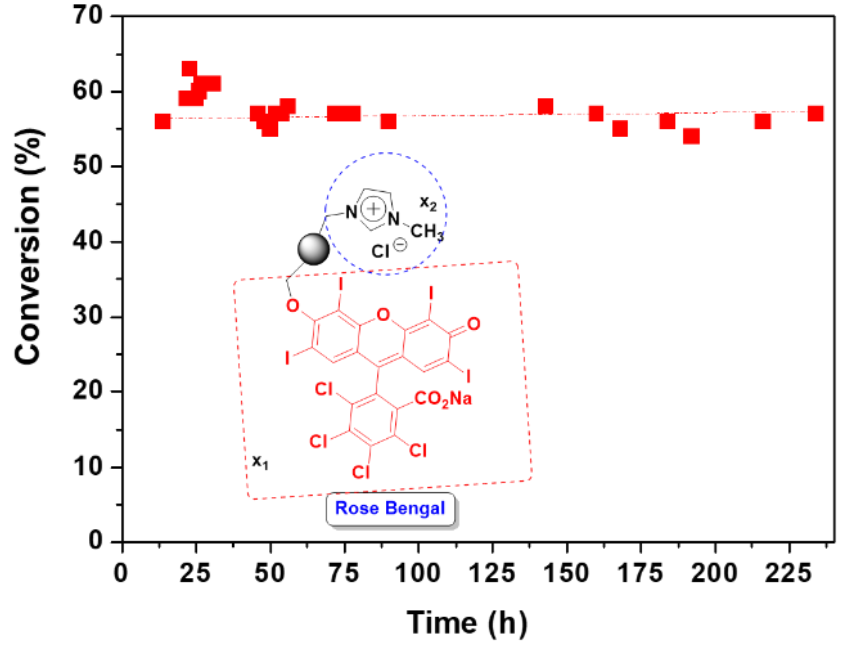

Figure 6. Conversion of SO *vs* time on stream obtained for the continuous flow reaction between SO and CO_2 at 150 ºC and 140 bars. 50 µl/min of CO_2 and 5 µl/min of SO; reactor 1.906 g of RB-SILLP **27**. Conversion calculated by ^{1}H-NMR. Selectivity > 99%.

Deactivation after several hour of operation under continuous use is a common trend for immobilized or heterogeneous catalysts.[18] In the case of the RB-SILLP **27**, no appreciable leaching of RB or decay on the catalytic activity was observed during this ten days of continuous use. Besides, the productivity of this system was 1.129 $g_{cyclocarbonate} \times g_{catalyst}^{-1} \times h^{-1}$, which is among the higher productivities reported so far under continuous flow conditions (Table SI.2).

7.3. Conclusions

The present results demonstrate that it is possible to develop a sustainable, cheap and easily accessible multifunctional heterogeneous catalyst using commercially available chloromethylated PS-DVB resins beads modified to introduce IL-like units. The simultaneous presence of RB fragments and residual water molecules acts in combination with supported ionic liquid like phases produce important synergies, effectively enhancing the catalytic activity of both micro and microporous polymer supported catalysts. Such systems are able to achieve high catalytic activity and excellent selectivity at both atmospheric and 10 bar CO_2 pressures. These heterogeneous systems can be systematically optimized considering the loading of the IL-like units, the substitution pattern at the imidazolium rings and polymer morphology. The resulting organcatalytic optimized supported systems allow reaching TON and TOF values of up to 83041 of 494 h^{-1} respectively. Those values are in line with the ones reported in the literature for systems based on transition metals and involving dual activation mechanisms. The fact that the catalytic systems presented here are metal free represents a clear advantage for a green and sustainability approach. Furthermore, these catalysts can be easily prepared and upscaled from simple and cheap commercially available resins and modifiers. Their high stability has been demonstrated using continuous flow systems, although for an efficient access to the catalytic sites, under those conditions. No appreciable loss of activity

was observed for at least ten days of continuous operation, which is a key property in the perspective of a large-scale application.

7.4. Experimental Section

Materials

All reagents were purchased from Sigma-Aldrich and used without further purification. ^{1}H and ^{13}C NMR experiments were carried out using Bruker Avance III HD 300 or 400 spectrometer (300 or 400 MHz for ^{1}H and 125 or 100 MHz for ^{13}C). The chemical shifts are given in delta (δ) values, using the residual solvent signal for reference.

General characterization protocols

Spectroscopic studies

Fourier Transform Infrared Spectra (FT-IR) spectra were acquired with a Pike single-reflection ATR diamond/ZnSe accessory in a JASCO FT/IR-4700 instrument.

Synthetic protocols

The synthesis and characterization of SILLPs and RB-SILLPs has been reported in references 21, 22 and 25.

General procedure for the synthesis of cyclic carbonate by CO_2 transformation: Batch experiments

Two different set-ups were used for the cyclocarboxylation of SO with CO_2. The first system, for the reactions under pressure, used a Berghof R-300 high pressure reactor connected to a pressurized CO_2 source and a back-pressure regulator from Jasco. The heater was first brought to the desired temperature of 100 ^oC. The reactor was then loaded with styrene oxide (1 mL) and catalyst (35.6 mg). The reactor was connected to the CO_2 pump and the back-pressure regulator and immersed in the bath. CO_2 was liquefied and pumped into the reactor up to the desired pressure, under stirring. After five hours of reaction, the high-pressure reactor was cooled down and depressurized to atmospheric pressure. Afterward, the reactor was opened and the contents collected using 1 mL of deuterated chloroform, to dissolve the reaction mixture. The catalyst is separated by filtration. ^1H NMR spectra were recorded. Experimental procedures were replicated for all experiments. The average deviation of styrene carbonate formation was less than 5%.

The second one, employed for the reaction at atmospheric pressure, used a round bottom flask with a CO_2 balloon (100% CO_2) as the gas supply. The same work up than before was used at the end of the reaction.

The signals δ (ppm) for SO are: 2.76 (t, 1H), 3.10 (t, 1H) 3.82 (t, 1H) for the CH and CH_2 groups and 7.22–7.38 (m, 5H) for the phenyl group. The signals δ (ppm) for the cyclic styrene carbonate are: 4.29 (t, 1H) and 4.82 (t,1H) for the CH_2 (methylene), 5.70 (t, 1H) for the CH (methine) and 7.22–7.38 (m, 6H) for the phenyl group. No further peaks were detected for all experiments. For all reactions performed, the selectivity was 100%, with no by-products formation.

Continuous flow experiments

SO was pumped using a Jasco HPLC pump at a rate of 5 µl/min. CO_2 was pumped with a refrigerated CO_2 Jasco pump at a flow rate of 50 µl/min. Once CO_2 and epoxide entered in contact in a mixer, they passed through a preheater and two fix-bed reactors charged with the corresponding catalyst. The reactors were in an oven to achieve the required experimental temperature. A Jasco back pressure regulator was connected at the outlet of the second reactor to establish the desired pressure. All required connections were made with stainless-steel 1/16 inch coil. The reaction stream of crude product was collected in a cold trap at the outlet of the back-pressure regulator. Samples were taken and analyzed by ^{1}H-NMR spectroscopy to determine the conversion and selectivity of the reaction.

7.5. Supplementary Information

Multifunctional polymers based on ionic liquid and Rose Bengal fragments for the conversion of CO_2 to carbonates

Table of Contents

Table SI.1. Structure and properties for the different SILLPs prepared.

Structure	Code	Type	Loading (meq/g)	R	R´	Water content [a] (%)	Swelling (%)[c]
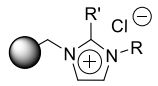	7a	Gel	1.01	CH_3	H	1.81	56
	8a	Macroporous	1.09	CH_3	H	3.46	-
	9a	Gel	0.97	CH_4H_9	H	1,27	69
	10a	Macroporous	1.94	CH_4H_9	H	2.62	-
	11a	Gel	0.88	$CH_{10}H_{21}$	H	1.27	81
	12a	Macroporous	0.95	$CH_{10}H_{21}$	H	2.10	-
	13b	Gel	3.18	CH_3	H	11.35	-
	14b	Macroporous	3.79	CH_3	H	15.14	-
	15b	Macroporous	3.71	CH_3	CH_3	-	-
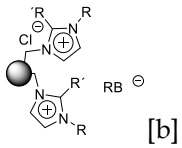 [b]	16a	Gel	1.01	CH_3	H	2.01	-
	17a	Macroporous	1.09	CH_3	H	3.50	-
	18a	Gel	0.97	CH_4H_9	H	-	-
	19a	Macroporous	1.94	CH_4H_9	H	2.60	-
	20a	Gel	0.88	$CH_{10}H_{21}$	H	1.17	-
	21a	Macroporous	0.95	$CH_{10}H_{21}$	H	2.10	-
	22b	Gel	3.18	CH_3	H	-	-
	23b	Macroporous	3.79	CH_3	H	-	-
	24b	Macroporous	3.71	CH_3	CH_3	-	-
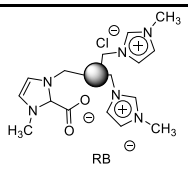	25b	Macroporous	3.68	CH_3	H	-	-
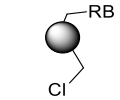	26	Macroporous	1.56	CH_3	H	-	-
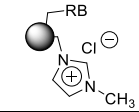	27	Macroporous	2.23	CH_3	H	-	-
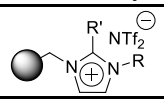	30a	Gel	1.1	CH_3	H	-	-
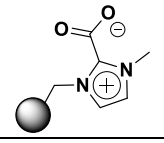	31b	Macroporous	3.67	CH_3	H		

[a] Water content calculated from TGA, after equilibration at rt during 24 h. [b] RB loading 3.92 x 10^{-2} µmol RB / g of polymer. [c] $Swelling = \left(\frac{Wet\ size - Dry\ size}{Dry\ size}\right) \cdot 10^2$

a)

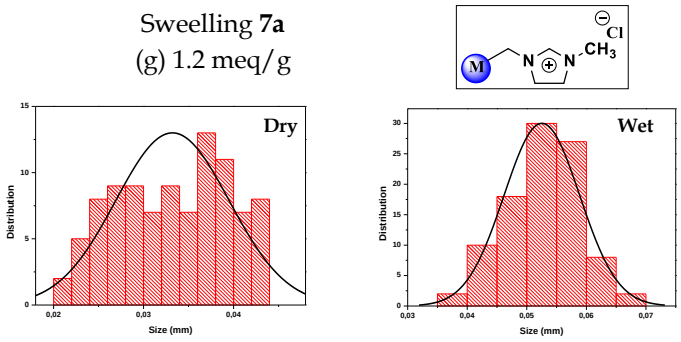

Swelling: 56%

b)

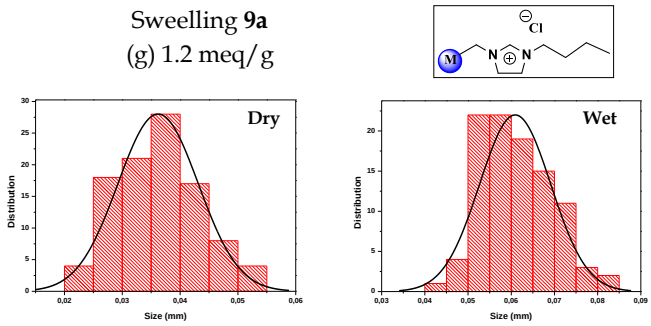

Swelling: 69%

c)

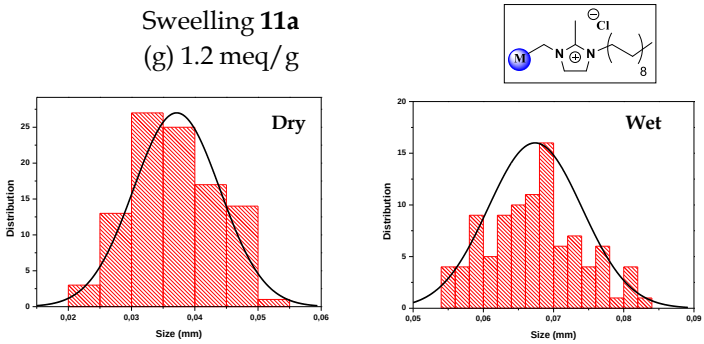

Swelling: 81%

Figure SI.1. Swelling of different RB-SILLPs resins in styrene oxide (SO) calculated as **(a) 7a**. **(b) 9a**. **(c) 11a.** $Swelling = \left(\frac{Wet\ size - Dry\ size}{Dry\ size}\right) \cdot 10^2$-For each resin, the size distribution diagram on the left corresponds to the dry state, while the one on the right correspond the size distribution in the presence of SO.

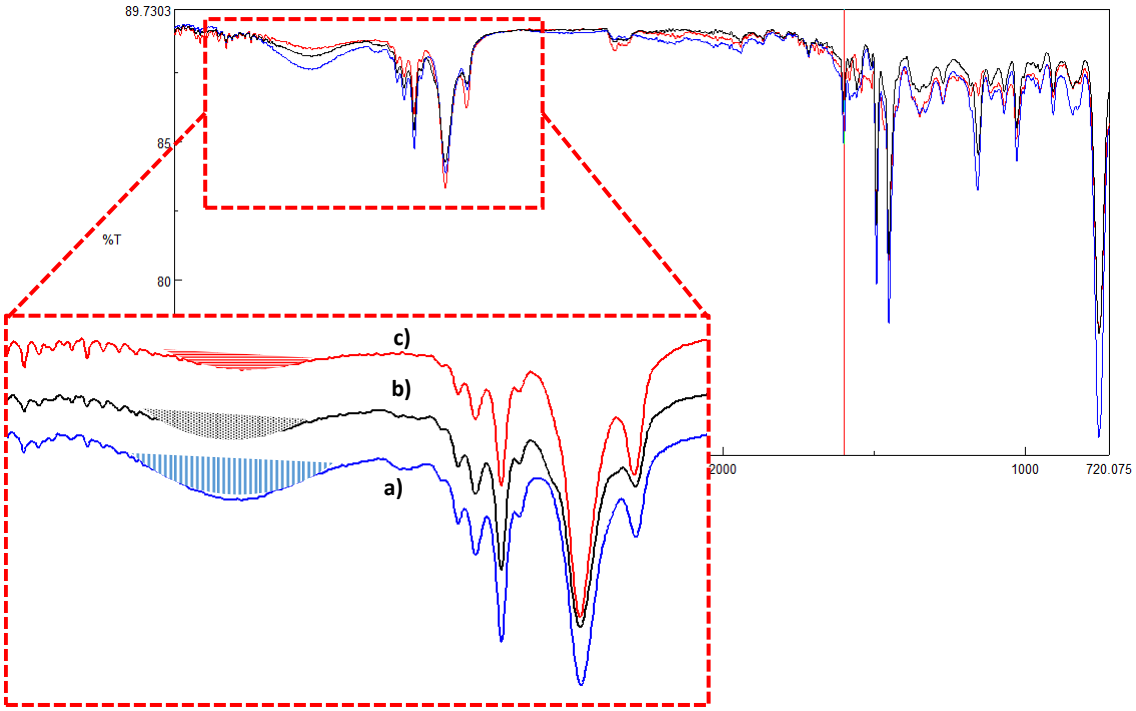

Figure SI.2. FT-IR-ATR spectra obtained for the RB-SILLPs of ν (O–H) region showing the uptake of water from air as for the different low loading gel-type PS-DVB resin with different substitution pattern. **(a) 16a** (methyl). **(b) 18a** (butyl). **(c) 20a** (2-methyl-decyl).

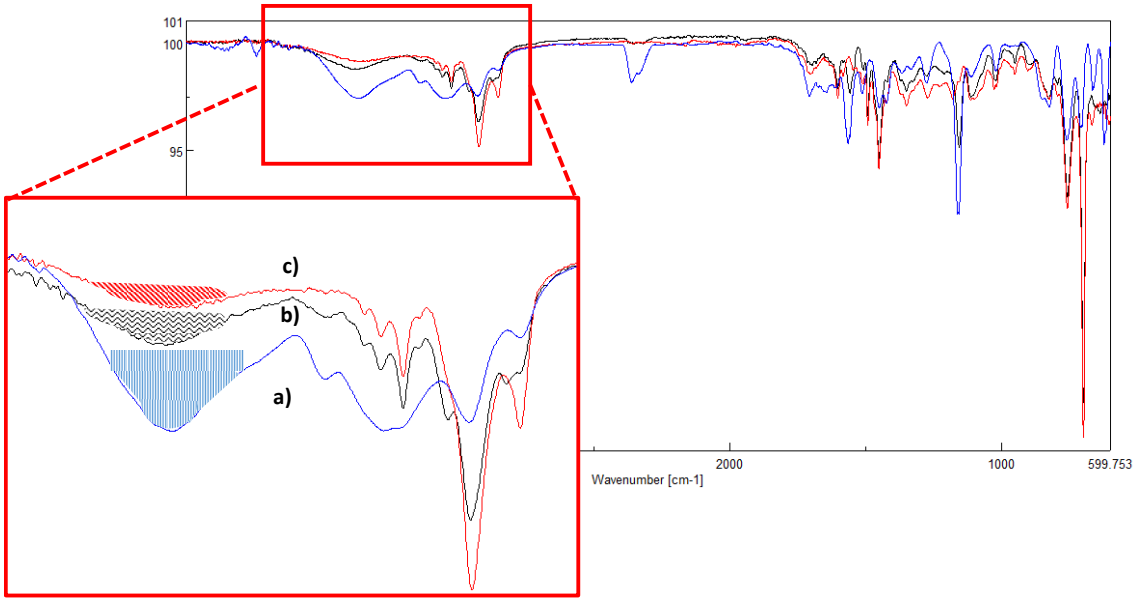

Figure SI.3. FT- IR-ATR spectra obtained for the RB-SILLPs of ν (O–H) region showing the uptake of water from air as for the different of low loading macroporous type PS-DVB resin with different substitution pattern. **(a) 17a** (methyl). **(b) 19a** (butyl). **(c) 21a** (2-methyl-decyl).

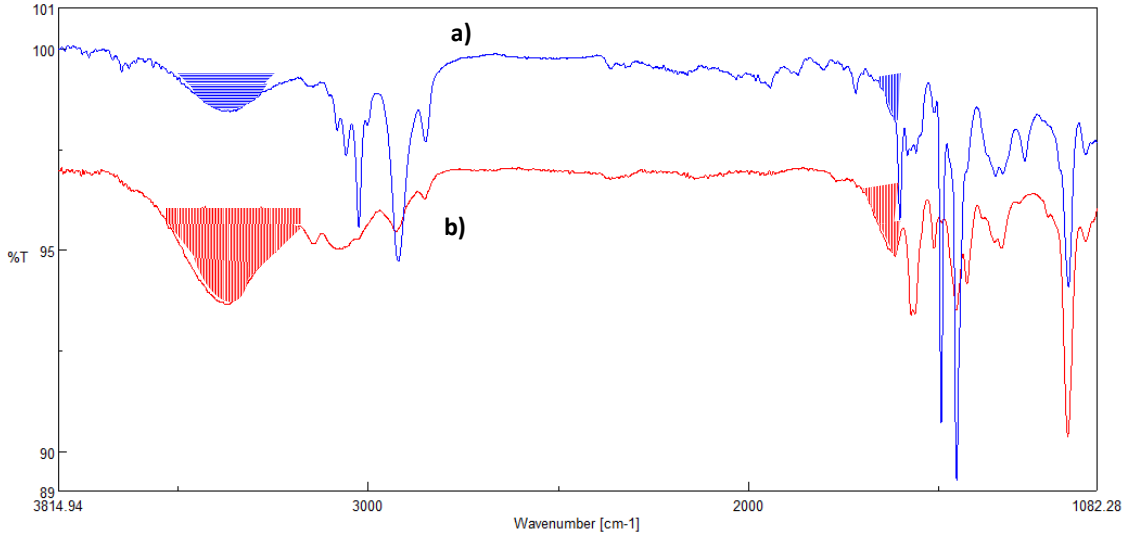

Figure SI.4. FT-IR-ATR spectra obtained for the RB-SILLPs of ν(O–H) region showing the uptake of water from air as for the different for the RB-SILLPs of gel type PS-DVB resins with different loading. **(a)** Low loading (**16a**). **(b)** High loading (**22b**).

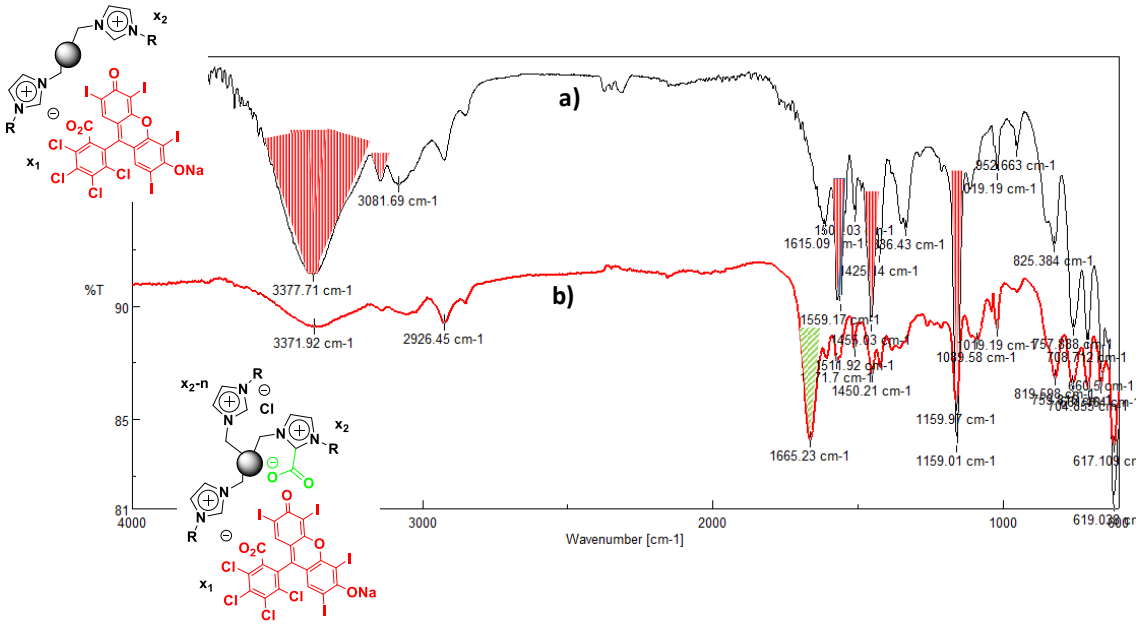

Figure SI.5. FT-IR-ATR spectra obtained for the RB-SILLP **23b (a)** before its use as catalyst. **(b)** after its use in the catalytic reaction (36.7 mg RB-SILLP **23b**) for 5 h at 100 ºC, 10 bar of CO_2 and using 1 mL epoxide.

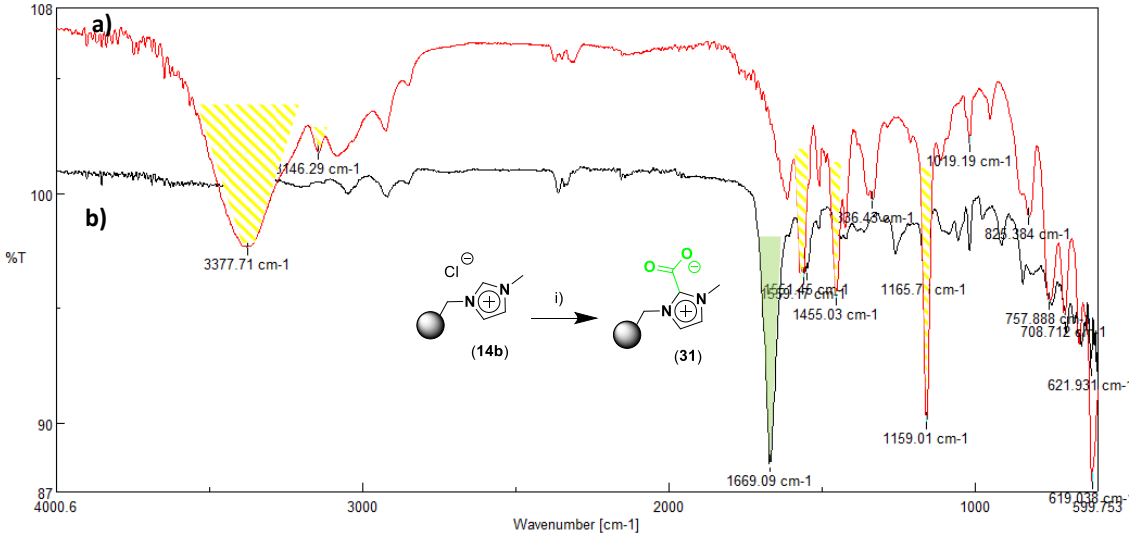

Figure SI.6. FT-IR-ATR spectra for the synthesis of the zwitterionic NHC−CO_2 polymer **31** from **14b** (from a high loading chlorometilated resin, macroporous). i) Resin **14b** in 1,0 mL of dry THF, 8.5 equivalents of KHMDS at 80 ºC and CO_2 (balloon). **(a) 14a**. **(b) 31** resin, high loading and macroporous.

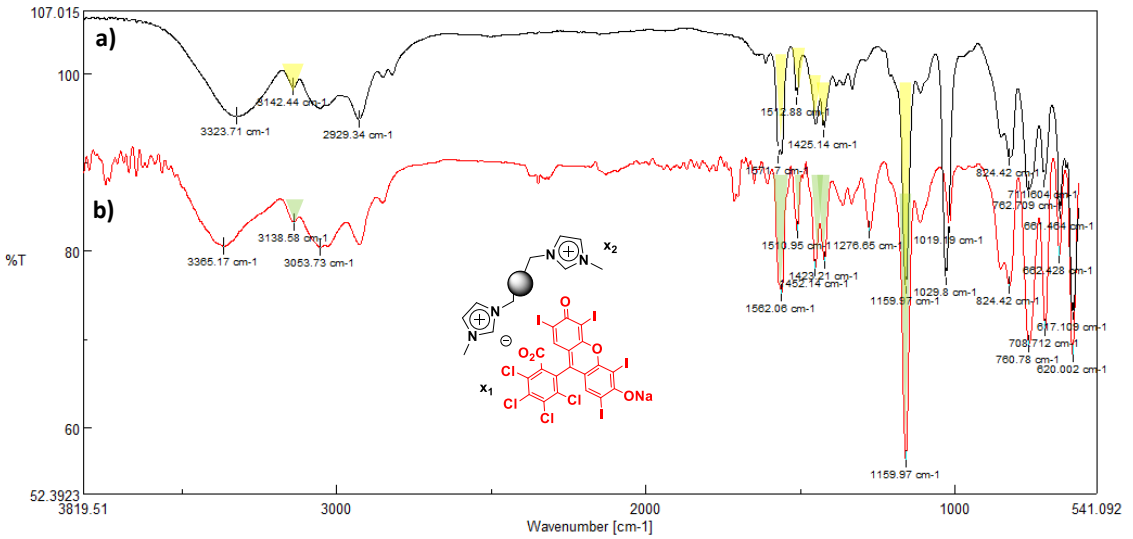

Figure SI.7. FT-IR-ATR obtained before and after the use of catalyst. **(a)** RB-SILLPs **17a** before **(b)** RB-SILLPs **17a** after. reaction conditions: solventless, 5 hours, 100 ºC, 10 bar CO_2, 1, mL epoxide and 36.7 mg catalyst.

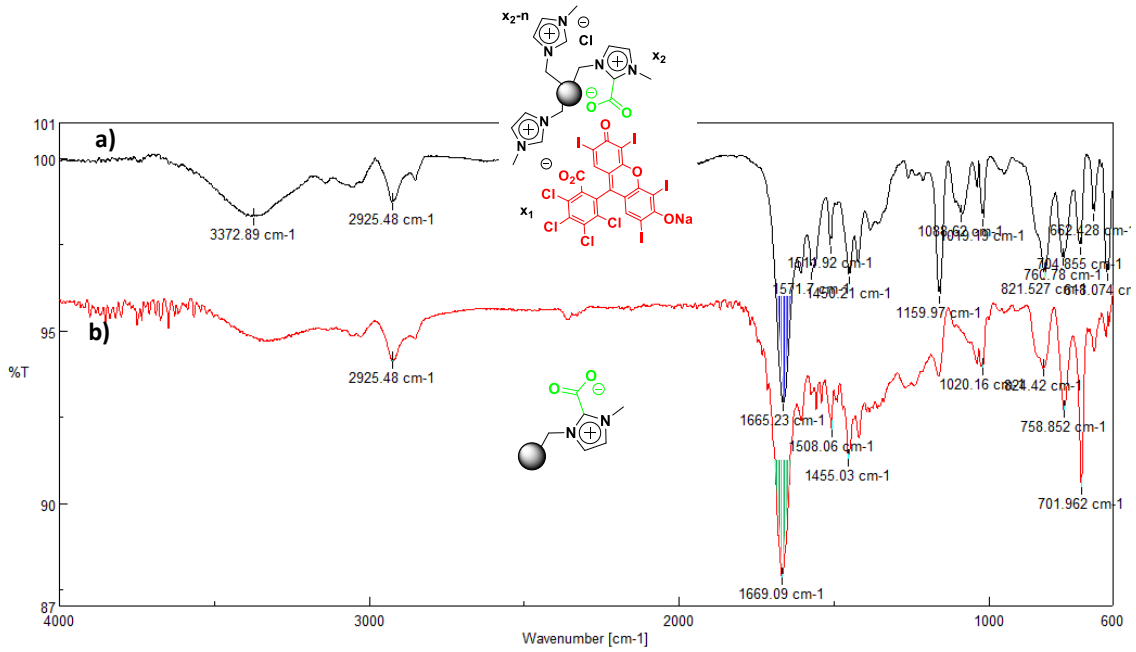

Figure SI.8. FT-IR-ATR spectra obtained for **(a)** RB-SILLP **25b (b) 31**, after their use in the catalytic reaction (36.7 mg) for 5 h at 100 ºC, 10 bar of CO_2 and using 1 mL epoxide.

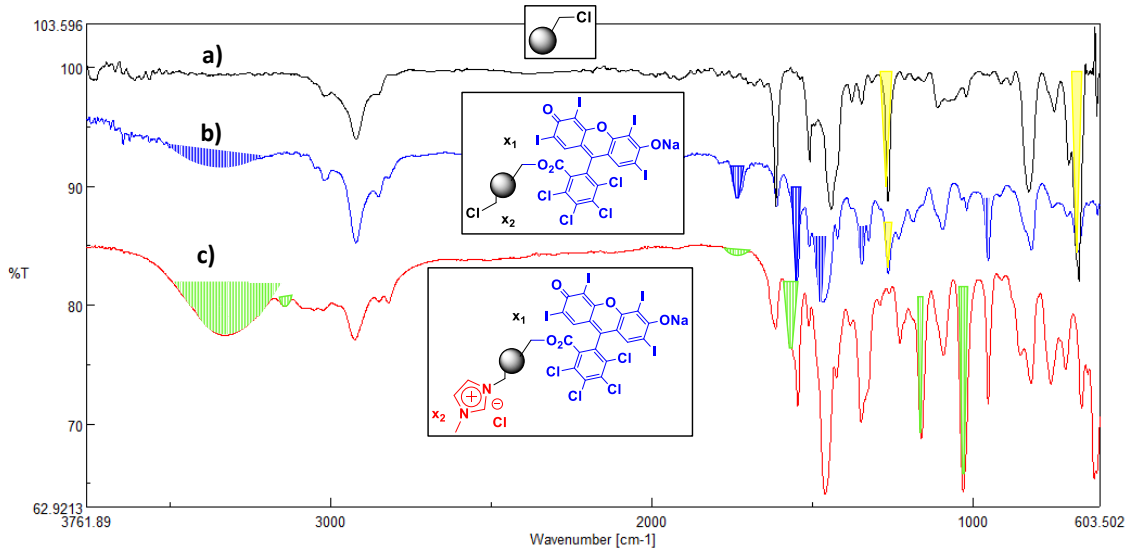

Figure SI.9. FT-IR-ATR spectra obtained for **(a)** Merrifield resin **2**. **(b)** resin **26**. **(c)** resin **27**.

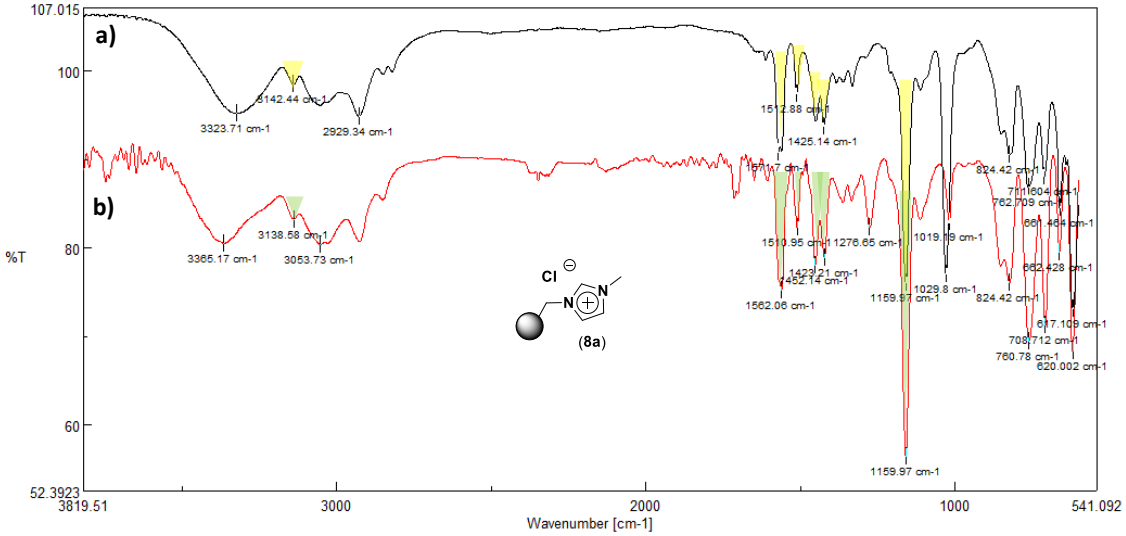

Figure SI.10. FT-IR-ATR spectra obtained for SILLP **8a** before **(a)** and after **(b)** the catalytic reaction (36.7 mg of catalyst) for 5 h at 100 ºC, 10 bar of CO_2 and using 1 mL epoxide.

Table SI.2. Comparison of SILPs **27** with some catalysts reported in the literature for cycloaddition of CO_2 in a continuous flow system.

Entry	Catalyst	(g)	Cocatalyst	Solvent	Substrate[a]	Flow Substrate (mL/min)	Flow CO_2 (mL/min)	Flow N_2 (mL/min)	Pressure (bar)	Temp. (°C)	Time / Activity (h)	Yield (%)	Prod.$_T$ ($g_{epoxide} \times g_{cat}^{-1} \times h^{-1}$)	Prod.$_{Exp}$ ($g_{epoxide} \times g_{cat}^{-1} \times h^{-1}$)	Leaching[b]
1	**27**	1.9	RB/H2O	-	SO	0.005	0.05	-	140	150	234	57	1.9808	1.1291	X
2	MCM-41/[Co(II)(salen)]	4	*n*-Bu_4NBr	-	EO	0.17	0.33	-	125	110	24	86	0.0901	0.775	X
3	Amorphous silica/$[(salem)Al]_2O$*t*Bu	0.43	-	-	EO	0.0025	0.017	0.042	1.01	150	6	57	0.3159	0.1801	✓
4	MCM-41/$[(salem)Al]_2O$*t*Bu	1.57	-	-	EO	0.0025	0.017	0.042	1.01	60	7	95	0.0865	0.0822	✓
5	Cs-P-Si-oxide	10	-	-	PO	0.05	0.2	-	140	200	3	50	0.0152	0.0076	✓
6	MOF MIL-101(Cr)	0.042	TBABr	Chlorobenzene	PO	0.25	4	-	50	100	5	80	1.0676	0.8541	✓
7	MOF MIL-101(Sc)	0.042	-	-	PO	0.25	4	-	50	100	5	57	1.0676	0.6085	✓

[a]: SO: Styrene oxide; EO = Ethylene Oxide; PO = Propylene Oxide.
[b]: X = No leaching; ✓= Leaching

Entry (References):
2. Lu, X.-B.; Xiau, J.-H.; He, R.; Jin, K.; Luo, L.-M.; Feng, X.-J. Chemical fixation of CO_2 to ethylene carbonate under supercritical conditions: continuous and selective. *Appl. Catal. Gen*. **2004**. *275*. 73–78.
3 & 4. North, M.; Villuendas, P.; Young, C. A Gas-phase flow reactor for ethylene carbonate synthesis from waste carbon dioxide. *Chem. Eur. J*. **2009**. *15*. 11454-11457.
5. Yasuda, H.; He, L.-H.; Takahashi, T.; Sakakura, T. Non-halogen catalysts for propylene carbonate synthesis from CO_2 under supercritical conditions. *Appl. Catal. Gen*. **2006**. *298*. 177-180.
6 & 7. James, B. R.; Boissonnault, J. A.; Wong-Foy, A. G.; Matzger, A. J.; Sanford, M. S. Structure activity relationships in metal-organic framework catalysts for the continuous flow synthesis of propylene oxide carbonate from CO_2 and propylene oxide. *RSC. Adv*. **2018**. *8*. 2132-2137.

CAPÍTULO VIII

Impresión 3D como herramienta facilitadora de técnicas emergentes. Conversión catalítica estable y más eficiente de CO_2 en procesos de flujo continuo usando reactores impresos basados en líquidos iónicos soportados

Resumen. El diseño exitoso de materiales avanzados basados en compuestos moleculares es muy complejo ya que requiere la creación y adaptación de geometrías macroscópicas complejas. Sin embargo, esto último se facilita con el uso de la impresión 3D. A continuación, se presenta el desarrollo de materiales avanzados obtenidos mediante impresión 3D, los cuales han sido modificados para modular el comportamiento catalítico como SILLPs. Los materiales han sido utilizados en la reacción de cicloadición del CO_2 a los epóxidos, como una ruta atractiva para obtener productos de alto valor agregado. Además, los materiales creados por impresión 3D permitieron trabajar en condiciones de flujo continuo y mediante su diseño digital proporcionaron una mejora en la productividad del producto final.

Chapter VIII. 3D Printing as *enabler* of enabling techniques. Stable and more efficient catalytic CO_2 conversion under continuous flow process using printed reactors based on supported ionic liquids

Abstract. The successful design of advanced materials based on molecular compounds is highly complex since it requires creation and adaptation of complexes macroscopic geometries. The latter, however, can be facilitated by using 3D printing. This work presents the development of advanced materials and devices through 3D printing, which have been modified to fine tuning the catalytic behavior of supported ionic liquid-like Phases (SILLPs).The materials have been used in the cycloaddition of CO_2 carbon dioxide to epoxides, which is an attractive route to provide high-added value products. In addition, the materials created by 3D printing allowed to work under continuous flow conditions. Their optimized digital design provided an improvement in the productivity for the desired molecular target.

Keywords: 3D printing • enabling technologies • catalysis • CO_2 conversion • flow chemistry

8.1. Introduction

Additive manufacturing, commonly known as 3D printing (3DP) is an emerging technology that facilitates the generation of complex geometries and is available for a variety of materials (i.e. polymers, ceramics and metals).[1,2] 3DP enables a big degree of design freedom and the possibility to generate tailored complex geometries that would not be possible, or would be very expensive, with traditional manufacturing techniques.[3] However, 3DP is much more than an emerging additive manufacturing technique as it can be considered as a facilitating technology for the

[1] Frazier, W. E. Metal Additive Manufacturing: A Review. *J. of Materi Eng and Perform.* **2014**, *23* (6), 1917–1928.
[2] Ligon, S. C.; Liska, R.; Stampfl, J.; Gurr, M.; Mülhaupt, R. Polymers for 3D Printing and Customized Additive Manufacturing. *Chem. Rev.* **2017**, *117* (15), 10212–10290.
[3] Hartings, M. R.; Ahmed, Z. Chemistry from 3D Printed Objects. *Nat. Rev. Chem.* **2019**, *3* (5), 305–314.

integration of the so-called *enabling techniques*.[4,5] Enabling techniques encompass traditional as well as new techniques (*i.e.* flow reactors, photochemistry, electrochemistry, chemo-, organo- or bio-catalysis, sensing, separation, ultrasounds, microwave irradiation, solid-phase assisted synthesis and new solvents), which have been developed to speed up synthetic transformations and, importantly, ease the workup as well as the isolation of products.[6,7,8] Thus, 3DP can be envisioned as an *enabler* of *enabling techniques* in the development of truly new advanced technological platforms. This is an emerging field, where only a few successful examples using 3DP technologies to integrate several enabling techniques have appeared in the literature. One of those examples is the demonstration of the availity of 3DP to integrate organic synthetic transformations (either chemo or biocatalytic) with flow processes.[9,10,11,12] The integration of new materials with Ionic Liquids (ILs) into discrete molecular devices capable

[4] Vasudevan, A.; Bogdan, A. R.; Koolman, H. F.; Wang, Y.; Djuric, S. W. Enabling Chemistry Technologies and Parallel Synthesis—Accelerators of Drug Discovery Programmes. In *Progress in Medicinal Chemistry*; Witty, D. R., Cox, B., Eds.; Elsevier, 2017; Vol. 56, pp 1–35.
[5] Fitzpatrick, D. E.; Battilocchio, C.; Ley, S. V. Enabling Technologies for the Future of Chemical Synthesis. *ACS Cent. Sci.* **2016**, *2* (3), 131–138.
[6] O'Brien, M.; Denton, R.; Ley, S. V. Lesser-Known Enabling Technologies for Organic Synthesis. *Synthesis*. **2011**, *2011* (8), 1157–1192.
[7] Wegner, J.; Ceylan, S.; Kirschning, A. Flow Chemistry – A Key Enabling Technology for (Multistep) Organic Synthesis. *Adv. Synth. Catal.* **2012**, *354* (1), 17–57.
[8] Kirschning, A.; Solodenko, W.; Mennecke, K. Combining Enabling Techniques in Organic Synthesis: Continuous Flow Processes with Heterogenized Catalysts. *Chem. Eur. J.* **2006**, *12* (23), 5972–5990.
[9] Peris, E.; Okafor, O.; Kulcinskaja, E.; Goodridge, R.; Luis, S. V.; Garcia-Verdugo, E.; O'Reilly, E.; Sans, V. Tuneable 3D Printed Bioreactors for Transaminations under Continuous-Flow. *Green Chem.* **2017**, *19* (22), 5345–5349.
[10] Sans, V. Emerging Trends in Flow Chemistry Enabled by 3D Printing: Robust Reactors, Biocatalysis and Electrochemistry. *Curr. Opin. Green Sustain. Chem.* **2020**, *25*, 100367.
[11] Rossi, S.; Puglisi, A.; Benaglia, M. Additive Manufacturing Technologies: 3D Printing in Organic Synthesis. *ChemCatChem.* **2018**, *10* (7), 1512–1525.
[12] Dragone, V.; Sans, V.; Rosnes, M. H.; Kitson, P. J.; Cronin, L. 3D-Printed Devices for Continuous-Flow Organic Chemistry. *Beilstein J. Org. Chem.* **2013**, *9* (1), 951–959.

of highly sophisticated functional operations for advanced applications is another of the emerging fields enabled by 3D printing technologies.[13]

Here, we report on our efforts to integrate, in a single platfform, solid-phase-assisted catalysis, flow chemistry and ILs for the activation and conversion of CO_2 in added value products. The special design of the materials obtained by 3DP are the key to integrate and transfer the optimised characteristic of the ILs at the molecular level to materials and macroscale devices able to capture, activate and convert CO_2, providing the required mixing to eliminate mass transfer limitations, which typically undermines catalytic behaviour of catalysts under flow conditions. The performance of the corresponding synthetic platform overpass those observed for active materials obtained by conventional methodologies.

8.2. Results and Discussion

Preparation of the monomeric inks and the 3D printing objects

In the search a straightforward and simple methodology for the preparation of functionalised 3DP polymeric devices, the commercial monomer glycidyl methacrylate (GMA) was envisioned as a suitable system for the formulation of functional monomeric inks. GMA copolymerizes with many conventional monomers and offers an economical means for introducing reactive functional groups into polymeric matrices, facilitating the development of functional materials for different applications.[14] The epoxy moiety allows different strategies for its

[13] Nulwala, H.; Mirjafari, A.; Zhou, X. Ionic Liquids and Poly(Ionic Liquid)s for 3D Printing – A Focused Mini-Review. *Eur. Polym. J.* **2018**, *108*, 390–398.
[14] Lee, H.; Neville, K. *Handbook of Epoxy Resins*; 1st ed.; McGraw-Hill, New York, 1967.

post-modification under mild and well-controlled conditions.[15,16] In the first attempt to obtain a functional ink allowing printing materials with epoxy functionalisation, a mixture of 90% w/w of GMA and 10% w/w of a commercially available 3DP ink (ELEGOO translucent LCD UV-Curing) was assayed. The mixture was polymerised by pouring the monomeric mixture into a mold and exposition to irradiation at 370 nm, using different amounts of phenylbis(2,4,6-trimethylbenzoyl)phosphine) oxide (BAPO) as the photoinitiator (Table SI.1). Suitable polymeric discs functionalised with epoxy groups were obtained in only two minutes (Figure 1). The polymeric discs were exposed to different organic solvents for one hour to evaluate their degree of swelling and stability. The degree of swelling in different solvents can provide an indication of crosslinked nature of the polymer.[17] Eight different solvents were tested (Table SI.2). The discs only showed a significant swelling (251.1 %, Table SI.2) in CH_2Cl_2, while they did not swell neither in polar solvents as water and MeOH nor in apolar solvents such toluene or hexane. DMF swelled the disc at a moderate extend (72.1%). The high swelling in CH_2Cl_2 can be related with a low crosslinking degree provided by the commercial ink. This high swelling in CH_2Cl_2 affected the structure of the disc and when after submerged during a prolonged time, the disc mechanical integrity was compromised. However, this effect was not observed for the other solvents, maintaining the discs their mechanical stability. It should be noted that a high degree of swelling is not recommendable for 3D structures obtained by 3DP for the applications

[15] Kalal, J.; Švec, F.; Maroušek, V. Reactions of Epoxide Groups of Glycidyl Methacrylate Copolymers. *J. polym. sci., Polym. symp.* **1974**, *47* (1), 155–166.
[16] Muzammil, E. M.; Khan, A.; Stuparu, M. C. Post-Polymerization Modification Reactions of Poly(Glycidyl Methacrylate)s. *RSC Adv.* **2017**, *7* (88), 55874–55884.
[17] Sherrington, D. C. Preparation, Structure and Morphology of Polymer Supports. *Chem. Commun.* **1998**, No. 21, 2275–2286.

considered here, as they will experiment significant volume changes, which are not optimal for the flow applications aimed.[18]

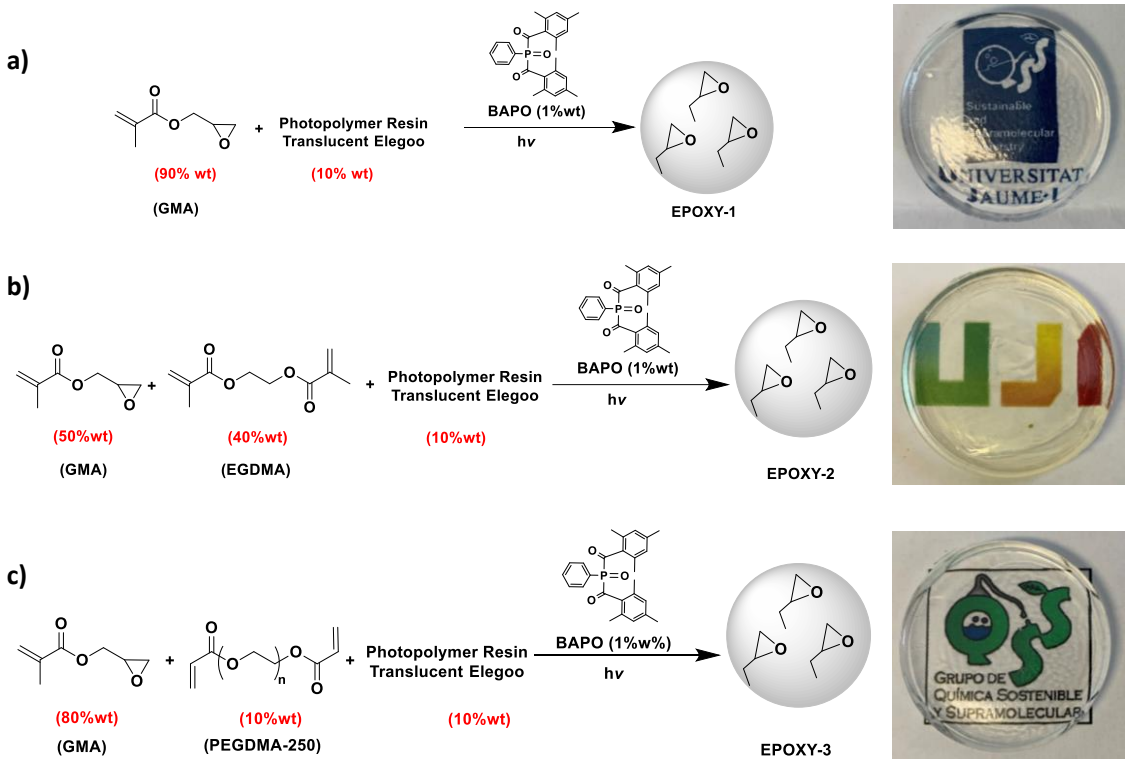

Figure. 1. Optimised compositions for the epoxy functionalised inks photopolymerizable at 370 nm using a 36 W UV lamp and pictures of the resulting polymeric discs.

The presence of an additional crosslinker should help to increase the mechanical stability of the disc and reduce the swelling of the polymer. Thus, different polymerisation mixtures containing a fixed amount of commercially available 3DP ink (10% w/w), different ratios of GMA and an additional crosslinking agent were assayed. Poly(ethylene glycol) dimethacrylate with an average M_n of 250 (PEGDMA-250) and ethylene

[18] Sans, V.; Karbass, N.; Burguete, M. I.; García-Verdugo, E.; Luis, S. V. Residence Time Distribution, a Simple Tool to Understand the Behaviour of Polymeric Mini-Flow Reactors. *RSC Adv.* **2012**, *2* (23), 8721–8728.

glycol dimethacrylate (EGDMA) were used as additional crosslinkers. The different mixtures assayed are summarised in Table SI.3 and Table SI.4. The degree of swelling in CH_2Cl_2 was selected as the reference to evaluate the effect of the different composition. In general, the polymeric discs prepared with PEGDMA-250 were slightly more elastic, due to the more flexible nature if this crosslinker. Figure 1 summarises the weight composition of the monomeric mixtures leading to polymer discs with low degree of swelling and good mechanical stability (Entry 7 of Table SI.3 and Entry 4 of Table SI.4).

Having demonstrated that these polymerisation mixtures can lead to mechanically stables epoxy functionalized polymeric disc, these formulations were printed into various 3D geometries. The initial attempt allowed the successful preparation of a simple 10 mm-tall square (30 x 30 mm) using a LED display photocuring 3D printing device. The printing parameters were set with an exposure time of 60 s per layer, irradiation of UV integrated light at 405 nm and 50 μm layer thickness. Optical images of the fabricated 3DP structures are depicted in Figure SI.1. The word "SILLPs" (Supported Ionic Liquid-like Phase) was also 3D printed with the monomeric ink composition used for the preparation of the discs **EPOXY-1** and **EPOXY-2** (Figure 2). To obtain objects with good definition, the exposure time per layer was increased to 120 s. The preparation of these simple 3D structures opens the possibility of the preparation of more challenging hierarchical 3DP objects.

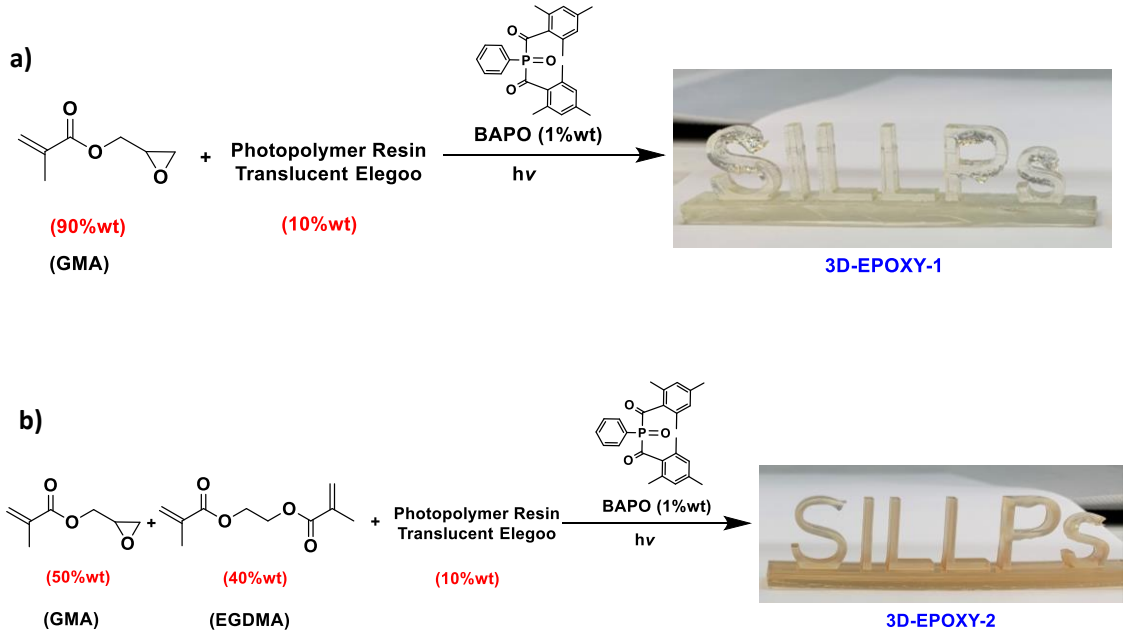

Figure **2**. Images of the word "SILLPs" obtained by 3DP using the optimised inks **EPOXY-1** and **EPOXY-2**. Exposure time: 120 s. Total printing time: 13 h 35 min.

Synthesis and characterisation of the Supported Ionic Liquid-Like Phases

The selection of the word "SILLPs" was not random. It has been demonstrated that in order to overcome some common drawbacks associated to the application of ILs in different processes (high cost, complex separations, some (eco)toxicological concerns, etc) the covalent functionalization of solid polymeric surfaces with IL-like moieties, the so-called Supported Ionic Liquid-like Phases (SILLPs), provides a suitable alternative. These materials maintain the main features of molecular ILs

(stability, tuneable polarity, hierarchical nanostructure, etc.).[19,20,21] Besides, the crosslinked polymeric backbones offer an additional design vector to optimize their macroscopic properties for a given process.[22] SILLPs have advantages when applied as "*self-organized solid ionic solvents*" for catalytic processes as they provide similar features than bulk ILs but simplify product isolation and recycling of the catalyst-IL-phase as well as eliminate (eco)toxicological concerns. In a similar way to liquid IL-phases, SILLPs can be also used to fine-tune the catalyst performance assisting the activation of the catalyst, generating novel catalytic species, improving catalyst stability, and influencing the selectivity. SILLPs have been applied with a wide range of catalysts including metal NPs,[23] photocatalysts,[24]

[19] Sans, V.; Karbass, N.; Burguete, M. I.; Compañ, V.; García-Verdugo, E.; Luis, S. V.; Pawlak, M. Polymer-Supported Ionic-Liquid-Like Phases (SILLPs): Transferring Ionic Liquid Properties to Polymeric Matrices. *Chem. Eur. J.* **2011**, *17* (6), 1894–1906.

[20] Karbass, N.; Sans, V.; Garcia-Verdugo, E.; Burguete, M. I.; Luis, S. V. Pd(0) Supported onto Monolithic Polymers Containing IL-like Moieties. Continuous Flow Catalysis for the Heck Reaction in near-Critical EtOH. *Chem. Commun.* **2006**, No. 29, 3095–3097.

[21] Burguete, M. I.; Galindo, F.; García-Verdugo, E.; Karbass, N.; Luis, S. V. Polymer Supported Ionic Liquid Phases (SILPs) versus Ionic Liquids (ILs): How much do they look alike. *Chem. Commun.* **2007**, No. 29, 3086–3088.

[22] Giacalone, F.; Gruttadauria, M. Covalently Supported Ionic Liquid Phases: An Advanced Class of Recyclable Catalytic Systems. *ChemCatChem.* **2016**, *8* (4), 664–684.

[23] (a) Burguete, M. I.; García-Verdugo, E.; Luis, S. V.; Restrepo, J. A. Preparation of Polymer-Supported Gold Nanoparticles Based on Resins Containing Ionic Liquid-like Fragments: Easy Control of Size and Stability. *Phys. Chem. Chem. Phys.* **2011**, *13* (33), 14831–14838. (b) Restrepo, J.; Lozano, P.; Burguete, M. I.; García-Verdugo, E.; Luis, S. V. Gold Nanoparticles Immobilized onto Supported Ionic Liquid-like Phases for Microwave Phenylethanol Oxidation in Water. *Catal. Today.* **2015**, *255*, 97–101. (c) Restrepo, J.; Porcar, R.; Lozano, P.; Burguete, M. I.; García-Verdugo, E.; Luis, S. V. Microwave-Assisted Selective Oxidation of 1-Phenyl Ethanol in Water Catalyzed by Metal Nanoparticles Immobilized onto Supported Ionic Liquid-like Phases. *ACS Catal.* **2015**, *5* (8), 4743–4750.

[24] Burguete, M. I.; Gavara, R.; Galindo, F.; Luis, S. V. New Polymer-Supported Photocatalyst with Improved Compatibility with Polar Solvents. Synthetic Application Using Solar Light as Energy Source. *Catal. Commun.* **2010**, *11* (13), 1081–1084.

organometallic catalysts,[25] biocatalysts,[26] and organocatalysts.[27] SILLP-based applications facilitate using columnar reactors under continuous flow conditions, compatible with the use of scFs as solvents.[28] They have the potential of developing multifunctional SILLPs[29] and SILLP-cocktails.[30]

A new family of SILLPs can be prepared by chemical post-modification of epoxy resins obtained either as discs or as 3DP polymeric objects. The modification was carried out through the nucleophilic ring opening of the epoxides in presence of the chloride salt of different N-alkyl-imidazole allowing for the simple introduction of a variety of IL-like moieties (Figure 3).[31] The modification was performed with methyl-, butyl-, octyl- and 1-decyl-2-methyl- imidazole.

[25] (a) Burguete, M. I.; García-Verdugo, E.; Garcia-Villar, I.; Gelat, F.; Licence, P.; Luis, S. V.; Sans, V. Pd Catalysts Immobilized onto Gel-Supported Ionic Liquid-like Phases (g-SILLPs): A Remarkable Effect of the Nature of the Support. *J. Catal.* **2010**, *269* (1), 150–160. (b) Gil, W.; Boczoń, K.; Trzeciak, A. M.; Ziółkowski, J. J.; Garcia-Verdugo, E.; Luis, S. V.; Sans, V. Supported N-Heterocyclic Carbene Rhodium Complexes as Highly Selective Hydroformylation Catalysts. *J. Mol. Catal. A: Chem.* **2009**, *309* (1), 131–136.

[26] (a) Lozano, P.; García-Verdugo, E.; Karbass, N.; Montague, K.; Diego, T. D.; Burguete, M. I.; Luis, S. V. Supported Ionic Liquid-Like Phases (SILLPs) for Enzymatic Processes: Continuous KR and DKR in SILLP–$ScCO_2$ Systems. *Green Chem.* **2010**, *12* (10), 1803–1810. (b) Lozano, P.; García-Verdugo, E.; Bernal, J. M.; Izquierdo, D. F.; Burguete, M. I.; Sánchez-Gómez, G.; Luis, S. V. Immobilised Lipase on Structured Supports Containing Covalently Attached Ionic Liquids for the Continuous Synthesis of Biodiesel in $ScCO_2$. *ChemSusChem.* **2012**, *5* (4), 790–798.

[27] (a) Burguete, M. I.; Erythropel, H.; Garcia-Verdugo, E.; Luis, S. V.; Sans, V. Base Supported Ionic Liquid-like Phases as Catalysts for the Batch and Continuous-Flow Henry Reaction. *Green Chem.* **2008**, *10* (4), 401–407. (b) Martín, S.; Porcar, R.; Peris, E.; Burguete, M. I.; García-Verdugo, E.; Luis, S. V. Supported Ionic Liquid-like Phases as Organocatalysts for the Solvent-Free Cyanosilylation of Carbonyl Compounds: From Batch to Continuous Flow Process. *Green Chem.* **2014**, *16* (3), 1639–1647.

[28] García-Verdugo, E.; Altava, B.; Burguete, M. I.; Lozano, P.; Luis, S. V. Ionic Liquids and Continuous Flow Processes: A Good Marriage to Design Sustainable Processes. *Green Chem.* **2015**, *17* (5), 2693–2713.

[29] Montolio, S.; Vicent, C.; Aseyev, V.; Alfonso, I.; Burguete, M. I.; Tenhu, H.; García-Verdugo, E.; Luis, S. V. AuNP–Polymeric Ionic Liquid Composite Multicatalytic Nanoreactors for One-Pot Cascade Reactions. *ACS Catal.* **2016**, *6* (10), 7230–7237.

[30] Sans, V.; Gelat, F.; Karbass, N.; Burguete, M. I.; García-Verdugo, E.; Luis, S. V. Polymer Cocktail: A Multitask Supported Ionic Liquid-Like Species to Facilitate Multiple and Consecutive C-C Coupling Reactions. *Adv. Synth. Catal.* **2010**, *352* (17), 3013–3021.

[31] Zhu, T.; Bi, W.; Row, K. H. A New Ionic Liquids-Based Monolithic Column for Determination of Caffeine and Theophylline. *J. Appl. Polym. Sci.* **2010**, *118* (6), 3425–3430.

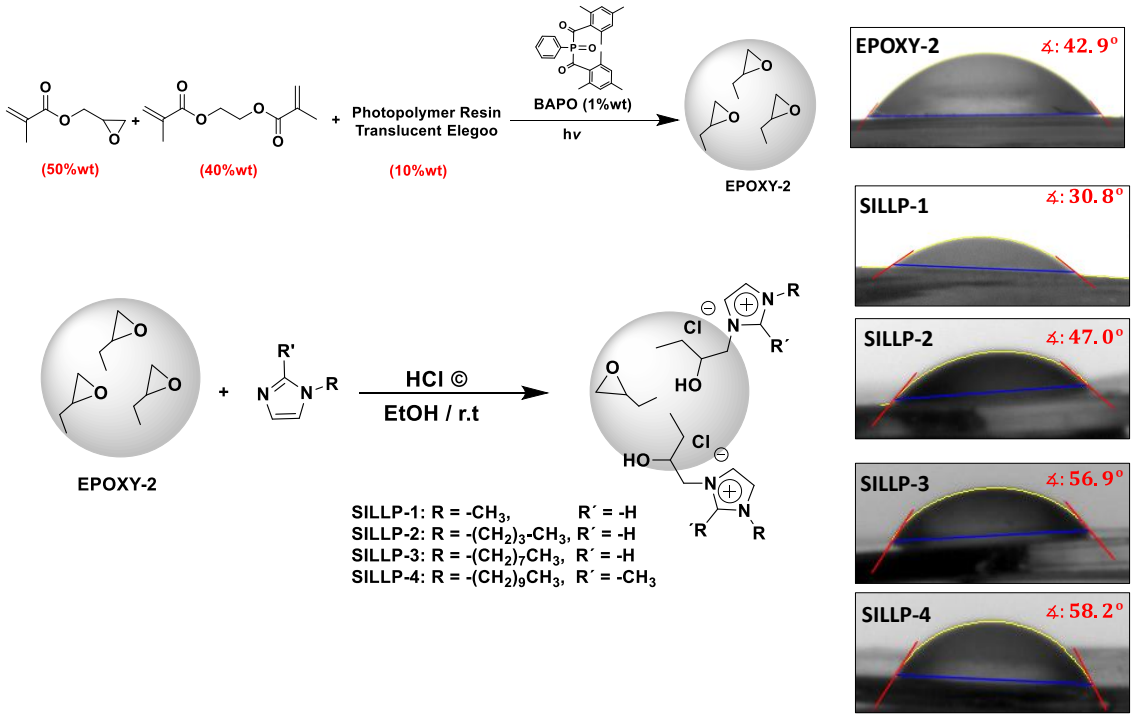

Figure 3. Preparation of SILLP-modified discs using different *N*-alkyl-imidazoles (**SILLP-1-SILLP-4**). The pictures show the water contact angle (WCA) of the modified discs.

The modification could be easily monitored by FT-IR-ATR. Figure SI.2 shows the spectra of the polymer before and after the chemical functionalisation. The first sign of a successful modification is the appearance of the peak associated with OH stretching at 3273 cm^{-1}, indicative of the aperture of the epoxy ring (Figure SI.2a). The ring opening was also confirmed by the almost complete disappearance of the peak at 905 cm^{-1} assignable to the C-O stretching in the epoxide (Figure SI.2b). The spectra also showed the presence of new peaks related to the imidazolium moiety at 3146 and 3111 cm^{-1} assigned to C_2–H stretching (low frequency component) and $C_{4,5}$–H stretching (high frequency component) together with signals at 1584 cm^{-1} and 1551 cm^{-1} (C=N ring stretching), 907 cm^{-1} (C–

C stretching) and at 700, 659 and 624 cm^{-1} (out-of-plane ring vibrations) (Figure SI.2).[32]

It should be noted that the penetration depth in the sample for FT-IR ATR experiments is typically between 0.5 and 2 μm, with the exact value determined by the wavelength of the light, the angle of incidence and the refraction indices of the ATR crystal and the medium being probed.[33] Thus, the data obtained from ATR spectroscopy only provided information about the modification of the surface.

To identify the extension of the surface modification, Raman confocal microscopy analyses of the samples were performed. This technique allows mapping the composition of the polymer with a penetration depth of *ca*. 200 μm. Figure 3 shows the mapping obtained for the disc **EPOXY-2** and the SILLP material prepared by its modification with butyl imidazole (**SILLP-1**) using different penetrations for the incident laser light. The Raman of the **EPOXY-2** ring reveals the presence of a single component on the entire depth evaluated. This main component, as expected, corresponds to the epoxy resin, with peaks at 1729 cm^{-1} (C=O) characteristic of the ester group of the acrylic monomers and at 1261 cm^{-1} and 911 cm^{-1} assignable to the epoxy groups (asymmetric and symmetric stretching respectively). However, the mapping of **SILLP-1** clearly shows the presence of two different and spatially separated components (Figure 4b).

[32] Paschoal, V. H.; Faria, L. F. O.; Ribeiro, M. C. C. Vibrational Spectroscopy of Ionic Liquids. *Chem. Rev.* **2017**, *117* (10), 7053–7112.
[33] Mirabella, F. M. *Internal Reflection Spectroscopy: Theory and Applications*; Marcel Dekker: New York, 1993.

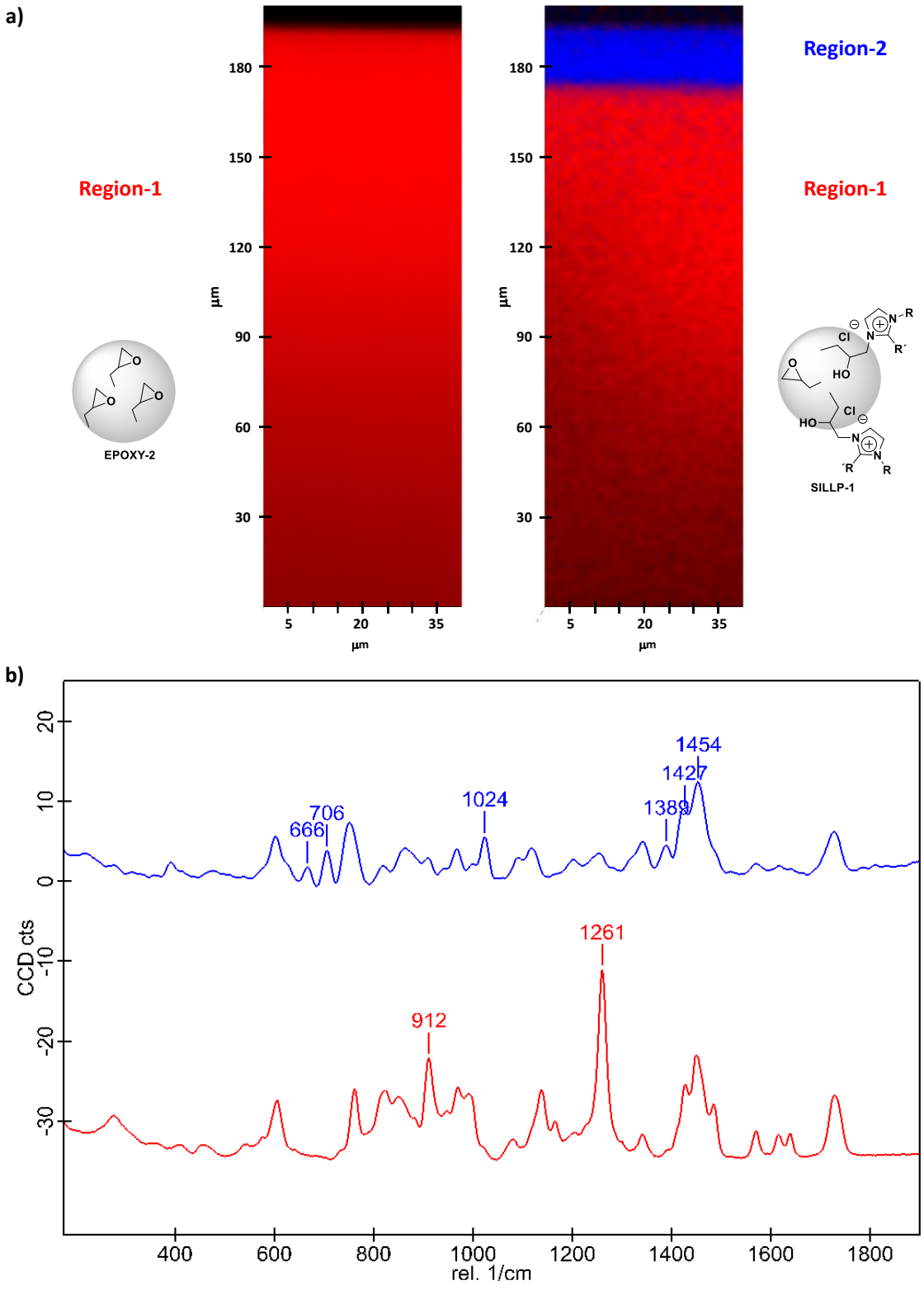

Figure 4. Raman confocal microscopy study of **EPOXY-2** and **SILLP-1** discs (excitation wavelength: 532 nm, laser power: 2.9 mW, objective magnification: 50x). a) Mapping for the initial 200 mm depth of the disc: black region corresponds to air, the blue region corresponds to the surface modification with imidazolium units, the red region corresponds to the unmodified epoxy region. b) Raman spectra corresponding to the blue (top) and red (bottom) regions.

The analysis of the spectra for the first component, which is found in a superficial thin layer of *ca*. 10 μm depth, reveals: i) a strong intensity decrease of the peaks assignable to the epoxy ring at 1261 cm^{-1} and 911 cm^{-1}, ii) the appearance of new peaks at 1025 cm^{-1} (C-H, in plane bending), 707 cm^{-1} and 667 cm^{-1} (C-C, out of plane ring vibrations) assignable to the imidazolium substitution, and iii) a significant change in the of 1500-1300 cm^{-1} region where the C=C and C=N bond stretching bands of imidazolium appear, specially the appearance of a peak at 1389 cm^{-1}.[32] This indicates that in the first layer the opening of the ring epoxy groups with methylimidazole has taken place. The second component matches with the single component found for the **EPOXY-2** resin. Hence, under the experimental conditions assayed, a superficial modification of *ca* 10 μm depth is achieved, which also explains the low loading of imidazolium units found by elemental analysis (Table 1).

The modification of the surface was also confirmed by performing water contact angle measurements (WCA, Figure 3), as the wettability of a solid surface changes with the chemical composition of the IL moieties attached to the solid surfaces.[34,35,36,37,38]

[34] Dong, Y.; Li, J.; Shi, L.; Wang, X.; Guo, Z.; Liu, W. Underwater Superoleophobic Graphene Oxide Coated Meshes for the Separation of Oil and Water. *Chem. Commun.* **2014**, *50* (42), 5586–5589.

[35] Zhao, Y.; Li, M.; Lu, Q. Tunable Wettability of Polyimide Films Based on Electrostatic Self-Assembly of Ionic Liquids. *Langmuir* **2008**, *24* (8), 3937–3943.

[36] (a) Lee, B.-S.; Lee, S.-G. Synthesis of Thiol-Functionalized Ionic Liquids and Formation of Self-Assembled Monolayer on Gold Surfaces: Effects of Alkyl Group and Anion on the Surface Wettability. *Bull. Korean Chem. Soc.* **2004**, *25* (10), 1531–1537. (b) Lee, B. S.; Chi, Y. S.; Lee, J. K.; Choi, I. S.; Song, C. E.; Namgoong, S. K.; Lee, S. Imidazolium Ion-Terminated Self-Assembled Monolayers on Au: Effects of Counteranions on Surface Wettability. *J. Am. Chem. Soc.* **2004**, *126* (2), 480–481.

[37] He, X.; Yang, W.; Pei, X. Preparation, Characterization, and Tunable Wettability of Poly(Ionic Liquid) Brushes via Surface-Initiated Atom Transfer Radical Polymerization. *Macromolecules.* **2008**, *41* (13), 4615–4621.

[38] Xin, B.; Hao, J. Superhydrophobic Self-Assembled Monolayers of Long-Chain Fluorinated Imidazolium Ionic Liquids. *RSC Adv.* **2012**, *2* (12), 5141–5146.

The resin **EPOXY-2** showed a WCA of 42.1º, which changed upon the modification with the corresponding alkyl imidazole. In the case of methyl imidazole, the WCA value was reduced in comparison with the unmodified epoxy polymer (from 42.1º to 30.8º) due to the introduction of more hydrophilic groups (OH and methylimidazolium chloride). However, the modification with more hydrophobic imidazoles, having longer alkyl chains, led to an increase of the WCA (47.0º, 56.9º and 58.2º for **SILLP-2**, **SILLP-3** and **SILLP-4**, respectively). This indicates that upon modification of the surface, the aliphatic chains are oriented towards the polymer/air interface. The WCA values are in good agreement with the wettability found for Au surfaces coated with monolayers of thiol-functionalized ILs.[39] These results not only confirmed the modification of the surface, but also that the nature of the N-alkyl-imidazole involved can be used to modulate the hydrophilicity/hydrophobicity of the surface. Noteworthy, the same modification methodology was also suitable for the introduction of N-alkyl-imidazolium moieties onto the surface of 3D objects obtained by 3D Printing.

Catalytic evaluation

The modified discs were tested as heterogeneous catalysts for the reaction between styrene oxide and CO_2 (Scheme 1). An initial catalytic screening was carried out by submerging **EPOXY-2** and **SILLPs 1-4** in styrene oxide and pressurising the reaction mixture at 10 bar and 100 ºC. The results obtained are summarised in Table 1. The reaction did not take place in the presence of the unmodified epoxy material (Entry 1, Table 1). Thus, the activity can be attributed to the presence of the imidazolium chloride

[39] Shen, Y.; Zhang, Y.; Zhang, Q.; Niu, L.; You, T.; Ivaska, A. Immobilization of Ionic Liquid with Polyelectrolyte as Carrier. *Chem. Commun.* **2005**, No. 33, 4193–4195.

fragments. All the supported salts provided an appreciable degree of conversion, with excellent selectivity (> 99%). Only in the case of the material functionalised with methylimidazole, the conversion degree was slightly lower (Entry 2, Table 1). In this case, the results were comparable with those for the analogous methylimidazole-derived SILLP prepared from a PS-DVD gel-type resin. The PS-DVB-SILLP provided a 39% conversion corresponding with a TON of 78, while the TON for the disc **SILLP-1** was 64.

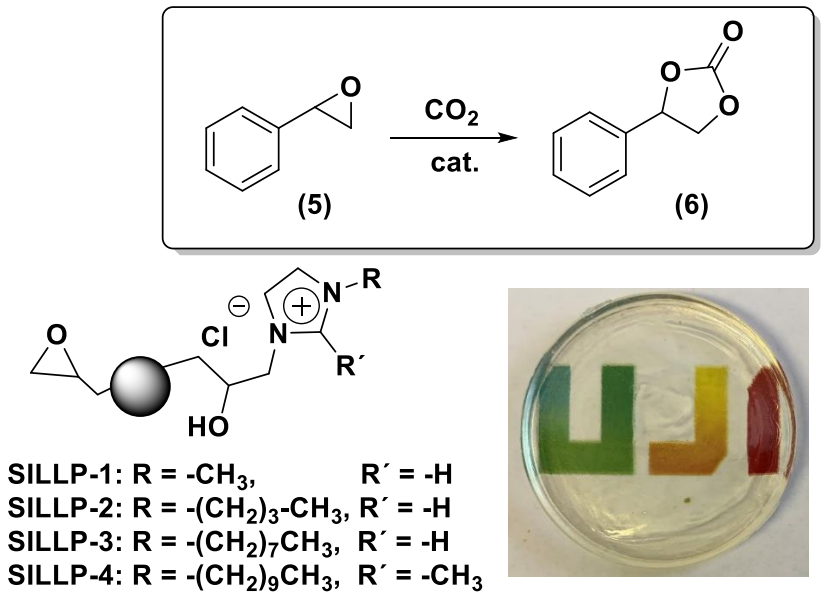

Scheme 1. Cycloaddition reaction of CO_2 to styrene epoxide catalyzed by SILLPs obtained by post-modification the **EPOXY-2** disc.

The conversion to carbonate increased with the length of the alkyl chain, with TON values following the order $C_8 > C_4 > C_1$. This trend has been reported in the literature for ILs in the liquid phase, where the reactivity for N-alkyl-methylimidazole follows the trend $C_8 > C_6 > C_4 > C_2$.[40] A similar

[40] Kawanami, H.; Sasaki, A.; Matsui, K.; Ikushima, Y. A Rapid and Effective Synthesis of Propylene Carbonate Using a Supercritical CO_2–Ionic Liquid System. *Chem. Commun.* **2003**, No. 7, 896–897.

trend has also been reported for the case of porous poly(ionic liquid)s, which were obtained by co-polymerisation of divinylbenzene and vinylimidazole followed by an alkylation step, where the catalyst's activity of the porous system increased for longer alkyl chains.[41] It is worth mentioning that the results obtained for the modified discs deviate from those observed for the case of PS-DVB-derived SILLPs and containing Rose Bengal,[42] for which the introduction of hydrophobic chains reduced the activity.

Table 1. Screening of SILLPs obtained by post-functionalisation of **EPOXY-2** discs as catalysts in the reaction between styrene oxide (**5**) and CO_2 to afford styrene carbonate (**6**).[a]

Entry	SILLP	IL Loading[b] [mmol g^{-1}]	TON	R	R´	Conv.[c] [%]
1	**EPOXY-2**	-	-	-	-	0
2	**SILLP-1**	0.076	64	CH_3	H	56
3	**SILLP-2**	0.088	75	$CH_3(CH_2)_3$	H	91
4	**SILLP-3**	0.091	88	$CH_3(CH_2)_7$	H	80
5	**SILLP-4**	0.071	106	$CH_3(CH_2)_9$	CH_3	86

[a] solventless, 12 h, 100 ^oC, 10 bar CO_2, 1 mL epoxide, 1.0 g cat. approx. [b] Imidazolium unit loading calculated by elemental analysis. [c] Calculated by ^{1}H-NMR. Selectivity > 99.9%.

[41] Dani, A.; Groppo, E.; Barolo, C.; Vitillo, J. G.; Bordiga, S. Design of High Surface Area Poly(Ionic Liquid)s to Convert Carbon Dioxide into Ethylene Carbonate. *J. Mater. Chem. A* **2015**, *3* (16), 8508–8518.

[42] See chapter VII. Multifunctional polymers based on ionic liquid and Rose Bengal fragments for the conversion of CO_2 to carbonates.

Integration onto flow devices

The former initial catalytic screening demonstrated the suitability of this methodology to transfer to the materials obtained by photo-polymerisation and post-modification the properties of the ILs at molecular level. The next step was to exploit the additive manufacturing techniques to develop devices allowing to integrate these systems for continuous flow application. 3DP allows the manufacture of polymeric devices with a total freedom of design. Hence, two simple monolithic structures based on the developed epoxy ink were designed and obtained. These structures could be accommodated in a commercially available Omnifit™ column (L: 15cm, Ø: 1.0cm) enabling their use under flow conditions (Figure 5c). Figure 5a and Figure SI.3 depict the two simple designs assayed. The design 1 (**3D-EPOXY-D1**) presents a square channel structure parallel to the long axis of the monolith. The design 2 (**3D-EPOXY-D2**) is identical to the design 1, with a network of square pores, but any layer of the structure is moved 90 degree with respect to the previous one. This renders a more intricate design in comparison with **3D-EPOXY-D1**. The two monolithic designs were obtained without any obvious defects or inhomogeneity (Figure 5b and 5c) by 3DP. After washed with isopropanol and cured in the oven for 24 h at 60 ^{o}C, the corresponding SILLPs were obtained by surface modification with butyl imidazolium units leading to **3D-SILLP-D1** and **3D-SILLP-D2**.

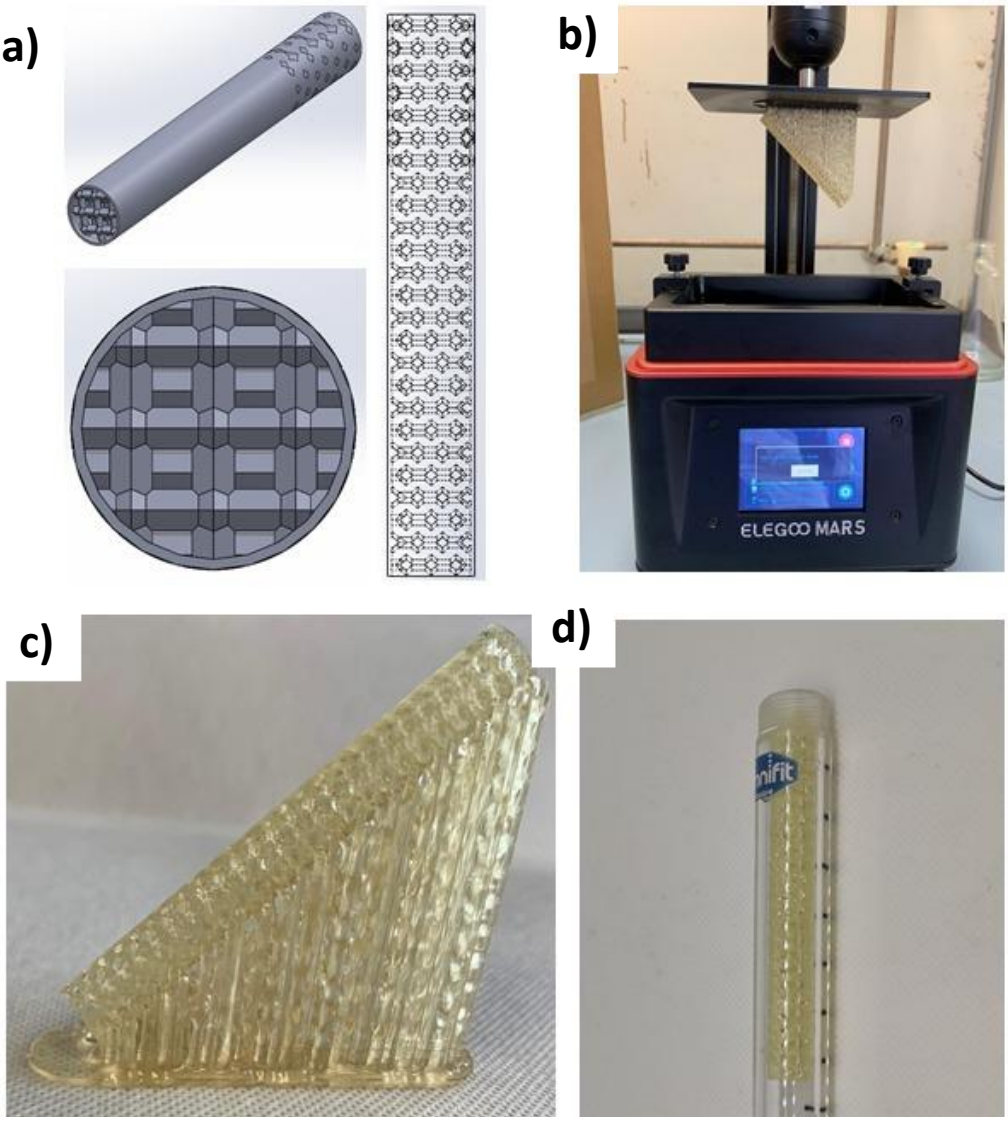

Figure 5. a) Computer-aided design (SolidWorks or CAD) monolith for **3D-EPOXY-2** with key geometric parameters being L (length) = 750 mm, W (with) = 90 mm, V (internal volume) = 3.44 mL for **3D-SILLP-D1** and 5.1 mL for **3D-SILLP-D2**. b) 3D object obtained by MARS 3D PRINTER, ELEGOO. c) 3D object monolithic column plus supporting polymerisation pillars after washing with isopropyl alcohol and curing at 60 ^{o}C for 24 h. **(d)** Omnifit™ column (L:15cm, Ø:1.0cm) holding the **3D-SILLP-D1/D2** for its application under flow conditions.

A continuous flow set-up was built as illustrated in Figure 6. Two pumps were used to deliver CO_2 and the epoxide to a mixer, forming a homogeneous mixture that then passes through a preheater to reach the reaction temperature before entering in contact with the supported catalyst. The reaction was performed using an oven temperature of 150 ^{o}C

but only modest pressure (20 bar) taking into the account the pressure limitation of the glass Omnifit reactor holder. Results were rather different depending of the monolithic design. Thus, the monolith **3D-SILLP-D1** provided a conversion of *ca*. 38%, while this value was increased to *ca*. 60% conversion for **3D-SILLP-D1**. It should be mentioned that both systems showed a remarkable stability without any activity deterioration, under flow conditions, during at least 5 days of continuous use.

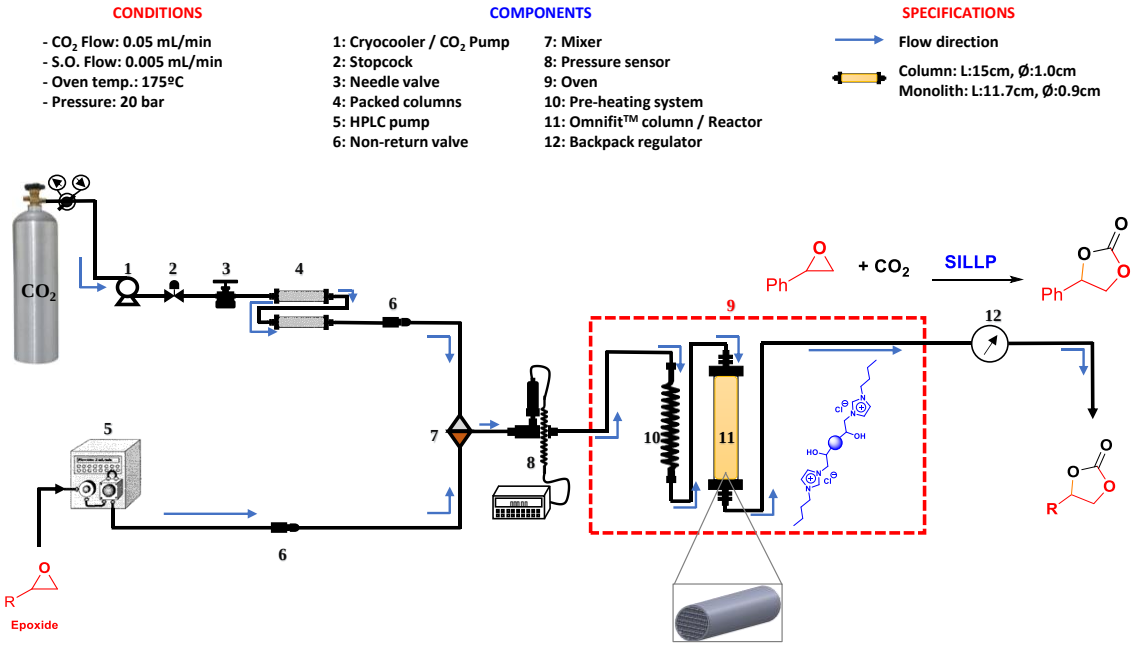

Figure 6. Schematic representation of the set-up for the continuous flow reactor.

The performance of the reactors was normalised taking into the account the catalyst loading, considering imidazolium unit as the active moiety, and the reactor volume. The productivity *vs* time on stream calculated in this way (Figure 7, g_{prod} mol_{im}^{-1} mL^{-1} h^{-1}) shows that, under the conditions employed, the performance can be significantly improved as a function of the monolith design.

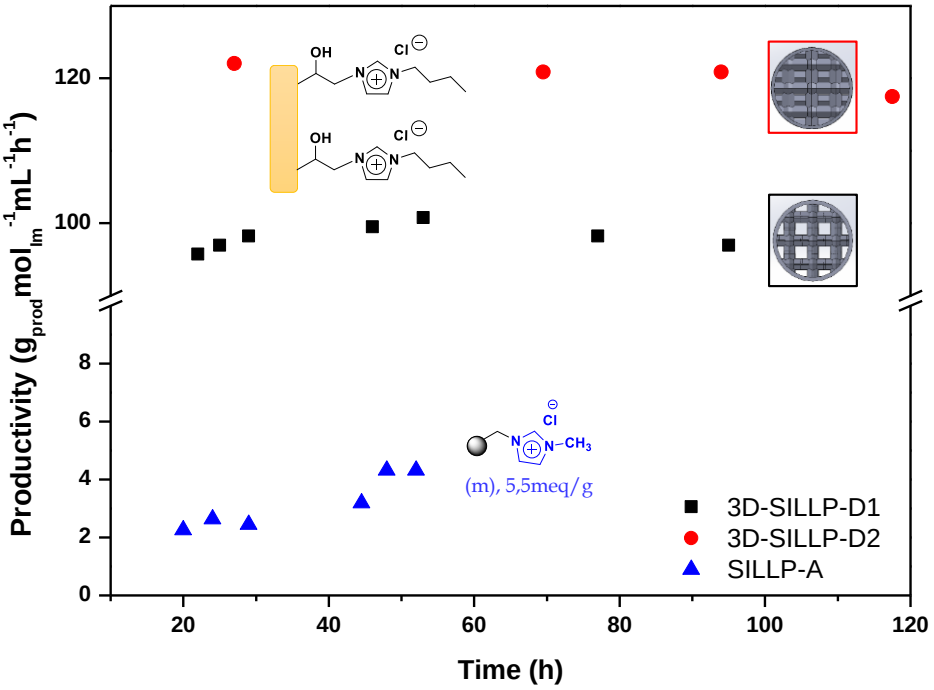

Figure 7. Productivity *vs* time on stream obtained for the continuous flow reaction between styrene oxide and CO_2 at 175 °C and 20 bars. Blue triangles: two coupled reactors filled with polymeric beads of **SILLP-A** (1.892 g). Black squares: **3D-SILLP-D1** (6.221g with 3.44 mL free volume). Red dots: **3D-SILLP-D2** (4.4503 g with 5.31 mL free volume). Conversion calculated by ^{1}H-NMR. Selectivity > 99%.

3D-SILLP-D2 achieved the highest conversions and productivity per imidazolium unit and reactor volume (*ca.* 120 *vs* 98 g of product · mol of imidazole^{-1} · mL^{-1} · h^{-1} for **3D-SILLP-D2** and **3D-SILLP-D1**, respectively). This can be explained for the more intricate design structure of **3D-SILLP-D2**. The design of **3D-SILLP-D2** is likely to provide enhanced fluid dynamics and distribution of the gas and liquid phases facilitating the contact with the catalytic surfaces and leading to the enhanced productivity in comparison with the **3D-SILLP-D1** with simpler fluid dynamics. Noteworthy, the systems based on the monolithic reactors prepared by 3DP provided an impressive improvement in comparison with the equivalent continuous flow system based on a fixed reactor packed with macroporous PS-DVB beads functionalised with methyl-imidazolium moieties (**SILLP-A**), which only yielded a modest productivity of 3.2 g of

product · mol of imidazole^{-1} · mL^{-1} · h^{-1}, even when the reaction was performed at higher pressure (140 bars). This difference can only be attributed to the different flow patterns defined by the reactor, as much as the results under batch conditions were very similar.

8.3. Conclusions

We have demonstrated that 3DP manufacturing can be efficiently used as an *enabler* to integrate different facilitating technologies such as solid phase supported catalysis, flow chemistry and ILs. The preparation and optimisation of an epoxy functionalised ink allowed the preparation of 3D objects. The surface of these objects was post-functionalised with IL-like units transferring the catalytic properties to the surface of these 3D objects. The great design freedom provided by this additive manufacturing technology was exploited to design continuous flow reactors with high stability (up to 5 days) and with enhanced activity profiles (up to three orders of magnitude) in comparison with conventional systems. The easy implementation and modification of the reactor design can be used as an essential element for the optimization of the catalytic processes under study.

8.4. Experimental Section

Materials

All reagents and solvents used were commercially available: Glycidyl methacrylate (97%, Aldrich), poly(ethylene glycol) dimethacrylate (97%, Aldrich), ethylene glycol dimethacrylate (98%, Aldrich), phenyl-bis-(2,4,6-

trimethylbenzoyl)phosphine oxide (97%, Aldrich), 1-methylimidazole (98%, Aldrich), 1-butylimidazole (98%, Aldrich), 1-octylimidazole (98%, Aldrich), 1-decyl-2-methylimidazole (97%, Aldrich), hydrochloric acid (37%, Scharlab), ink (ELEGOO translucent LCD UV-Curing), styrene oxide (97%, Aldrich). All the solvents were used as received from Scharlab.

General characterization protocols

^{1}H and ^{13}C NMR experiments were carried out using a Bruker Avance III HD 300 or 400 spectrometer (300 or 400 MHz for ^{1}H and 125 or 100 MHz for ^{13}C). The chemical shifts are given in delta (δ) values, using the residual solvent signal for reference. Fourier Transform Infrared (FT-IR) spectra were acquired with a Pike single-reflection ATR diamond/ZnSe accessory in a JASCO FT/IR-4700 instrument. The Raman spectra were acquired with a *Raman Confocal Microscope apyron (WITec)* with three optical fibers connected to the laser sources to excite the samples (532nm) with long pass filters and two optimized spectrometers, the first for the visible range with an EMCCD ultra-high efficiency detector and the second one optimized for the NIR region with a high efficiency CCD detector and equipped with different Zeiss optical lenses (x10, x20 LD, x50 LD, x100 (LD: long focal length)). Wettability of discs was determined by using a static contact angle goniometer in open air (Phoenix150, Surface Electro Optics).

Synthetic protocols

Synthesis of the Epoxy-1 disc

Phenyl-bis-(2,4,6-trimethylbenzoyl)phosphine oxide (1% w regarding to GMA) was added to glycidyl methacrylate (90% w) and then the commercial translucent

photopolymer resin (10% w) was added to this mixture. The polymerization was carried out by depositing 1.0 mL of the resulting solution into a circular glass mold and exposing the mixture to a 370 nm lamp. After 2 min. a solid disc was obtained that was extracted from the mold and washed with IPA (3 x 5 mL) and cured at 60 ºC for 24 h.

Synthesis of the Epoxy-2 disc

Phenyl-bis-(2,4,6-trimethylbenzoyl)phosphine oxide (1% w regarding to GMA) was added to a mixture of glycidyl methacrylate (50% w) and ethylene glycol dimethacrylate (40% w) and then the commercial translucent photopolymer resin (10% w) was added to this mixture. The polymerization was carried out by depositing 1.0 mL of the resulting solution into a circular glass mold and exposing the mixture to a 370 nm lamp. After 2 min. a solid disc was obtained that was extracted from the mold and washed with IPA (3 x 5 mL) and cured at 60 ºC for 24 h.

Synthesis of the Epoxy-3 disc

Phenyl-bis-(2,4,6-trimethylbenzoyl)phosphine oxide (1% w regarding to GMA) was added to a mixture of glycidyl methacrylate (80% w) and poly(ethylene glycol) dimethacrylate (10% w) and then the commercial translucent photopolymer resin (10% w) was added to this mixture. The polymerization was carried out by depositing 1.0 mL of the resulting solution into a circular glass mold and exposing the mixture to a 370 nm lamp. After 2 min. a solid disc was obtained that was extracted from the mold and washed with IPA (3 x 5 mL) and cured at 60 ºC for 24 h.

Synthesis of SILLP-1-4 discs

A 5.0 mL of solution of chloride salt of corresponding alkyl-imidazole (6.5 mol L^{-1}) was added to the disc. The reaction mixture was maintained with orbital shaking (125 rpm) for 24 h at rt. Finally, the disc was washed with IPA (3 x 5 mL) and dried at 60 ºC for 24 h.

Synthesis of 3DP objects with EPOXY-1 composition

The printer tank was filled with 50.0 mL a monomeric solution containing 90% by weight of glycidyl methacrylate and 10% by weight of the commercial translucent photopolymer ink. This solution contains 1% by weight of the photoinitiator (Phenyl-bis-(2,4,6-trimethylbenzoyl)phosphine oxide) regarding to GMA. The 3D structure was obtained according the digital design downloaded in the printer. Once the 3D structure was printed, the object was extracted from the build platform, washed with IPA (3 x 25 mL) and cured at 60 ºC for 24 h.

Synthesis of 3DP objects with EPOXY-2 composition

The printer tank was filled with 50.0 mL a monomeric solution containing 50% by weight of glycidyl methacrylate, 40% by weight of ethylene glycol dimethacrylate and 10% by weight of the commercial translucent photopolymer ink. This solution contains 1% by weight of the photoinitiator (Phenyl-bis-(2,4,6-trimethylbenzoyl)phosphine oxide) regarding to GMA. The 3D structure was obtained according the digital design downloaded in the printer (cube or letters). Once the 3D structure was printed, the object was extracted from the platform, washed with IPA (3 x 25 mL) and cured at 60 ºC for 24 h.

Printing Parameters of 3DP objects

Cube: 60 s exposure time, 120 s bottom time, 3 h 59 min total printing time.

SILLPs Letters: 120 s exposure time, 120 s bottom time, 13 h 35 min total printing time.

Synthesis of "monolith" 3D-EPOXY-D1 and 3D-EPOXY-D2

The printer tank was filled with 50.0 mL a monomeric solution containing 50% by weight of glycidyl methacrylate, 40% by weight of ethylene glycol dimethacrylate and 10% by weight of the commercial translucent photopolymer ink. This solution contains 1% by weight of the photoinitiator (Phenyl-bis-(2,4,6-trimethylbenzoyl)phosphine oxide) regarding to GMA. The 3D structure was obtained according the digital design downloaded in the printer (**3D-EPXOXY-D1** and **3D-EPXOXY-D2)**. Once the 3D monolithic structure was printed, the object was extracted from the platform, washed with IPA (3 x 25 mL) and cured at 60 ºC for 24 h.

Printing parameters: 120 s exposure time, 120 s bottom time, total printing time: 44 h 38 min.

Synthesis of "monolith" 3D-SILLP-D1 and 3D-SILLP-D2

A solution of the chloride salt of butyl imidazole (6.5 mol L^{-1}) was added to the 3D printed object. The reaction mixture was left in contact with the polymer at room temperature and under orbital shaking (125rpm) for 24 h. Finally, the 3D object was washed with IPA (3 x 25 mL) and dried at 60 ºC for 24 h.

General procedure for the reaction of styrene oxide and CO_2: Batch experiments

For the reactions under pressure, a Verghof R-300 high pressure reactor connected to a pressurized CO_2 source and a back-pressure regulator from Jasco was used. The heater was first brought to the desired temperature (100 ^oC). The reactor was then loaded with styrene oxide (1 mL) and the catalyst (1.0 g aprox.). The reactor was connected to the CO_2 pump and the back-pressure regulator and immersed in the bath. CO_2 was liquefied and pumped into the reactor up to the desired pressure, under stirring. After 12 h, the high-pressure reactor was cooled down and depressurized. Afterwards, the reactor was opened, and the contents collected using 1 mL of deuterated chloroform to dissolve the reaction mixture. The catalyst was separated by decantation. Experimental procedures were replicated for all experiments. The average deviation of styrene carbonate formation was less than 5%.

Continuous flow experiments

Styrene oxide was pumped using a Jasco HPLC pump at a rate of 5 μL min^{-1}. CO_2 was pumped with a refrigerated CO_2 Jasco pump at a flow rate of 50 μL min^{-1}. Once CO_2 and epoxide entered in contact in a mixer, they passed through a preheater and the catalytic reactor(s) maintained in an oven to achieve the required experimental temperature. A Jasco back pressure regulator was connected at the outlet of the reactor to establish the desired pressure. All required connections were made with stainless-steel 1/16-inch coil. The reaction stream of crude product was collected in a cold trap at the outlet of the back-pressure regulator. Samples were taken and analyzed by ^{1}H-NMR spectroscopy to determine the conversion and selectivity of the reaction.

8.5. Supplementary Information

3D Printing as *enabler* of enabling techniques. Stable and more efficient catalytic CO_2 conversion under continuous flow process using printed reactors based on supported ionic liquids

Table of Contents.

Table SI.1. Initial composition of poly-epoxy resins (**EPOXY-1**) and polymerization time[a]

Entry	EPOXY-1	GMA [%]	Photopolymer resin[b] [%]	BAPO[c] [%]	BAPO[d] [%]	Loading[e] [mmol g^{-1}]	Pol. time[f] [min.]
1	A	90	10	1.0	0.9	6.3	2.0
2	B	90	10	0.5	0.4	6.3	5.5
3	C	90	10	5.0	4.5	6.3	3.0

[a] In % w/w. [b] Commercial photopolymer resin Elegoo translucent. [c] Photoinitiator BAPO, w% regarding to glycidyl methacrylate (GMA). [d] % w regarding to the total mix. [e] Theoretical epoxide unit loading. [f] Polymerization time using a UV lamp of 36 W, gel curing, wavelength of highest peak: 370nm. The polymerization time is defined, as the time required the monomeric solution to evolve from a liquid to a solid state. To determine the polymerization time the polymerization mixture was exposed to the light using 30 seconds cycles until verifying that it became completely solid. Once the disc was solid, it was removed from the mold, washed with IPA (3 x 5 mL) and cured for 24 hours at 60 °C.

Table SI.2. Swelling of poly-epoxy disc **EPOXY-1** in different solvents.[a]

Entry	Solvent	Dry Mass [g]	Wet mass [g]	Swelling[b] [%]
1	2-Me-THF	1.0371	1.0319	-0.5[c]
2	DMF	1.0522	1.8105	72.1
3	Styrene oxide	1.0400	1.1475	10.3
4	MeOH	1.1718	1.2040	2.7
5	Hexane	1.0365	1.0377	0.1
6	Toluene	1.0856	1.1205	3.2
7	miliQ® H_2O	1.0574	1.0620	0.4
8	CH_2Cl_2	1.1256	3.9515	251.1

[a] Swelling time: 1 h. [b]. $Swelling = \left(\frac{Wet\ mass - Dry\ mass}{Dry\ mas}\right) \cdot 10^2$. [c] The weight loss is due to partial solubility.

Table SI.3. Composition of poly-epoxy (**EPOXY-2**) using ethylene glycol dimethacrylate (EDGMA) as the crosslinker.[a]

Entry	EPOXY-2	GMA [%]	EDGMA [%]	Photopolymer resin[b] [%]	BAPO[c] [%]	Loading[d] [mmol g^{-1}]	Pol. time[e] [min.]	Swelling[f] [%]
1	A	90	0	10	1	6,3	2	251
2	B	90	10	0	1	6,3	4	140
3	C	85	5	10	1	5,9	2	154
4	D	80	10	10	1	5,6	2	101
5	E	70	20	10	1	4,9	2	12
6	F	60	30	10	1	4,2	2	34
7	G	50	40	10	1	3,5	2	10
8	H	45	45	10	1	3,1	2	8

[a] In % w/w. [b] Commercial photopolymer resin Elegoo. [c] Photoinitiator BAPO, w% regarding to glycidyl methacrylate. [d] Theoretical epoxide unit loading. [e] Polymerization time using a UV lamp of 36 W, gel curing, wavelength of highest peak: 370nm. The polymerization time is defined, as the time required the monomeric solution to evolve from a liquid to a solid state. To determine the polymerization time the polymerization mixture was exposed to the light using 30 seconds cycles until verifying that it became completely solid. Once the disc was solid, it was removed from the mold, washed with IPA (3 x 5mL) and cured for 24 hours at 60 °C. [f] Swelling in CH_2Cl_2. Swelling time: Entry 1: 60 min.; 2-4: 30 min.; 5: 150 min.; 6-8: 1140min. The **EPOXY-2.G** and **EPOXY-2.H** do not break. $Swelling = \left(\frac{Wet\ mass - Dry\ mass}{Dry\ mass}\right) \cdot 10^2$

Table SI.4. Composition of poly-epoxy (**EPOXY-3**) using poly(ethylene glycol) dimethacrylate with average M_n of 250 (PEGDMA-250) as the crosslinker.[a]

Entry	EPOXY-3	GMA [%]	PEGDMA-250 [%]	Photopolymer resin[b] [%]	BAPO[c] [%]	Loading[d] [mmol g^{-1}]	Pol. time[e] [min.]	Swelling[f] [%]
1	A	90	0	10	1	6.3	2	251
2	B	90	10	0	1	6.3	4	218
3	C	85	5	10	1	5.9	4	168
4	D	80	10	10	1	5.6	4	63
5	E	70	20	10	1	4.9	3	134
6	F	60	30	10	1	4.2	2	61
7	G	50	40	10	1	3.5	2	49
8	H	45	45	10	1	3.1	2	20

[a] In % w/w. [b] Commercial photopolymer resin Elegoo. [c] Photoinitiator (BAPO), w% regarding to glycidyl methacrylate. [d] Theoretical epoxide unit loading. [e] Polymerization time using a UV lamp of 36 W, gel curing, wavelength of highest peak: 370nm. The polymerization time is defined, as the time required the monomeric solution to evolve from a liquid to a solid state. To determine the polymerization time the polymerization mixture was exposed to the light using 30 seconds cycles until verifying that it became completely solid. Once the disc was solid, it was removed from the mold, washed with IPA (3 x 5 mL) and cured for 24 hours at 60 °C. [f] Swelling in CH_2Cl_2. Swelling time: Entry 1: 60 min.; 2-5: 30 min.; 6: 120 min.; 7-8: 180min. All the **EPXOY-3** break. $Swelling = \left(\frac{Wet\ mass - Dry\ mass}{Dry\ mass}\right) \cdot 10^2$

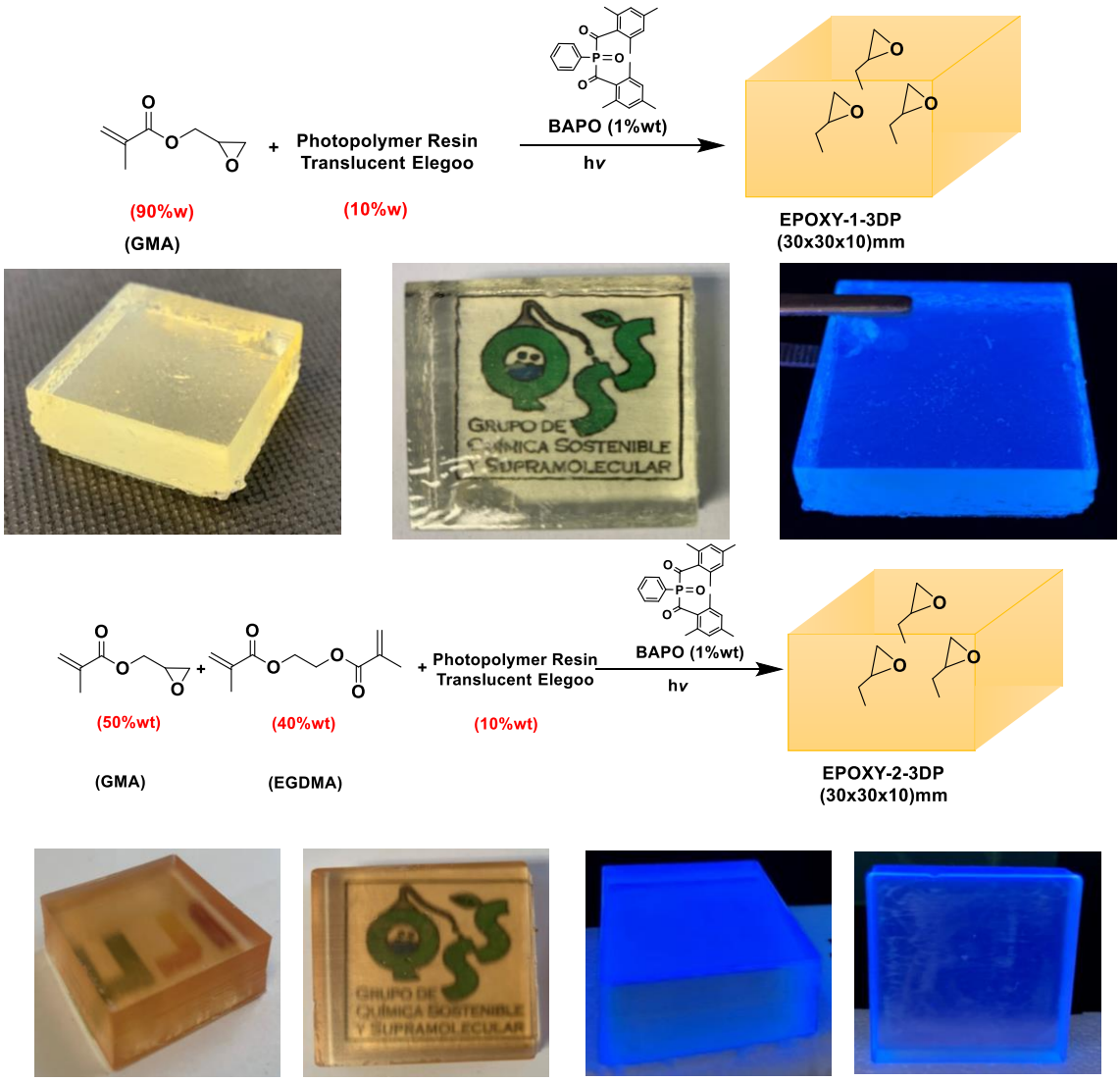

Figure SI.1. Pictures of the EPOXY resins obtained as 3D square objects by 3D printing. Top: Exposure time: 60 s. Bottom Exposure time: 120 s. Total printing time: 3 h 59 min. 33 s.

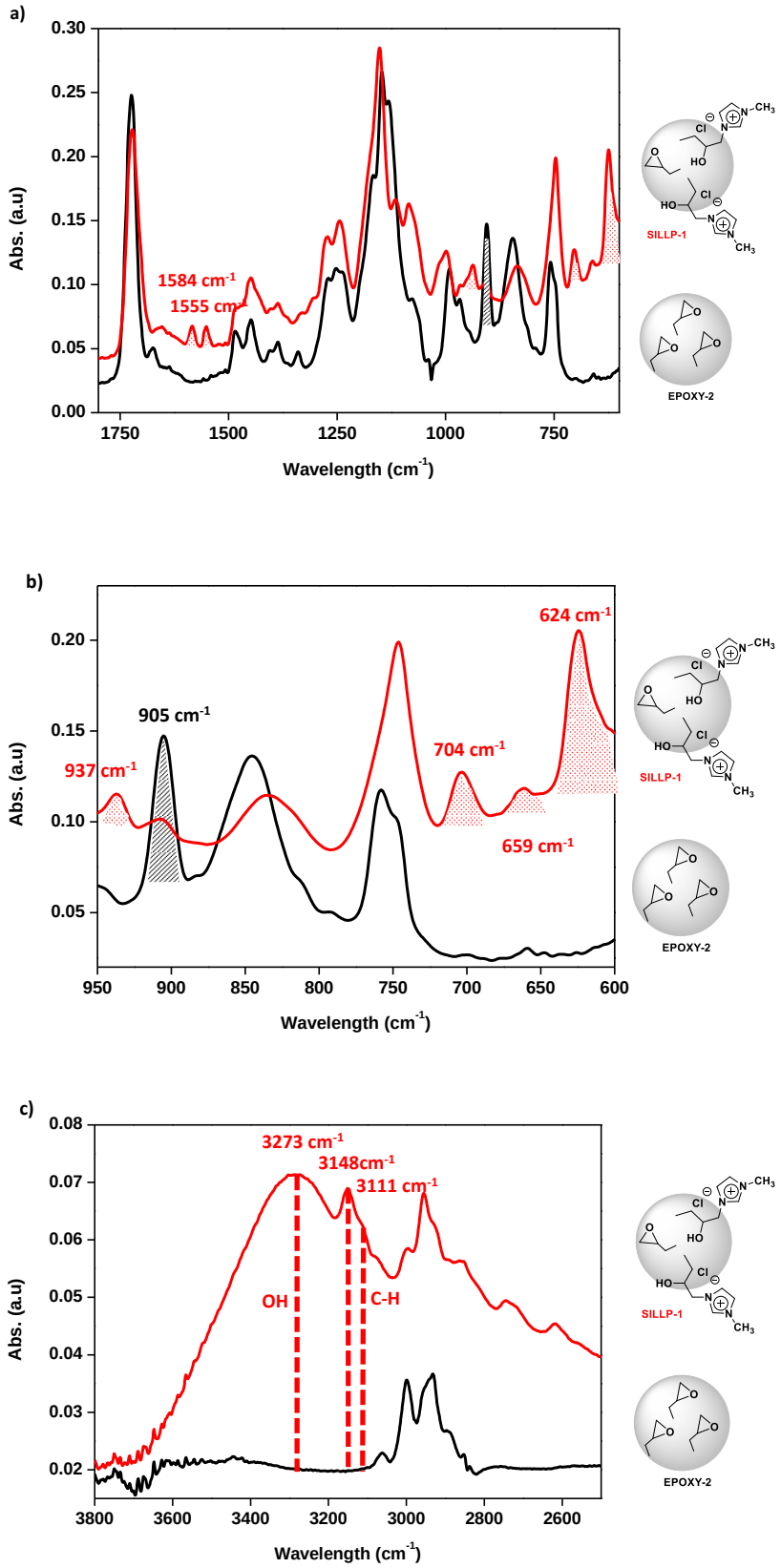

Figure SI.2. FT-IR-ATR of the **EPOXY-2** modified with methylimidazole. a) 1800-600 cm^{-1} region. b) 3800-2500 cm^{-1} region. c) 950-600 cm^{-1} region. Black: **EPOXY-2**. Red: **SILLP-1**.

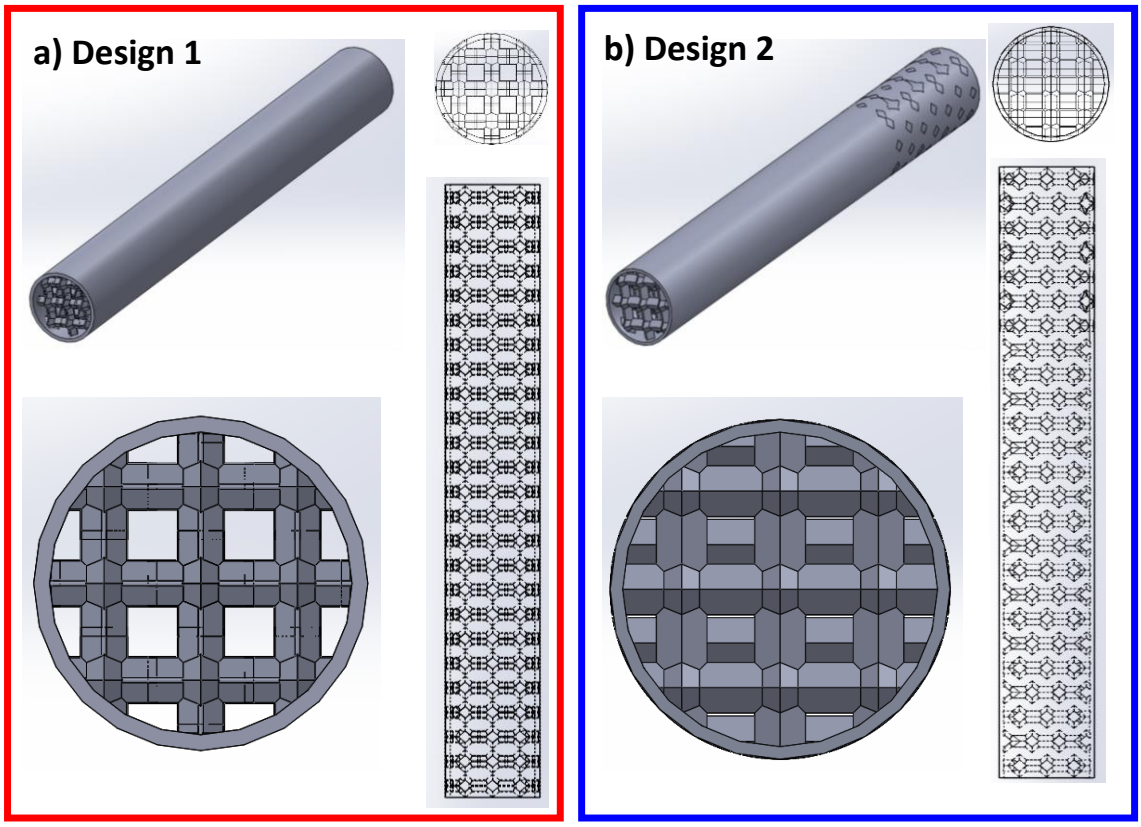

Figure SI.3. Digital design of the monolithic matrials. **(a)** Design 1 (**3D-EPOXY-D1**) square channel structure parallel to the long axis of the monolith (L: 750mm, Ø: 90mm). **(b)** Design 2 (**3D-EPOXY-D1**) a network of square pores moved 90 degree with respect to the previous one. (L: 750mm, Ø: 90mm).

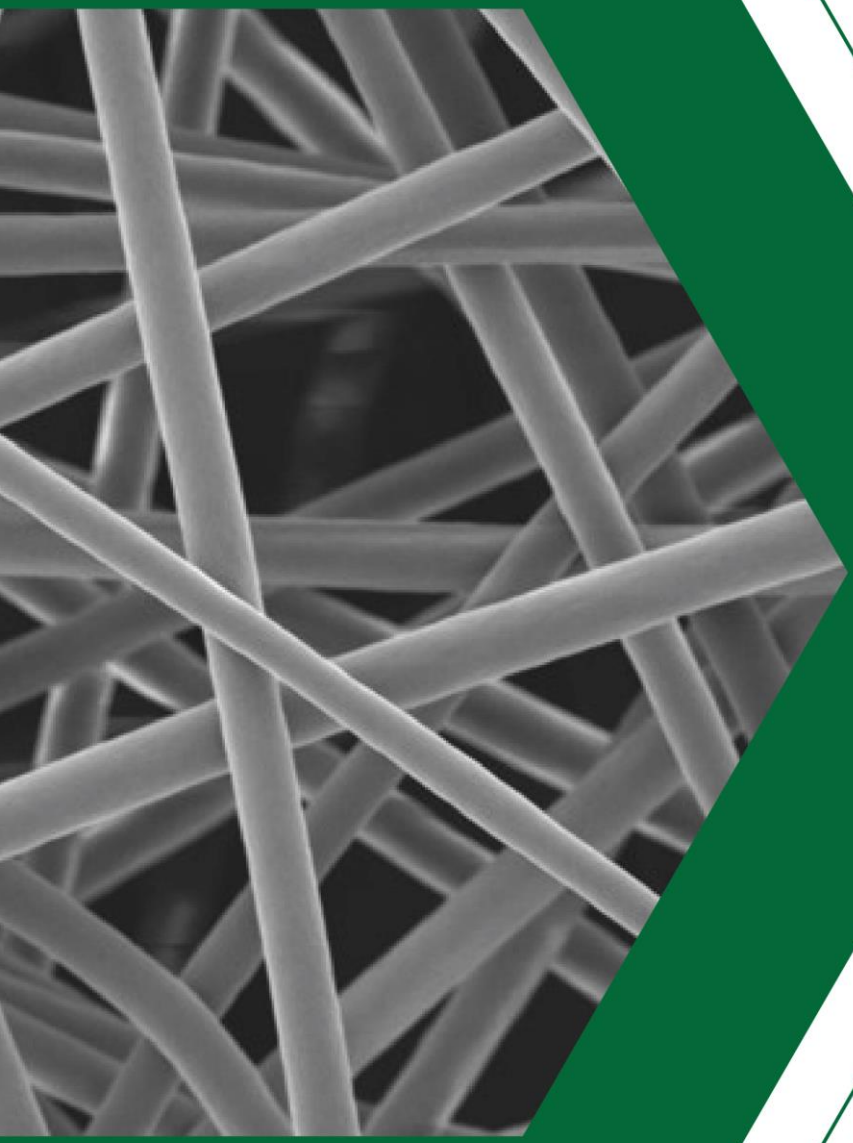

CAPÍTULO IX

Conclusiones

Capítulo IX. Conclusiones

9.1. Conclusiones generales

En el desarrollo de esta tesis Doctoral se han descrito las conclusiones específicas obtenidas en cada capítulo, por lo que en esta sección se destacaran las conclusiones generales obtenidas en el conjunto del trabajo de investigación.

1. Se ha demostrado que la combinación de polímeros funcionalizados con unidades de líquido iónico, líquidos iónicos zwiterionicos y sales de $LiNTf_2$, da lugar a materiales conductores de iones de interés. Las propiedades de dichos materiales dependen de la composición molecular de los diferentes componentes. Mediante la optimización de la composición de estos sistemas se obtienen materiales con una alta conductividad iónica, buenas propiedades mecánicas y alta estabilidad térmica.

2. Se ha demostrado que los polímeros que contienen en su estructura unidades de tiolactona permiten la obtención de materiales con diferentes niveles de funcionalización y entrecruzamiento. Estos materiales se pueden obtener empleando técnicas convencionales, pero también utilizando sistemas simples de flujo continuo o con técnicas más complejas como el electrohilado. Dependiendo de la metodología empleada se pueden crear materiales con diferentes propiedades morfológicas. Así, el empleo de condiciones de flujo continuo permite la preparación de polímeros funcionalizados en forma de *beads*, mientras que el electrohilado da lugar a nanofibras en forma de membranas, lo que permite ajustar la morfología de los materiales se puede ajustar en función de la aplicación a desarrollar.

3. El empleo de la técnica de electrohilado ha permitido la fabricaron de nanofibras poliméricas de PIL/PVP obtenidas en forma de membranas. La

presencia en los PILs de unidades de tiolactona permite obtener por post-modificación química nuevas membranas con diferente funcionalización y

niveles de entrecruzamiento en las nanofibras. Bajo las condiciones de modificación adecuadas, es posible obtener una nueva generación de membranas que conservan la morfología de las fibras nanoestructuradas y que poseen propiedades muy interesantes para su aplicación en la detección de aminas volátiles y como catalizadores en la reacción de cicloadición del CO_2 a epóxidos.

4. Se han desarrollado materiales poliméricos que contienen fases soportadas semejantes a líquidos iónicos derivados de imidazolio (SILLPs) que permiten la inmovilización del Rosa de Bengala como fotocatalizador. La presencia de las unidades del líquido iónico no solo da la posibilidad de modular la actividad catalítica de las unidades de Rosa de Bengala sino que también proporcionan a dichas unidades un microambiente específico que ajusta la accesibilidad de los reactivos y de los sustratos a los centros activos. Estos sistemas se han evaluado como (foto)catalizadores en la reacción del ácido 2-furóico con oxígeno singlete y en la reacción de cicloadición del CO_2 a epóxidos, demostrándose que es posible preparar materiales catalíticos más activos y estables, con propiedades modulables y con bajo coste económico.

5. El empleo del diseño digital y la impresión 3D ha permitido el desarrollo de materiales funcionalizados poliméricos con morfologías tridimensionales complejas. La presencia de grupos epóxido en la superficie de estos materiales permite su modificación con unidades de líquido iónico. Estas unidades transfieren a estos materiales las propiedades moleculares de los líquidos iónicos. Así, se han podido obtener materiales 3D que pudieron actuar como sistemas catalíticos eficientes en la reacción de cicloadición de CO_2 a epóxidos, obteniendo altos rendimientos y una estabilidad prolongada.

6. El empleo del diseño digital ha permitido obtener estructuras 3D complejas que aplicadas a sistemas de reacción bifásico gas-líquido consiguen mejorar la

fluidodinámica del sistema en comparación con los sistemas tradicionales (lecho fijo empaquetado con *beads*) mejorando la eficiencia de la reacción de cicloadición de CO_2 a epóxidos en términos de productividad.

7. En este trabajo se ha demostrado que es posible realizar el diseño y síntesis de materiales poliméricos multifuncionales con propiedades modulables y morfologías complejas integrando una serie de tecnologías novedosas como los sistemas en flujo continuo, el electrohilado y la impresión 3D. El empleo de técnicas de fabricación avanzada, como las mencionadas anteriormente, permite obtener materiales con aplicaciones interesantes como la detección aminas volátiles y la catálisis. Tanto el diseño de los materiales sintetizados como el desarrollo de sus aplicaciones se han llevado a cabo de acuerdo con los "Principios de la Química Verde".

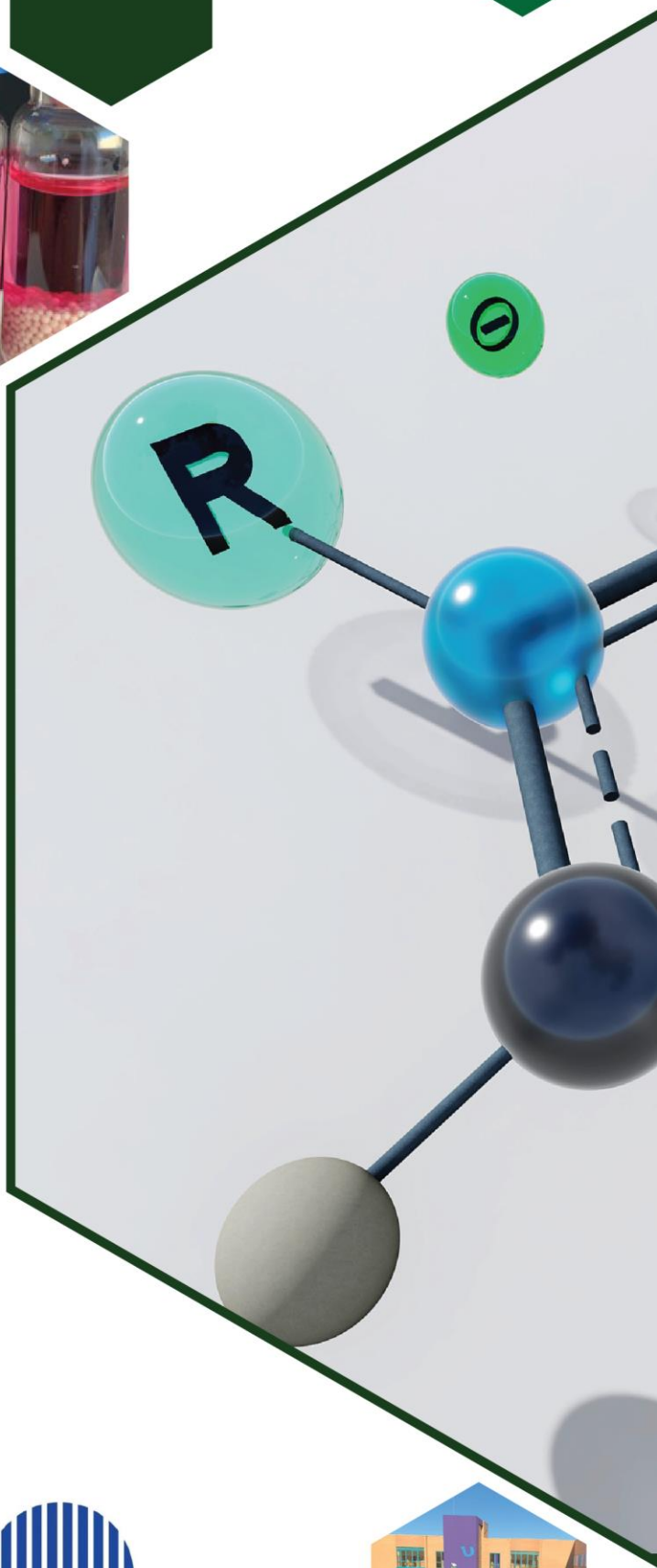

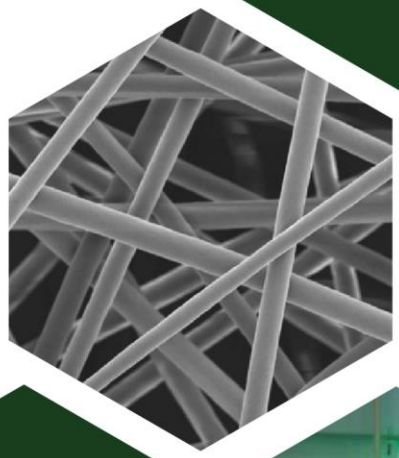

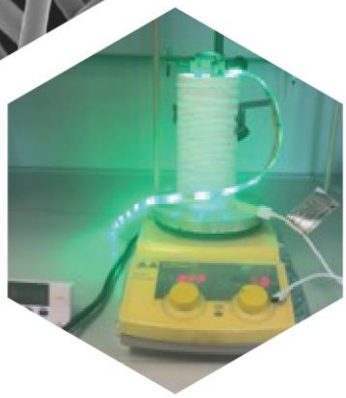

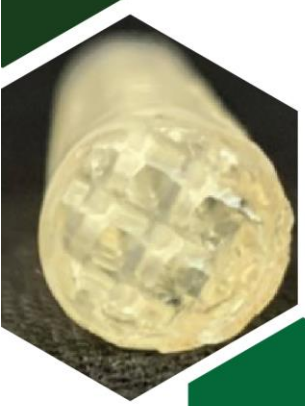

Sustainable and Supramolecular Chemistry

UNIVERSITAT JAUME·I

UNED